SANDIA REPORT
SAND2022-5515
Printed April 2022

Sandia National Laboratories

HYSPLIT/MACCS Atmospheric Dispersion Model Technical Documentation and Benchmark Analysis

Prepared by: D.J. Clayton*, N.E. Bixler*, and K.L. Compton**

* Sandia National Laboratories
** United States Nuclear Regulatory Commission (NRC)

Prepared by
Sandia National Laboratories
Albuquerque, New Mexico
87185 and Livermore,
California 94550

Issued by Sandia National Laboratories, operated for the United States Department of Energy by National Technology & Engineering Solutions of Sandia, LLC.

Available to DOE and DOE contractors from
U.S. Department of Energy
Office of Scientific and Technical Information
P.O. Box 62
Oak Ridge, TN 37831

Telephone: (865) 576-8401
Facsimile: (865) 576-5728
E-Mail: reports@osti.gov
Online ordering: http://www.osti.gov/scitech

Available to the public from
U.S. Department of Commerce
National Technical Information Service
5301 Shawnee Rd
Alexandria, VA 22312

Telephone: (800) 553-6847
Facsimile: (703) 605-6900
E-Mail: orders@ntis.gov
Online order: https://classic.ntis.gov/help/order-methods/

ABSTRACT

The nuclear accident consequence analysis code MACCS has traditionally modeled dispersion during downwind transport using a Gaussian plume segment model. MACCS is designed to estimate consequence measures such as air concentrations and ground depositions, radiological doses, and health and economic impacts on a statistical basis over the course of a year to produce annual-averaged output measures. The objective of this work is to supplement the Gaussian atmospheric transport and diffusion (ATD) model currently in MACCS with a new option using the HYSPLIT model. HYSPLIT/MACCS coupling has been implemented, with HYSPLIT as an alternative ATD option. The subsequent calculations in MACCS use the HYSPLIT-generated air concentration, and ground deposition values to calculate the same range of output quantities (dose, health effects, risks, etc.) that can be generated when using the MACCS Gaussian ATD model. Based on the results from the verification test cases, the implementation of the HYSPLIT/MACCS coupling is confirmed.

This report contains technical details of the HYSPLIT/MACCS coupling and presents a benchmark analysis using the HYSPLIT/MACCS coupling system. The benchmark analysis, which involves running specific scenarios and sensitivity studies designed to examine how the results generated by the traditional MACCS Gaussian plume segment model compare to the new, higher fidelity HYSPLIT/MACCS modeling option, demonstrates the modeling results that can be obtained by using this new option. The comparisons provided herein can also help decision-makers evaluate the potential benefit of using results based on higher fidelity modeling with the additional computational burden needed to perform the calculations. Three sensitivity studies to investigate the potential impact of alternative modeling options, regarding 1) input meteorological data set, 2) method to estimate stability class, and 3) plume dispersion model for larger distances, on consequence results were also performed. The results of these analyses are provided and discussed in this report.

ACKNOWLEDGEMENTS

Pat Santiago provided the NRC management oversight at the onset of this project, followed by Jon Barr, Tamara Bloomer and Luis Betancourt. Keith Compton provided technical oversight and edited materials provided by the SNL technical contributors, as well as organized and led the peer review process. Jon Barr was the NRC Project Manager at the inception of the project, and was succeeded by Salman Haq, who oversaw successful completion of the project.

Many thanks to the peer review panel for all their work to review the initial documentation and provide meaningful comments. The panel was comprised of Damien Didier, head of the Environmental Dispersion Modeling for Accidental Consequences Section at the Institut de Radioprotection et de Sûreté Nucléaire; Dr. Steven Hanna, a consultant with extensive experience in atmospheric dispersion modeling; and Dr. Chris Owen, who is the Model Development Team lead for the US Environmental Protection Agency's AERMOD Modeling System. This report is significantly improved due to their review.

In addition, the authors extend their appreciation to Roland Draxler, Glenn Rolph, Ariel Stein, Tianfeng Chai, and Mark Cohen from the National Oceanic and Atmospheric Administration (NOAA) Air Resources Laboratory (ARL), who supported the integration of HYSPLIT with MACCS by responding to questions, updating software, reviewing progress, and suggesting alternatives. This group also created software to implement a polar coordinate system for calculating air concentrations and ground depositions, which is now the standard option used when coupling HYSPLIT with MACCS.

CONTENTS

LIST OF FIGURES

LIST OF TABLES

ACRONYMS AND TERMS

Acronym/Term	Definition
ADP	Automated Data Processing
ARL	Air Resources Laboratory
ATD	Atmospheric Transport and Diffusion
Bq	Becquerel
CCDF	Complementary Cumulative Distribution Function
CRAC	Calculation of Reactor Accident Consequences
EA	Environmental Assessments
EF	Early Fatality
EIS	Environmental Impact Statement
EPA	Environmental Protection Agency
HYSPLIT	HYbrid Single-Particle Lagrangian Integrated Trajectory
KI	Potassium Iodide
LCF	Latent Cancer Fatality
MACCS	Nuclear accident consequence analysis code
NAM	North American Mesoscale
NARR	North American Regional Reanalysis
NCEP	National Centers for Environmental Prediction
NOAA	National Oceanic and Atmospheric Administration
NPP	Nuclear Power Plant
NRC	Nuclear Regulatory Commission
PRA	Probabilistic Risk Assessment
SAMA	Severe Accident Mitigation Alternatives
SAMDA	Severe Accident Mitigation Design Alternative
SOARCA	State of the Art Consequence Analysis
WRF	Weather Research and Forecasting

This page left blank

1. INTRODUCTION

The nuclear accident consequence analysis code MACCS was developed by Sandia National Laboratories for the U.S. NRC with the main purpose of simulating and analyzing the impacts of severe nuclear accidents at nuclear power plants on the surrounding population and environment. MACCS is used to perform probabilistic health and economic consequence assessments of nuclear power plants by examining the site-specific meteorological conditions that may occur over the course of a year and producing complementary cumulative distribution functions (CCDF) for a variety of consequence measures with annual statistics. Mean and selected percentile results of these measures, taken over the course of the year, are used to characterize the CCDF produced by the code. MACCS achieves this by modeling the following:

- atmospheric dispersion and plume depletion,
- probabilistic treatment of meteorology,
- dosimetry,
- protective actions for the emergency phase, intermediate phase, and long-term phase,
- societal and economic costs, and
- radiogenic health effects (both early and latent).

MACCS is used by U.S. nuclear power plant (NPP) license renewal applicants to support the plant specific evaluation of severe accident mitigation alternatives (SAMAs) as part of the applicant's environmental report for license renewal. MACCS is also used in severe accident mitigation design alternatives (SAMDA) analyses and severe accident consequence analyses for environmental impact statements (EIS) and environmental assessments (EA) for new reactor applications. The NRC uses MACCS in its cost-benefit assessments supporting regulatory analyses that evaluate potential new regulatory requirements for existing reactors. This update supports these regulatory applications with an alternative atmospheric dispersion model to improve the MACCS capabilities for modeling atmospheric dispersion for potentially complex airflows such as lake or sea breezes, river valleys, or transport and diffusion over long distances. MACCS models are described in a series of reports published by the NRC (H-N Jow, et al., 1990; Chanin and Young, 1998; and Bixler et al., 2021).

The MACCS code is divided into the ATMOS, EARLY, and CHRONC modules. The ATMOS module performs the calculations for atmospheric transport, diffusion, and deposition, as well as the radioactive decay that occurs prior to release and while the material is in the atmosphere. The EARLY module performs the calculations, including the effects of emergency response, related to the early (emergency) phase. The exposure pathways considered during this period are cloudshine, groundshine, direct inhalation of the plume, and resuspension inhalation. Protective actions that can be modeled in MACCS for the early phase include evacuation, sheltering, use of potassium iodide (KI), and population relocation based on dose projections (Chanin and Young, 1998). The cost of protective actions implemented in the early phase is captured in the CHRONC module. The CHRONC module also simulates exposures that occur following the emergency phase and estimates the economic costs of the long-term protective actions. CHRONC calculates the individual health effects that result from external exposure to contaminated ground and from inhalation of resuspended materials. Population doses and health effects caused by the consumption of contaminated food and water by individuals who could reside both in and out of the area of interest are also calculated in CHRONC.

The atmospheric transport and diffusion (ATD) model in ATMOS is a Gaussian plume segment model, which dates to the various incarnations of the MACCS code and its predecessors, i.e., Calculation of Reactor Accident Consequences (CRAC) (US NRC, 1975), CRAC2 (Ritchie et al.

1983), MACCS (Chanin et al. 1990), and MACCS2 (Chanin and Young, 1998), including the most current versions of the MACCS code suite. With the Gaussian plume segment model, releases of material to the atmosphere are divided into successive plume segments, usually of one to ten hours in duration, and each segment is modeled as if it is traveling in a straight-line with an assumed Gaussian distribution of concentration in both crosswind and vertical directions. The Gaussian plume segment ATD model chosen for MACCS has served well over the years and has proven to be adequate for performing Probabilistic Risk Assessments (PRAs), which are less demanding in terms of ATD fidelity than emergency response tools. PRA analyses evaluate future, hypothetical accidents and, therefore, it is impossible to know the meteorological characteristics at the time of the accident, other than in a statistical sense. As a result, analysts assume that future meteorology will be like past meteorology and that adequate statistical sampling of past meteorology provides a statistical understanding of the consequences that might occur from a potential future accident. Furthermore, the results that are most commonly used in a PRA analysis are annual mean values over the possible meteorological conditions that occur in the course of a representative year. It has been shown that annual mean results calculated by the MACCS Gaussian plume segment model compare reasonably well with higher fidelity models (Molenkamp et al., 2004).

Two of the principal advantages of a Gaussian plume segment model over a higher fidelity model are the required computational time and the minimal requirements on meteorological data. These two advantages were almost certainly part of the consideration when MACCS and its predecessors were created. However, these advantages are less significant today than they were in the 1970s through 1990s when the initial development of the MACCS code and its predecessors was done. Now, it is possible to use a higher fidelity model in terms of both computational time and meteorological data requirements. These higher fidelity models may be more suitable for some situations, such as complex terrain, complex or transient wind fields, or long-distance transport.

The National Oceanic and Atmospheric Administration's (NOAA's) HYbrid Single-Particle Lagrangian Integrated Trajectory (HYSPLIT) model is a state-of-the-art complete system for computing simple air parcel trajectories, and complex dispersion and deposition simulations (Draxler and Hess, 1997; Draxler and Hess, 1998; Draxler, 1999; Stein et al., 2015). The initial development of HYSPLIT was a result of a joint effort between NOAA and Australia's Bureau of Meteorology. The NOAA HYSPLIT model has been chosen for integration with MACCS because it offers both puff and particle dispersion models, accepts a wide variety of high-quality publicly available meteorological data, is well documented and widely used, offers graphical capabilities, and its source code is publicly-available. Furthermore, NOAA has supplied exemplary support to the MACCS developers and has guided many of the decisions on how to implement the model in MACCS

1.1. Objective

The objective of this report is to document the technical components and the implementation of the HYSPLIT/MACCS coupled model. This coupled model is not intended to replace the Gaussian ATD model currently in MACCS (ATMOS), but to supplement MACCS with a new ATD model option. ATMOS has been and continues to be the primary model for performing consequence analyses in support of PRAs. The documentation of the implementation is provided to describe how the coupling was achieved and to show the results of verification tests performed on the HYSPLIT/MACCS coupling.

A benchmark analysis, which compares the results of the traditional MACCS Gaussian plume segment model against the higher fidelity HYSPLIT/MACCS results for specific scenarios and sensitivity studies is also documented in this report. This comparative exercise has several purposes. First, it serves as an initial analysis using the HYSPLIT/MACCS coupling to demonstrate the

modeling results that can be obtained from using this new option. This provides a practical test of the implementation and provides information on the differences in the model input data and computational resources needed to exercise the new capability. Second, it serves as a further test of the hypothesis tested in (Molenkamp et al., 2004) that the results of a simple Gaussian plume segment model are sufficient for purposes of estimating expected values of consequence measures when averaged over a broad set of meteorological conditions (e.g., one year). Ultimately, the purpose of this benchmarking study is to illustrate the application of the new capabilities and inform decisions on when it may be appropriate to choose the Gaussian model versus the HYSPLIT model for specific applications. Because some applications may be substantially different from these benchmarking comparisons, this study does not draw general conclusions regarding which ATD modeling option should be used. It should also be noted that, with the introduction of the new capability, the logistical challenge of comparing the simple Gaussian model against the more advanced model is considerably reduced. Users are encouraged to perform their own studies to determine which modeling approach best suits their needs in terms of model fidelity and computational expense.

As this report is limited in scope and because MACCS can be used for a wide range of applications, the conclusions in this report should be considered in light of the purpose of the analysis to be conducted.

1.2. Report Organization

This report documents the technical components of the implementation of the HYSPLIT model as an option for MACCS. A brief overview of the technical basis for both the traditional MACCS Gaussian plume segment model and the HYSPLIT ATD model are provided in the remainder of Section 1. The verification of the implementation of the HYSPLIT/MACCS option is discussed in Section 2. Section 3 contains the plan for the benchmark analyses, and the results of the benchmark calculations and discussion are reported in Section 4. This is followed by the results of an additional set of sensitivity studies in Section 5 and a summary in Section 6.

1.3. Atmospheric Dispersion Model Overview

1.3.1. Gaussian Plume Segment Model

MACCS has traditionally modeled dispersion during downwind transport using a Gaussian plume segment model. The material released to the atmosphere is divided into successive plume segments and each segment is modeled as a plume traveling in a straight-line with an assumed Gaussian distribution of concentration in both crosswind and vertical directions. Thus, the crosswind and vertical dimensions of each plume segment are expressed in terms of crosswind (σ_y) and vertical (σ_z) standard deviations of the normal concentration distributions that characterize a Gaussian plume. The Gaussian equations implemented in MACCS are derived assuming that, in the along-wind direction, turbulent velocities are negligible compared with the mean wind speed. That is, along-wind dispersion, σ_x, is assumed to be zero. An option in MACCS is to use power-law functions to define σ_y and σ_z, and these have the form:

$$\sigma_{yi} = a_i \cdot (x/x_0)^{b_i}$$
$$\sigma_{zi} = c_i \cdot (x/x_0)^{d_i} \qquad \text{(Equation 1)}$$

Where

σ_{yi} = lateral dispersion parameter for stability class, *i*, which is the standard deviation of a Gaussian distribution (m).

σ_{zi} = vertical dispersion parameter for stability class, *i*, which is the standard deviation of a Gaussian distribution (m).
x = downwind distance from the virtual source location (m).
a_i, b_i = linear and exponential coefficients in the power-law expressions for crosswind dispersion. Subscript, *i*, represents stability class. Units for these coefficients are m and dimensionless, respectively.
c_i, d_i = linear and exponential coefficients in the power-law expressions for vertical dispersion. Subscript, *i*, represents stability class. Units for these coefficients are m and dimensionless, respectively.
x_0 = unit of length, 1 m.

MACCS also allows dispersion lookup tables to be used to define the dispersion parameters, but this option is not employed in the analyses described in this report and so they are not discussed here. A detailed discussion of this option can be found in (Bixler et al., 2021).

(Hanna, 2002) recommended that plume dispersion beyond 30 km (19 mi) be based on time of travel, not on distance from the source to the receptor. MACCS allows the user to implement this recommendation. The basis for the recommended distance, 30 km (19 mi), is that the measurements from field experiments upon which dispersion tables are based have a limit of about 30 km (19 mi). In the MACCS implementation, the user must select the downwind distance at which the code switches from distance-based dispersion to time-based dispersion. The user must also select a linear coefficient for the time-based dispersion model. Hanna recommends a distance of 30 km (19 mi) and a linear coefficient value of 0.5 m/s. A virtual source approach is used to ensure continuity in the crosswind dispersion parameter across the transition. The following equation describes the time-based model:

$$\sigma_y = \begin{cases} a\left(\dfrac{x}{x_0}\right)^b & x < x_c \\ a_c t & x \geq x_c \end{cases} \qquad \text{(Equation 2)}$$

Where

σ_y = value of crosswind dispersion (m).
a = linear coefficient for distance-based, crosswind dispersion (m).
x = downwind distance from the virtual source (m).
x_0 = unit of length, 1 m.
b = exponential parameter for distance-based, crosswind dispersion (dimensionless).
x_c = distance from the source (m) at which the dispersion model switches from distance- to time-based formulations (CYDIST in MACCS). The default value is 30 km (19 mi) based on (Hanna, 2002).
a_c = linear coefficient for time-based, crosswind dispersion (m/s) (CYCOEF in MACCS). The default value is 0.5 m/s based on (Hanna, 2002).
t = time since the plume was released from the virtual source (s) at the current wind speed.

During downwind transport, atmospheric turbulence causes plume segments to expand in all directions with the rate of expansion increasing when atmospheric turbulence increases. Vertical expansion of the plume is increased by larger values of surface heating by the sun (convective turbulence) and by increased wind speed and surface roughness (mechanical turbulence) and constrained by the ground and by inversion layers and mixing height. Crosswind spreading of the plume along the y-direction is unconstrained but is proportional to turbulent intensity. The effective crosswind dimensions of a plume segment may be increased by lateral meander of the plume about its

centerline trajectory. Turbulent expansion in the wind direction is neglected in the MACCS implementation. Thus, the along-wind dimension of the plume segment is the wind speed multiplied by the time duration of the emissions contributing to the segment.

The Gaussian plume segment model assumes that the dispersion of gas molecules and aerosol particles in the plume during its downwind transport can be modeled as a correlated random walk that generates a normal distribution for air concentration in the vertical and crosswind directions. Mechanical turbulence and thermal gradients within the mixing layer can cause vertical and horizontal (crosswind) plume dispersion to differ significantly and therefore these quantities must be calculated separately.

The size of a Gaussian plume in the vertical and crosswind directions is defined by the standard deviations (σ_y and σ_z) of the normal distributions of concentrations. When unconstrained by the ground or by inversion layers, the Gaussian plume equation has the following form:

$$\chi(x,y,z) = \frac{Q}{2\pi u \sigma_y \sigma_z} \exp\left[-\frac{1}{2}\left(\frac{y}{\sigma_y}\right)^2\right] \exp\left[-\frac{1}{2}\left(\frac{z-h}{\sigma_z}\right)^2\right] \qquad \text{(Equation 3)}$$

Where

$\chi(x,y,z)$ = time-integrated air concentration (Bq·s/m^3) at downwind location (x, y, z). x is distance in the downwind dimension, y is distance in the crosswind dimension, and z is distance in the vertical dimension. The interval used for integration is the duration of emissions contributing to the individual plume segment.

Q = released activity (Bq).

u = mean wind speed (m/s).

h = stabilized height of the plume centerline (m).

Once a plume has expanded sufficiently in the vertical dimension so that further vertical expansion is constrained by the ground and/or the capping inversion layer, Equation (3) is no longer applicable. To treat restricted growth in the vertical dimension, the ground and the inversion layer are treated as impenetrable, reflecting boundaries. Mathematically, reflection is included by the addition of mirror image sources above the inversion layer and below the plane of the ground. This produces the following equation, which is used in MACCS to calculate the time-integrated, plume-centerline, air concentration, $\chi(x, y = 0, z = h)$, the time-integrated, ground-level, air concentration under the plume centerline, $\chi(x, y = 0, z = 0)$, as well as off-centerline concentrations in the crosswind direction, from the time a plume segment is released until the vertical distribution of the segment becomes uniform between the ground and capping inversion layer (becomes well mixed in the vertical dimension):

$$\chi(x,y,z) = \frac{Q}{2\pi u \sigma_y \sigma_z} exp\left[-\frac{1}{2}\left(\frac{y}{\sigma_y}\right)^2\right] \sum_{n=-\infty}^{\infty} \left\{ exp\left[-\frac{1}{2}\left(\frac{z-h+2nH}{\sigma_z}\right)^2\right] + exp\left[-\frac{1}{2}\left(\frac{z+h+2nH}{\sigma_z}\right)^2\right]\right\}$$

(Equation 4)

Where

H = height (m) of the capping inversion layer, i.e., the height of the mixing layer.

At each spatial interval along the plume's trajectory, MACCS tests for the occurrence of a uniform concentration distribution in the vertical direction (well-mixed plume between the ground and the capping inversion layer) using the criterion of when $H/\sigma_z < 0.03$. This criterion approximately corresponds to the requirement that the results of Equation (4) would be within 1% as a uniform concentration distribution in the vertical direction. Once a uniform vertical distribution is attained, Equation (4) reduces to the following equation:

$$\chi(x, y=0, z) = \frac{Q}{\sqrt{2\pi}\sigma_y uH} \exp\left[-\frac{1}{2}\left(\frac{y}{\sigma_y}\right)^2\right] \quad \text{(Equation 5)}$$

MACCS estimates the initial mixing layer height by linear interpolation between the minimum and the maximum values for the season of the year, based on the time of day. The minimum value is used from just after sunset to sunrise. The maximum value is achieved at sunset. The mixing layer height increases (if not already at the maximum) during the morning to afternoon up to the maximum. Once the maximum mixing layer height is attained, it is held constant for the duration of the plume segment travel time as it transports through the grid.

Buoyant plume segments can rise to heights greater than their initial release height. In MACCS, plume rise is calculated using equations recommended by (Briggs, 1973; Hanna et al., 1982). The calculated plume rise depends on the windspeed, the atmospheric stability, and the initial plume buoyancy and is limited by the mixing layer height. When windspeeds are high, a buoyant plume segment that is released into a strong building wake is unable to rise above the wake. In MACCS, the ability of the buoyant plumes segments to rise above building wakes is based on the wind speed (u), buoyancy flux (F) and building height (H_b), based on the following inequality proposed by (Briggs, 1973).

$$u > \left(\frac{9.09F}{H_b}\right)^{1/3} \quad \text{(Equation 6)}$$

If the inequality is satisfied, the plume is modeled with zero plume rise. The buoyancy flux (F) is the calculated as 8.69 x 10^{-6} m^4/s^3/W times the rate of release of sensible heat (in W).

The model for building wake effects typically used in MACCS assumes that the initial distance scales of the plume are based on the dimensions of the building or complex of buildings from which the release emits. The standard guidance is to assume that ground-level concentrations at the edges of the building and the concentration directly above the centerline at the top of the building are 10% of the centerline plume concentration (Turner, 1970). This guidance translates into assuming the initial σ_y = 0.23 x building width and the initial σ_z = 0.47 x building height.

During downwind transport, radioactive decay and build-up of radioactive daughters of each radionuclide in the plume segment are evaluated using the Bateman equation. Decay chains of up to six members can be represented in MACCS. Decay and build-up are calculated from time zero (reactor shutdown) and continue through the modeled timeframe.

Dry deposition is modeled in MACCS using Chamberlain's source depletion method (Chamberlain, 1953; Hosker, 1974; Karlsson, 1982), modified to allow treatment of particle size distribution and capping of vertical expansion by the mixing height. The ground deposition is calculated as the product of the ground-level air concentration and the dry deposition velocity. The method neglects the effects of deposition on the shape of the vertical distribution of contaminants in the plume. The effects of a particle-size distribution are accounted for by specifying dry-deposition velocities for each aerosol size. The dry deposition velocity is assumed spatially and temporally constant throughout the calculation. The user specifies the dry deposition velocity to be used for each particle size bin.

Deposition of reactive vapors is also modeled using a deposition velocity. Nonreactive gases (e.g., noble gases) are typically modeled assuming that there is no deposition.

In MACCS, wet deposition is modeled as a rapid, first-order rate process, using the model of (Brenk and Vogt, 1981). The depletion rate due to wet deposition is proportional to the amount of contaminant in the plume segment and the washout coefficient, which is a function of the precipitation intensity. As plume segments may span multiple spatial elements, MACCS apportions the wet deposition over all spatial elements traversed wholly or partially by a plume segment during a rainstorm.

Incorporating the above processes, MACCS determines the ground-level air concentration and ground deposition of a radionuclide for each spatial element and for each plume segment. The results from a set of plume segments are then summed together to determine the overall ground-level, time-integrated, air concentration (in units of $Bq \cdot s/m^3$) and ground deposition (in units of $Bq \cdot s/m^2$) for each radionuclide. The integration is over the entire duration of plume passage. The integral concentrations and depositions can be output from the ATMOS module in MACCS.

The spatial domain is user-defined within MACCS by specifying the number of radial intervals, the number of compass sectors, and the radial distance from the release point (i.e., from the center of the polar coordinate system,) for each radial interval. Definition of a spatial grid for modeling involves consideration of the objectives of the analysis and the limitations of the models used by MACCS. The analyst can designate up to 35 radial distances in MACCS. Grid spacing is typically at finer intervals close to the site, with larger intervals being more appropriate at longer distances. A logarithmic spacing (or roughly so) is commonly used to define the radial distances. The spatial grid is an important element of the overall model. Factors that may affect the grid definition include (but are not limited to) the distance to the site boundary, the population distribution around the site, the areas over which different emergency response actions may be taken, the spatial range of applicability of the ATD model, and the range over which consequence results are desired. The domain is assumed flat (i.e., no terrain-height corrections).

1.3.2. HYSPLIT

Several advanced ATD models were assessed for coupling with MACCS. The essential features for selection included the ability to treat Lagrangian puffs or particles, the incorporation of three-dimensional wind fields, the availability of the executable and source code, and validation evidence for the model. It was desirable that the model support a variety of gridded weather data formats and could facilitate graphical post-processing. Based on these criteria, HYSPLIT was selected for coupling with MACCS.

HYSPLIT (Draxler and Hess, 1997; Draxler and Hess, 1998; Draxler, 1999; Stein et al., 2015) is used for both research applications and emergency response events that require modeling the transport and dispersion of harmful pollutants in the atmosphere. The model is designed to support a wide range of simulations related to the ATD modeling of pollutants and hazardous materials, as well as the deposition of these materials onto the Earth's surface. Some of the applications include tracking and forecasting the release of radioactive material, volcanic ash, wildfire smoke, and other pollutants (such as mercury) from various stationary emission sources.

In HYSPLIT, the dispersion of a pollutant can be calculated using either puff or particle modes. Hybrid puff/particle modes are also available, which can treat dispersion as a mixture of puff and particle modes. In puff mode, puffs expand until they exceed the size of the meteorological grid cell (either horizontally or vertically) and then split into several new puffs, each with its share of the pollutant mass. The particle mode advects a fixed number of particles through the model domain with the mean wind field and spreads the particles using a random turbulent component. One of the

hybrid modes retains the particle treatment in the vertical where greater resolution has significant impact and uses the puff mode in the horizontal where the greater fidelity of the particle mode is not as impactful. This gains some of the fidelity of the particle mode, but also saves computation time. For this analysis, the HYSPLIT Lagrangian particle model was selected as a starting point as that is the default mode when running a HYSPLIT calculation. Comparisons with the other modes is reserved for future studies.

HYSPLIT includes the option of specifying the heat content (buoyancy flux) of the release. When that option is used, HYSPLIT uses the plume rise equations recommended by (Briggs, 1973; Hanna et al., 1982). The calculated plume rise height then replaces the specified release height for the initial position of the puff/particle, i.e., final plume rise is assumed to be instantaneous.

Radioactive decay can be represented in HYSPLIT and radionuclide daughter production modules have been incorporated into HYSPLIT. Given a chain of decay beginning with a parent radionuclide, the model can calculate the additional radiological activity due to in-growth of daughter products using the Bateman equations. The radioactive decay can be modeled for each aerosol. The mass of the radionuclide in the air and deposited onto the ground are then decreased based on the calculated decay. Correspondingly, the mass of the daughter product in the air and deposited on the ground are increased.

In HYSPLIT, dry deposition is either explicitly defined as a deposition velocity or computed using the resistance method (Draxler and Hess, 1998) and information about the nature of the surface. Deposition is computed in HYSPLIT only when the bottom of the puff or the particle center position is within the surface layer. The mass deposited is calculated by assuming a uniform vertical concentration distribution in the deposition layer adjacent to the ground. Mass is then removed from the puff/particle and the same mass is apportioned (deposited) onto the ground surface.

Wet deposition is divided into two processes, those in which the polluted air is continuously ingested into a cloud from a polluted boundary layer and those in which rain falls through a polluted layer (Draxler and Hess, 1998). For particulate pollutants, the simplifying assumption of a scavenging ratio is assumed for pollutants located within a cloud layer and a scavenging coefficient is used for pollutant removal in rain below a cloud layer. Wet removal can be defined for soluble gases by specifying its Henry's Law coefficient. Gaseous wet removal only occurs for the fraction of the pollutant below the cloud top.

Incorporating the above processes, HYSPLIT determines air concentrations (at user specified levels) and ground depositions for each pollutant modeled. The air concentrations and ground depositions are cumulative measures from all the puffs/particles in the simulation. A complete description of the HYSPLIT modeling system is provided in (Draxler and Hess, 1997).

1.4. Weather Sampling

The primary purpose of MACCS is to analyze the potential consequences of a hypothetical accident that could occur in the future. Because of the hypothetical nature of a future accident, it is impossible to know what the weather might be at the time of the accident. To account for the natural variability of weather, MACCS evaluates the statistical nature of potential consequences for a set of weather trials (of several hours each) based on archived weather data. A fundamental assumption is that the statistical nature of future weather is essentially the same as past weather. Since weather gradually changes over time due to natural cycles and potentially from anthropogenic forcing, it is generally preferable to use recent weather data rather than older data to perform weather sampling.

MACCS is configured to examine the variability in consequences over a period of one year using archived weather data. The computed consequences are presented in the form of a CCDF. The

CCDF produced by the code is based on sampling of a year of weather data. The same methods are used whether the Gaussian or HYSPLIT ATD model options are selected. The choice of one year ensures that seasonal variations are treated fairly in a statistical sense. However, annual variations in rainfall, wind rose, or other climatological characteristics may not be adequately treated with only one year of weather data. As a result, analysts may be compelled to evaluate consequences with multiple years of weather data. At this time, MACCS requires these evaluations to be performed one year at a time.

The concept of weather sampling is to pair a set of representative weather events with one or more atmospheric release events. Both the weather and the characteristics of the release can, and almost always do, change over time. The composition, rate, aerosol size distribution, and other characteristics of the atmospheric release generally evolve over the duration of the hypothetical accident. Likewise, the weather evolves over the period during which the released contaminants are transported through the atmosphere. A weather trial is specified by choosing the point in time during a year when the hypothetical atmospheric release begins. From this point in time forward, the weather evolves according to the archived data and simultaneously the release characteristics evolve according to a precalculated source term, which depends on the type of reactor, presumed initiating event, operator actions, and other assumptions.

Traditionally, the weather data used by MACCS are one-hour averages, which add up to 8,760 data points to define the weather for a 365-day year. A complete set of weather trials would be to pair the start of a release with each hour of weather data in the archived weather file, creating 8,760 weather trials. However, experience indicates that evaluating a subset of the 8,760 potential weather trials produces statistically representative results with adequate accuracy, with the benefit of reduce computational expense. The reduced set of weather trials approach is most often used when the computational expense (i.e., evaluation time and disk space) is large relative to the resources available. For example, severe accident uncertainty or sensitivity analyses may be undertaken in which the annual weather sampling must be repeated hundreds to thousands of times to understand the influence of non-meteorological input parameters on annual average consequence results. The statistics that are needed, e.g., mean, 5th percentile, and 95th percentile, have an impact on how many weather trials are required to produce acceptably accurate results. Over the past 10 or so years, a method has emerged that has been shown to produce adequate accuracy results over a broad range of statistical results. This method uses what is referred to as nonuniform weather bin sampling and is described in more detail below.

One method supported by MACCS is called stratified random sampling. It produces a set of weather trials that are equally probable. With this method, one or more weather trials are selected randomly for each day of the year. The user specifies how many samples are to be selected from each day. The method thus creates sets of weather trials that are multiples of 365.

The second method is called weather bin sampling. It is a type of importance sampling in which weather events that have a larger contribution to the overall consequences can be sampled more heavily than those that do not. The method constructs unequal probabilities for each of the weather trials so that those that are sampled more heavily are assigned lower probabilities, as discussed below. Ultimately, the method properly accounts for the statistical nature of the results but with fewer weather trials than are required for stratified random sampling to obtain comparable statistical accuracy.

Weather bin sampling begins by assigning each hour of weather data to a weather bin according to four characteristics: 1) precipitation rate, 2) distance a plume segment travels before precipitation starts, 3) stability class, and 4) wind speed. Some of the binning characteristics are predefined in MACCS and some are selected by the user. Wind direction is also a key variable that affects

consequences. However, the MACCS weather bin sampling algorithm assumes that a sufficient set of samples within each of the meteorologically-defined weather bins is available to adequately represent the wind rose, i.e., the likelihood of the wind blowing in each compass direction for that bin.

So-called rain bins are considered important because of the potential for a plume segment containing a large activity to travel to a population center and then for precipitation to begin, creating a local hotspot that aligns with the population center. Other bins include weather sequences for which precipitation does not occur close to the plant. Those (non-rain) bins group weather sequences according to stability class and wind speed, which have important effects on peak air concentrations and inhalation exposures at short distances. Once the weather data are binned, the algorithm randomly selects a set of weather trials from each bin.

Performing a set of weather trials with the Gaussian plume segment model in MACCS relies on the use of weather sequences, which are sequences of successive hourly values of the weather conditions, beginning at a certain time, contained in a meteorological file (i.e., wind speed, wind direction, stability class, and precipitation). The concept of a weather trial when using the HYSPLIT option is completely analogous to the weather trial concept used in the traditional MACCS Gaussian plume segment model, except that gridded weather data are used in place of single weather tower data to drive atmospheric dispersion, and these weather data may not be hourly. A weather sequence in MACCS is more complex than just a point value of weather data. A weather sequence is defined by the starting hour of weather data from the meteorological data file. However, the weather sequence uses as much sequential data from the meteorological data file as required to transport all plume segments through and out of the computational grid. An overall atmospheric release (source term) can be described by up to 500 plume segments, each of which can start at a different time after the beginning of the release. Each plume segment can travel in a different direction, and it is affected by the hourly data (i.e., wind speed, stability class, and precipitation rate) taken from the weather file starting with the hour of its release from the source location and continuing until it exits the computational grid. Both the traditional MACCS Gaussian plume segment option and the HYSPLIT option allow wind speed, stability class, and precipitation rate to change for each plume segment as it transports through the grid; however, when using the MACCS Gaussian plume segment option, a plume segment continues in the same direction once it begins.

MACCS allows two variations for performing weather bin sampling. The first is uniform sampling, which means that the same number of weather samples are drawn for each weather bin. The second is nonuniform weather bin sampling, for which the user determines the specific number of samples to draw from each weather bin. Nonuniform weather bin sampling has emerged as a best practice option over the past 10 or so years because it allows the user to perform a minimum number of weather trials from each bin but to perform more weather trials for the bins that are more heavily populated and thus more likely to occur. Current practice is to use 10% of the number in the bin, with a minimum of 12 trials (or all the trials in a bin) (Bixler et al., 2014, Bixler et al., 2021). This results in a total of about 1,000 weather trials out of the 8,760 potential weather trials to represent a year of weather data. Previous evaluations have found that this method produces a mean that is within one or two percent of the value obtained by performing all 8,760 possible weather trials. 5th and 95th percentile results tend to have larger errors but are considered statistically adequate considering the uncertainties inherent in performing a consequence analysis.

The probability of each weather bin, i.e., the probability that weather falls into the category represented by the bin, is equal to the number of weather trials in the bin divided by those in the complete year, or 8,760. The probability of a weather trial drawn from a bin depends on the total number of weather trials drawn from that bin. The collection of weather trials drawn from a bin are intended to represent the bin and, therefore, the collection is assigned the same probability as the bin

they represent. Thus, the probability of each weather trial is the inverse of the number of trials drawn from its bin times the probability of the bin, as shown in the following equation:

$$P_{wt,B} = \frac{P_B}{N_{S,B}} = \frac{N_B}{N_{wt} \cdot N_{S,B}} \quad \text{(Equation 7)}$$

Where

$P_{wt,B}$ = probability of a weather trial drawn from bin B.
P_B = probability of the weather category represented by bin B.
$N_{S,B}$ = number of samples or trials drawn from bin B.
N_B = total number of potential weather trials contained in bin B.
N_{wt} = total number of weather trials (8,760).

From Equation 7, it is straightforward to demonstrate that the sum of the probabilities of the set of weather trials is unity, as it should be.

Once a set of weather trials are run, a statistical characterization of those results is constructed in the form of a CCDF representing the variability of each consequence measure of interest due to the variability in weather conditions over the course of the year. The statistical results are built by constructing a vector of probabilities for each weather trial and a corresponding vector of results for each consequence measure. A statistical characterization is created by performing the following steps:

1. The mean for each consequence measure is constructed by taking the dot product of the probability vector and the vector of consequence results. In other words, the mean (or expected value) is the sum of the products of the corresponding elements in the two vectors.
2. The first step in calculating percentile results, such as the 5th and 95th percentiles used in this report, is to reorder the entries of the vector of consequence results from smallest to largest. The vector of probabilities is reordered in the same fashion so that frequencies and consequence results are maintained as ordered pairs.
3. Next, a third vector is created from the running sum of the reordered probability vector to create a cumulative probability for each consequence result. To calculated percentile statistics, the cumulative probability (a fraction) is converted to a cumulative percentile.
4. Finally, desired percentile values are interpolated from consecutive entries in the result vector by locating the cumulative percentile values that span the desired percentile and performing a linear interpolation between the corresponding values in the result vector.

The statistical characterization described in the previous steps is valid regardless of whether the results are equally probable or not, so it works for each of the weather sampling schemes described above.

The most common approaches when creating cumulative probabilities are to (1) assign the first value in the vector of cumulative probabilities to be the first probability and the last value to be unity or (2) the first value to be zero, in which case the last value comes out to be unity minus the first probability. Both options introduce some bias, albeit the bias diminishes as the number of samples increases. An alternative method that is more correct statistically is to construct a vector of cumulative probabilities that neither includes values of zero nor unity. This can be achieved by scaling each of the values in approach (1) by $\frac{N_T}{N_T+1}$, where N_T is the total number of weather trials, i.e., $N_T = \sum_B N_B$. For the case when the weather trials are equally probable, this creates the same spacing between zero and the first cumulative probability as between the last cumulative probability and unity, which are both equal to $\frac{1}{N_T+1}$. This is the method currently used in MACCS.

The previous discussion of the nonuniform weather bin sampling method the method used in this report for both the Gaussian and the HYSPLIT ATD model options. Because the same sampling method is used for both ATD options, the same set of weather trials is selected for both options, which ensures consistency in this aspect of the comparison.

2. IMPLEMENTATION

The implementation of the HYSPLIT code into MACCS is discussed below. First, the overall conceptual framework of how HYSPLIT is coupled with MACCS is presented. Next, the verification of the implementation of HYSPLIT into MACCS is shown. Finally, the lessons learned during the implementation and verification are discussed.

2.1. Conceptual Framework

As discussed above, the implementation strategy for incorporating HYSPLIT into MACCS is to provide a database of air concentration and ground deposition values, generated by HYSPLIT, that can be queried by MACCS to use in subsequent consequence calculations. The database should be created with the appropriate spatial and temporal resolution for the intended analysis. Historically, the atmospheric transport calculations within MACCS were accomplished in the ATMOS module using a Gaussian plume segment model described in the preceding section. When the HYSPLIT option is selected, instead of MACCS performing atmospheric transport, diffusion, and deposition calculations to determine the transient air concentration and ground deposition values, the results of the equivalent HYSPLIT calculations are used. The subsequent calculations in MACCS use the HYSPLIT generated air concentration and ground deposition values to calculate the same output quantities (dose, health effects, risks, etc.) that have traditionally been generated using the ATMOS Gaussian ATD model.

The conceptual framework for coupling MACCS and HYSPLIT is shown below in Figure 2-1. The light blue rectangles in the figure correspond to input/output data files and the green rectangles correspond to computer codes. Each of the individual pieces of the framework are discussed in more detail below.

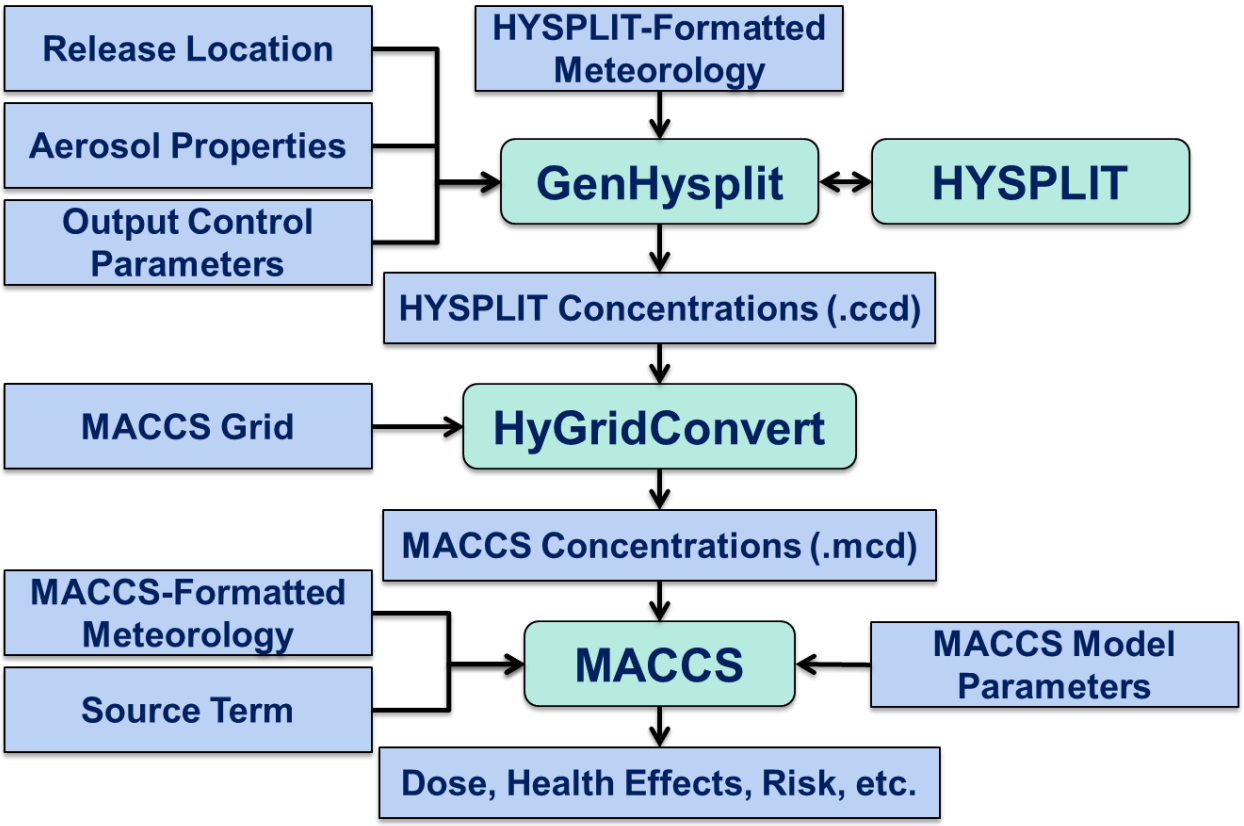

Figure 2-1. Conceptual framework for HYSPLIT/MACCS coupling

2.1.1. GenHysplit

To conduct and organize the HYSPLIT ATD calculations, an overarching program has been developed, called GenHysplit. GenHysplit is configured as a stand-alone program. GenHysplit collects input values, runs the requested HYSPLIT calculations, and consolidates the set of output files containing transient, source term independent, air concentration and ground deposition values. Several data sources are needed to conduct the analyses. These include meteorology, aerosol properties, release location, and parameters that control the output to be created. The flow of information for GenHysplit is displayed in Figure 2-2.

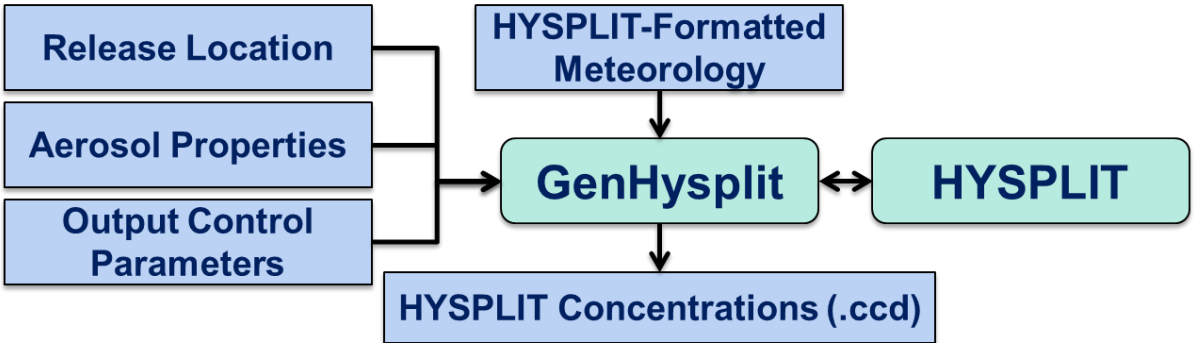

Figure 2-2. GenHysplit information flow diagram

HYSPLIT requires specially preformatted meteorological data. Gridded meteorological data, on a latitude-longitude grid or one of three conformal (Polar, Lambert, Mercator) map projections, are required at regular time intervals. The GenHysplit input file requires that both the type of

meteorological data and the time period of interest be specified. The user selects a meteorological data set that corresponds with the intended analysis. Meteorological data sets compatible with HYSPLIT can be found on an ftp site maintained by the NOAA Air Resources Laboratory (ARL) (NOAA, 2017).

The properties of the aerosols and gases are needed to determine dispersion and deposition characteristics in HYSPLIT (see Section 1.3.2). Multiple aerosol sizes and gases can be represented in the HYSPLIT simulation by Lagrangian particles, Gaussian puffs, or hybrids of the two. Information on the aerosols, such as their diameters and densities, are supplied to GenHysplit through an input file. Multiple aerosol diameters are typically used, where each aerosol has different atmospheric transport properties (e.g., deposition velocity). GenHysplit is configured to supply the required parameters to HYSPLIT to model gases. Deposition of aerosols and gases by dry deposition, wet deposition, both, and neither are supported by HYSPLIT. The user selects the aerosol and gas representation and transport properties that correspond with the intended analysis.

The atmospheric transport begins at the release location. One key aspect of the release is the stabilized height. In principle, the stabilized release height depends on the initial release height, the buoyancy of the plume, and atmospheric conditions. (Neither MACCS nor HYSPLIT currently treat plume rise from an initial momentum flux.) The option to specify multiple stabilized release heights for the database is supported in GenHysplit. This provides the capability in MACCS to model a source term that has a changing release height or buoyancy during its release duration. Two approaches to specifying the effect of buoyancy are available to the user. The first is to specify a set of specific stabilized release heights. The second is to specify a set of rates of release of sensible energy and then allow HYSPLIT to determine the stabilized release height based on the input energies and meteorological data at the time of the release. Each release height or rate of release of sensible energy requires a separate calculation with HYSPLIT.

Currently, HYSPLIT treats buoyant releases as starting at ground level, even if the release is from a stack, and does not have a model to determine when a plume segment is brought to the ground due to building wake effects. The HYSPLIT option is less general than in MACCS, where the initial height of release, rate of release of sensible heat, and effect of a building wake are all treated. The user selects the release height representation that corresponds with the intended analysis.

The HYSPLIT calculations are configured for a "normalized release," which is a one becquerel (Bq) release of a conservative (i.e, non-decaying) tracer species for each aerosol size of interest over a one-hour time-period. This normalized release approach is valid if the processes in the model are linear (e.g., no chemical reactions or transformations during transport). In this application, MACCS takes the HYSPLIT results for a conservative tracer as input and subsequently accounts for non-linear effects such radioactive decay and ingrowth.

The specification of the output control parameters for GenHysplit defines the resolution and extent of the output air concentration and ground deposition in both space and time, which should be chosen to support the intended subsequent MACCS calculations. For example, a MACCS analysis may require that each one-hour release of tracer material be tracked for up to three days out to distances of 500 km and the three days of air concentration and ground deposition information are needed on 15-minute intervals. MACCS treats evacuation of the public, which may overlap with the period of atmospheric release. During the evacuation period, transient air concentrations and ground depositions are needed to estimate exposures of the evacuees. The air concentrations and ground depositions are calculated in HYSPLIT by time-integrating the results over the specified period and dividing by the duration of the period. Time-integrated air concentrations and ground depositions can then be calculated as the products of the HYSPLIT average air concentrations and ground

depositions and the duration of the period. The specified period should divide an hour evenly (i.e., 1, 2, 3, 4, 5, 6, 10, 12, 15, 20, 30, or 60 minutes).

GenHysplit is configured to use the HYSPLIT options of either uniformly spaced rectangular or polar output grids for the ground-level air concentration and ground deposition. The mapping between two polar grids generally introduces less numerical dilution and is the recommended option versus using the HYSPLIT rectangular output grid. The capability to use multiple output grids that increase in span and spacing in HYSPLIT has been incorporated into GenHysplit. The concentration grid is defined by specifying the output grid type and size, and a base grid size and spacing. The base grid size determines the distance from the release location to the edge of the base grid in each direction. The base grid spacing determines the size of the grid cells within the base grid, which generates either a rectangular grid with $\Delta x = \Delta y$ = the specified spacing or a polar grid with 128 equally spaced sectors and Δr = the specified spacing. The number of grids used in the HYSPLIT simulation is determined by comparing the base grid and the output grid. The base grid size and spacing are repeatedly multiplied by two until the output grid size is reached or exceeded. This results in multiple concentration grids, each with increasing extent and spacing up to the desired output grid size. The largest grid matches the specified output grid size. For example, a base grid defined with a size of 10 km with a 1-km spacing and an output grid defined with a size of 50 km would generate four grids. The first grid would span 10 km from the release location with a 1-km grid resolution. The second grid would span 20 km from the release location with a 2-km grid resolution. The third grid would span 40 km from the release with a 4-km grid resolution. The fourth grid would span 50 km from the release with a 5-km grid resolution. The combination of these grids together contains the results of the HYSPLIT calculations with a grid resolution of 1 km out to 10 km, 2 km between 10 km and 20 km, 4 km between 20 km and 40 km, and 5 km between 40 km and 50 km. This capability facilitates configuring a finer resolution near the point of release and coarser resolution further out where a fine resolution is not needed. The user selects the grid size and resolution that corresponds with the intended analysis.

Because the physical processes are linear in the modeling system, the air concentration and ground deposition for each grid cell and time period can be scaled to represent any source term from the modeled location. It should be noted that while plume segments may be released from different elevations, multiple release locations in the same calculation are not currently supported in MACCS. All releases are assumed to originate at the center of the spatial grid. Modeling a source term during any hour of a 365-day year requires 8,760 simulations of the "normalized release" for each release height or rate of energy release. Within a single simulation, all aerosol sizes and deposition options are represented. Most commonly, the deposition options of interest are to include both dry and wet deposition for each of the aerosol sizes, usually ten, plus a single non-depositing gas representing noble gases.

An example GenHysplit input file is shown in Appendix A. One of the resultant sets of HYSPLIT input files generated from the sample GenHysplit input file are also shown in Appendix A. The GenHysplit input file shows the options that are configurable. The HYSPLIT options are either defined by the values in the GenHysplit input file or otherwise by the default HYSPLIT values hardcoded into GenHysplit or HYSPLIT.

The output from GenHysplit is a set of files with suffix .ccd that contain normalized air concentration and ground deposition values on the specified output grid(s) for each time period during the entire duration of the calculation. For an analysis in which one 365-day year of meteorological data is provided, the output from GenHysplit is a set of 8,760 .ccd files. Each file contains the air concentrations and ground depositions of the requested set of aerosol-size and deposition variations at the defined spatial and temporal resolution. For the example described above with a one-hour

release of tracer material that is tracked for up to three days on 15-minute intervals, each of the 8,760 .ccd files contains 288 values (15-minute intervals over three days) of ground-level air concentrations and ground depositions for each grid cell and aerosol-size and deposition variations. Each of the 288 values are associated with one of the 15-minute intervals during the three-day duration of the calculation. If multiple (in space) stabilized heights or rates of release of sensible energy are specified, then the output from GenHysplit is a set of 8,760 .ccd files for each release height or rate of release of sensible energy.

2.1.2. HyGridConvert

Like many modeling systems in which outputs from one model are used as inputs for another, MACCS/HYSPLIT coupling requires that the results from HYSPLIT be converted for use in MACCS. HyGridConvert is a program developed to convert the output file sets from HYSPLIT, generated by GenHysplit, into a format required by MACCS. HyGridConvert is configured to be called within WinMACCS or run as a stand-alone program. The flow of information for HyGridConvert is shown in Figure 2-3.

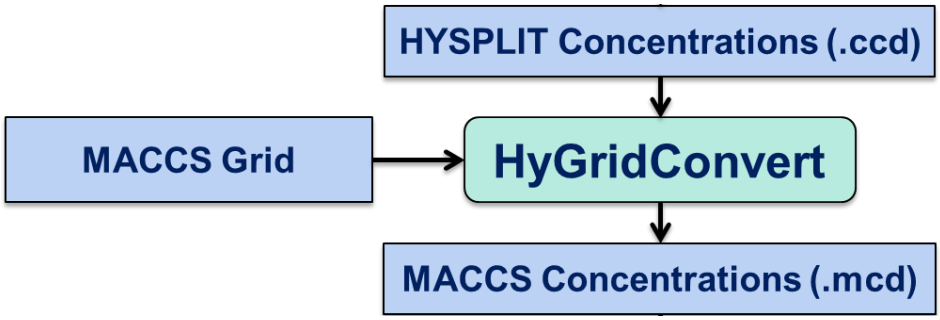

Figure 2-3. HyGridConvert information flow diagram

MACCS uses a user-defined, non-uniform, polar grid for consequence calculations. Typically, the MACCS grid is logarithmically spaced in the radial dimension so that resolution is finer near the origin of release and coarser far away, accounting for specific distances or regions of interest that need to be reported. HYSPLIT generates results on a uniform rectangular or polar grid. HyGridConvert calculates the air concentration and ground deposition values for the specified non-uniform polar grid for MACCS for each file in the set of .ccd files. An illustration comparing a non-uniform (exaggerated for illustration purposes) polar MACCS grid (green) to a uniform rectangular HYSPLIT grid (blue) and a uniform polar HYSPLIT grid (orange) are shown in Figure 2-4. Each MACCS grid cell may encompass parts of many HYSPLIT grid cells or could also be entirely contained within a single HYSPLIT grid cell. HyGridConvert determines a mapping relationship between each of the HYSPLIT grid cells and MACCS grid cells. The MACCS grid size and resolution selected should match the intended analysis and need not necessarily match the HYSPLIT grid.

HyGridConvert uses an area-weighted average of the appropriate HYSPLIT grid cells to determine the air concentration and ground deposition value for each MACCS grid cell. The first step in the algorithm, if the multiple HYSPLIT output grid option was used in GenHysplit, is to determine the finest HYSPLIT grid resolution available for each MACCS grid cell. The algorithm assumes that the air concentration and ground deposition within each HYSPLIT grid cell is uniform in space for each time interval. Next, the area-based weighting factor for each HYSPLIT grid cell, relative to each MACCS grid cell is determined. Once the set of weighting factors is determined, HyGridConvert applies the weighting factors to each file within the file set. For a case where 8,760 .ccd files were generated, this results in a set of 8,760 .mcd files that can be used by MACCS.

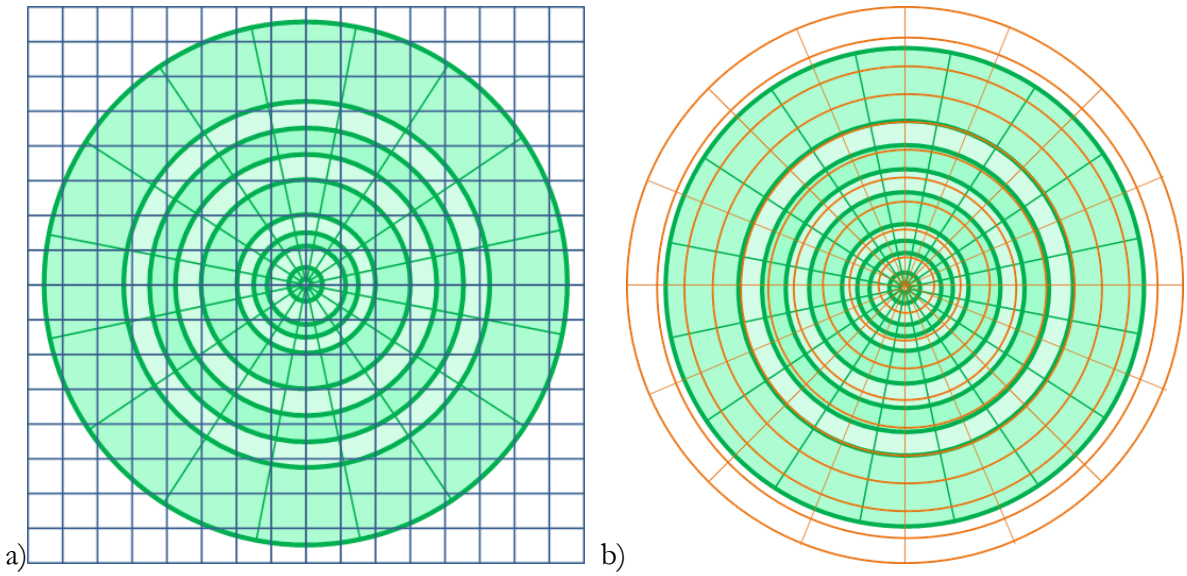

Figure 2-4. Comparison of a non-uniform polar MACCS grid to a) a uniform rectangular HYSPLIT grid and b) a uniform polar HYSPLIT grid

Conversion of HYSPLIT output files to MACCS input files is maintained as a separate step to allow a user to use the same HYSPLIT output files for multiple MACCS grids. If the user needs to modify the MACCS grid, only the conversion step with HyGridConvert needs to be repeated, versus restarting the process with GenHysplit. Since HyGridConvert runs much faster than GenHysplit, this capability is very useful.

2.1.3. MACCS

With the HYSPLIT concentration files formatted for use in MACCS by HyGridConvert (i.e., the .mcd files) and with the other required MACCS input files, MACCS can evaluate consequences. The flow of information for MACCS is shown in Figure 2-5. The MACCS-formatted meteorological file, source term information and MACCS model parameter inputs are needed when using both the Gaussian ATD model and the HYSPLIT/MACCS coupled model. The outputs from MACCS are nearly the same with the HYSPLIT ATD option as compared with the Gaussian ATD option. Some outputs generated with the Gaussian ATD model option, such as the air concentration at the centerline of a Gaussian plume, are not available when using the HYSPLIT option.

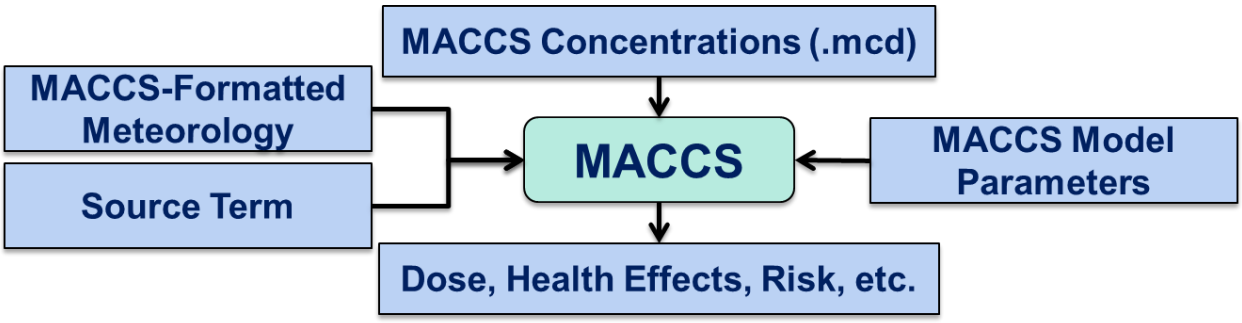

Figure 2-5. MACCS information flow diagram

With the option of the Gaussian ATD model, the wind speed and direction, precipitation rate, and stability class in the MACCS-formatted meteorological file are used to:

- Determine the atmospheric transport and diffusion of each plume segment.
- Determine the plume rise for each plume segment.
- Determine evacuation locations and speeds.
- Bin the weather for the weather bin sampling options.

With the option of the HYSPLIT model, the wind speed and direction, precipitation rate, and stability class in the MACCS-formatted meteorological file are used to:

- Determine the plume rise for each plume segment (if assessed by MACCS instead of HYSPLIT).
- Determine evacuation locations and speeds.
- Bin the weather for the weather bin sampling options.

Three options are available in MACCS for treating meteorological data: fixed start time, weather bin sampling, and stratified random sampling. These three options are compatible with the original Gaussian and HYSPLIT ATD models. For all three meteorological sampling options, both the Gaussian and the HYSPLIT ATD options require a formatted meteorological file for MACCS. A utility to generate the MACCS-formatted meteorological file from the same gridded meteorological data used for the HYSPLIT calculations has been created (MacMetGen) and is discussed in the next section. Using this utility ensures consistency between the meteorological input used for HYSPLIT and MACCS.

The MACCS-formatted meteorological file contains data for wind speed, wind direction, stability class, and precipitation rate for each hour (optionally 15- or 30-min periods) over the course of a year at the release location. On the other hand, the time frame required for the MACCS concentration (.mcd) files when using the HYSPLIT ATD option depends on the sampling option as follows:

1. For the fixed start time option, the time frame for the source term to be modeled determines the number of MACCS concentration files (.mcd) needed. For example, to model a source term that has a total release duration of four days requires a minimum of 96 (4 days × 24 hours per day) hours of MACCS concentration files (.mcd), which begin at the same hour as the selected start time. This meteorological option is useful when modeling a specific event and allows for a smaller set of MACCS concentration files compared with the other two options.
2. For the weather bin and stratified random sampling options, MACCS concentration files (.mcd) that span at least one year are needed. Additional files for the last few days of the year before and the first few days of the following year can also be included to avoid reusing the current year of data for releases that start before the beginning of the year or continue past the end of the year. When only a year of data is provided, source terms that span across the beginning or end of the year are modeled assuming the meteorological data for the previous and subsequent years are the same as for the modeled year. The MACCS-formatted meteorological file is used to perform the weather binning step in MACCS when that option is selected.

MACCS combines the normalized air concentration and ground deposition values from the MACCS concentration files (.mcd) with the desired source term. First, the source term is divided into one-hour plume segments. Each one-hour plume segment is then associated with a single MACCS concentration file (.mcd). For source terms that do not start or end on the hour, the first and/or last

segment are adjusted to account for the partial hour. For each release segment, the normalized air concentration and ground deposition values for each aerosol bin are multiplied by the release amount during that hour for each different radionuclide and aerosol bin. The radioactive decay and ingrowth that would occur up to the time in the calculation is also accounted for in this step. MACCS does not account for any changes in physical form or chemical reactions. This results in an array of air concentration and ground deposition values as a function of radionuclide, grid cell, and time. This is the required information for MACCS to perform consequence calculations for dose, health effects, risk, economic consequences, etc.

2.1.4. MacMetGen

MACCS uses a formatted meteorological file that contains data for wind speed, wind direction, stability class, and precipitation rate for each hour of a year at the release location. This is one of the inputs to MACCS shown in Figure 2-1 and Figure 2-5. Typically, this formatted meteorological file is generated from observational meteorological data at a site. A utility to capture these same data from the meteorological data sets compatible with HYSPLIT has been created. This MACCS-formatted meteorological file generator is called MacMetGen and it has been designed to be configurable by the user. MacMetGen ensures consistency between the meteorological information used in HYSPLIT and MACCS[1]. The flow of information for MacMetGen is shown in Figure 2-6.

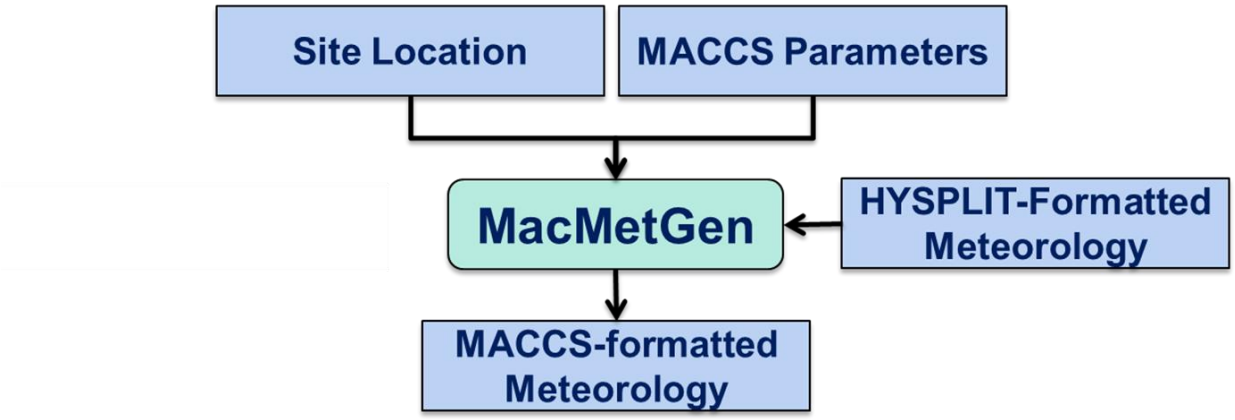

Figure 2-6. MacMetGen information flow diagram

The input meteorological data used by MacMetGen are the same as those used by HYSPLIT. Meteorological data sets compatible with HYSPLIT can be found on an ftp site maintained by the NOAA Air Resources Laboratory (ARL) (NOAA, 2017). The site location determines where in the meteorological field the wind direction, wind speed, and precipitation data are extracted. Spatial interpolation based on proximity to the surrounding grid points is used. Interpolation in time is also performed if needed. The MACCS parameters define the period for the entries, number of sectors used in the discretization of wind direction, and method to determine stability class used to create the MACCS-formatted meteorological file. The extracted wind speeds, precipitation rates, and stability classes in the MACCS-formatted meteorological file are then used in MACCS in the weather binning

[1] It may be noted that while many modern ATD models (including HYSPLIT) have moved away from the use of classes to represent atmospheric stability, MACCS requires a class-based stability, for binning weather sequences for sampling, for determining plume rise, and (if exercised) for use in the Gaussian plume segment model in ATMOS. MacMetGen uses the same meteorological data that is used by HYSPLIT but has a variety of options for estimating a stability class from that data.

algorithm with the weather bin sampling options. The calculated stability class is also used in MACCS to determine the plume rise for each plume segment.

MacMetGen has three methods to determine stability class to allow the user flexibility based on the available data. The first method is called Delta Temperature Delta Z (height) (DTDZ), which determines the stability class based on the vertical temperature gradient near the surface of the Earth. This value is compared with the criteria shown in Table 2-1 (US NRC, 2007) to determine the stability class.

The second method to determine stability class is called Turner's method, which is based on net radiation index, wind speed and cloud cover. This method uses the procedure outlined in (US EPA, 2000) and shown in Figure 2-7, using the criteria shown in Figure 2-8 and Figure 2-9. Not all meteorological data files support this option.

The third method to determine stability class is called Solar Radiation/Delta Temperature (SRDT), which is based on the amount of solar radiation, wind speed, and vertical temperature gradient near the surface of the Earth. "The SRDT method retains the basic structure and rationale of Turner's method while obviating the need for observations of cloud cover and ceiling" (US EPA, 2000). With this method, the stability class is determined using the criteria shown below in Figure 2-10.

Table 2-1. Stability class as a function of vertical temperature gradient (US NRC, 2007)

Vertical Temperature Gradient Delta T/Delta Z [K/100 m]	Stability Class
< -1.9	1 (A)
-1.9 to -1.7	2 (B)
-1.7 to -1.5	3 (C)
-1.5 to -0.5	4 (D)
-0.5 to 1.5	5 (E)
1.5 to 4.0	6 (F)
> 4.0	7 (G)

Procedure for Determining the Net Radiation Index

1. If the total cloud[1] cover is 10/10 and the ceiling is less than 7000 feet, use net radiation index equal to 0 (whether day or night).

2. For nighttime: (from one hour before sunset to one hour after sunrise):
   (a) If total cloud cover ≤ 4/10, use net radiation index equal to -2.
   (b) If total cloud cover > 4/10, use net radiation index equal to -1.

3. For daytime:
   (a) Determine the insolation class number as a function of solar altitude from Table 6-5.
   (b) If total cloud cover ≤5/10, use the net radiation index in Table 6-4 corresponding to the isolation class number.
   © If cloud cover >5/10, modify the insolation class number using the following six steps.
      (l) Ceiling <7000 ft, subtract 2.
      (2) Ceiling ≥7000 ft but <16000 ft, subtract 1.
      (3) total cloud cover equal 10/10, subtract 1. (This will only apply to ceilings ≥7000 ft since cases with 10/10 coverage below 7000 ft are considered in item 1 above.)
      (4) If insolation class number has not been modified by steps (1), (2), or (3) above, assume modified class number equal to insolation class number.
      (5) If modified insolation class number is less than 1, let it equal 1.
      (6) Use the net radiation index in Table 6-4 corresponding to the modified insolation class number.

Figure 2-7. Procedure for Using Turner's Method (US EPA, 2000)

Table 6-4

Turner's Key to the P-G Stability Categories

Wind Speed		Net Radiation Index						
(knots)	(m/s)	4	3	2	1	0	-1	-2
0,1	0 - 0.7	1	1	2	3	4	6	7
2,3	0.8 - 1.8	1	2	2	3	4	6	7
4,5	1.9 - 2.8	1	2	3	4	4	5	6
6	2.9 - 3.3	2	2	3	4	4	5	6
7	3.4 - 3.8	2	2	3	4	4	4	5
8,9	3.9 - 4.8	2	3	3	4	4	4	5
10	4.9 - 5.4	3	3	4	4	4	4	5
11	5.5 - 5.9	3	3	4	4	4	4	4
≥ 12	≥ 6.0	3	4	4	4	4	4	4

Figure 2-8. Turner's Key to the P-G Stability Categories, extracted from (US EPA, 2000)

Table 6-5

Insolation Class as a Function of Solar Altitude

Solar Altitude Φ (degrees)	Insolation	Insolation Class Number
60 < Φ	strong	4
35 < Φ ≤ 60	moderate	3
15 < Φ ≤ 35	slight	2
Φ ≤ 15	weak	1

Figure 2-9. Insolation Class as a Function of Solar Altitude, extracted from (US EPA, 2000)

Table 6-7

Key to Solar Radiation Delta-T (SRDT) Method for Estimating Pasquill-Gifford (P-G) Stability Categories

DAYTIME

	Solar Radiation (W/m^2)			
Wind Speed (m/s)	≥ 925	925 - 675	675 - 175	< 175
< 2	A	A	B	D
2 - 3	A	B	C	D
3 - 5	B	B	C	D
5 - 6	C	C	D	D
≥ 6	C	D	D	D

NIGHTTIME

	Vertical Temperature Gradient	
Wind Speed (m/s)	< 0	≥ 0
< 2.0	E	F
2.0 - 2.5	D	E
≥ 2.5	D	D

Figure 2-10. Key to Solar Radiation Delta-T Method for Estimating Pasquill-Gifford Stability Categories, extracted from (US EPA, 2000)

2.2. Verification Tests

The verification of the implementation of the HYSPLIT results into MACCS is documented in this report. In this report, the term "verification" is used in the sense of verifying that the coupling of MACCS and HYSPLIT has been implemented as intended but does not address comparisons of model predictions with field observations. The test cases were designed to verify the correct coupling between HYSPLIT and MACCS. Test cases are set up to directly demonstrate the intended coupling between the codes and the intended usage of the HYSPLIT results in MACCS for calculating consequence results. These test cases attempt to verify correct coupling and usage by comparing output quantities from a HYSPLIT/MACCS calculation with a calculation run with HYSPLIT as a standalone code. The results are expected to be within numerical precision or rounding (within 0.1%) unless otherwise noted.

For each test case, the initial release was assumed to be 10^{14} Bq of a single radionuclide, Am-241 (unless otherwise specified). Am-241 was selected due to its relatively long half-life (433 years), compared with atmospheric transport times, which minimizes any effect of radioactive decay for these test cases. It should be noted that this is not a realistic assumption for nuclear reactor accidents, but

rather a simplifying assumption to facilitate testing. The releases were assumed to emanate at a fixed height of 10 m, with no nearby buildings.

The test cases are designed to build upon one another by progressively adding more complexity. The test cases progress: 1) from a single plume segment to multiple plume segments; 2) from a single aerosol with a fixed deposition velocity to multiple aerosols, each with the deposition velocity calculated based on their size; 3) from a constant simple weather field to spatially and temporally varying weather; 4) from insignificant radioactive decay to significant radioactive decay; and 5) from a stationary (non-evacuation) population to an evacuating population. The increase in complexity for each test case is illustrated below in Table 2-2.

Table 2-2. Complexities included in test cases

Test Case	Multiple Plume Segments	Multiple Aerosol Sizes & Deposition	Spatially & Temporally Varying Weather	Radioactive Decay	Evacuation
1					
2	X				
3	X	X			
4	X	X	X		
5				X	
6	X	X	X		X

For each test case, atmospheric dispersion outputs are compared for the HYSPLIT/MACCS coupled and HYSPLIT standalone calculations. The atmospheric dispersion output metrics are integrated over the entire period of plume passage and include:

- Peak (around the compass) time-integrated air concentration (χ/Q, s/m^3) over a 1000-km radius
- Peak (around the compass) ground concentration (D/Q, $1/m^2$) over a 1000-km radius
- Cumulative (as a function of distance from the release) land areas (km^2) that exceed various levels of ground deposition over a 1000-km radius

These outputs from the HYSPLIT/MACCS coupled and HYSPLIT standalone calculations should match within 0.1% if the coupling between HYSPLIT and MACCS has been implemented correctly. Some differences in results can arise because of numerical precision or rounding differences between HYSPLIT and MACCS.

The peak air concentration is the maximum value of the time-integrated (over the entire period of plume passage), surface-layer, air concentration around the compass at a given distance from the source. The peak ground deposition is the maximum value of the deposition on the ground around the compass at a specified distance. These values are normalized by dividing by the initial activity of the source to obtain the value of χ/Q. The peak air concentration and ground deposition are calculated by examining the air concentration and ground deposition in each sector ($1/64^{th}$ of the compass) and selecting the largest value at each distance from the site. Air concentration and ground deposition were chosen because they are used to determine the potential consequences. Furthermore, they are a direct measure of the atmospheric dispersion calculations.

The cumulative land areas that exceed various levels of ground deposition are the total surface areas of land that have enough deposition to be above a specified activity per unit area. It is calculated by determining the contamination level of each grid cell (within the specified distance) and if it is above the specified level, adding the area of the grid cell to the total. Two ground deposition levels are used,

100 μCi/m^2 and 1,000 μCi/m^2. Because these curves represent a cumulative quantity, they should increase with distance from the site until they reach the distance at which the deposition level is no longer exceeded, at which distance the curve will exhibit a plateau. It should be noted that these ground deposition levels are used to facilitate testing and do not necessarily reflect specific regulatory requirements. The land area that exceeds various levels of ground deposition was selected as a direct measure of the atmospheric dispersion calculations that reflects the spatial extent of ground deposition predicted by the model.

The test cases are also designed to verify the correct usage of the HYSPLIT results within MACCS. The test cases are configured to use the air concentration at each location to determine ionizing radiation doses to individuals at those locations (i.e. no resuspension or groundshine pathways modeled). It should be noted that this is not a realistic assumption for nuclear reactor accidents, but rather a simplification to facilitate the consequence calculations for the HYSPLIT standalone calculations. Other consequence metrics are derived in MACCS based on doses. For each test case, the peak dose output is compared for the HYSPLIT/MACCS coupled and HYSPLIT standalone calculations. The consequence output metric used was:

- Peak (around the compass) ionizing radiation dose (Sv) over the region

The peak dose results for the HYSPLIT/MACCS coupled and HYSPLIT standalone calculations should match within 0.1% if the coupling between HYSPLIT and MACCS has been implemented correctly. Some differences in results can arise due to the differences in peak air concentrations.

The peak ionizing radiation dose is the maximum value of the dose to an individual assumed to be standing around the compass at a given distance. It is calculated by examining the individual dose in each sector (1/64th of the compass) and selecting the largest value at each distance from the site. The peak dose was selected as a metric because it is directly calculated from the peak air concentration and is often reported in analyses performed for NRC applications.

2.2.1. Verification Test Case 1

Test Case 1 is designed as a simple problem for which the models should match within 10%, given the correct coupling of HYSPLIT results with MACCS. A constant meteorological field was used with the following characteristics:

- 4 m/s wind to the west
- Stability class D (neutrally-stable conditions)
- Mixing height of 1.5 km
- No precipitation (no wet deposition)

A fixed, single deposition velocity, 0.3 cm/s, was used for all aerosols. The release was modeled as a single, one-hour plume segment and then tracked for five days to ensure passage of the plume over the entire computational grid.

The peak air concentration, peak ground deposition, and land areas that exceed 100 μCi/m^2 and 1,000 μCi/m^2 comparisons for Test Case 1 are shown in Figure 2-11 through Figure 2-14. The figures also contain the ratio of the HYSPLIT standalone results to the HYSPLIT/MACCS at each distance. Comparing the HYSPLIT/MACCS and HYSPLIT standalone model results for all the above quantities shows agreement with differences of <0.1%, verifying the implementation of the HYSPLIT/MACCS coupling for this simple case. Both calculations show the decreasing peak air concentration and ground deposition with distance, as well as the increasing land areas contaminated above the ground deposition levels with distance. Concerning land area contaminated above 1,000

μCi/m^2, a plateau is seen after 100 km in Figure 2-14. At this distance, the dispersion of the release is sufficient that the ground deposition is below the threshold and no additional land area is contaminated above the threshold.

The peak ionizing radiation dose comparison for Test Case 1 is shown in Figure 2-15. Comparing the HYSPLIT/MACCS and HYSPLIT standalone model results for peak individual dose shows agreement with differences of <0.1%, verifying the correct usage of the HYSPLIT results in MACCS for this simple case.

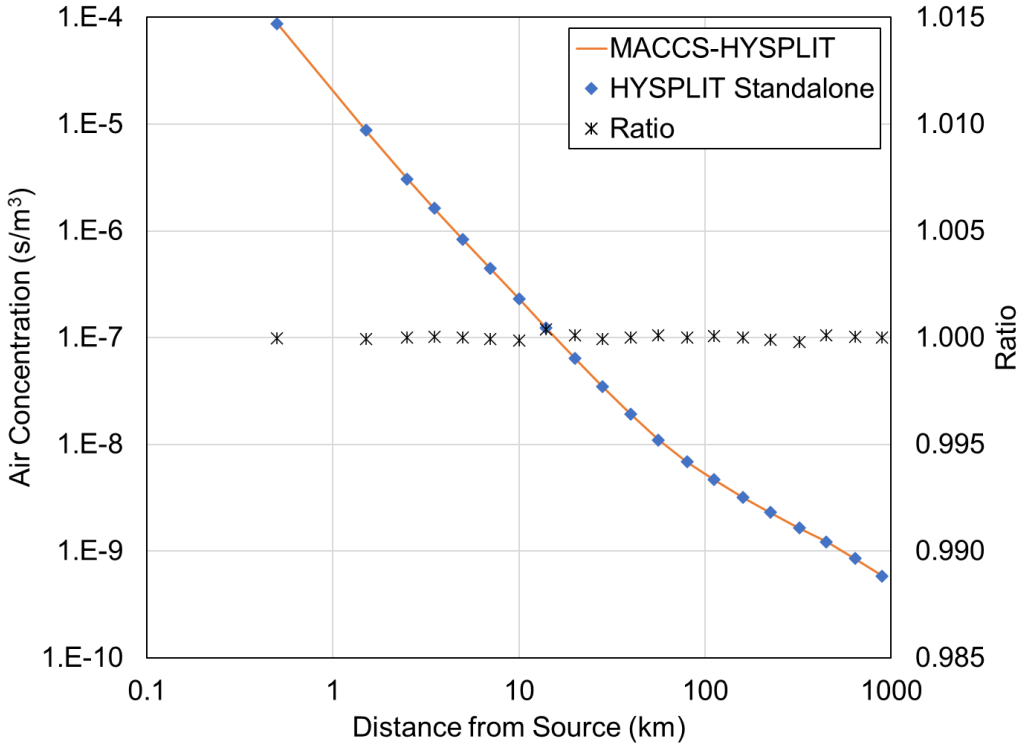

Figure 2-11. Test Case 1 comparison of peak air concentration

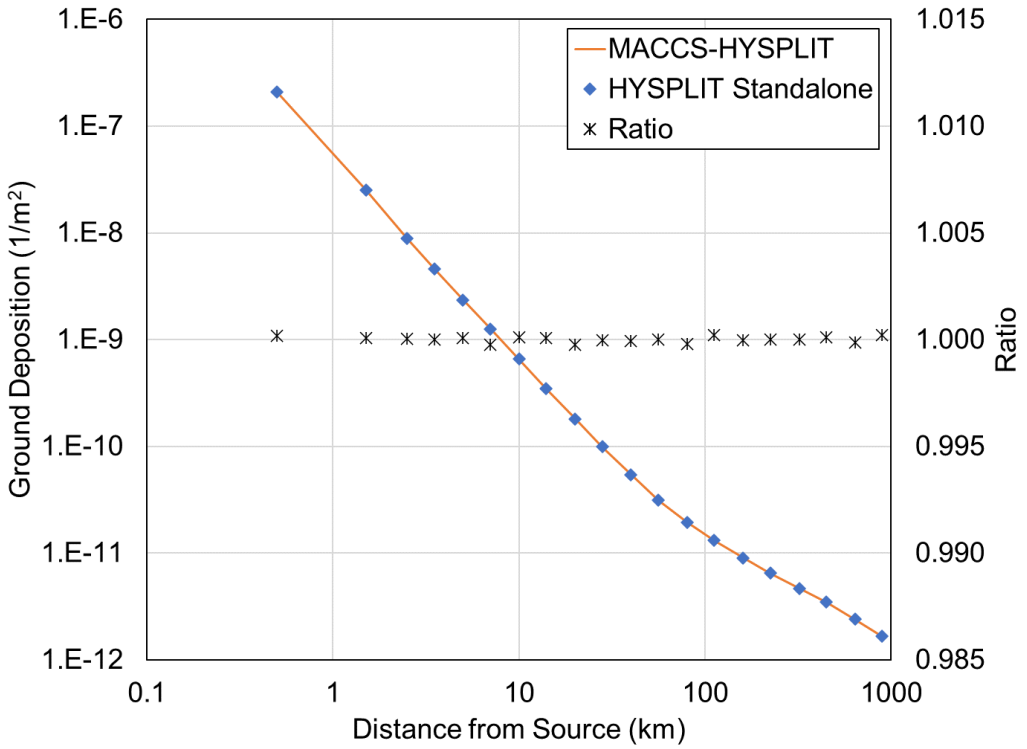

Figure 2-12. Test Case 1 comparison of peak ground deposition

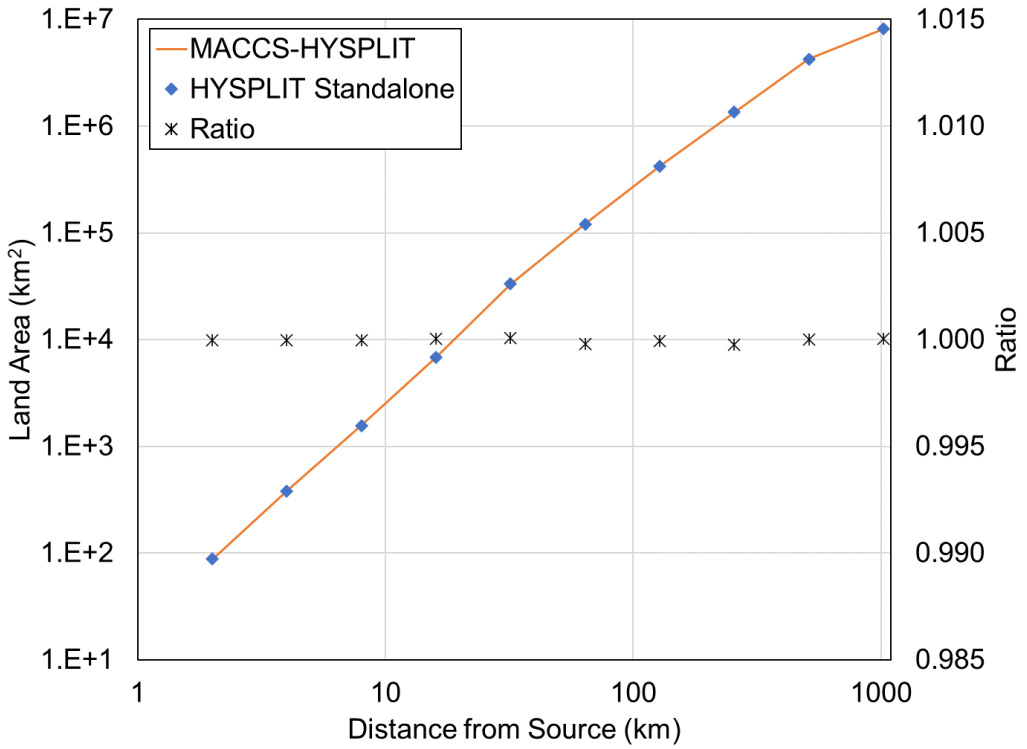

Figure 2-13. Test Case 1 comparison of land areas that exceed 100 μCi/m²

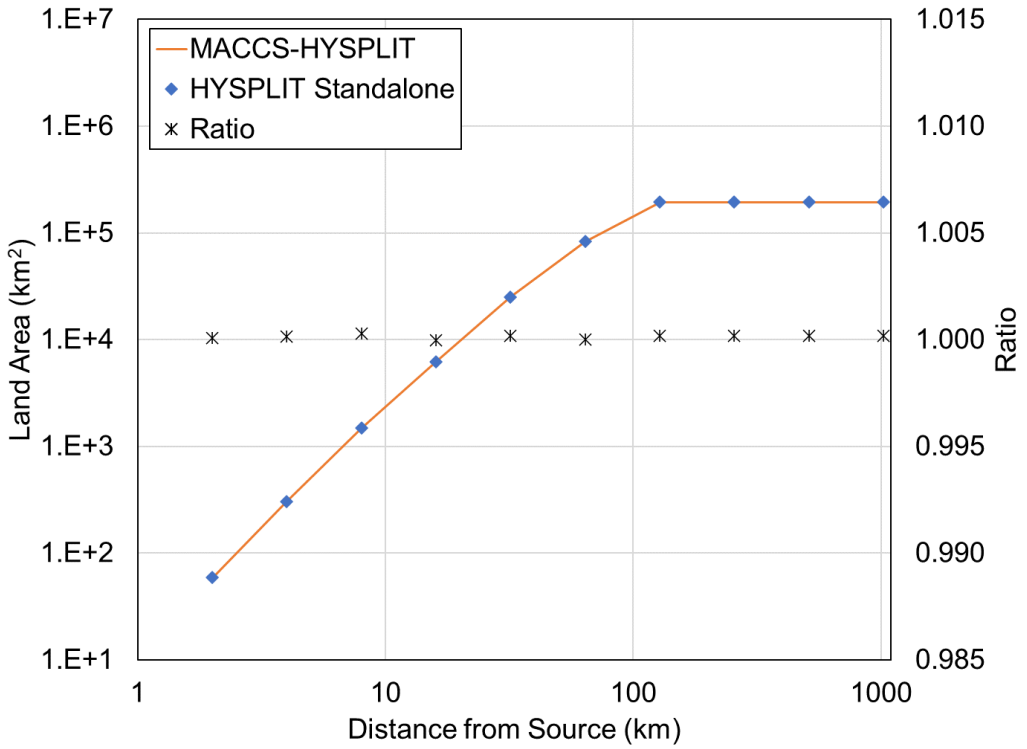

Figure 2-14. Test Case 1 comparison of land areas that exceed 1,000 μCi/m²

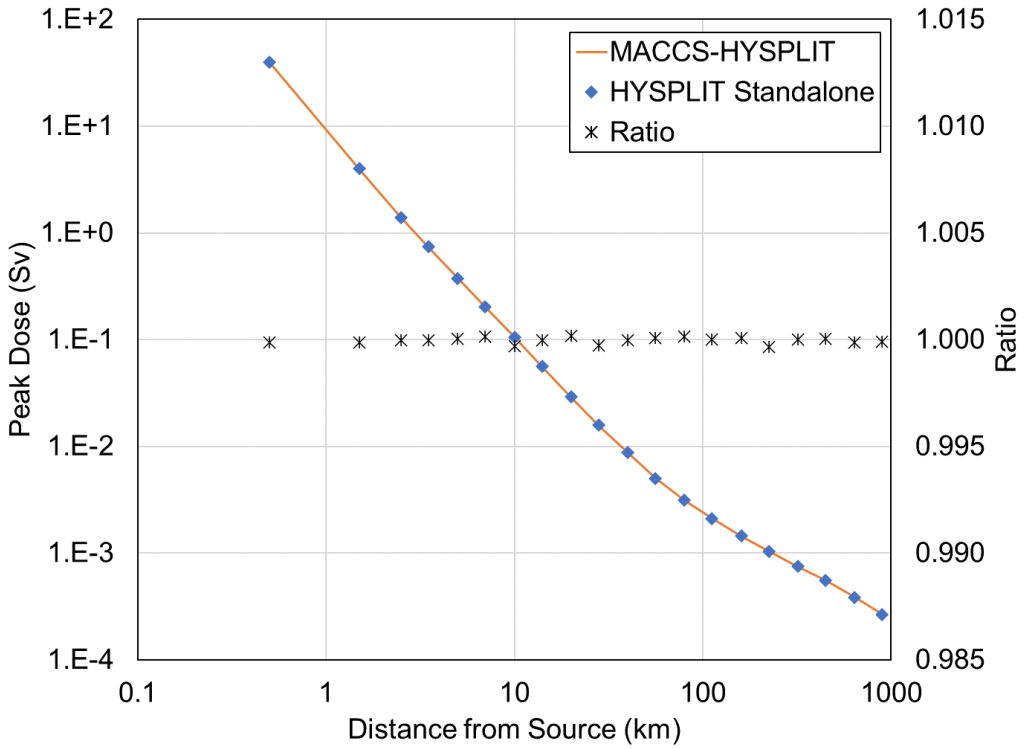

Figure 2-15. Test Case 1 comparison of peak individual dose

2.2.2. *Verification Test Case 2*

Test Case 2 is designed to build upon Test Case 1 by modeling multiple plume segments. Test Case 2 uses the same parameters as Test Case 1, with one modification. Instead of a single one-hour release, two plume segments were modeled. The first plume segment begins at time zero, lasts for one hour, and contains 10^{14} Bq of Am-241. The second plume segment begins at hour three, lasts for three hours and contains 0.75×10^{14} Bq of Am-241. The releases are tracked for five days.

The peak air concentration, peak ground deposition, and land areas that exceed 100 μCi/m^2 and 1,000 μCi/m^2 comparisons for Test Case 2 are shown in Figure 2-16 through Figure 2-19. Comparing the HYSPLIT/MACCS and HYSPLIT standalone model results for all the above quantities shows agreement with differences of <0.1%, verifying the implementation of the HYSPLIT/MACCS coupling with multiple plume segments. Both calculations show the decreasing peak air concentration and ground deposition with distance, as well as the increasing land areas contaminated above the ground deposition levels with distance. Concerning land area contaminated above 1,000 μCi/m^2, a plateau is seen after 200 km in Figure 2-19. At this distance, the dispersion of the release is sufficient that the ground deposition is below the threshold and no additional land area is contaminated above the threshold.

The peak ionizing radiation dose comparison for Test Case 2 is shown in Figure 2-20. Comparing the HYSPLIT/MACCS and HYSPLIT standalone model results for peak individual dose shows agreement with differences of <0.1%, verifying the correct usage of the HYSPLIT results in MACCS with multiple plume segments.

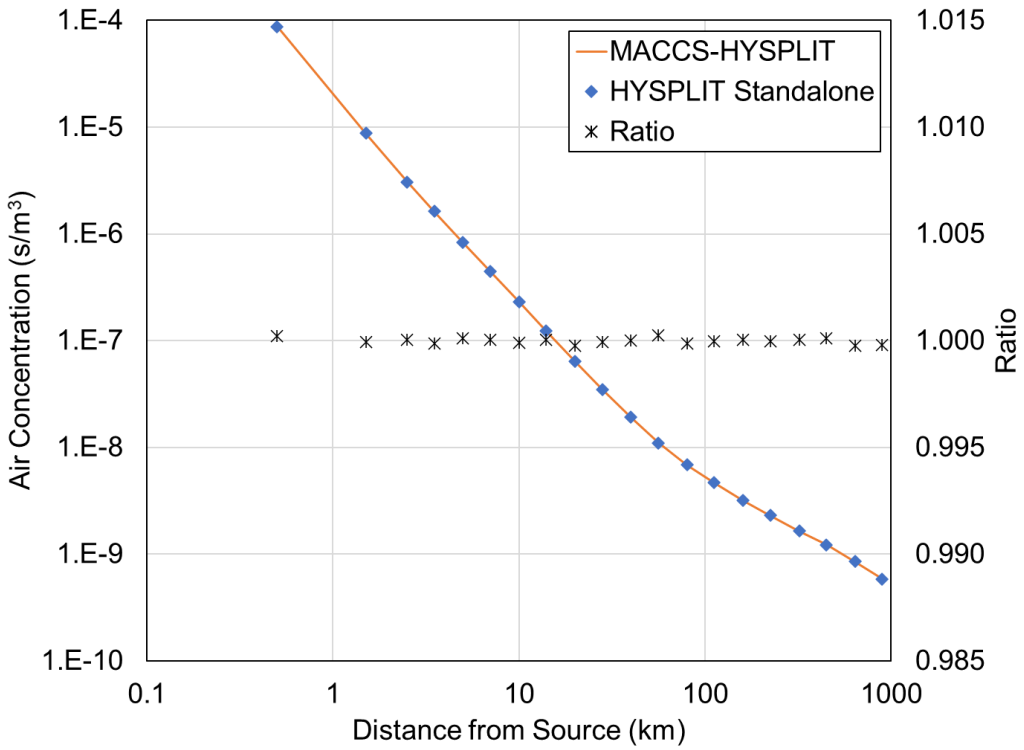

Figure 2-16. Test Case 2 comparison of peak air concentration

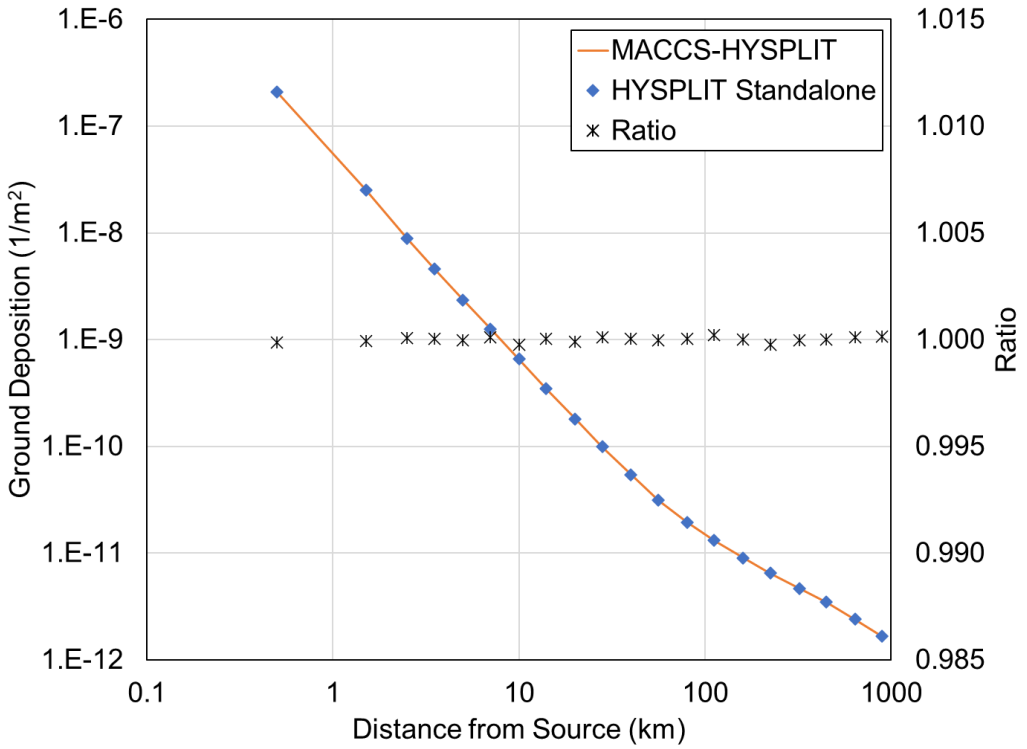

Figure 2-17. Test Case 2 comparison of peak ground deposition

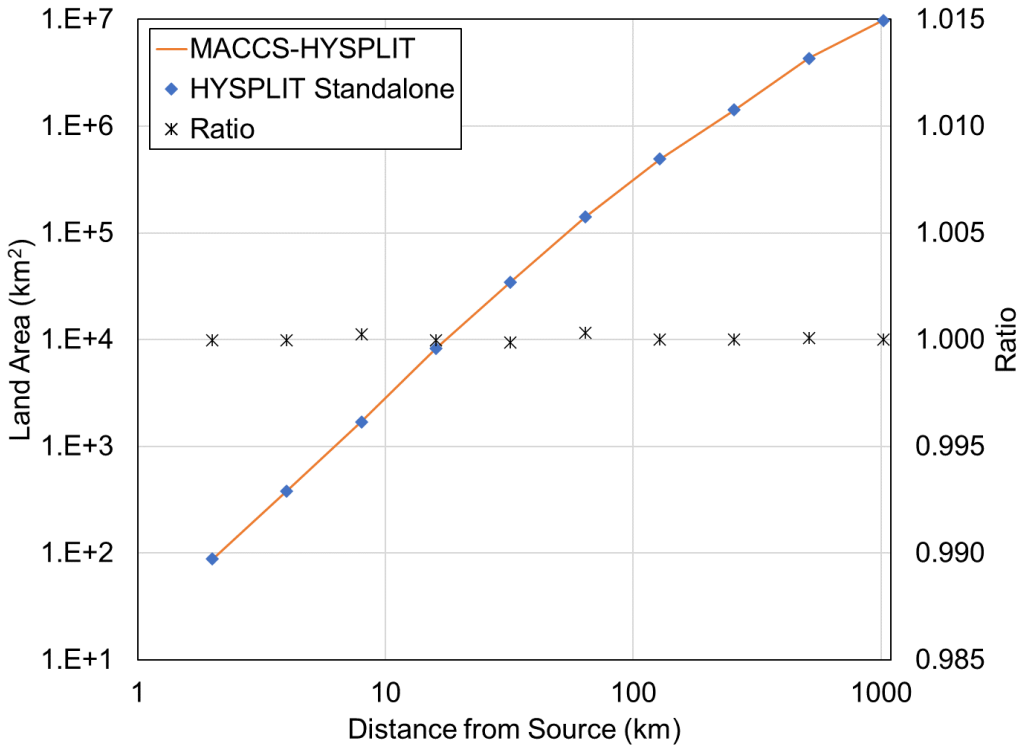

Figure 2-18. Test Case 2 comparison of land areas that exceed 100 μCi/m²

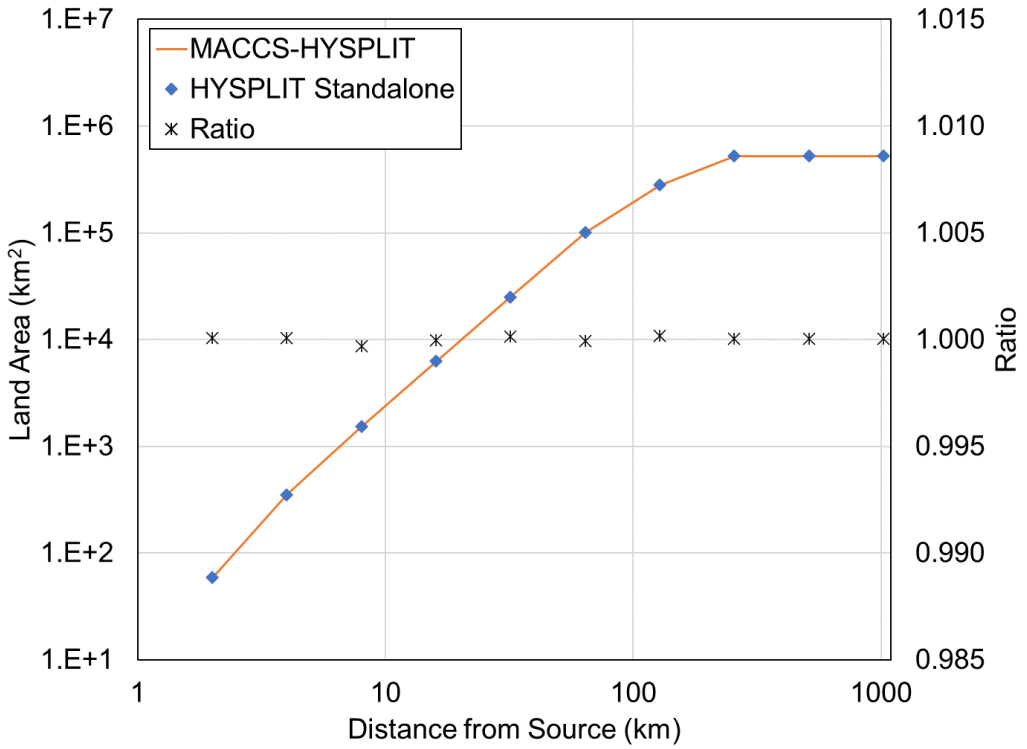

Figure 2-19. Test Case 2 comparison of land areas that exceed 1,000 μCi/m²

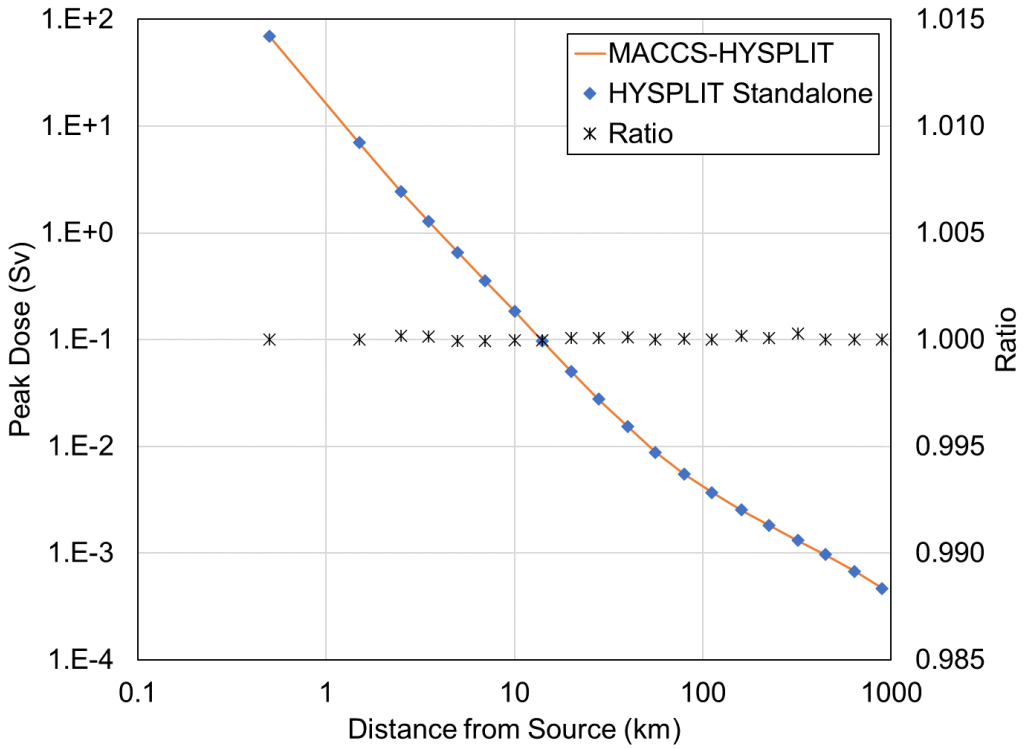

Figure 2-20. Test Case 2 comparison of peak individual dose

2.2.3. *Verification Test Case 3*

Test Case 3 is designed to build upon Test Case 2 by modeling multiple aerosol sizes. Test Case 3 uses the same parameters as Test Case 2, with one modification. Instead of using a single deposition velocity for the aerosols, the resistance model within HYSPLIT was used for each of ten aerosol sizes. The HYSPLIT resistance model calculates the deposition of the aerosol while accounting for the aerosol size, gravitational settling, ground surface roughness, and atmospheric conditions. The ten sizes used in Test Case 3 are shown in Table 2-3.

Table 2-3. Test Case 3 aerosol sizes

Aerosol Diameter (μm)
0.15
0.29
0.53
0.99
1.84
3.43
6.38
11.9
22.1
41.2

The air concentration, ground deposition, and land areas that exceed 100 $\mu Ci/m^2$ and 1,000 $\mu Ci/m^2$ comparisons for Test Case 3 are shown in Figure 2-21 through Figure 2-24. Comparing the HYSPLIT/MACCS and HYSPLIT standalone model results for all the above quantities shows agreement with differences of <0.1%, verifying the implementation of the HYSPLIT/MACCS coupling with the addition of multiple aerosol sizes. As expected, both calculations show the decreasing peak air concentration and ground deposition with distance, as well as the increasing land areas contaminated above the ground deposition levels with distance. The decrease in slope of the ground deposition curve seen near 300 km shown in Figure 2-22 shows how the resistance model within HYSPLIT can vary with distance as the surface roughness of the ground changes with distance. Concerning land area contaminated above 1,000 $\mu Ci/m^2$, a plateau is seen after 200 km in Figure 2-24. At this distance, the dispersion of the release is sufficient that the ground deposition is below the threshold and no additional land area is contaminated above the threshold.

The peak ionizing radiation dose comparison for Test Case 3 is shown in Figure 2-25. Comparing the HYSPLIT/MACCS and HYSPLIT standalone model results for peak individual dose shows agreement with differences of <0.1%, verifying the correct usage of the HYSPLIT results in MACCS with the addition of multiple aerosol sizes.

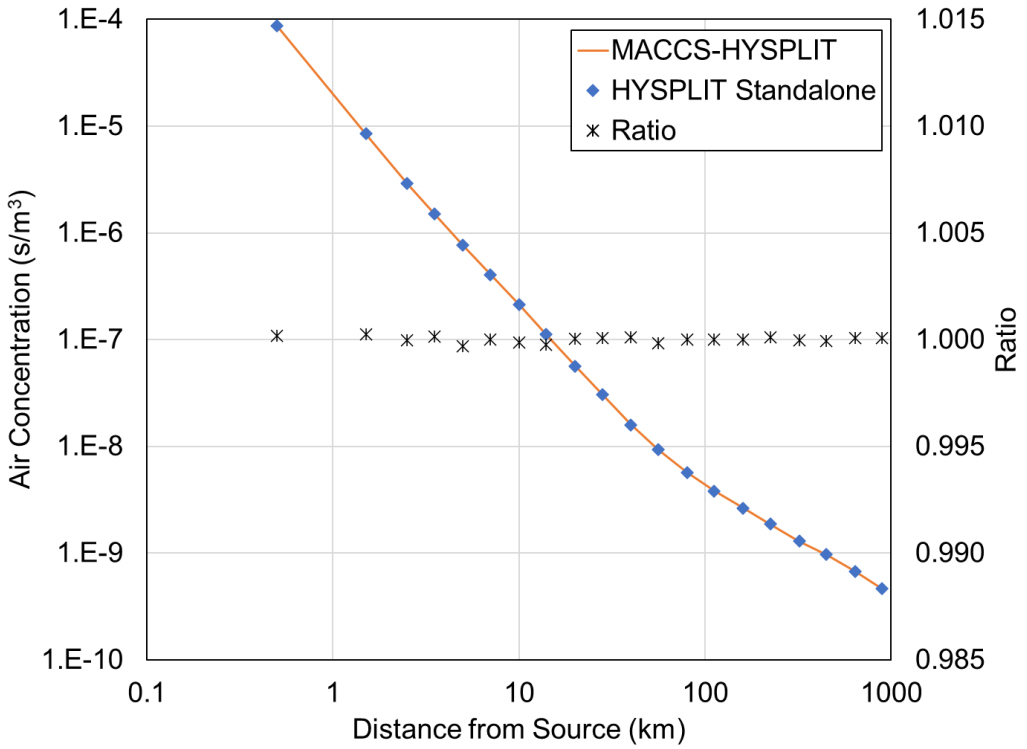

Figure 2-21. Test Case 3 comparison of peak air concentration

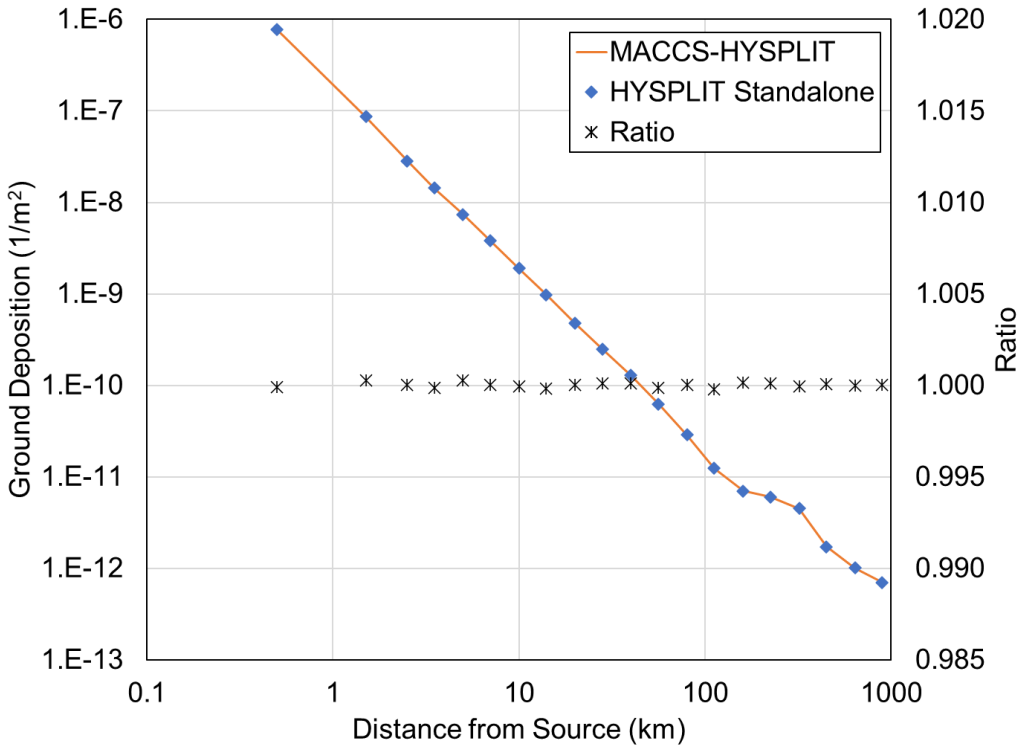

Figure 2-22. Test Case 3 comparison of peak ground deposition

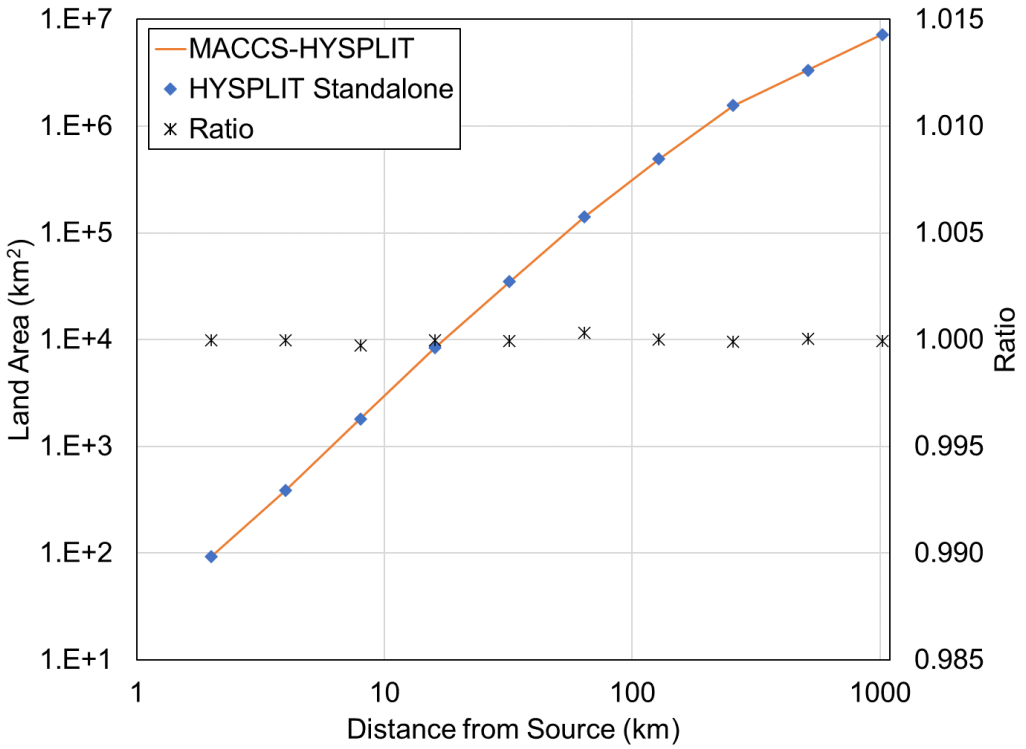

Figure 2-23. Test Case 3 comparison of land areas that exceed 100 μCi/m²

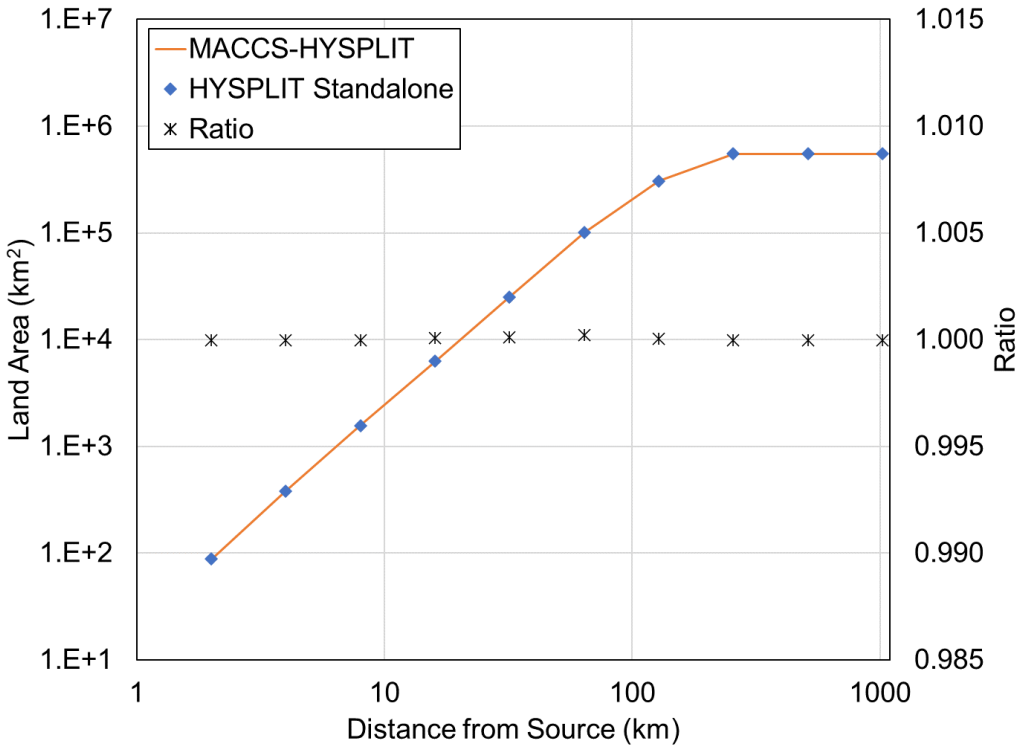

Figure 2-24. Test Case 3 comparison of land areas that exceed 1,000 μCi/m²

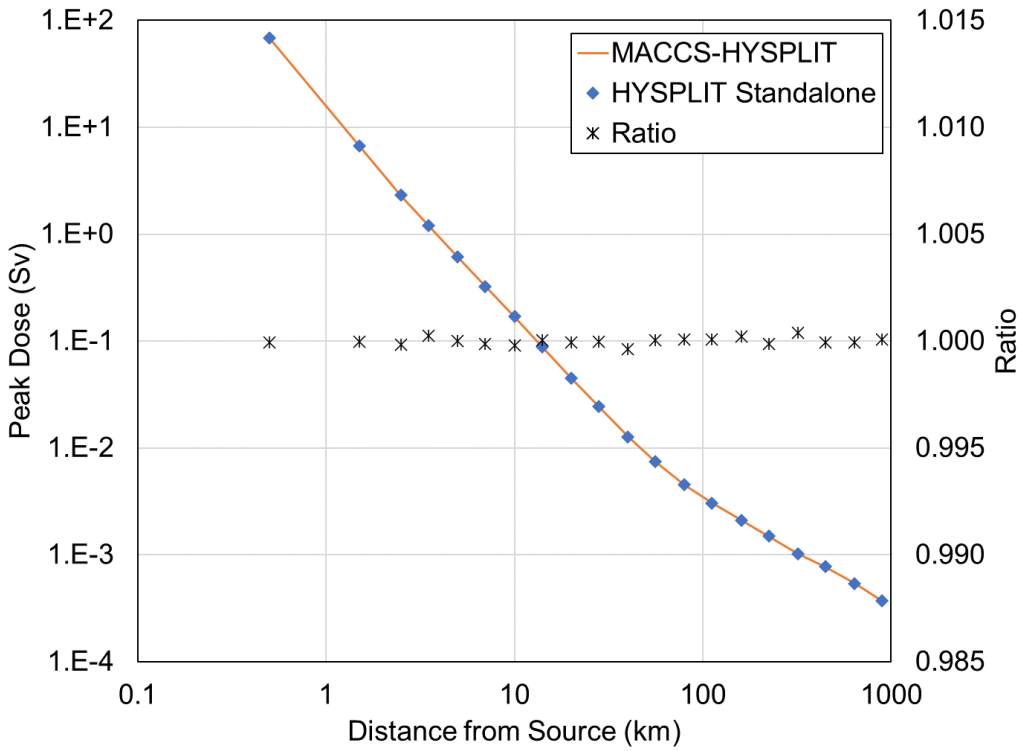

Figure 2-25. Test Case 3 comparison of peak individual dose

2.2.4. Verification Test Case 4

Test Case 4 is designed to build upon Test Case 3 by including spatially and temporally varying weather conditions. Test Case 4 uses the same parameters as Test Case 3, with one modification. Instead of using a constant weather field, meteorological data from the North American Mesoscale (NAM) 12-km files for 2009 (NOAA, 2017) were used in the HYSPLIT calculations. The wind direction and speed at the release location for the first 48 hours used in Test Case 4 are shown in Figure 2-26. The wind direction and speed vary spatially as well (data every 12 km) and are used in the HYSPLIT calculations, but for simplicity, only the data at the release location are shown in Figure 2-26. At the release location, the wind starts out blowing toward ESE, shifting to NE and then back toward ESE over the 48 hours. Additionally, the wind speed begins near 10 m/s, slowing down almost to 3 m/s, and then increases almost to 10 m/s.

The air concentration, ground deposition, and land areas that exceed 100 μCi/m^2 and 1,000 μCi/m^2 comparisons for Test Case 4 are shown in Figure 2-27 through Figure 2-30. Comparing the HYSPLIT/MACCS and HYSPLIT standalone model results for all the above quantities shows agreement with differences of <0.1%, verifying the implementation of the HYSPLIT/MACCS coupling when using spatially and temporally varying weather conditions. Both calculations show the decreasing peak air concentration and ground deposition with distance, as well as the increasing land areas contaminated above the ground deposition levels with distance. The air concentration as a function of distance in Figure 2-27 shows how the changing of the wind speed and direction over time can impact dispersion. The ground deposition as a function of distance in Figure 2-28 shows how the resistance model within HYSPLIT can vary with distance as the surface roughness of the ground changes. Concerning land area contaminated above 1,000 μCi/m^2, a plateau is seen after 500 km in Figure 2-30. At this distance, the dispersion of the release is sufficient that the ground deposition is below the threshold and no additional land area is contaminated above the threshold.

The peak ionizing radiation dose comparison for Test Case 4 is shown in Figure 2-31. Comparing the HYSPLIT/MACCS and HYSPLIT standalone model results for peak individual dose shows agreement with differences of <0.1%, verifying the correct usage of the HYSPLIT results in MACCS when using spatially and temporally varying weather conditions.

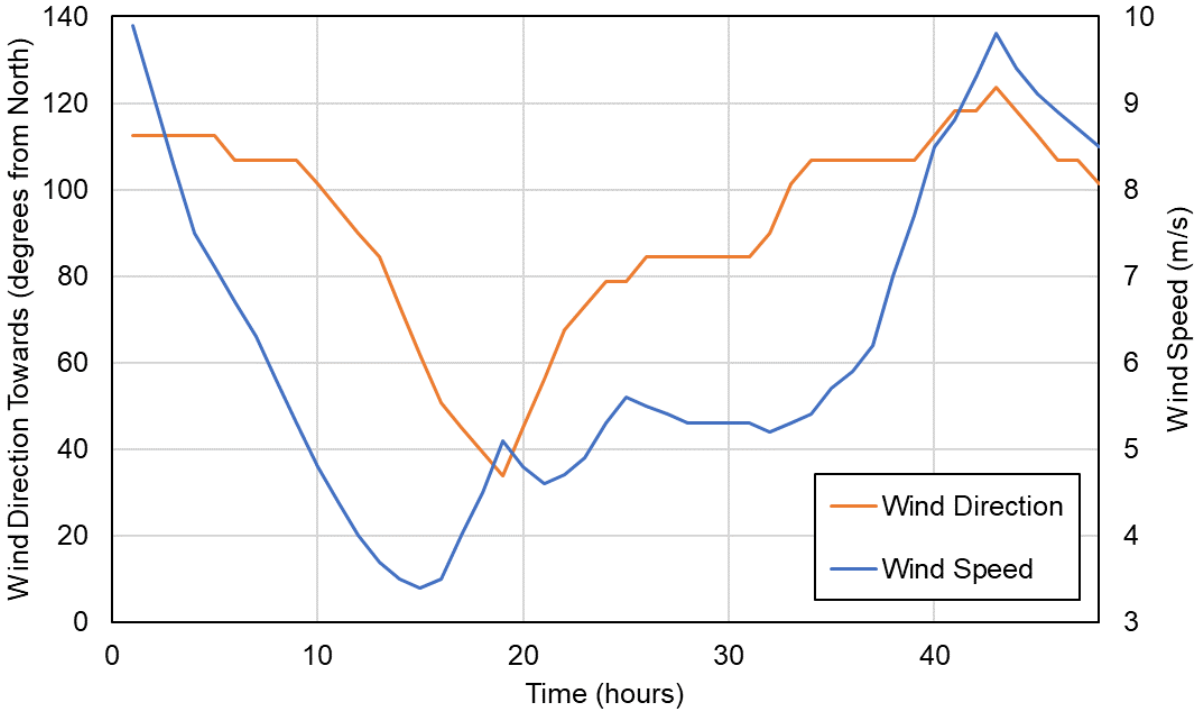

Figure 2-26. Wind directions and speeds used in Test Case 4

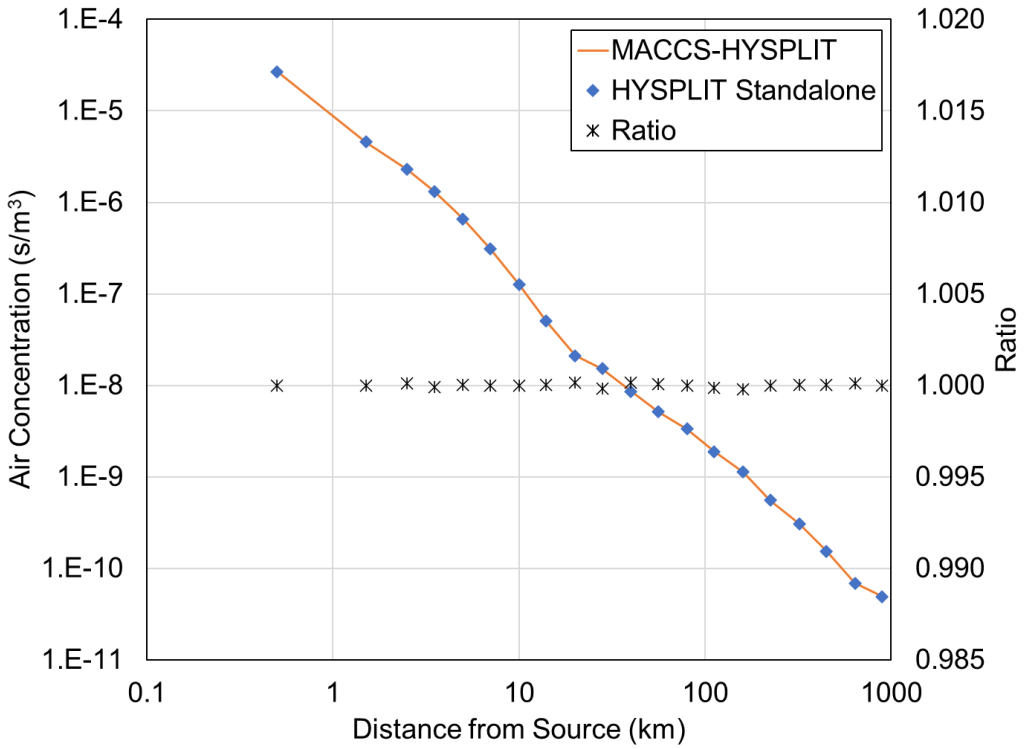

Figure 2-27. Test Case 4 comparison of peak air concentration

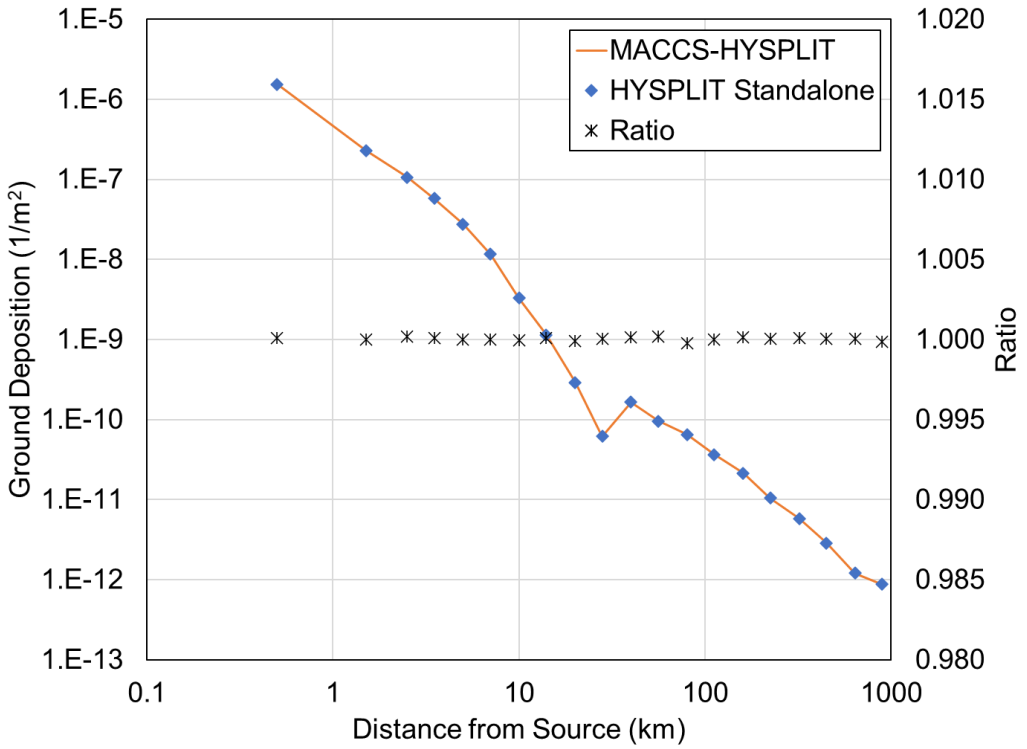

Figure 2-28. Test Case 4 comparison of peak ground deposition

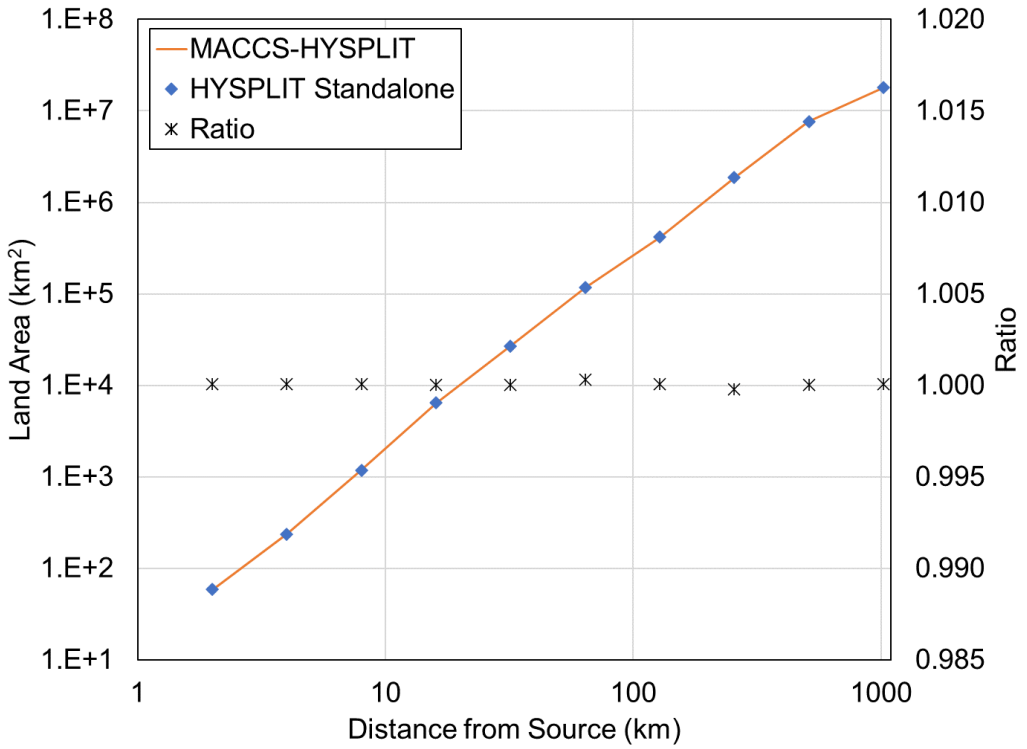

Figure 2-29. Test Case 4 comparison of land areas that exceed 100 μCi/m²

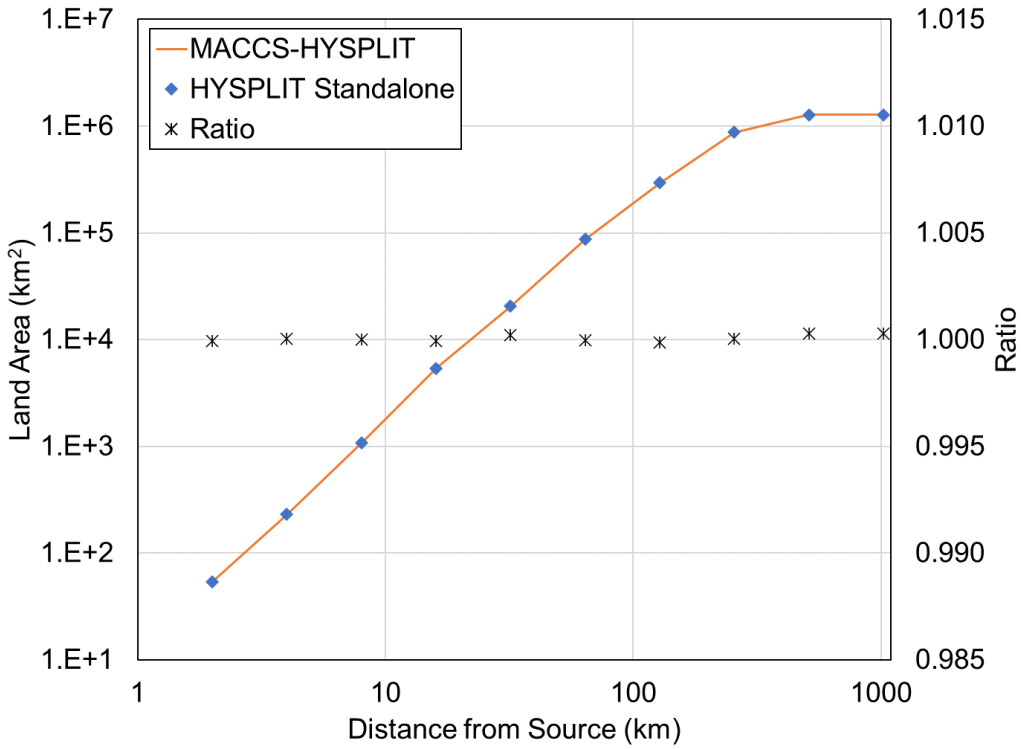

Figure 2-30. Test Case 4 comparison of land areas that exceed 1,000 μCi/m²

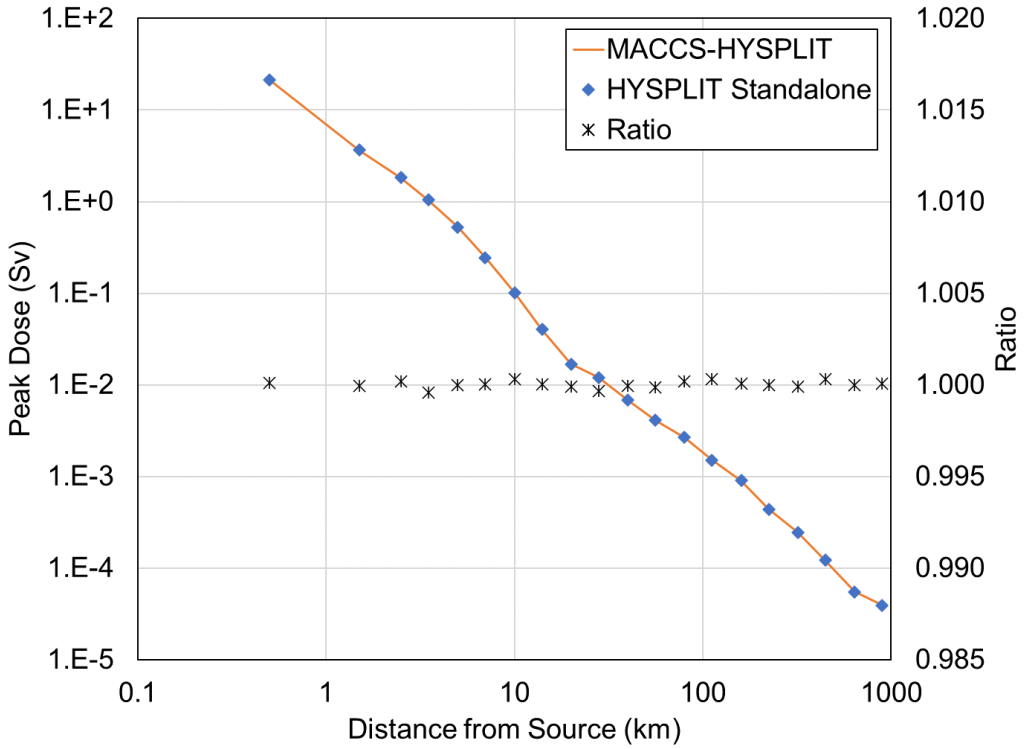

Figure 2-31. Test Case 4 comparison of peak individual dose

2.2.5. Verification Test Case 5

Test Case 5 is designed to build upon Test Case 1 by modeling radioactive decay. Test Case 5 utilized the same parameters as Test Case 1, with one modification. Instead of a release of 10^{14} Bq of Am-241, a release of 10^{14} Bq of La-142 is modeled. La-142 has a radioactive half-life of 92.5 minutes, about five orders of magnitude shorter than the half-life of Am-241 (433 years). The half-life of La-142 is also about an order of magnitude smaller than the time of travel of the modeled plume across the domain, meaning that it is short enough to have a significant effect on air concentrations within the time frame of atmospheric transport.

The air concentration, ground deposition, and land areas that exceed 100 μCi/m^2 and 1,000 μCi/m^2 comparisons for Test Case 5 are shown in Figure 2-32 through Figure 2-35. Comparing the HYSPLIT/MACCS and HYSPLIT standalone model results for all the quantities shows agreement within <2% for both the peak air concentration and ground deposition and within <0.1% for land areas exceeding the thresholds, verifying the implementation of the HYSPLIT/MACCS coupling with radioactive decay. The differences between the peak air concentration and ground deposition are higher for this test case than the others due to the differences in the numerical precision in MACCS and HYSPLIT when calculating radioactive decay. As expected, both calculations show the decreasing peak air concentration and ground deposition with distance, as well as the increasing land areas contaminated above the ground deposition levels with distance. Both the peak air concentration and ground deposition significantly decrease (more than ten orders of magnitude by 1,000 km) with distance compared with the previous test cases as multiple half-lives are required to travel out to long distances (>100 km). Concerning land area contaminated above 100 and 1,000 μCi/m^2, a plateau is seen after 100 km in Figure 2-34 and after 50 km in Figure 2-35, respectively. At this distance, the dispersion and radioactive decay of the release is sufficient that the ground deposition is below the threshold and no additional land area is contaminated above the threshold.

The peak ionizing radiation dose comparison for Test Case 5 is shown in Figure 2-36. Comparing the HYSPLIT/MACCS and HYSPLIT standalone model results for peak individual dose shows agreement with differences of <2% (equivalent to the air concentration agreement), verifying the correct usage of the HYSPLIT results in MACCS with radioactive decay. The last point in the HYSPLIT/MACCS calculation is reported as zero since it is below 1.E-20 (lower bound in MACCS) and hence is not shown in the figure.

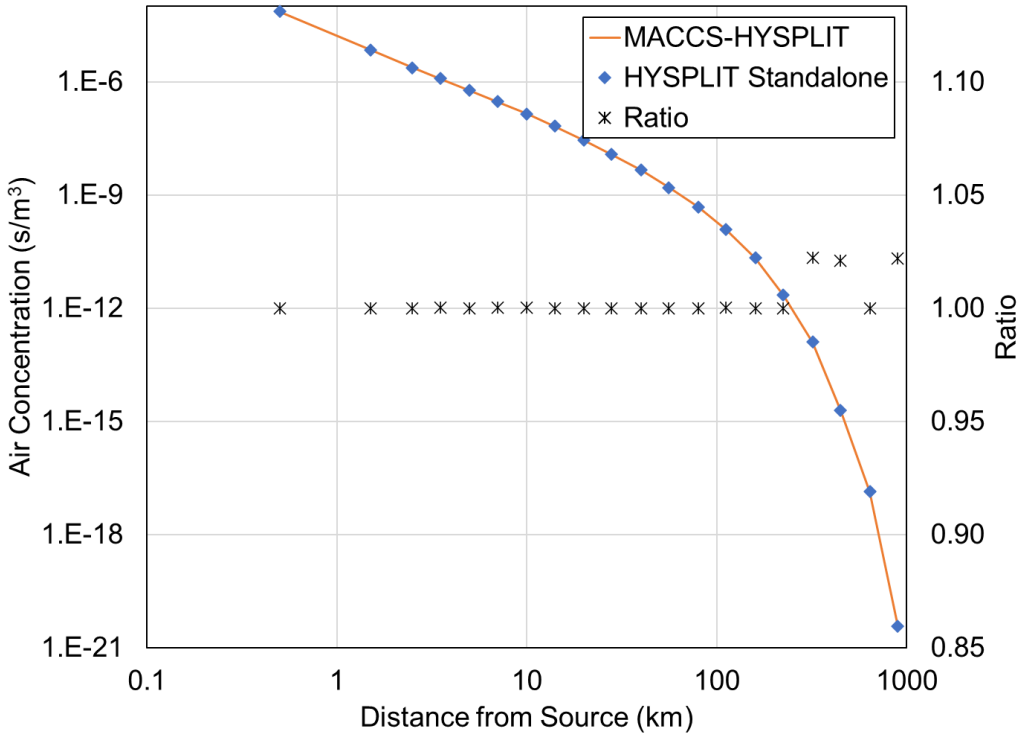

Figure 2-32. Test Case 5 peak air concentration coupling comparison

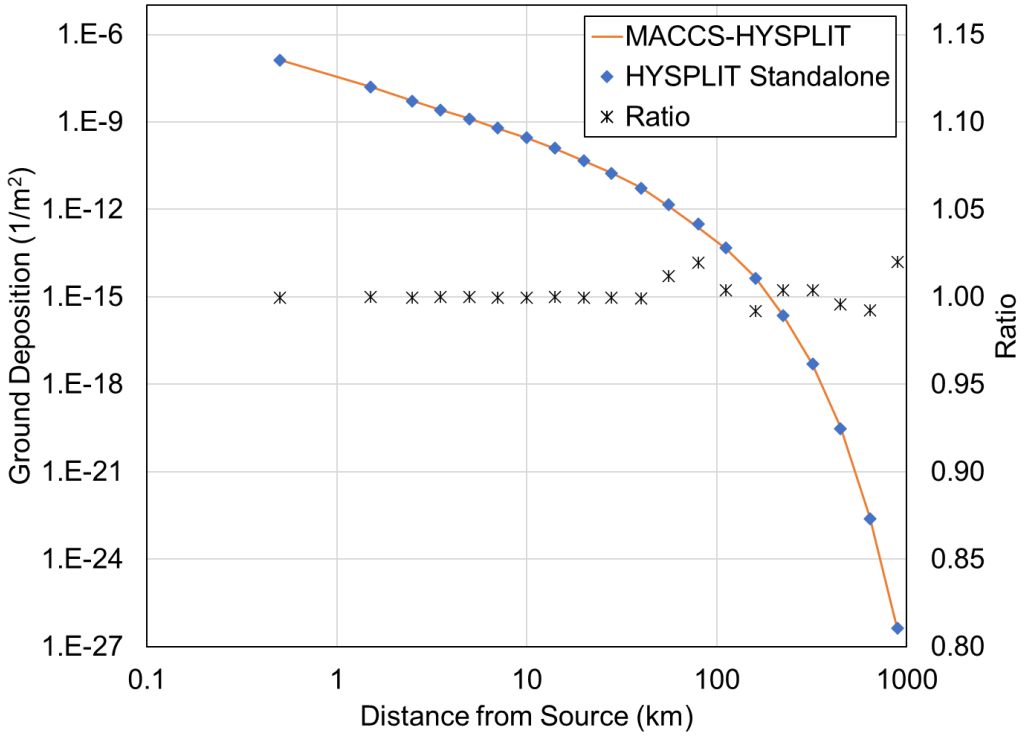

Figure 2-33. Test Case 5 peak ground deposition coupling comparison

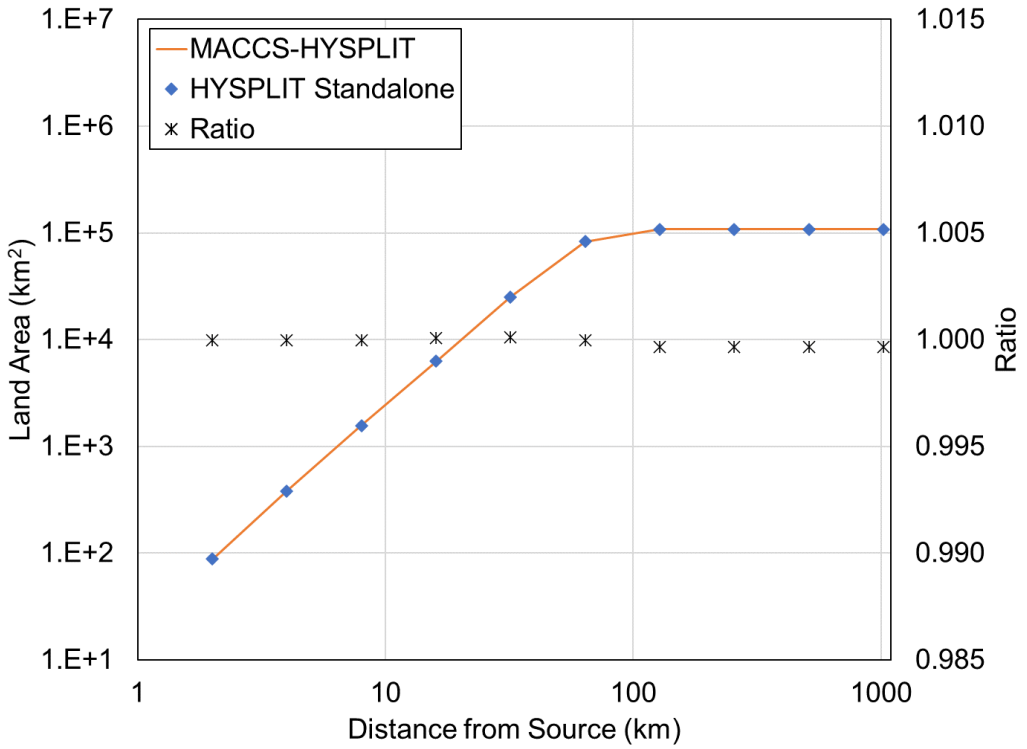

Figure 2-34. Test Case 5 land areas that exceed 100 μCi/m² coupling comparison

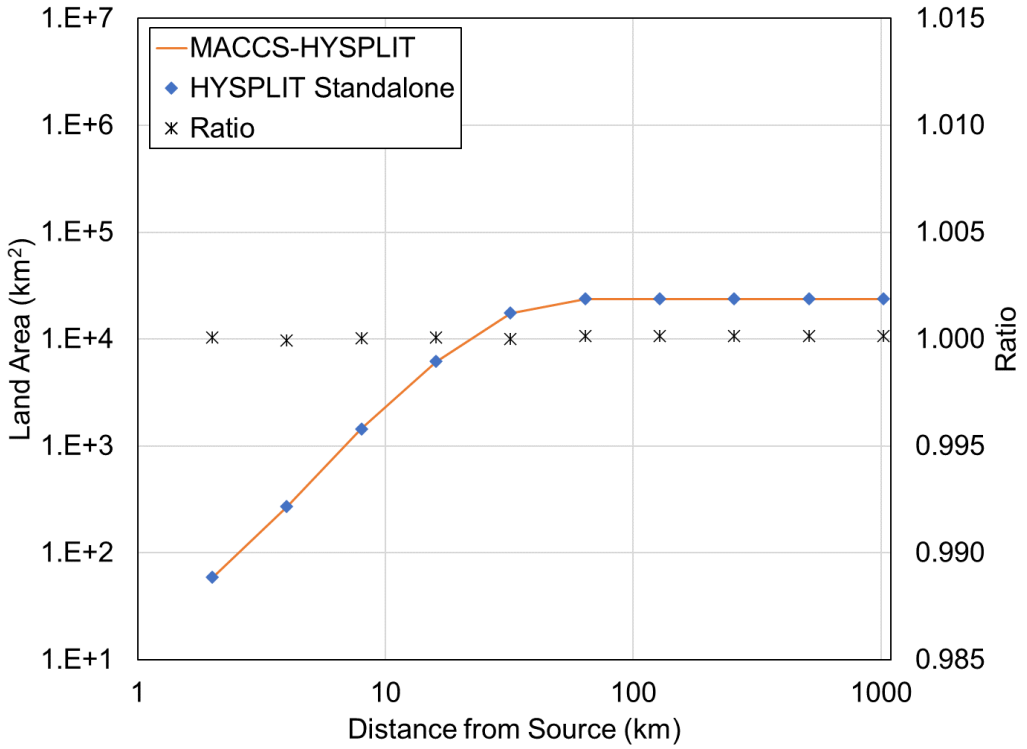

Figure 2-35. Test Case 5 land areas that exceed 1,000 μCi/m² coupling comparison

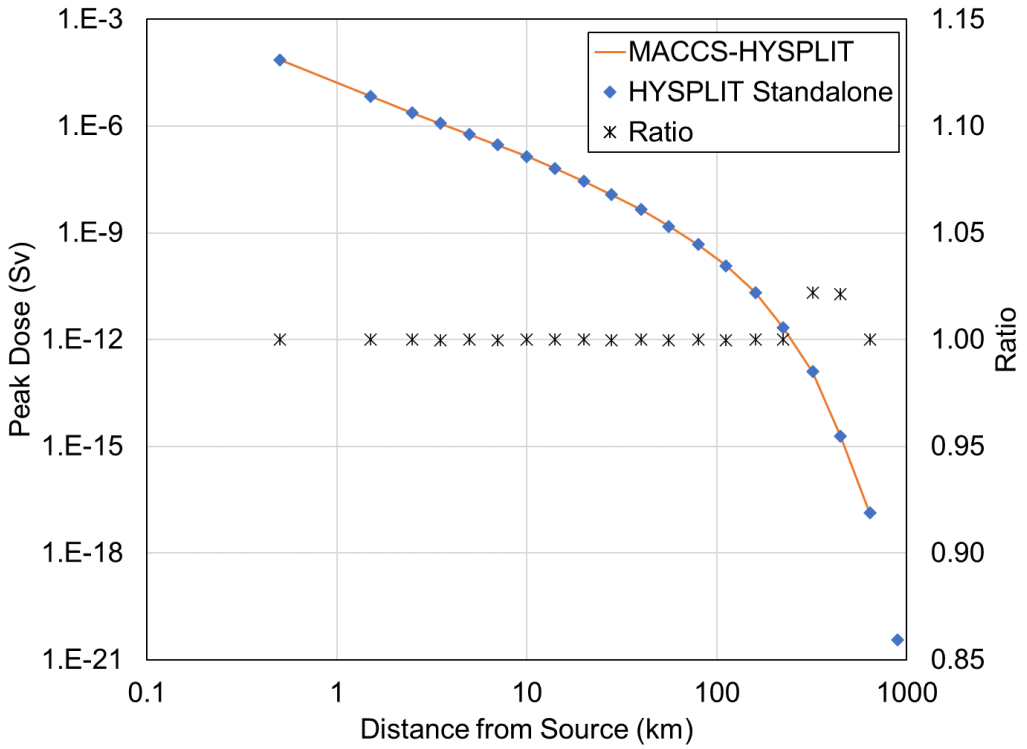

Figure 2-36. Test Case 5 comparison of peak individual dose

2.2.6. *Verification Test Case 6*

Test Case 6 is designed to build upon Test Case 4 by including model algorithms for evacuation. One purpose of this test case is to verify that the time-dependence of the plume concentrations on the grid are implemented properly. Another purpose is to verify that the plume concentrations are used correctly by the sheltering and evacuation algorithms. Test Case 6 uses the same parameters as Test Case 4, with one modification. Instead of using a constant population density with no movement of individuals, half of the individuals within 16 km of the release location are configured to shelter in place during the passage of the plume segments and then evacuate (Cohort 1) and the other half are configured to evacuate before any plume reaches their location (Cohort 2). No one evacuates beyond 16 km.

The air concentration, ground deposition, and land areas that exceed 100 μCi/m^2 and 1,000 μCi/m^2 are identical to those for Test Case 4 and are shown in Figure 2-27 through Figure 2-30. The peak ionizing radiation dose comparison for Test Case 6 is shown in Figure 2-37. Comparing the HYSPLIT/MACCS and HYSPLIT standalone model results for peak individual dose shows agreement with differences of <0.1%. Since Cohort 1 sheltered during the plume segments passage and then evacuated, a lower dose is expected at distances <16 km. Since Cohort 2 evacuated before either plume, a zero dose is expected at distances <16 km. Figure 2-37 shows a comparison between the individual doses for the two cohorts modeled in this test case with the previous scenario of no evacuation modeled in Test Case 4. As seen in the figure, the doses to individuals within 16 km of the release location for Cohort 1 are lower than for no evacuation and for Cohort 2 they are zero. Furthermore, the dose results are identical to those for Test Case 4 (no evacuation) at distances >16 km. This verifies the correct usage of the HYSPLIT results in MACCS when modeling evacuations.

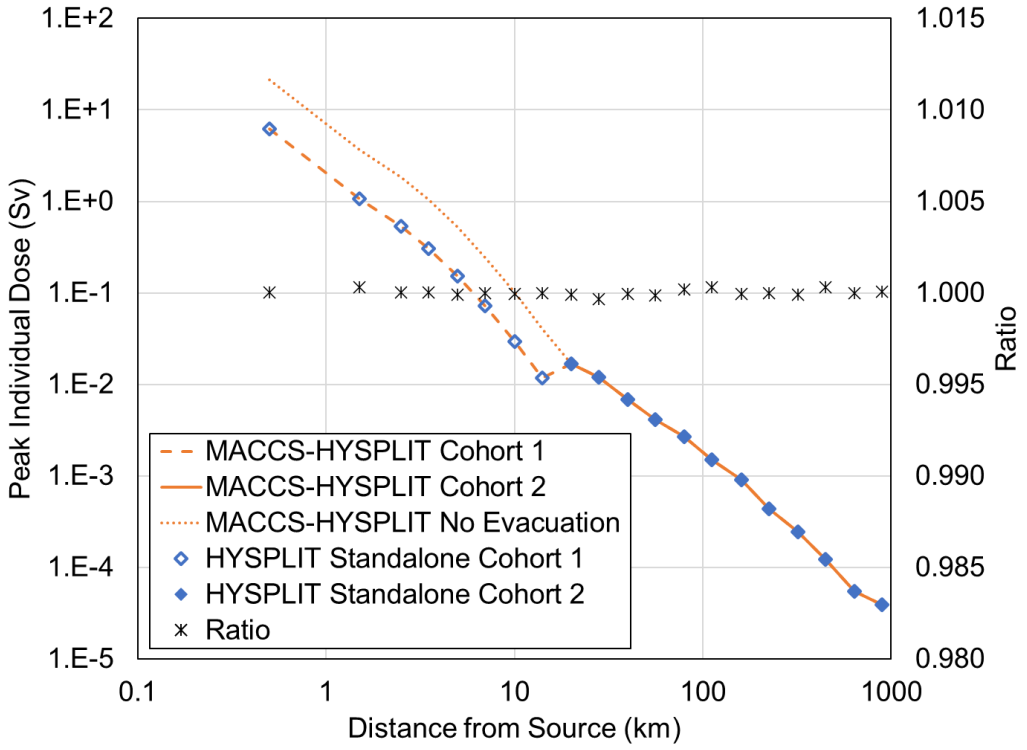

Figure 2-37. Test Case 6 comparison of peak individual dose

2.2.7. Summary

The implementation strategy for incorporating HYSPLIT into MACCS is to provide a database of air concentration and ground deposition values, generated by HYSPLIT, that can be queried by MACCS for use in subsequent consequence calculations. Based on the results from the verification test cases, the implementation of the HYSPLIT results into MACCS is confirmed. The comparisons of air concentration and ground deposition from the HYSPLIT/MACCS coupled calculations with the HYSPLIT standalone calculations in Test Cases 1 through 6 show they match within the acceptance criteria, confirming the correct coupling of HYSPLIT and MACCS. The comparison of the peak dose output for the HYSPLIT/MACCS coupled and HYSPLIT standalone calculations in all six test cases match within the acceptance criteria. This confirms the correct usage of the HYSPLIT results in MACCS.

3. BENCHMARK ANALYSIS PLAN

In this and subsequent chapters, a model comparison exercise is described. This benchmark analysis involves running specific scenarios and sensitivity studies in which the results from the Gaussian plume segment model are compared to the results of the HYSPLIT/MACCS model. The benchmarking exercise has several purposes. First, it serves as an initial analysis using the HYSPLIT/MACCS coupling to demonstrate the modeling results that could be obtained from using this new option. This provides a practical test of the implementation and provides information on the differences in the data and computational resources needed to exercise the new capability. Second, it serves as a further test of the hypothesis explored in (Molenkamp et al., 2004) that the results of a simple Gaussian plume segment model are sufficient for purposes of estimating expected values of consequence measures when averaged over a broad set of meteorological conditions (e.g., one year). As stated in NUREG/CR-2300, "*When calculating complementary cumulative distribution functions, the Gaussian model is used many times to simulate a number of weather conditions. It is intuitively reasonable to expect that there will be a certain element of 'swings and roundabouts' in that the calculations in which the consequences are overestimated will compensate for those in which the consequences are underestimated. This has never been proved with scientific rigor, but to the extent that the deviations from the Gaussian model are random, it is a reasonable expectation*" (US NRC, 1983). That hypothesis was tested in (Molenkamp et al., 2004), which explained that the justification for use of the Gaussian model "*has been that only average or expected values of metrics of interest are needed for the NRC's purposes and that a simplified model, by averaging metrics of interest obtained using numerous weather sequences one-by-one, compensates for the loss of structure in the meteorology that occurs away from the point of release.*" The objective of that study was to "*determine if the average ATD results from these codes are sufficiently close that more complex models are not required for the NRC purposes of planning, cost-benefit, and PRA are different enough that one or both of the NRC codes should be modified to provide more rigorous ATD. The decision will be made by the NRC using results of this study and other factors, most notably run time and input requirements*" (Molenkamp et al., 2004). That study found that, for the single site studied, differences in the annual average exposure and deposition results between MACCS and an advanced model (ADAPT/LODI) were nearly all within a factor of two out to a distance of 100 miles.

The following benchmark study extends that comparison by including a wider array of consequence measures, longer distances, multiple sites, and 5th and 95th percentile results in addition to the mean. The extension to a broader set of consequence measures is to ensure that the level of agreement observed for the atmospheric transport outputs such as peak integrated air concentration, peak ground deposition, and area exceeding deposition thresholds is indicative of the level of agreement for measures more typically used in consequence analyses, such as estimates of health effects, population doses, and economic impacts. The extension to longer distances allows testing of the hypothesis that there are no "cliff-edge" effects in the comparisons at distances beyond 100 mi. The extension to multiple sites allows examination of whether the results of (Molenkamp et al., 2004) were specific to the site that was selected (a relatively flat site in Oklahoma with no large water bodies) or whether the conclusions extend to some sites with potentially more complex wind fields.

Ultimately, the purpose of this comparative study is to illustrate the application of the new capabilities and inform decisions on when it may be appropriate to choose the Gaussian ATD model versus the HYSPLIT ATD model for specific applications. Because some applications may be substantially different from these benchmarking comparisons, this study does not attempt to draw general conclusions. It should be noted that with the introduction of the new capability, the logistical challenge of comparing the simple Gaussian ATD model against a more advanced model is considerably reduced. Users are encouraged to perform their own studies to determine which modeling approach best suits their needs in terms of model fidelity and computational expense.

3.1. Source Terms

For this benchmark exercise, two different source terms are modeled. The first source term (ST #1) is a NUREG-1150 historic source term (US NRC, 1990). It consists of two plume segments: a large, initial puff release, followed by a smaller, longer duration tail. The second source term (ST #2) is based on one of the State-of-the-Art Reactor Consequence Analyses (SOARCA) of a short-term station blackout (US NRC, 2012). This source term is more delayed and prolonged than the one from NUREG-1150. This source term also includes considerably more plume segments (42), each of which may travel in a different direction depending upon the wind direction at the time of release. The time histories for the two source terms are shown in Figure 3-1. The initial peak for ST #1 is about five times higher than for ST #2 and the subsequent release rate near ten times lower for ST #2. The time until initial release is ten longer for ST #2 and the total duration of the release is five times longer for ST #2.

Both source terms use the MACCS2 Sample Problem A (Chanin and Young, 1998) core inventory. The distribution of aerosol sizes was estimated using the MELCOR code and is typical of a nuclear reactor accident. The overall release fraction shown in Figure 3-1 is calculated by summing the product of the activity of each of the 69 modeled isotopes in the core at the time of reactor shutdown (i.e., the inventory) and their respective release fractions and dividing by the total core inventory of all 69 isotopes. These two source terms were selected due to their different time histories (and different numbers of plume segments used to represent the release) to illustrate the potential dependence of the comparative results on source term.

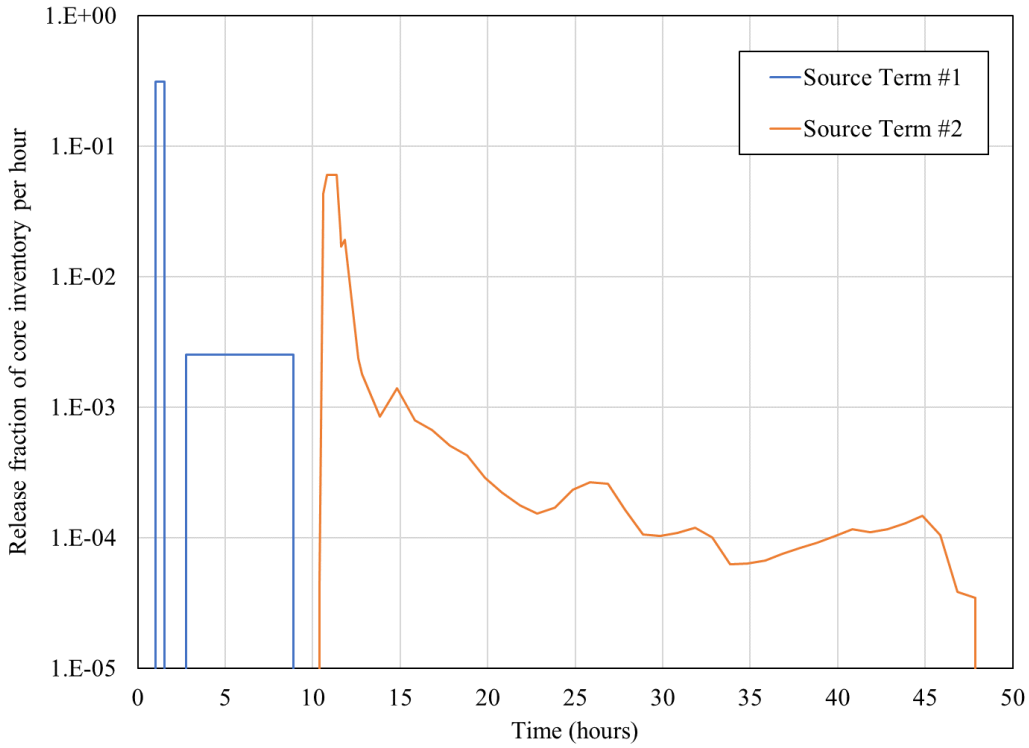

Figure 3-1. Time histories for the source terms used in the benchmark analysis

3.2. Site Data

Site-specific meteorological, population, and economic data are used in this benchmark analysis. A set of five sites, summarized in Table 3-1, were selected to demonstrate the potential range of results for a representative set of regions.

Table 3-1. Summary of selected sites

Site Identifier	Description
A	Large river valley
B	Central midwestern plain
C	Dry western region
D	Atlantic coast with potential for sea breezes
E	Southeast river valley influenced by Bermuda high

Population and economic region data for each site were determined using SecPop with 2010 Census data and 2012 County data (Weber and Bixler, 2014). A population multiplier of 1.02076, and an economic multiplier of 1.0535 are used to adjust the values to the same year with these values as an estimate for the year 2015.

Gridded model output meteorological data were obtained from an ftp site maintained by the NOAA ARL. The NAM 12-km meteorological database is run four times a day, i.e., at 00, 06, 12, and 18 UTC. Model output for the analysis time and a 3-hour forecast is converted to a 12-km Lambert conformal grid (614 by 428 cells). Data at 26 pressure levels (vertical) are included for seven variables: height, temperature, relative humidity, turbulent kinetic energy, and u, v, and w wind velocities. This produces a three hourly, 12-km data set for North America, which is made available as daily files online at the ARL server via ftp (NOAA, 2017). The NAM 12-km data set can capture complex meteorological scenarios (e.g., land/sea breeze, valley flows, etc.) given they are on length scales around 12 km or greater.

Meteorological data were extracted from the NAM 12-km data set for the year 2008 for each of the five sites and converted with MacMetGen to generate a MACCS-formatted meteorological data file representative of each site. The gridded model output information on the 12 km grid was interpolated to the site location using the same algorithms used in HYSPLIT. The MACCS Gaussian plume segment model used the MACCS-formatted meteorological data file, whereas the full NAM 12-km data set was used for the HYSPLIT ATD model calculations. These data are used in this benchmark study in place of site observations to provide as much consistency as possible between the two ATD options so that any differences in results would be due to differences in the two ATD modeling approaches rather than due to differences in meteorological data.

The main meteorological characteristics from the MACCS-formatted meteorological data files for the five sites are compared below. Figure 3-2 shows the distribution of wind directions (as interpolated from the NAM 12-km dataset) over the course of one year (2008) for the five sites from the NAM 12-km data sets. Note that the directions that the wind blows **towards** are shown in Figure 3-2, which is the convention used in the MACCS Gaussian ATD model. Sites A and B have the highest propensities for winds blowing towards north. Site C has a larger likelihood of winds blowing to the northeast. Site D has a larger likelihood of winds blowing towards the west because of sea breezes influenced by its location along the Atlantic seacoast. Site E appears to alternate between a northeastern and southwestern wind. Wind directions for Site A are strongly influenced by the directions of the river valleys along which it is located. Wind directions for Site E are due to the shifting locations of the Bermuda high.

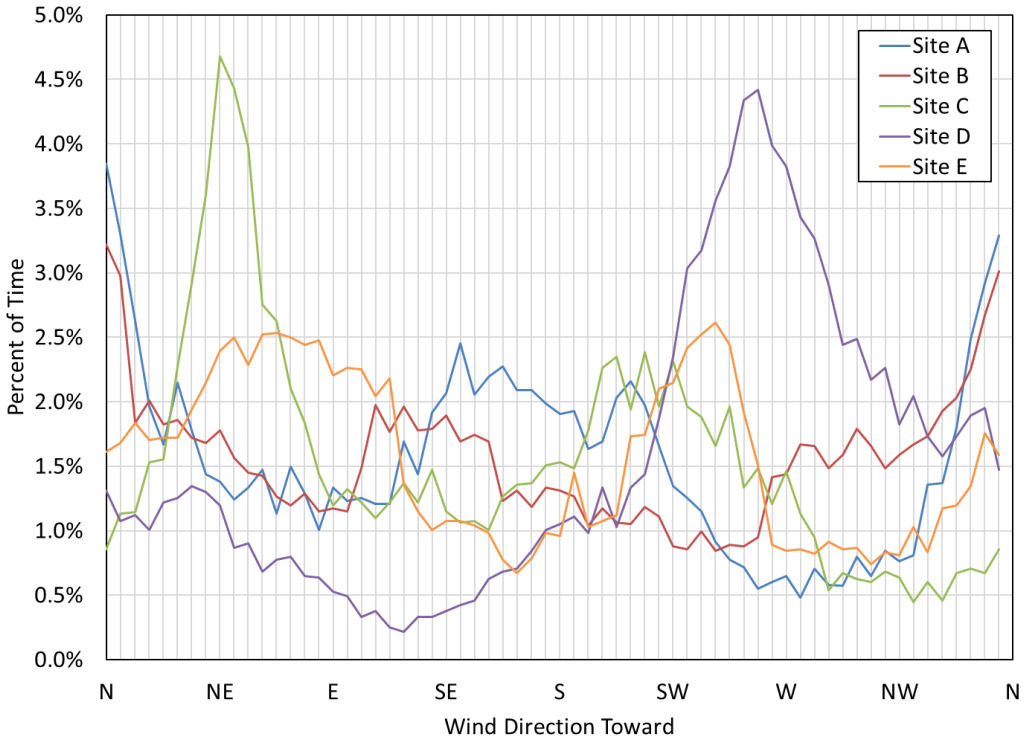

Figure 3-2. Distribution of wind directions over the course of a year for the five sites derived from the NAM 12-km data set

Figure 3-3 shows the average wind speed as a function of wind direction for the five sites. In general, Sites A and C have the lowest wind speeds, while Site D has the highest wind speeds. Figure 3-4 displays the average stability class as a function of wind direction for the five sites. The stability class is shown ranging from 1 (A, unstable) to 7 (G, stable) and was calculated based on the vertical temperature gradient at the site using the DTDZ method (criteria shown in Table 1 of [US NRC, 2007]). The sensitivity of the benchmark analysis results to the method to determine stability class is explored in Section 5.2. The stability class appears to correlate with wind direction for Site C, but to be relatively independent of wind direction for the other sites. Sites A, B, and E have similar average stability classes, while Site D tends more toward unstable conditions. Figure 3-5 shows the distribution of stability class as a function of time of day for the five sites.

Figure 3-6 shows the average precipitation rate as a function of wind direction for the five sites. Total precipitation over the course of the selected year for Site A, Site B, Site C, Site D, and Site E are 42 in, 43 in, 8 in, 39 in, and 30 in, respectively. Site C has the lowest amount of precipitation. Site A appears to have the highest precipitation rate when winds are toward the west. The peak precipitation rate for Site B is largely distributed between southern, southwestern, and western directions. Sites D and E show similar precipitation rates to each other apart from a few peaks.

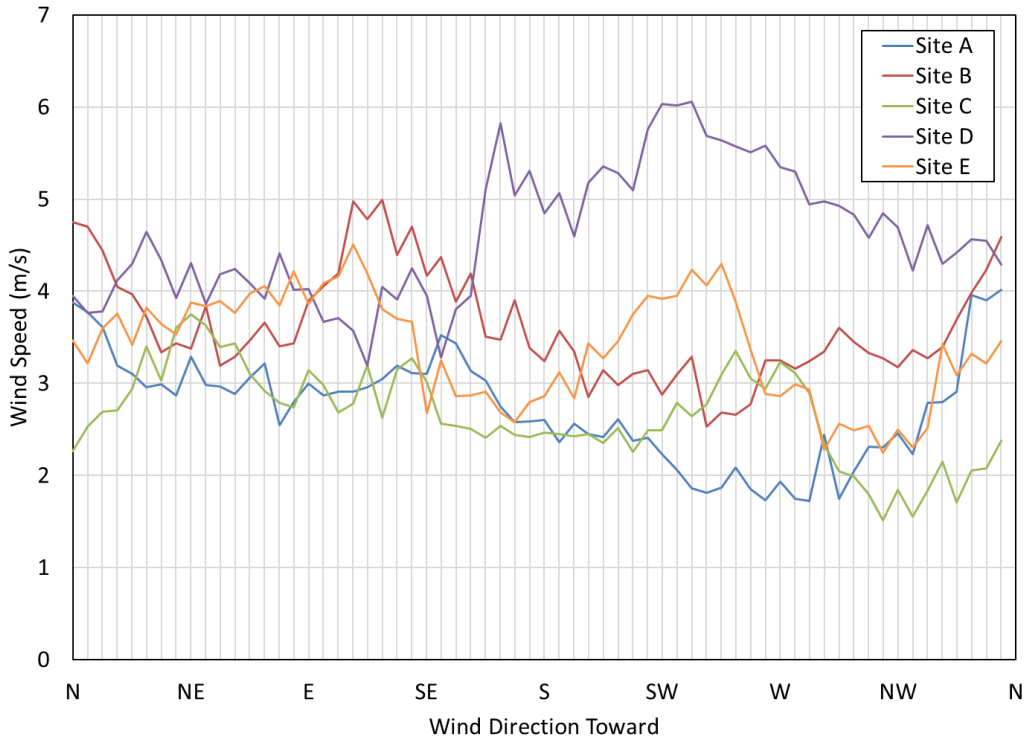

Figure 3-3. Average wind speed as a function of wind direction for the five sites derived from the NAM 12-km data set

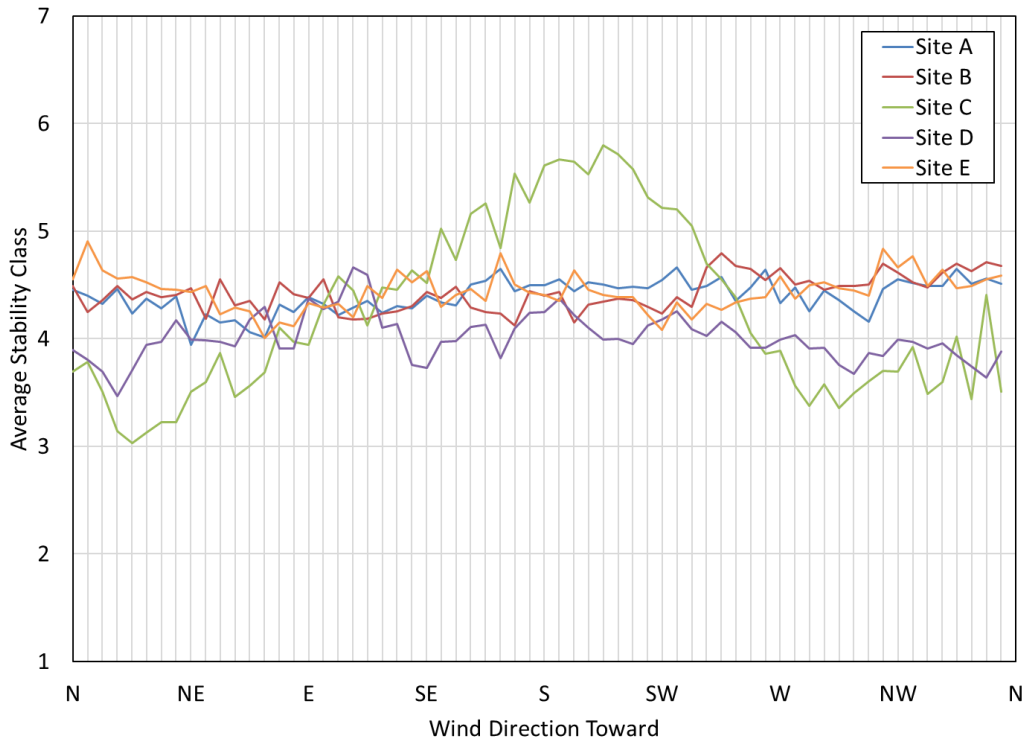

Figure 3-4. Average stability class as a function of wind direction for the five sites derived from the NAM 12-km data set

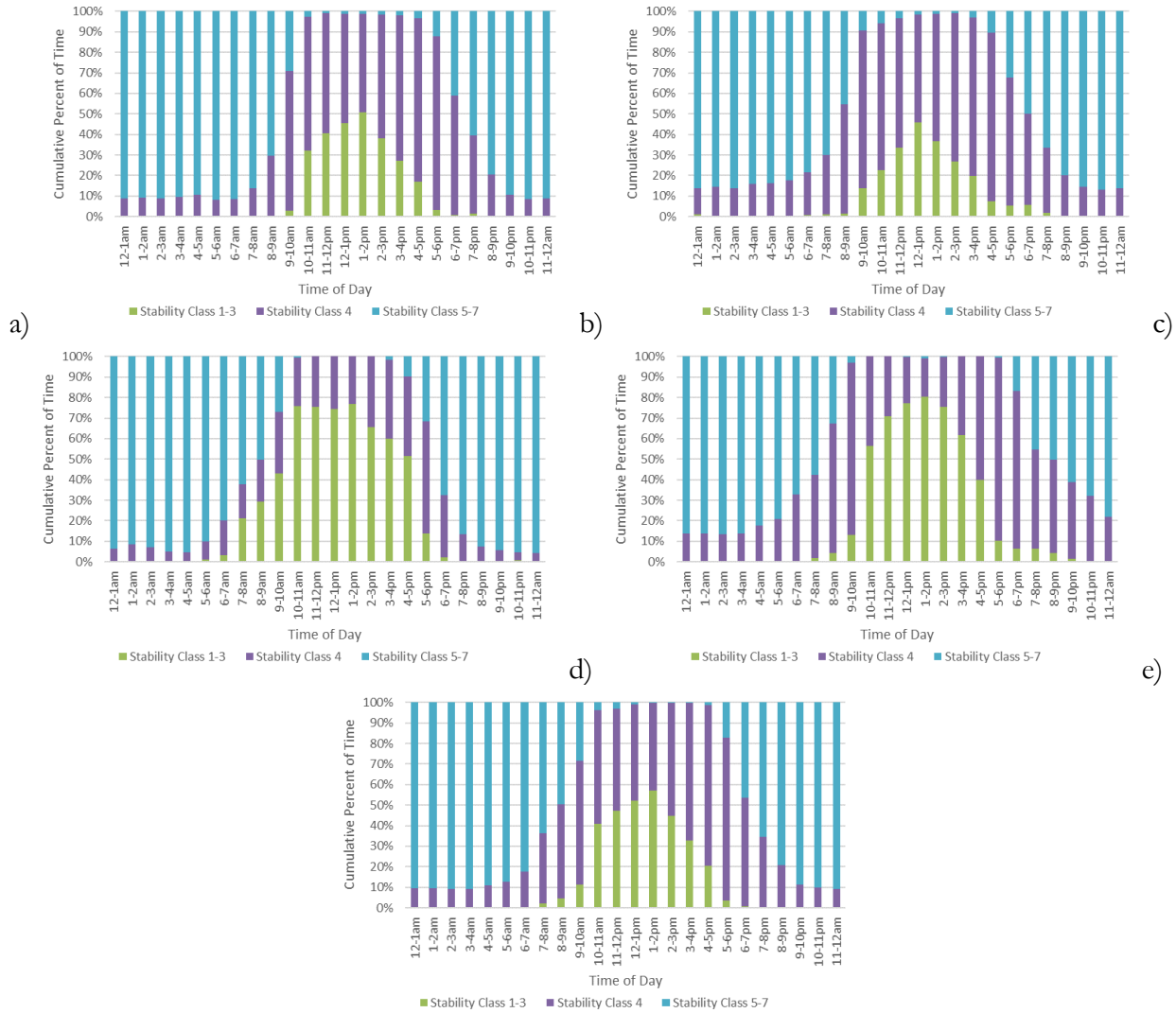

Figure 3-5. Stability class distribution as a function of time of day for a) Site A, b) Site B, c) Site C, d) Site D, and e) Site E derived from the NAM 12-km data set

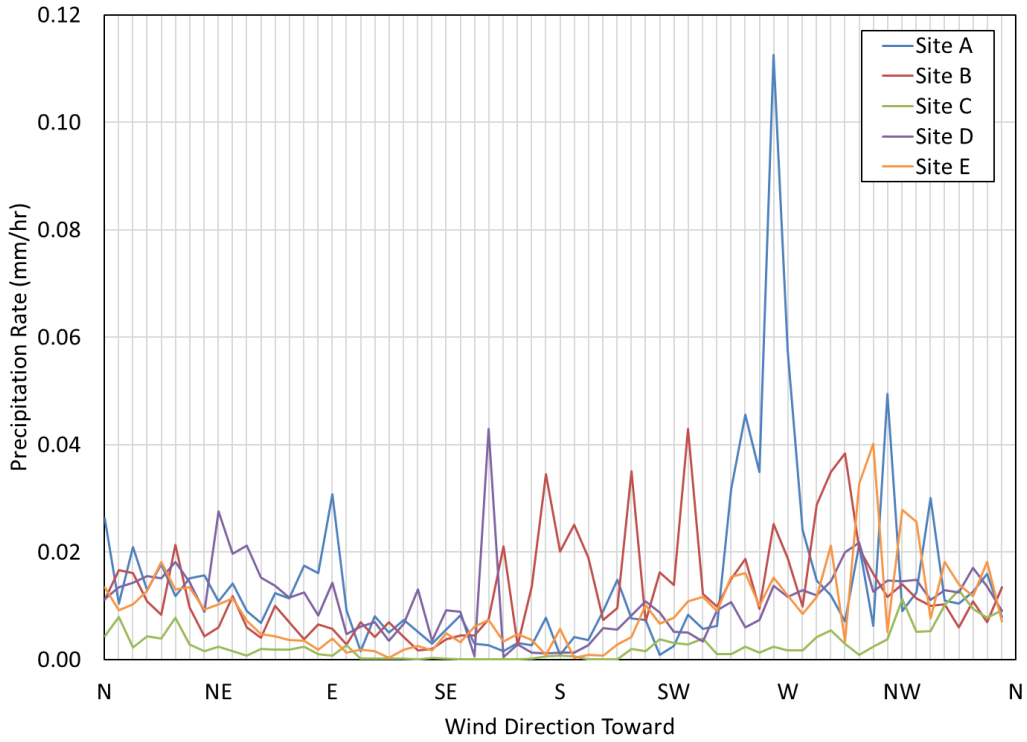

Figure 3-6. Average precipitation rate as a function of wind direction for the five sites derived from the NAM 12-km data set

3.3. Grid Definition

The spatial domain is defined by the user within MACCS by selecting the number of radial intervals, the number of compass sectors, and the radial distance from the release point, (i.e., from the center of the polar coordinate system,) for each radial interval. For the benchmark analysis, the same grid definition is used for all five sites. The origin of each grid was centered on the respective site location. The MACCS grid for this analysis contains 29 radial intervals and 64 compass sectors. The radial distance from the release point for each interval is shown in Table 3-2.

Table 3-2. MACCS grid radial distances

Radial Interval	Radial Distance
1	0.16 km (0.10 mi)
2	0.56 km (0.35 mi)
3	1.21 km (0.75 mi)
4	1.61 km (1.00 mi)
5	2.16 km (1.35 mi)
6	3.22 km (2.00 mi)
7	4.02 km (2.50 mi)
8	4.83 km (3.00 mi)
9	6.44 km (4.00 mi)
10	8.05 km (5.00 mi)
11	12.1 km (7.50 mi)
12	16.1 km (10.0 mi)
13	20.1 km (12.5 mi)
14	24.1 km (15.0 mi)
15	32.2 km (20.0 mi)

Radial Interval	Radial Distance
16	40.2 km (25.0 mi)
17	48.3 km (30.0 mi)
18	64.4 km (40.0 mi)
19	80.5 km (50.0 mi)
20	112.7 km (70.0 mi)
21	160.9 km (100 mi)
22	241.4 km (150 mi)
23	321.9 km (200 mi)
24	442.6 km (275 mi)
25	563.3 km (350 mi)
26	684.0 km (425 mi)
27	804.7 km (500 mi)
28	1,207 km (750 mi)
29	1,609 km (1,000 mi)

The radial intervals have a finer resolution near the release location and become coarser in the outer domain. A value of 1,609 km (1,000 mi) was selected as the outer boundary because it was used in some historical analyses, e.g., NUREG-1150. Also, this choice facilitates comparisons between the Gaussian ATD and HYSPLIT/MACCS models to test the hypothesis that there are no "cliff-edge" effects in the comparisons at longer distances. The selection of 64 compass sectors provides the highest degree of grid angular resolution currently available in MACCS and allows for relatively good resolution of results such as peak air concentration and peak individual dose.

For the HYSPLIT calculations, multiple polar grids with 128 compass sectors each and uniformly spaced radial distances are used to evaluate air concentrations and ground depositions for 15-min intervals. The nine HYSPLIT grids are shown in Table 3-3 with their specifications[2]. The results on the HYSPLIT grids are then interpolated onto the MACCS grid (Table 3-2) using HyGridConvert (see Section 2.1.2). The HYSPLIT/MACCS benchmark calculations use the same MACCS grid as the Gaussian ATD model calculations.

Table 3-3. HYSPLIT grid parameters

Grid #	Spacing	Span
0	0.5 km	10 km
1	1.0 km	20 km
2	2.0 km	40 km
3	4.0 km	80 km
4	8.0 km	160 km
5	16.0 km	320 km
6	32.0 km	640 km
7	64.0 km	1,280 km
8	80.5 km	1,610 km

The grid shown in Table 3-3 demonstrates the computational savings of the nested, multi-polar-grid approach. The nested grid used in this benchmark includes 20 radial intervals per computational grid for a total of 180 intervals. Using a 0.5 km spacing over the entire computational grid would have used 3,220 intervals. Thus, less than 6% of the number of grid cells are used with the multi-grid approach as would have been required using a single-grid approach.

3.4. ATD Model Definition

The model-specific options for the Gaussian ATD and HYSPLIT/MACCS models are discussed in this section. In general, the options are selected to mirror the typical choices used in NRC applications. Note that the options selected for this benchmark analysis may not be optimal for other applications. The user should conduct similar studies to determine the best choices for their application.

[2] It may be noted that with the MACCS resolution for the first 3-4 intervals, the initial grid spacing of 0.5 km spacing with 50 m layer thickness produces only a coarse representation of results within the first several MACCS grid intervals. This spacing is a current HYSPLIT limitation due to the limit of a one-minute time step in the code.

3.4.1. Gaussian ATD Model Configuration

The Gaussian ATD model results are based on the following choices:

- A power-law representation of the Pasquill-Gifford dispersion curves is used for dispersion, (as described in Section 1.3.1), with Tadmor-Gur coefficients (Dobbins, 1979).
- Unless noted otherwise, calculations use time-based dispersion beyond 30 km downwind.
- Deposition is calculated using the set of deposition velocities shown in Table 3-4.
- Stabilized plume height is calculated using the standard Briggs model in MACCS.
- Initial dispersion parameters are based on a release from a building that is 50 m high by 40 m wide.
- Weather data extracted from the 2008 NAM 12-km meteorological data at the site location is used over the computational domain out to a radius of 1,600 km (1,000 mi). The data are extracted from the same 2008 NAM 12-km meteorological data set that is used with the MACCS/HYSPLIT model.

Table 3-4. Deposition velocities used with Gaussian ATD model

Aerosol Diameter (μm)	Deposition Velocity (cm/s)
0.15	7.87e-2
0.29	5.92e-2
0.53	6.66e-2
0.99	1.01e-1
1.84	1.87e-1
3.43	3.80e-1
6.38	7.63e-1
11.9	1.37e+0
22.1	1.97e+0
41.2	2.90e+0

3.4.2. HYSPLIT/MACCS Model Configuration

HYSPLIT is configurable. There are several options in the HYSPLIT model that are thought to potentially affect the results of the benchmark analysis. These options are investigated to explore choices for the benchmark analysis discussed above. These include two options to specify stabilized plume height, the number of Lagrangian particles to use in the simulations, the height of the surface layer used to evaluate surface air concentrations, and the area source size. The results of the investigation and model choices are discussed below. The HYSPLIT model results use the following:

- Dispersion is estimated using default parameters in HYSPLIT. The release is from a point source.
- Deposition is estimated using the aerosol diameters shown in Table 3-4. Aerosol densities are assumed to be 1.0 g/cm^3. The resistance model in HYSPLIT is used to estimate deposition velocities.
- The surface layer thickness used for the concentration grid is 50 m at all distances, which means that surface air concentration is calculated by accounting for all the particles below this height.

- The 2008 NAM 12-km meteorological data set are used over the entire computational domain.

3.4.2.1. Stabilized Plume Height

Both MACCS and HYSPLIT include models for plume buoyancy based on (Briggs, 1973). The current implementation allows the options to use MACCS to estimate a stabilized plume height or to use the HYSPLIT model to estimate plume rise. Because the current implementation uses precalculated HYSPLIT results, both options are implemented using a binned approach. The bin levels are constructed by the user and may include as many bins as needed. The bins either contain a set of stabilized release heights or a set of rates of sensible heat release. With the first option, MACCS calculates the stabilized height, accounting for the initial height of release and plume buoyancy, considering the current stability class, and selects the bin that most closely matches the calculated value. The MACCS calculation also considers the possibility that the plume is insufficiently buoyant to rise after being impacted by the building wake. With the second option, MACCS simply passes the rate of release of sensible heat to HYSPLIT and lets HYSPLIT calculate the stabilized plume height. Currently, the HYSPLIT model assumes that buoyant releases occur at ground level and does not account for either elevated release locations or downwash in the building wake.

While the Briggs model for plume rise is essentially the same in MACCS as it is in HYSPLIT, there are four significant differences in the treatment of plume rise that can cause predictions to be different.

- As mentioned above, MACCS considers the possibility that the plume is not buoyant enough to rise after being impacted by the building wake; HYSPLIT assumes plume rise to the stabilized height under all conditions.
- MACCS uses seasonal values for mixing height to restrict the rise of the plume, i.e., the plume is not allowed to rise above the mixing height; HYSPLIT uses information from the gridded weather file to determine rise height, which for the NAM 12-km data used in this benchmark study has values that can change over the course of each day.
- MACCS uses a bent-over plume model in the nearfield to define the shape of the plume; HYSPLIT assumes instantaneous plume rise up to its stabilized height. This difference in treatment can affect near-field results but has no effect at distances beyond which stabilized plume height is achieved (generally by downwind distances of one or two km). This difference is not relevant to the discussion here, which is focused on how to best account for plume buoyancy when using the HYSPLIT model with MACCS. It is relevant for the comparisons between the HYSPLIT and Gaussian results shown in Section 4.
- MACCS accounts for the initial release height plus the rise height; HYSPLIT assumes that the initial height is zero when it calculates rise height.

Based on the discussion above, the option to run HYSPLIT with a set of stabilized plume heights is selected rather than with a set of rates of release of sensible heat. This option uses the MACCS model for plume buoyancy to determine the stabilized height for each plume segment. The calculated height for each release is then matched against a precalculated set of release heights using the HYSPLIT model, which are chosen to be 10 m, 50 m, 100 m, and 200 m in this benchmark analysis. MACCS selects one of the HYSPLIT results for each plume segment, using the arithmetic means of each successive pair as boundaries (e.g., heights between 75 m and 150 m use the 100 m results). The advantages of this choice are that MACCS accounts for the initial height of release and

for the possibility that the building wake affects the plume rise, whereas HYSPLIT does neither of these things; the disadvantage is that HYSPLIT uses current data from the gridded weather file to restrict plume rise height, whereas MACCS uses seasonal data. In general, the plume rise has the largest effect in the nearfield, with a diminishing effect at longer distances.

3.4.2.2. Number of Lagrangian Particles

The number of Lagrangian particles used to represent released aerosols is a HYSPLIT model parameter that was investigated to determine a reasonable value for the benchmark analyses. The number of Lagrangian particles is specified on a particles per minute basis for each aerosol bin in GenHysplit. A test case was run using 10 particles per minute per aerosol bin and compared with the same case increasing the total number of particles by 2x, 5x, and 10x. Comparisons between the peak air concentration and ground deposition showed little differences (maximum of 10%), even at distances up to 1,600 km (1,000 miles). In general, computational run time increases in proportion to the number of particles in the simulation and increases more when memory limitations are reached. Since increasing the number of particles increases the run time without significantly improving results, 10 particles per minute per aerosol bin is selected as the number of Lagrangian particles per aerosol bin for the benchmark analyses. This results in about 6,000 Lagrangian particles (10 particles per minute per aerosol bin x 60 minutes x 10 aerosol bins) for each one-hour plume segment.

Another method for evaluating the number of Lagrangian particles to use in a simulation is to determine the number of particles that pass through each grid volume over the averaging time. In general, Lagrangian particle dispersion models target 10 to 100 particles in each grid volume. The actual dispersion is much more complex than the discussion below. For example, there are more particles near the center of the plume than the edges (both horizontal and vertical), but the discussion assumes that they are uniformly distributed. Over the 15-minute averaging time used in this analysis, 1,500 Lagrangian particles (10 particles per minute per aerosol bin x 15 minutes x 10 aerosol bins) would pass through a radius. Bounding the horizontal dispersion to spread the plume segment over $1/16^{th}$ of the compass (22.5 degrees), results in four sectors for the particles to distribute throughout. Assuming a uniform vertical dispersion and a 1,000 m mixing layer height, $1/20^{th}$ of the particles would be in the 50 m surface layer. Using these assumptions, the 1,500 Lagrangian particles would be spread over four sectors and contain $1/20^{th}$ of the particles, for an average of 19 particles passing through each grid volume over the averaging time, within the Lagrangian particle dispersion model target.

3.5. Evacuation Scheme

Evacuation is considered within 16 km of each site. The evacuation scheme used for all the benchmark cases includes five cohorts. Cohorts 1 to 4 use radial evacuation; Cohort 5 (0.5% of the population) was modeled as non-evacuating. The four evacuating cohorts have the following delays:

- Cohort 1 – evacuation begins 5,400 s after accident initiation
- Cohort 2 – evacuation begins 11,700 s after accident initiation
- Cohort 3 – evacuation begins 19,800 s after accident initiation
- Cohort 4 – evacuation begins 27,900 s after accident initiation

Cohort 1 represents the early evacuation of 10% of the population. Cohort 2 represents the early middle evacuation of 40% of the population. Cohort 3 represented the later middle evacuation of 40% of the population. Cohort 4 represents a late evacuating tail (9.5% of the population) of the evacuation.

3.6. Output Measures

The combination of sites and source terms lead to a total of ten cases in this analysis. For each site/source term combination, a MACCS calculation using the MACCS Gaussian ATD model option and one using the HYSPLIT ATD model option were performed. Uniform weather bin sampling, with 40 samples per bin, is used to explore the variability of the meteorology for each site, generating a range of results. For each output quantity, the mean and the 5th and 95th percentiles are used to quantify the range of the results. The output quantities are grouped into two categories, ATD results and consequence results.

3.6.1. ATD Outputs

The following list indicates the atmospheric dispersion results that are compared:

- Peak (around the compass) normalized, time-integrated, ground-level, air concentration (χ/Q, s/m^3) as a function of distance from the site (Peak Air)
- Peak (around the compass) normalized ground concentration (D/Q, 1/m^2) as a function of distance from the site (Peak Ground)
- Normalized cumulative land areas that exceed various levels of ground deposition (unitless) (Land Area)

The statistics for these metrics are evaluated over a one-year period. That is, we are not looking for the peak concentrations for a single release period scenario. For each output quantity, the mean and the 5th and 95th percentiles over the one-year period are used to quantify the range of the results.

The peak air concentration is the maximum value of the normalized, time-integrated, ground-level, air concentration (or dilution) around the compass at a given distance. The peak ground deposition is the maximum value of the normalized deposition on the ground around the compass at a given distance. These values are normalized by dividing by the released activity. Air concentration and ground deposition were chosen as important metrics because many of the consequences are calculated from one or both of them. Furthermore, they are the most direct outputs from the atmospheric dispersion calculations.

The land areas that exceed various levels of ground deposition are the total surface areas of land that have sufficient deposition to be above a specified activity per unit area. The area is calculated by determining the contamination level of each grid cell out to 800 km (500 mi), checking whether it is above the specified level, and when it is, adding the area of the grid cell to the total. The normalized values are determined by dividing by the area from the Gaussian calculation that exceeds 1 μCi/m^2. This too is for a one-year period. The mean and the 5th and 95th percentiles over the one-year period are used to quantify the range of the results. The land area that exceeds various levels of ground deposition was selected as a direct output from the atmospheric transport and dispersion calculations that is used in subsequent consequence calculations by MACCS.

3.6.2. Consequence Outputs

Consequence measures are selected as outputs in addition to the ATD measures since ATD measures may not always predict trends of consequence measures, due to the non-linear nature of many consequence measures. Furthermore, these additional measures expand the on results presented in (Molenkamp et al., 2004). The following list shows the consequence results that are compared in this benchmark:

- Normalized peak dose (unitless) as a function of distance (Peak Dose)
- Early fatality risk (unitless) within a circular area near the point of release (EF Risk)
- Normalized regional population doses (unitless) (Pop Dose)
- Latent cancer fatality risk (unitless) over region (LCF Risk)
- Normalized, regional economic loss (unitless) (Econ Loss)

As is the case for the ATD outputs, the statistics for these metrics are all evaluated over a one-year period. For each output quantity, the mean and the 5^{th} and 95^{th} percentiles over the one-year period are used to quantify the range of the results.

The peak dose is the maximum value of the ionizing radiation dose to an individual around the compass at a given distance. It is calculated by examining the individual ionizing radiation dose in each sector and selecting the largest value for each distance from the site. For this comparison, it is normalized by dividing by the value from the Gaussian model at 0.85 mi. The peak dose was selected as an important metric because it is used to determine several of the emergency response measures modeled in MACCS.

The early fatality risk is the number of predicted early fatalities divided by the population with a specified distance from the site. This provides a measure of the average early fatality risk to an individual within that region. Normalized values are determined by dividing by the corresponding values from the Gaussian calculation at 1 mi. Early fatality risk depends on the ionizing radiation dose to a target organ, but the response is highly nonlinear. When the dose is below a threshold for that organ, the risk is zero. Above the threshold dose, the response follows a Weibull function, which has a sigmoidal shape.

The population dose within a specified distance from the site is the sum of the calculated individual ionizing radiation doses multiplied by the number of individuals who would receive that ionizing radiation dose within the specified distance. The total latent cancer fatality risk within a specified distance from the site is the number of predicted latent cancer fatalities divided by the population within that distance. This provides a measure of the average cancer fatality risk to an individual within that region. Normalized values are determined by dividing by the corresponding values from the Gaussian calculation at 10 mi. When a zero value is estimated for the Gaussian calculation, the value from the HYSPLIT calculation is used to normalize and only occurred for one of the site/source term cases. Early fatality risk, population dose, and latent cancer fatality risk are chosen as important metrics because they are often reported in consequence analyses performed for NRC applications.

The regional economic loss is the total economic cost to perform remedial actions needed to return the area to a usable state. Economic loss includes per diem costs associated with individuals displaced over the short term, one-time moving costs for individuals displaced over the long term, costs to decontaminate land and property, costs associated with loss of use of property, condemnation costs for property that cannot be restored to usability, and costs to dispose of farm crops. The normalized values are determined by dividing by the Gaussian value at 10 mi. Economic losses are closely related to the land areas contaminated above specific threshold levels. The regional economic loss is selected as an important consequence metric because it is used in cost-benefit analyses.

This page left blank

4. BENCHMARK ANALYSIS RESULTS

The results of the benchmark analyses are presented below. First the computational requirements are discussed. Next, figures showing results for the ten site/source term combinations compare the Gaussian and HYSPLIT ATD models. The five sites chosen for this benchmark are shown in Table 3-1 and the two source terms are illustrated in Figure 3-1. In the following subsections, the results for each site/source term combination are shown as a series of plots for each of the selected consequence measures. A brief description of the results is repeated at the beginning of each subsection as an aid to the reader. In these plots, the annual statistics for these measures are shown with different colors, where the annul mean values are in black, the annual 5th percentile values are shown in blue, and the annual 95th percentile values are shown in green. HYSPLIT results are shown as dashed lines and Gaussian model results are shown as solid lines. The normalized results are shown as a function of distance, rather than the ratio of Gaussian and HYSPLIT results, to allow for the trends with distance to be observed. A summary of interpretations from the results is found in the final subsection.

Because this analysis involves the comparison of two completely different methods for estimating atmospheric dispersion, there is no expectation of close (<10%) agreement of the results. The purpose of this benchmark is to investigate the similarities, differences, and trends between the two models. The expectation is that nearly all results should be within a factor of ten and most results should be within a factor of two, as reported previously in (Molenkamp et al., 2004). As previously noted, the primary objective of this benchmarking exercise is to illustrate the application of the new capabilities and inform decisions on when it may be appropriate to choose the MACCS Gaussian model versus the MACCS/HYSPLIT coupled model for specific applications. Because some applications may be substantially different from these benchmarking comparisons, this study does not attempt to draw general conclusions regarding which option may be considered the preferred approach for all possible applications. Users are encouraged to independently evaluate which modeling approach best suits their specific needs in terms of model fidelity and computational expense.

4.1. Computational Requirements

The codes and versions for the software used in the benchmark analyses are shown in Table 4-1. GenHysplit requires a python interpreter and parallel processing package. For the benchmark analysis, GenHysplit and HYSPLIT were run in a Linux RedHat environment with a python interpreter and OpenMPI. HyGridConvert, MacMetGen, MACCS, SecPop, and WinMACCS were run in a Windows 7 environment. Each is a separate executable that does not require any other packages to run.

Table 4-1. Software used in benchmark analyses

Code	Version
GenHysplit	1.2.0
HyGridConvert	1.2.0
HYSPLIT	5.0.0
MacMetGen	1.0.0
MACCS	4.0
SecPop	4.3.0
WinMACCS	4.0

Using the HYSPLIT ATD option adds substantial computational costs compared with the Gaussian ATD option. For example, for each site GenHysplit took 36 hours running on 720 processors to generate the HYSPLIT concentration files (*.ccd), generating a total of 35,136 files and storage of 500-600 GB per site. Another 14 hours were needed to run HyGridConvert for each site to generate the set of *.mcd files, which require ~200 GB more disk storage. Furthermore, the MACCS run time is longer when using the HYSPLIT ATD option. It is a function of the input/output speeds and depends on the communication speed between the device storing the *.mcd files and the computer running the calculations. The MACCS run time also depends on the number of plume segments in the source term. For example, it took about 5 hours for the MACCS/HYSPLIT calculations using ST #1 for each site; it took 28 hours using ST #2. The same calculations with MACCS using the Gaussian ATD option took 90 seconds for ST #1 and 22 minutes for ST #2

4.2. Site A

4.2.1. Source Term #1

The comparison between the Gaussian and HYSPLIT ATD model results for Site A, ST #1 (from Sample Problem A), for peak air concentration, peak ground deposition, land contamination area, peak dose, early fatality risk, population dose, latent cancer fatality risk, and economic loss (as described in Section 3.6) are shown in Figure 4-1 through Figure 4-8. The annual statistics for these measures are shown with different colors, where the mean values are in black, the 5th percentile values are shown in blue, and the 95th percentile values are shown in green. HYSPLIT results are shown as dashed lines and Gaussian model results are shown as solid lines. The normalized results are shown as a function of distance, rather than the ratio of Gaussian and HYSPLIT results, to allow for the trends with distance to be observed. Some results are zero for early fatality risk, so they cannot be shown on the log scale used in the figures. Note that the change in slope at about 19 mi for the Gaussian ATD model curves is caused by the switch from distance- to time-based dispersion models. Discussion of the difference seen in these figures is provided below in Section 4.7.

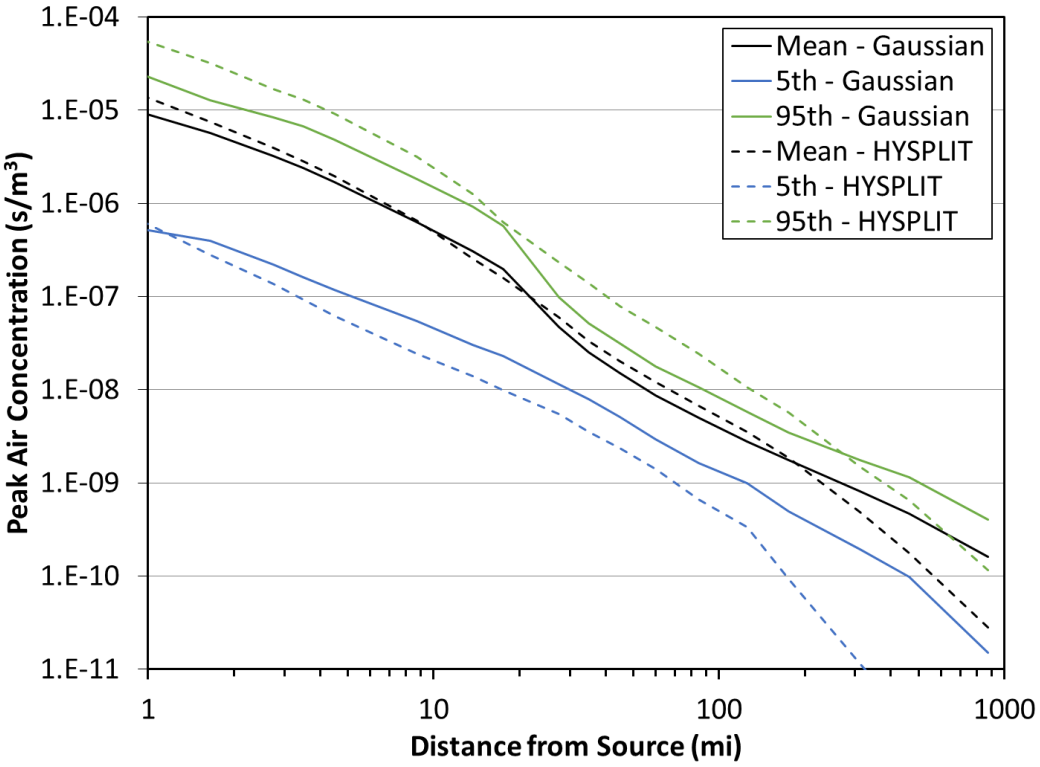

Figure 4-1. Benchmark Site A, ST #1, peak air concentration comparison

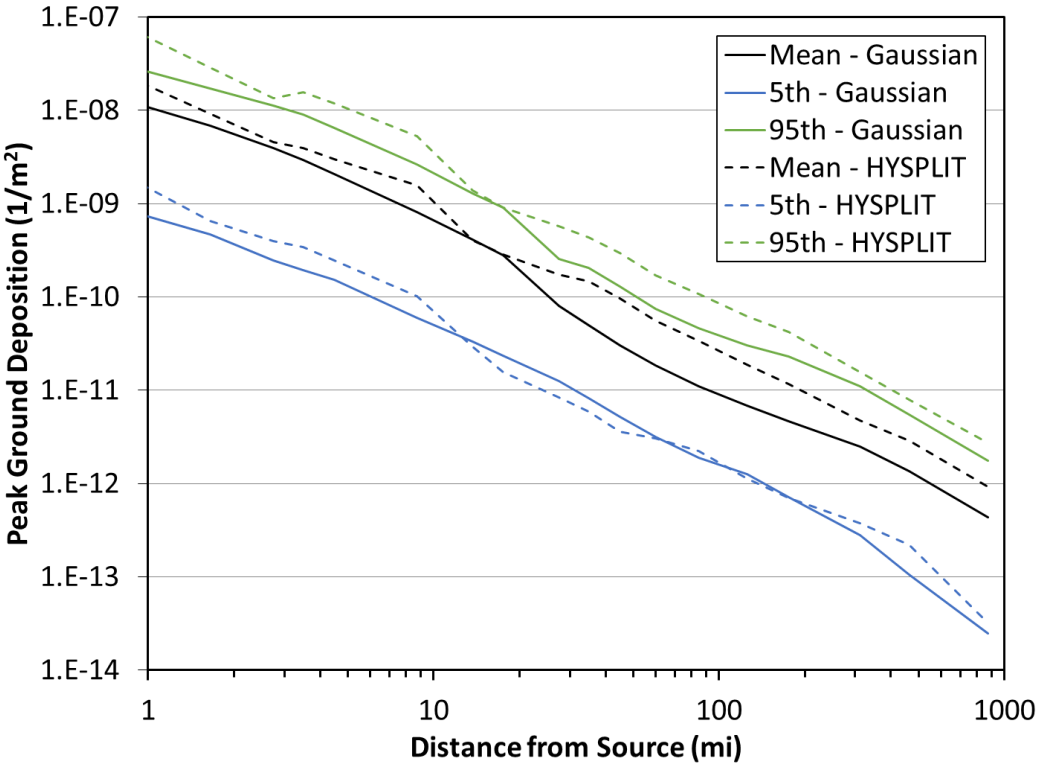

Figure 4-2. Benchmark Site A, ST #1, peak ground deposition comparison

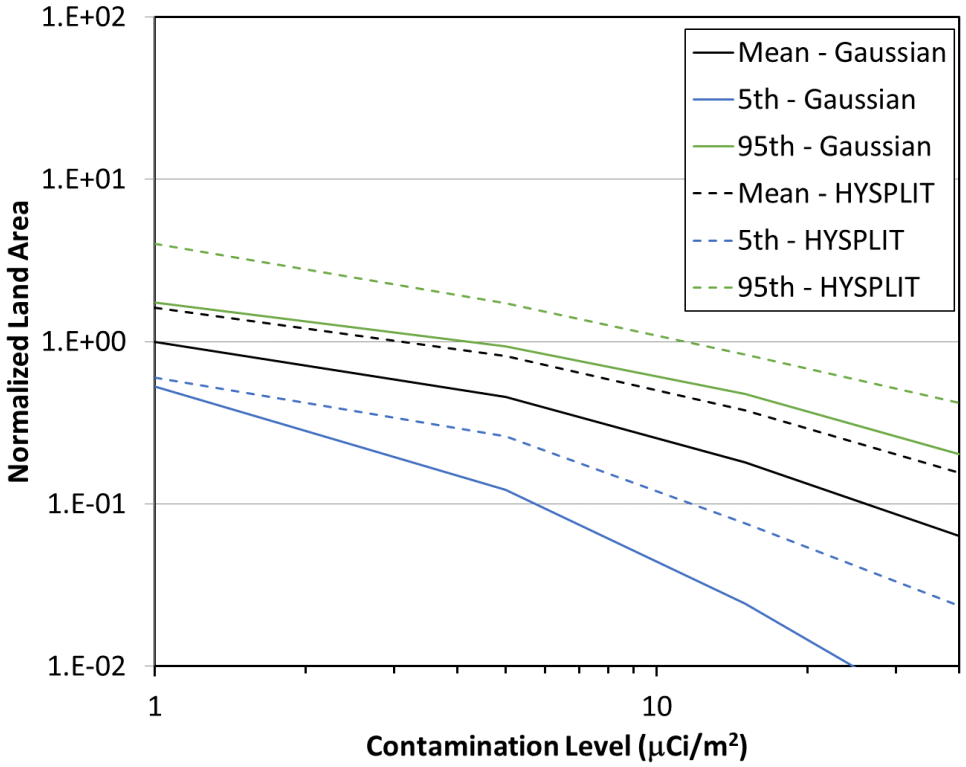

Figure 4-3. Benchmark Site A, ST #1, land contamination area within 805 km (500 mi) comparison

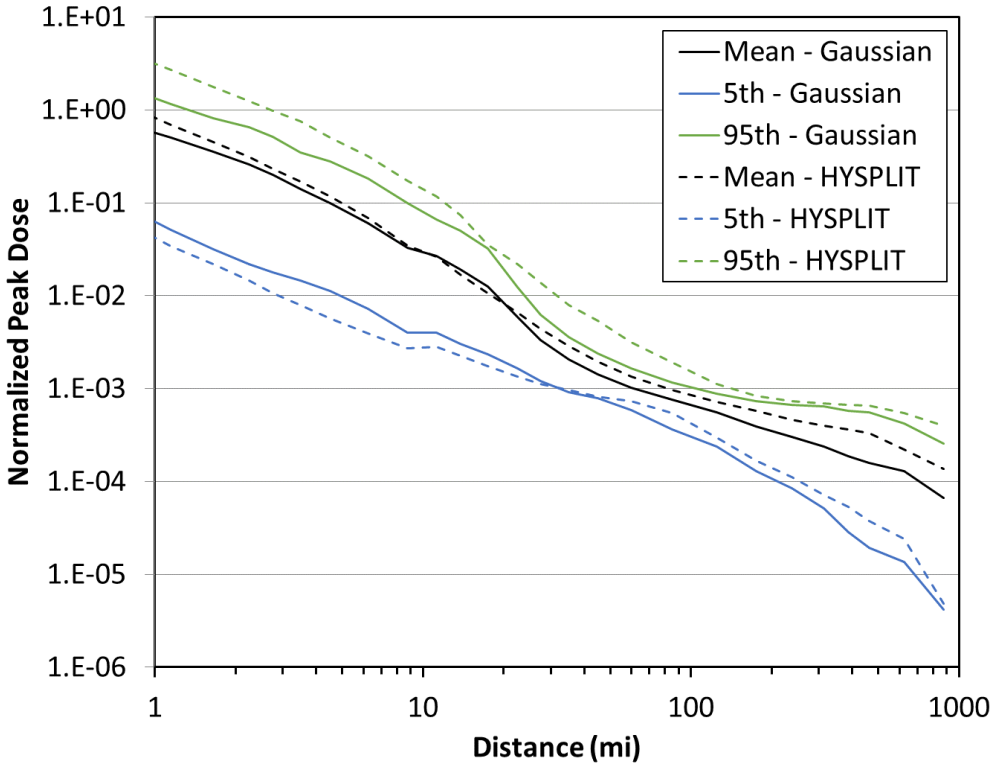

Figure 4-4. Benchmark Site A, ST #1, peak dose comparison

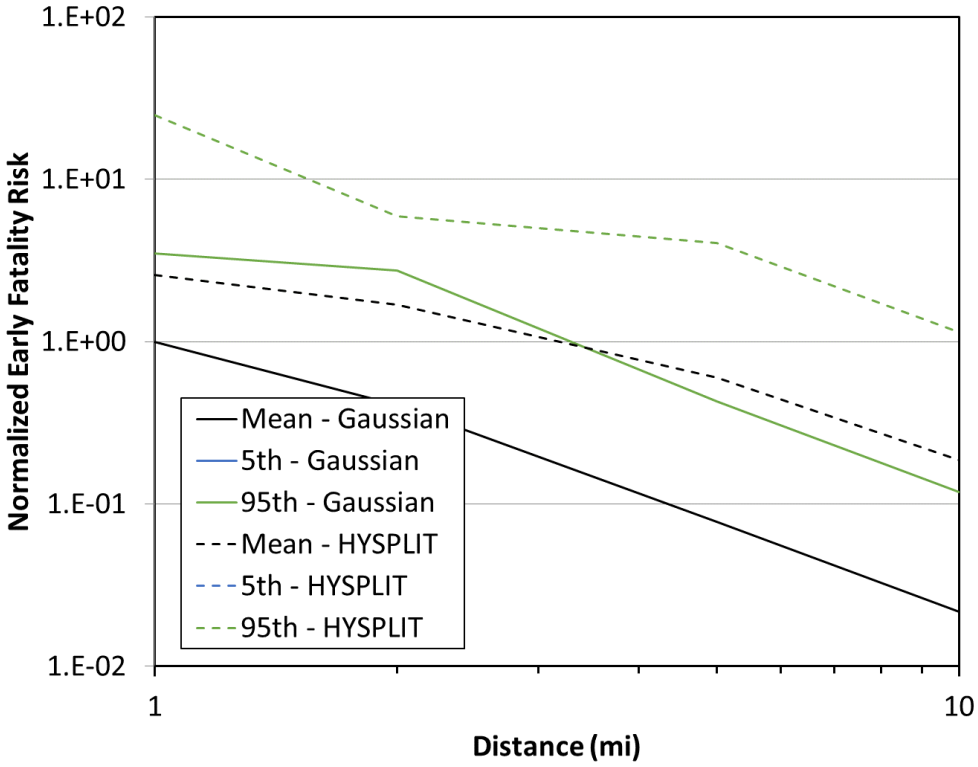

Figure 4-5. Benchmark Site A, ST #1, early fatality risk comparison

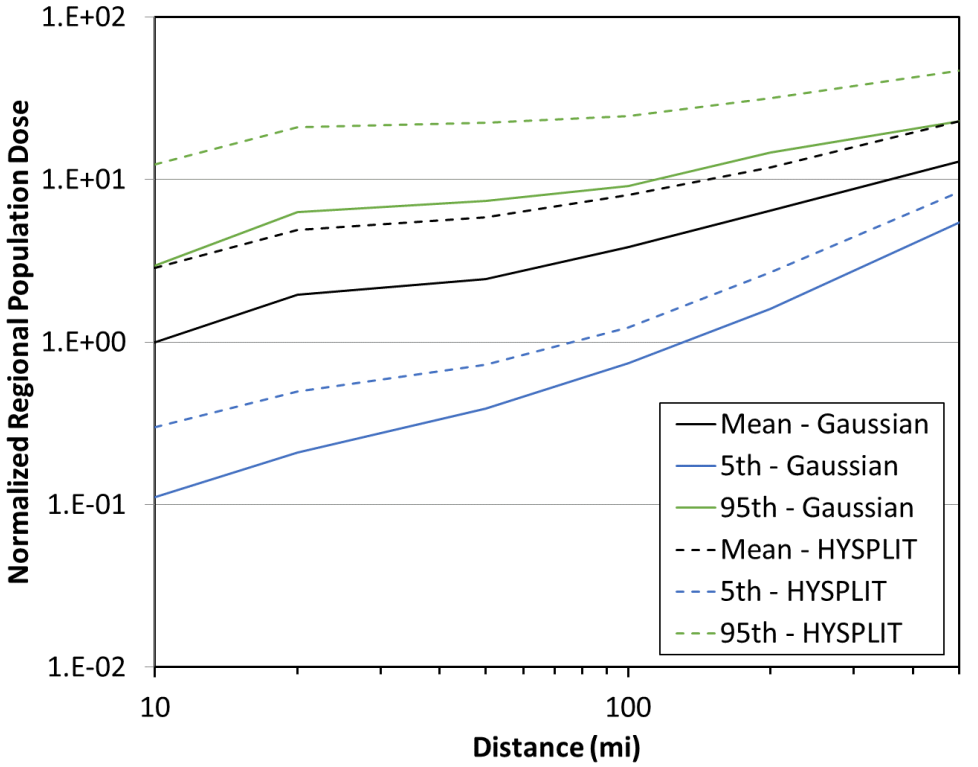

Figure 4-6. Benchmark Site A, ST #1, population dose comparison

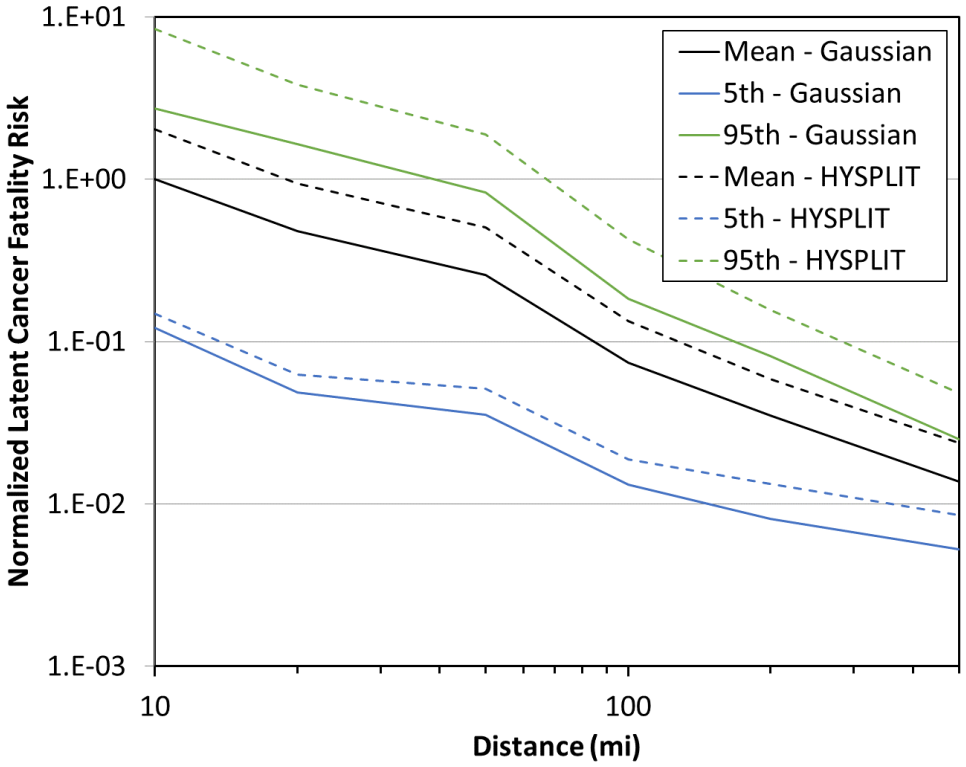

Figure 4-7. Benchmark Site A, ST #1, latent cancer fatality risk comparison

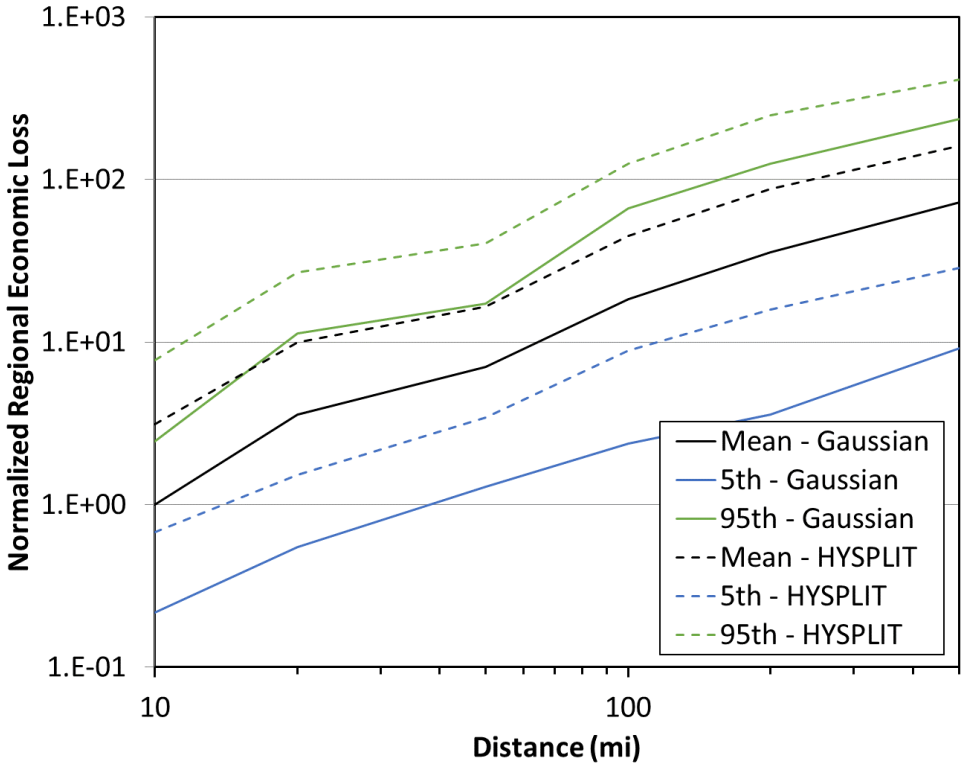

Figure 4-8. Benchmark Site A, ST #1, economic loss comparison

4.2.2. Source Term #2

The comparison between the Gaussian and HYSPLIT ATD model results for Site A, ST #2 for peak air concentration, peak ground deposition, land contamination area, peak dose, early fatality risk, population dose, latent cancer fatality risk, and economic loss (as described in Section 3.6) are shown in Figure 4-9 through Figure 4-16. The annual statistics for these measures are shown with different colors, where the mean values are in black, the 5th percentile values are shown in blue, and the 95th percentile values are shown in green. HYSPLIT results are shown as dashed lines and Gaussian model results are shown as solid lines. The normalized results are shown as a function of distance, rather than the ratio of Gaussian and HYSPLIT results, to allow for the trends with distance to be observed. Some results are zero for early fatality risk, so they cannot be shown on the log scale used in the figures. Note that the sharp jumps in peak dose in Figure 4-12 and some other figures below correspond to evacuation of the population within 10 miles but not beyond. Discussion of the difference seen in these figures is provided below in Section 4.7.

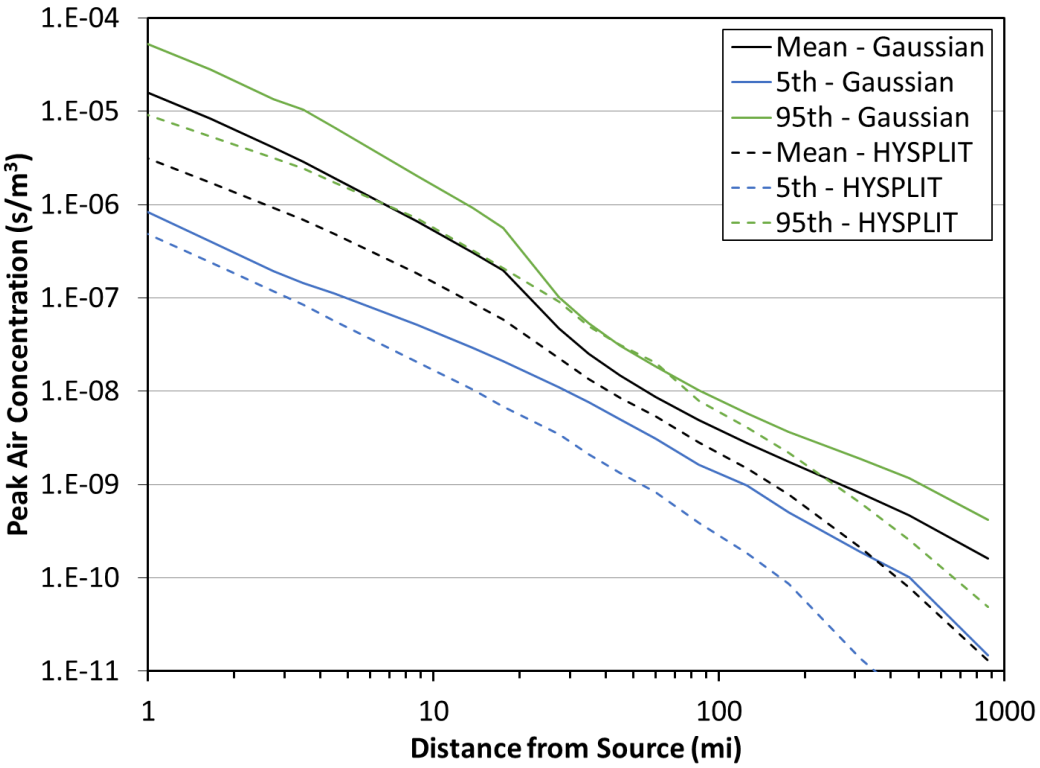

Figure 4-9. Benchmark Site A, ST #2, peak air concentration comparison

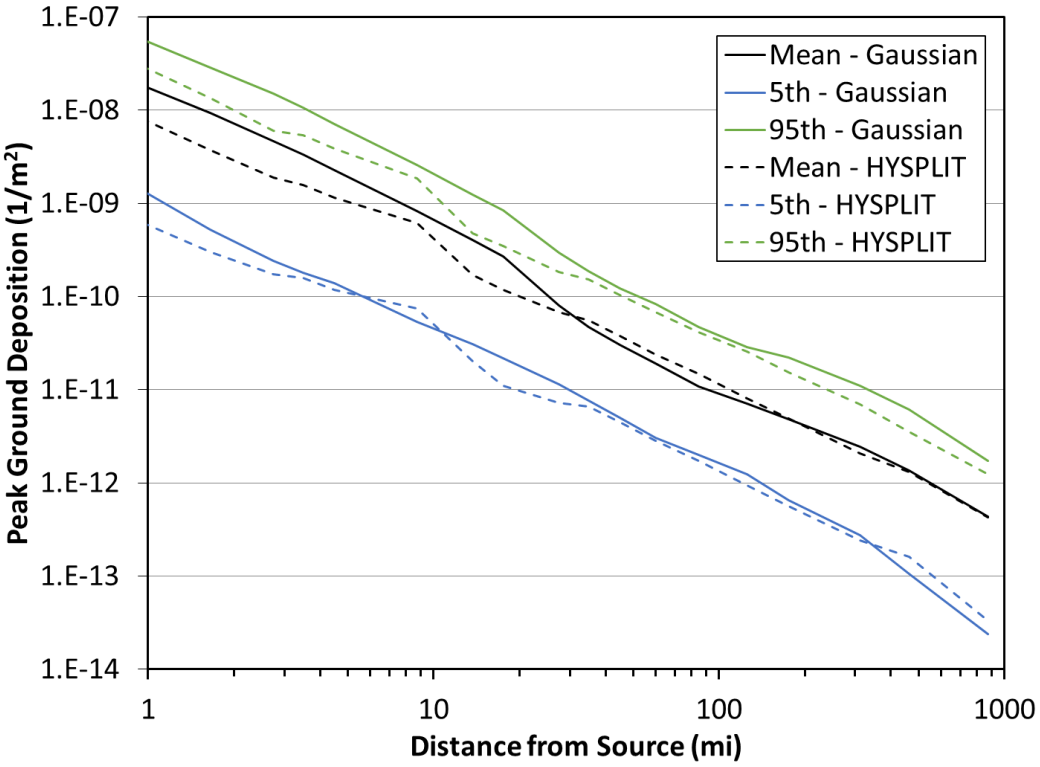

Figure 4-10. Benchmark Site A, ST #2, peak ground deposition comparison

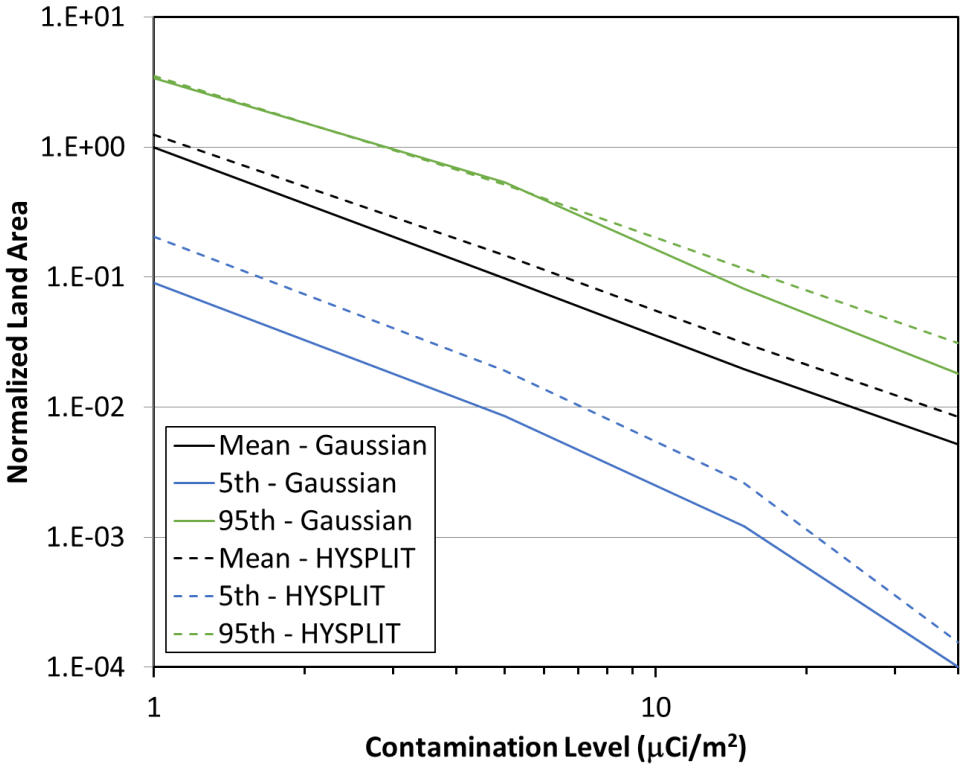

Figure 4-11. Benchmark Site A, ST #2, land contamination area within 805 km (500 mi) comparison

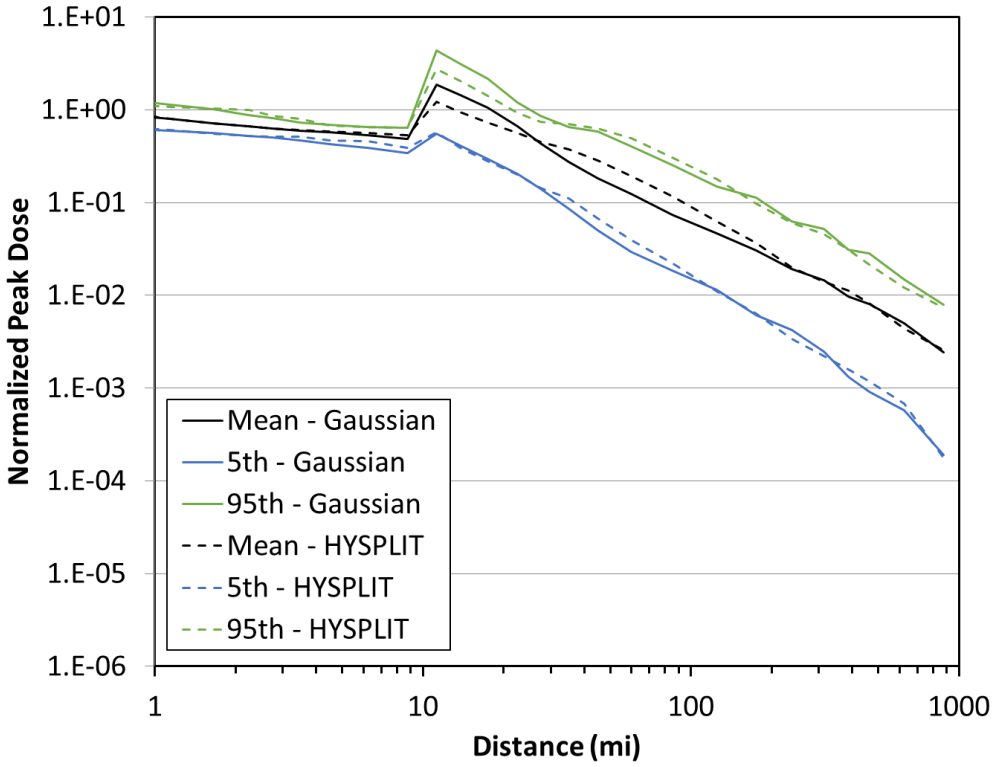

Figure 4-12. Benchmark Site A, ST #2, peak dose comparison

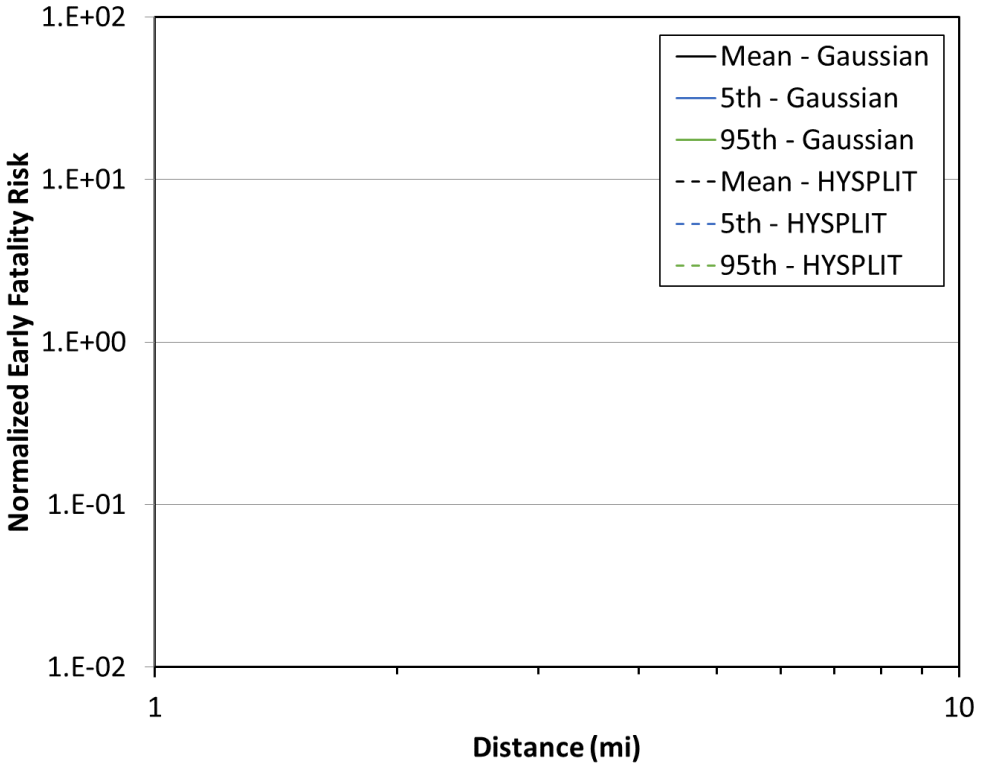

Figure 4-13. Benchmark Site A, ST #2, early fatality risk comparison

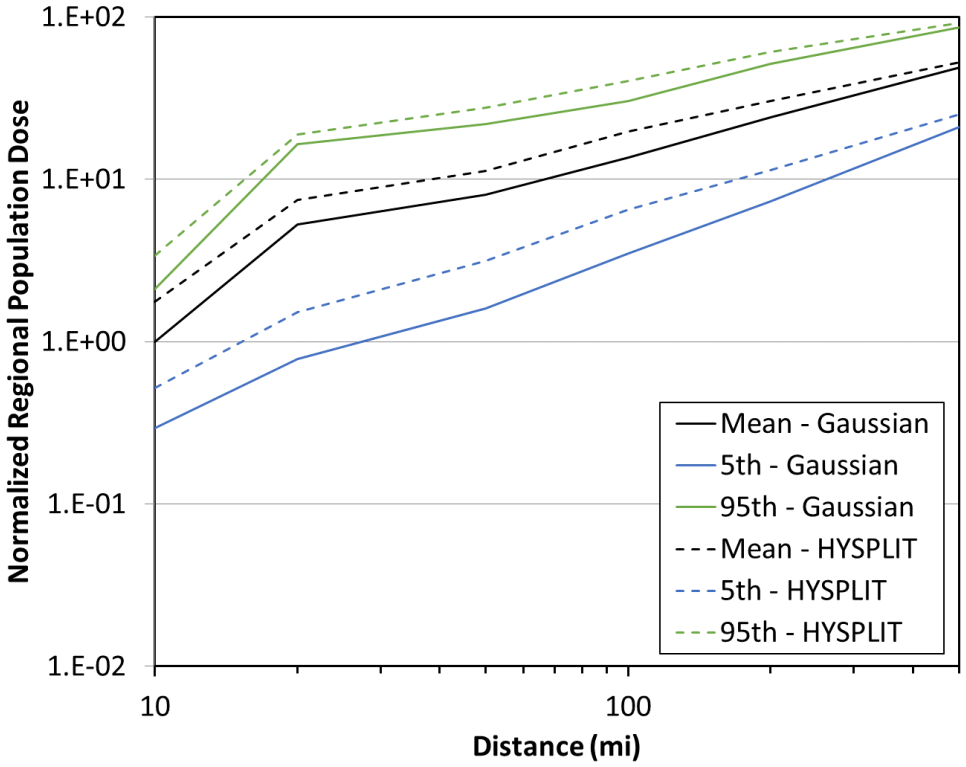

Figure 4-14. Benchmark Site A, ST #2, population dose comparison

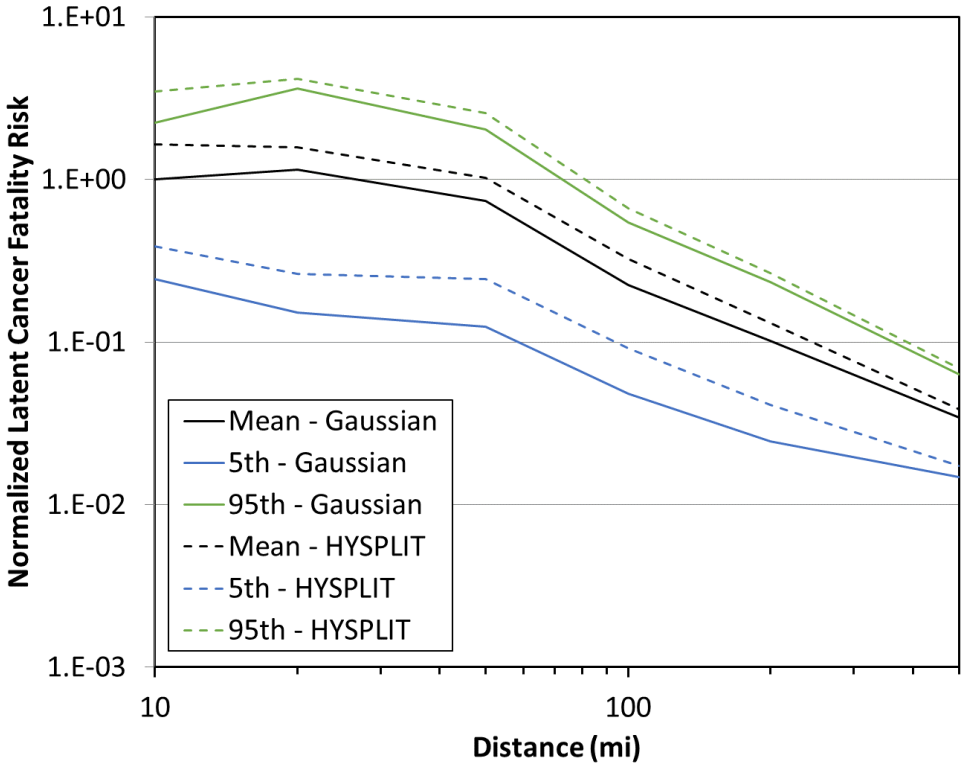

Figure 4-15. Benchmark Site A, ST #2, latent cancer fatality risk comparison

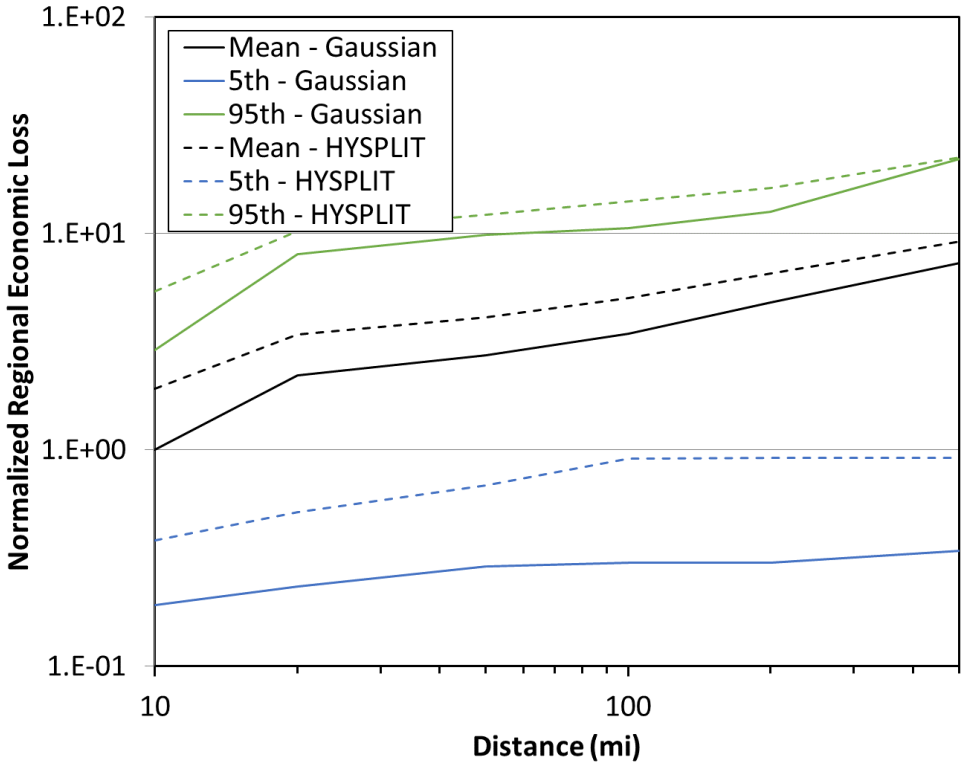

Figure 4-16. Benchmark Site A, ST #2, economic loss comparison

4.3. Site B

4.3.1. Source Term #1

The comparison between the Gaussian and HYSPLIT ATD model results for Site B, ST #1 for peak air concentration, peak ground deposition, land contamination area, peak dose, early fatality risk, population dose, latent cancer fatality risk, and economic loss (as described in Section 3.6) are shown in Figure 4-17 through Figure 4-24. The annual statistics for these measures are shown with different colors, where the mean values are in black, the 5th percentile values are shown in blue, and the 95th percentile values are shown in green. HYSPLIT results are shown as dashed lines and Gaussian model results are shown as solid lines. The normalized results are shown as a function of distance, rather than the ratio of Gaussian and HYSPLIT results, to allow for the trends with distance to be observed. Some results are zero for early fatality risk, so they cannot be shown on the log scale used in the figures. For Site B, there are no individuals within two miles of the site, which results in a calculated zero fatality risk. Discussion of the difference seen in these figures is provided below in Section 4.7.

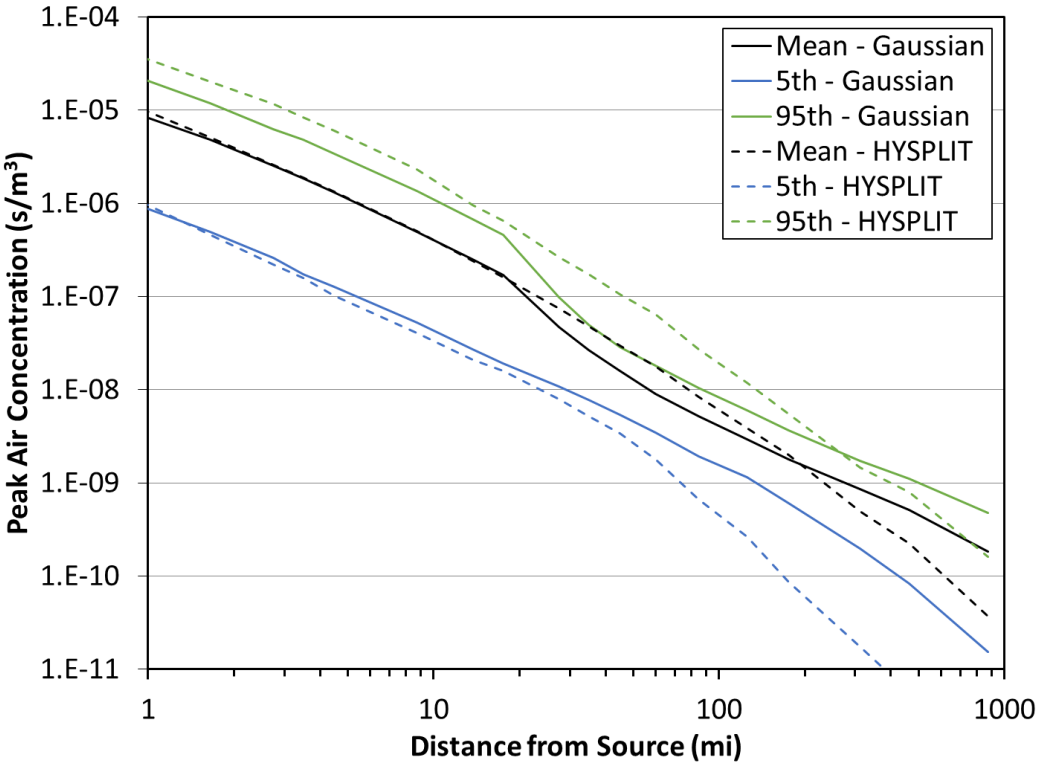

Figure 4-17. Benchmark Site B, ST #1, peak air concentration comparison

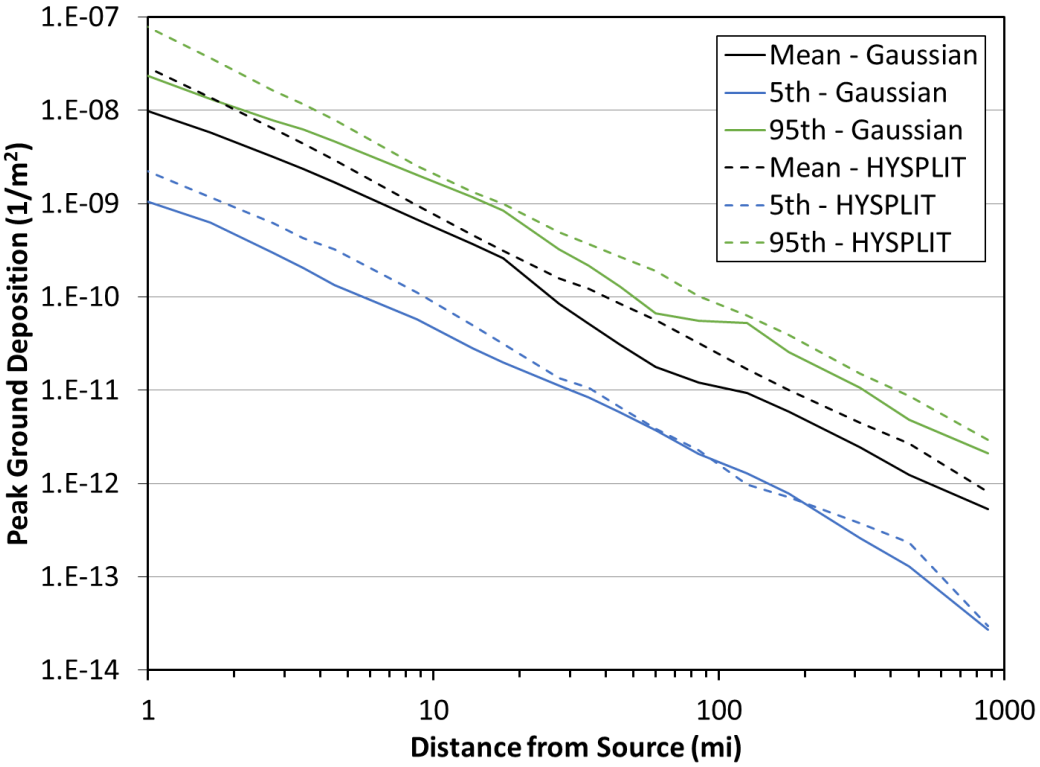

Figure 4-18. Benchmark Site B, ST #1, peak ground deposition comparison

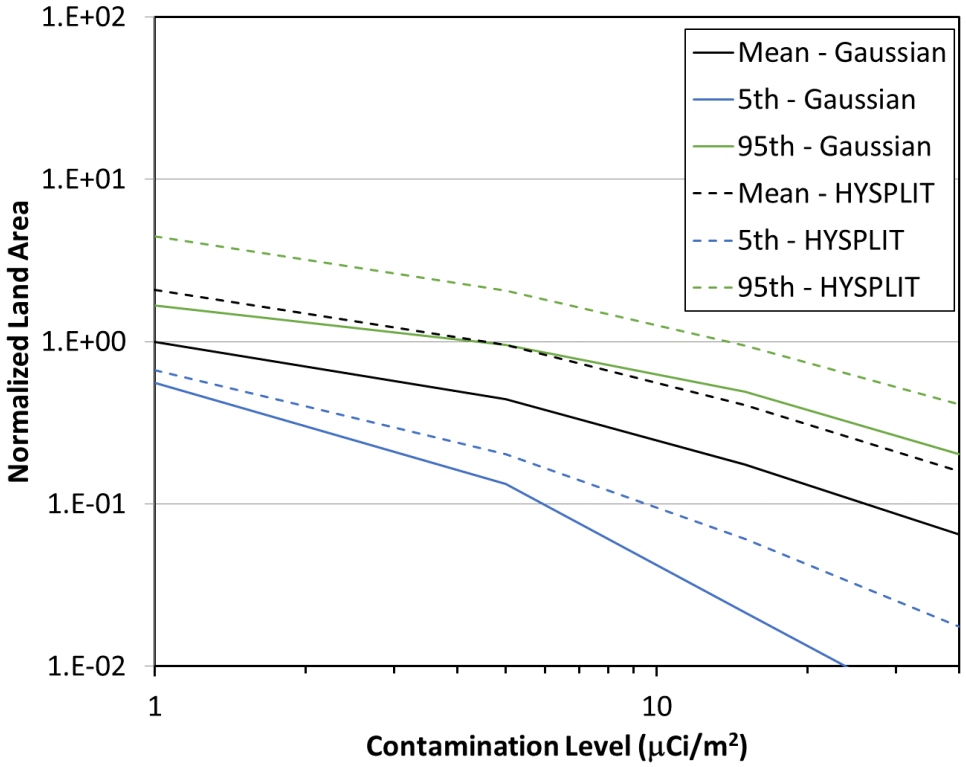

Figure 4-19. Benchmark Site B, ST #1, land contamination area within 805 km (500 mi) comparison

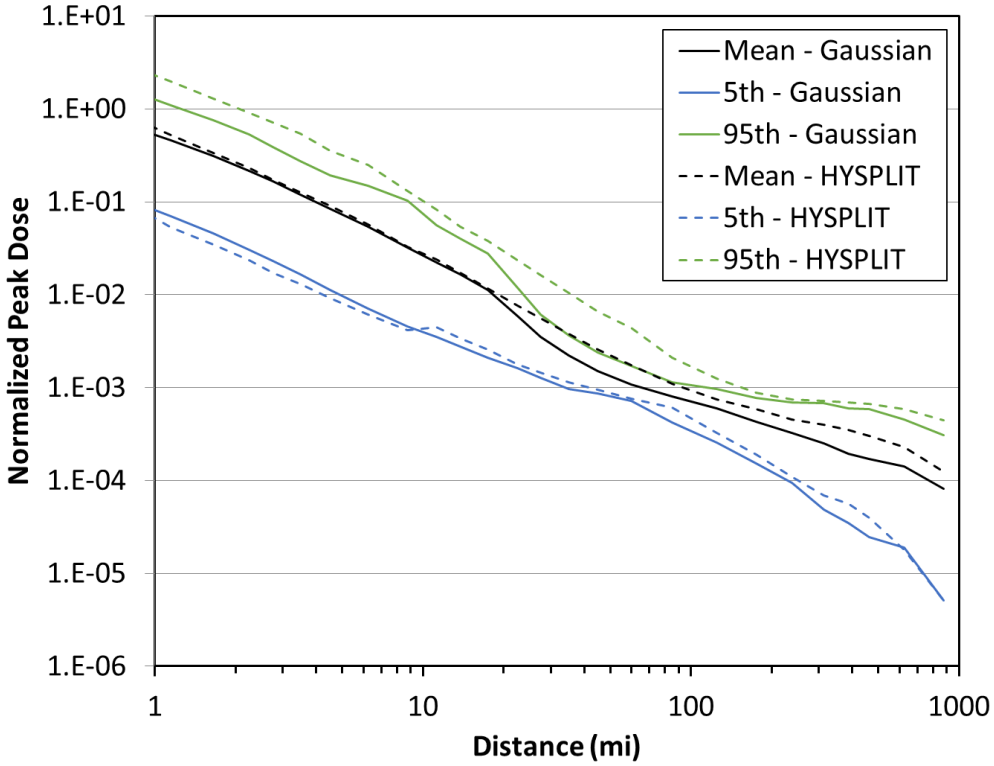

Figure 4-20. Benchmark Site B, ST #1, peak dose comparison

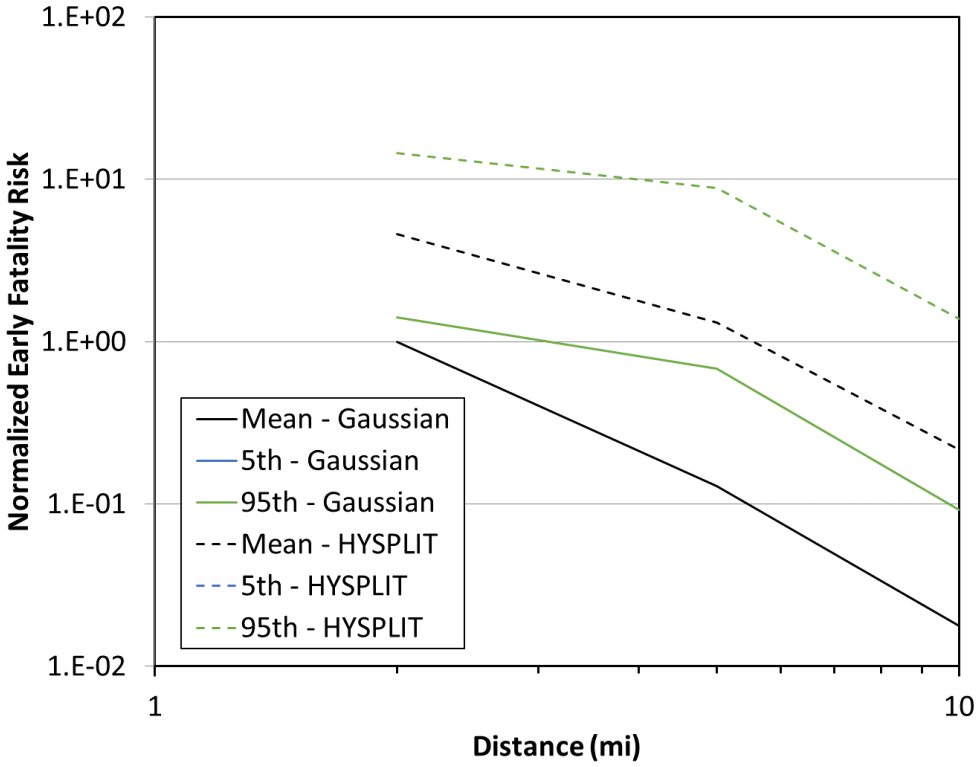

Figure 4-21. Benchmark Site B, ST #1, early fatality risk comparison

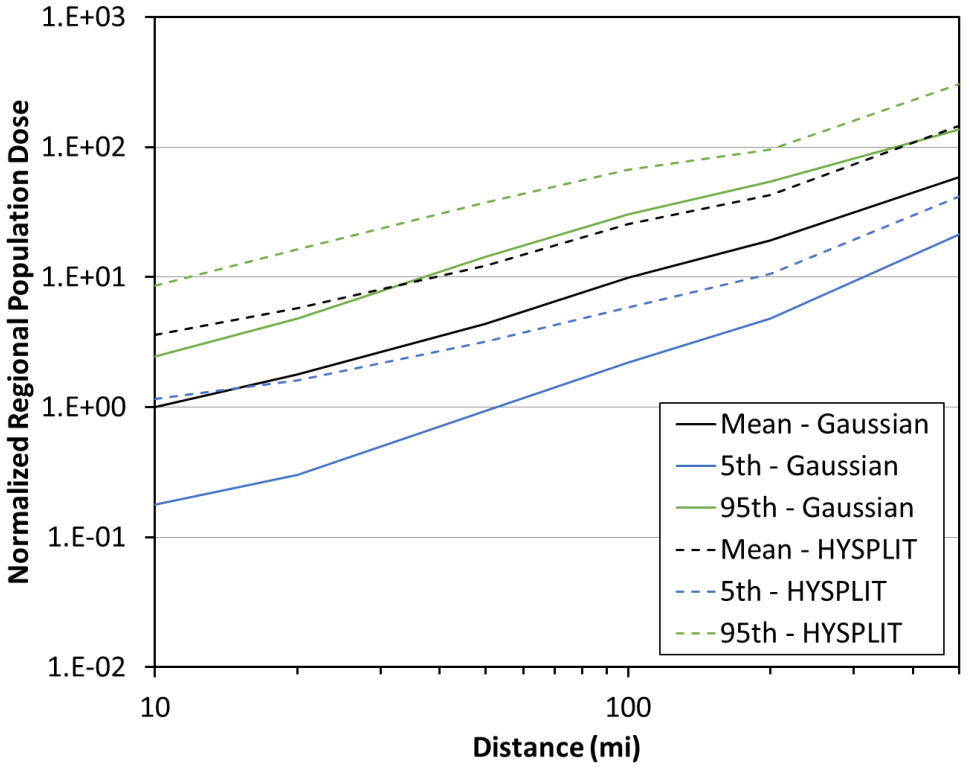

Figure 4-22. Benchmark Site B, ST #1, population dose comparison

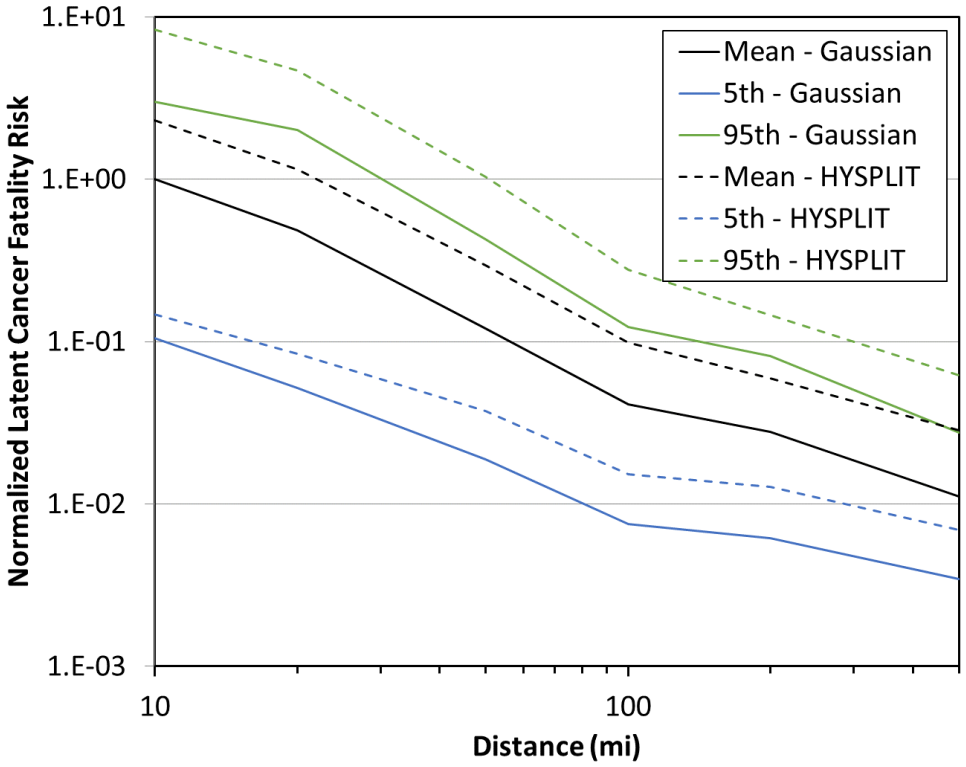

Figure 4-23. Benchmark Site B, ST #1, latent cancer fatality risk comparison

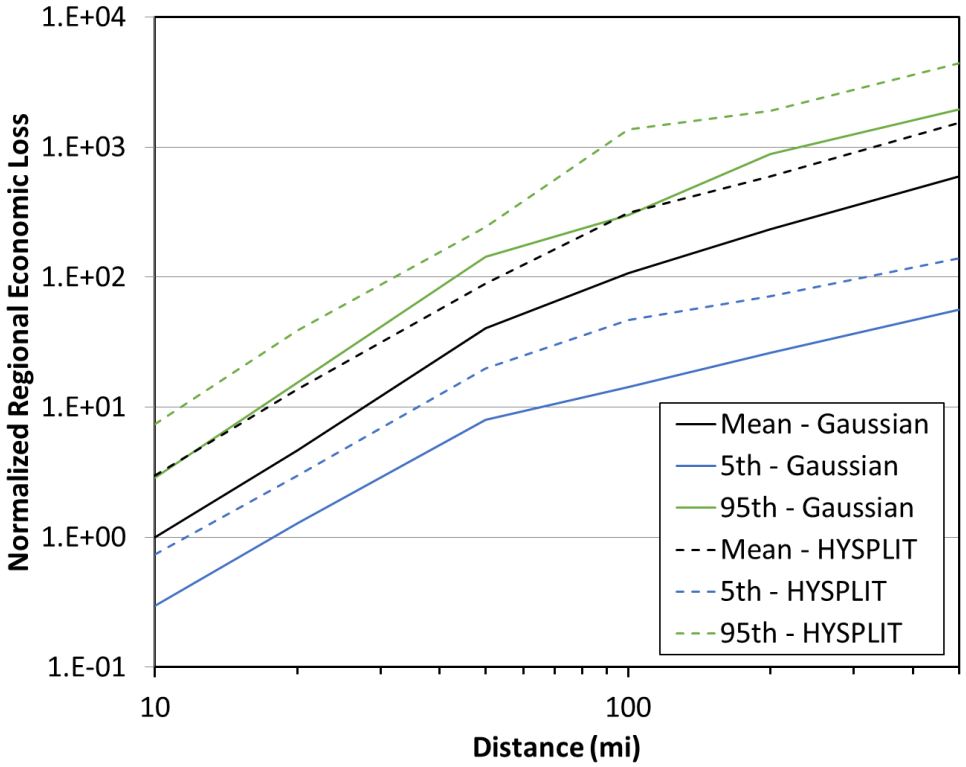

Figure 4-24. Benchmark Site B, ST #1, economic loss comparison

4.3.2. Source Term #2

The comparison between the Gaussian and HYSPLIT ATD model results for Site B, ST #2 for peak air concentration, peak ground deposition, land contamination area, peak dose, early fatality risk, population dose, latent cancer fatality risk, and economic loss (as described in Section 3.6) are shown in Figure 4-25 through Figure 4-32. The annual statistics for these measures are shown with different colors, where the mean values are in black, the 5th percentile values are shown in blue, and the 95th percentile values are shown in green. HYSPLIT results are shown as dashed lines and Gaussian model results are shown as solid lines. The normalized results are shown as a function of distance, rather than the ratio of Gaussian and HYSPLIT results, to allow for the trends with distance to be observed. Some results are zero for early fatality risk, so they cannot be shown on the log scale used in the figures. In Figure 4-29, the single, normalized curve for the HYSPLIT ATD mean early fatality risk represents extremely small (essentially zero) values; the corresponding Gaussian results are zero. Discussion of the difference seen in these figures is provided below in Section 4.7.

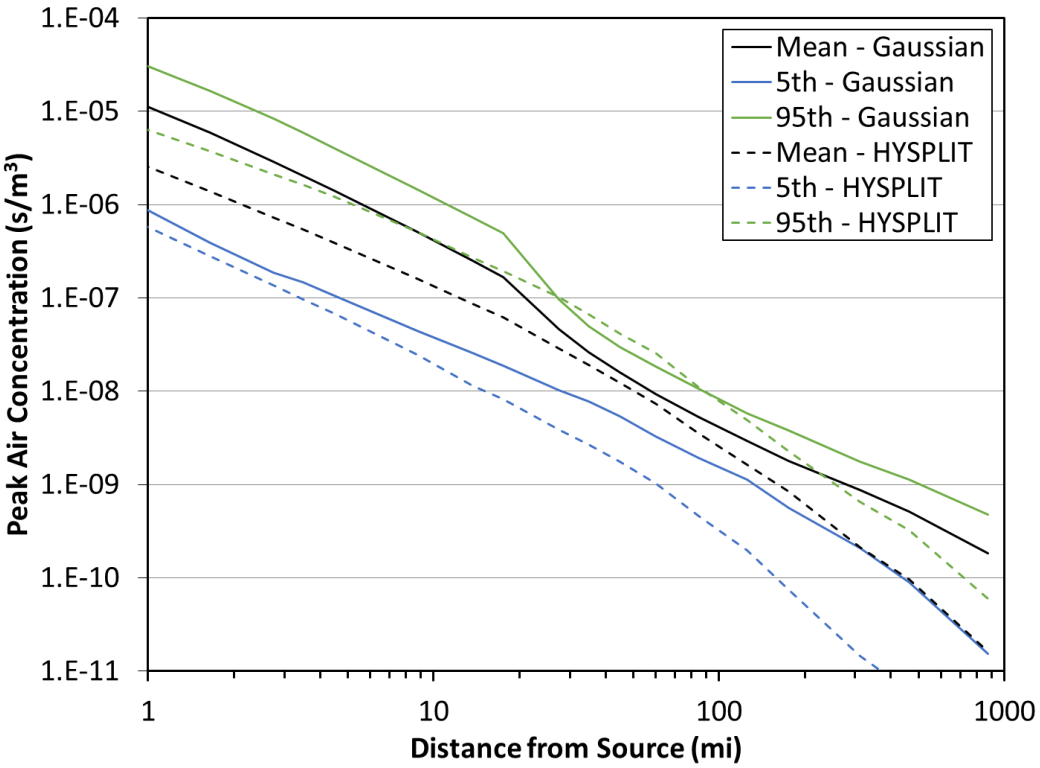

Figure 4-25. Benchmark Site B, ST #2, peak air concentration comparison

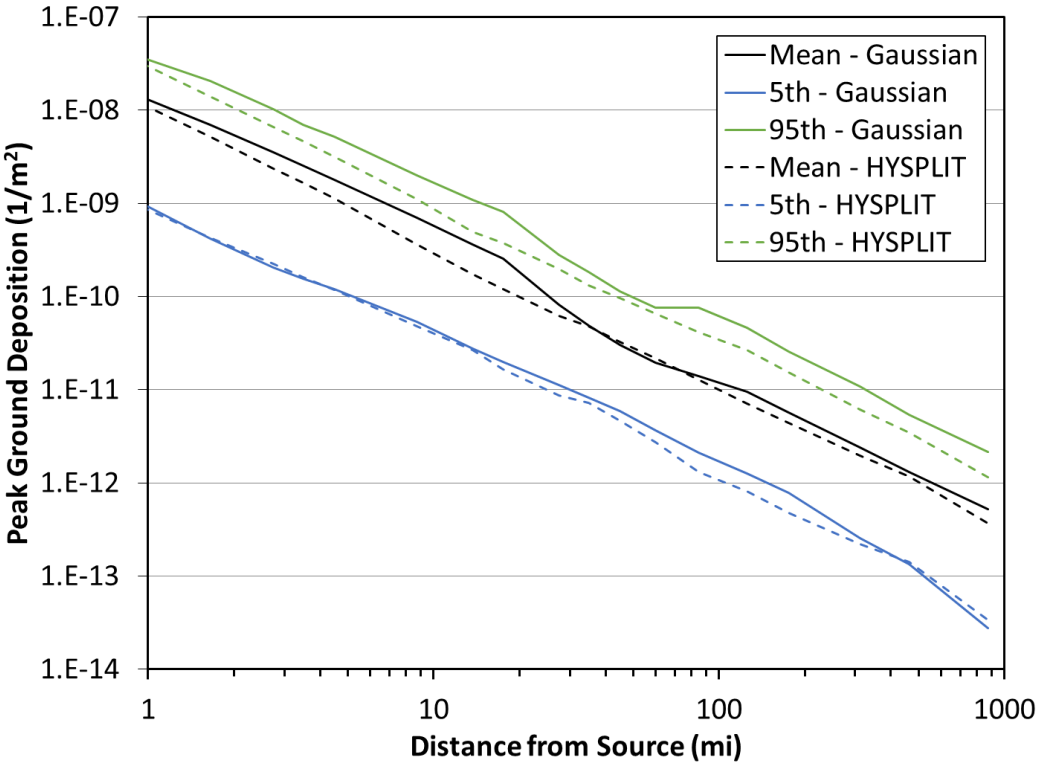

Figure 4-26. Benchmark Site B, ST #2, peak ground deposition comparison

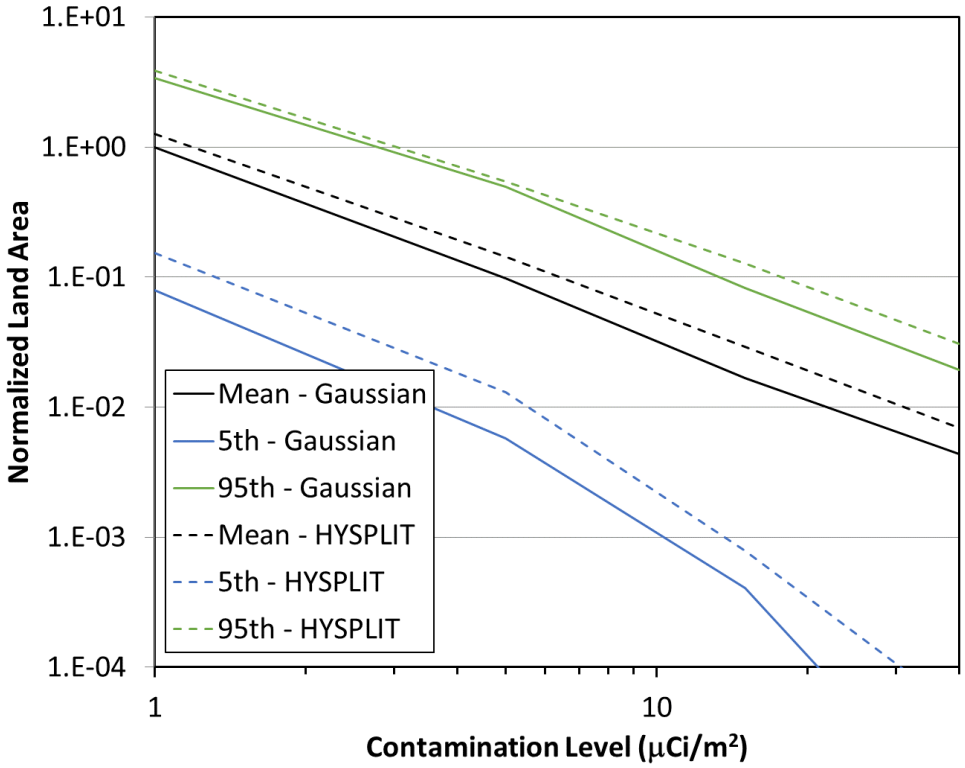

Figure 4-27. Benchmark Site B, ST #2, land contamination area within 805 km (500 mi) comparison

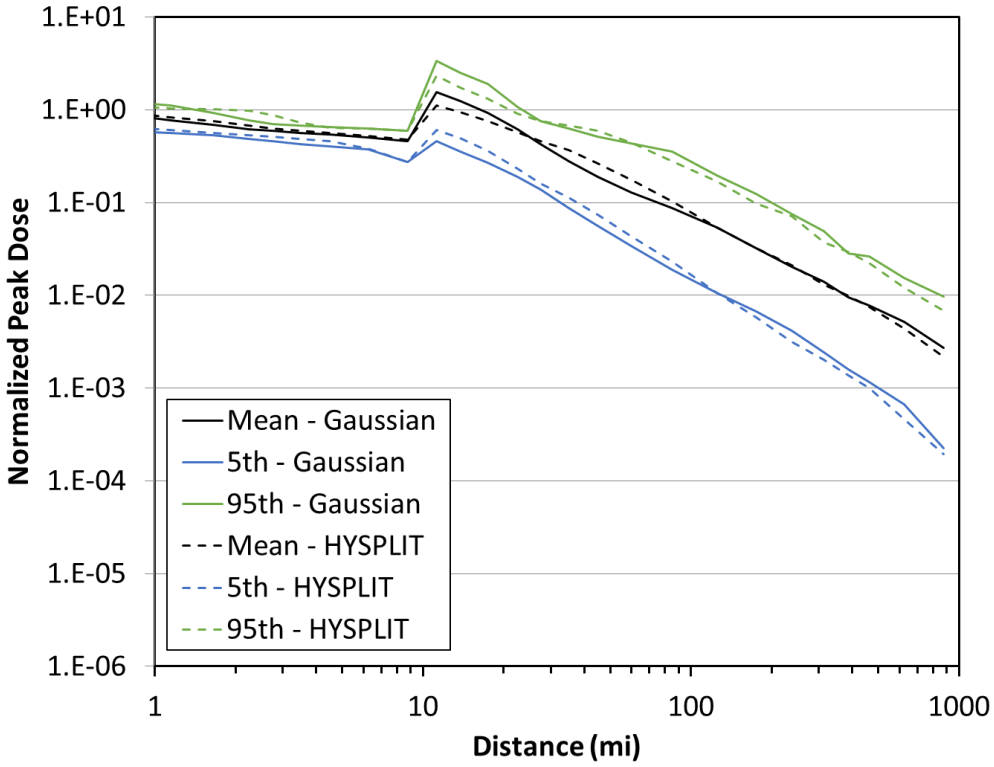

Figure 4-28. Benchmark Site B, ST #2, peak dose comparison

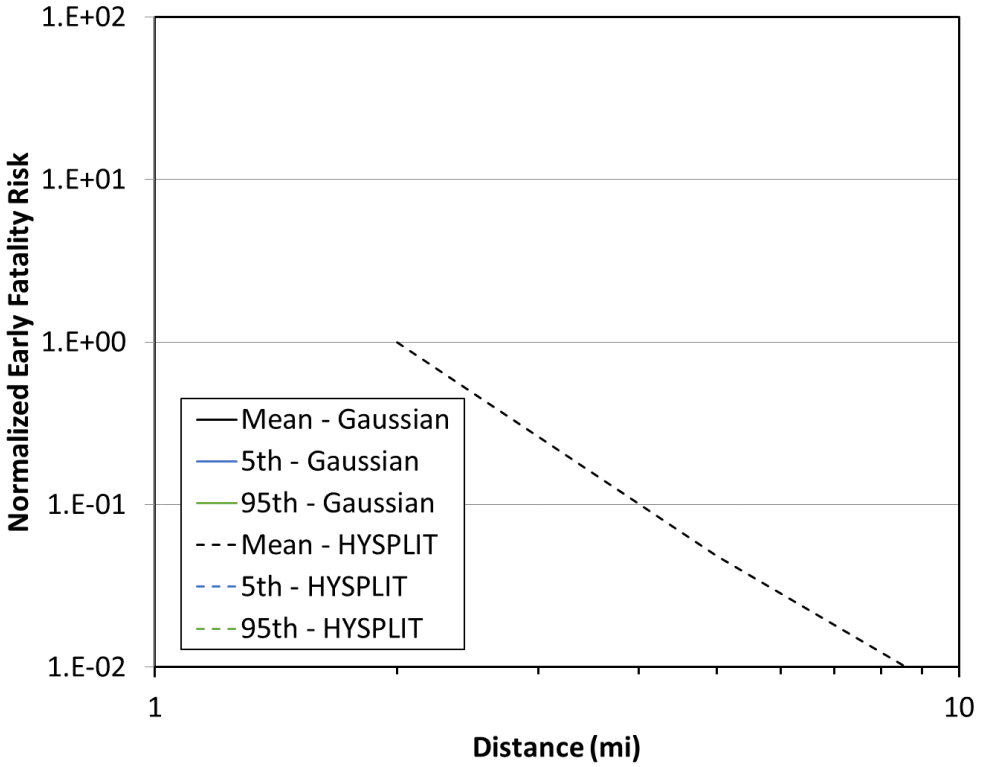

Figure 4-29. Benchmark Site B, ST #2, early fatality comparison

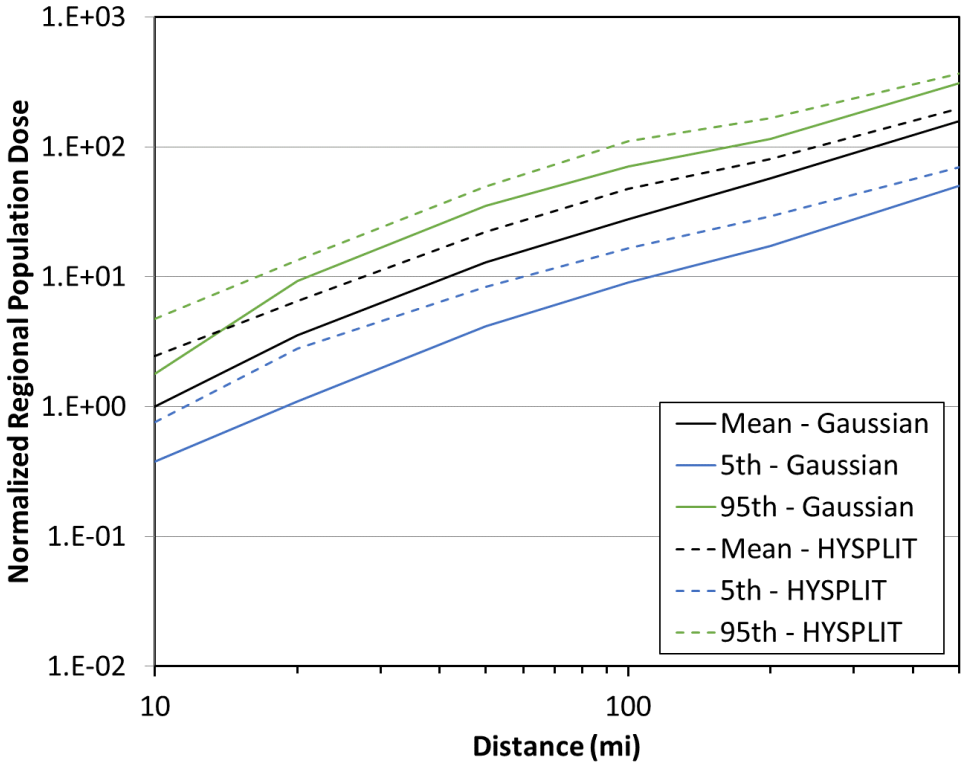

Figure 4-30. Benchmark Site B, ST #2, population dose comparison

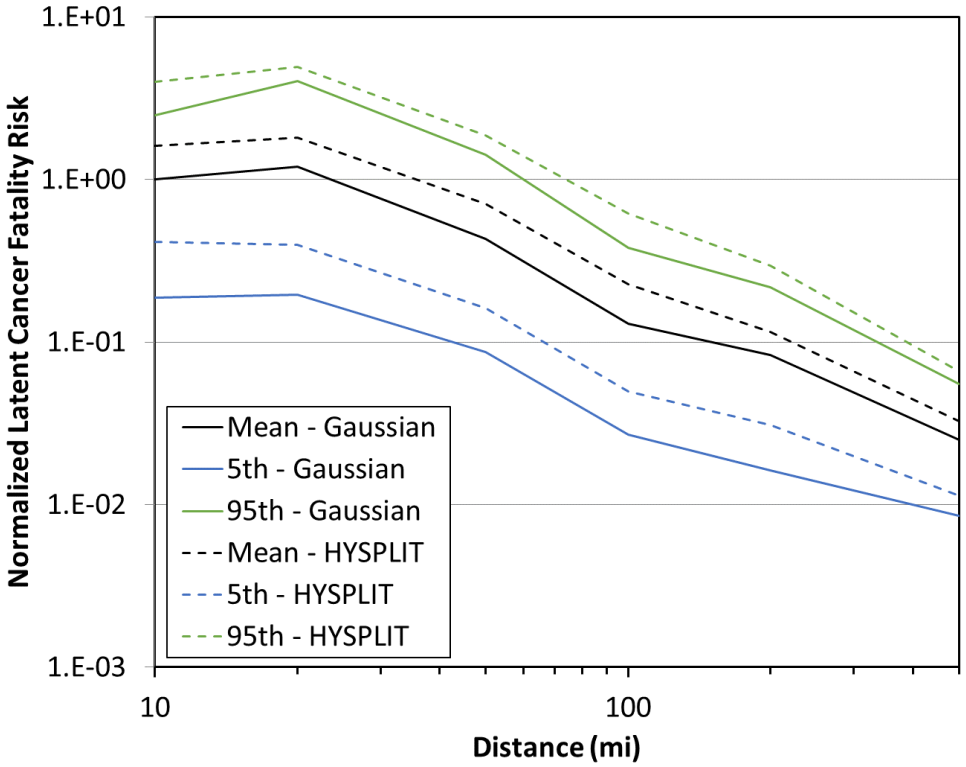

Figure 4-31. Benchmark Site B, ST #2, latent cancer fatality risk comparison

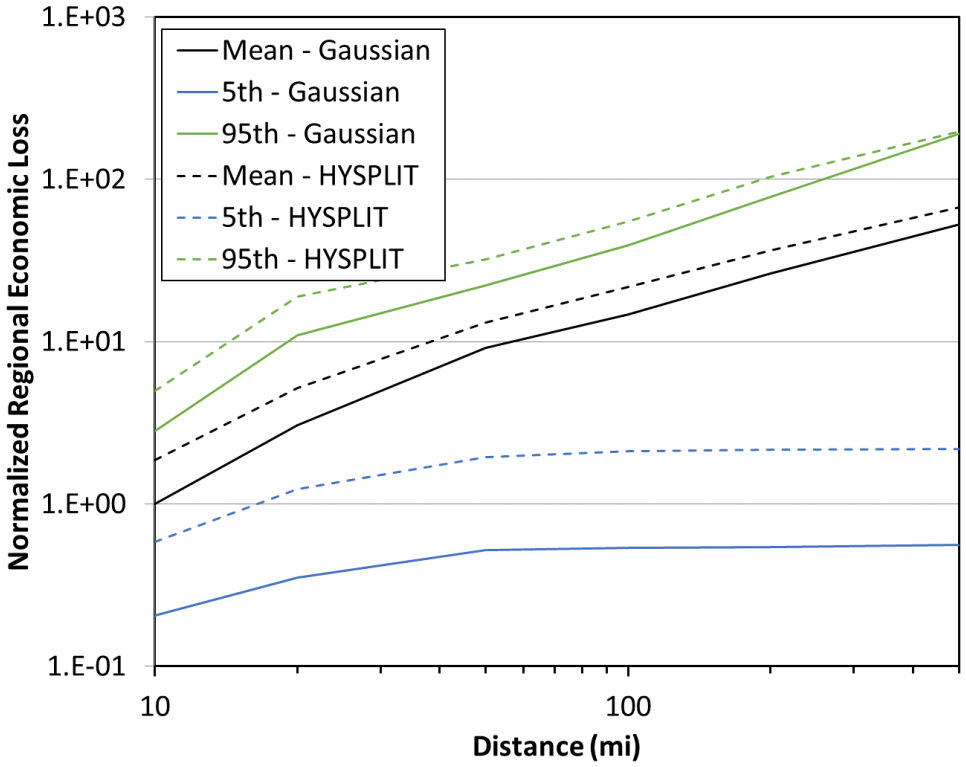

Figure 4-32. Benchmark Site B, ST #2, economic loss comparison

4.4. Site C

4.4.1. Source Term #1

The comparison between the Gaussian and HYSPLIT ATD model results for Site C, ST #1 for peak air concentration, peak ground deposition, land contamination area, peak dose, early fatality risk, population dose, latent cancer fatality risk, and economic loss (as described in Section 3.6) are shown in Figure 4-33 through Figure 4-40. The annual statistics for these measures are shown with different colors, where the mean values are in black, the 5th percentile values are shown in blue, and the 95th percentile values are shown in green. HYSPLIT results are shown as dashed lines and Gaussian model results are shown as solid lines. The normalized results are shown as a function of distance, rather than the ratio of Gaussian and HYSPLIT results, to allow for the trends with distance to be observed. Some results are zero for early and latent cancer fatality risk, so they cannot be shown on the log scale used in the figures. Discussion of the difference seen in these figures is provided below in Section 4.7.

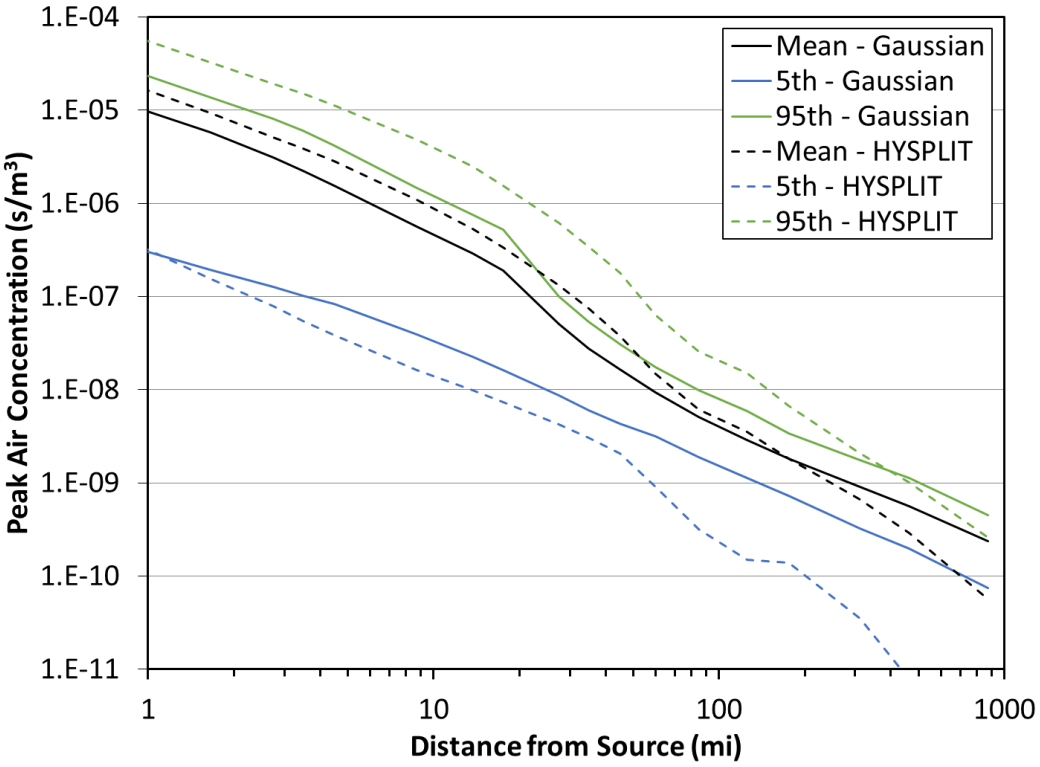

Figure 4-33. Benchmark Site C, ST #1, peak air concentration comparison

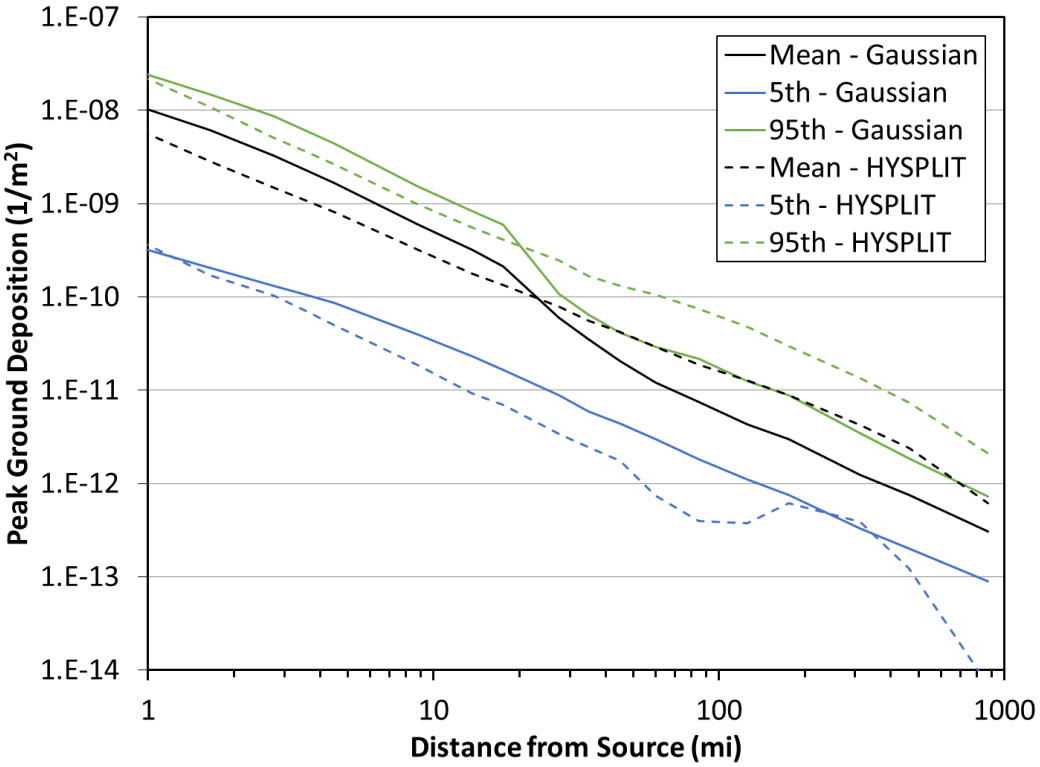

Figure 4-34. Benchmark Site C, ST #1, peak ground deposition comparison

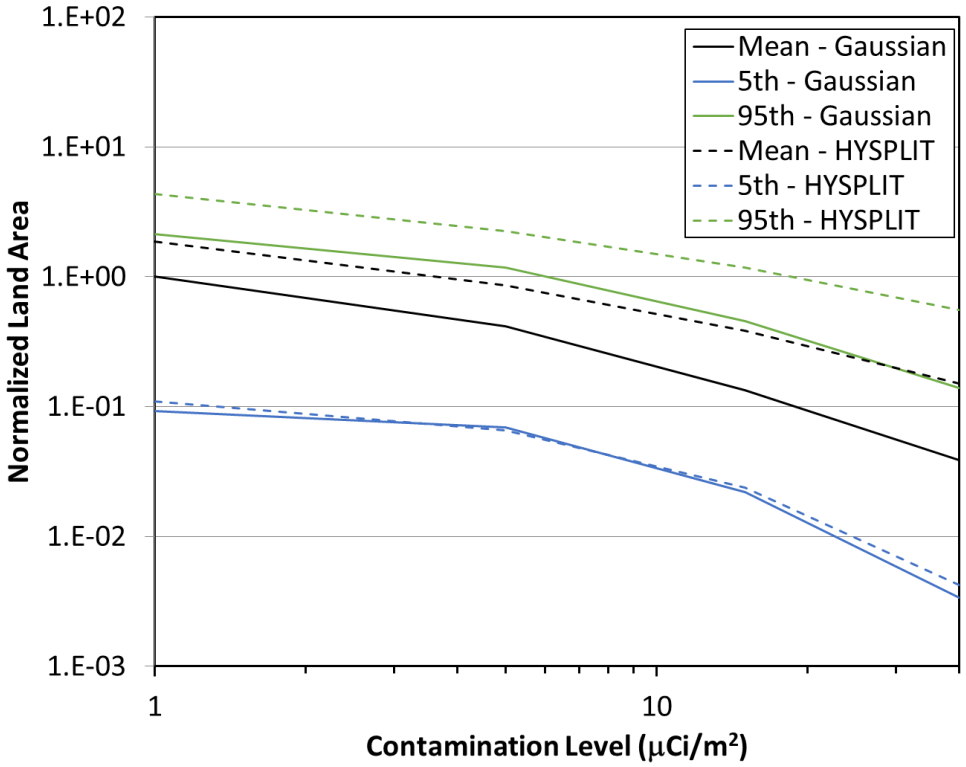

Figure 4-35. Benchmark Site C, ST #1, land contamination area within 805 km (500 mi) comparison

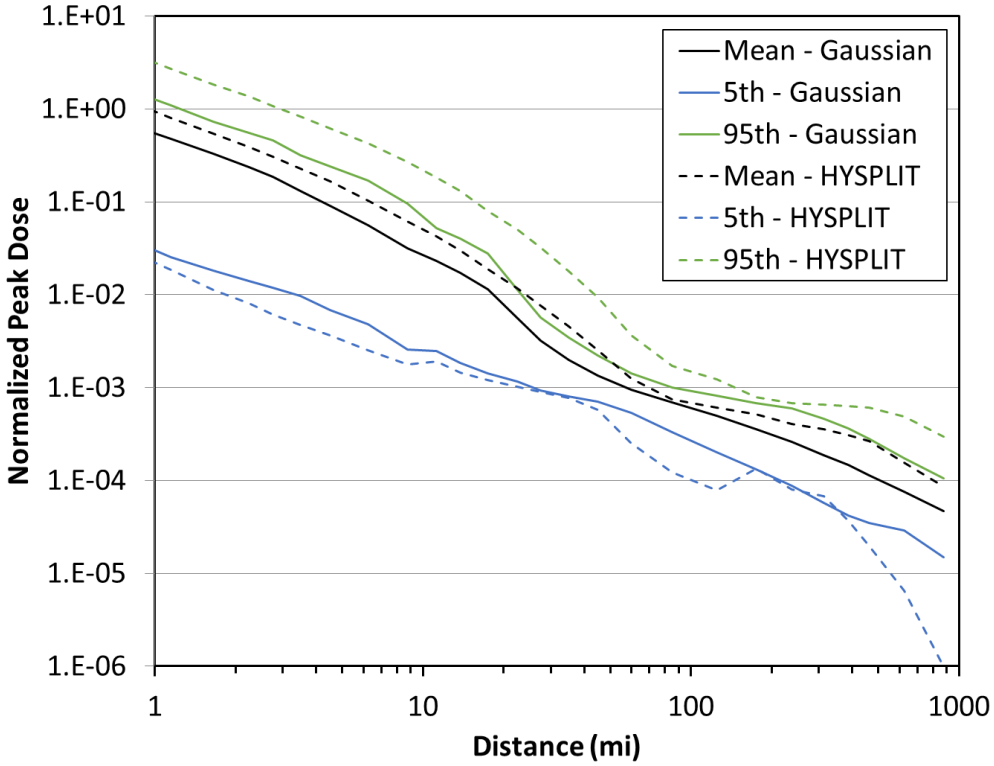

Figure 4-36. Benchmark Site C, ST #1, peak dose comparison

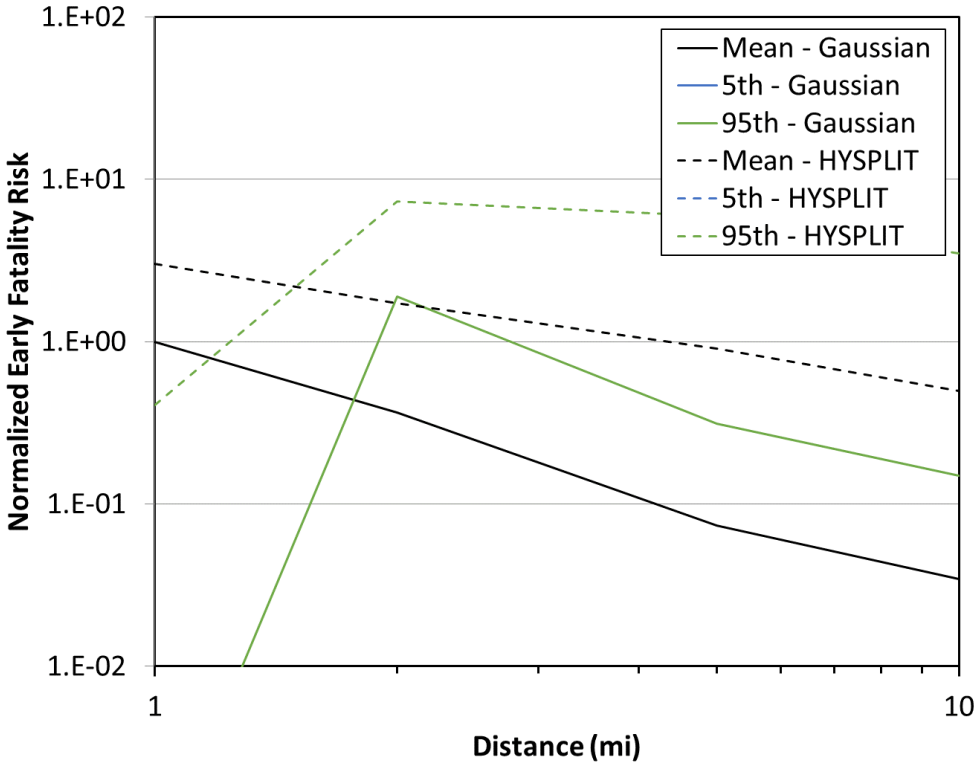

Figure 4-37. Benchmark Site C, ST #1, early fatality comparison

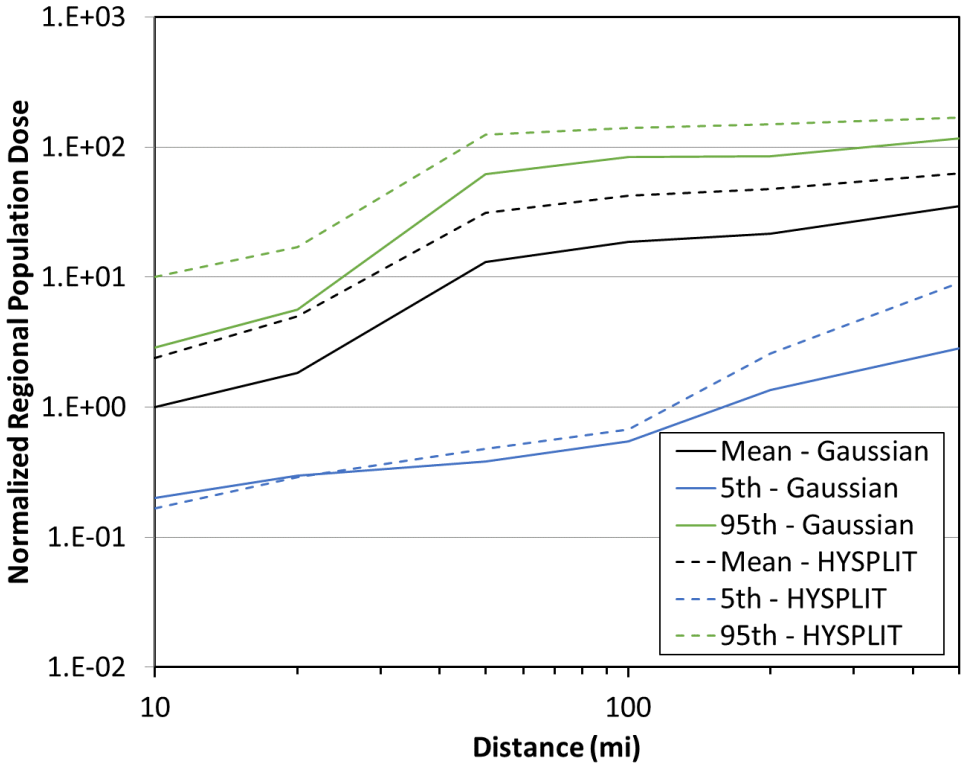

Figure 4-38. Benchmark Site C, ST #1, population dose comparison

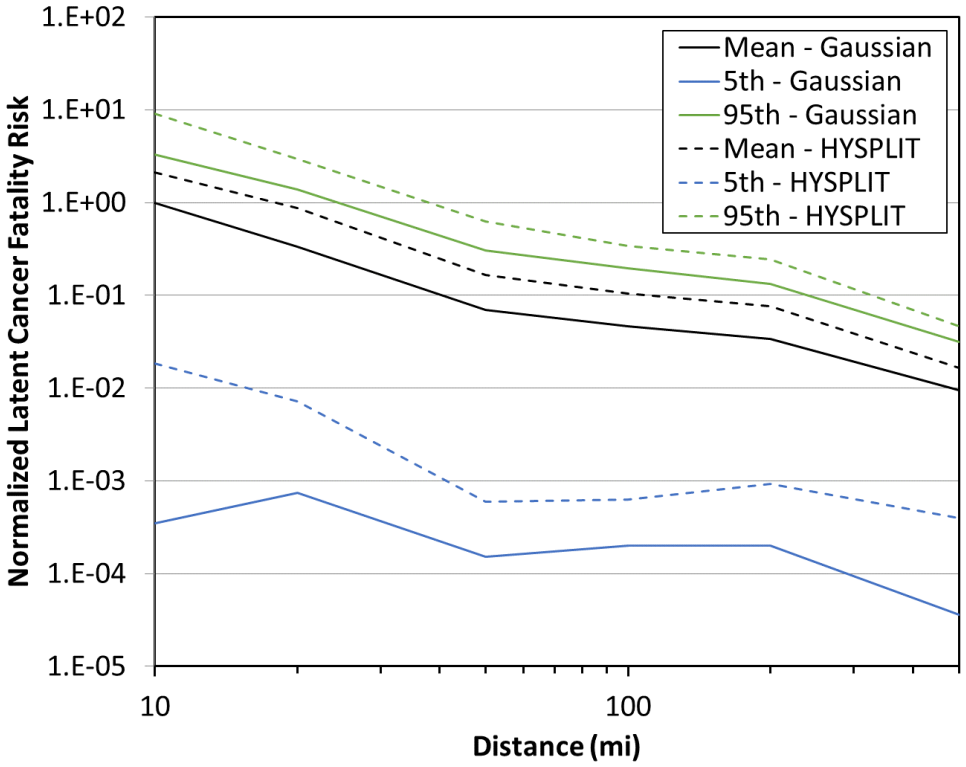

Figure 4-39. Benchmark Site C, ST #1, latent cancer fatality risk comparison

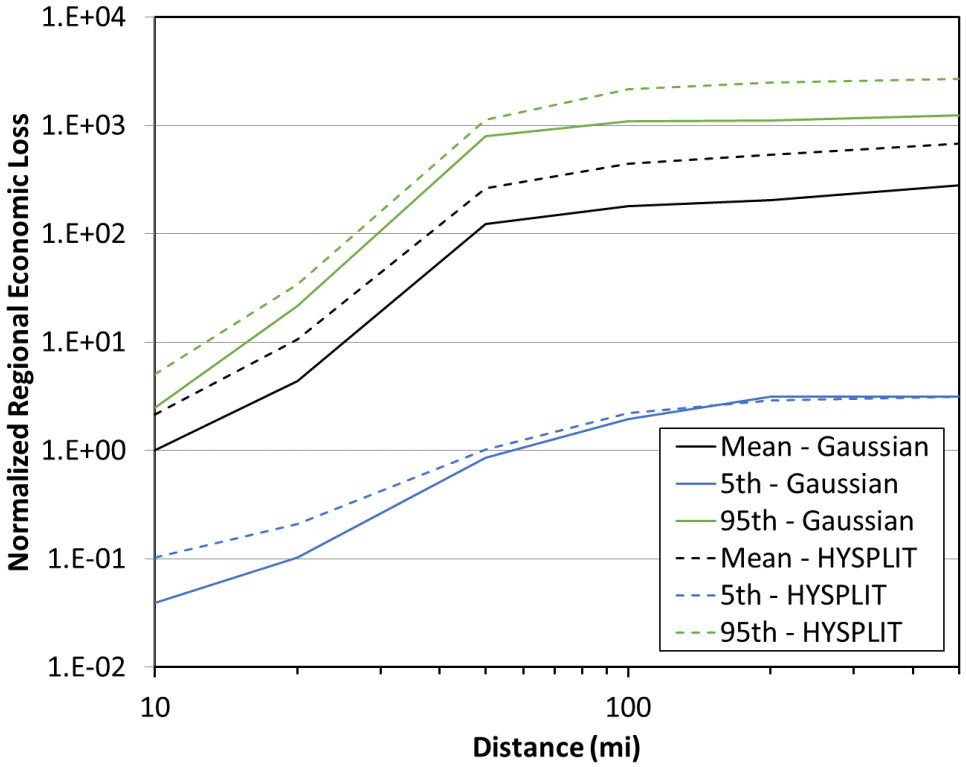

Figure 4-40. Benchmark Site C, ST #1, economic loss comparison

4.4.2. Source Term #2

The comparison between the Gaussian and HYSPLIT ATD model results for Site C, ST #2 for peak air concentration, peak ground deposition, land contamination area, peak dose, early fatality risk, population dose, latent cancer fatality risk, and economic loss (as described in Section 3.6) are shown in Figure 4-41 through Figure 4-48. The annual statistics for these measures are shown with different colors, where the mean values are in black, the 5th percentile values are shown in blue, and the 95th percentile values are shown in green. HYSPLIT results are shown as dashed lines and Gaussian model results are shown as solid lines. The normalized results are shown as a function of distance, rather than the ratio of Gaussian and HYSPLIT results, to allow for the trends with distance to be observed. Some results are zero for early fatality risk, so they cannot be shown on the log scale used in the figures. Discussion of the difference seen in these figures is provided below in Section 4.7.

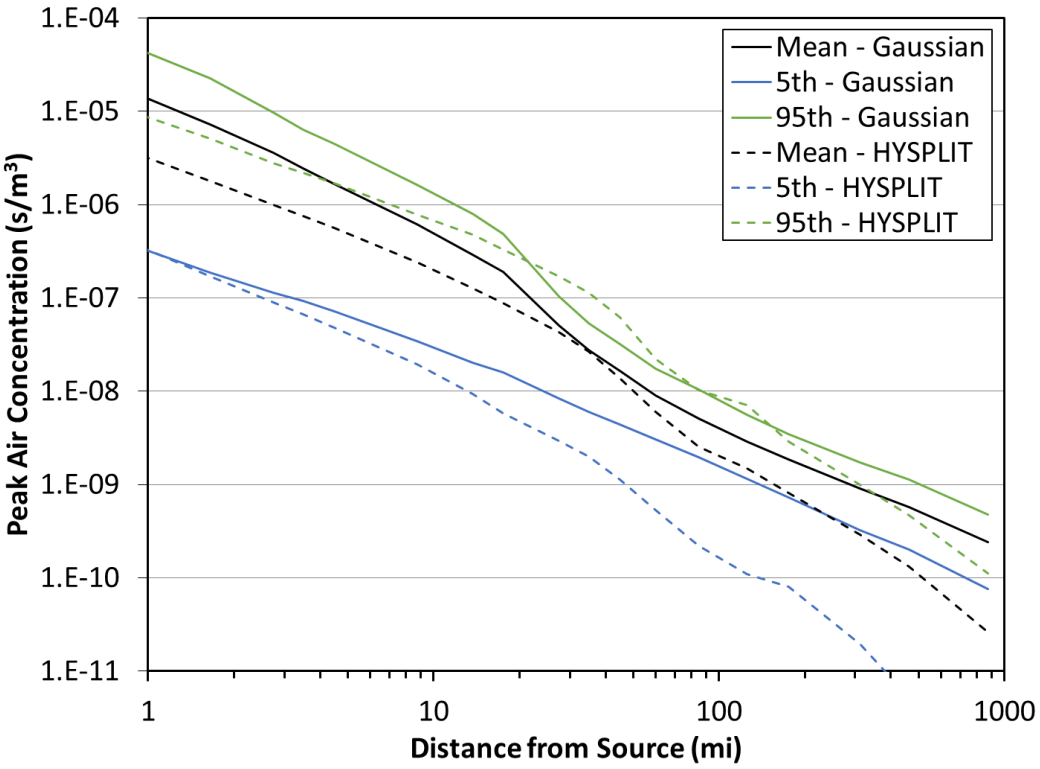

Figure 4-41. Benchmark Site C, ST #2, peak air concentration comparison

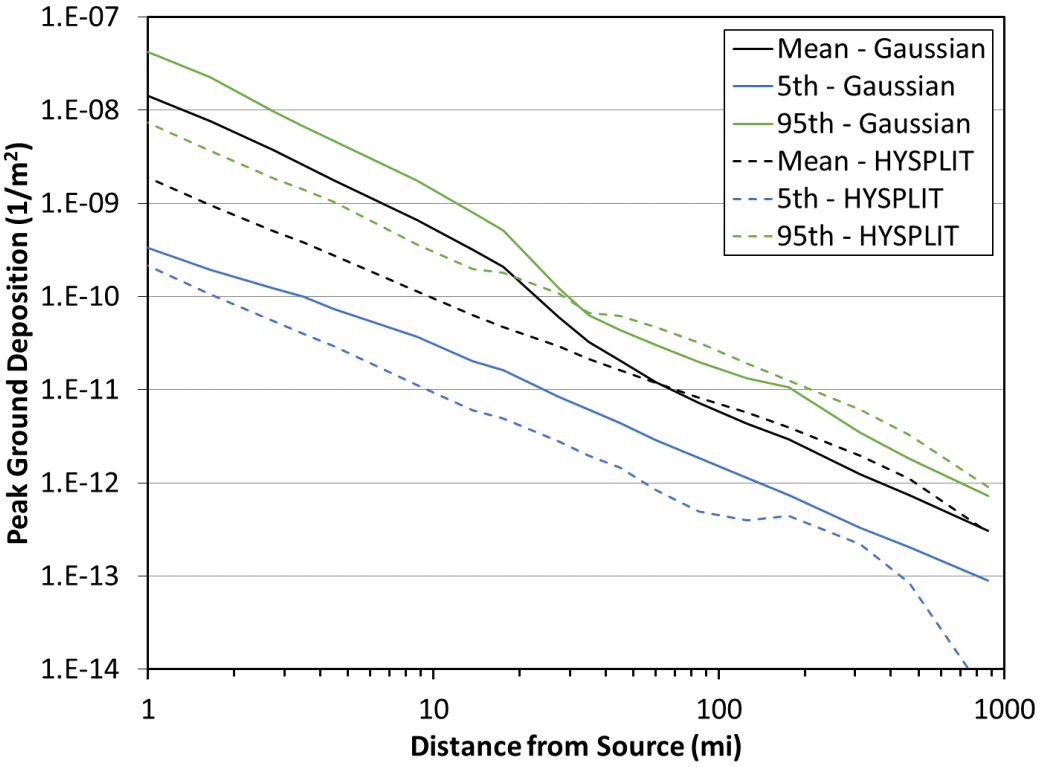

Figure 4-42. Benchmark Site C, ST #2, peak ground deposition comparison

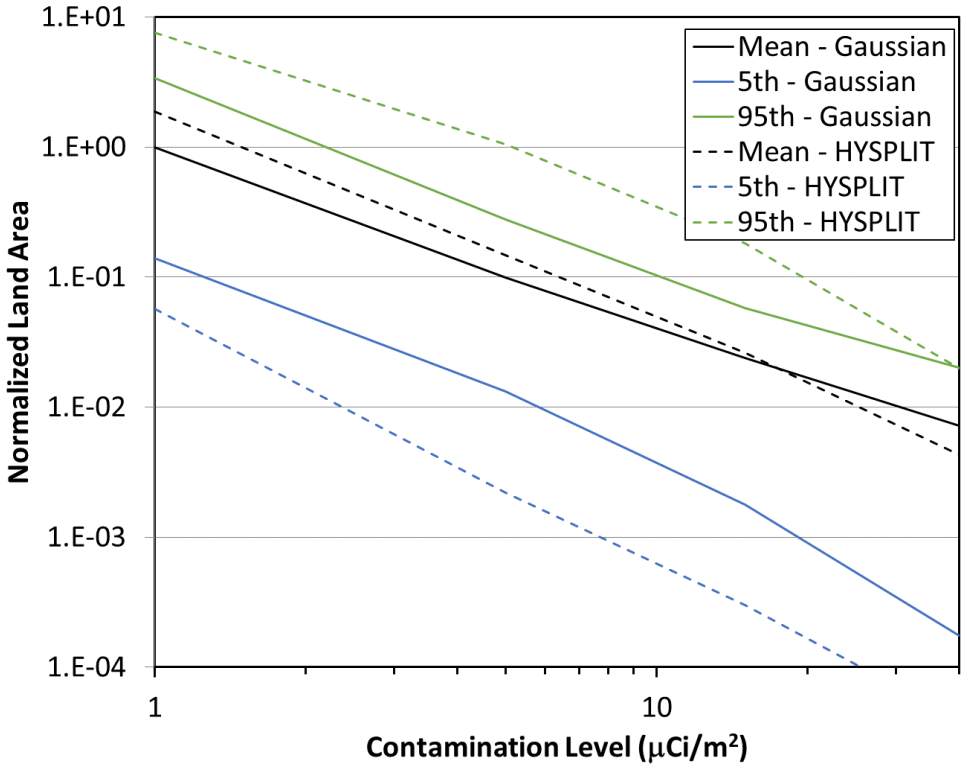

Figure 4-43. Benchmark Site C, ST #2, land contamination area within 805 km (500 mi) comparison

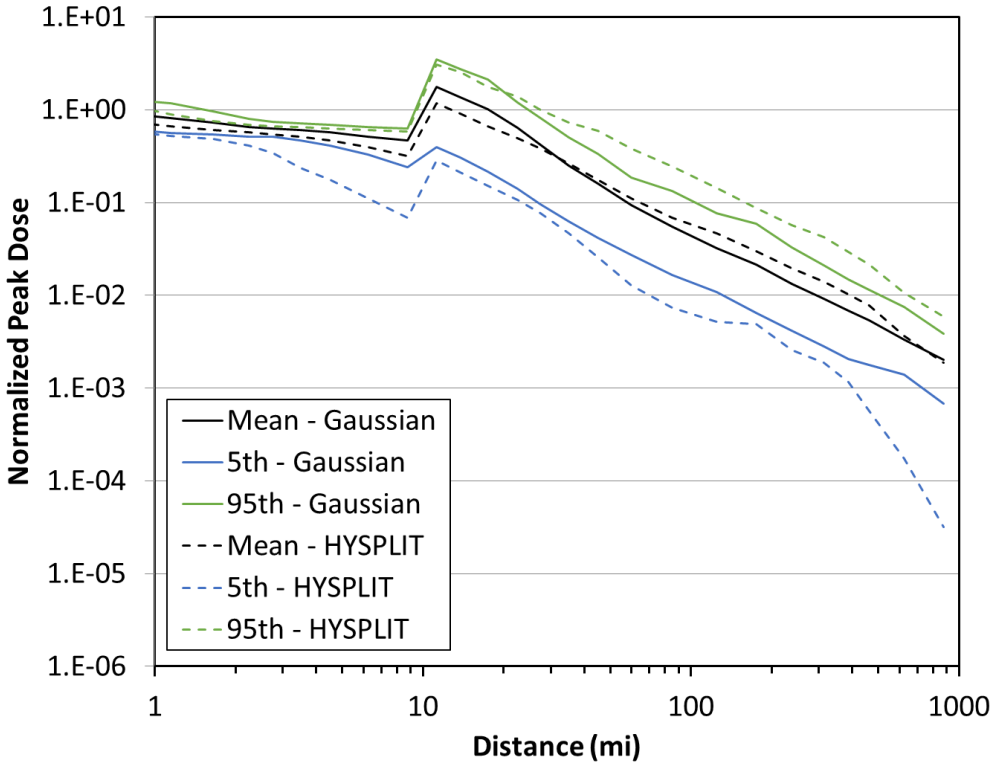

Figure 4-44. Benchmark Site C, ST #2, peak dose comparison

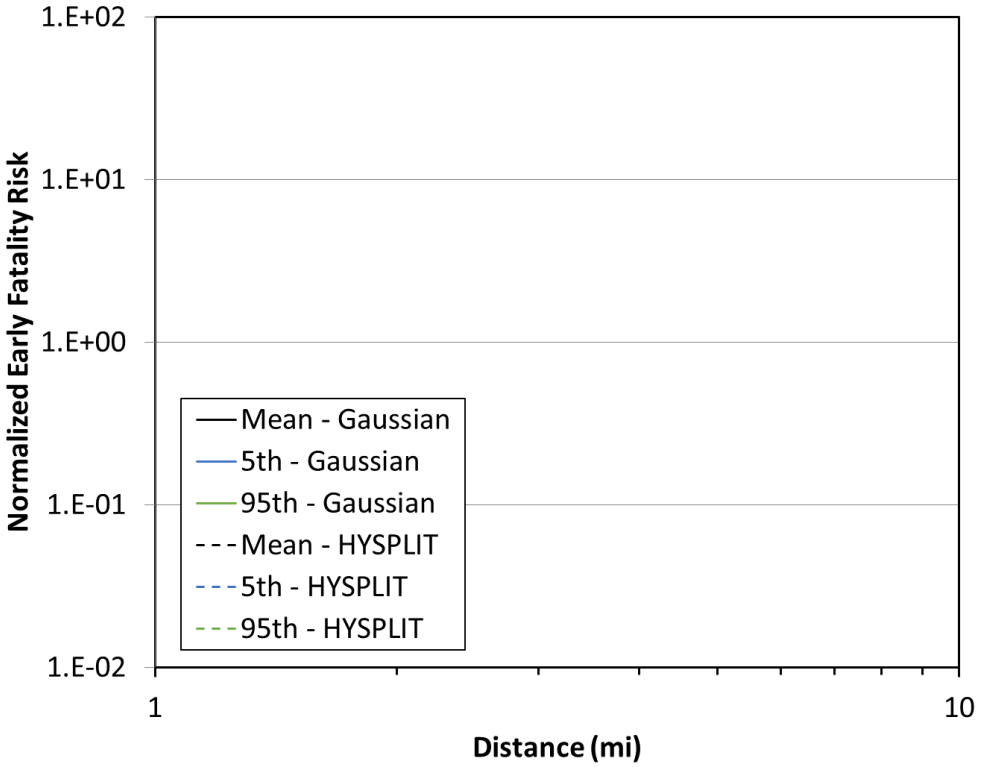

Figure 4-45. Benchmark Site C, ST #2, early fatality risk comparison

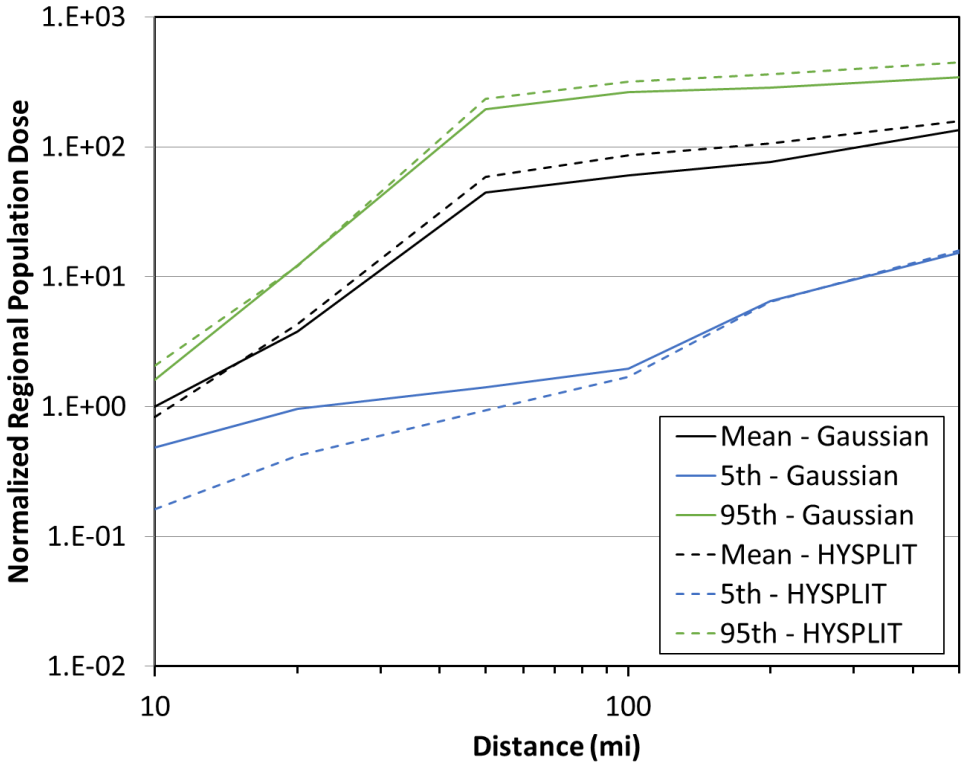

Figure 4-46. Benchmark Site C, ST #2, population dose comparison

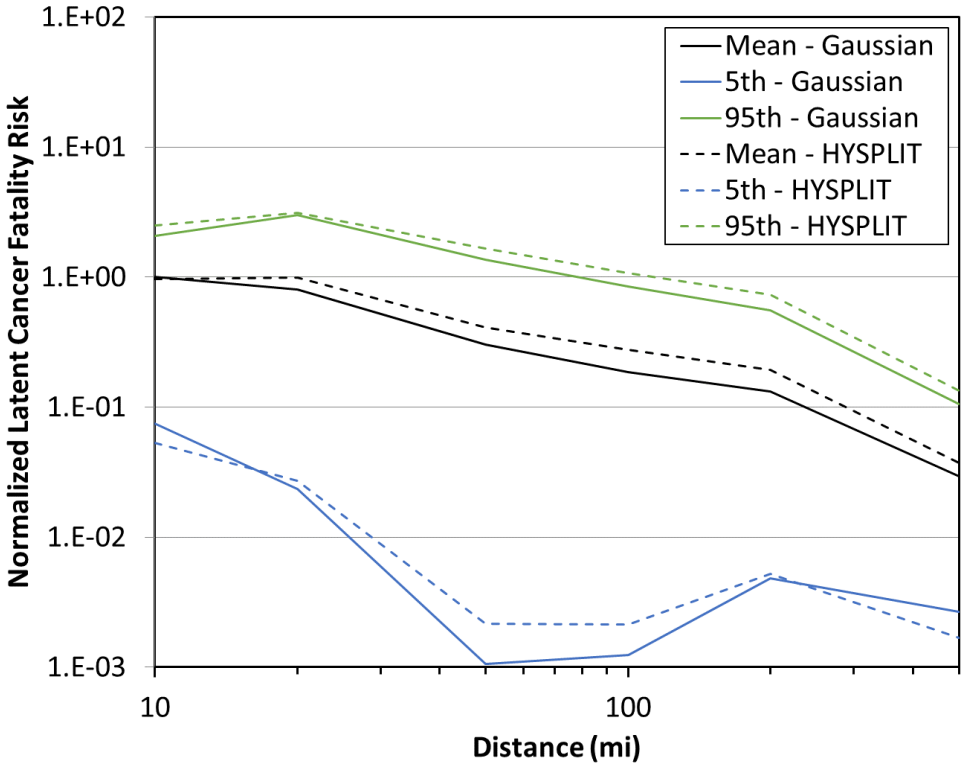

Figure 4-47. Benchmark Site C, ST #2, latent cancer fatality risk comparison

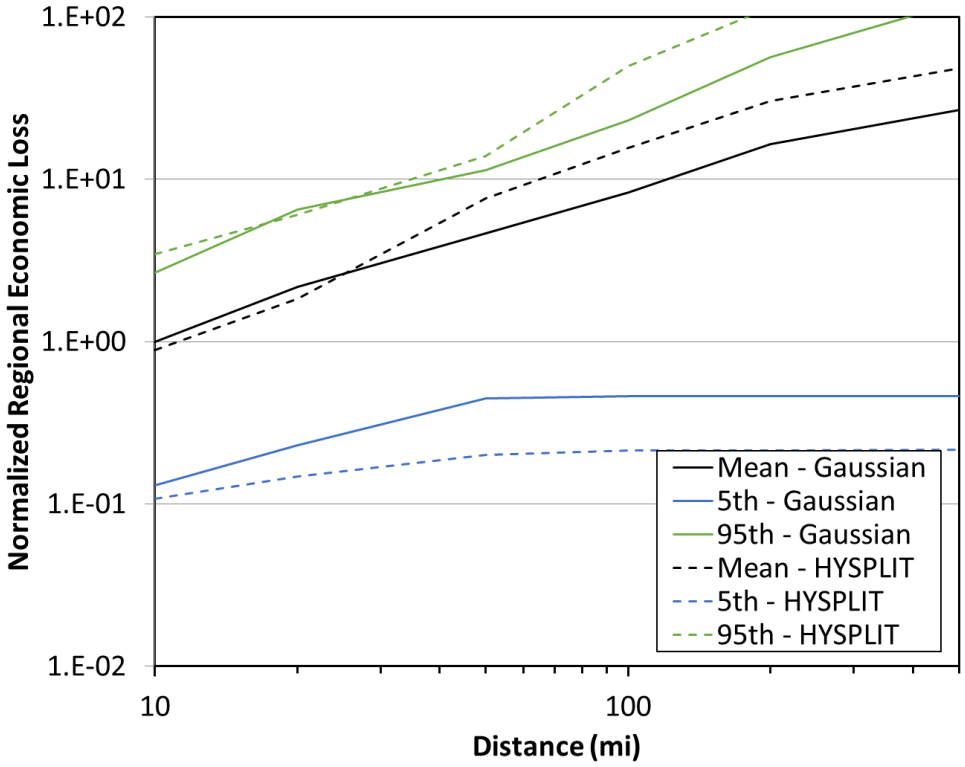

Figure 4-48. Benchmark Site C, ST #2, economic loss comparison

4.5. Site D

4.5.1. Source Term #1

The comparison between the Gaussian and HYSPLIT ATD model results for Site D, ST #1 for peak air concentration, peak ground deposition, land contamination area, peak dose, early fatality risk, population dose, latent cancer fatality risk, and economic loss (as described in Section 3.6) are shown in Figure 4-49 through Figure 4-56. The annual statistics for these measures are shown with different colors, where the mean values are in black, the 5th percentile values are shown in blue, and the 95th percentile values are shown in green. HYSPLIT results are shown as dashed lines and Gaussian model results are shown as solid lines. The normalized results are shown as a function of distance, rather than the ratio of Gaussian and HYSPLIT results, to allow for the trends with distance to be observed. Some results are zero for early and latent cancer fatality risk, so they cannot be shown on the log scale used in the figures. For Site D, there are no individuals within five miles of the site, which results in a calculated zero early fatality risk at shorter distances. Discussion of the difference seen in these figures is provided below in Section 4.7

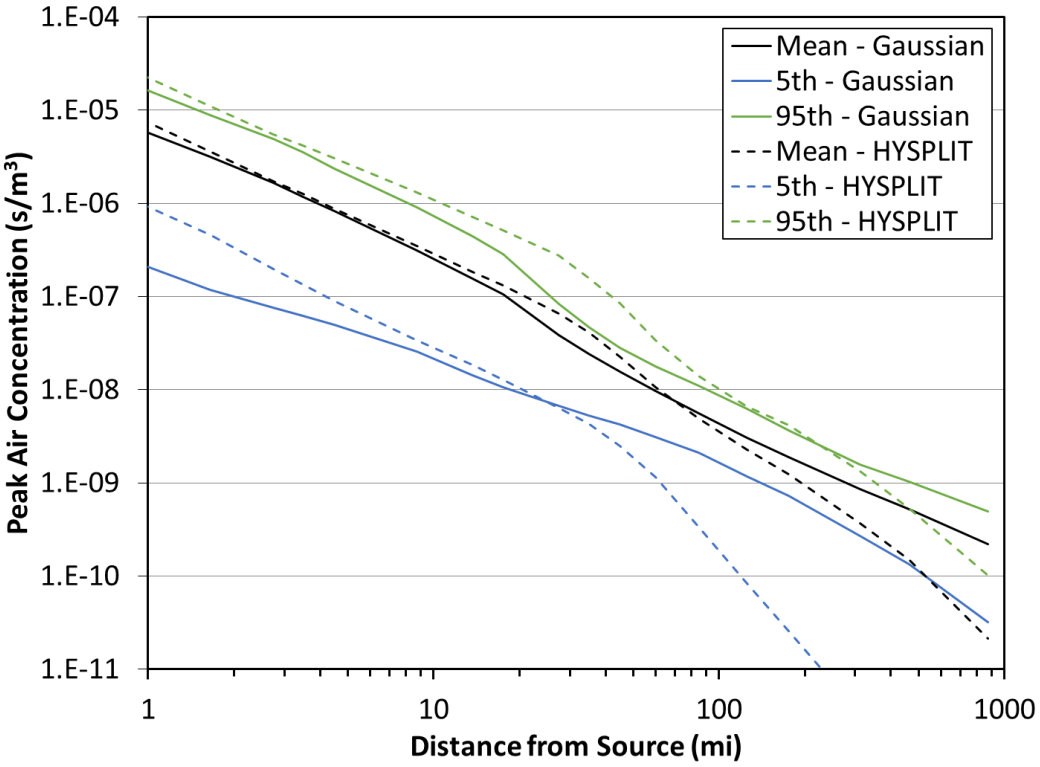

Figure 4-49. Benchmark Site D, ST #1, peak air concentration comparison

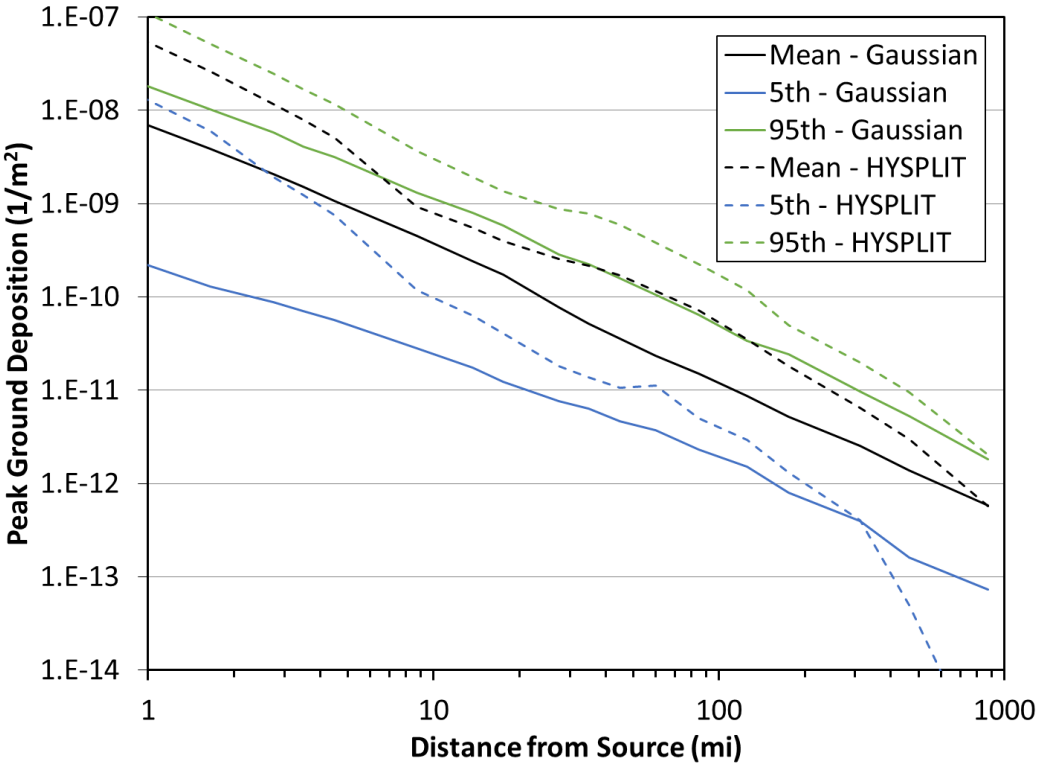

Figure 4-50. Benchmark Site D, ST #1, peak ground deposition comparison

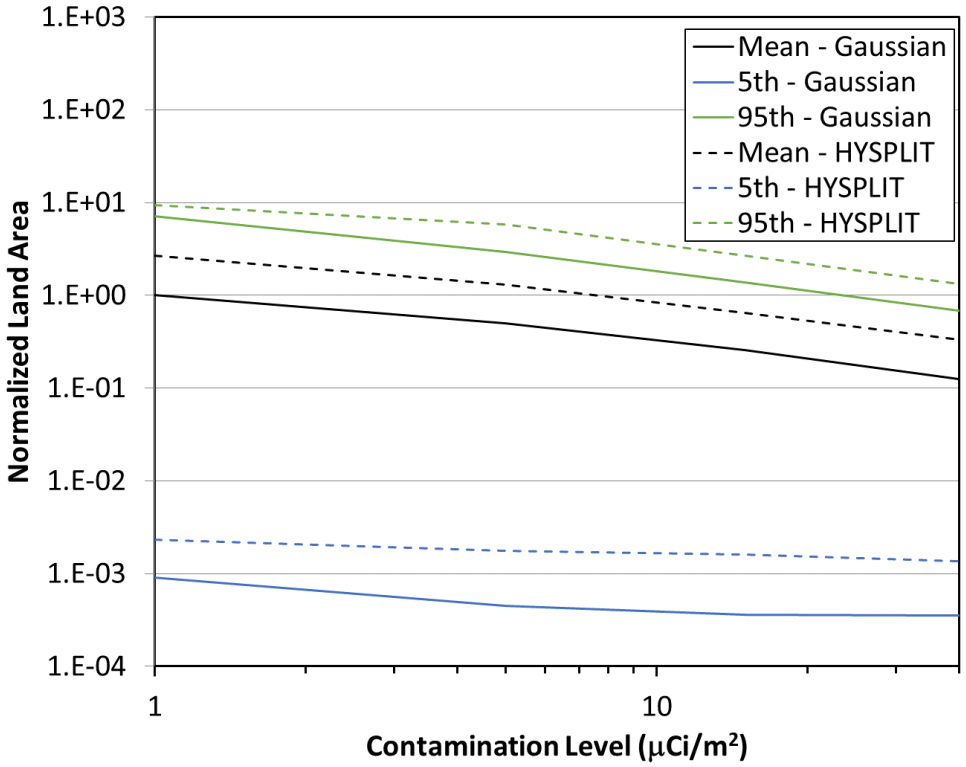

Figure 4-51. Benchmark Site D, ST #1, land contamination area within 805 km (500 mi) comparison

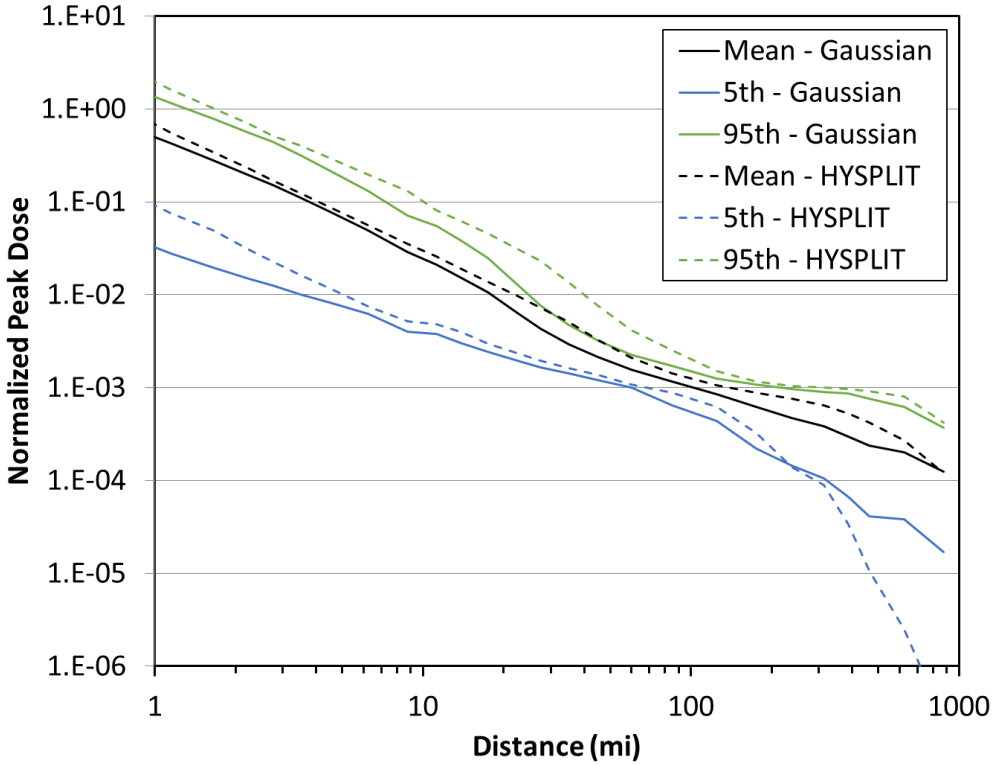

Figure 4-52. Benchmark Site D, ST #1, peak dose comparison

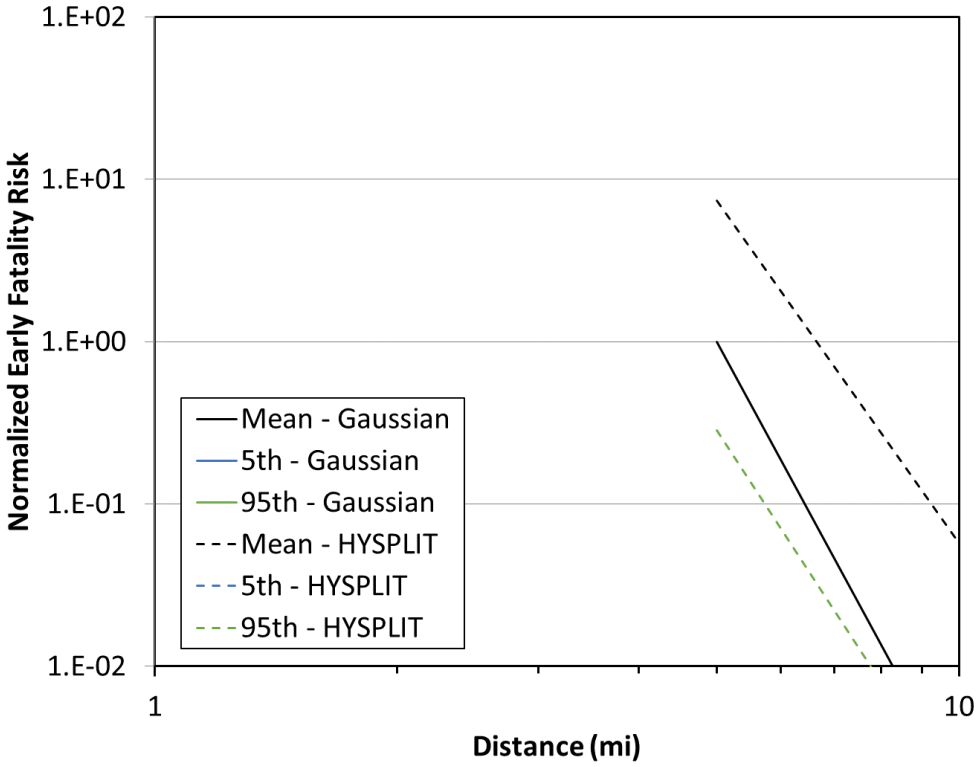

Figure 4-53. Benchmark Site D, ST #1, early fatality risk comparison

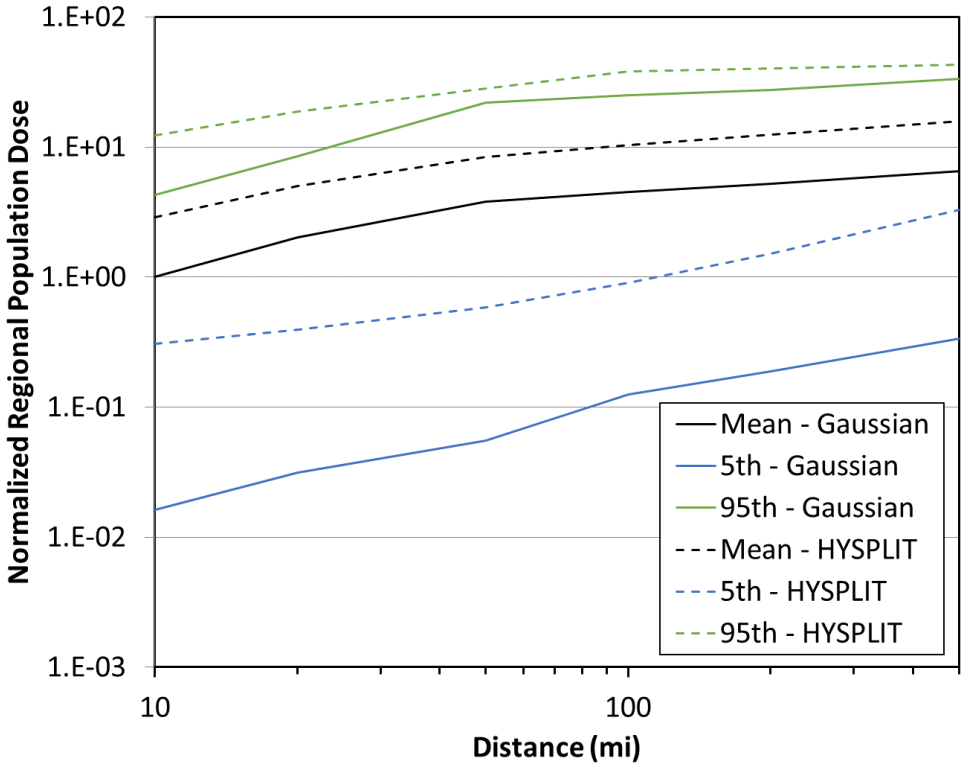

Figure 4-54. Benchmark Site D, ST #1, population dose comparison

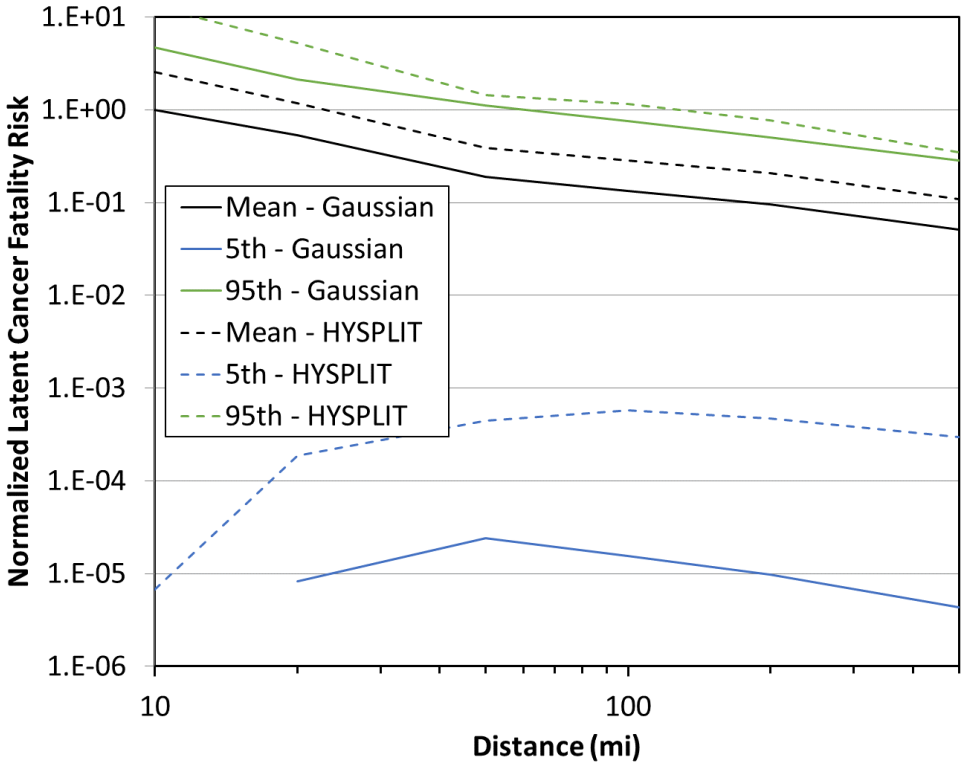

Figure 4-55. Benchmark Site D, ST #1, latent cancer fatality risk comparison

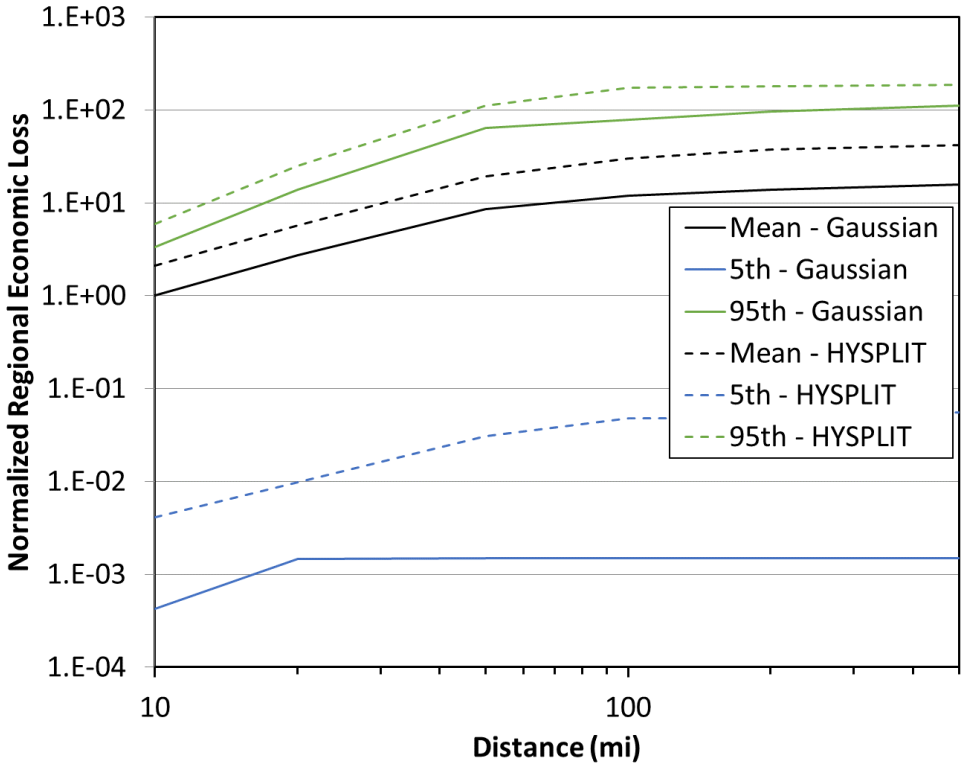

Figure 4-56. Benchmark Site D, ST #1, economic loss comparison

4.5.2. Source Term #2

The comparison between the Gaussian and HYSPLIT ATD model results for Site D, ST #2 for peak air concentration, peak ground deposition, land contamination area, peak dose, early fatality risk, population dose, latent cancer fatality risk, and economic loss (as described in Section 3.6) are shown in Figure 4-57 through Figure 4-64. The annual statistics for these measures are shown with different colors, where the mean values are in black, the 5th percentile values are shown in blue, and the 95th percentile values are shown in green. HYSPLIT results are shown as dashed lines and Gaussian model results are shown as solid lines. The normalized results are shown as a function of distance, rather than the ratio of Gaussian and HYSPLIT results, to allow for the trends with distance to be observed. Some results are zero for early fatality risk, so they cannot be shown on the log scale used in the figures. Discussion of the difference seen in these figures is provided below in Section 4.7.

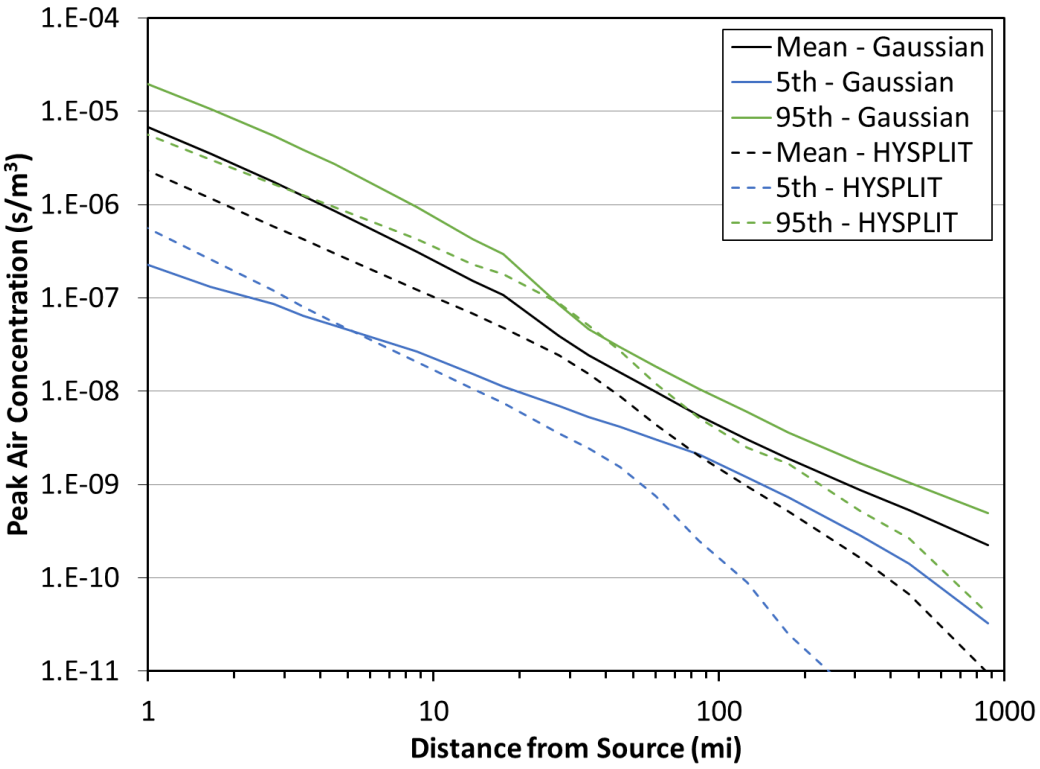

Figure 4-57. Benchmark Site D, ST #2, peak air concentration comparison

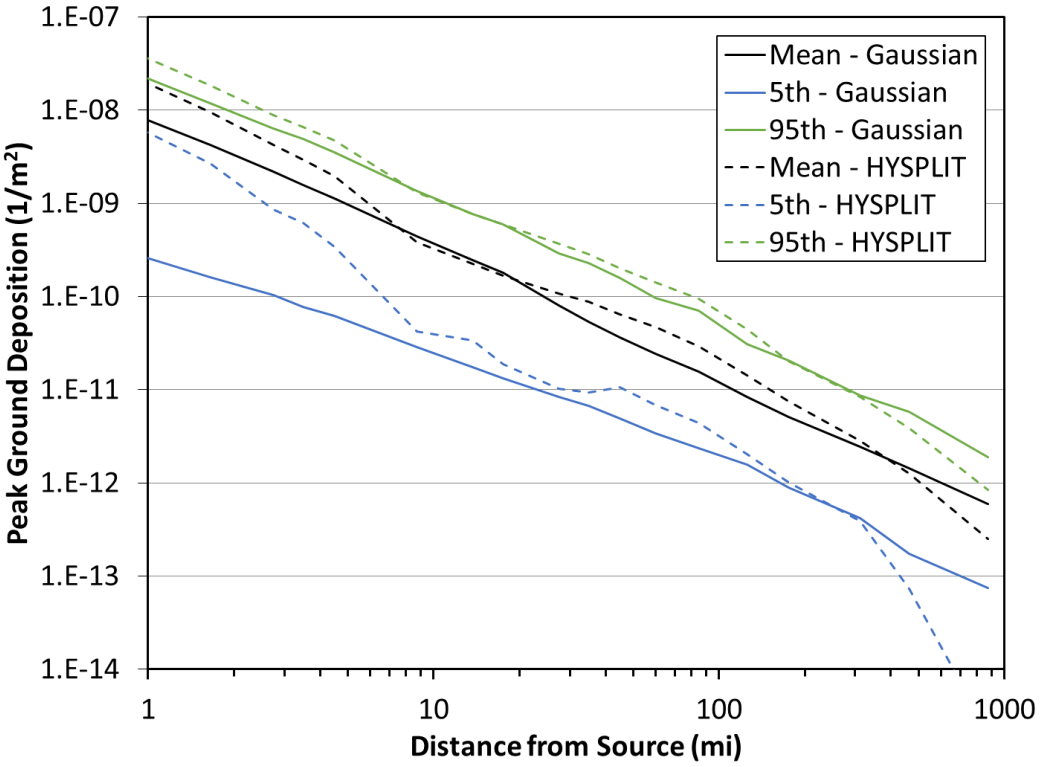

Figure 4-58. Benchmark Site D, ST #2, peak ground deposition comparison

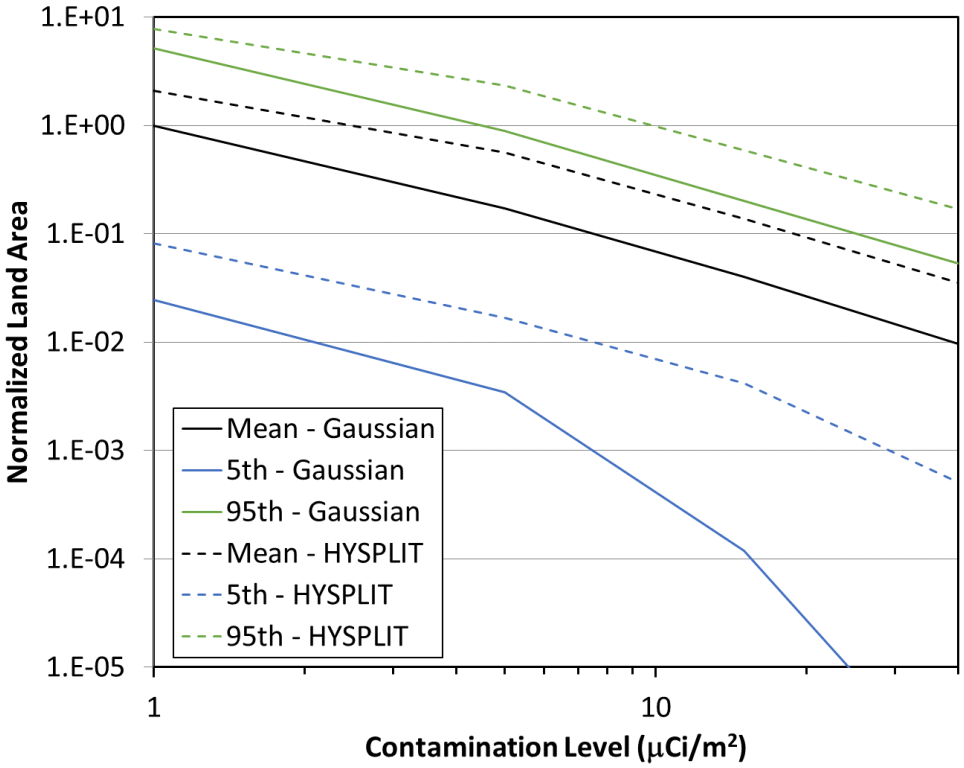

Figure 4-59. Benchmark Site D, ST #2, land contamination area within 805 km (500 mi) comparison

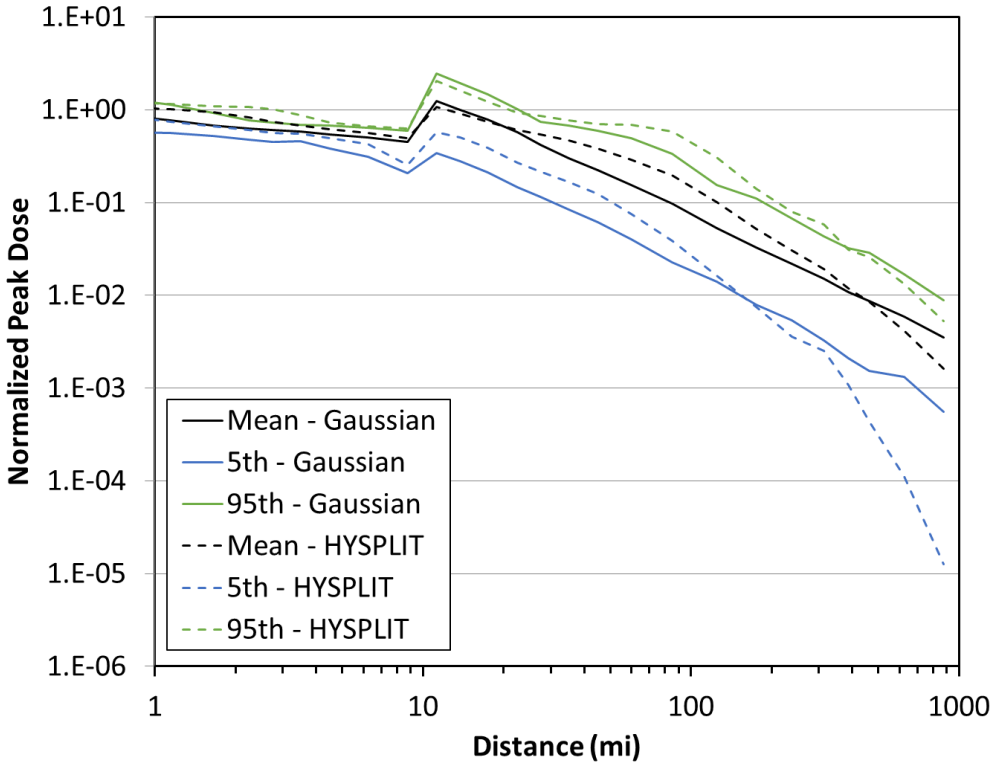

Figure 4-60. Benchmark Site D, ST #2, peak dose comparison

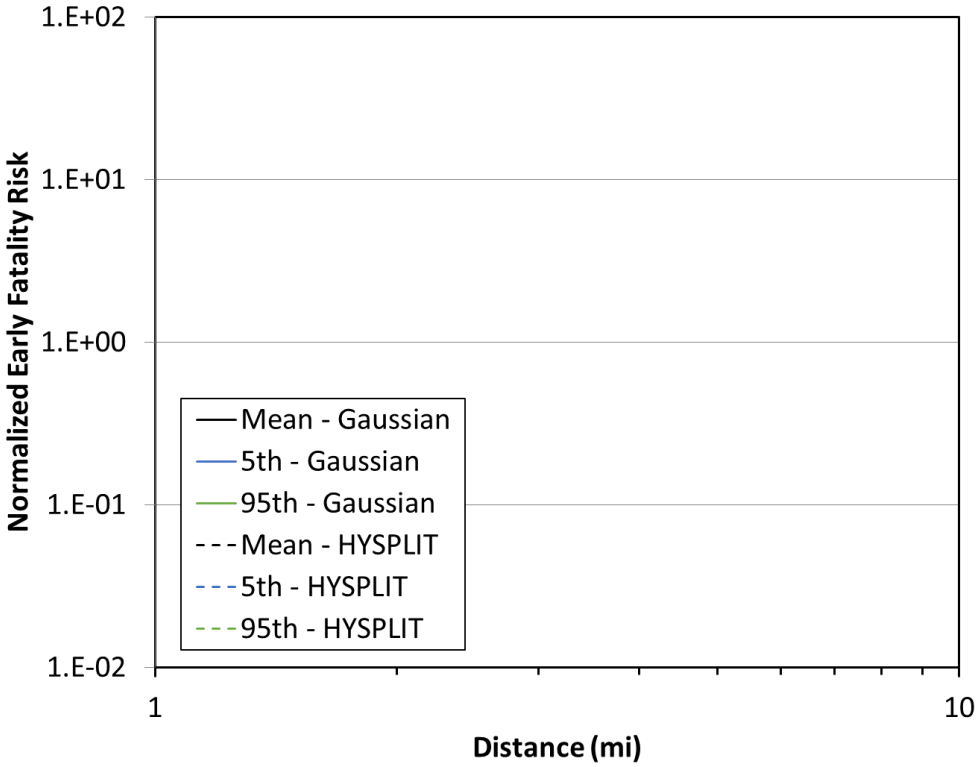

Figure 4-61. Benchmark Site D, ST #2, early fatality risk comparison

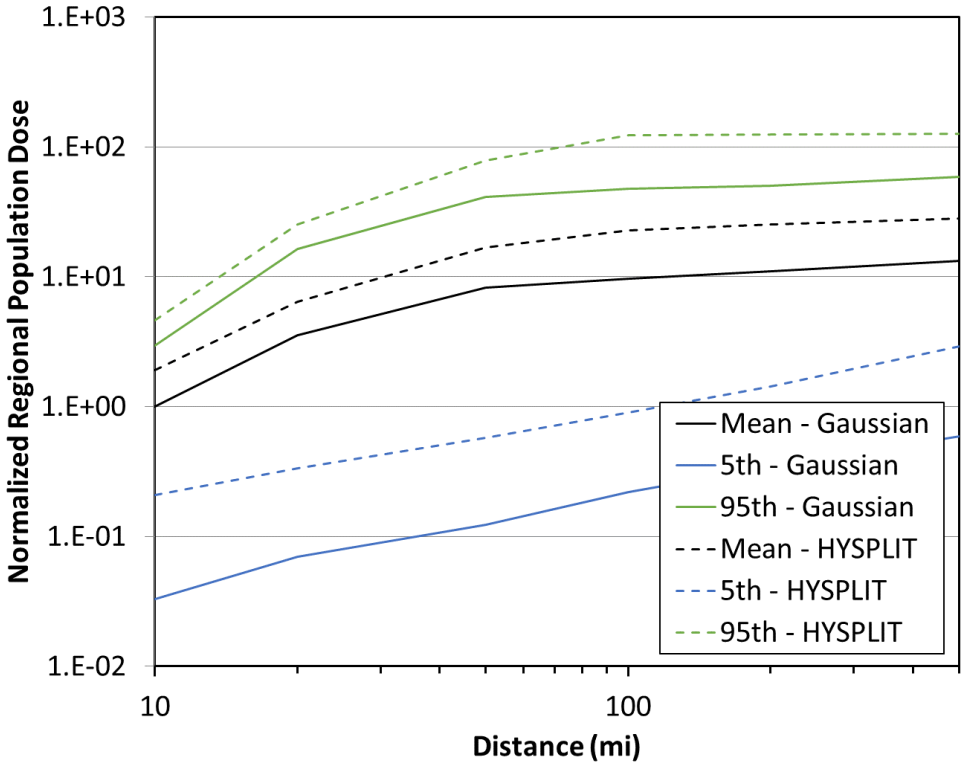

Figure 4-62. Benchmark Site D, ST #2, population dose comparison

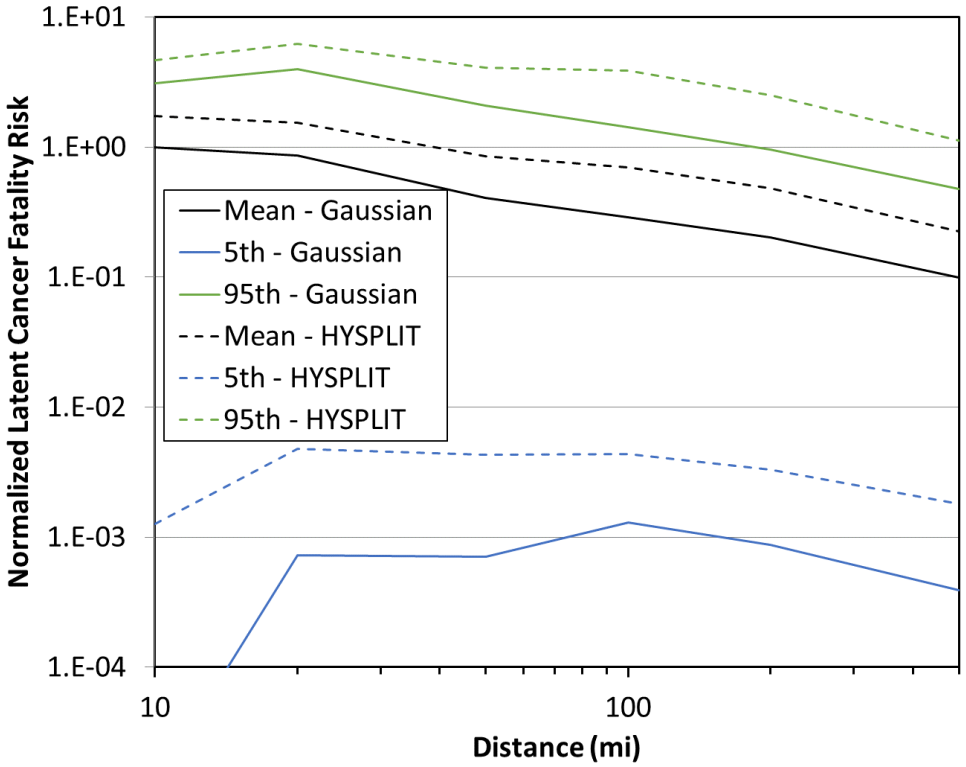

Figure 4-63. Benchmark Site D, ST #2, latent cancer fatality risk comparison

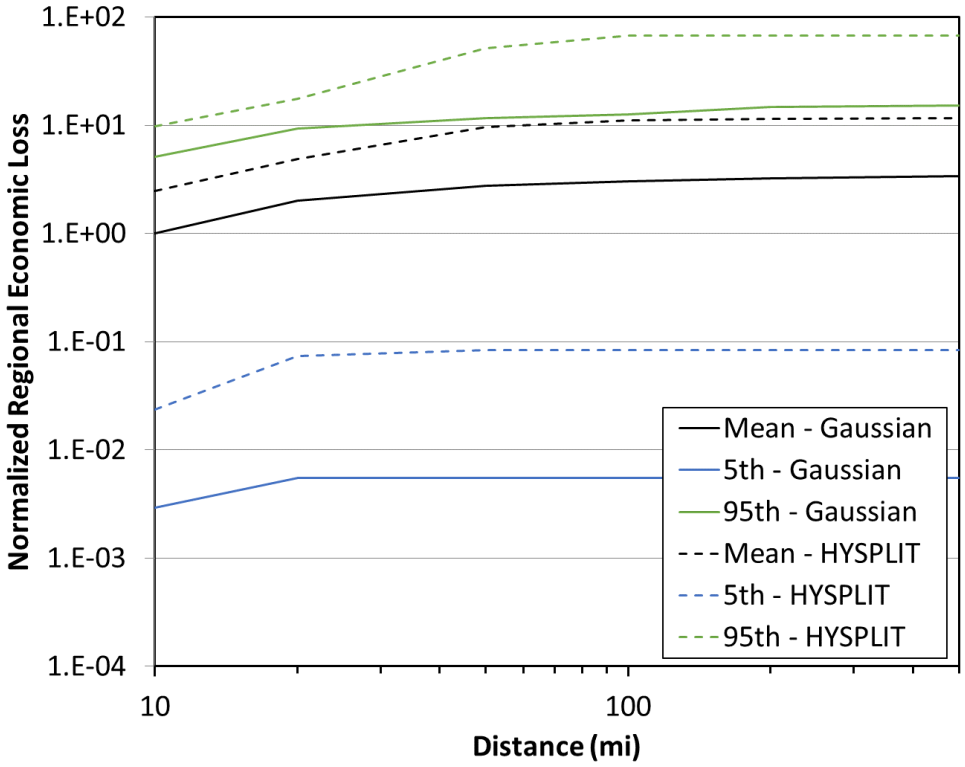

Figure 4-64. Benchmark Site D, ST #2, economic loss comparison

4.6. Site E

4.6.1. Source Term #1

The comparison between the Gaussian and HYSPLIT ATD model results for Site E, ST #1 for peak air concentration, peak ground deposition, land contamination area, peak dose, early fatality risk, population dose, latent cancer fatality risk, and economic loss (as described in Section 3.6) are shown in Figure 4-65 through Figure 4-72. The annual statistics for these measures are shown with different colors, where the mean values are in black, the 5th percentile values are shown in blue, and the 95th percentile values are shown in green. HYSPLIT results are shown as dashed lines and Gaussian model results are shown as solid lines. The normalized results are shown as a function of distance, rather than the ratio of Gaussian and HYSPLIT results, to allow for the trends with distance to be observed. Some results are zero for early and latent cancer fatality risk, so they cannot be shown on the log scale used in the figures. Discussion of the difference seen in these figures is provided below in Section 4.7.

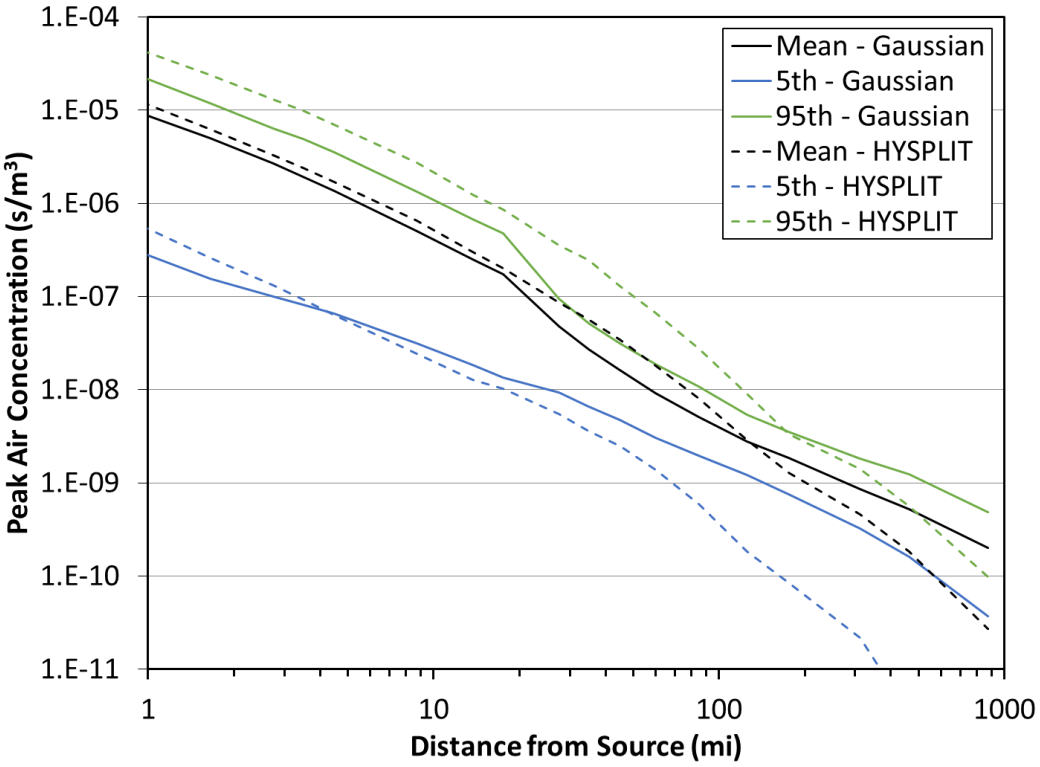

Figure 4-65. Benchmark Site E, ST #1, peak air concentration comparison

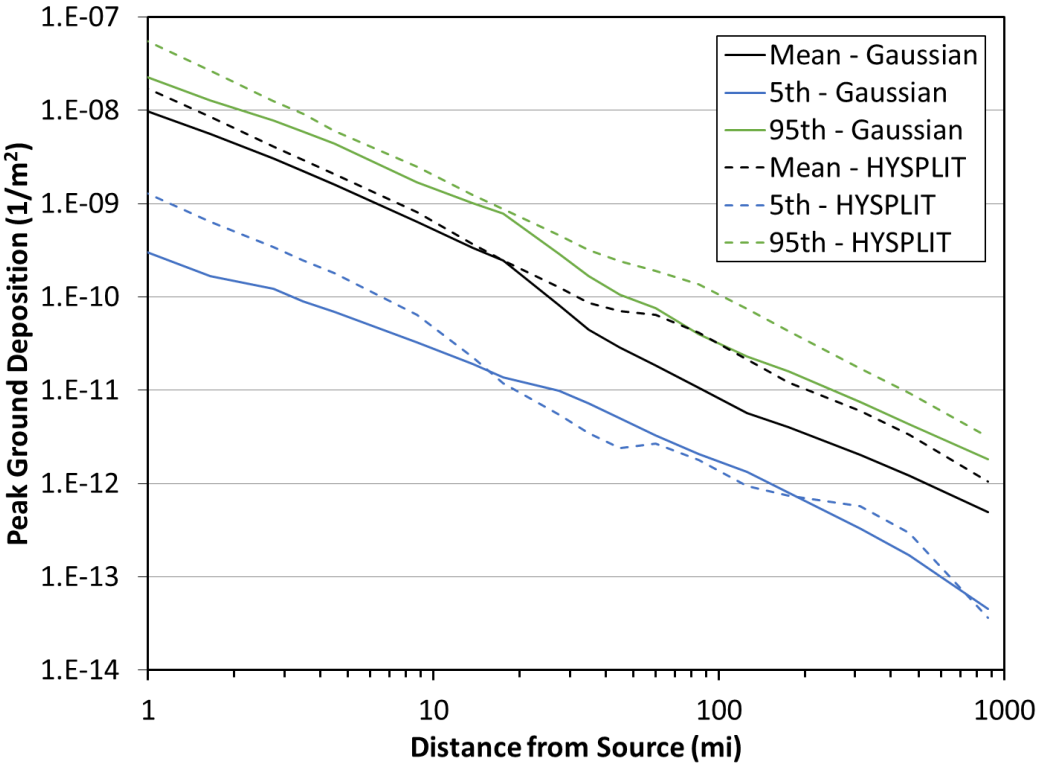

Figure 4-66. Benchmark Site E, ST #1, peak ground deposition comparison

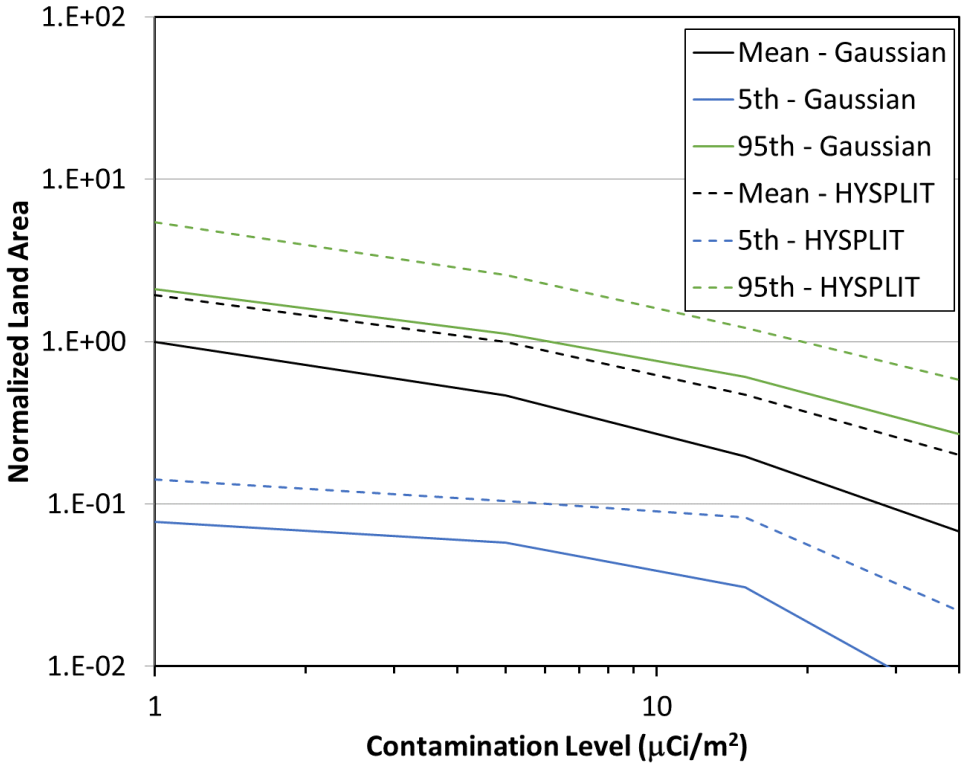

Figure 4-67. Benchmark Site E, ST #1, land contamination area within 805 km (500 mi) comparison

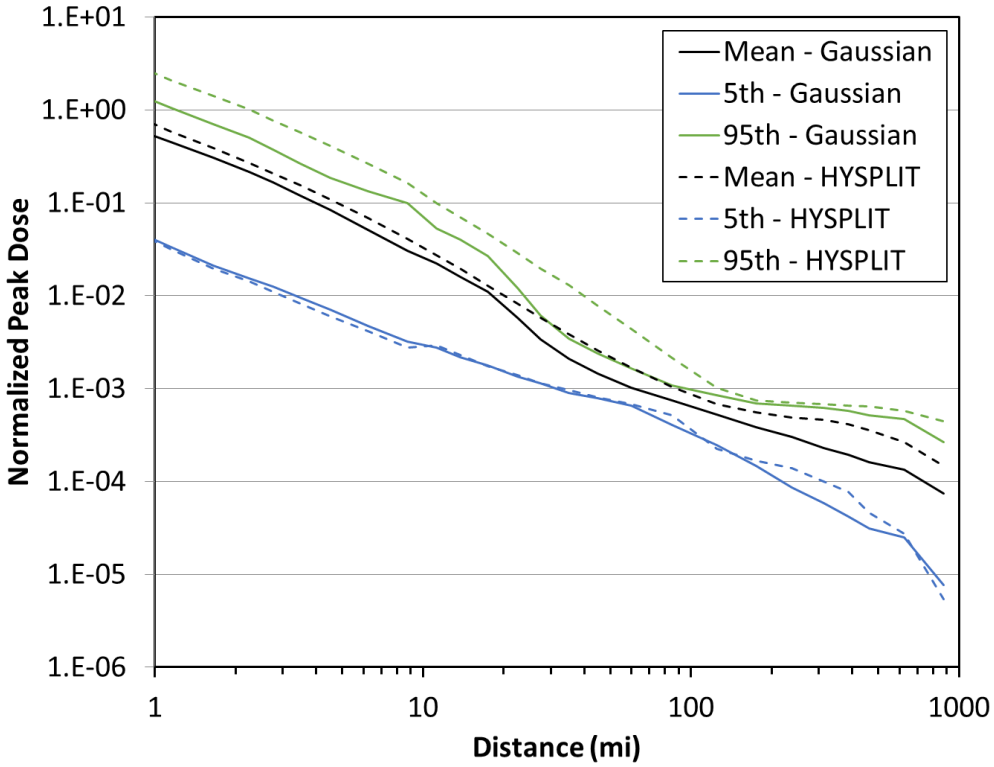

Figure 4-68. Benchmark Site E, ST #1, peak dose comparison

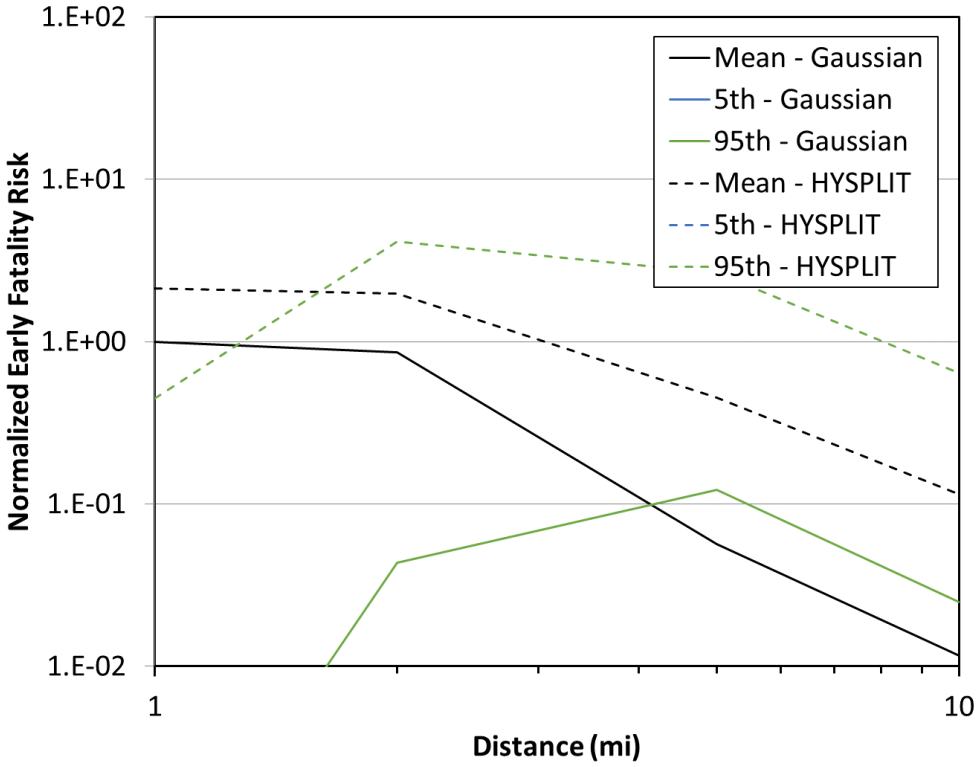

Figure 4-69. Benchmark Site E, ST #1, early fatality risk comparison

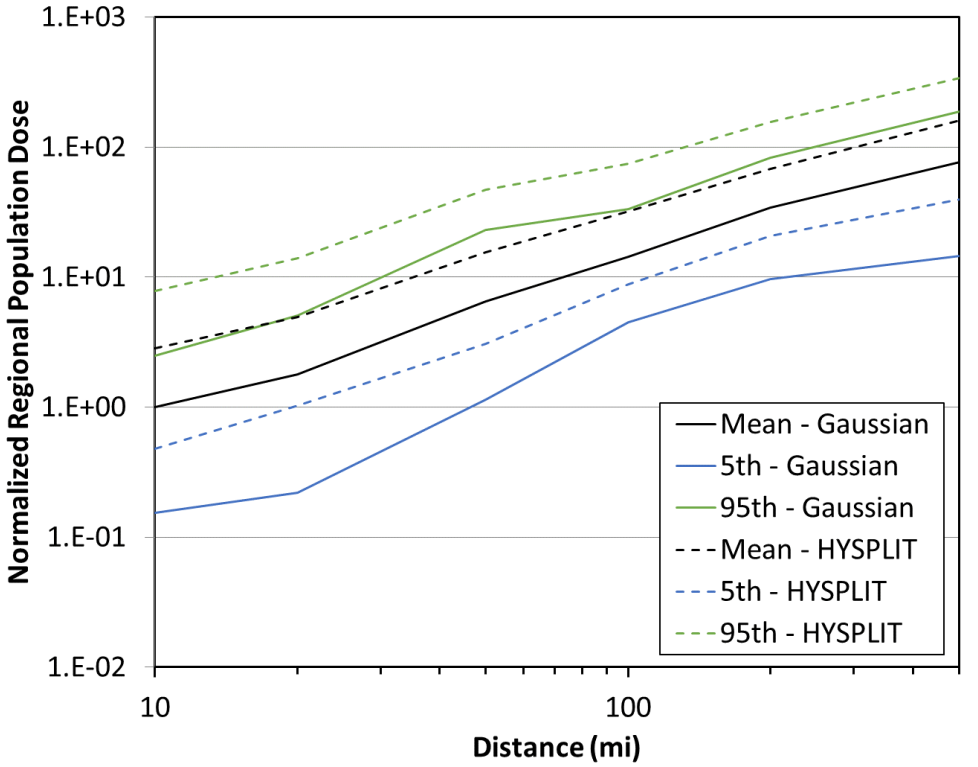

Figure 4-70. Benchmark Site E, ST #1, population dose comparison

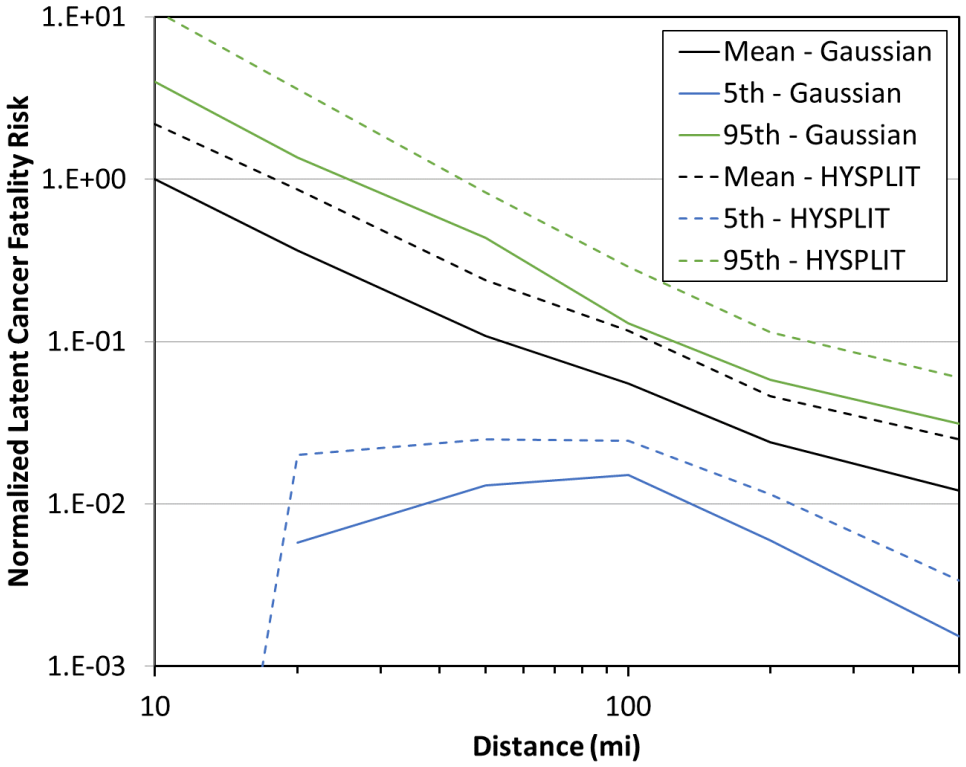

Figure 4-71. Benchmark Site E, ST #1, latent cancer fatality risk comparison

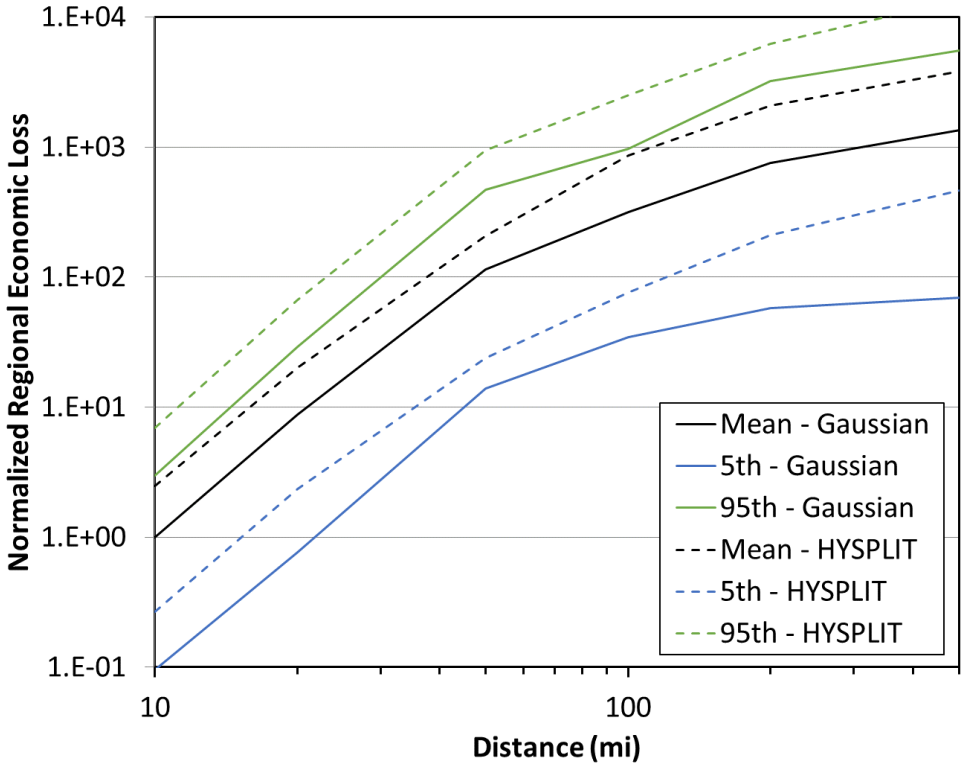

Figure 4-72. Benchmark Site E, ST #1, economic loss comparison

4.6.2. Source Term #2

The comparison between the Gaussian and HYSPLIT ATD model results for Site E, ST #2 for peak air concentration, peak ground deposition, land contamination area, peak dose, early fatality risk, population dose, latent cancer fatality risk, and economic loss (as described in Section 3.6) are shown in Figure 4-73 through Figure 4-80. The annual statistics for these measures are shown with different colors, where the mean values are in black, the 5th percentile values are shown in blue, and the 95th percentile values are shown in green. HYSPLIT results are shown as dashed lines and Gaussian model results are shown as solid lines. The normalized results are shown as a function of distance, rather than the ratio of Gaussian and HYSPLIT results, to allow for the trends with distance to be observed. Some results are zero for early and latent cancer fatality risk, so they cannot be shown on the log scale used in the figures. Discussion of the difference seen in these figures is provided below in Section 4.7.

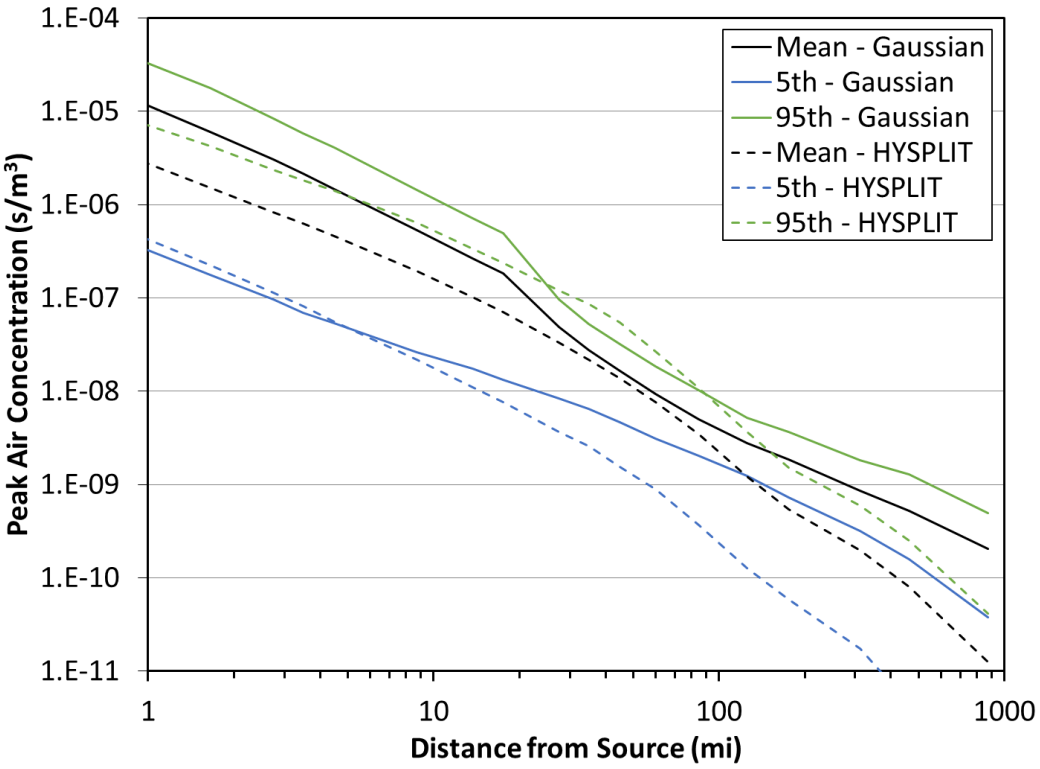

Figure 4-73. Benchmark Site E, ST #2, peak air concentration comparison

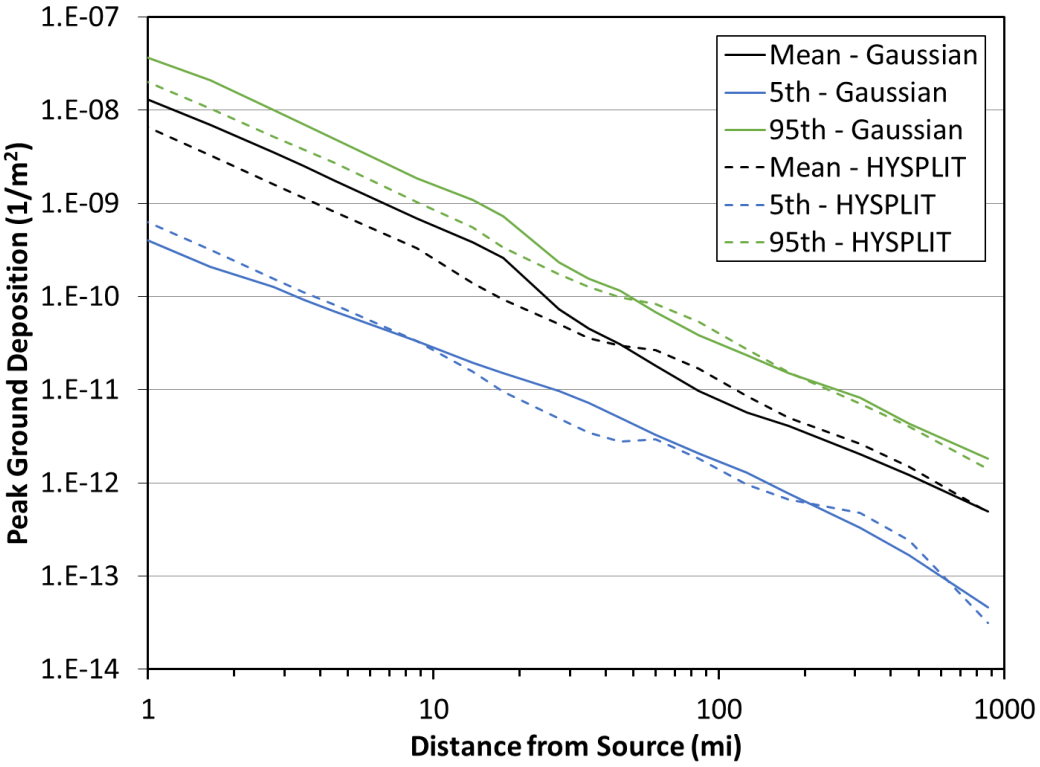

Figure 4-74. Benchmark Site E, ST #2, peak ground deposition comparison

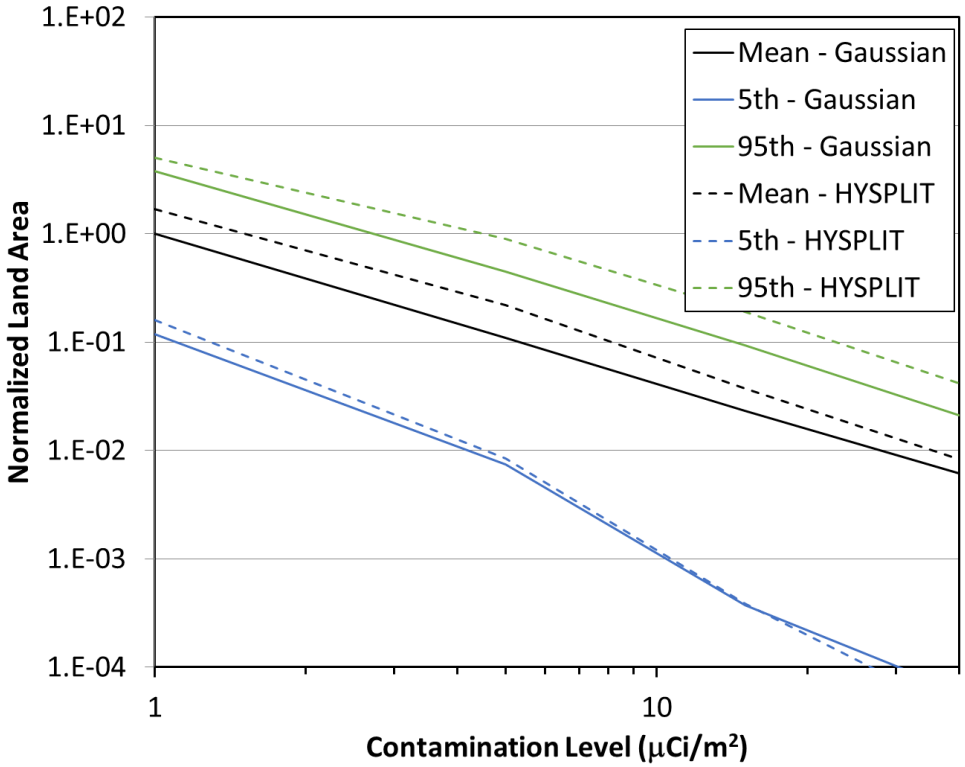

Figure 4-75. Benchmark Site E, ST #2, land contamination area within 805 km (500 mi) comparison

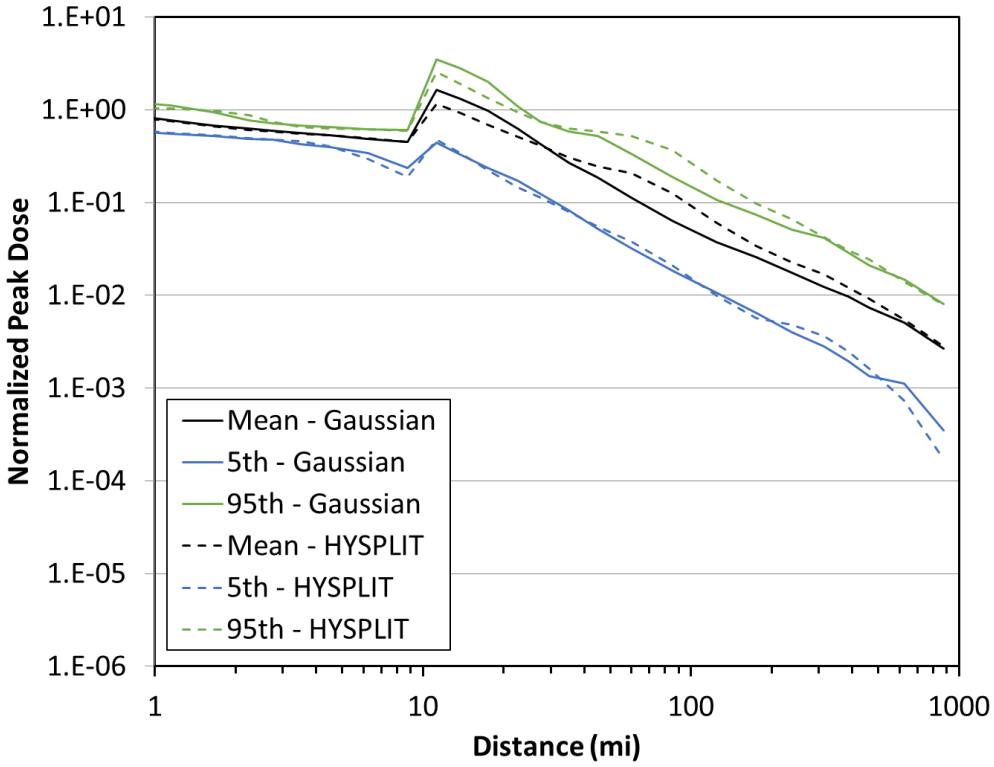

Figure 4-76. Benchmark Site E, ST #2, peak dose comparison

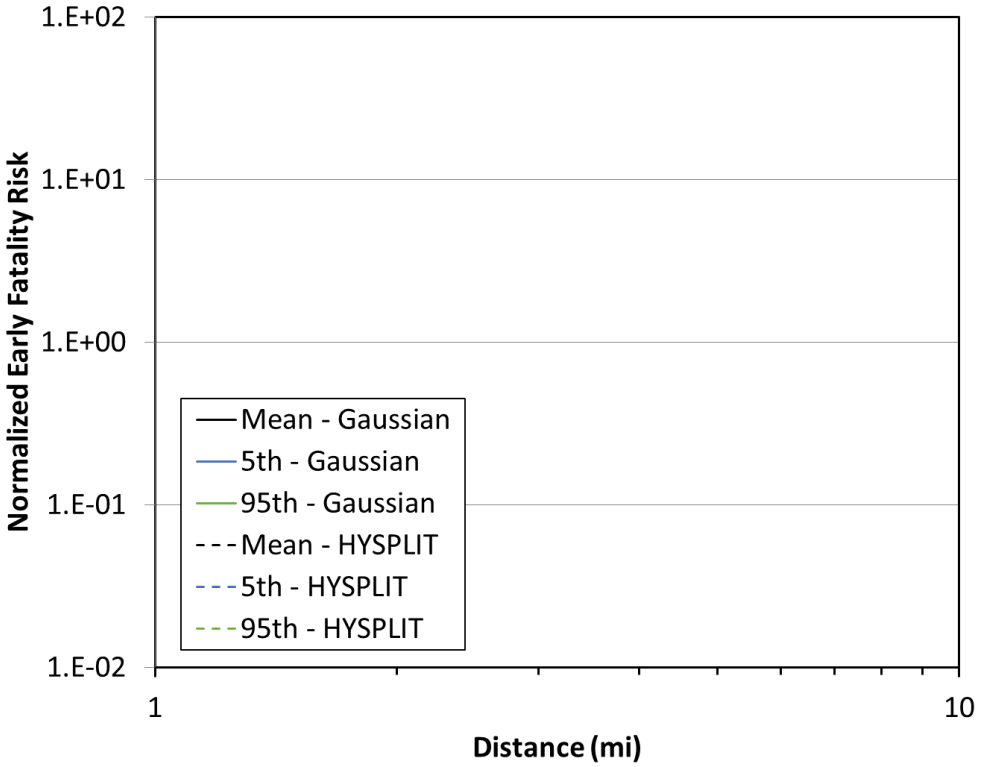

Figure 4-77. Benchmark Site E, ST #2, early fatality risk comparison

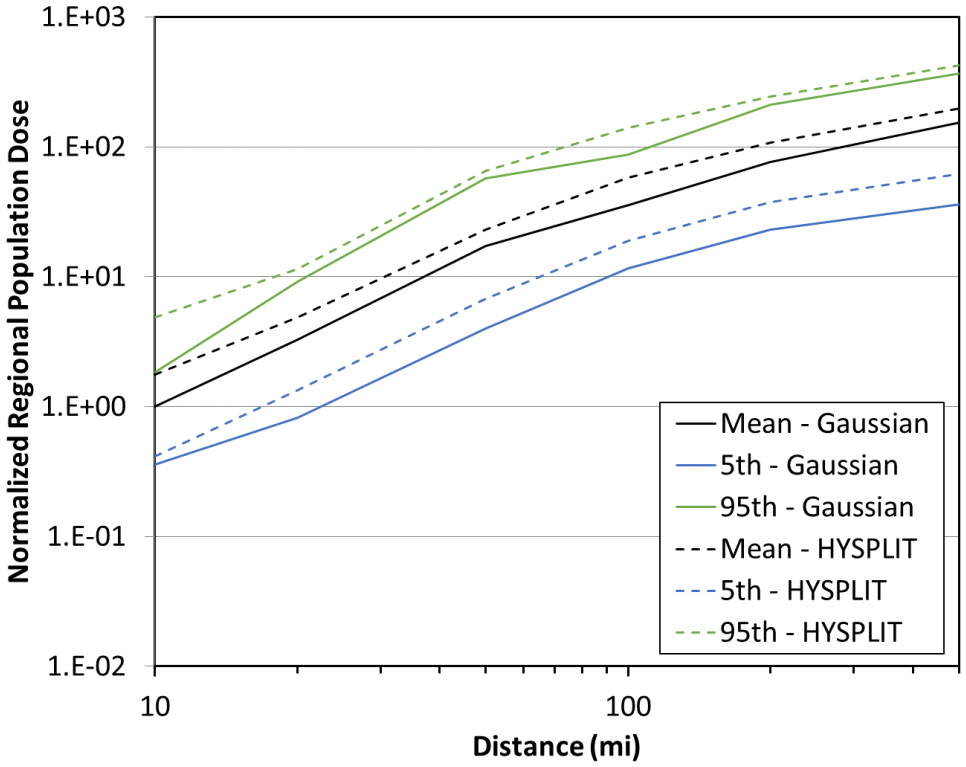

Figure 4-78. Benchmark Site E, ST #2, population dose comparison

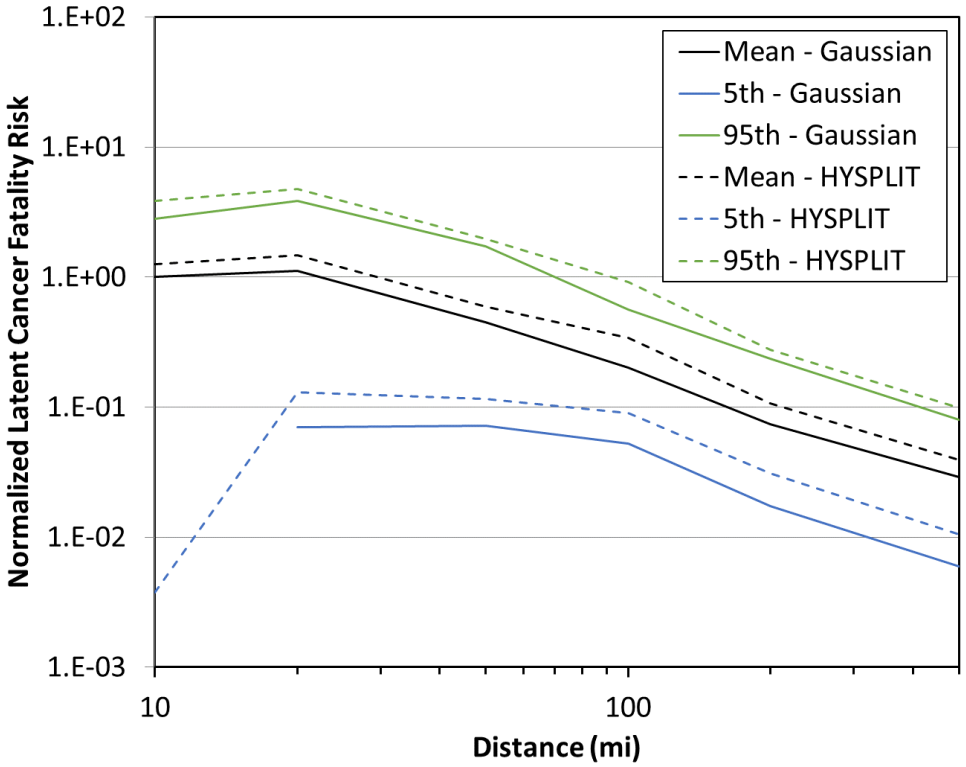

Figure 4-79. Benchmark Site E, ST #2, latent cancer fatality risk comparison

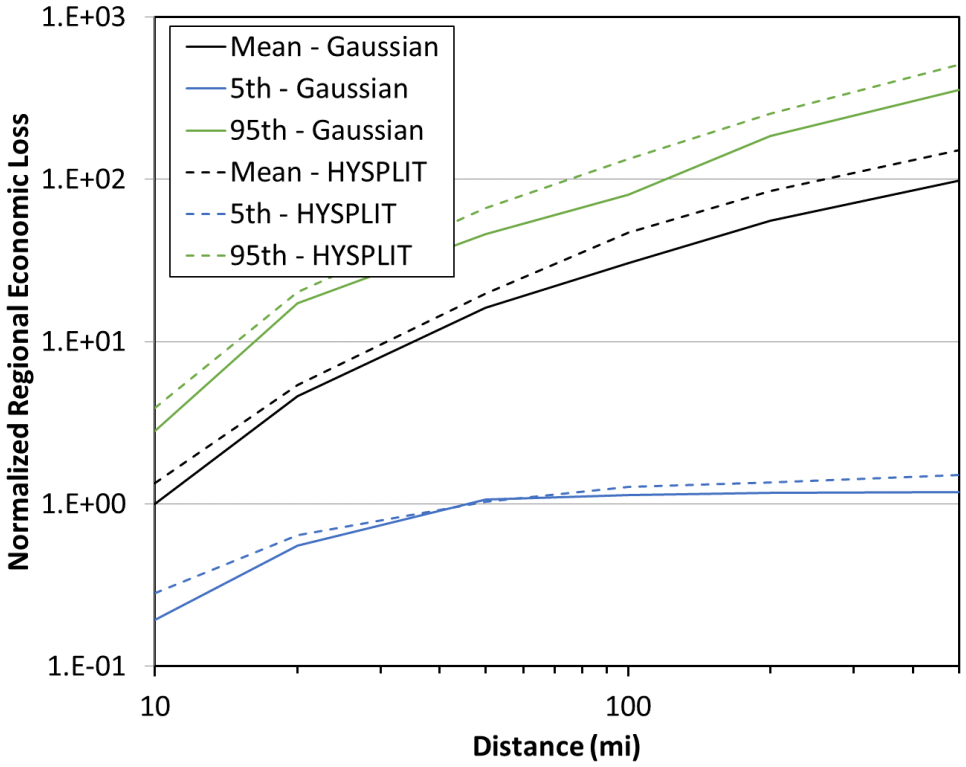

Figure 4-80. Benchmark Site E, ST #2, economic loss comparison

4.7. Interpretations of Benchmark Comparison Results

This section provides a comprehensive analysis of the results in the multiple figures presented in the previous sections (Sections 4.2 through 4.6). For these figures, the ratios of the annual average results for the HYSPLIT ATD model to the Gaussian ATD model are calculated for each output metric as a function of distance. The averages of these ratios, along with their minimums and maximums are delineated between nearfield (here defined to be from the site out to a radius of 48 km [30 mi]) and far field (beyond 48 km [30 mi] from the site out to 805 km [500 mi]) below in Table 4-2 and Table 4-3, respectively. The columns represent the outputs in the figures presented above. EF risk is purely a nearfield result and hence is only shown in Table 4-2. The land areas contaminated above a specific level are not delineated by distance and so are only shown in the far field results in Table 4-3. For source term #2, EF risk was calculated as zero and so a ratio could not be calculated.

Table 4-2. Nearfield ratios of the annual average results for the HYSPLIT ATD model to the Gaussian ATD model, shown as [Average (Minimum | Maximum)]

Site/ Source	Near Field						
	Peak Air	Peak Ground	Peak Dose	Pop Dose	LCF Risk	Econ Loss	EF Risk
A/1	1.1 (0.8|1.3)	1.4 (1.0|2.1)	1.1 (0.9|1.4)	2.7 (2.5|2.8)	2.0 (2.0|2.0)	3.0 (2.8|3.1)	5.8 (2.6|8.6)
B/1	1.1 (1.0|1.6)	1.7 (1.2|2.4)	1.1 (1.0|1.6)	3.4 (3.2|3.6)	2.3 (2.3|2.4)	3.0 (3.0|3.0)	9.0 (4.6|12.2)
C/1	1.9 (1.6|2.6)	0.6 (0.4|1.3)	1.8 (1.6|2.4)	2.6 (2.4|2.7)	2.4 (2.1|2.6)	2.3 (2.2|2.4)	8.6 (3.0|14.3)
D/1	1.2 (1.1|1.7)	4.0 (2.1|6.8)	1.3 (1.1|1.7)	2.7 (2.5|2.9)	2.4 (2.2|2.5)	2.1 (2.1|2.1)	20.0 (7.4|32.6)
E/1	1.3 (1.2|1.8)	1.3 (1.0|1.6)	1.3 (1.2|1.7)	2.8 (2.8|2.8)	2.3 (2.2|2.4)	2.4 (2.3|2.5)	5.5 (2.1|9.8)
A/2	0.3 (0.2|0.5)	0.5 (0.4|0.8)	0.9 (0.6|1.1)	1.6 (1.4|1.8)	1.5 (1.4|1.6)	1.7 (1.5|1.9)	a
B/2	0.3 (0.2|0.6)	0.6 (0.5|0.8)	1.0 (0.7|1.1)	2.1 (1.8|2.4)	1.6 (1.5|1.6)	1.8 (1.7|1.9)	a
C/2	0.4 (0.2|0.8)	0.2 (0.1|0.5)	0.8 (0.7|0.9)	1.0 (0.8|1.1)	1.1 (1.0|1.2)	0.9 (0.8|0.9)	a
D/2	0.4 (0.3|0.6)	1.5 (0.9|2.3)	1.1 (0.9|1.4)	1.9 (1.8|1.9)	1.8 (1.7|1.8)	2.5 (2.4|2.5)	a
E/2	0.4 (0.3|0.7)	0.5 (0.4|0.7)	0.9 (0.7|1.0)	1.6 (1.5|1.8)	1.3 (1.3|1.3)	1.3 (1.2|1.4)	a

[a]Data not available to compute ratio

Table 4-3. Far field ratios of the annual average results for the HYSPLIT ATD model to the Gaussian ATD model, shown as [Average (Minimum | Maximum)]

Site/ Source	Far Field						
	Peak Air	Peak Ground	Peak Dose	Pop Dose	LCF Risk	Econ Loss	Land Area
A/1	1.1 (0.4|1.4)	2.7 (1.9|3.2)	1.5 (1.3|2.1)	2.0 (1.8|2.4)	1.8 (1.7|2.0)	2.4 (2.2|2.5)	2.0 (1.6|2.5)
B/1	1.3 (0.4|2.0)	2.3 (1.7|3.1)	1.6 (1.3|1.8)	2.5 (2.2|2.8)	2.4 (2.1|2.6)	2.6 (2.2|2.9)	2.3 (2.1|2.5)
C/1	1.4 (0.5|2.7)	2.6 (1.6|3.5)	1.7 (1.1|2.3)	2.2 (1.8|2.4)	2.1 (1.8|2.4)	2.4 (2.1|2.6)	2.7 (1.9|3.9)
D/1	0.9 (0.3|1.7)	3.9 (2.2|5.0)	1.5 (1.2|1.8)	2.3 (2.2|2.4)	2.1 (2.0|2.2)	2.5 (2.3|2.7)	2.6 (2.5|2.7)
E/1	1.3 (0.4|2.1)	3.0 (1.9|3.8)	1.7 (1.3|2.2)	2.2 (2.0|2.4)	2.1 (1.9|2.2)	2.5 (1.8|2.8)	2.4 (1.9|3.0)
A/2	0.5 (0.2|0.6)	1.1 (0.9|1.4)	1.3 (1.0|1.6)	1.3 (1.1|1.4)	1.3 (1.1|1.4)	1.4 (1.3|1.5)	1.5 (1.2|1.6)
B/2	0.6 (0.2|0.8)	0.9 (0.7|1.1)	1.1 (0.9|1.4)	1.5 (1.3|1.7)	1.5 (1.3|1.8)	1.4 (1.3|1.5)	1.5 (1.3|1.7)
C/2	0.6 (0.2|1.0)	1.2 (0.7|1.6)	1.3 (1.1|1.5)	1.3 (1.2|1.4)	1.4 (1.3|1.5)	1.8 (1.6|1.9)	1.3 (0.6|1.9)
D/2	0.4 (0.1|0.6)	1.6 (0.9|1.9)	1.5 (1.0|2.0)	2.2 (2.1|2.3)	2.3 (2.1|2.4)	3.5 (3.4|3.7)	3.1 (2.1|3.6)
E/2	0.5 (0.2|0.8)	1.3 (0.8|1.7)	1.4 (1.1|2.0)	1.4 (1.3|1.6)	1.5 (1.3|1.7)	1.5 (1.2|1.5)	1.7 (1.4|2.0)

General results determined by examining the comparisons between the Gaussian and HYSPLIT ATD model calculations for the five sites and two source terms are discussed below. Caution should be used in generalizing these interpretations to other sites or consequence metrics. The interpretations in this section summarize the trends from the results above.

1. The level of agreement between annual average results from the Gaussian and HYSPLIT ATD model is very similar to the results shown in NUREG/CR-6853 (Molenkamp et al., 2004), with the current study having a wider set of metrics and a longer distance range. It is important to note that this study examined only the comparison of annual statistics; the level of agreement between the two models may be quite different if these comparisons were evaluated for individual weather trials. Note the consistent trend in all metrics discussed below. On average, the HYSPLIT ATD model generally (but not always) predicts larger peak air concentrations and ground depositions than the Gaussian ATD model. The HYSPLIT ATD model also generally predicts larger consequences (e.g., doses, health effects, land areas contaminated, and economic effects). The differences between the Gaussian and HYSPLIT ATD model results was generally more pronounced with ST#1

than with ST#2. This shows that the level of agreement can be systematically affected by the source term being evaluated. The trends as a function of distance for the output quantities also agree between the two models:

a. Annual average peak air concentrations are higher (with an average of 1.3) for the HYSPLIT ATD model compared with the Gaussian ATD model for ST #1 in the nearfield and at 4 out of 5 sites in the far field. For ST #2 the peak air concentration is always lower (with an average ratio of 0.5) for the HYSPLIT ATD model compared with the Gaussian ATD model in both the near and far field. This indicates that the nature of the source term has an impact on peak air concentration trends.
b. Annual average peak ground depositions in the nearfield, are higher (with an average ratio of 2.1) at 4 out of 5 sites for ST #1 and lower (with an average ratio of 0.5) at 4 out of 5 sites for ST #2 for the HYSPLIT ATD model compared with the Gaussian ATD model. In the far field, they are the higher (with an average ratio of 2.9) at all five sites for ST #1 and higher (with an average ratio of 1.3) at 4 out of 5 sites for ST #2. This indicates that the nature of the source term has an impact on ground deposition trends.
c. Annual average peak dose in the nearfield, are higher (with an average ratio of 1.3) for ST #1 and lower or equal (with an average ratio of 0.9) at 4 out of 5 sites for ST #2 for the HYSPLIT ATD model compared with the Gaussian ATD model. Peak dose is higher in all cases in the far field (with an average ratio of 1.6 and 1.3 for ST #1 and ST #2, respectively,) with the HYSPLIT ATD model.
d. Annual average population doses in the nearfield are higher (with an average ratio of 2.8) for the HYSPLIT ATD model compared with the Gaussian ATD model for ST #1. For ST #2, the HYSPLIT ATD model predicts higher or equal (with an average ratio of 1.6) nearfield population doses. This indicates that there is a source term/site dependence in the trends of nearfield population dose predictions. For the far field, the HYSPLIT ATD model predicts higher population doses in all cases (with an average ratio of 2.2 and 1.5 for ST #1 and ST #2, respectively).
e. Annual average latent cancer fatality risks are consistently higher (with an average ratio of 2.3 and 1.5 for ST #1 and ST #2, respectively,) for the HYSPLIT ATD model in the nearfield. They are also consistently higher (with an average ratio of 2.1 and 1.6 for ST #1 and ST #2, respectively,) in the far field as well.
f. Annual average economic loss in the nearfield is consistently predicted to be higher (with an average ratio of 2.6) for the HYSPLIT ATD model with ST #1. For ST #2, 4 out of 5 sites are higher (with an average ratio of 1.8) for the HYSPLIT ATD model. This indicates that there is a significant source term dependence on the trend for economic loss in the nearfield. For the far field, the HYSPLIT ATD model consistently predicts larger economic loss (with an average ratio of 2.4 and 1.9 for ST #1 and ST #2, respectively).
g. Annual average early fatality risk is predicted to be the larger (with an average ratio of 9.8) than the HYSPLIT ATD model for all cases for ST #1. All EF risks are predicted to be zero for ST #2.
h. Land contamination area is consistently predicted to be higher (with an average ratio of 2.4 and 1.8 for ST #1 and ST #2, respectively,) for the HYSPLIT ATD model with both STs.

2. While there are changes in trends between annual average results from the predictions of the Gaussian and HYSPLIT ATD models between the near and far fields for some of the

consequence metrics considered in this study, there is no clear distance at which the Gaussian model seems to systematically diverge (greater than an order of magnitude) from the HYSPLIT ATD model. This highlights the difficulty in quantitatively identifying a specific distance limit beyond which Gaussian ATD models should not be used to estimate average annual consequences over variable weather. However, this study does not examine applications of Gaussian ATD models for specific weather sequences, where it is anticipated that these models may not produce acceptably accurate results at longer distances for some meteorological sequences (e.g., a sea breeze scenario or a cold front passage scenario). The process of averaging consequences over a full annual cycle of weather variability appears to largely compensate for inaccuracies in the use of Gaussian ATD models for specific weather sequences.

3. 5^{th} and 95^{th} percentile annual results shown in the benchmark results also follow the same trends for the Gaussian and HYSPLIT ATD models. However, they are often farther apart than the mean results, as expected.
4. Changes in annual average consequence results do not correlate directly with the changes in the annual average peak air concentration and peak ground deposition. For example, the far field, ST #2 results show an average ratio of 0.4 for the annual average peak air concentration and 0.7 for the annual average peak ground deposition, while the annual average peak individual dose had an average ratio of 0.9 and the annual average population dose had an average ratio of 1.6, both higher than either the annual average peak air concentration or peak ground deposition. The consequence output ratios show a strong dependence on sites and source terms.
5. The zero early fatality risks for ST #2 are due to the relatively small, delayed, and protracted nature of the source term. Early fatalities only occur when acute doses exceed a threshold level for a type of early fatalities. The delayed nature of the source terms calculated in the SOARCA project allows time for radioactive decay of several shorter-lived radionuclides. The protracted nature of these source terms allows for wind shifts that reduce peak doses to any individual. Combined with relatively small releases of radionuclides, the analyses show that the likelihood of early fatalities for these source terms is essentially zero regardless of the ATD model option used.
6. One of the differences between ST #1 and ST #2 is that the rate of release of sensible heat in ST #1 is relatively large for the initial "puff" release (plume segment 1), which also carried most of the radionuclides. This should have caused more of the radionuclides to be carried further downwind than in ST #2. This may have accounted for at least some of the differences in trends between the two STs in the nearfield.

5. SENSITIVITY STUDIES

The results from a set of sensitivity studies are presented in this section. These sensitivity studies test whether the relationship between the HYSPLIT and Gaussian ATD calculations illustrated in Section 4 is affected by:

1. the source of the meteorological data set used for the HYSPLIT or Gaussian ATD calculations;
2. the MacMetGen stability class determination method used to generate the MACCS-formatted meteorological file for the Gaussian ATD calculations (HYSPLIT ATD calculations do not use stability classes); and
3. whether the long-range Gaussian dispersion model plume spread coefficients are expressed as a function of time or distance.

The same consequence metrics shown for the benchmark analyses (as described in Section 3.6) are shown here in the sensitivity studies. Two of the five sites were selected for the sensitivity studies as a reduced set for simplicity. Site A was selected because a meteorological data file created from local weather-tower measurements was available. Site D was selected to evaluate the effect of different meteorology on the trends. It should be noted that the sensitivity studies are variants of the Gaussian model and don't affect the parameterization of the HYSPLIT model. The sensitivity to the source of the meteorological data set study includes HYSPLIT runs but does not change the parameterization of the HYSPLIT model. They are all therefore cases to test the hypothesis that trajectory averaging will result in reasonable agreement (approximately a factor of two) between the traditional MACCS Gaussian ATD model and the higher-fidelity MACCS/HYSPLIT coupled ATD model for computing consequence distributions.

5.1. Meteorological Data Source

The first sensitivity study investigates the potential differences that could arise in the results due to the source of meteorological input data. In addition to the NAM 12-km 2008 meteorological data set (labeled as NAM12) used in the benchmark analyses, two other meteorological data sets are evaluated to demonstrate the potential impact on atmospheric dispersion modeling and resulting consequences. This sensitivity analysis is conducted for Site A (a large river valley) and Site D (a site on the Atlantic coast with potential for sea breezes). This analysis provides perspective on the magnitude of the differences in the benchmark analyses.

The first alternative meteorological data set (labeled as WRF27) is created using the Weather Research and Forecasting (WRF) model (Skamarock et al., 2008), using the North American Regional Reanalysis (NARR) data set as initial conditions, and nudged by the observational data from the National Centers for Environmental Prediction (NCEP) Automated Data Processing (ADP) global surface data sets. Model output for each hour is converted to a 27-km Lambert conformal grid centered over North America (216 x 174 cells). Data at 34 sigma levels (vertical) are included for six variables: pressure, temperature, u, v, and w wind velocities, and relative humidity. This produces an hourly, 27-km resolution, data set for North America that is put into a daily file and made available online at the ARL server via ftp (NOAA, 2017). Meteorological data were extracted from the WRF27 database for the year 2008 for Sites A and D and converted to a MACCS-formatted (single weather station) meteorological data file. The full WRF27 database was used for the HYSPLIT ATD model calculations. This meteorological data set can only capture complex meteorological behavior (e.g., land/sea breeze, valley flows, etc.) at length scales around 27 km or greater.

The second alternative meteorological data set is generated from local weather-tower data from 2008 (labeled as Site) for Site A only. No site file for Site D was available. Meteorological data at one-hour intervals include surface wind direction, wind speed, stability class, and precipitation rate. This data set only supports Gaussian ATD model calculations; it does not contain sufficient information to support HYSPLIT ATD model calculations. This meteorological data set cannot capture complex meteorological behavior (e.g., land/sea breeze, valley flows, etc.) for which the wind field is a function of location on the grid.

To capture complex meteorological behavior (e.g., land/sea breeze, valley flows, etc.) at finer length scales, a finer resolution meteorological data set is required. One approach to generate this finer resolution meteorological data set is to start with the WRF27 data set as initial and boundary conditions and use WRF to calculate finer resolution data sets. The WRF runs could be nudged with local observational data to improve the evaluation of complex wind fields. Performing a WRF analysis would significantly increase the overall computation cost of the analysis and should be balanced against the needed level of fidelity for an application. For this sensitivity study, no WRF analyses were performed to provide higher resolution meteorological data.

The three sources of data (NAM12, WRF27, and site observational data) support two HYSPLIT calculations (NAM12 and WRF27), using the 3-dimensional, transient, gridded data sets, and three Gaussian calculations using the extracted single-weather-station data from the two gridded data sets plus the local observational data. The meteorological characteristics from the MACCS-formatted meteorological data files for the three meteorological data sets for Site A and the two meteorological data sets for Site D are compared below.

Figure 5-1 and Figure 5-2 show the distribution of wind direction over the course of a year for the three meteorological data sets for Site A and for the two meteorological data sets for Site D. The wind direction distribution is similar between the NAM12 and WRF27 data sets. The observational data set has much higher peaks for SSW and NNE winds compared with the NAM12 and WRF27 data sets. This may be because the resolution of the two gridded data sets is insufficient to capture the river-valley effects near the site.

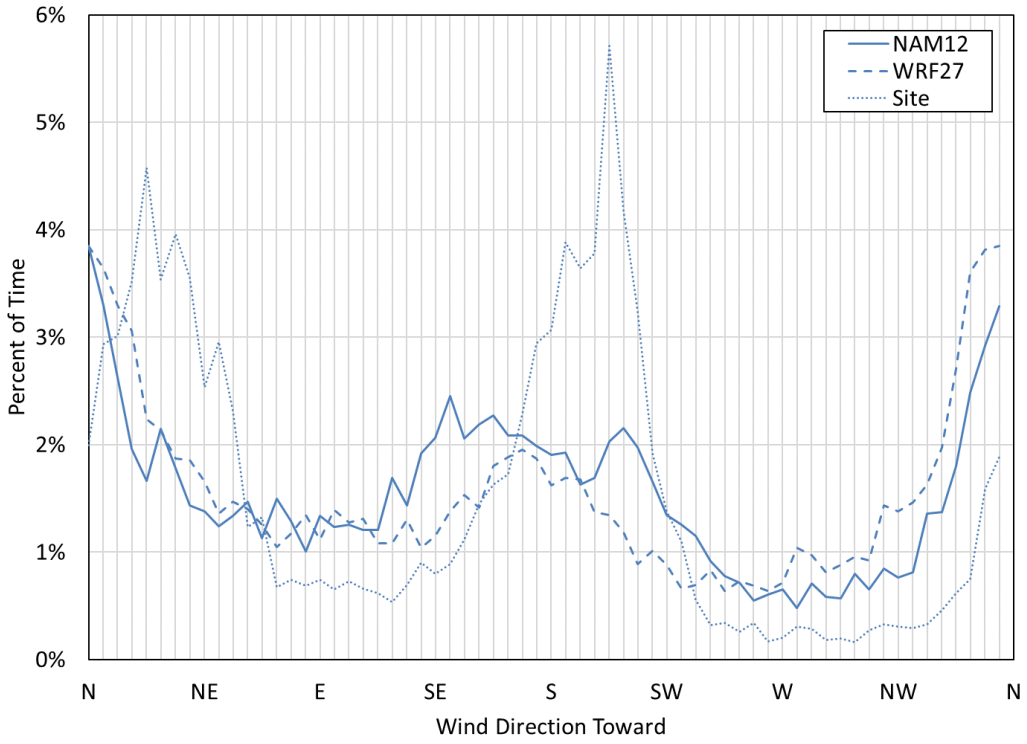

Figure 5-1. Distribution of wind direction over the course of a year for the three meteorological data sets for Site A

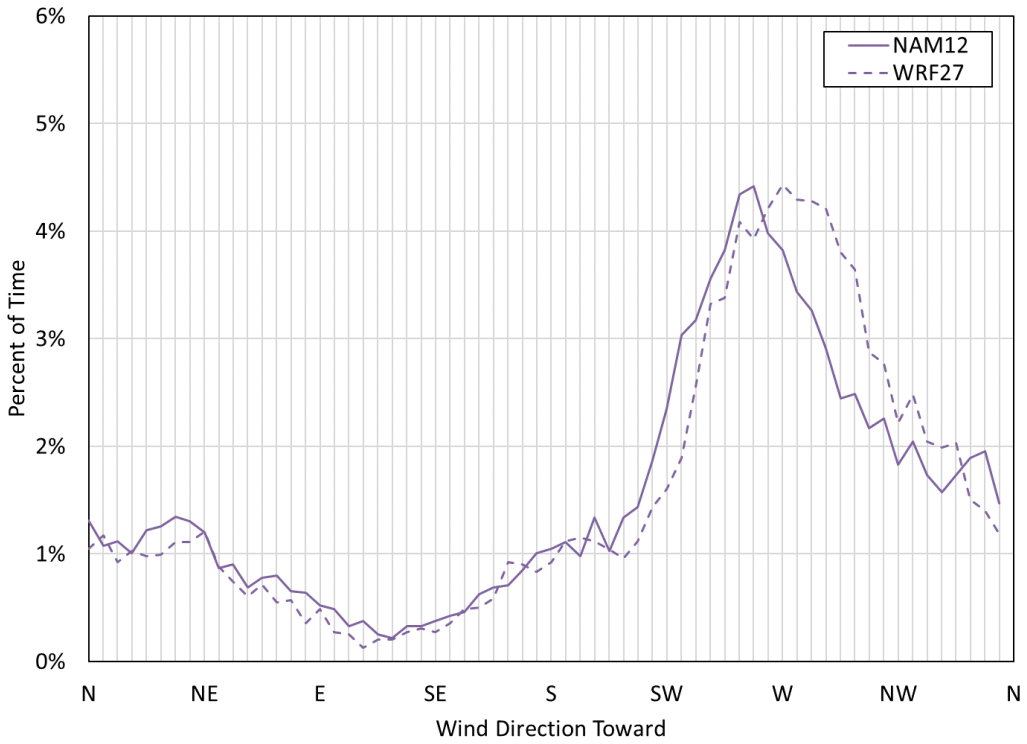

Figure 5-2. Distribution of wind direction over the course of a year for the two meteorological data sets for Site D

Figure 5-3 and Figure 5-4 illustrate the average wind speed as a function of wind direction for the three meteorological data sets for Site A and for the two meteorological data sets for Site D. In general, the NAM12 data set has the highest wind speeds, the Site data set has the lowest wind speeds, and the WRF27 data set is between the other two.

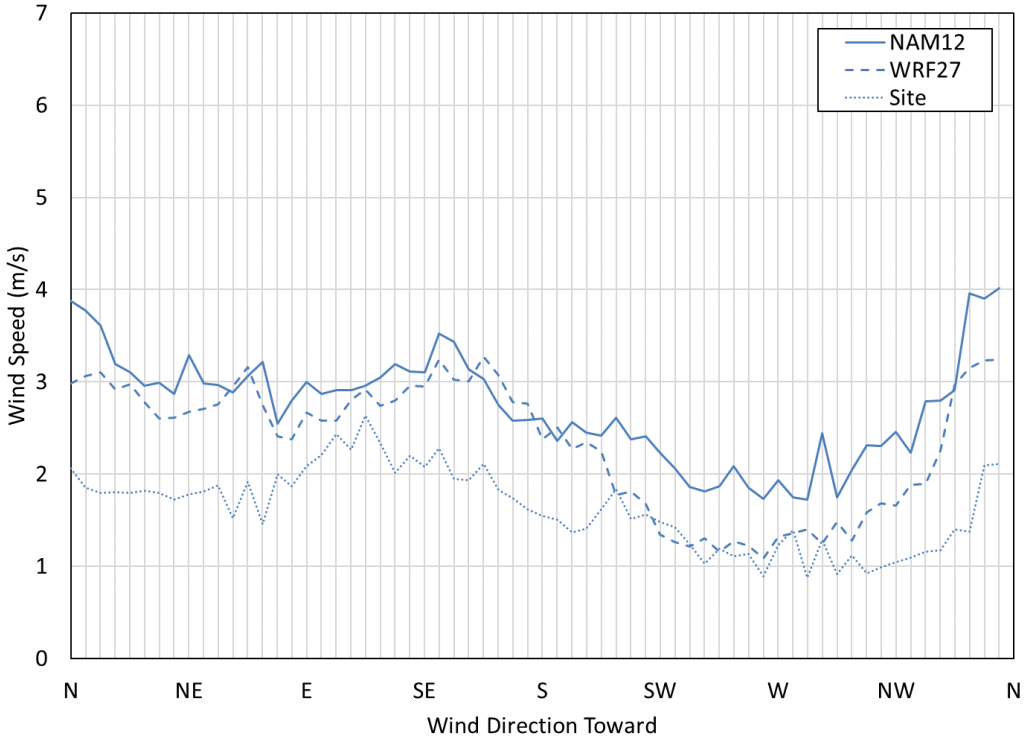

Figure 5-3. Average wind speed as a function of wind direction for the three meteorological data sets for Site A

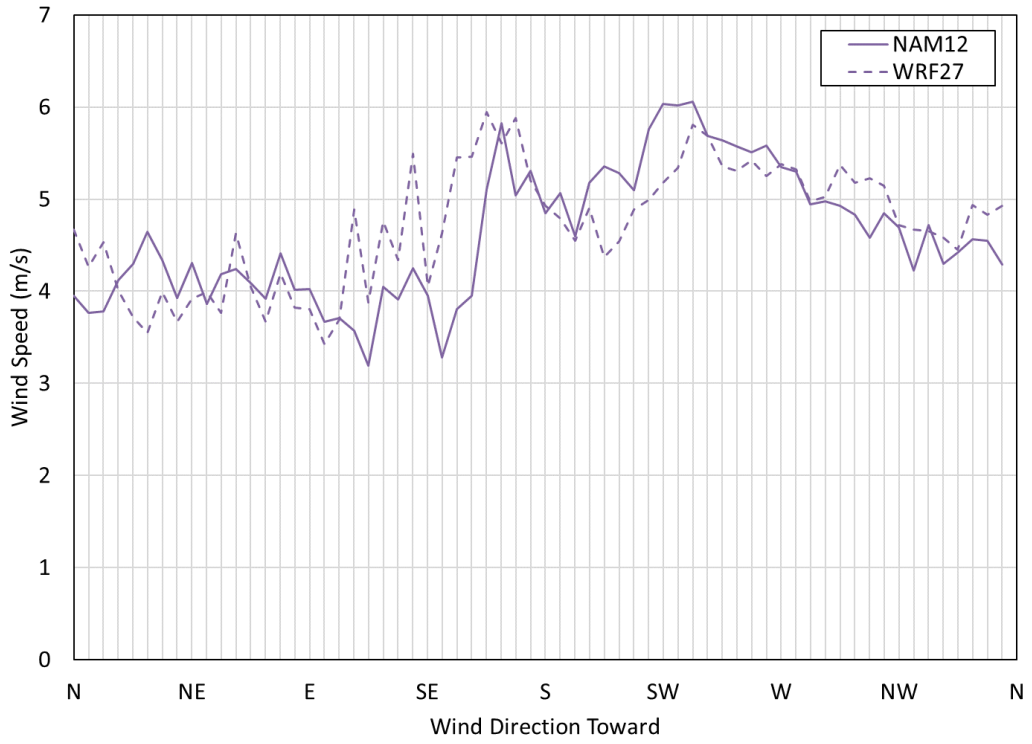

Figure 5-4. Average wind speed as a function of wind direction for the two meteorological data sets for Site D

Figure 5-5 and Figure 5-6 display the average stability class as a function of wind direction for the three meteorological data sets for Site A and Site D, respectively. The stability class is shown ranging from 1 (A, unstable) to 7 (G, stable) and was calculated based on the temperature gradient above the site (DTDZ) using the criteria in (US NRC, 2007) applied to both the NAM12 and WRF27 data sets. For Site A, the NAM12 and Site data sets have similar stability class distributions and the WRF27 data set tends toward more stable conditions compared with the NAM12 and Site data sets when the wind is blowing towards western directions. For Site D, the NAM12 data set tends toward more stable conditions compared with the WRF27 data set for all wind directions. Figure 5-7 and Figure 5-8 show the distribution of stability class as a function of time of day for the three data sets for Site A and two data sets for Site D, respectively.

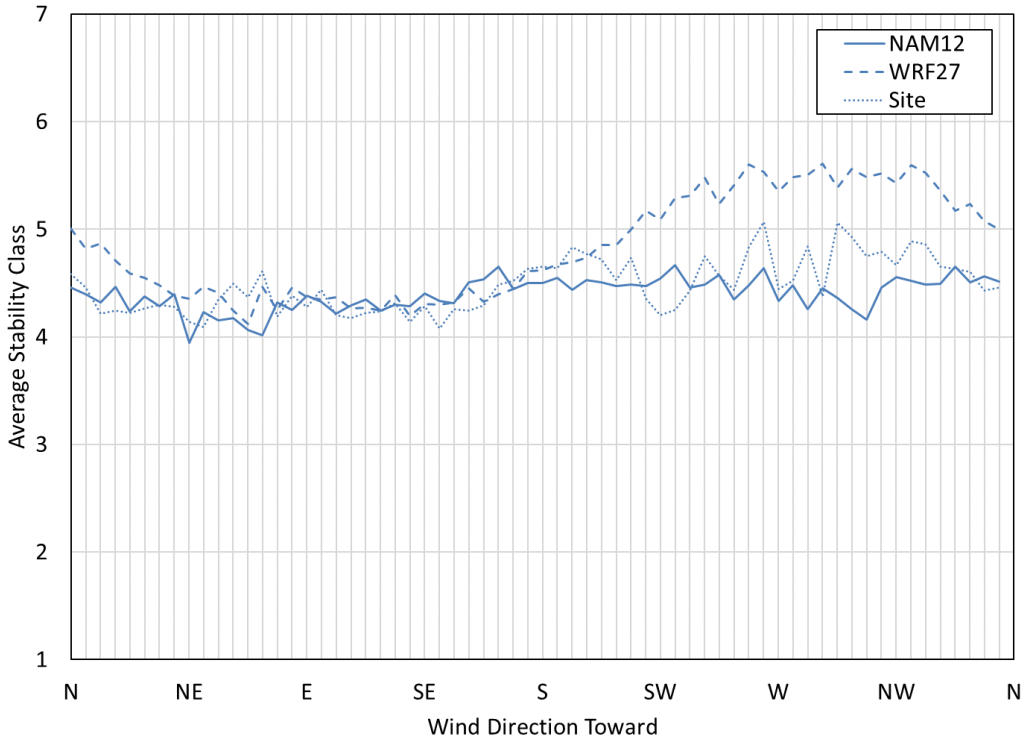

Figure 5-5. Average stability class as a function of wind direction for the three meteorological data sets for Site A

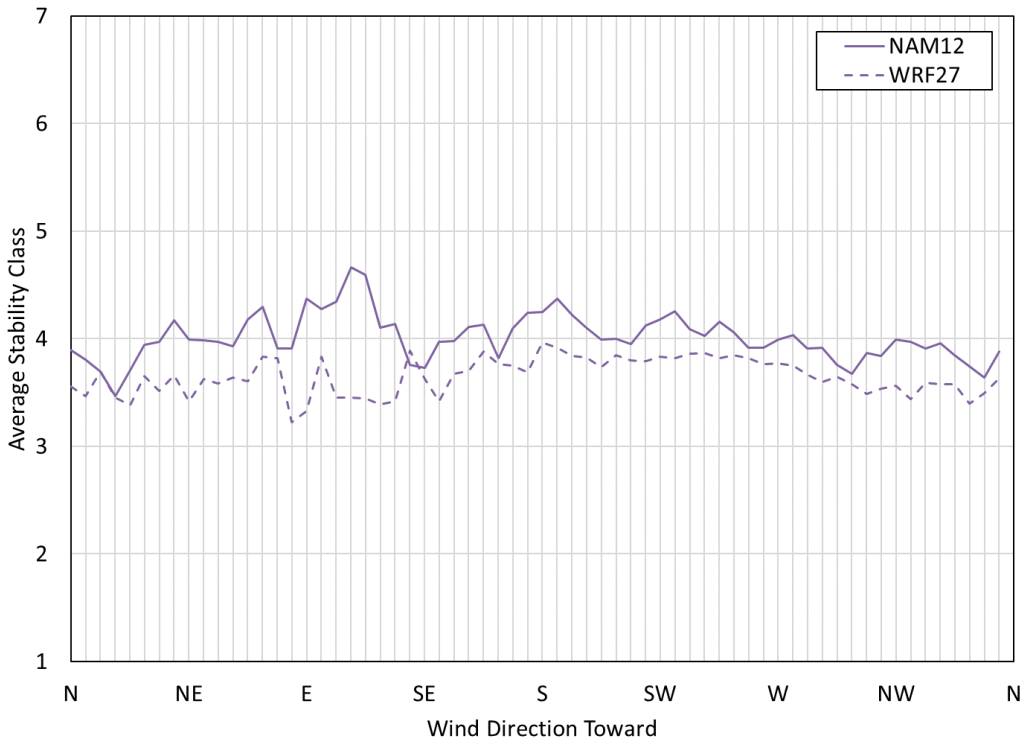

Figure 5-6. Average stability class as a function of wind direction for the two meteorological data sets for Site D

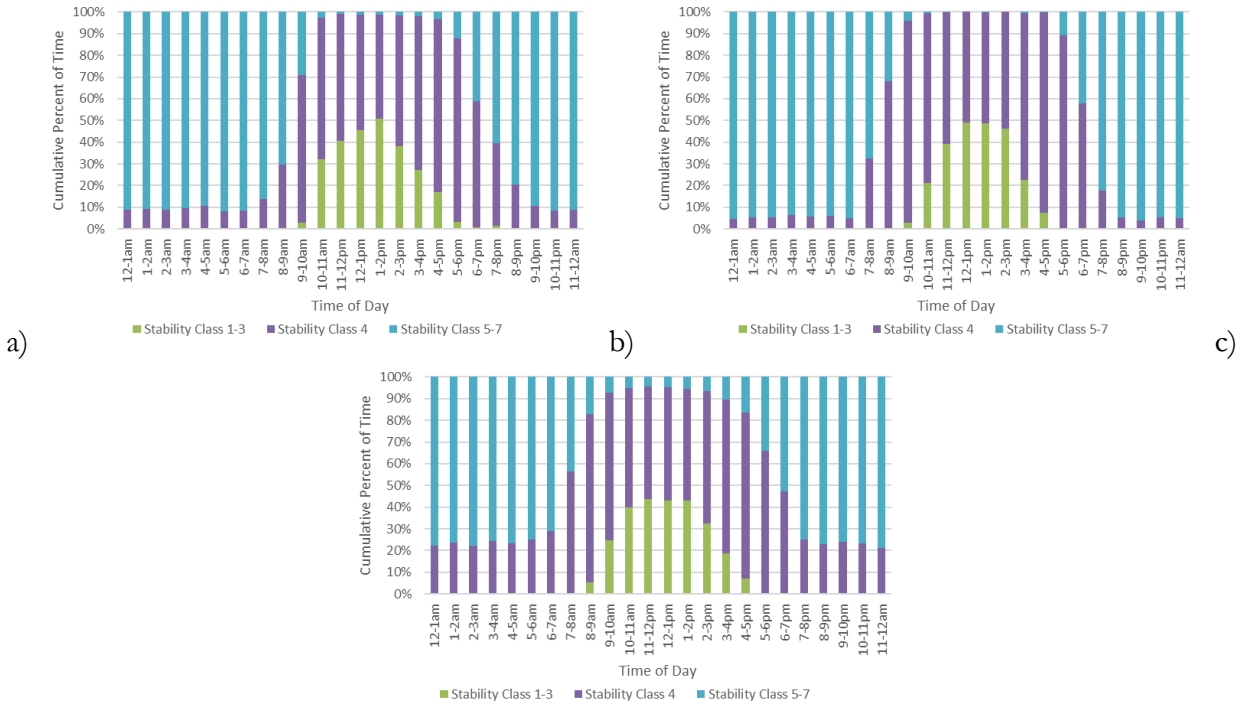

Figure 5-7. Stability class distribution as a function of time of day for the a) NAM12, b) WRF27, and c) Site meteorological data sets for Site A

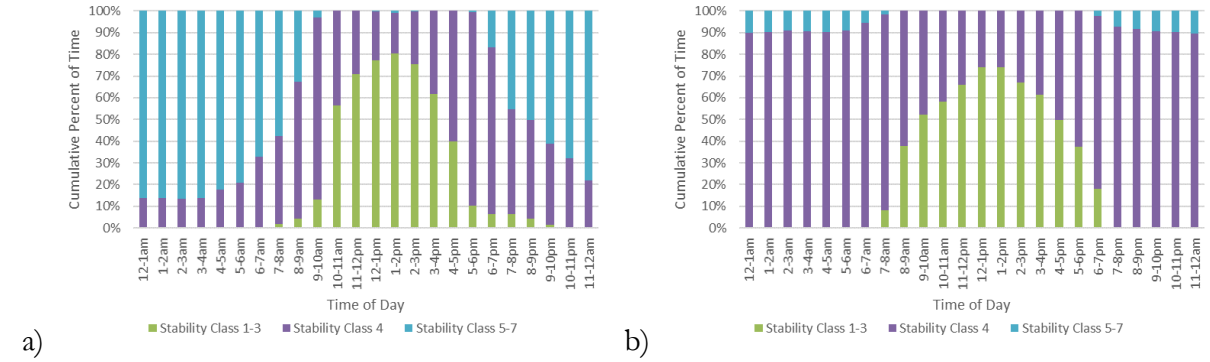

Figure 5-8. Stability class distribution as a function of time of day for the a) NAM12, and b) WRF27 data sets for Site D

Figure 5-9 and Figure 5-10 show the average precipitation rate as a function of wind direction for the three meteorological data sets for Site A and two meteorological data sets for Site D, respectively. For Site A, the total precipitation over the year for the NAM12, WRF27, and Site data sets are 42 in, 16 in, and 40 in, respectively. For Site D, the total precipitation over the year for the NAM12 and WRF27 data sets are 39 in and 16 in, respectively. The WRF27 data set has the lowest amount of precipitation. The NAM12 data set appears to have the highest precipitation rate when the wind is towards the west for Site A and towards the south-southeast direction for Site D. There is no significant peak in the precipitation rate for the Site data set.

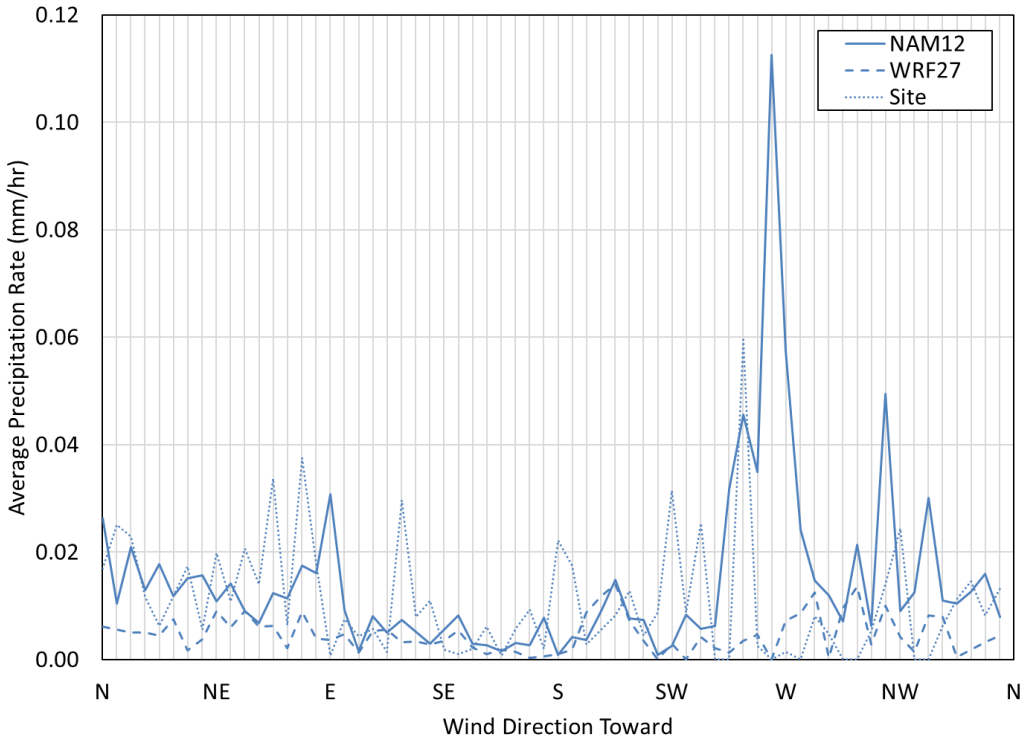

Figure 5-9. Average precipitation rate as a function of wind direction for the three meteorological data sets for Site A

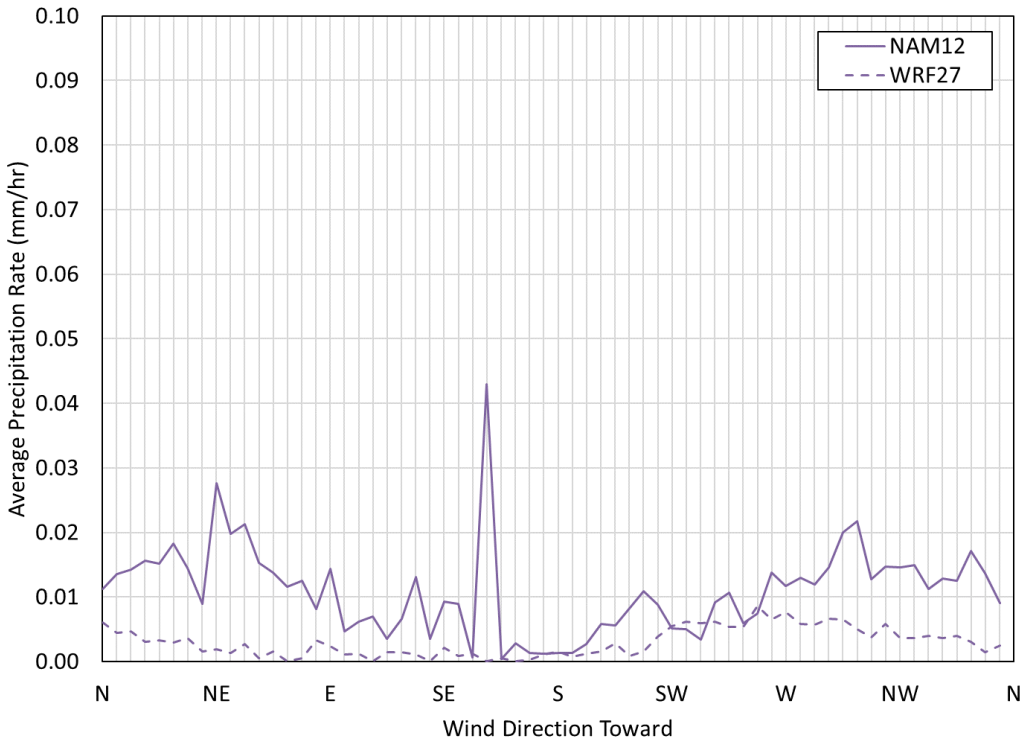

Figure 5-10. Average precipitation rate as a function of wind direction for the two meteorological data sets for Site D

The comparisons below are presented first for the Gaussian ATD model and subsequently for the HYSPLIT ATD model. The first comparison shows the results from the Gaussian ATD model runs with both source terms for the three meteorological data sets for Site A and the NAM12 and WRF27 meteorological data sets for Site D. The second comparison shows the results from the HYSPLIT ATD model runs with the NAM12 and WRF27 meteorological data sets for both source terms for the two sites.

5.1.1. Gaussian Comparison

5.1.1.1. Site A

5.1.1.1.1. Source Term #1

Results for the Gaussian ATD model for Site A with ST #1 using the three meteorological data sets are compared for peak air concentration, peak ground deposition, land contamination area, peak dose, early fatality risk, population dose, latent cancer fatality risk, and economic loss (as described in Section 3.6) in Figure 5-11 through Figure 5-18. The annual statistics for these measures are shown with different colors, where the mean values are in black, the 5th percentile values are shown in blue, and the 95th percentile values are shown in green. HYSPLIT results are shown as dashed lines and Gaussian model results are shown as solid lines. The normalized results are shown as a function of distance, rather than the ratio of Gaussian and HYSPLIT results, to allow for the trends with distance to be observed. Some results are zero for early fatality risk, so they cannot be shown on the log scale used in the figures. Discussion of the difference seen in these figures is provided below in Section 5.1.3.

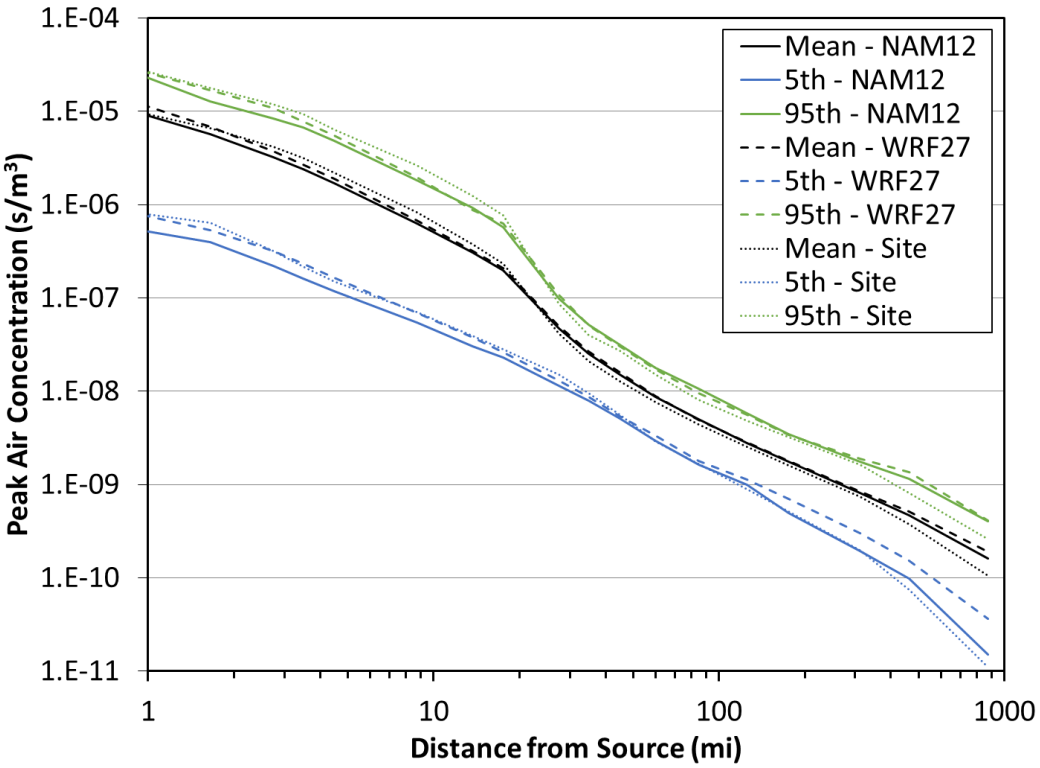

Figure 5-11. Comparison of peak air concentration for the three meteorological data sets at Site A with ST #1 using the Gaussian ATD model

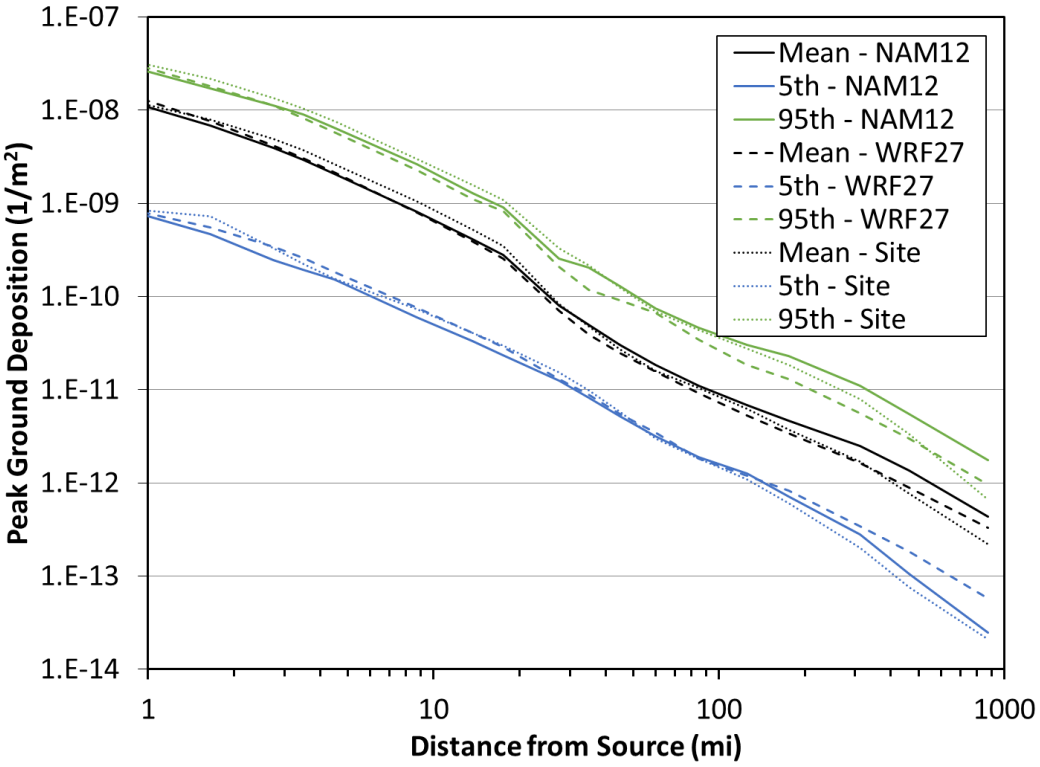

Figure 5-12. Comparison of peak ground deposition for the three meteorological data sets at Site A with ST #1 using the Gaussian ATD model

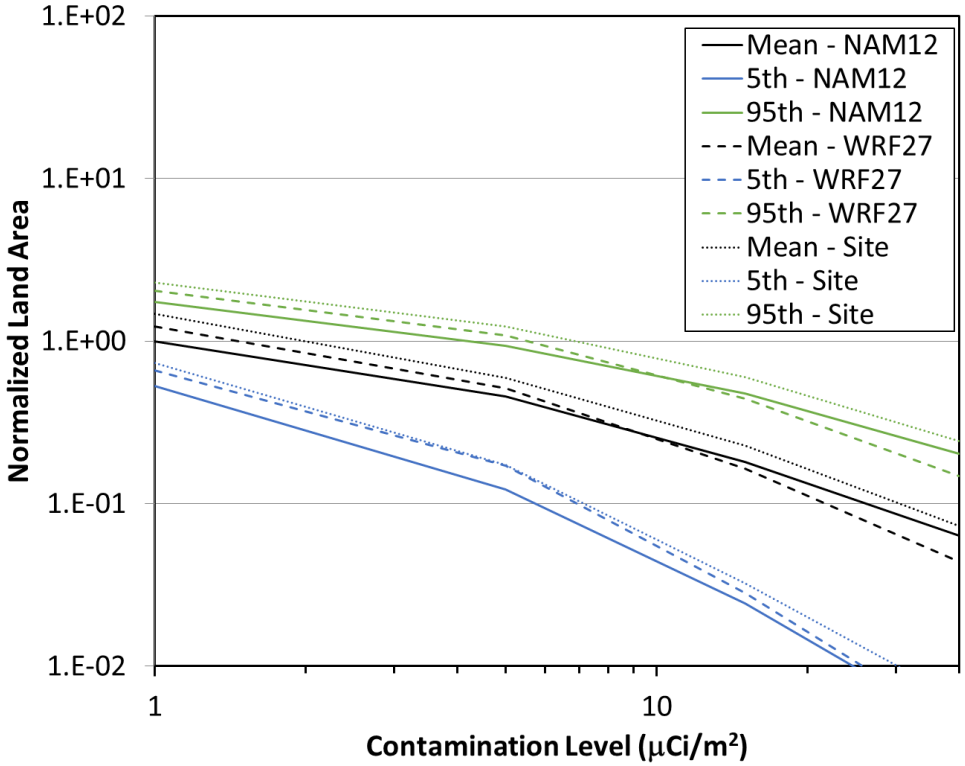

Figure 5-13. Comparison of land contamination area for the three meteorological data sets at Site A with ST #1 using the Gaussian ATD model

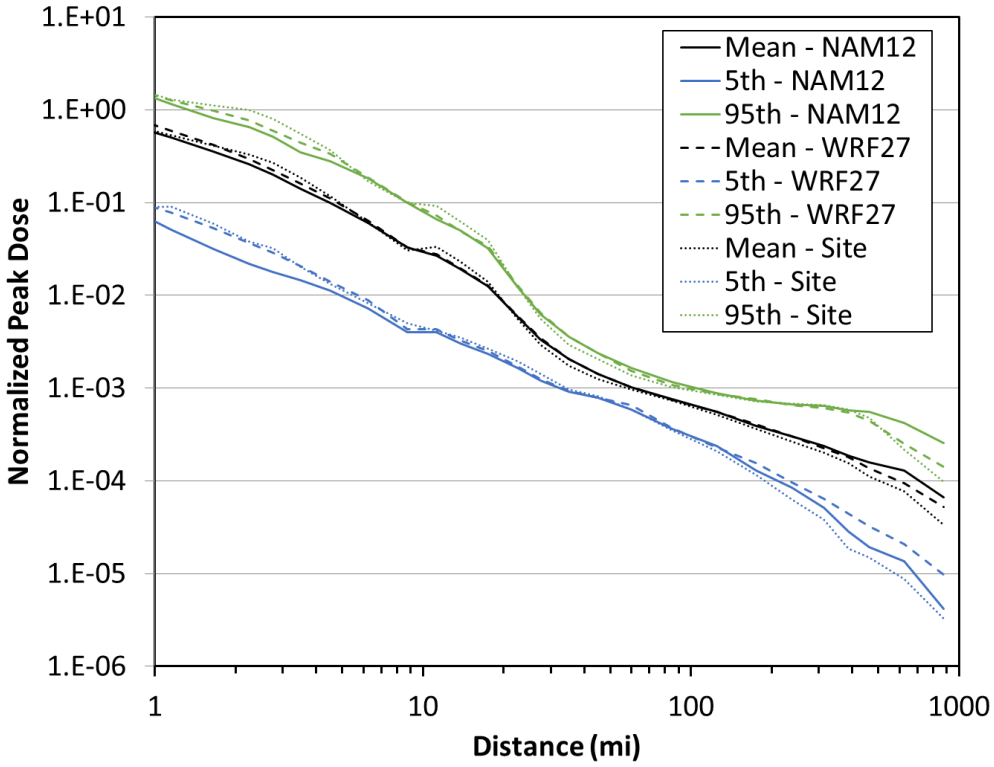

Figure 5-14. Comparison of peak dose for the three meteorological data sets at Site A with ST #1 using the Gaussian ATD model

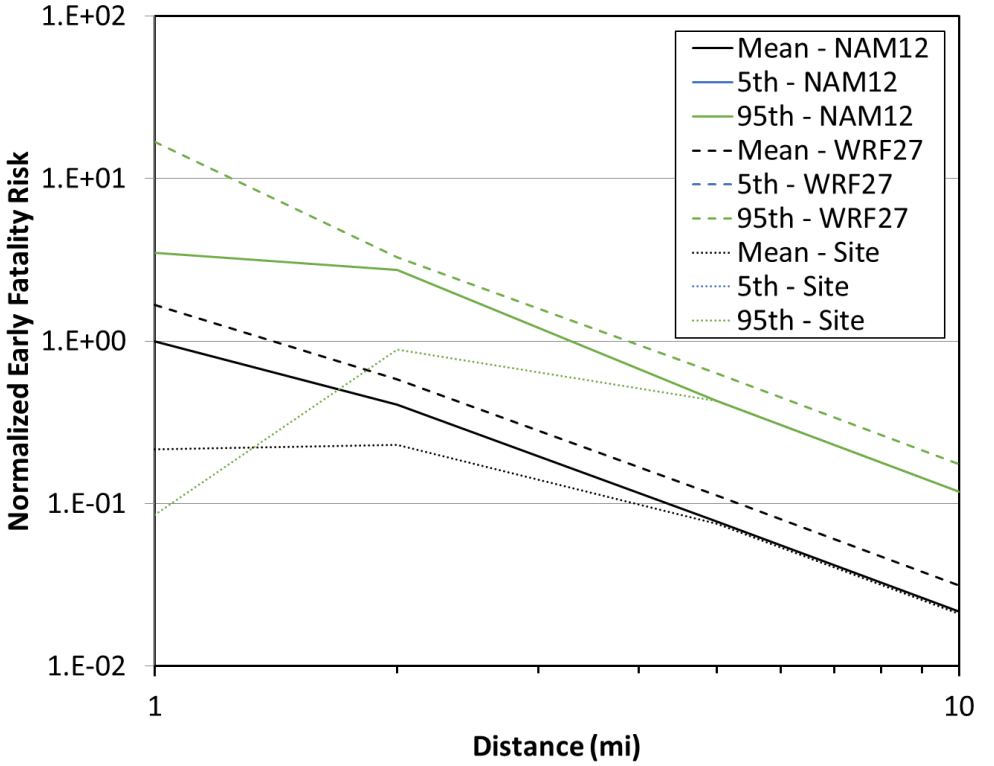

Figure 5-15. Comparison of early fatality risk for the three meteorological data sets at Site A with ST #1 using the Gaussian ATD model

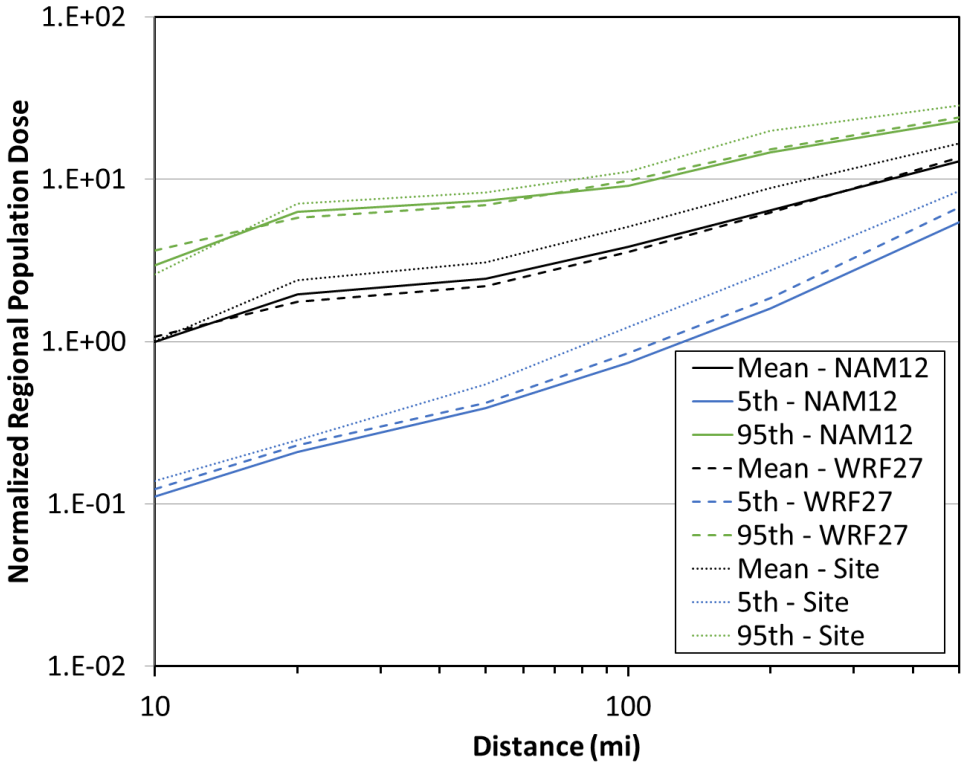

Figure 5-16. Comparison of population dose for the three meteorological data sets at Site A with ST #1 using the Gaussian ATD model

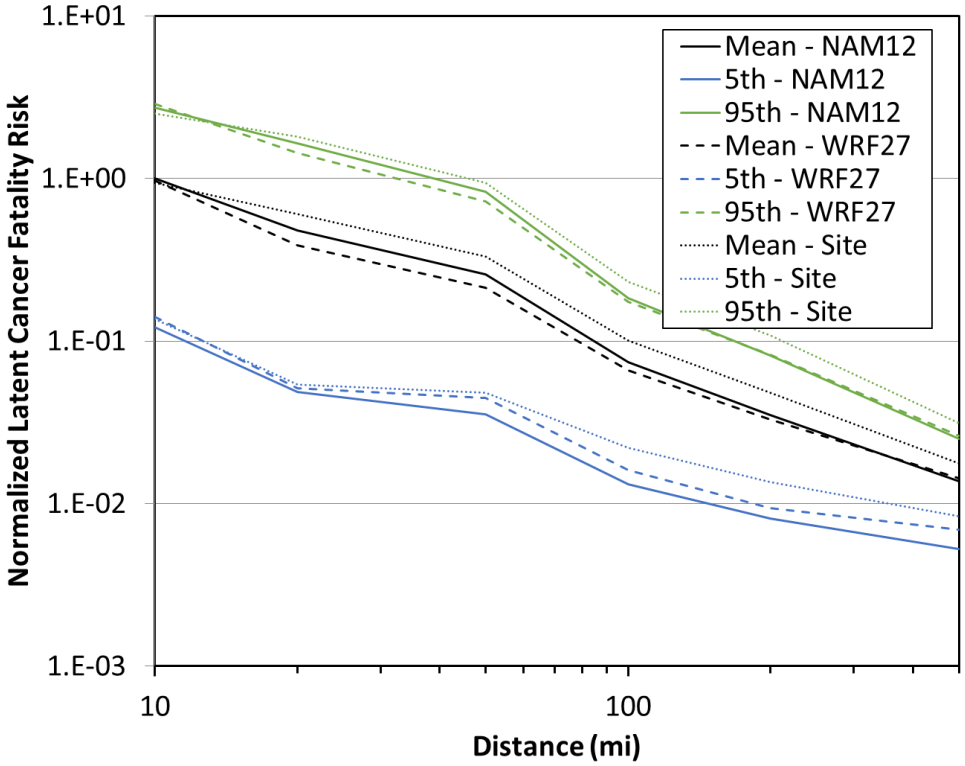

Figure 5-17. Comparison of latent cancer fatality risk for the three meteorological data sets at Site A with ST #1 using the Gaussian ATD model

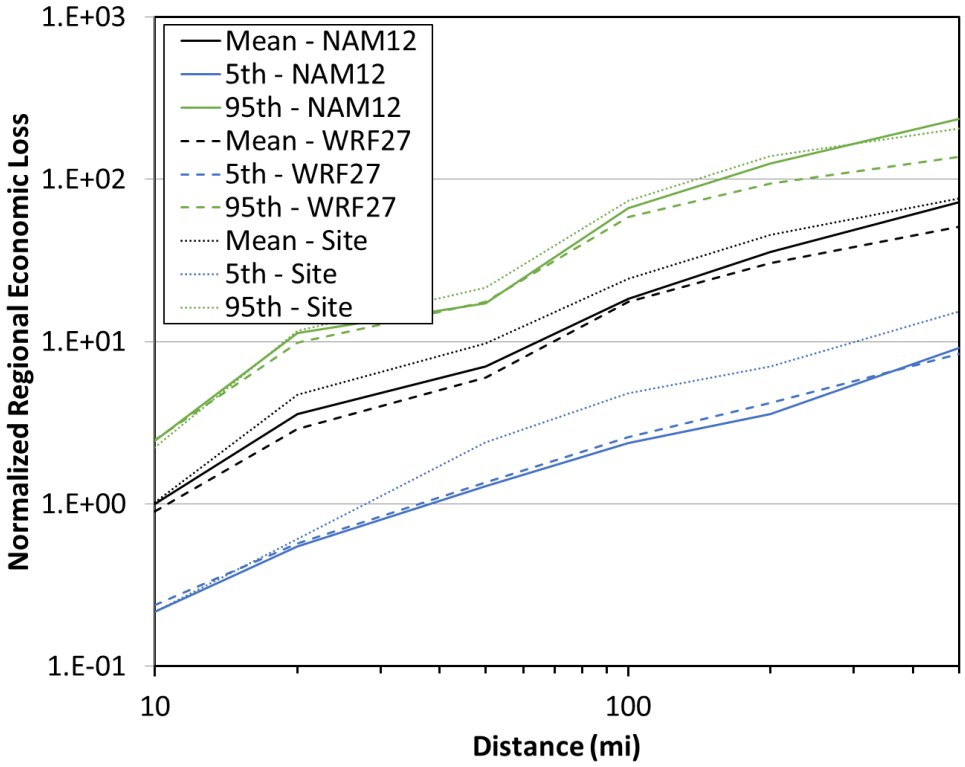

Figure 5-18. Comparison of economic loss for the three meteorological data sets at Site A with ST #1 using the Gaussian ATD model

5.1.1.1.2. Source Term #2

Results for the Gaussian ATD model for Site A with ST #2 using the three meteorological data sets are compared for peak air concentration, peak ground deposition, land contamination area, peak dose, early fatality risk, population dose, latent cancer fatality risk, and economic loss (as described in Section 3.6) in Figure 5-19 through Figure 5-26. The annual statistics for these measures are shown with different colors, where the mean values are in black, the 5th percentile values are shown in blue, and the 95th percentile values are shown in green. HYSPLIT results are shown as dashed lines and Gaussian model results are shown as solid lines. The normalized results are shown as a function of distance, rather than the ratio of Gaussian and HYSPLIT results, to allow for the trends with distance to be observed. Some results are zero for early fatality risk, so they cannot be shown on the log scale used in the figures. Discussion of the difference seen in these figures is provided below in Section 5.1.3.

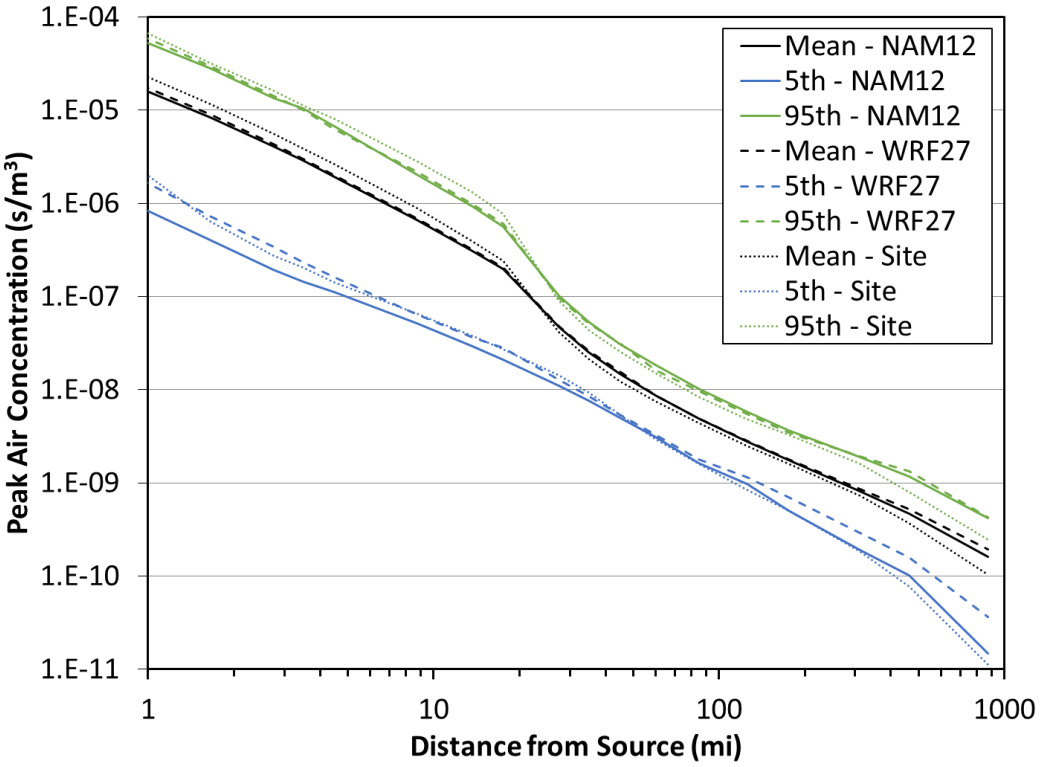

Figure 5-19. Comparison of peak air concentration for the three meteorological data sets at Site A with ST #2 using the Gaussian ATD model

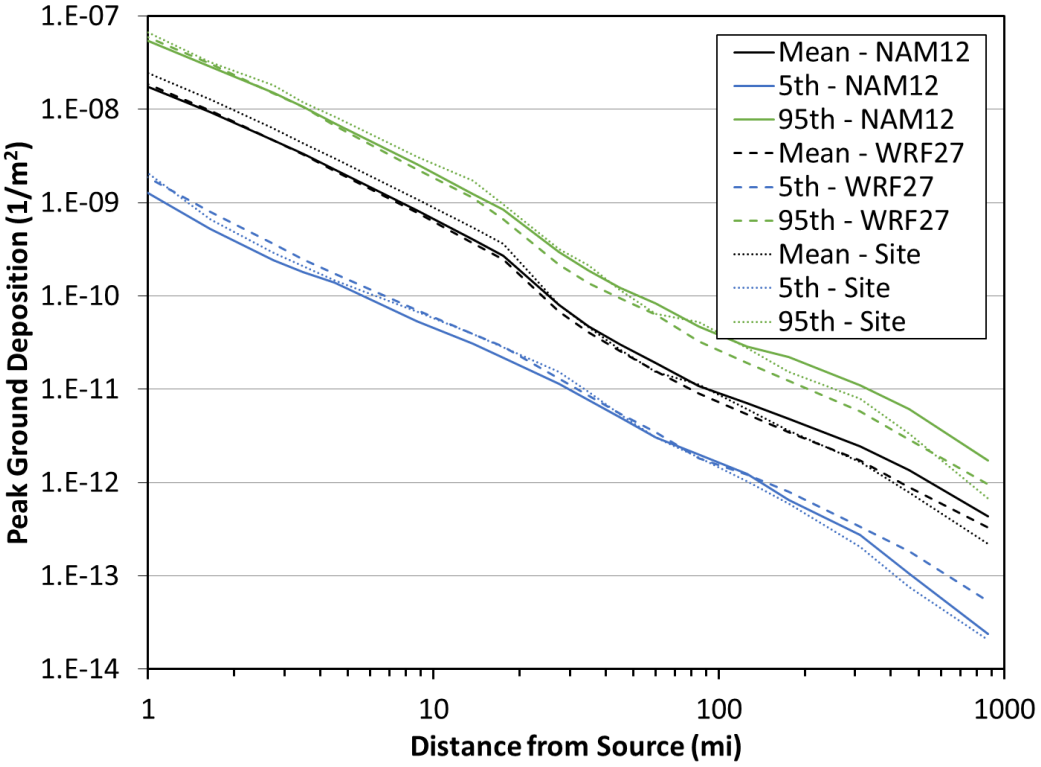

Figure 5-20. Comparison of peak ground deposition for the three meteorological data sets at Site A with ST #2 using the Gaussian ATD model

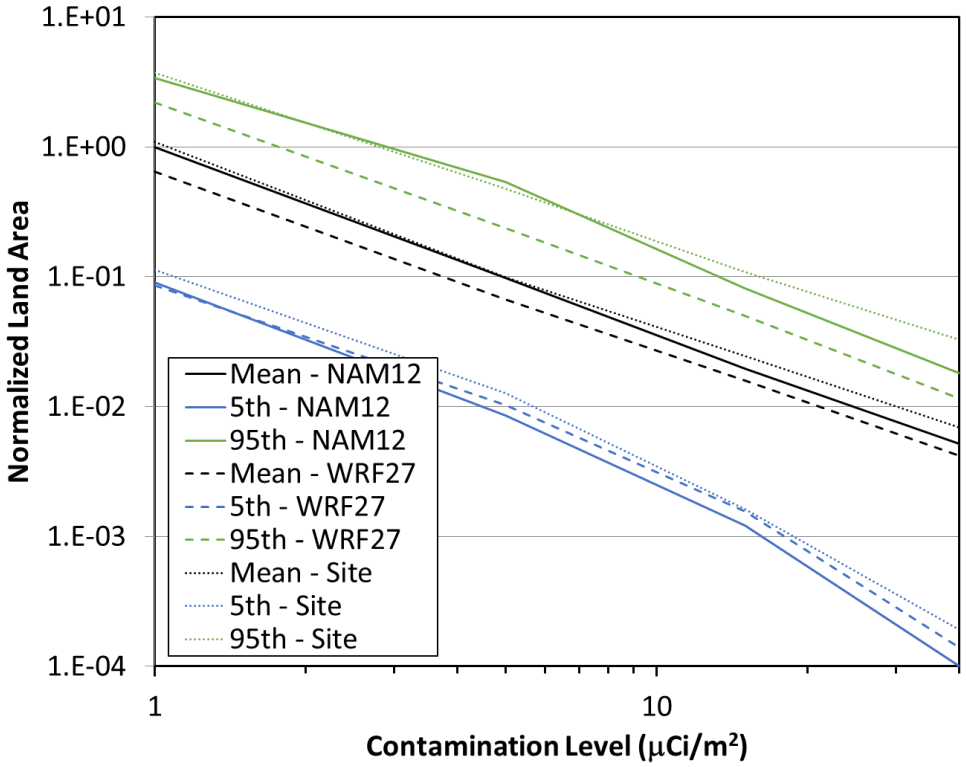

Figure 5-21. Comparison of land contamination area for the three meteorological data sets at Site A with ST #2 using the Gaussian ATD model

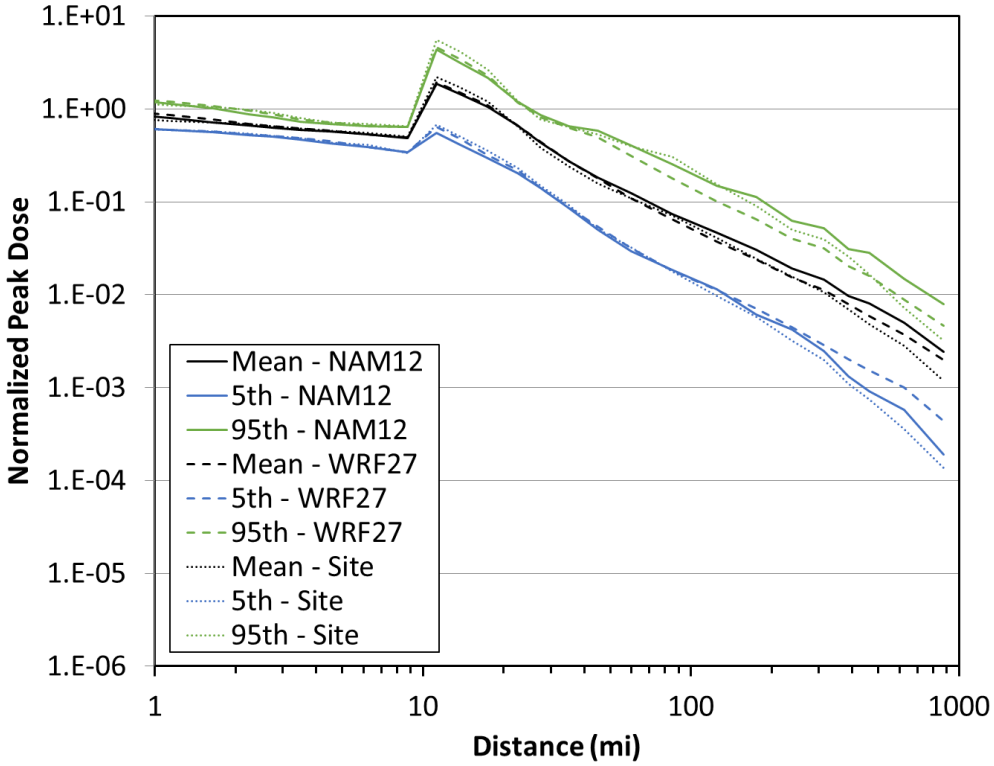

Figure 5-22. Comparison of peak dose for the three meteorological data sets at Site A with ST #2 using the Gaussian ATD model

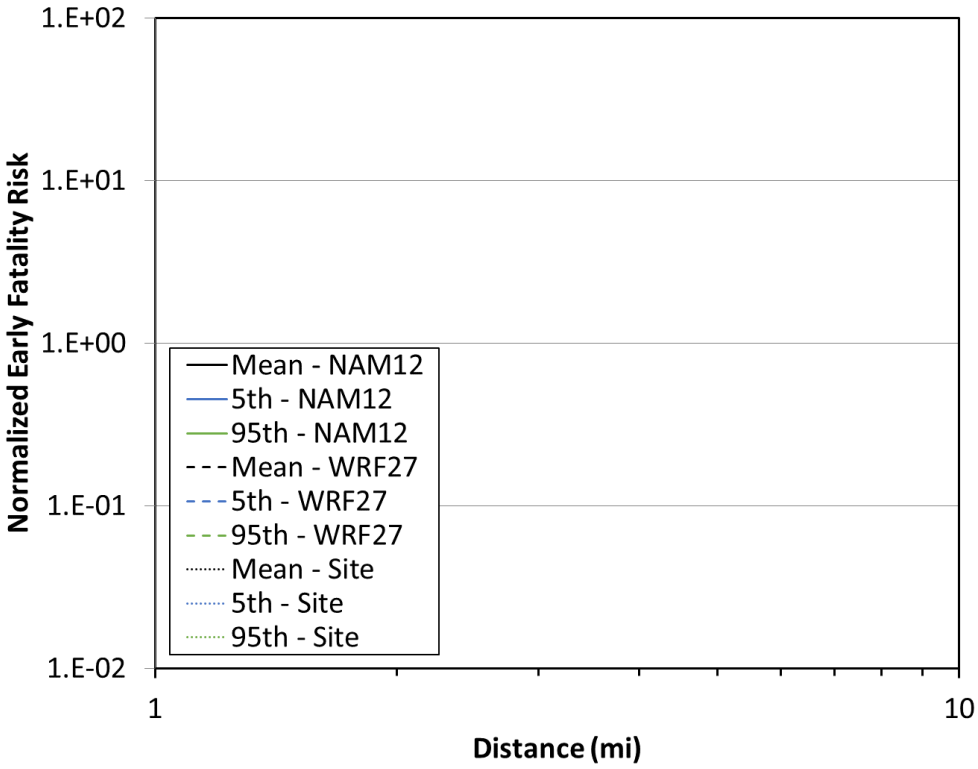

Figure 5-23. Comparison of early fatality risk for the three meteorological data sets at Site A with ST #2 using the Gaussian ATD model

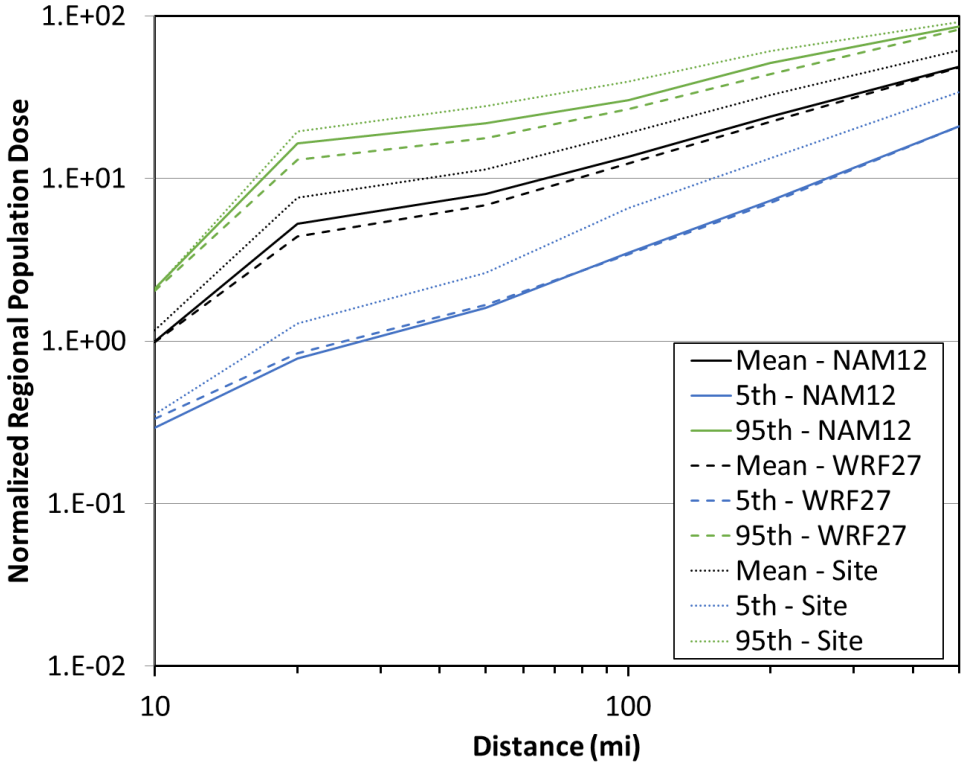

Figure 5-24. Comparison of population dose for the three meteorological data sets at Site A with ST #2 using the Gaussian ATD model

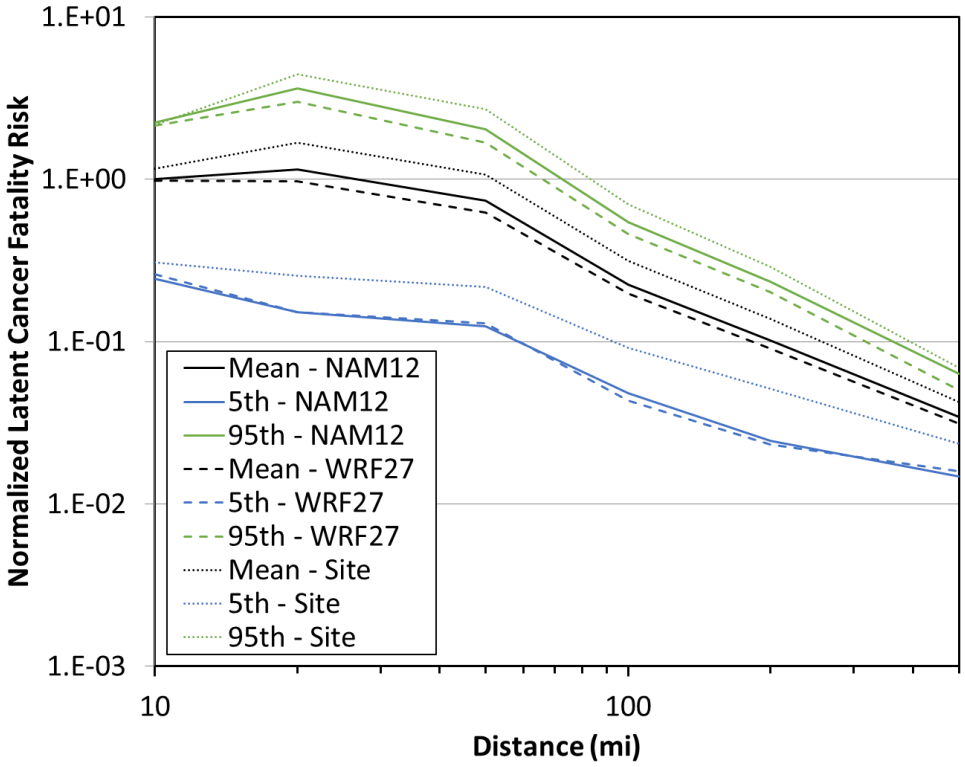

Figure 5-25. Comparison of latent cancer fatality risk for the three meteorological data sets at Site A with ST #2 using the Gaussian ATD model

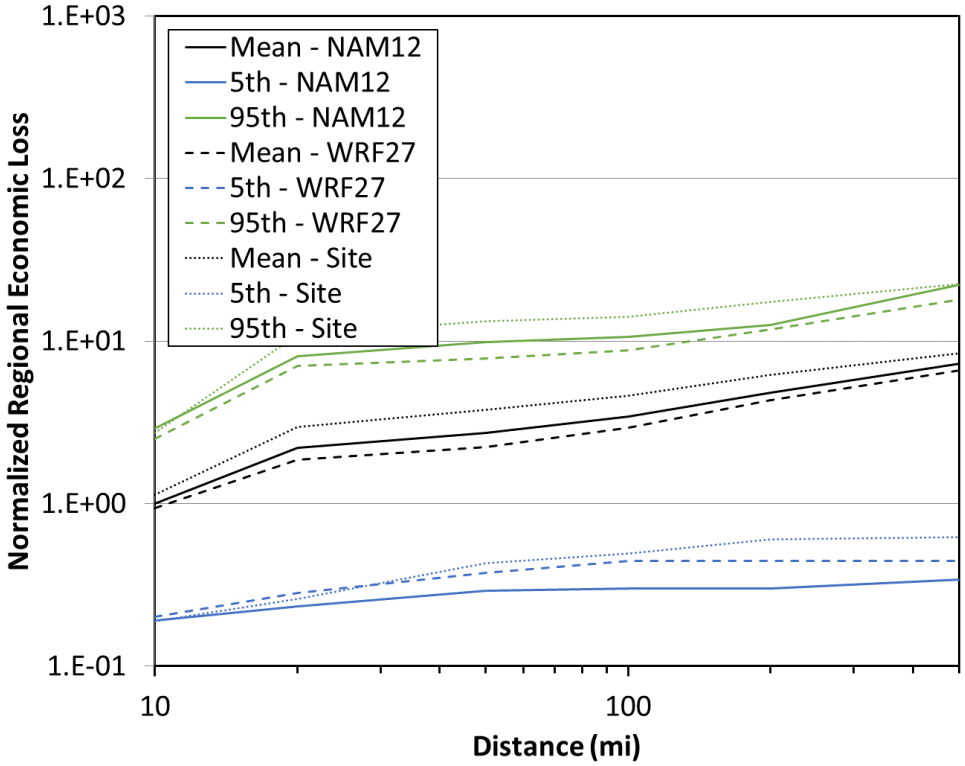

Figure 5-26. Comparison of economic loss for the three meteorological data sets at Site A with ST #2 using the Gaussian ATD model

5.1.1.2. Site D

5.1.1.2.1. Source Term #1

Results for the Gaussian ATD model for Site D with ST #1 using the two meteorological data sets are compared for peak air concentration, peak ground deposition, land contamination area, peak dose, early fatality risk, population dose, latent cancer fatality risk, and economic loss (as described in Section 3.6) in Figure 5-27 through Figure 5-34. The annual statistics for these measures are shown with different colors, where the mean values are in black, the 5th percentile values are shown in blue, and the 95th percentile values are shown in green. HYSPLIT results are shown as dashed lines and Gaussian model results are shown as solid lines. The normalized results are shown as a function of distance, rather than the ratio of Gaussian and HYSPLIT results, to allow for the trends with distance to be observed. Some results are zero for early fatality risk, so they cannot be shown on the log scale used in the figures. Discussion of the difference seen in these figures is provided below in Section 5.1.3.

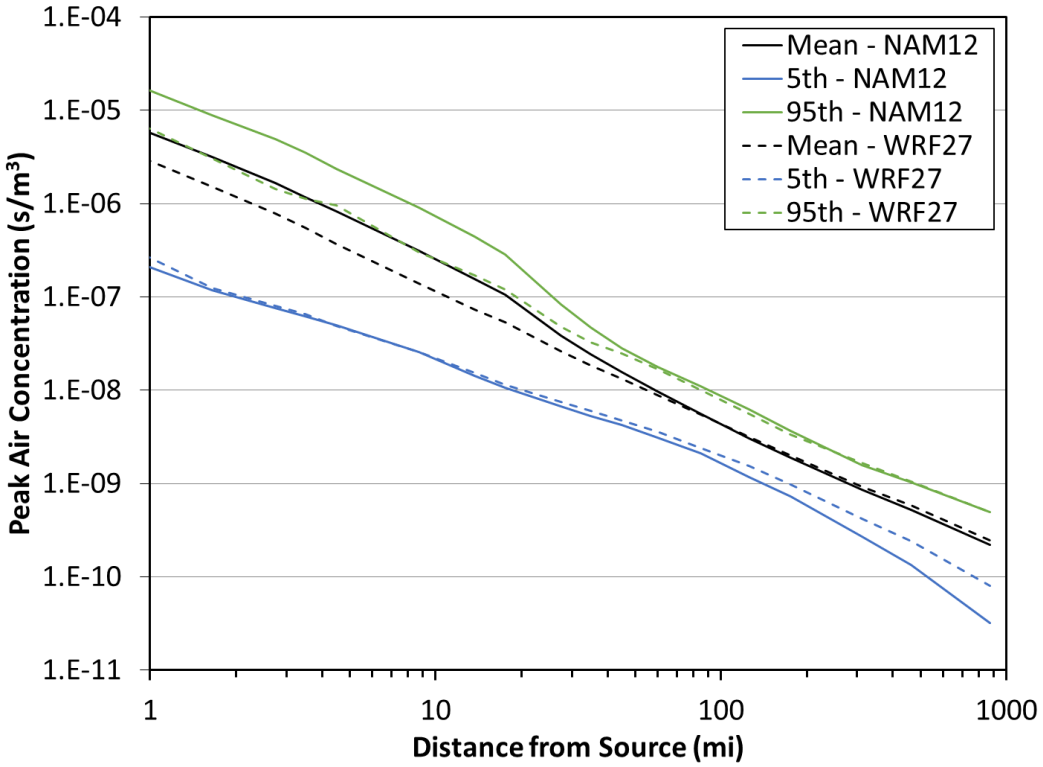

Figure 5-27. Comparison of peak air concentration for the two meteorological data sets at Site D with ST #1 using the Gaussian ATD model

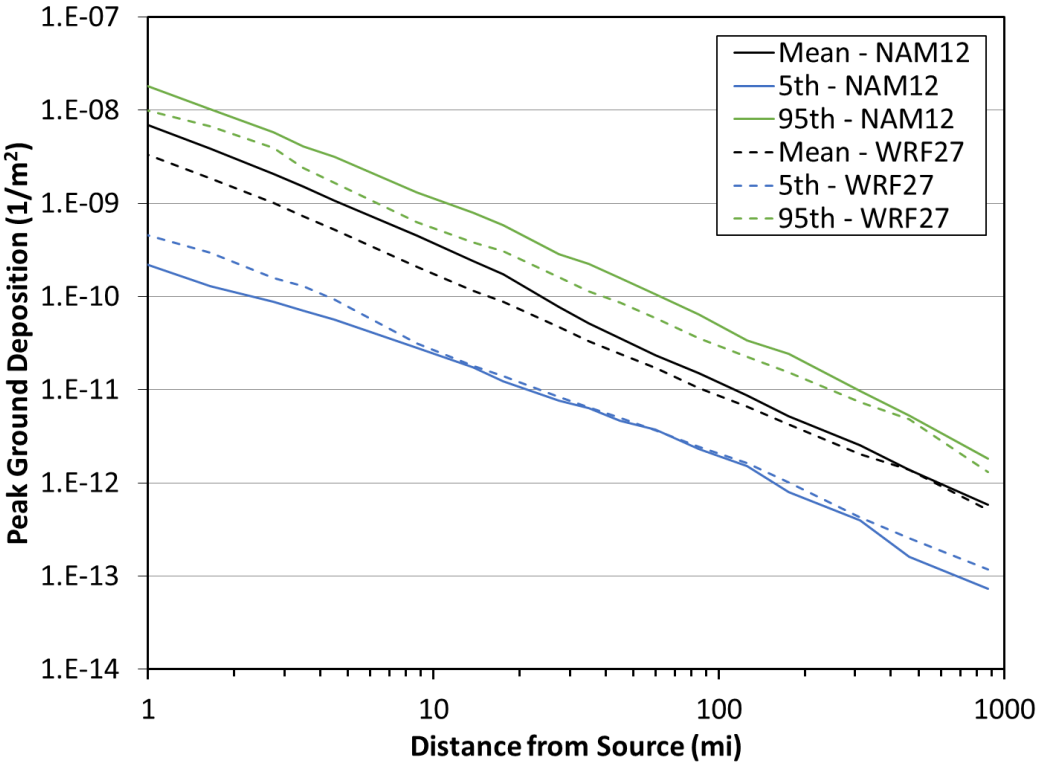

Figure 5-28. Comparison of peak ground deposition for the two meteorological data sets at Site D with ST #1 using the Gaussian ATD model

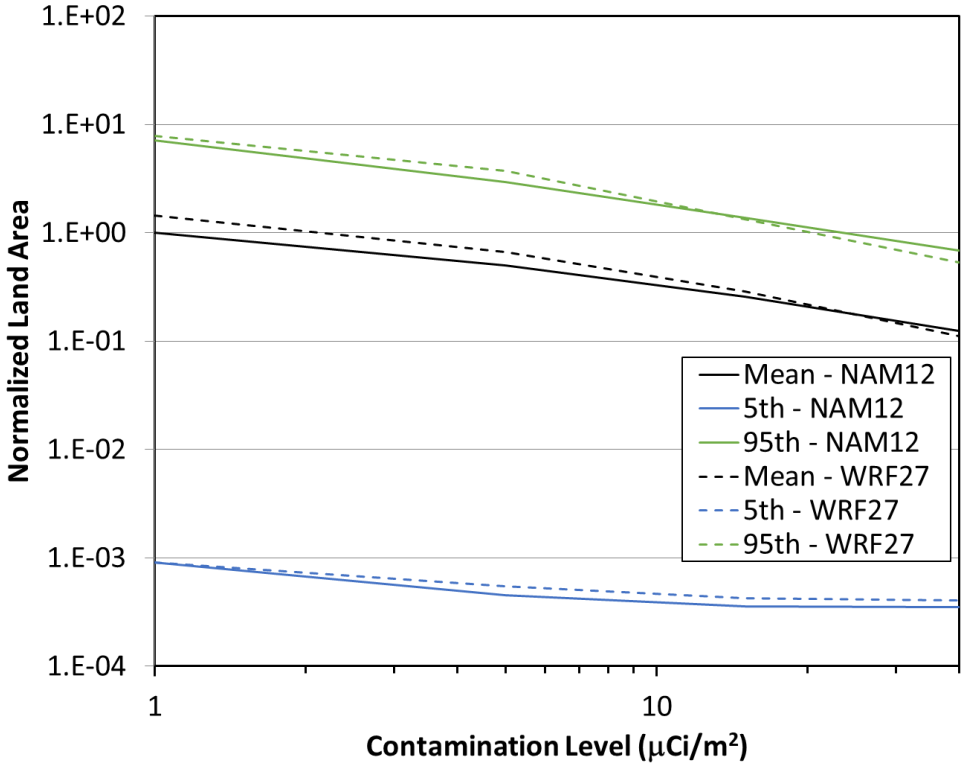

Figure 5-29. Comparison of land contamination area for the two meteorological data sets at Site D with ST #1 using the Gaussian ATD model

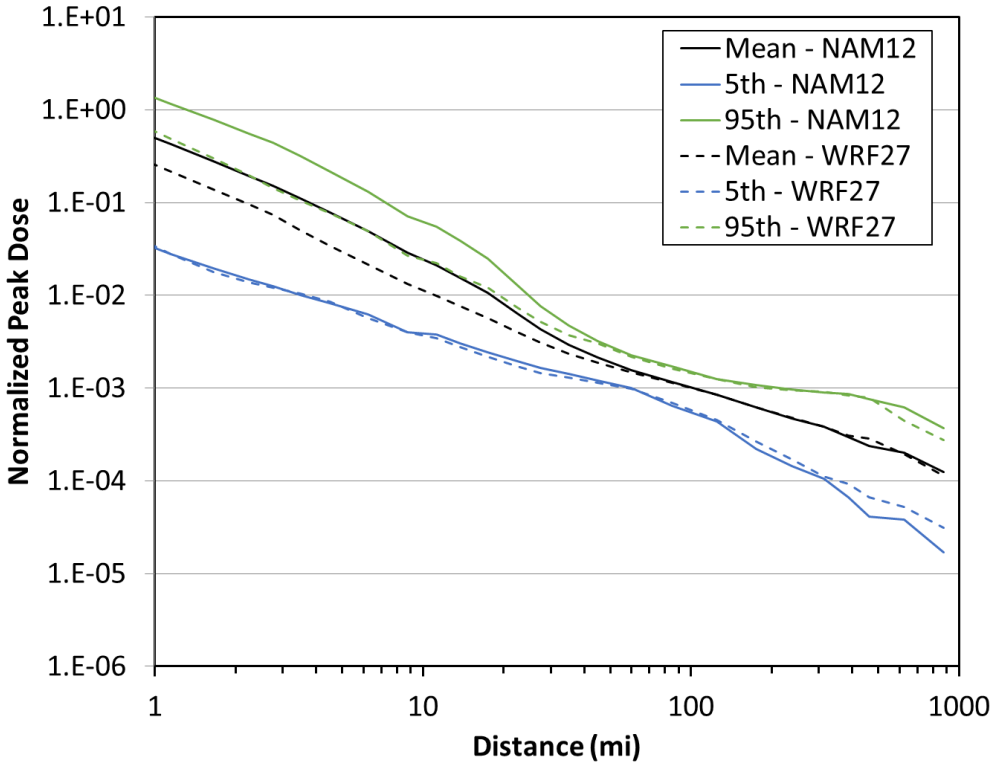

Figure 5-30. Comparison of peak dose for the two meteorological data sets at Site D with ST #1 using the Gaussian ATD model

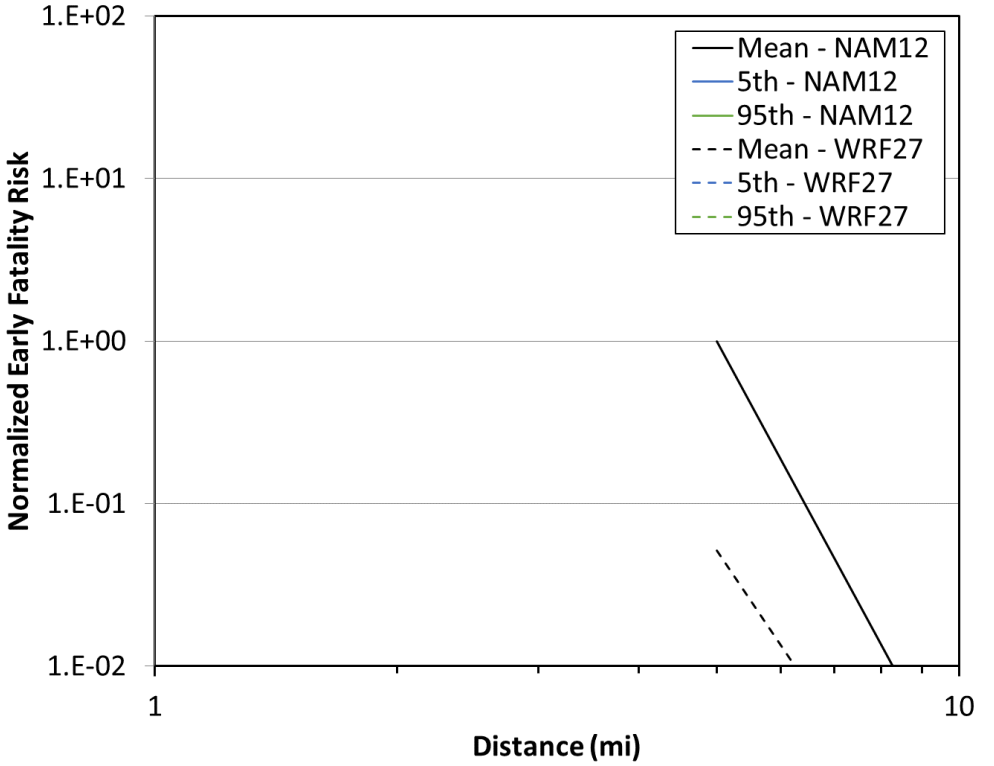

Figure 5-31. Comparison of early fatality risk for the two meteorological data sets at Site D with ST #1 using the Gaussian ATD model

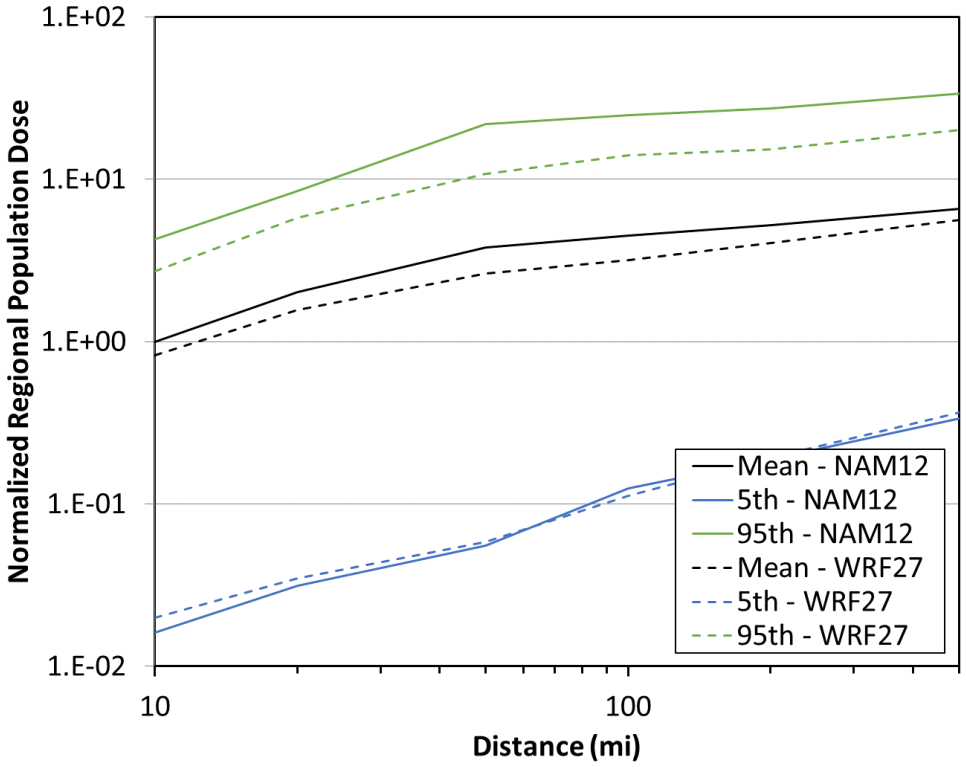

Figure 5-32. Comparison of population dose for the two meteorological data sets at Site D with ST #1 using the Gaussian ATD model

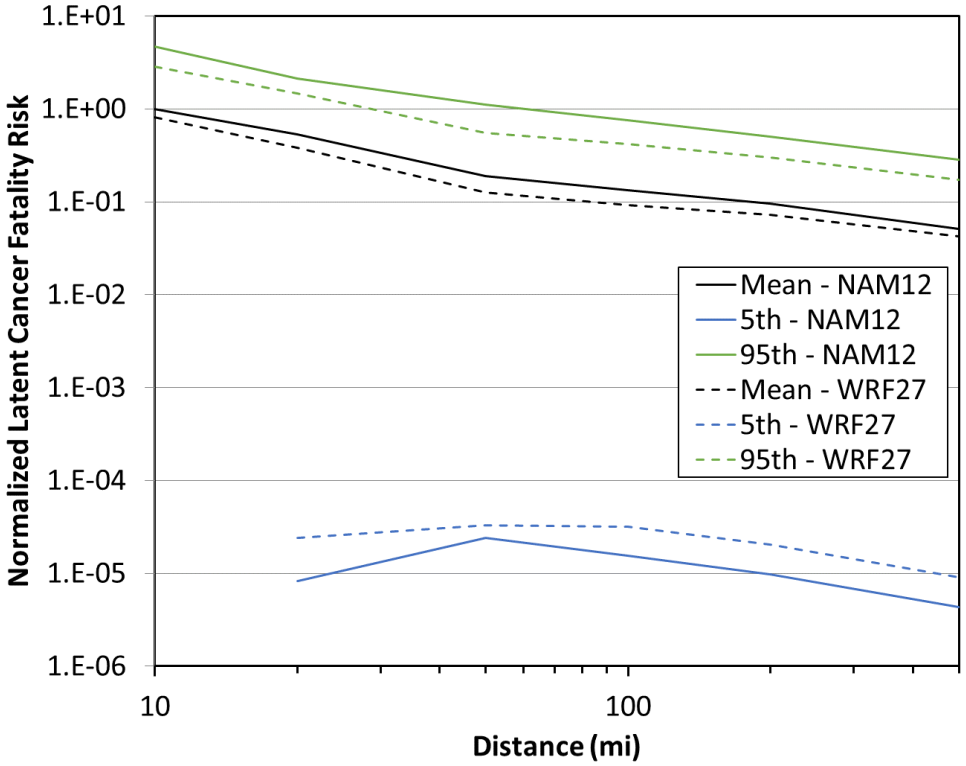

Figure 5-33. Comparison of latent cancer fatality risk for the two meteorological data sets at Site D with ST #1 using the Gaussian ATD model

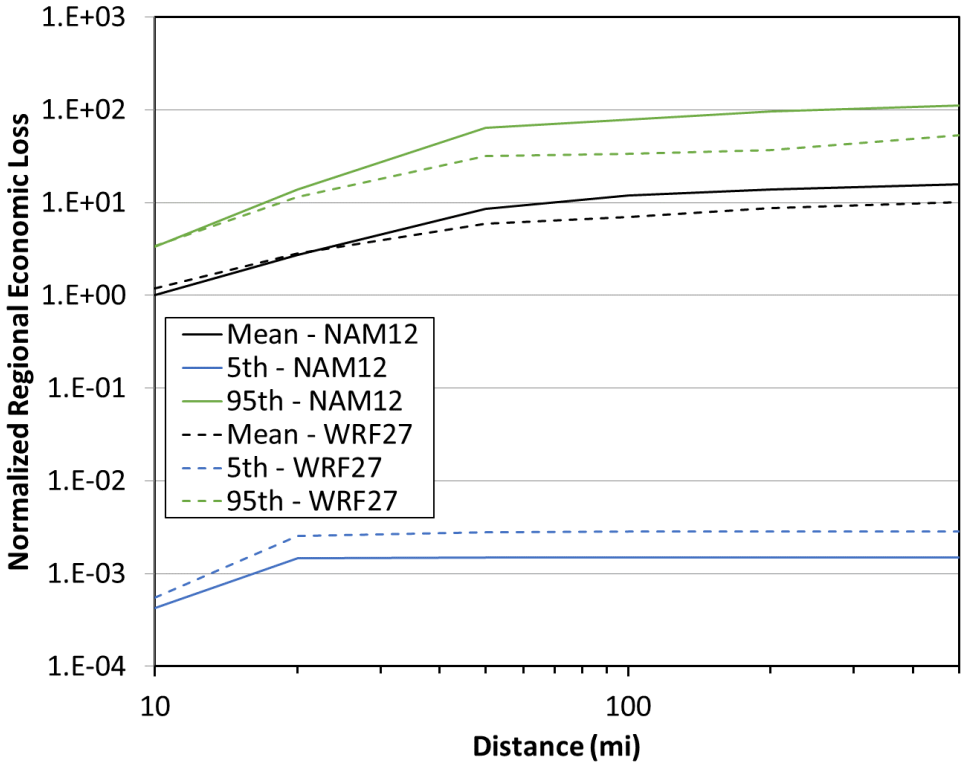

Figure 5-34. Comparison of economic loss for the two meteorological data sets at Site D with ST #1 using the Gaussian ATD model

5.1.1.2.2. Source Term #2

Results for the Gaussian ATD model for Site D with ST #2 using the two meteorological data sets are compared for peak air concentration, peak ground deposition, land contamination area, peak dose, early fatality risk, population dose, latent cancer fatality risk, and economic loss (as described in Section 3.6) in Figure 5-35 through Figure 5-42. The annual statistics for these measures are shown with different colors, where the mean values are in black, the 5th percentile values are shown in blue, and the 95th percentile values are shown in green. HYSPLIT results are shown as dashed lines and Gaussian model results are shown as solid lines. The normalized results are shown as a function of distance, rather than the ratio of Gaussian and HYSPLIT results, to allow for the trends with distance to be observed. Some results are zero for early fatality risk, so they cannot be shown on the log scale used in the figures. Discussion of the difference seen in these figures is provided below in Section 5.1.3.

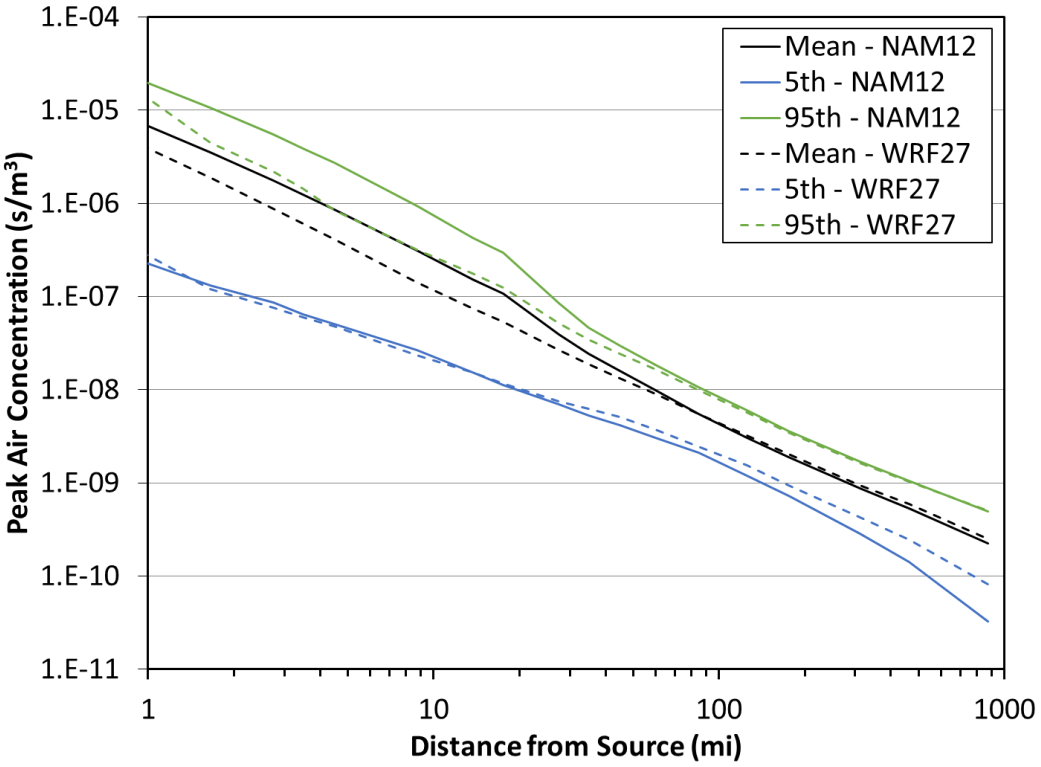

Figure 5-35. Comparison of peak air concentration for the two meteorological data sets at Site D with ST #2 using the Gaussian ATD model

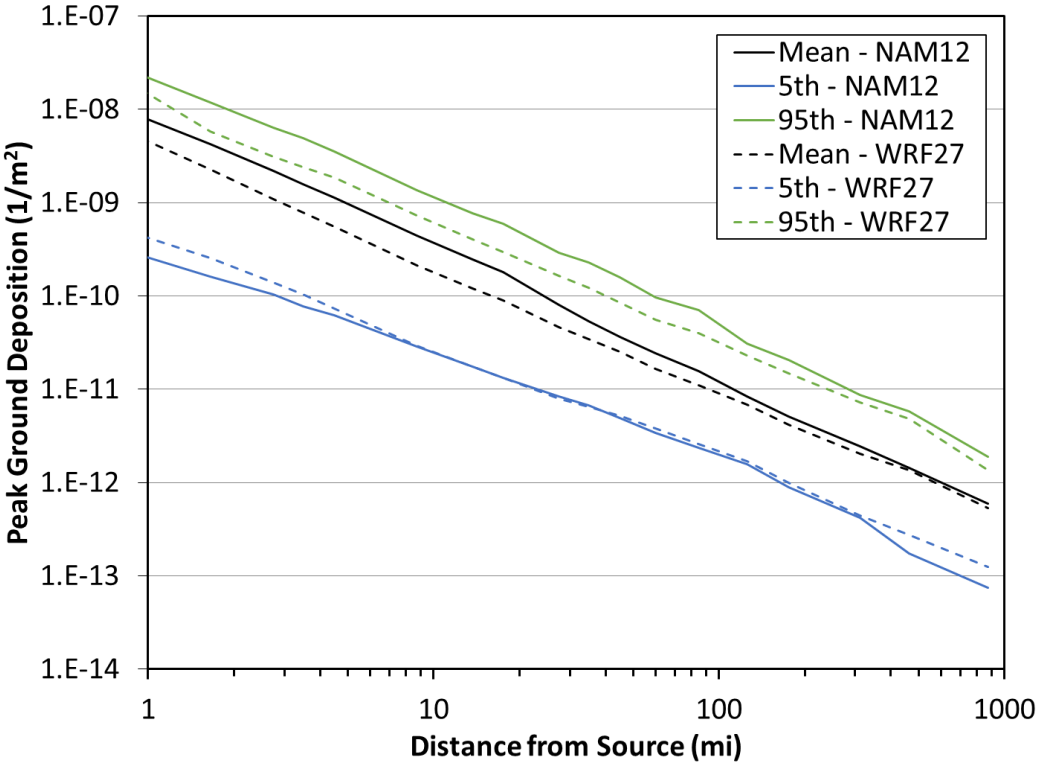

Figure 5-36. Comparison of peak ground deposition for the two meteorological data sets at Site D with ST #2 using the Gaussian ATD model

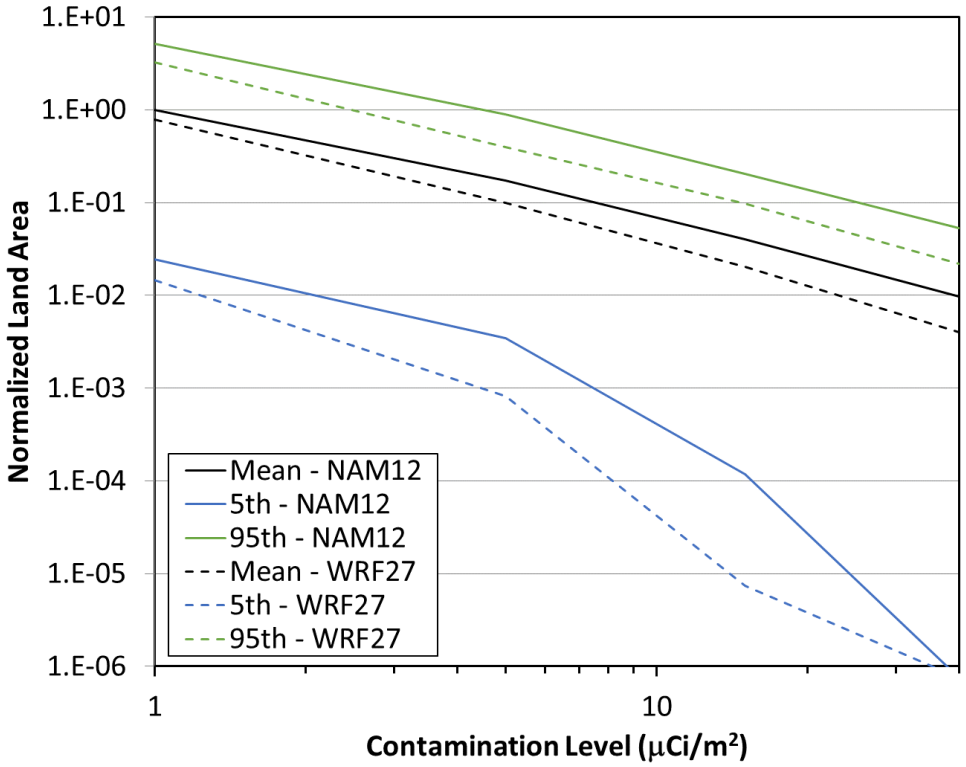

Figure 5-37. Comparison of land contamination area for the two meteorological data sets at Site D with ST #2 using the Gaussian ATD model

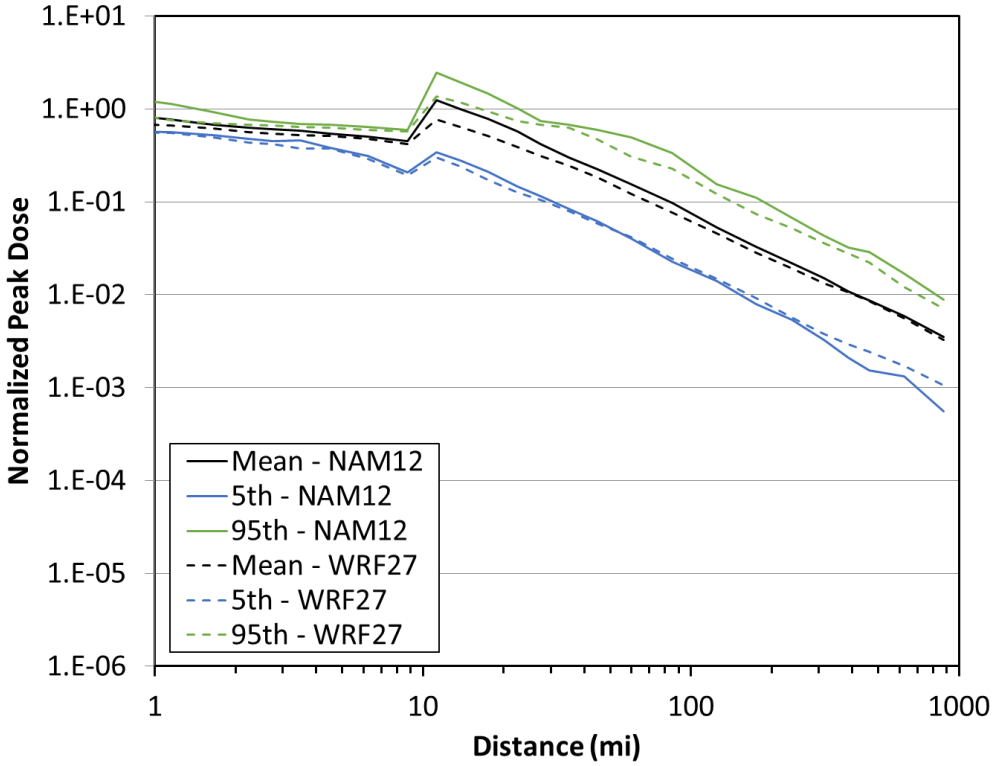

Figure 5-38. Comparison of peak dose for the two meteorological data sets at Site D with ST #2 using the Gaussian ATD model

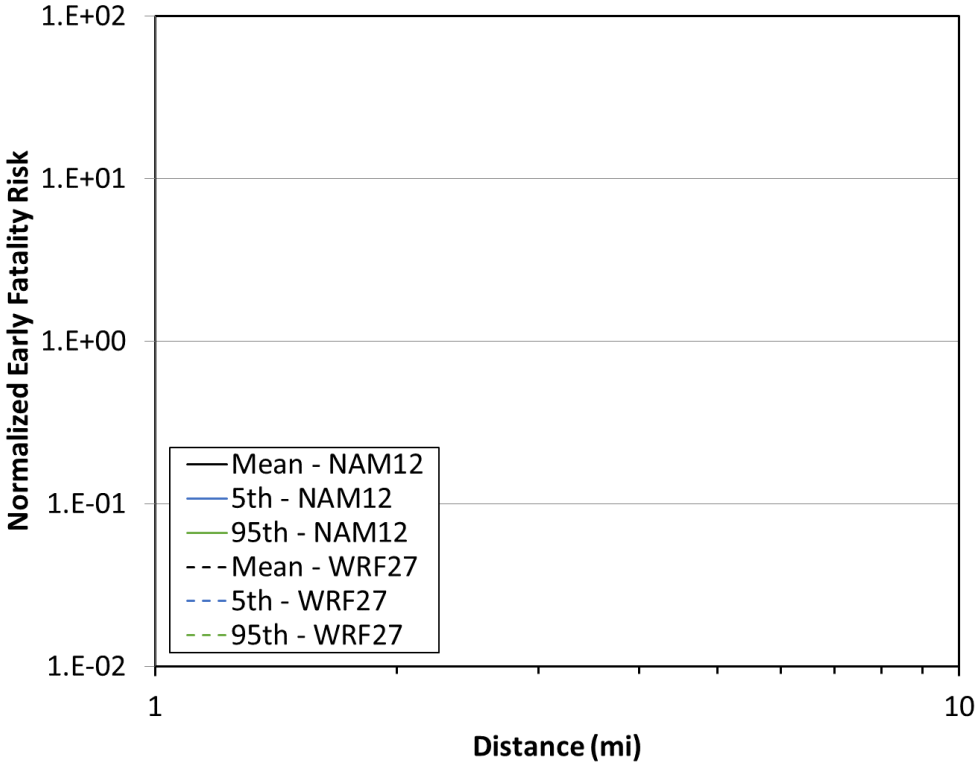

Figure 5-39. Comparison of early fatality risk for the two meteorological data sets at Site D with ST #2 using the Gaussian ATD model

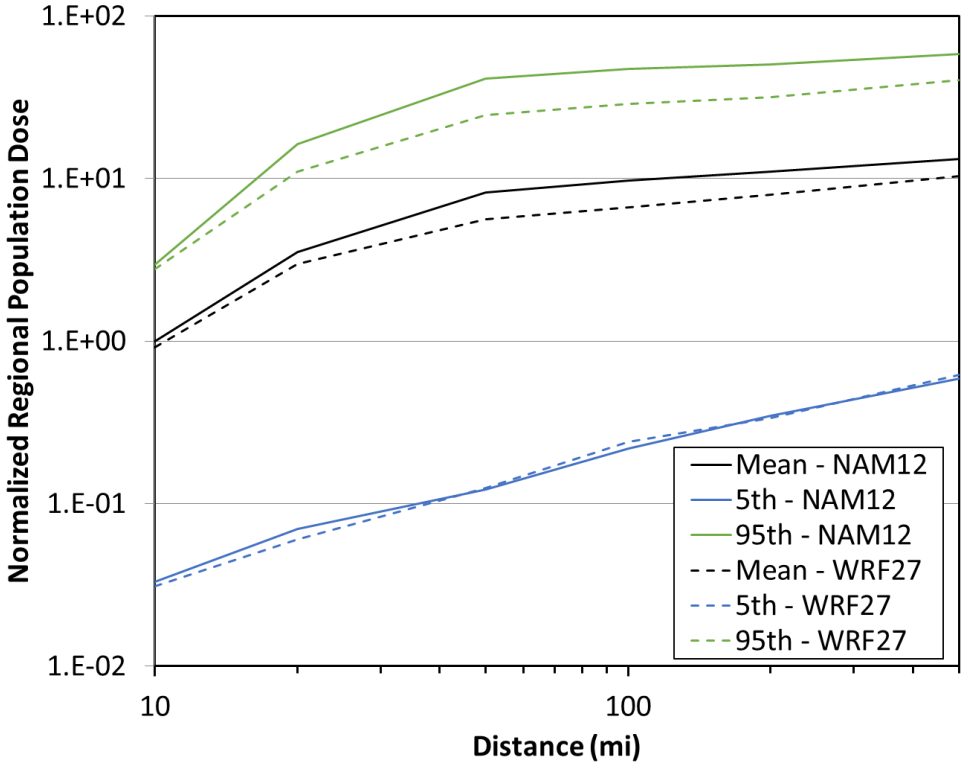

Figure 5-40. Comparison of population dose for the two meteorological data sets at Site D with ST #2 using the Gaussian ATD model

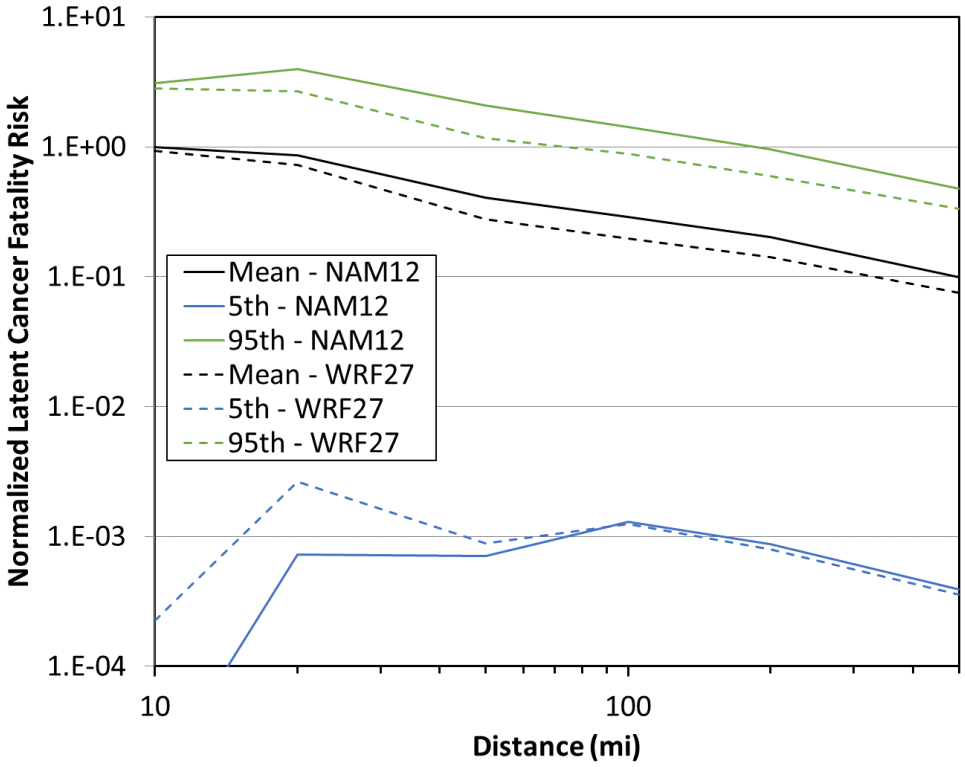

Figure 5-41. Comparison of latent cancer fatality risk for the two meteorological data sets at Site D with ST #2 using the Gaussian ATD model

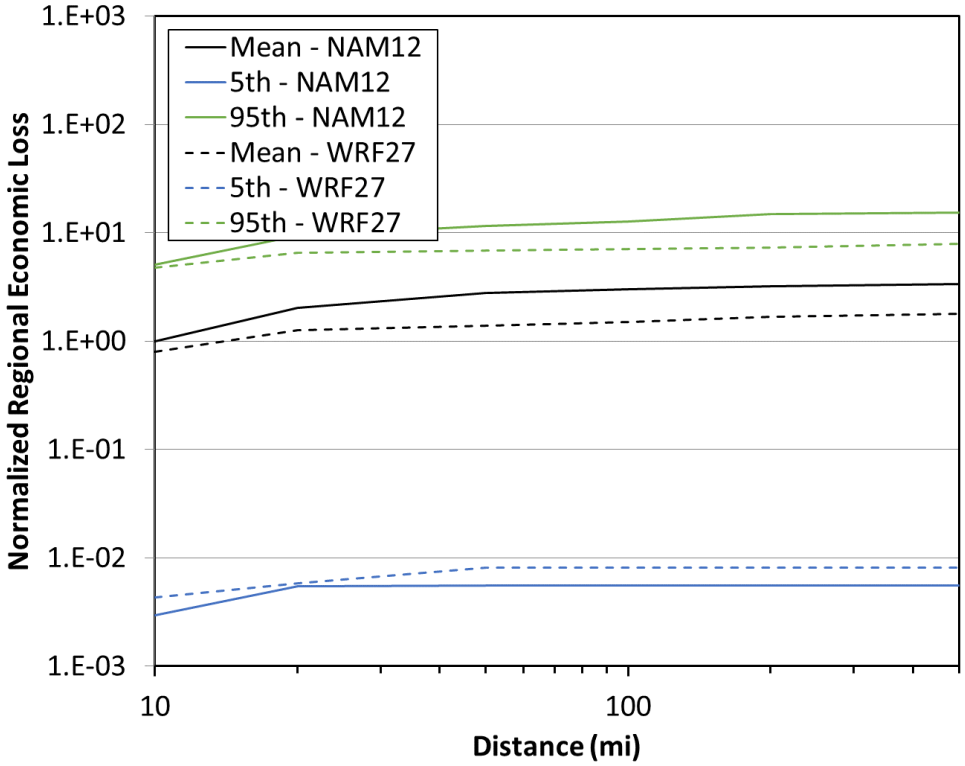

Figure 5-42. Comparison of economic loss for the two meteorological data sets at Site D with ST #2 using the Gaussian ATD model

5.1.2. HYSPLIT Comparison

5.1.2.1. Site A

5.1.2.1.1. Source Term #1

Results for the HYSPLIT ATD model for Site A with ST #1 using the NAM12 and WRF27 data sets are compared for peak air concentration, peak ground deposition, land contamination area, peak dose, early fatality risk, population dose, latent cancer fatality risk, and economic loss (as described in Section 3.6) in Figure 5-43 through Figure 5-50. The annual statistics for these measures are shown with different colors, where the mean values are in black, the 5th percentile values are shown in blue, and the 95th percentile values are shown in green. HYSPLIT results are shown as dashed lines and Gaussian model results are shown as solid lines. The normalized results are shown as a function of distance, rather than the ratio of Gaussian and HYSPLIT results, to allow for the trends with distance to be observed. Some results are zero for early fatality risk, so they cannot be shown on the log scale used in the figures. Discussion of the difference seen in these figures is provided below in Section 5.1.3.

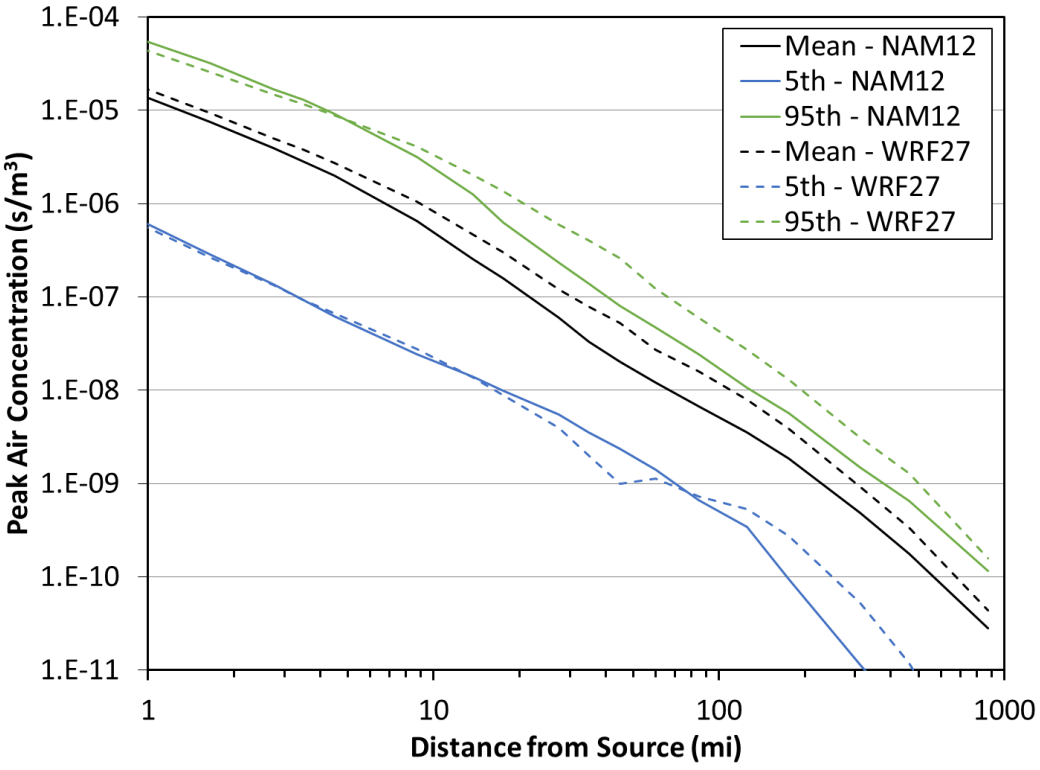

Figure 5-43. Comparison of peak air concentration for two meteorological data sets at Site A with ST #1 using the HYSPLIT ATD model

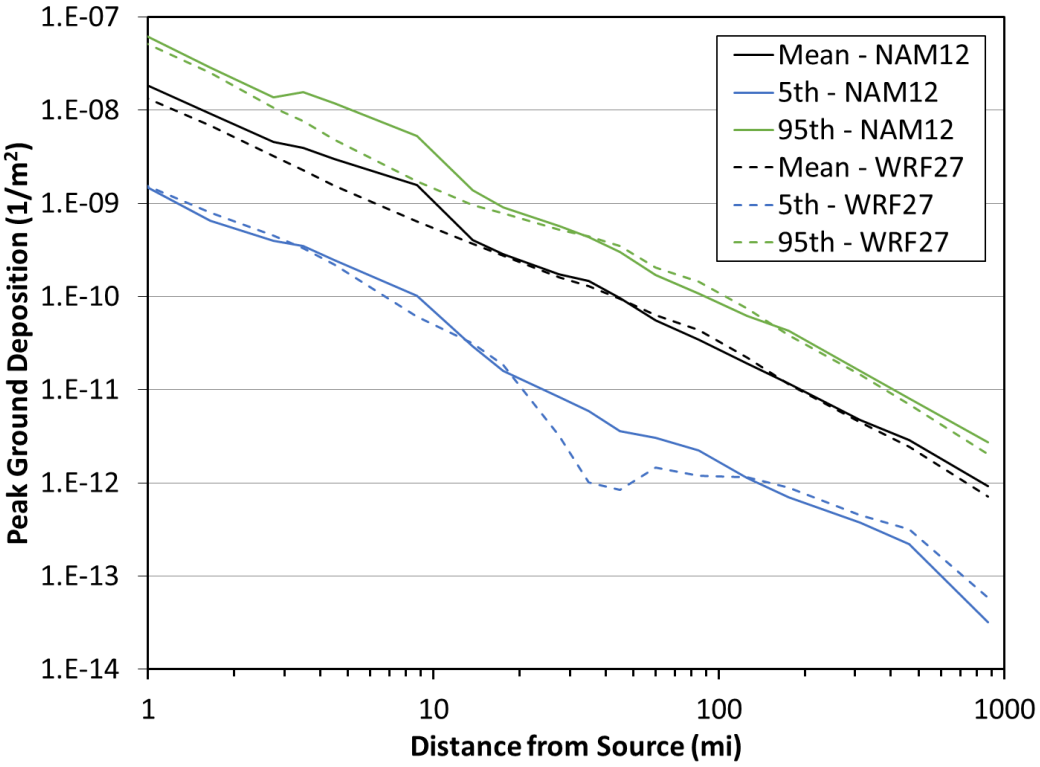

Figure 5-44. Comparison of peak ground deposition for two meteorological data sets at Site A with ST #1 using the HYSPLIT ATD model

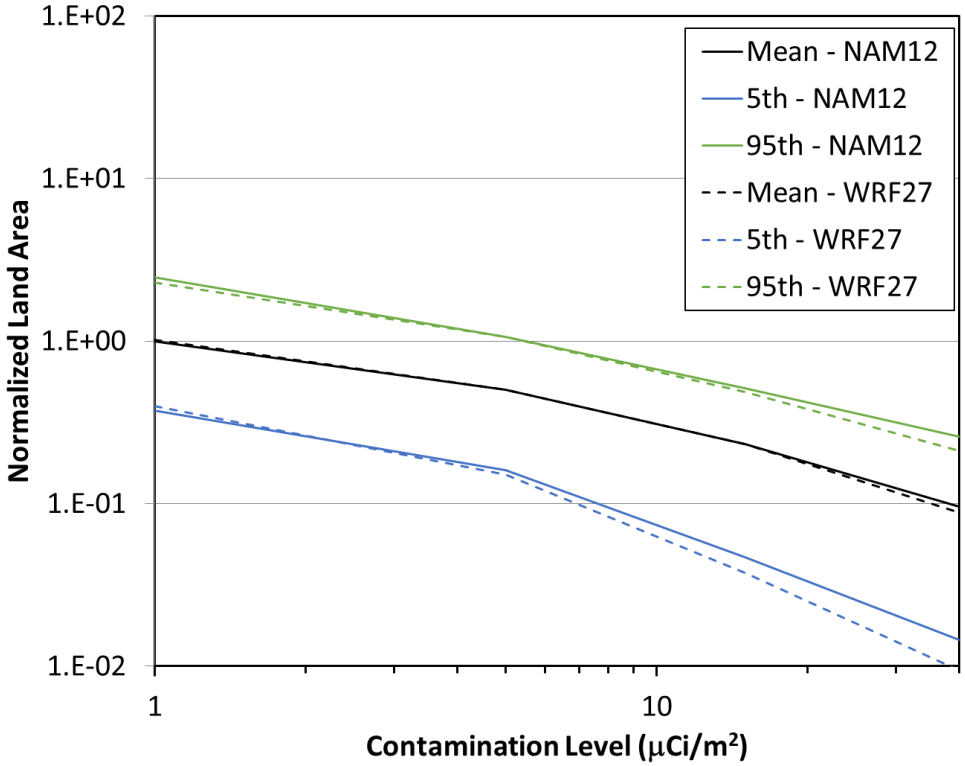

Figure 5-45. Comparison of land contamination area for two meteorological data sets at Site A with ST #1 using the HYSPLIT ATD model

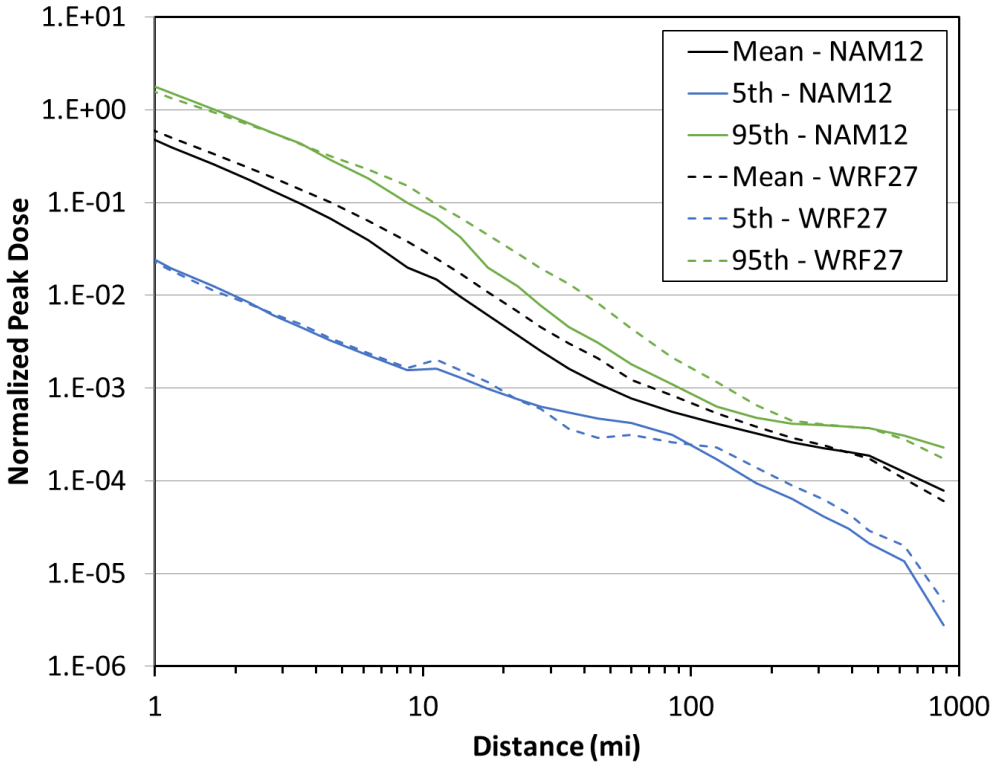

Figure 5-46. Comparison of peak dose for two meteorological data sets at Site A with ST #1 using the HYSPLIT ATD model

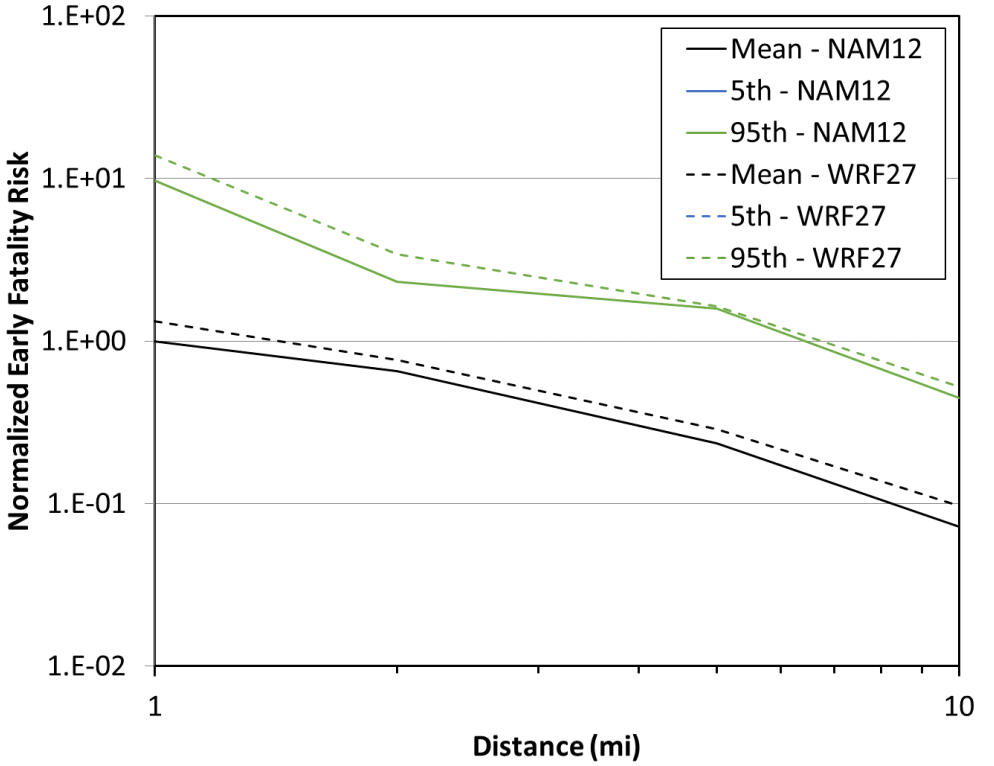

Figure 5-47. Comparison of early fatality risk for two meteorological data sets at Site A with ST #1 using the HYSPLIT ATD model

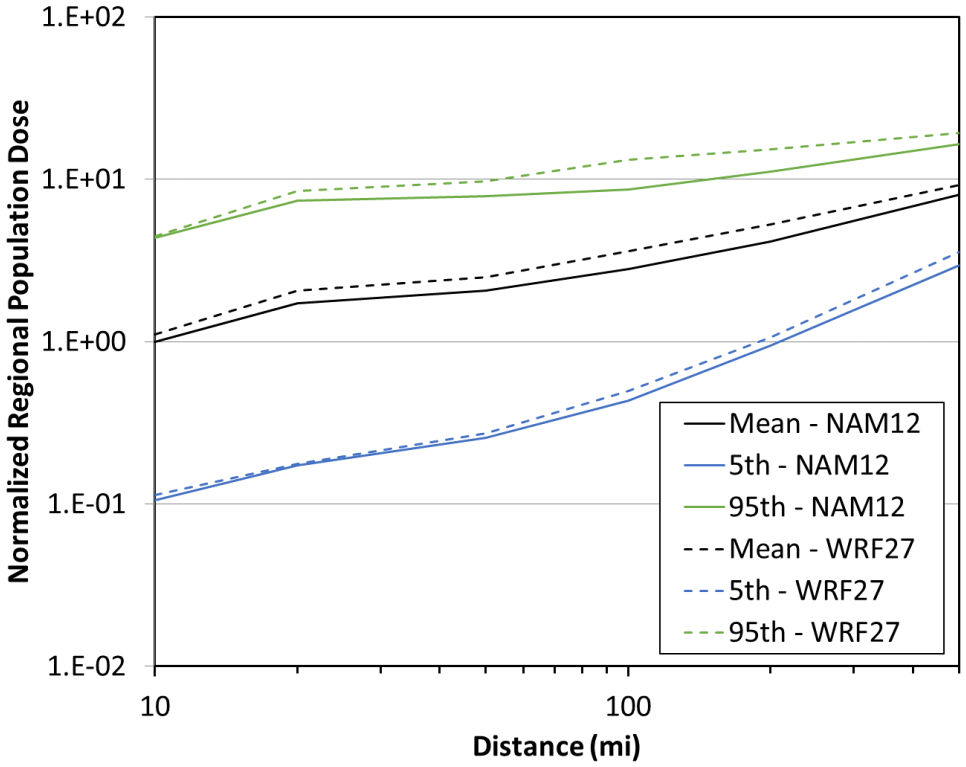

Figure 5-48. Comparison of population dose for two meteorological data sets at Site A with ST #1 using the HYSPLIT ATD model

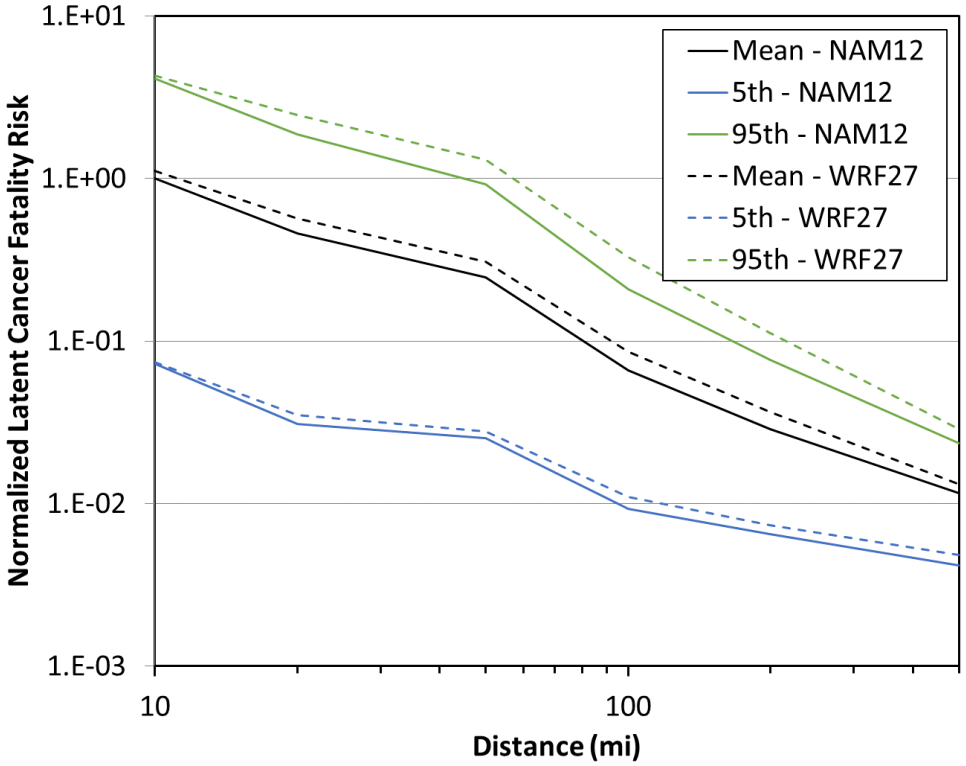

Figure 5-49. Comparison of latent cancer fatality risk for two meteorological data sets at Site A with ST #1 using the HYSPLIT ATD model

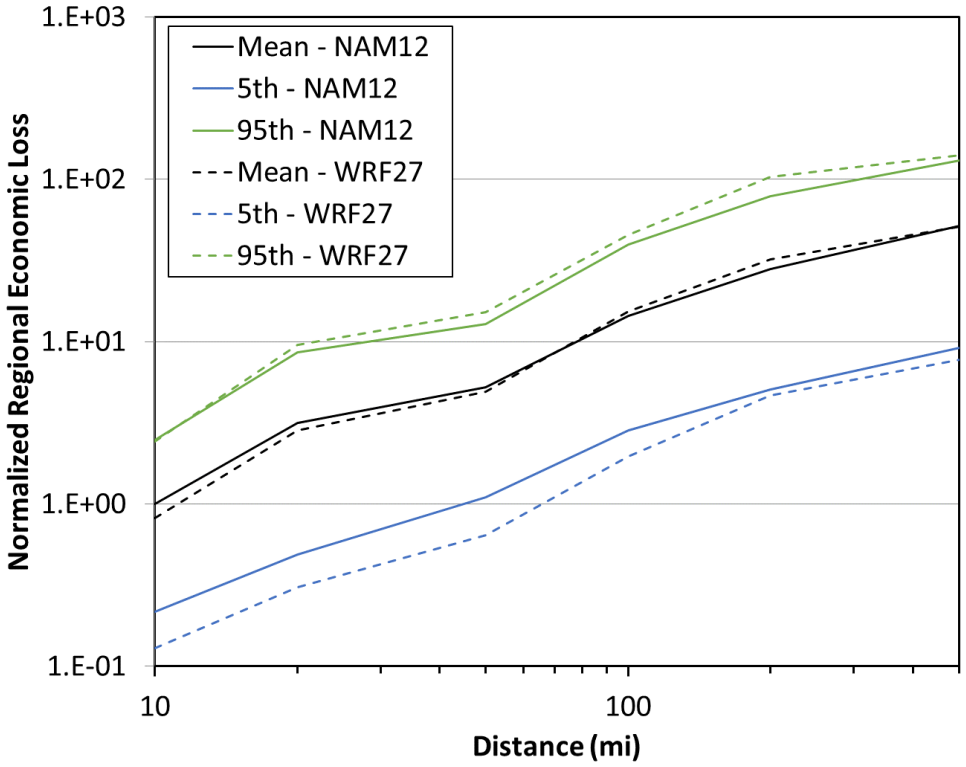

Figure 5-50. Comparison of economic loss for two meteorological data sets at Site A with ST #1 using the HYSPLIT ATD model

5.1.2.1.2. Source Term #2

Results for the HYSPLIT ATD model for Site A with ST #2 using the NAM12 and WRF27 data sets are compared for peak air concentration, peak ground deposition, land contamination area, peak dose, early fatality risk, population dose, latent cancer fatality risk, and economic loss (as described in Section 3.6) in Figure 5-51 through Figure 5-58. The annual statistics for these measures are shown with different colors, where the mean values are in black, the 5th percentile values are shown in blue, and the 95th percentile values are shown in green. HYSPLIT results are shown as dashed lines and Gaussian model results are shown as solid lines. The normalized results are shown as a function of distance, rather than the ratio of Gaussian and HYSPLIT results, to allow for the trends with distance to be observed. Some results are zero for early fatality risk, so they cannot be shown on the log scale used in the figures. Discussion of the difference seen in these figures is provided below in Section 5.1.3.

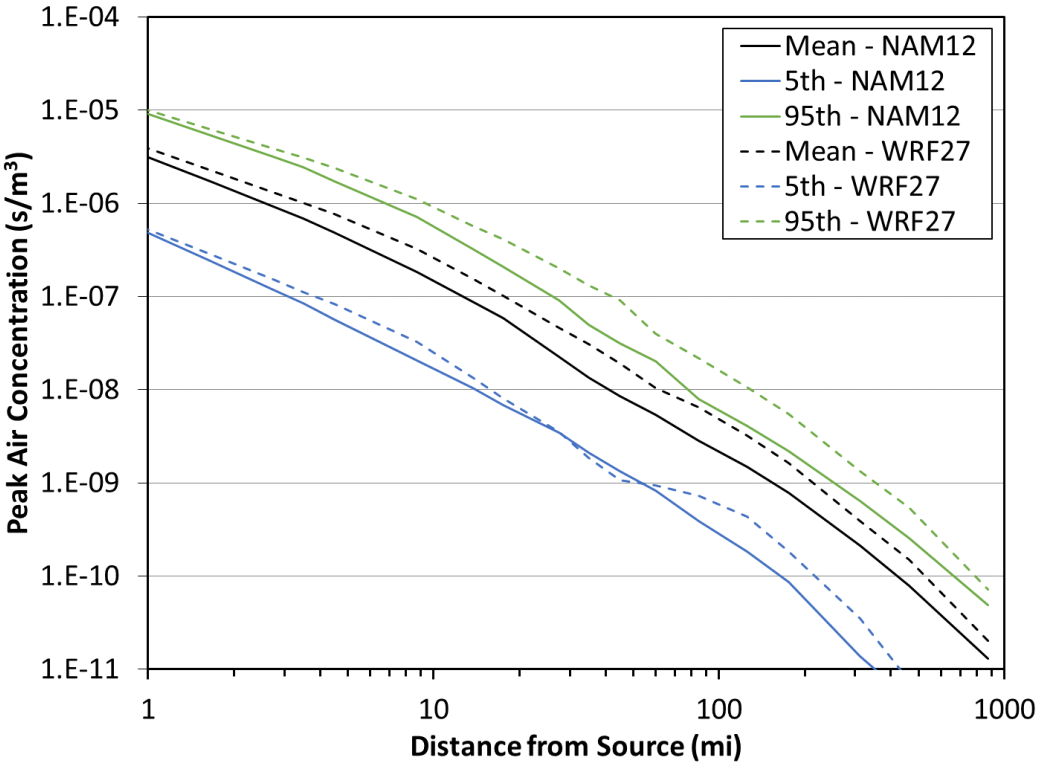

Figure 5-51. Comparison of peak air concentration for two meteorological data sets at Site A with ST #2 using the HYSPLIT ATD model

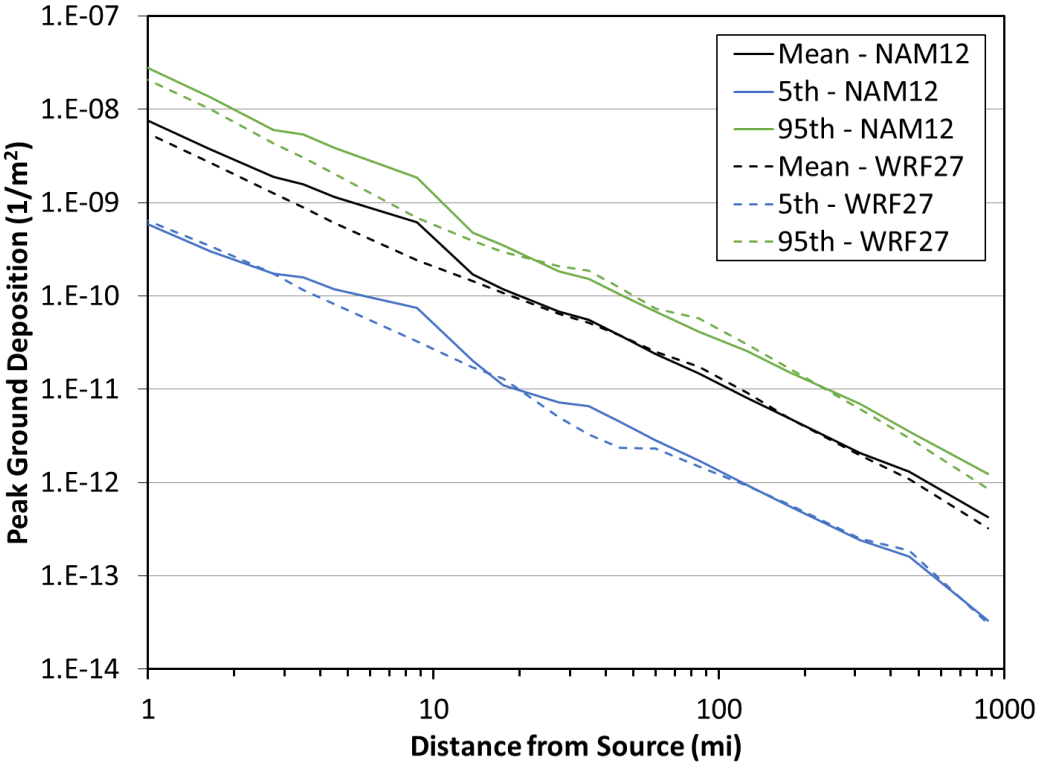

Figure 5-52. Comparison of peak ground deposition for two meteorological data sets at Site A with ST #2 using the HYSPLIT ATD model

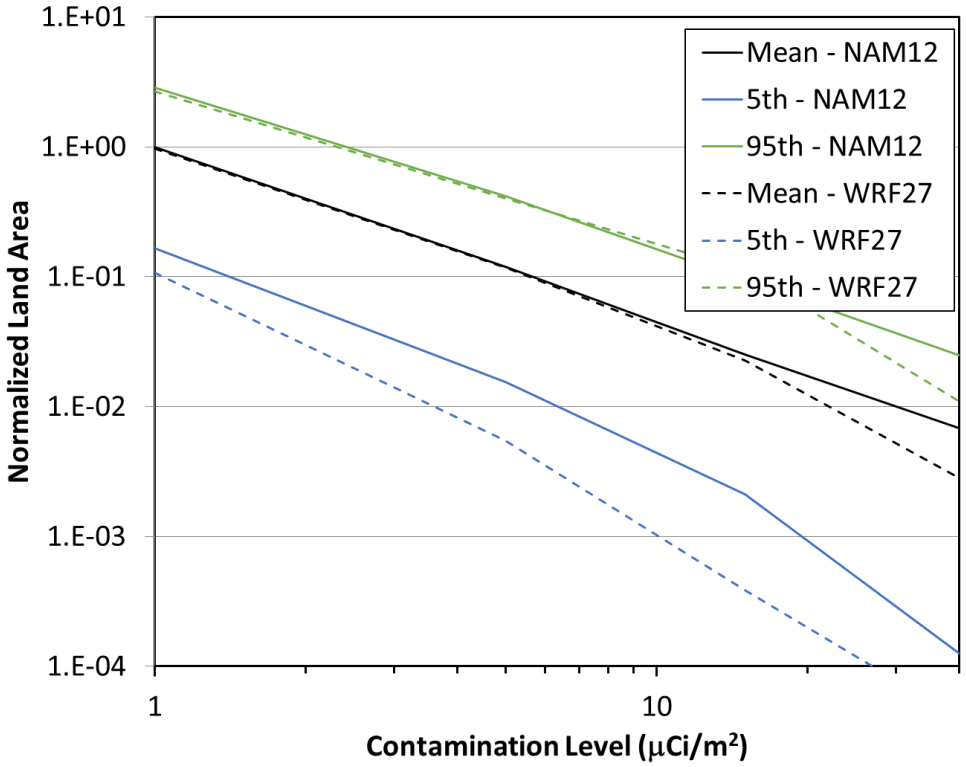

Figure 5-53. Comparison of land contamination area for two meteorological data sets at Site A with ST #2 using the HYSPLIT ATD model

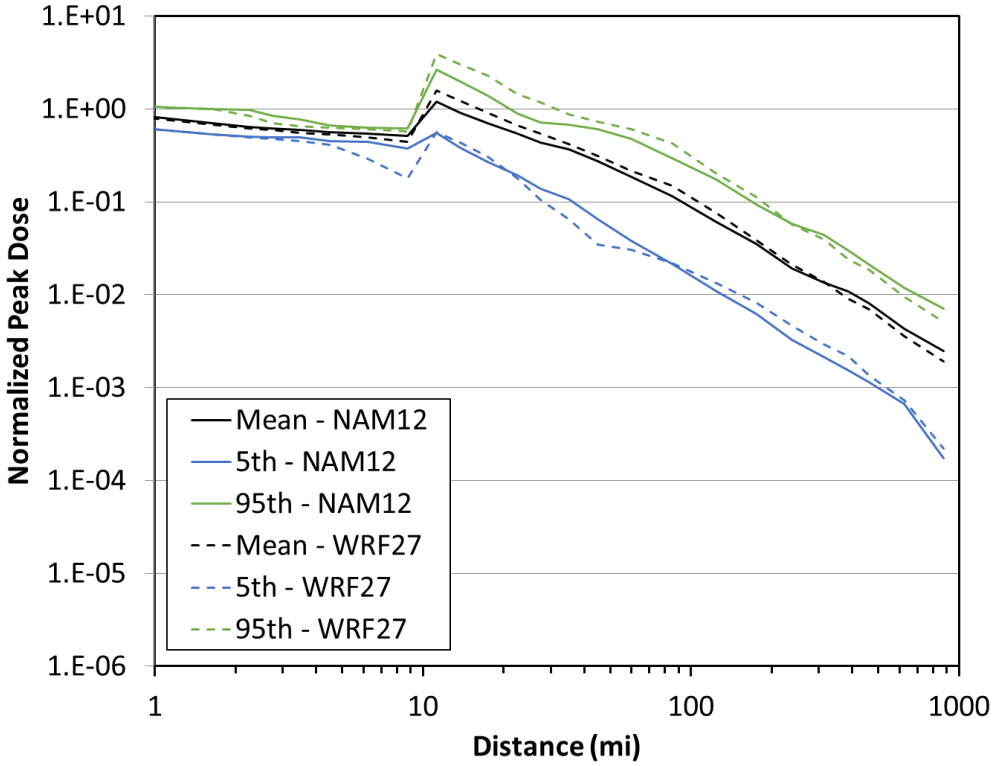

Figure 5-54. Comparison of peak dose for two meteorological data sets at Site A with ST #2 using the HYSPLIT ATD model

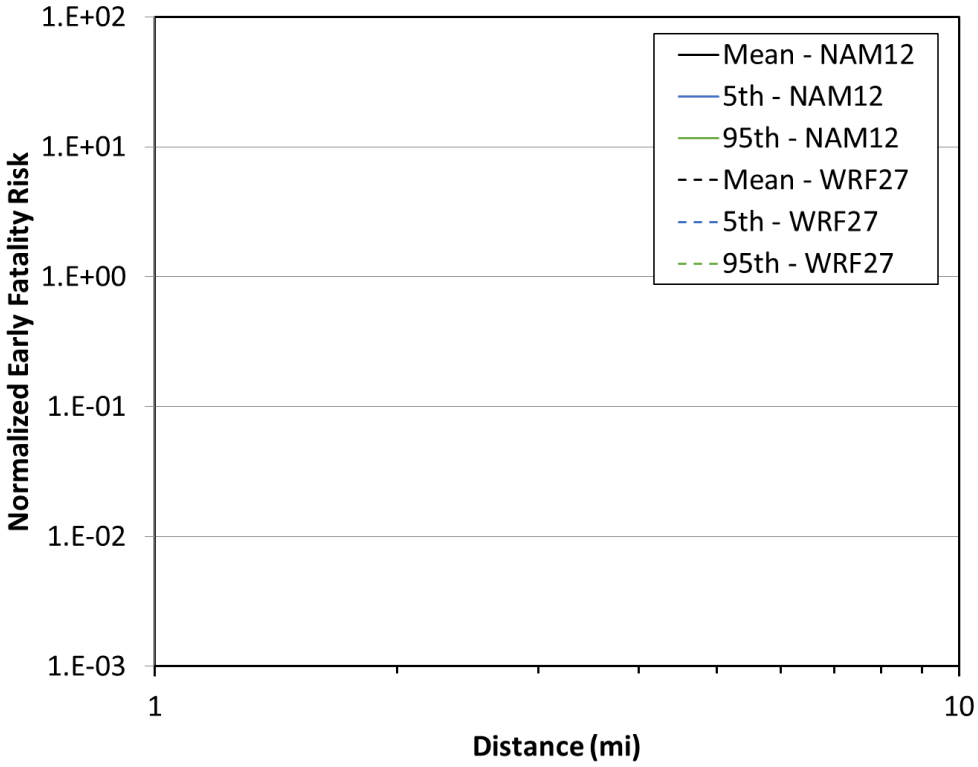

Figure 5-55. Comparison of early fatality risk for two meteorological data sets at Site A with ST #2 using the HYSPLIT ATD model

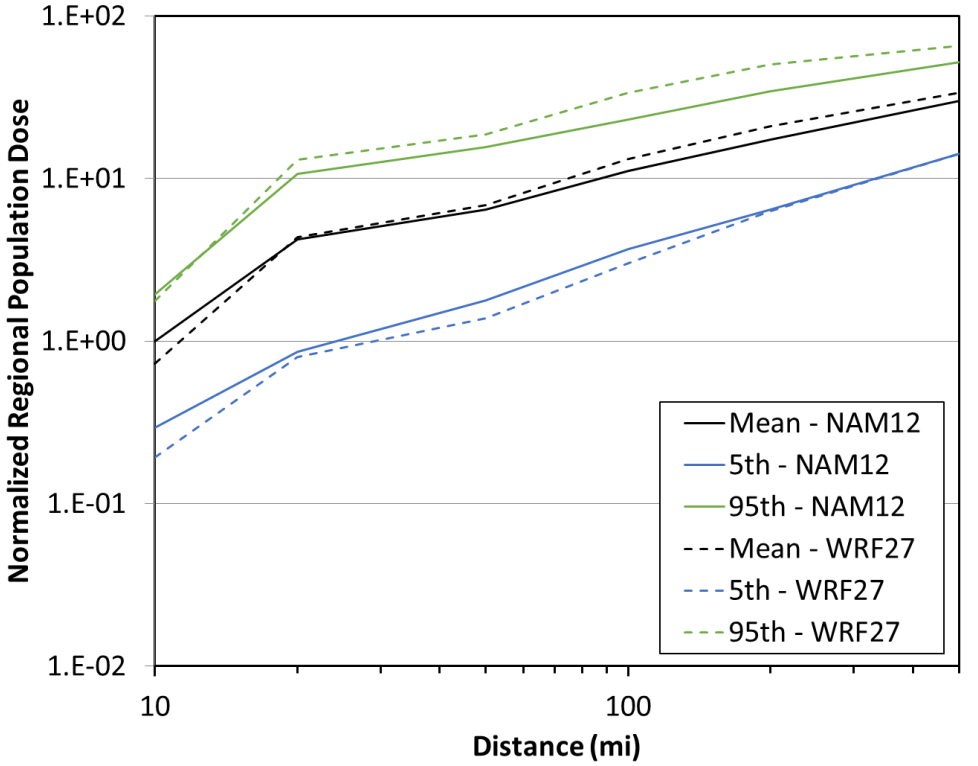

Figure 5-56. Comparison of population dose for two meteorological data sets at Site A with ST #2 using the HYSPLIT ATD model

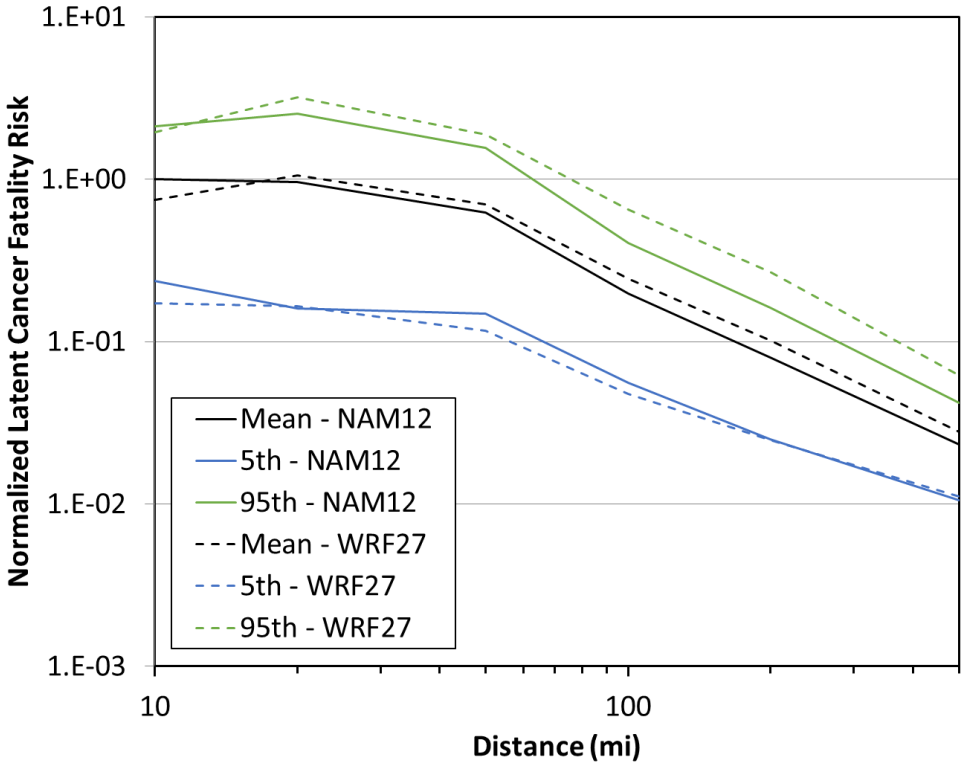

Figure 5-57. Comparison of latent cancer fatality risk for two meteorological data sets at Site A with ST #2 using the HYSPLIT ATD model

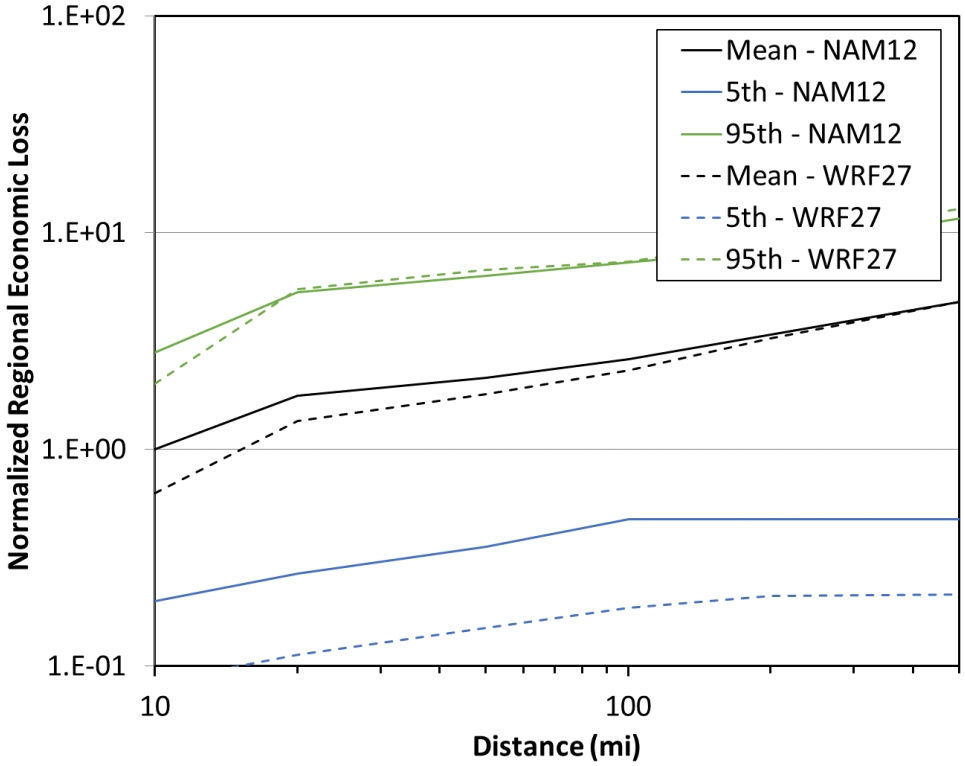

Figure 5-58. Comparison of economic loss for two meteorological data sets at Site A with ST #2 using the HYSPLIT ATD model

5.1.2.2. Site D

5.1.2.2.1. Source Term #1

Results for the HYSPLIT ATD model for Site D with ST #1 using the NAM12 and WRF27 data sets are compared for peak air concentration, peak ground deposition, land contamination area, peak dose, early fatality risk, population dose, latent cancer fatality risk, and economic loss (as described in Section 3.6) in Figure 5-59 through Figure 5-66. The annual statistics for these measures are shown with different colors, where the mean values are in black, the 5th percentile values are shown in blue, and the 95th percentile values are shown in green. HYSPLIT results are shown as dashed lines and Gaussian model results are shown as solid lines. The normalized results are shown as a function of distance, rather than the ratio of Gaussian and HYSPLIT results, to allow for the trends with distance to be observed. Some results are zero for early fatality risk, so they cannot be shown on the log scale used in the figures. Discussion of the difference seen in these figures is provided below in Section 5.1.3.

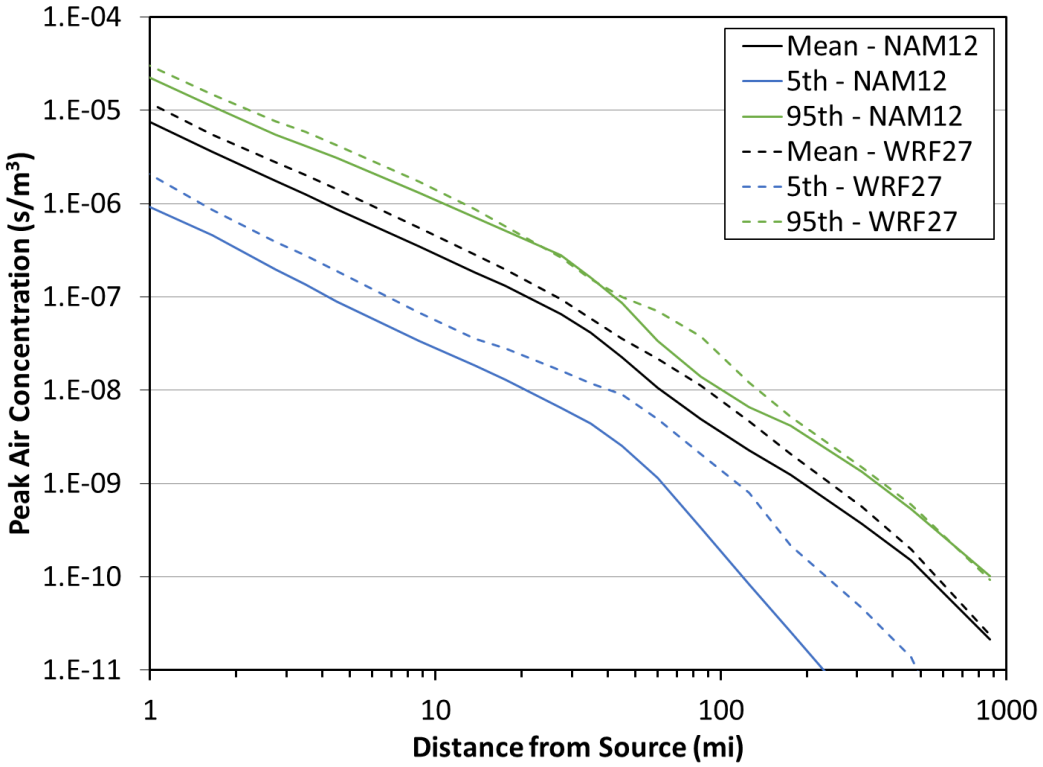

Figure 5-59. Comparison of peak air concentration for two meteorological data sets at Site D with ST #1 using the HYSPLIT ATD model

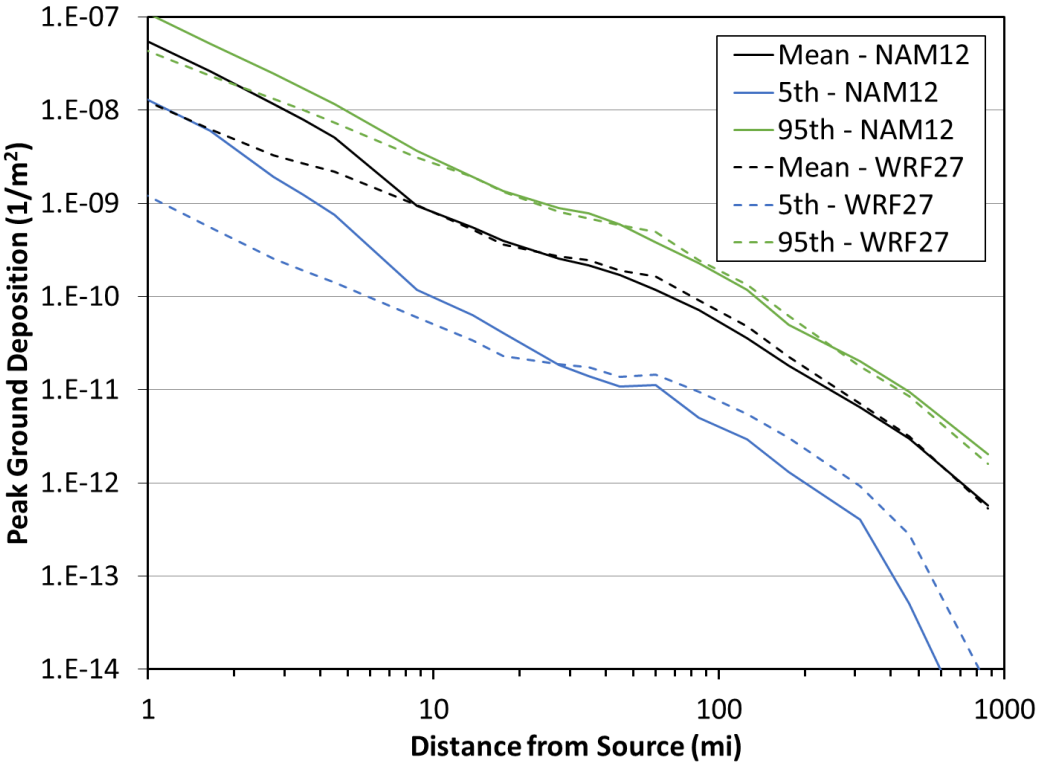

Figure 5-60. Comparison of peak ground deposition for two meteorological data sets at Site D with ST #1 using the HYSPLIT ATD model

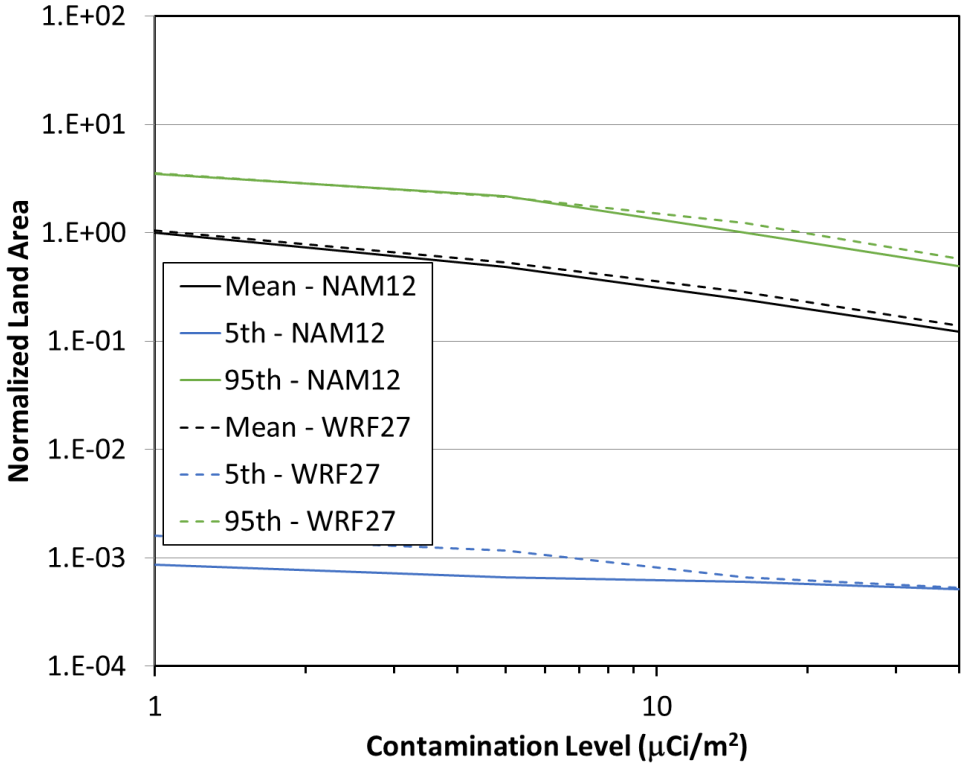

Figure 5-61. Comparison of land contamination area for two meteorological data sets at Site D with ST #1 using the HYSPLIT ATD model

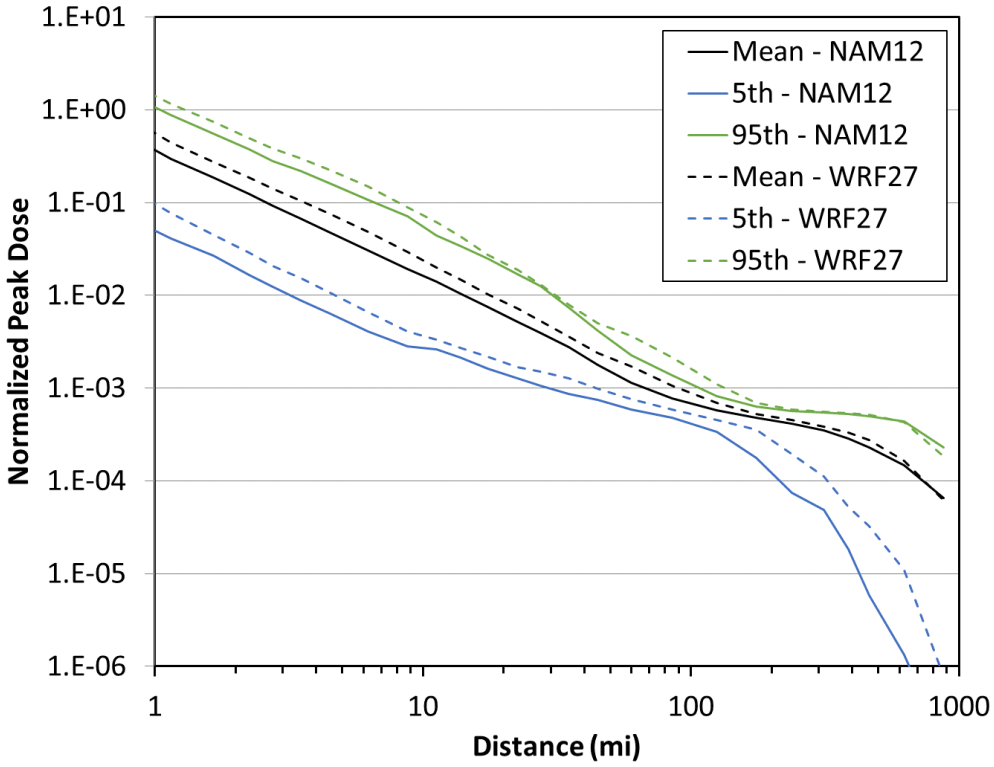

Figure 5-62. Comparison of peak dose for two meteorological data sets at Site D with ST #1 using the HYSPLIT ATD model

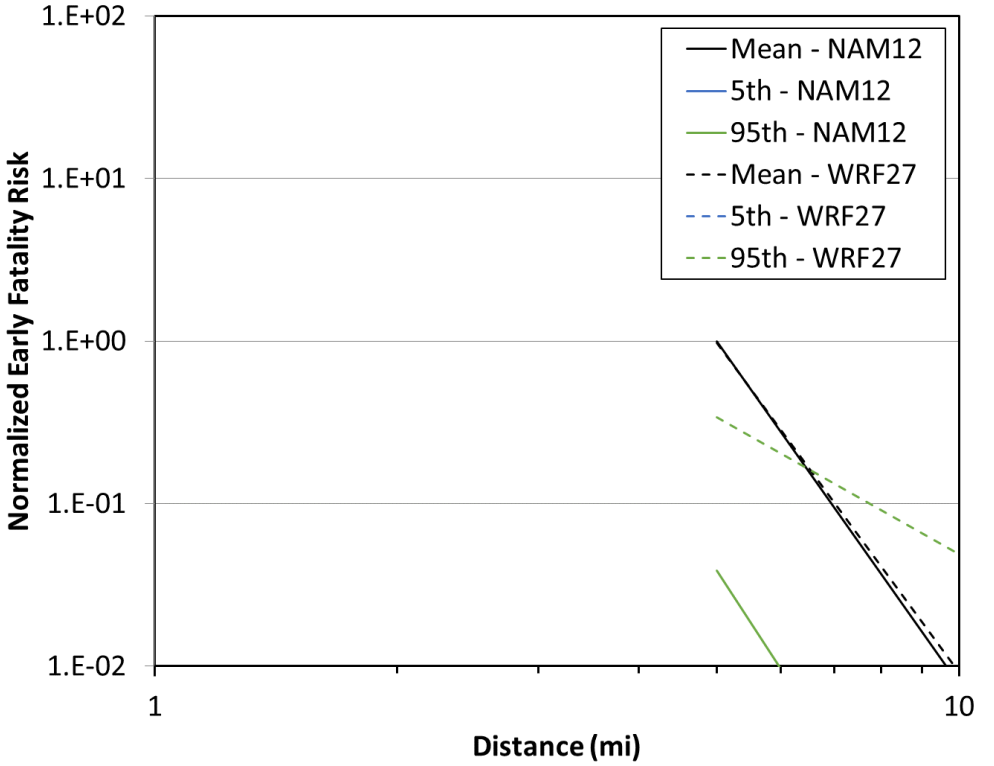

Figure 5-63. Comparison of early fatality risk for two meteorological data sets at Site D with ST #1 using the HYSPLIT ATD model

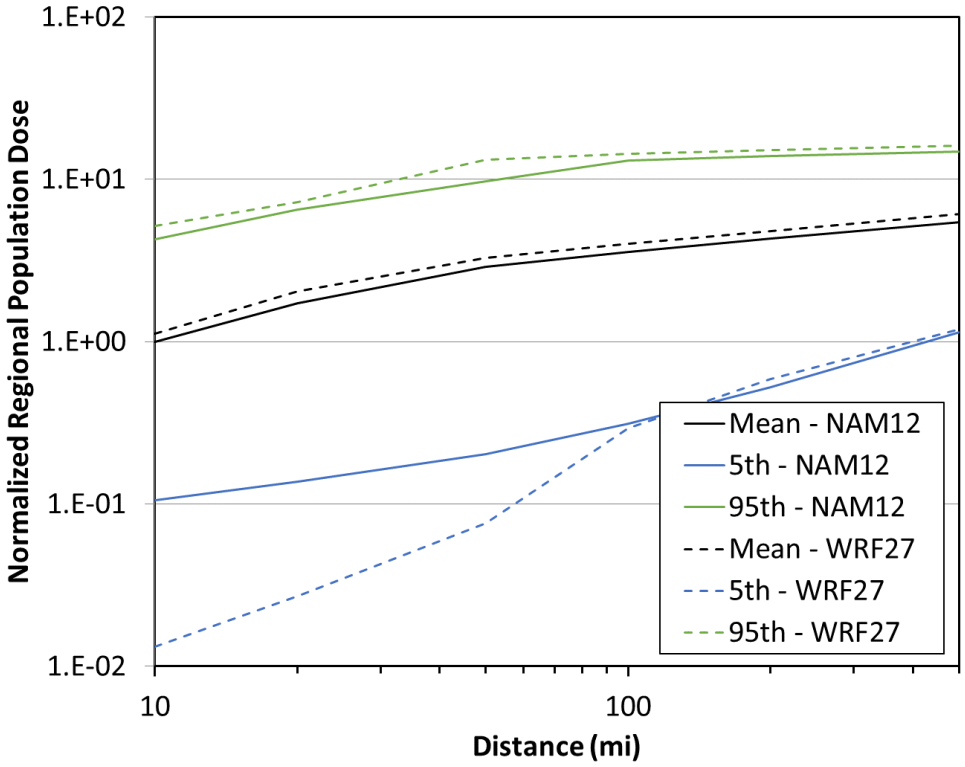

Figure 5-64. Comparison of population dose for two meteorological data sets at Site D with ST #1 using the HYSPLIT ATD model

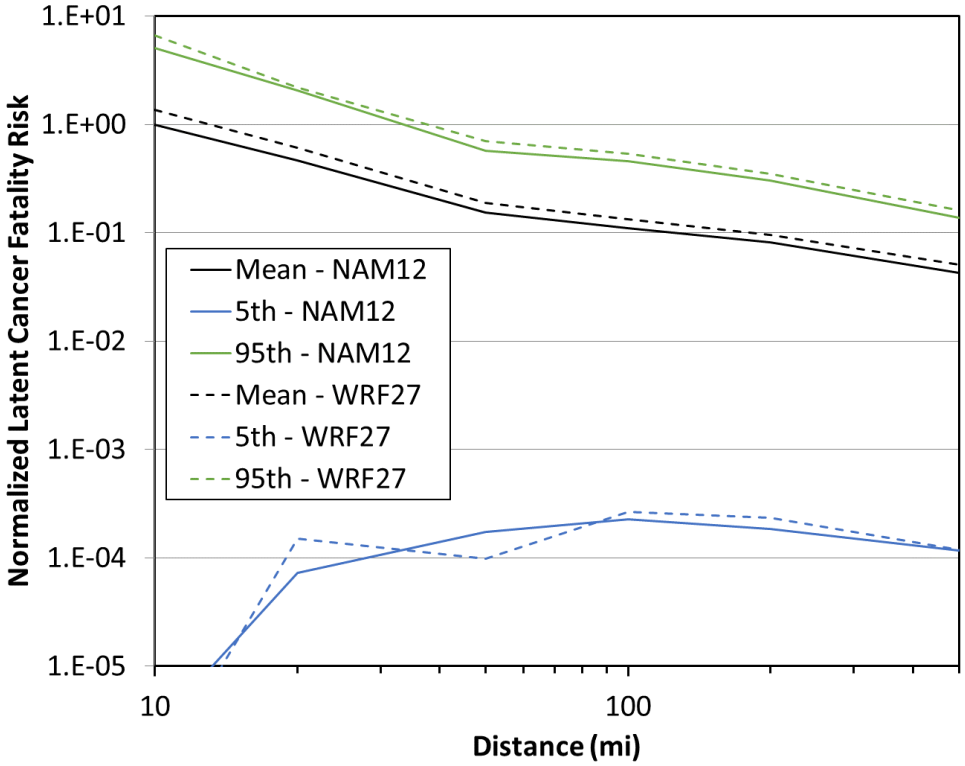

Figure 5-65. Comparison of latent cancer fatality risk for two meteorological data sets at Site D with ST #1 using the HYSPLIT ATD model

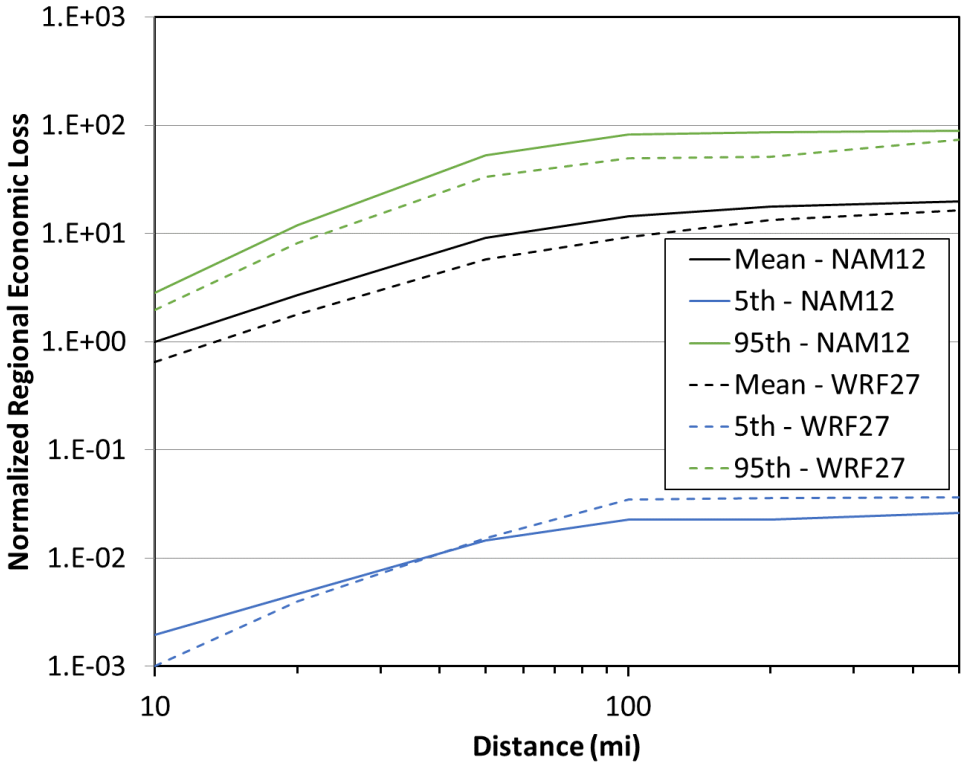

Figure 5-66. Comparison of economic loss for two meteorological data sets at Site D with ST #1 using the HYSPLIT ATD model

5.1.2.2.2. Source Term #2

Results for the HYSPLIT ATD model for Site D with ST #2 using the NAM12 and WRF27 data sets are compared for peak air concentration, peak ground deposition, land contamination area, peak dose, early fatality risk, population dose, latent cancer fatality risk, and economic loss (as described in Section 3.6) in Figure 5-67 through Figure 5-74. The annual statistics for these measures are shown with different colors, where the mean values are in black, the 5th percentile values are shown in blue, and the 95th percentile values are shown in green. HYSPLIT results are shown as dashed lines and Gaussian model results are shown as solid lines. The normalized results are shown as a function of distance, rather than the ratio of Gaussian and HYSPLIT results, to allow for the trends with distance to be observed. Some results are zero for early fatality risk, so they cannot be shown on the log scale used in the figures. Discussion of the difference seen in these figures is provided below in Section 5.1.3.

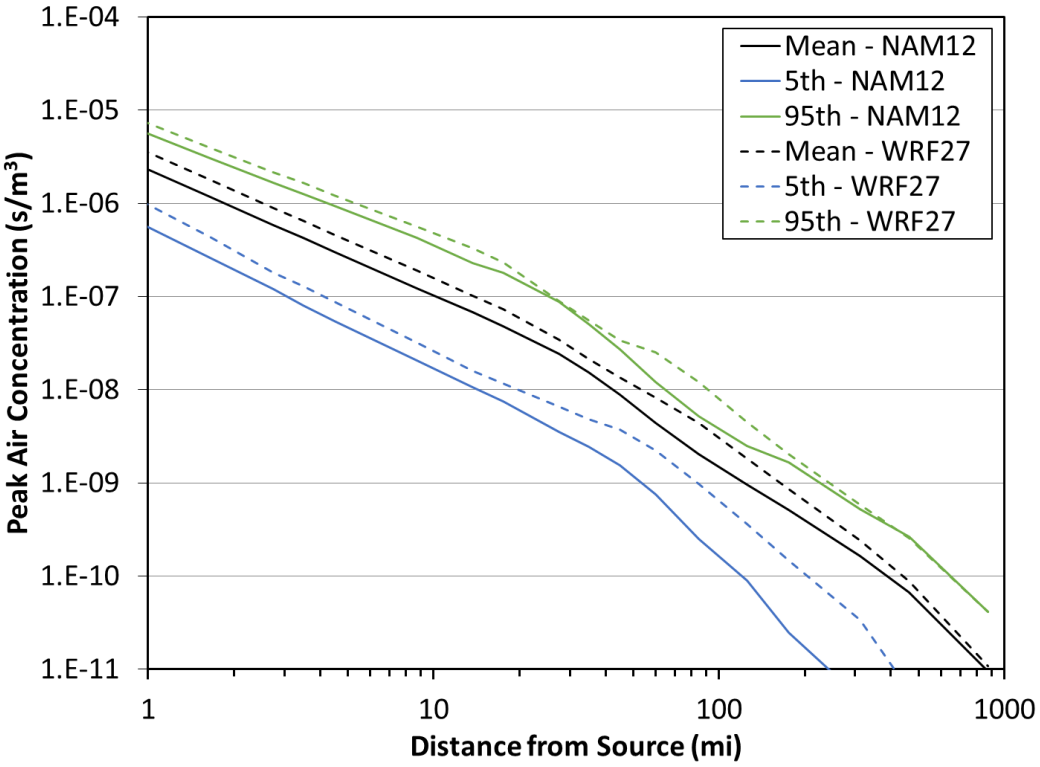

Figure 5-67. Comparison of peak air concentration for two meteorological data sets at Site D with ST #2 using the HYSPLIT ATD model

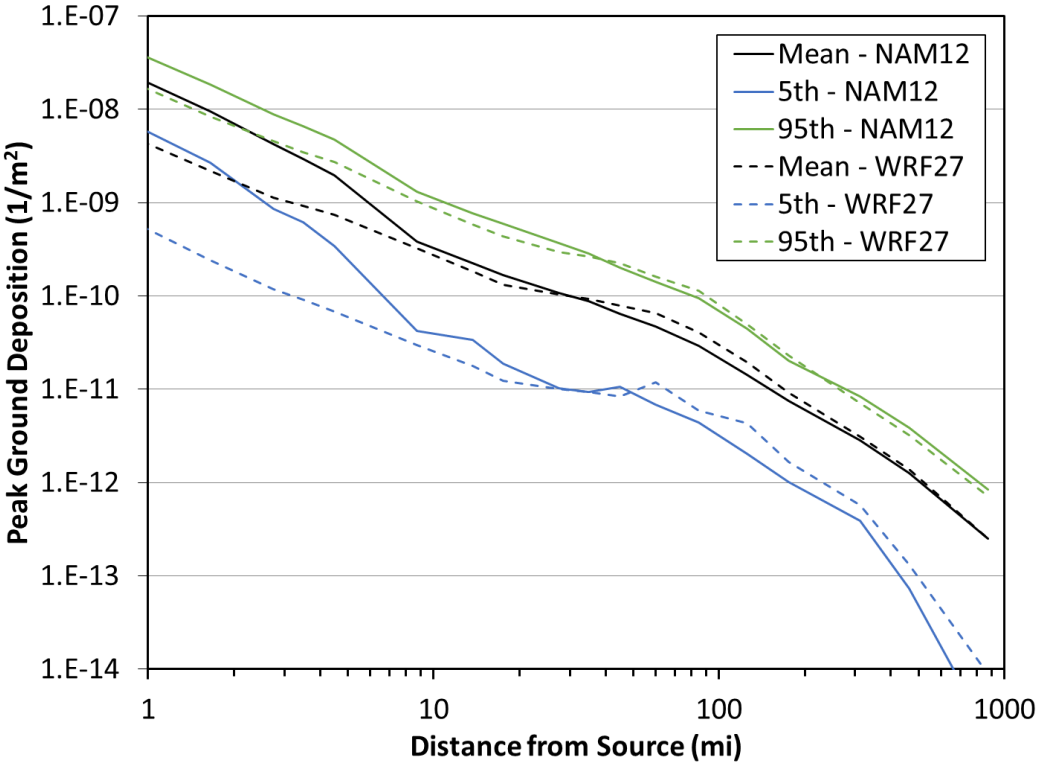

Figure 5-68. Comparison of peak ground deposition for two meteorological data sets at Site D with ST #2 using the HYSPLIT ATD model

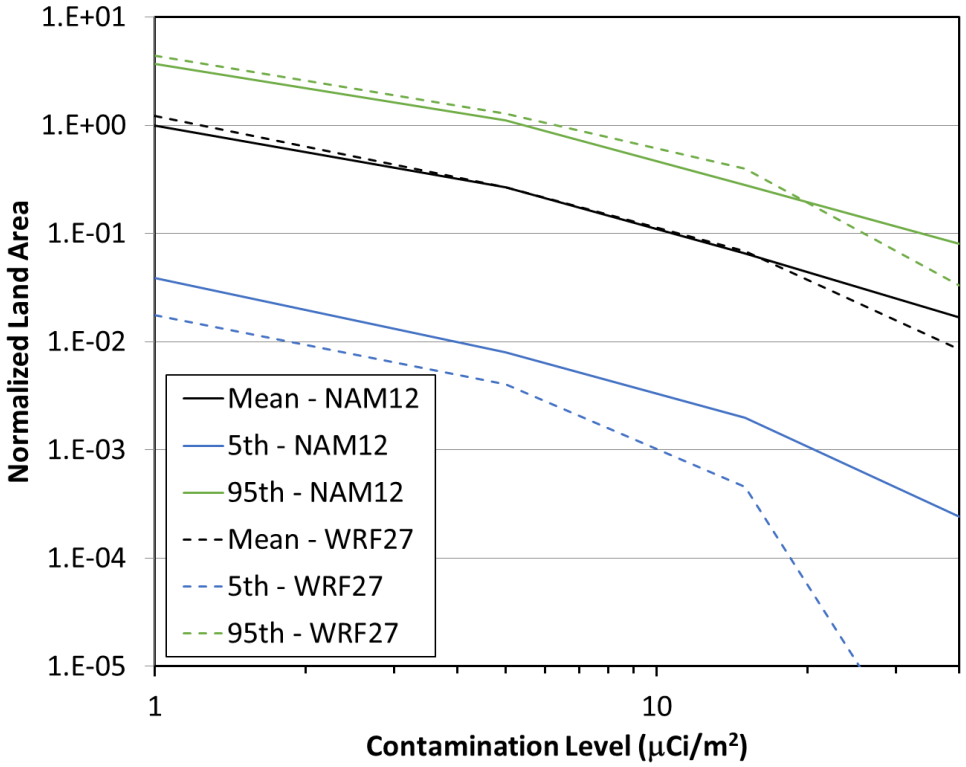

Figure 5-69. Comparison of land contamination area for two meteorological data sets at Site D with ST #2 using the HYSPLIT ATD model

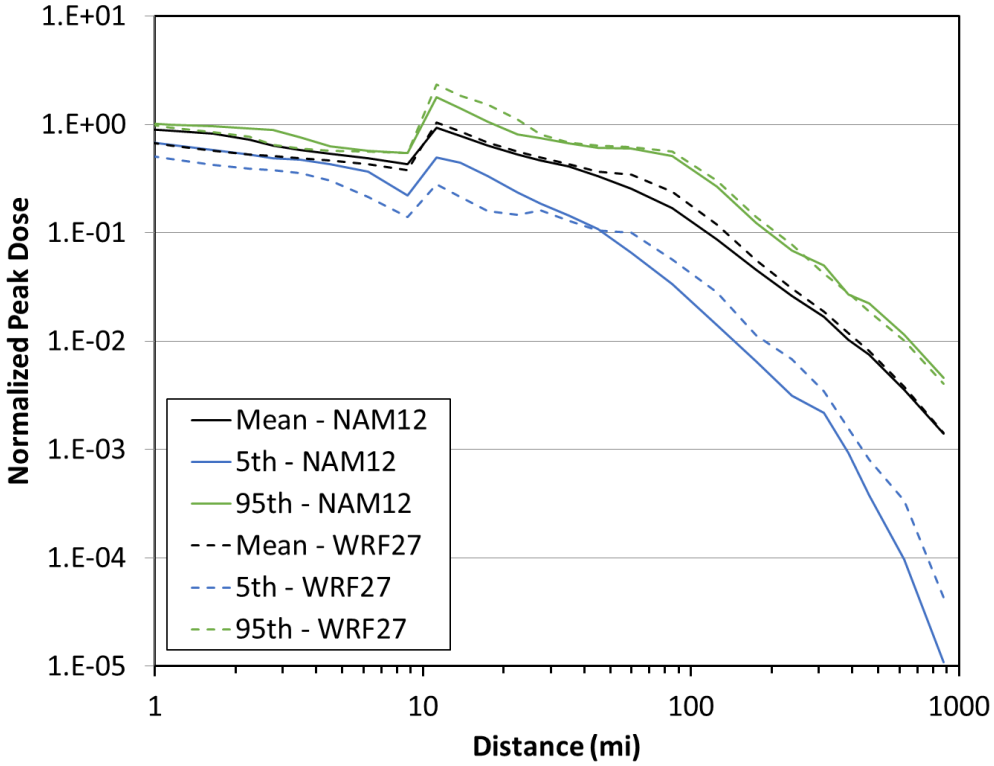

Figure 5-70. Comparison of peak dose for two meteorological data sets at Site D with ST #2 using the HYSPLIT ATD model

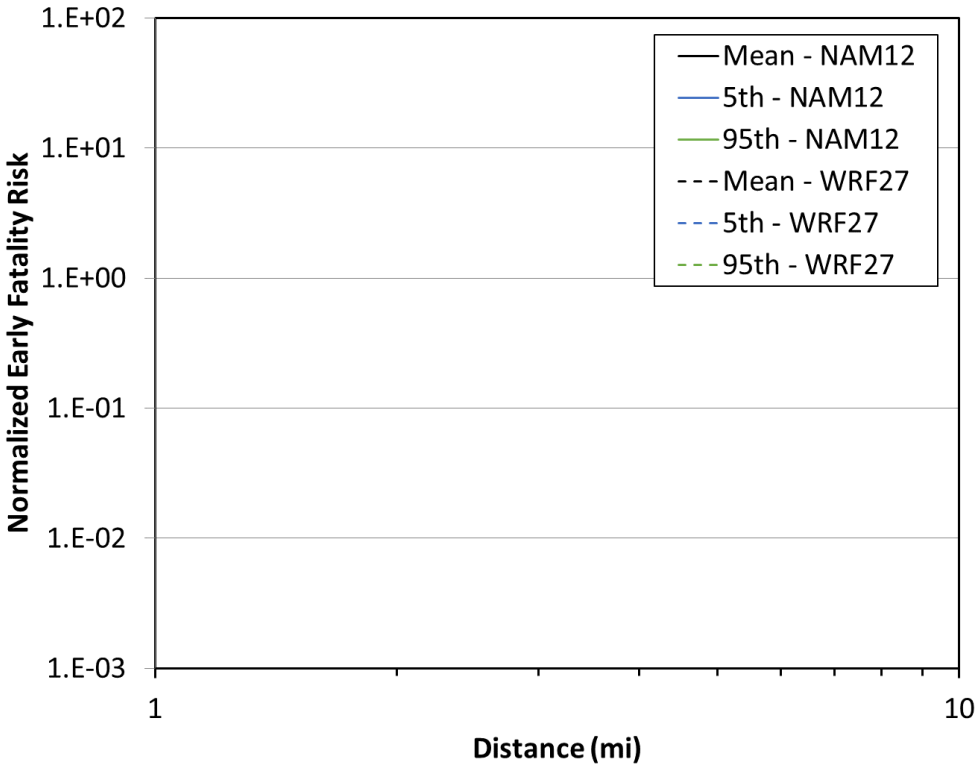

Figure 5-71. Comparison of early fatality risk for two meteorological data sets at Site D with ST #2 using the HYSPLIT ATD model

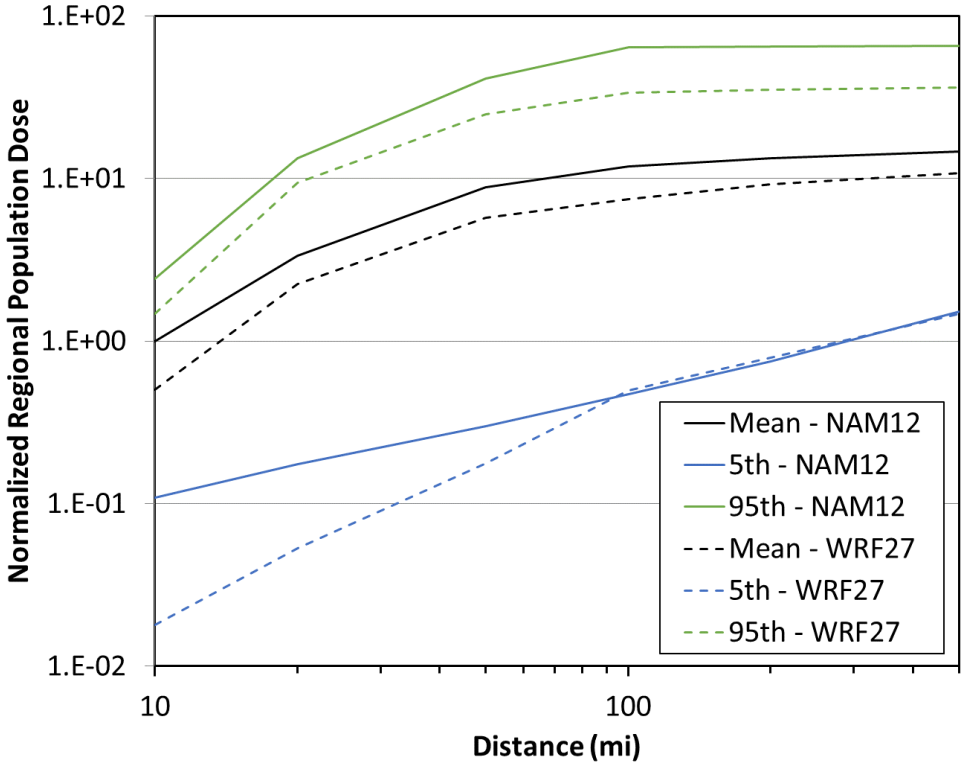

Figure 5-72. Comparison of population dose for two meteorological data sets at Site D with ST #2 using the HYSPLIT ATD model

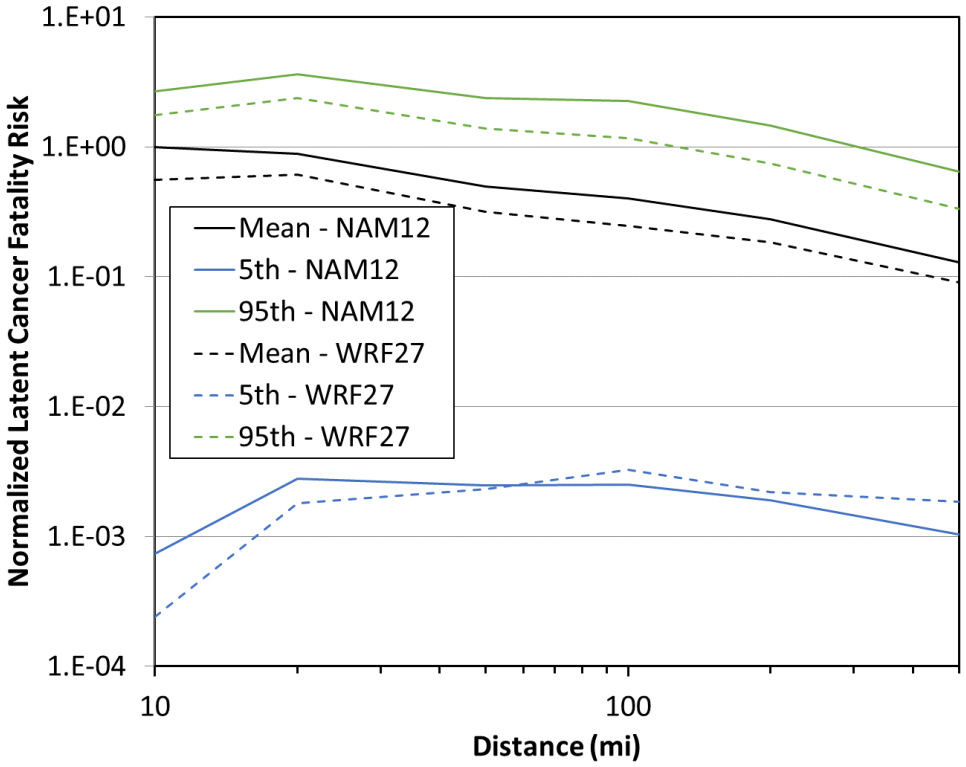

Figure 5-73. Comparison of latent cancer fatality risk for two meteorological data sets at Site D with ST #2 using the HYSPLIT ATD model

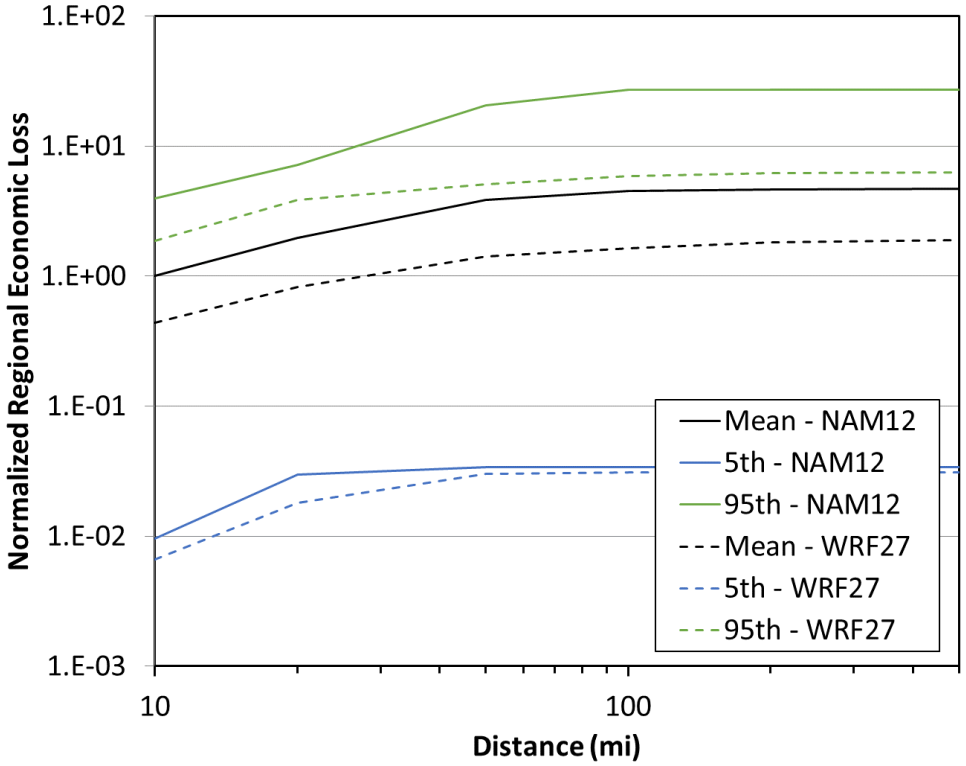

Figure 5-74. Comparison of economic loss for two meteorological data sets at Site D with ST #2 using the HYSPLIT ATD model

5.1.3. *Interpretations of Meteorological Data Source Sensitivity*

This section provides a comprehensive analysis of the results in the multiple figures presented in the previous sections (Sections 5.1.1 through 5.1.2). For the figures in Section 5.1.1, the ratios of the annual average results over the weather input options for the Gaussian calculations with the WRF27 meteorological data set to those for the NAM12 meteorological data set are determined for each output metric as a function of distance. In addition, the ratios of the annual average results over the weather input options for the Gaussian calculations with the Site meteorological data set to those for the NAM12 meteorological data set are determined for each output metric as a function of distance. The averages of these ratios, along with their minimums and maximums from the site out to 805 km (500 mi) are shown in Table 5-1 and Table 5-2, respectively. Table 5-1 shows the relationship of Gaussian model results using a meteorological file derived from the 2008 WRF27 data set as opposed to a meteorological file derived from the 2008 NAM12 data set. Table 5-2 shows the relationship of Gaussian model results using a meteorological file derived from 2008 meteorological observations at the site as opposed to a meteorological file derived from the 2008 NAM12 data set. For the figures in Section 5.1.2, the ratios of the annual average results over the weather input options for the HYSPLIT calculations with the WRF27 meteorological data set to those for the NAM12 meteorological data set are determined for each output metric as a function of distance. The averages of these ratios, along with their minimums and maximums from the site out to 805 km (500 mi) are shown in Table 5-3. Table 5-3 shows the relationship of HYSPLIT model results using the 2008 WRF27 data set as opposed to the 2008 NAM12 data set. The columns represent the outputs in the figures presented above for all distances; i.e., there is no break down between nearfield and far field. For source term #2, EF risk was calculated as zero and so a ratio couldn't be calculated.

Table 5-1. Ratios of the Gaussian annual average results using a weather file derived from the WRF27 meteorological data set to those using a weather file derived from the NAM12 data set, shown as [Average (Minimum | Maximum)]

Site/ Source	Peak Air	Peak Ground	Peak Dose	Pop Dose	LCF Risk	Econ Loss	EF Risk	Land Area
A/1	1.1 (1.0|1.2)	0.9 (0.7|1.1)	1.0 (0.9|1.2)	1.0 (0.9|1.1)	0.9 (0.8|1.0)	0.8 (0.7|1.0)	1.5 (1.4|1.7)	1.0 (0.7|1.2)
D/1	0.7 (0.4|1.1)	0.6 (0.5|1.0)	0.7 (0.4|1.2)	0.8 (0.7|0.9)	0.7 (0.7|0.8)	0.8 (0.6|1.2)	0.1 (0.1|0.2)	1.2 (0.9|1.4)
A/2	1.0 (1.0|1.1)	0.9 (0.6|1.0)	0.9 (0.7|1.1)	0.9 (0.8|1.0)	0.9 (0.8|1.0)	0.9 (0.8|0.9)	a	0.7 (0.6|0.8)
D/2	0.7 (0.5|1.1)	0.6 (0.5|1.0)	0.8 (0.6|1.0)	0.8 (0.7|0.9)	0.8 (0.7|0.9)	0.6 (0.5|0.8)	a	0.6 (0.4|0.8)

[a]Data not available to compute ratio

Table 5-2. Ratios of the Gaussian annual average results using a weather file derived from the site meteorological data set to those using a weather file derived from the NAM12 data set, shown as [Average (Minimum | Maximum)]

Site/ Source	Peak Air	Peak Ground	Peak Dose	Pop Dose	LCF Risk	Econ Loss	EF Risk	Land Area
A/1	1.0 (0.8|1.3)	1.0 (0.6|1.3)	1.0 (0.7|1.4)	1.2 (1.0|1.4)	1.2 (0.9|1.4)	1.2 (1.0|1.4)	0.7 (0.2|1.0)	1.3 (1.1|1.5)
A/2	1.1 (0.8|1.4)	1.1 (0.6|1.4)	0.9 (0.6|1.2)	1.3 (1.2|1.4)	1.3 (1.2|1.5)	1.3 (1.1|1.4)	a	1.2 (1.0|1.3)

[a]Data not available to compute ratio

Table 5-3. Ratios of the HYSPLIT annual average results using the WRF27 meteorological data set to those using the NAM12 data set, shown as [Average (Minimum | Maximum)]

Site/ Source	Peak Air	Peak Ground	Peak Dose	Pop Dose	LCF Risk	Econ Loss	EF Risk	Land Area
A/1	1.9 (1.2|2.6)	0.9 (0.4|1.3)	1.5 (0.9|1.9)	1.2 (1.1|1.3)	1.2 (1.1|1.3)	1.0 (0.8|1.1)	1.3 (1.2|1.3)	1.0 (0.9|1.0)
D/1	1.6 (1.3|2.3)	0.9 (0.2|1.4)	1.4 (1.1|1.6)	1.1 (1.1|1.2)	1.2 (1.2|1.4)	0.7 (0.6|0.8)	1.1 (1.0|1.2)	1.1 (1.1|1.2)
A/2	1.9 (1.3|2.3)	0.9 (0.4|1.2)	1.1 (0.8|1.3)	1.1 (0.7|1.2)	1.1 (0.7|1.3)	0.8 (0.6|1.0)	a	0.8 (0.4|1.0)
D/2	1.6 (1.3|2.2)	0.9 (0.2|1.4)	1.0 (0.7|1.4)	0.6 (0.5|0.7)	0.6 (0.6|0.7)	0.4 (0.4|0.4)	a	0.9 (0.5|1.2)

[a]Data not available to compute ratio

General results determined by examining the comparisons between the Gaussian and HYSPLIT ATD model calculations for the three meteorological data sets for Site A and the two meteorological data sets for Site D and two source terms are discussed below. Caution should be used in generalizing these interpretations to other sites or consequence metrics. The interpretations in this section summarize the trends from the results above.

1. The level of agreement between annual average results from the Gaussian ATD model when using a weather file derived from the three meteorological data sets is within plus or minus 50% with both source terms and for all consequence metrics. The trends in the level of agreement as a function of distance also agree between the three meteorological data set options. Differences resulting from the source of meteorological data are on the order of half the differences between the Gaussian and HYSPLIT ATD consequence metrics shown in the Section 4.7.
2. The levels of agreement from the Gaussian ATD model with the Site meteorological data set are generally about equal or greater than those with the corresponding NAM12-derived weather file results for both source terms for the consequence metrics: population dose, latent caner fatality risk, contaminated land area, and economic loss. The WRF27-dervied weather file results are generally lower than or equal to the NAM12-dervied weather file results for both source terms and all output quantities.
3. The levels of agreement between annual average results from the HYSPLIT ATD model for the NAM12 and WRF27 meteorological data sets, two source terms, and all output quantities are within 60%, except for peak air concentration for Site A at a ratio of 1.9. The trends as a function of distance for the output quantities agree as well.

5.2. Method to Determine Stability Class

The second sensitivity study explores the effect of the method used to estimate stability class for the MacMetGen-generated meteorological file on the model outputs. For the benchmark analyses, the stability class for the MacMetGen-generated meteorological file was determined from the NAM12 meteorological data set using the vertical temperature gradient over the lower 200 m at the site (labeled DTDZ) using the criteria shown in Table 1 of (US NRC, 2007). This method was compared with two alternative methods to determine the stability class for MACMETGEN-generated meteorological file. Each of these options were exercised using data from the 2008 NAM12 meteorological data and were used with the MACCS Gaussian ATD model option.

- The first option for determining stability class is the traditional DTDZ method that was used for the analyses shown in Section 4.
- The second option, labeled SRDT, is an alternative method that uses the wind speed, time of day, solar radiation flux, and the vertical temperature gradient at the site from the NAM12

meteorological data file to apply a method that replicates Turner's method, but does not require cloud cover information (US EPA, 2000) for stability class. This method was selected because cloud cover information is not available in the NAM12 2008 meteorological data set.

- The third option, label VMIX, is an alternative method that uses a routine that is included with HYSPLIT, called VMIXING with the default options (Draxler and Hess, 1997; Draxler and Hess, 1998; Draxler, 1999; Stein et al., 2015), which determines the stability class from the wind speed and turbulent kinetic energy.

Figure 5-75 and Figure 5-76 display the average stability class as a function of wind direction for the three stability class options at Site A and Site D, respectively. The average stability class is shown, based on hourly values from 1 (A) to 7 (G). Figure 5-77 and Figure 5-78 show the distribution of stability class as a function of time of day for the three options for Site A and Site D, respectively. For both sites, the DTDZ option is dominated (54% and 41% of the year for Site A and D, respectively,) by stable conditions (5 [E] to 7 [G]), while the VMIX options is dominated (47% and 43% of the year for Site A and D, respectively,) by unstable conditions (1 [A] to 3 [C]). The SRDT option is dominated (39% and 73% of the year for Site A and D, respectively,) by neutral conditions.

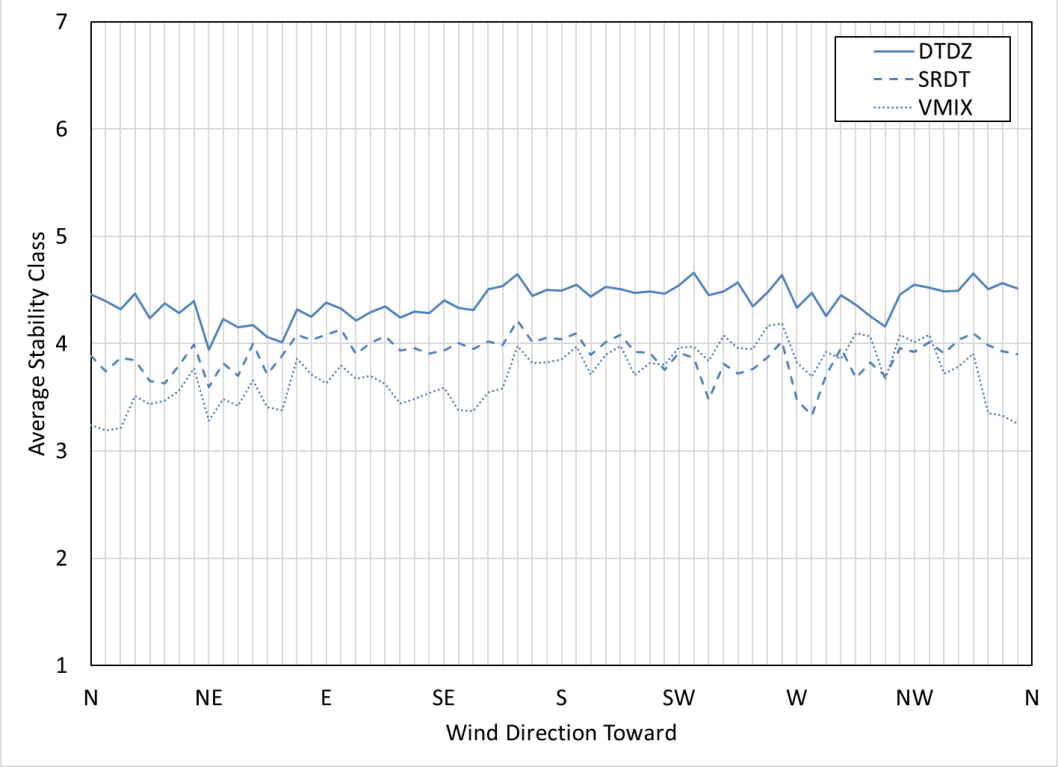

Figure 5-75. Average stability class as a function of wind direction for the three methods to determine stability class for Site A

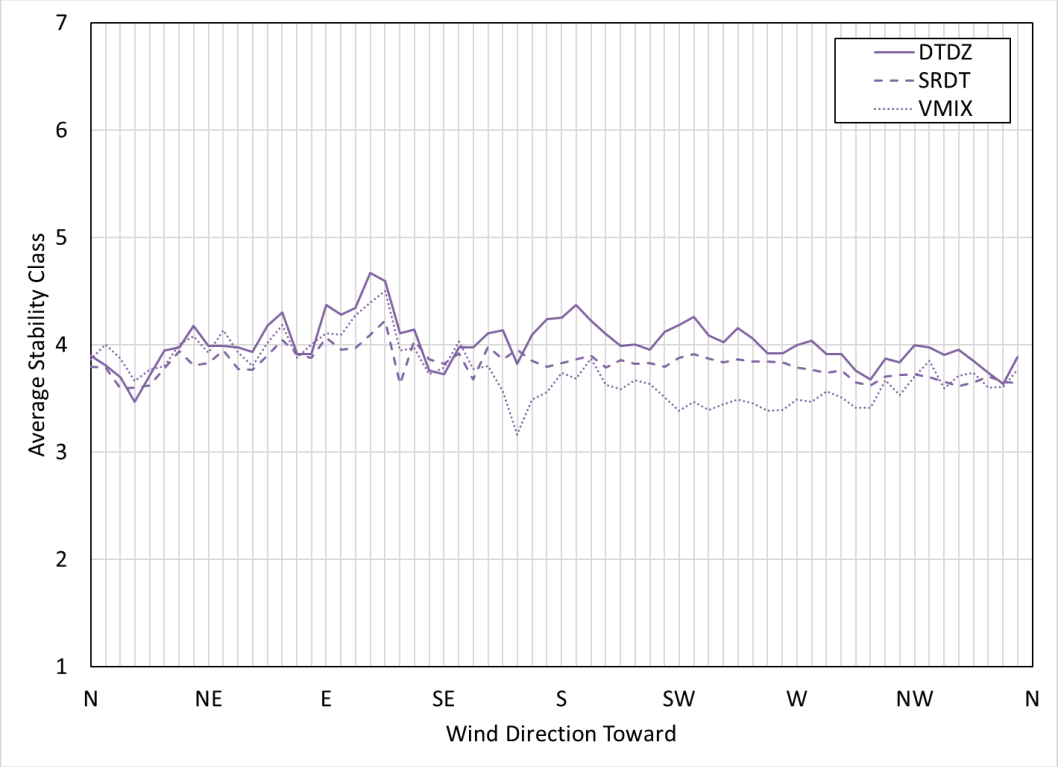

Figure 5-76. Average stability class as a function of wind direction for the three methods to determine stability class for Site D

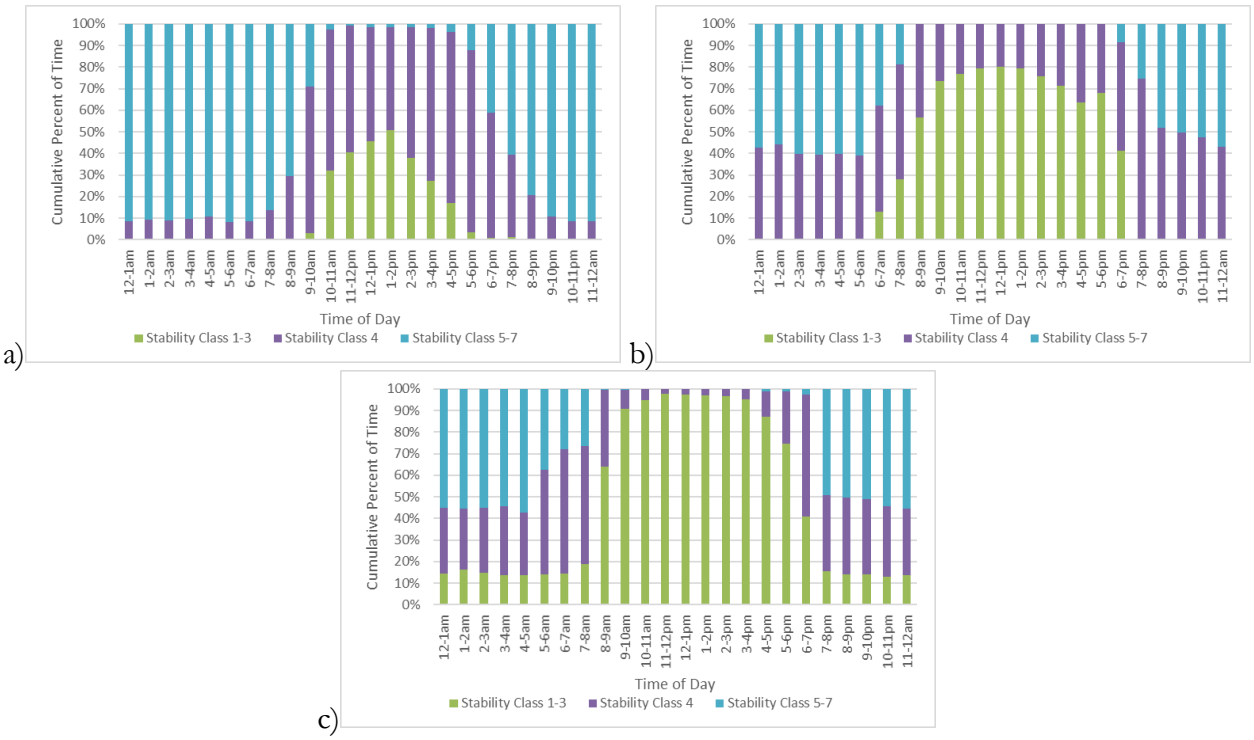

Figure 5-77. Stability class distribution as a function of time of day for the a) DTDZ, b) SRDT, and c) VMIX stability class methods for Site A

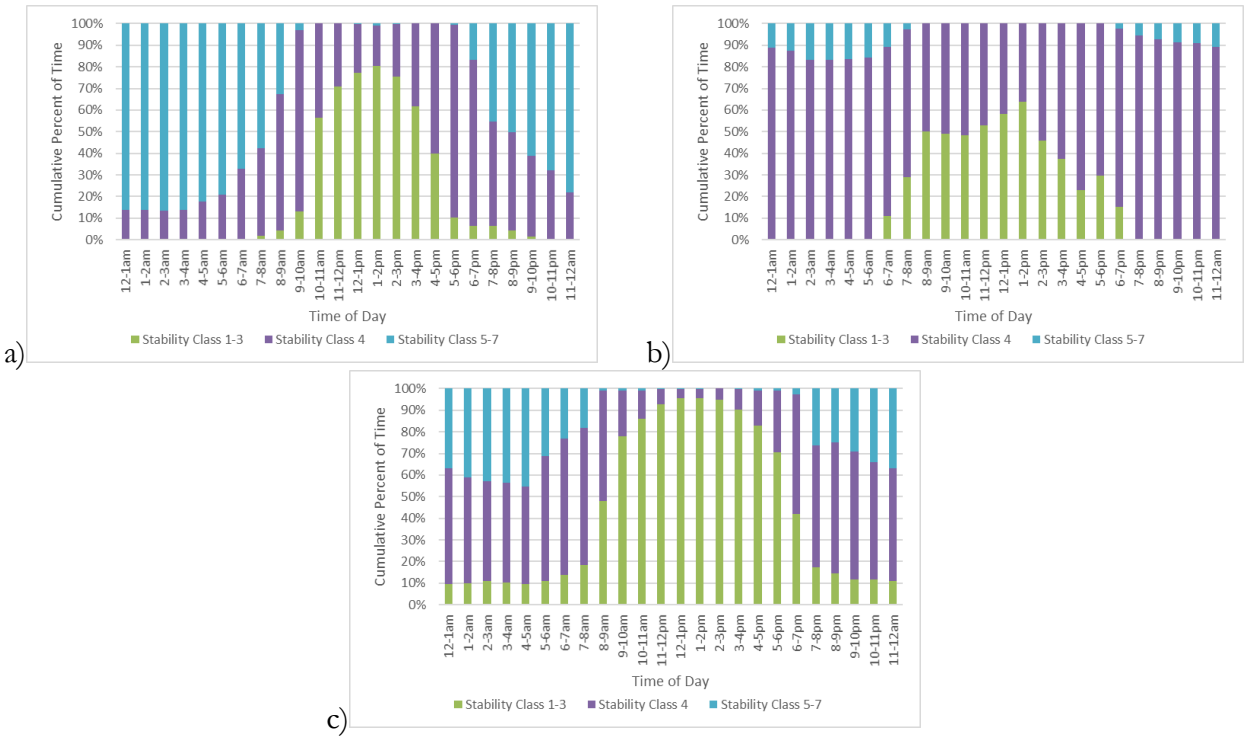

Figure 5-78. Stability class distribution as a function of time of day for the a) DTDZ, b) SRDT, and c) VMIX stability class methods for Site D

The comparisons in the following sections show the results using the MACCS Gaussian ATD model with the three stability class methods for both source terms for both Site A and Site D. Wind direction, wind speed, and precipitation rates are the same for all three cases and are shown as the NAM12 curves in Figure 5-1 and Figure 5-2, Figure 5-3 and Figure 5-4, and Figure 5-9 and Figure 5-10, respectively.

5.2.1. Site A

5.2.1.1. Source Term #1

Results for peak air concentration, peak ground deposition, land contamination area, peak dose, early fatality risk, population dose, latent cancer fatality risk, and economic loss (as described in Section 3.6) using the Gaussian ATD model at Site A with ST #1 are compared for the DTDZ, SRDT, and VMIX stability class methods in Figure 5-79 through Figure 5-86. The annual statistics for these measures are shown with different colors, where the mean values are in black, the 5th percentile values are shown in blue, and the 95th percentile values are shown in green. HYSPLIT results are shown as dashed lines and Gaussian model results are shown as solid lines. The normalized results are shown as a function of distance, rather than the ratio of Gaussian and HYSPLIT results, to allow for the trends with distance to be observed. Some results are zero for early fatality risk, so they cannot be shown on the log scale used in the figures. Discussion of the difference seen in these figures is provided below in Section 5.2.3.

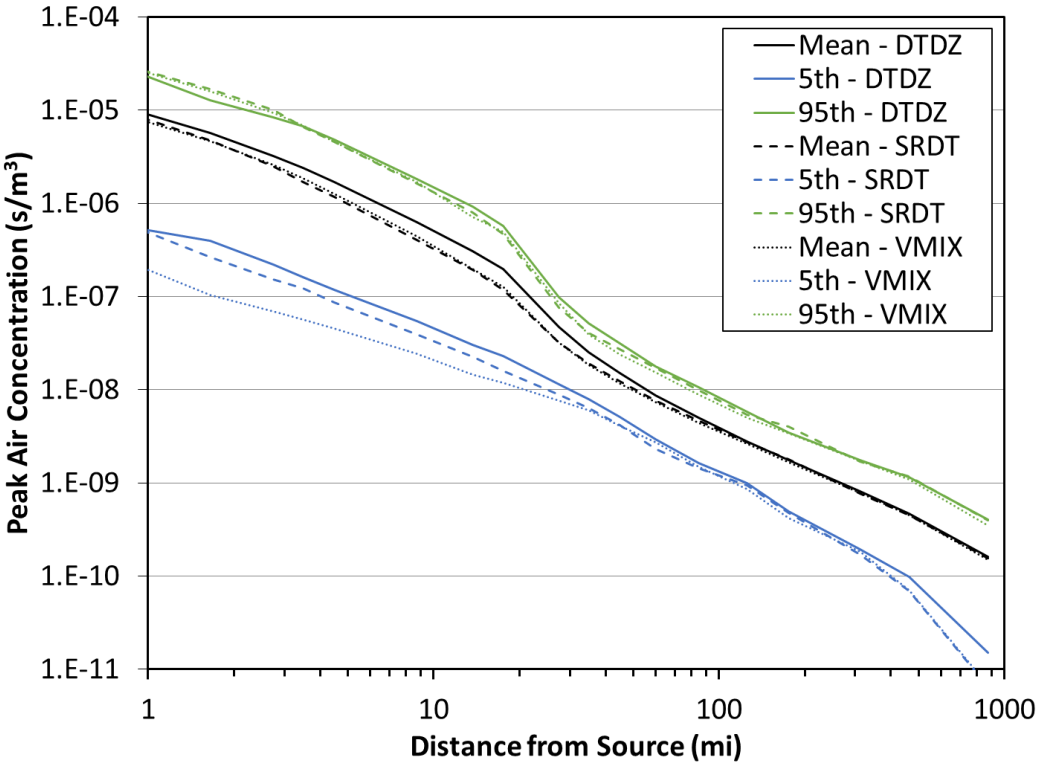

Figure 5-79. Peak air concentration comparison for three stability class methods (Site A, ST #1)

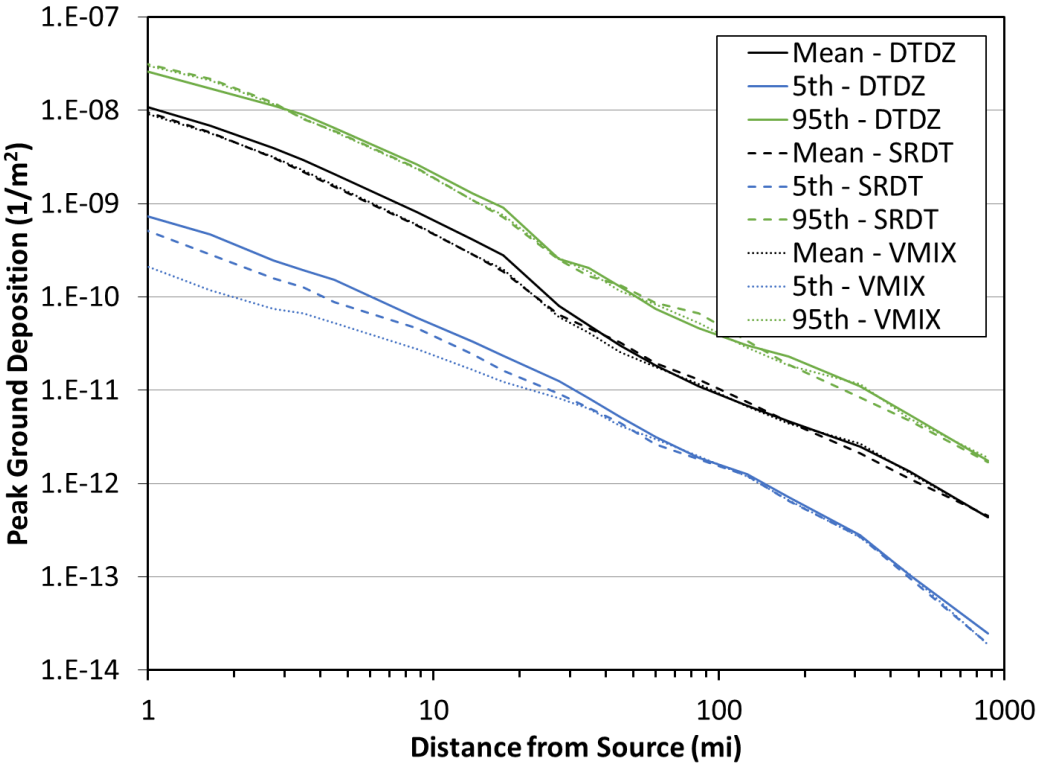

Figure 5-80. Peak ground deposition comparison for three stability class methods (Site A, ST #1)

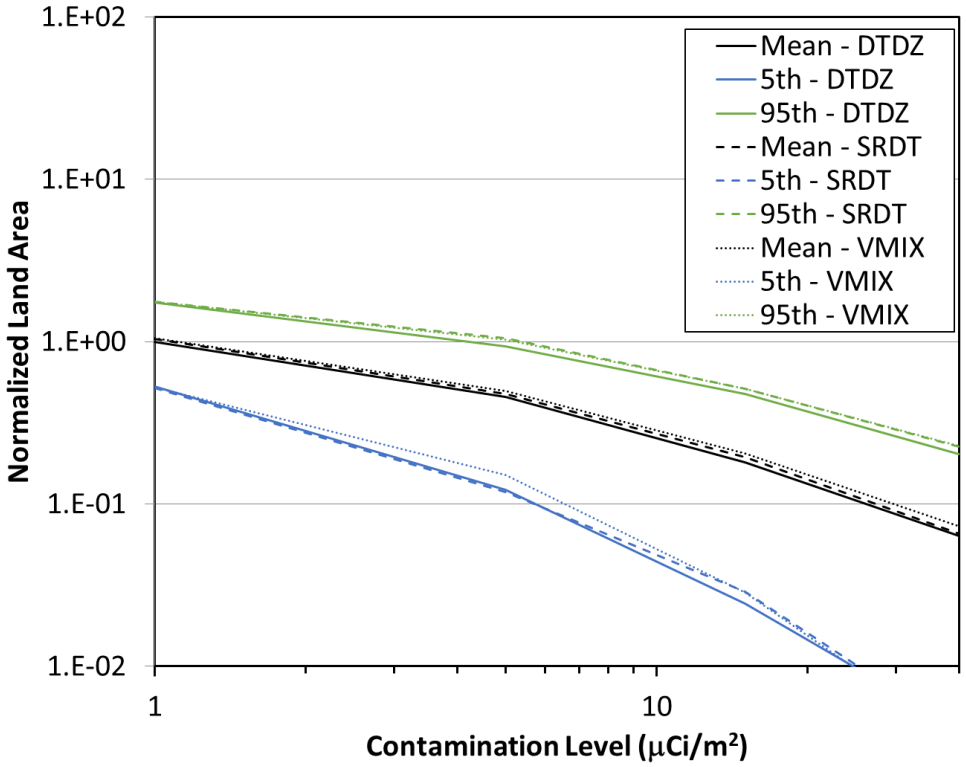

Figure 5-81. Land contamination area within 805 km (500 mi) comparison for three stability class methods (Site A, ST #1)

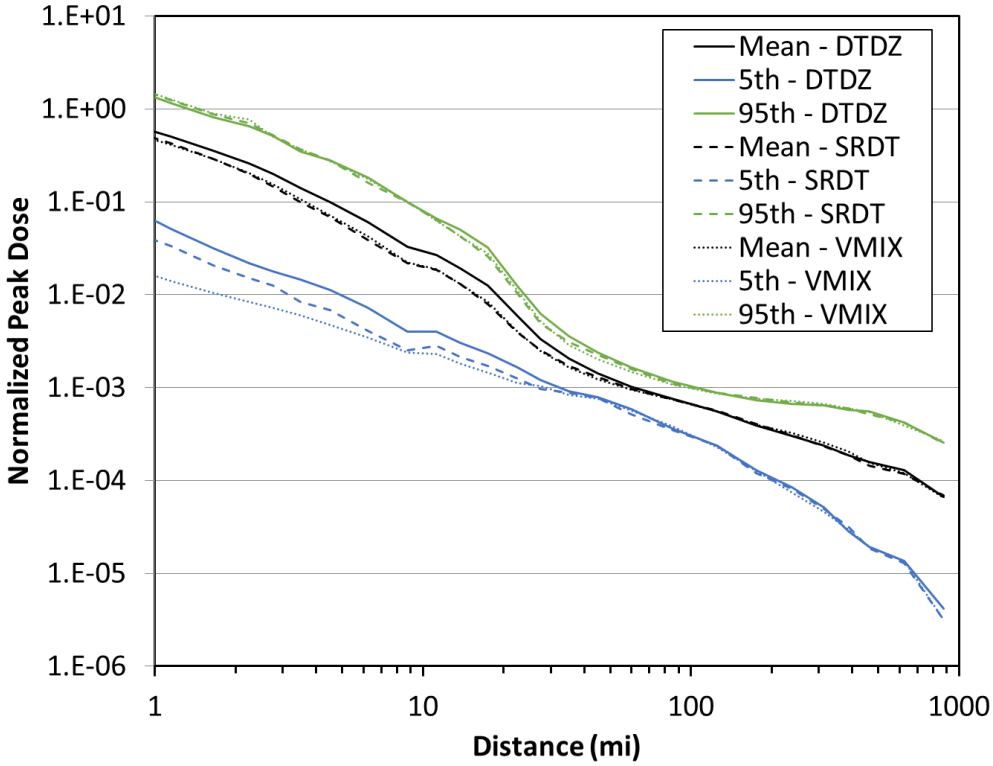

Figure 5-82. Peak dose comparison for three stability class methods (Site A, ST #1)

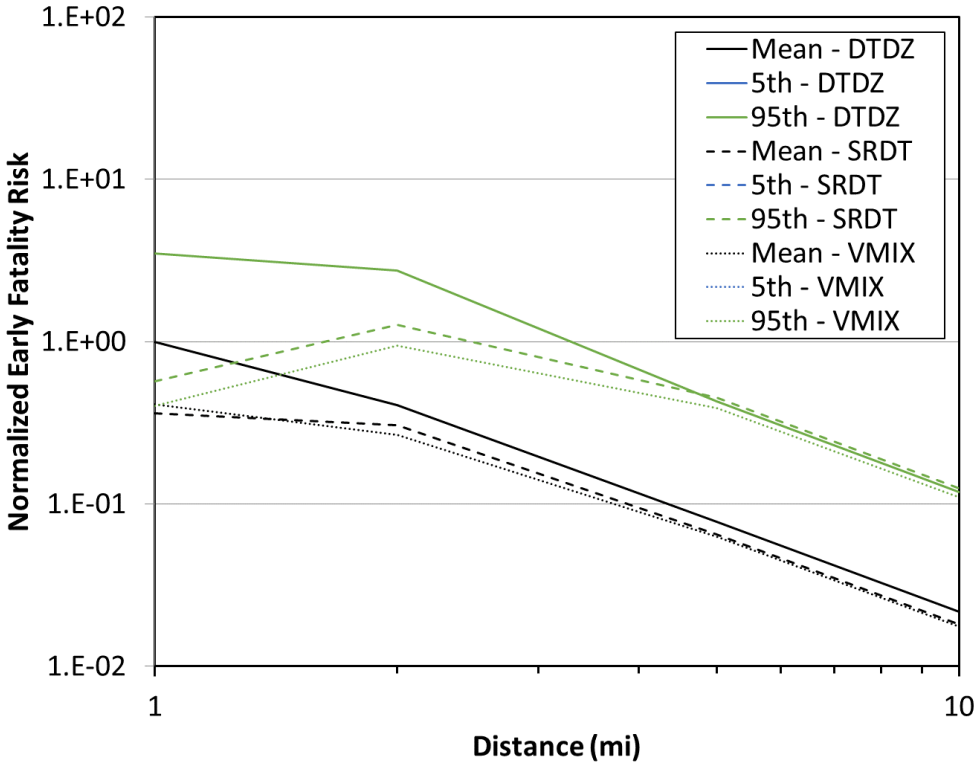

Figure 5-83. Early fatality risk comparison for three stability class methods (Site A, ST #1)

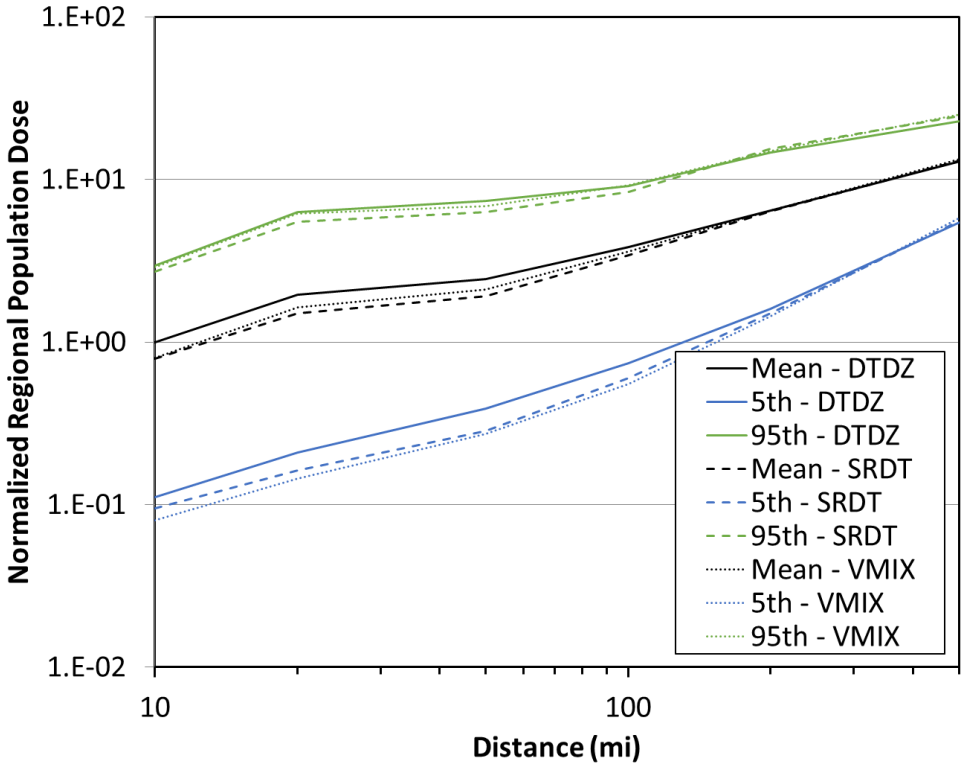

Figure 5-84. Population dose comparison for three stability class methods (Site A, ST #1)

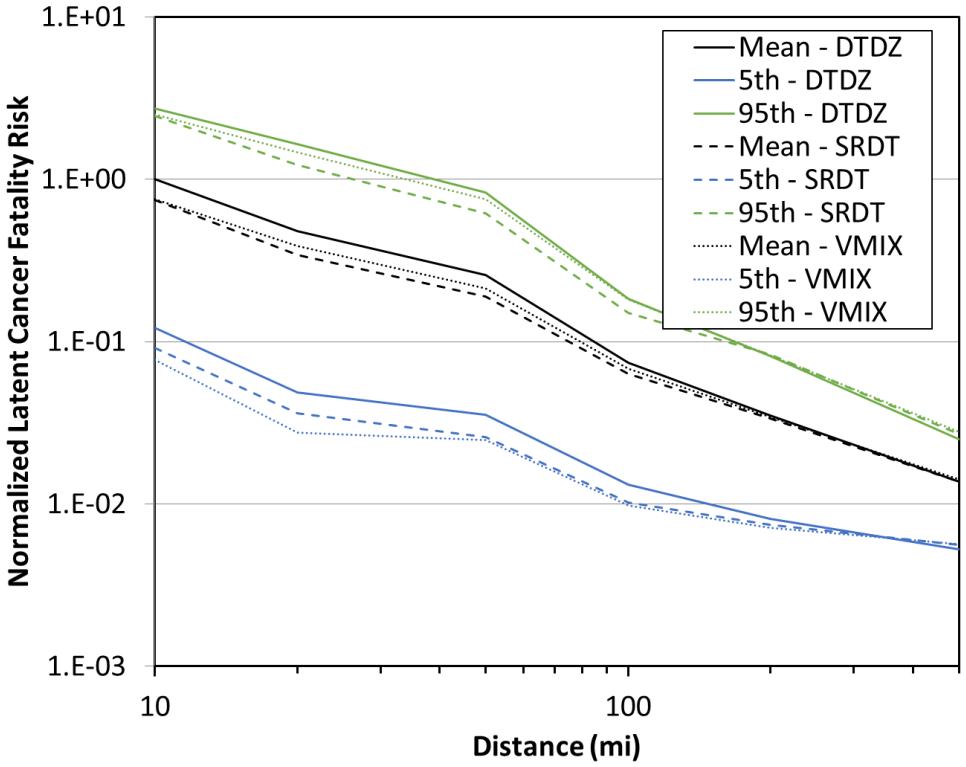

Figure 5-85. Latent cancer fatality risk comparison for three stability class methods (Site A, ST #1)

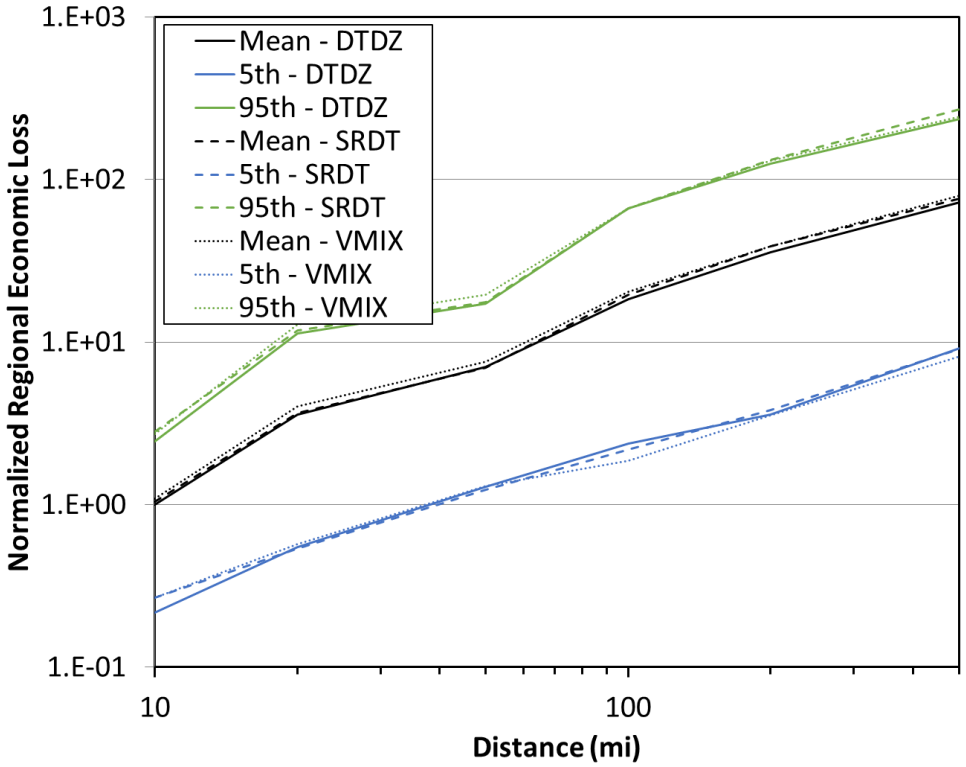

Figure 5-86. Economic loss comparison for three stability class methods (Site A, ST #1)

5.2.1.2. Source Term #2

Results for peak air concentration, peak ground deposition, land contamination area, peak dose, early fatality risk, population dose, latent cancer fatality risk, and economic loss (as described in Section 3.6) using the Gaussian ATD model at Site A with ST #2 are compared for the DTDZ, SRDT, and VMIX stability class methods in Figure 5-87 through Figure 5-94. The annual statistics for these measures are shown with different colors, where the mean values are in black, the 5th percentile values are shown in blue, and the 95th percentile values are shown in green. HYSPLIT results are shown as dashed lines and Gaussian model results are shown as solid lines. The normalized results are shown as a function of distance, rather than the ratio of Gaussian and HYSPLIT results, to allow for the trends with distance to be observed. Some results are zero for early fatality risk, so they cannot be shown on the log scale used in the figures. Discussion of the difference seen in these figures is provided below in Section 5.2.3.

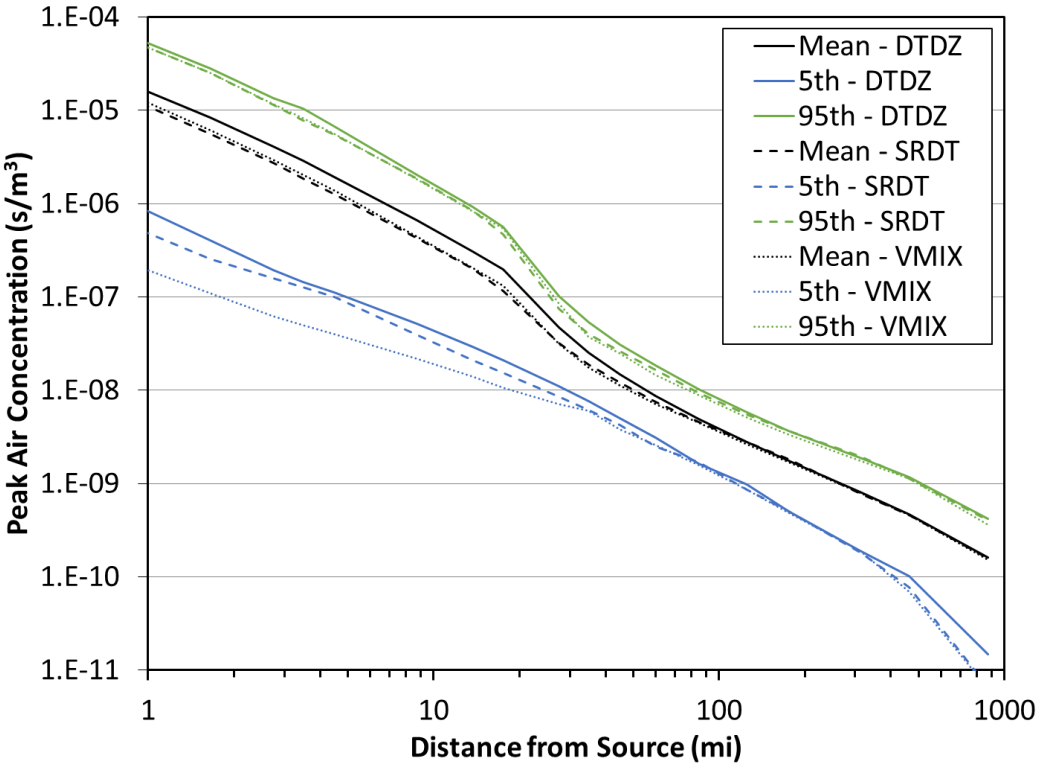

Figure 5-87. Peak air concentration comparison for three stability class methods (Site A, ST #2)

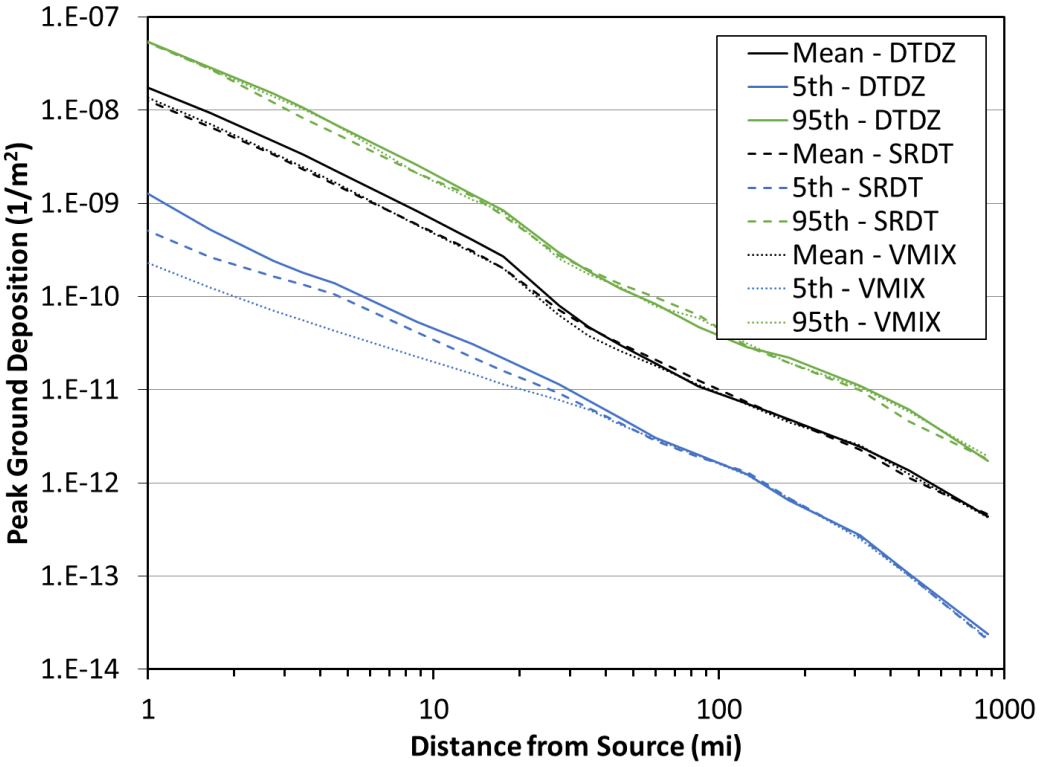

Figure 5-88. Peak ground deposition comparison for three stability class methods (Site A, ST #2)

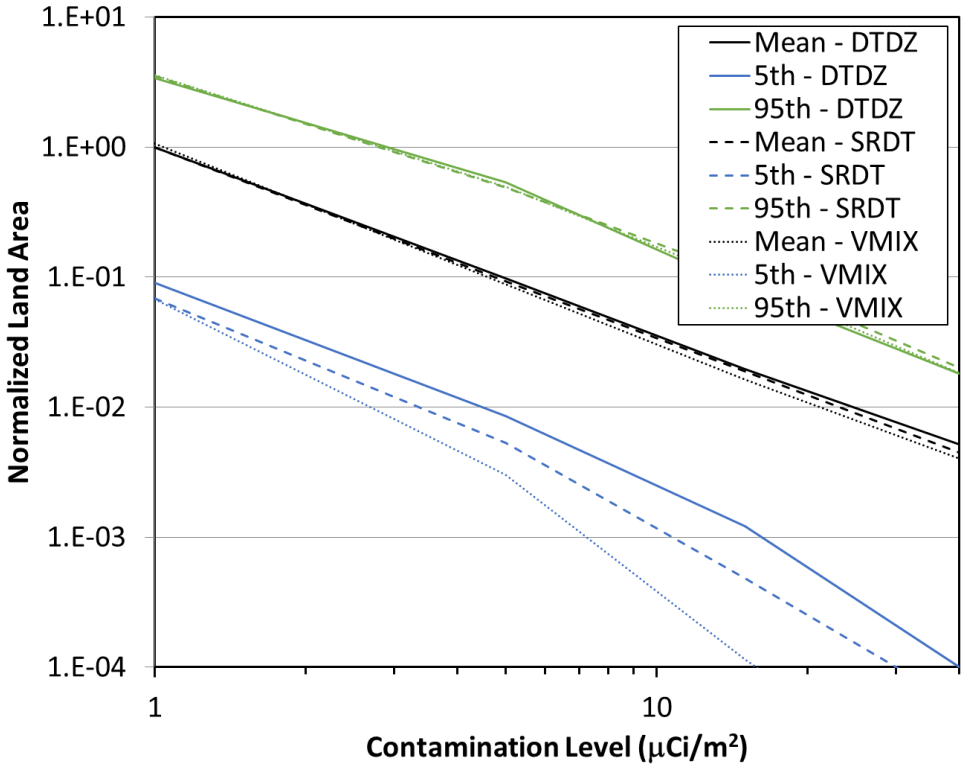

Figure 5-89. Land contamination area within 805 km (500 mi) comparison for three stability class methods (Site A, ST #2)

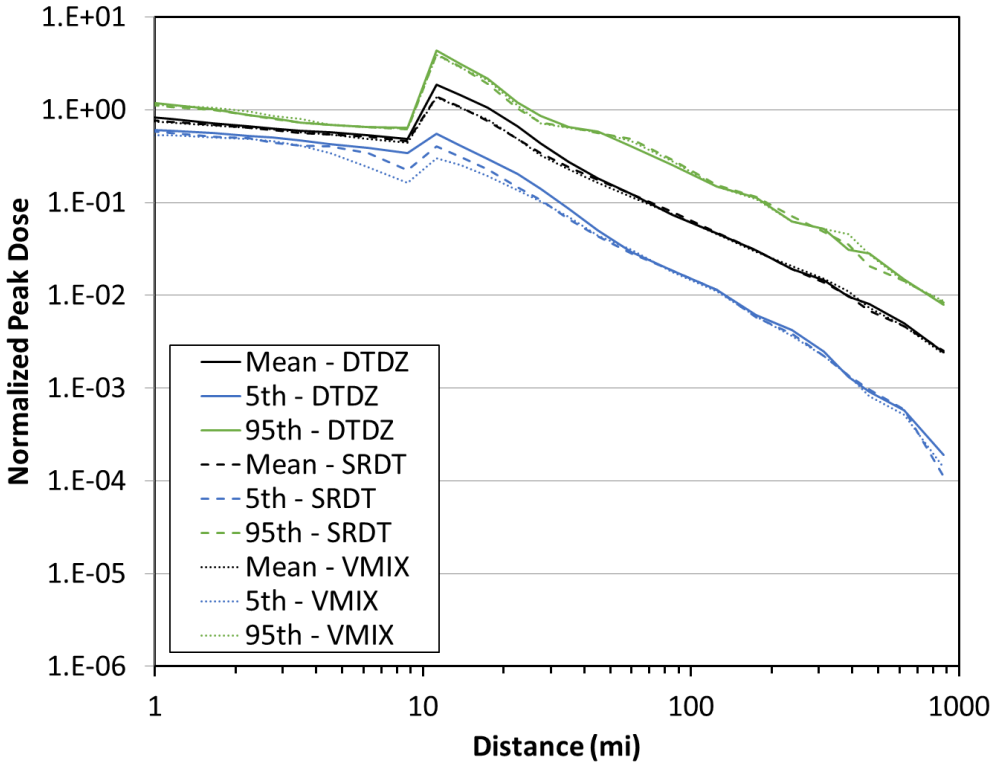

Figure 5-90. Peak dose comparison for three stability class methods (Site A, ST #2)

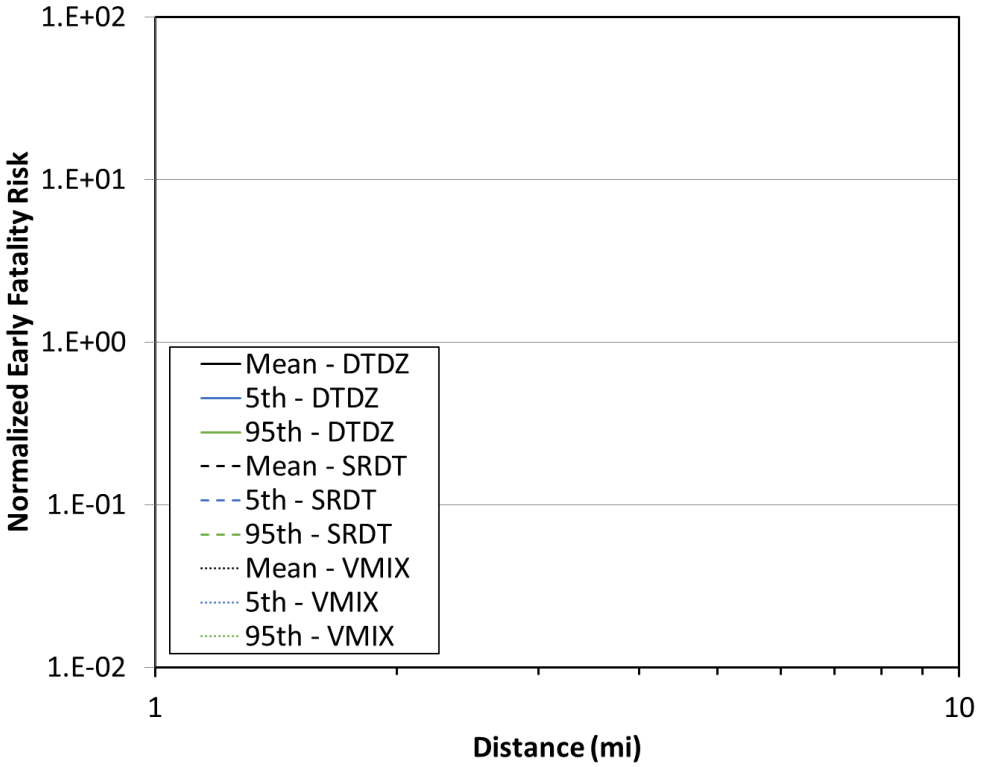

Figure 5-91. Early fatality risk comparison for three stability class methods (Site A, ST #2)

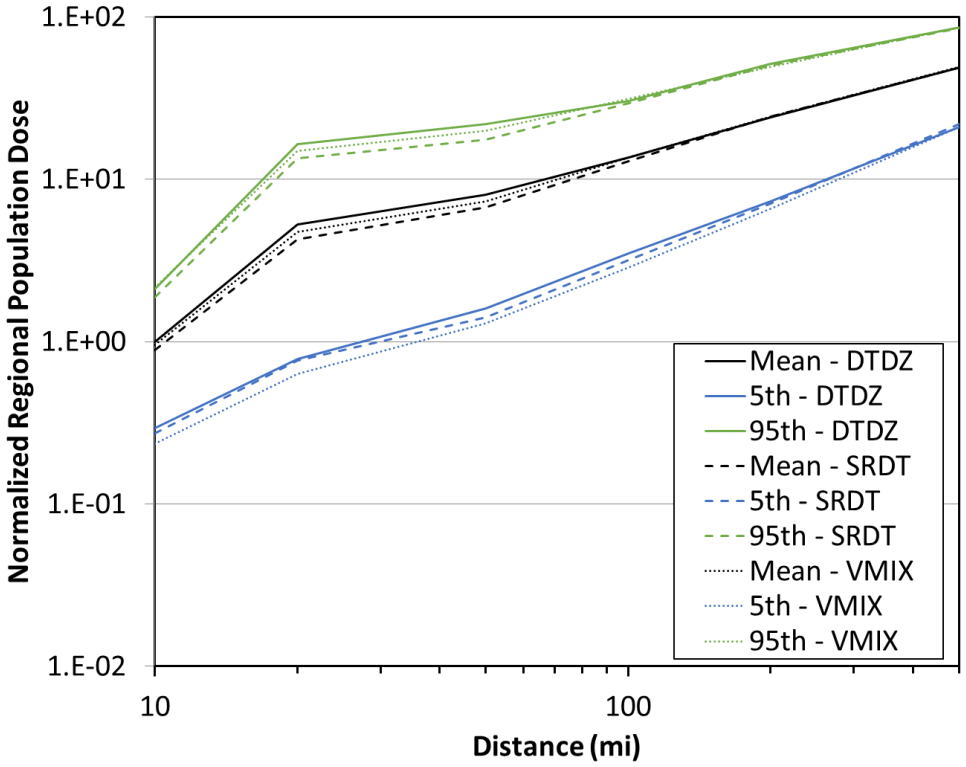

Figure 5-92. Population dose comparison for three stability class methods (Site A, ST #2)

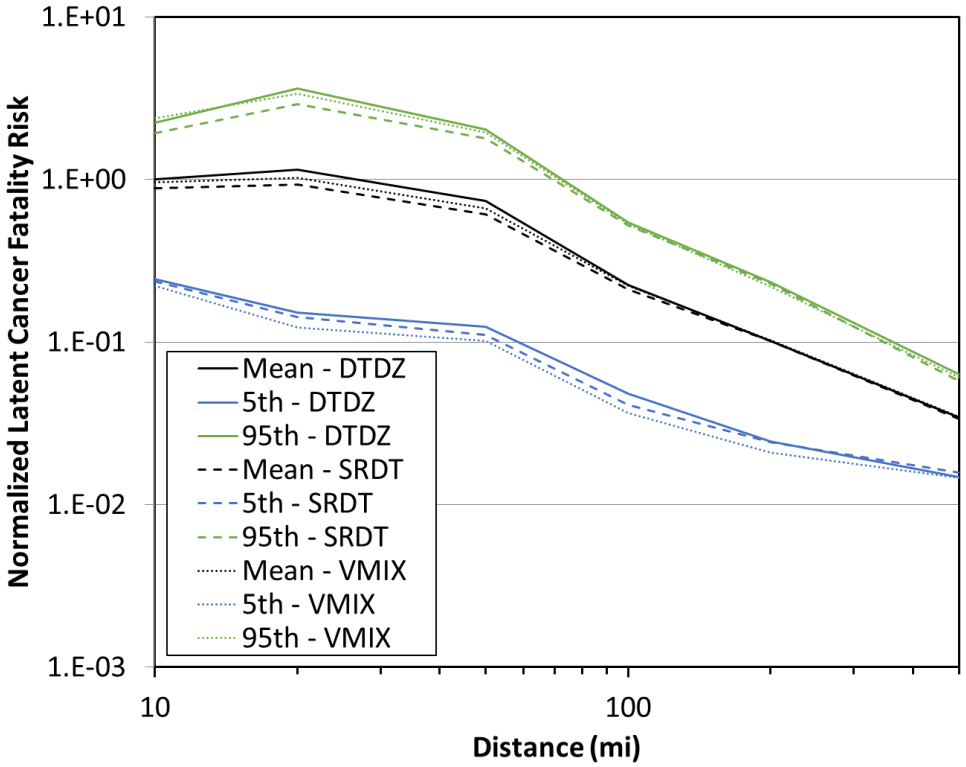

Figure 5-93. Latent cancer fatality risk comparison for three stability class methods (Site A, ST #2)

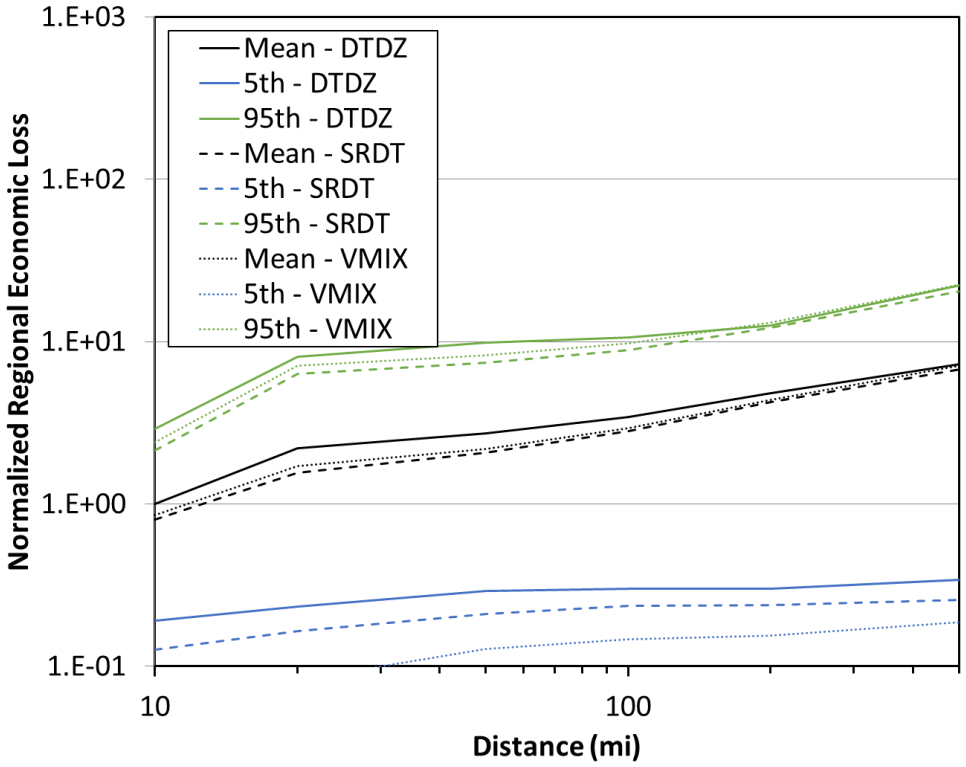

Figure 5-94. Economic loss comparison for three stability class methods (Site A, ST #2)

5.2.2. Site D

5.2.2.1. Source Term #1

Results for peak air concentration, peak ground deposition, land contamination area, peak dose, early fatality risk, population dose, latent cancer fatality risk, and economic loss (as described in Section 3.6) using the Gaussian ATD model at Site D with ST #1 are compared for the DTDZ, SRDT, and VMIX stability class methods in Figure 5-95 through Figure 5-102. The annual statistics for these measures are shown with different colors, where the mean values are in black, the 5th percentile values are shown in blue, and the 95th percentile values are shown in green. HYSPLIT results are shown as dashed lines and Gaussian model results are shown as solid lines. The normalized results are shown as a function of distance, rather than the ratio of Gaussian and HYSPLIT results, to allow for the trends with distance to be observed. Some results are zero for early fatality risk, so they cannot be shown on the log scale used in the figures. Discussion of the difference seen in these figures is provided below in Section 5.2.3.

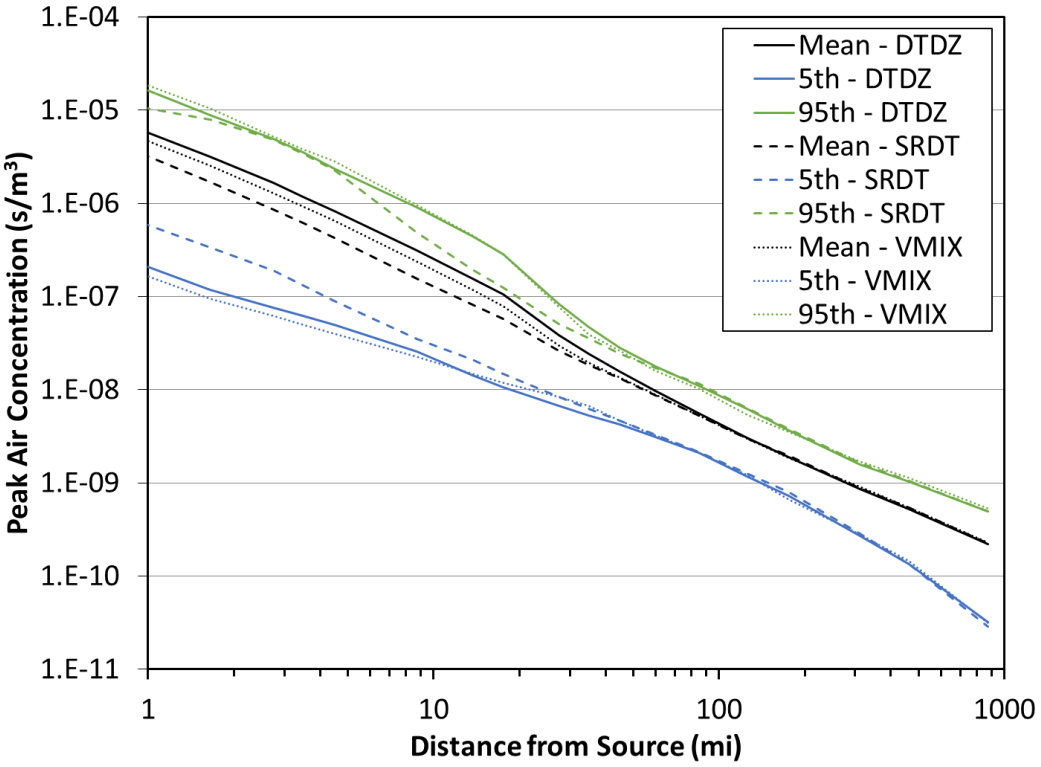

Figure 5-95. Peak air concentration comparison for three stability class methods (Site D, ST #1)

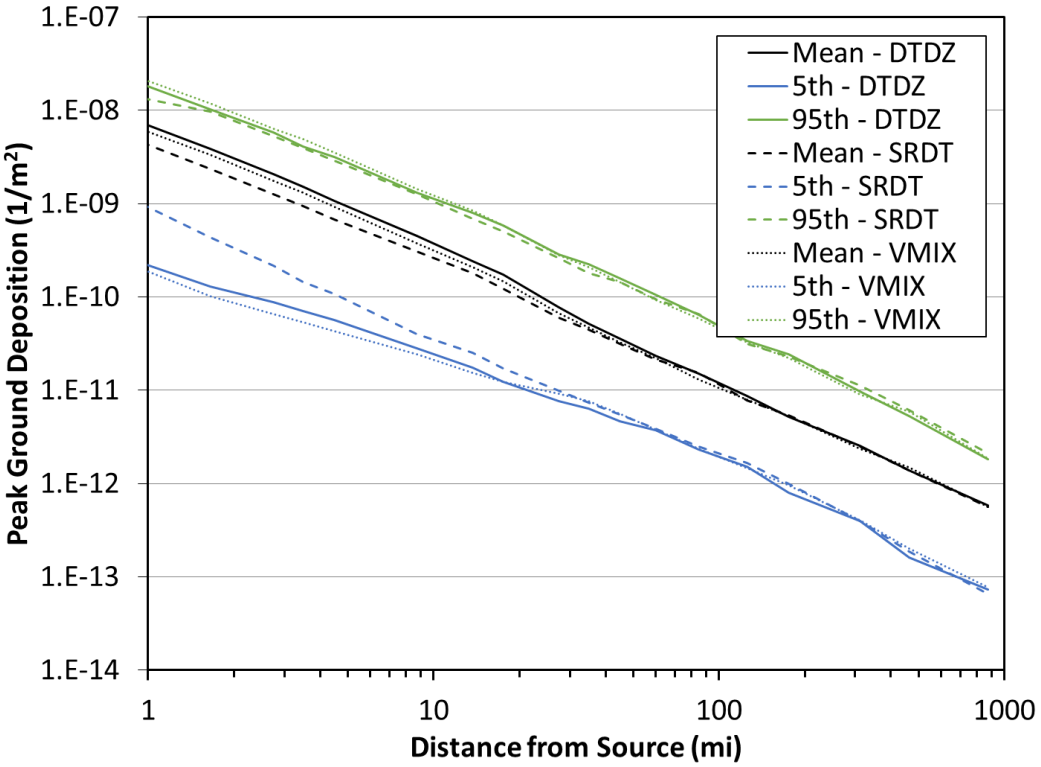

Figure 5-96. Peak ground deposition comparison for three stability class methods (Site D, ST #1)

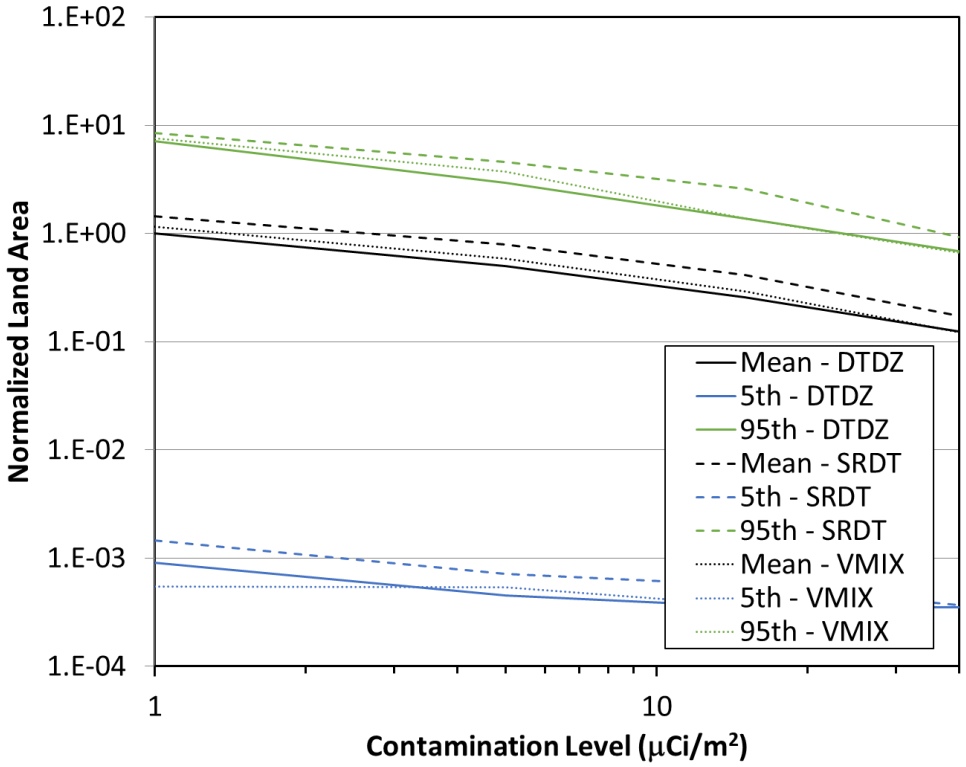

Figure 5-97. Land contamination area within 805 km (500 mi) comparison for three stability class methods (Site D, ST #1)

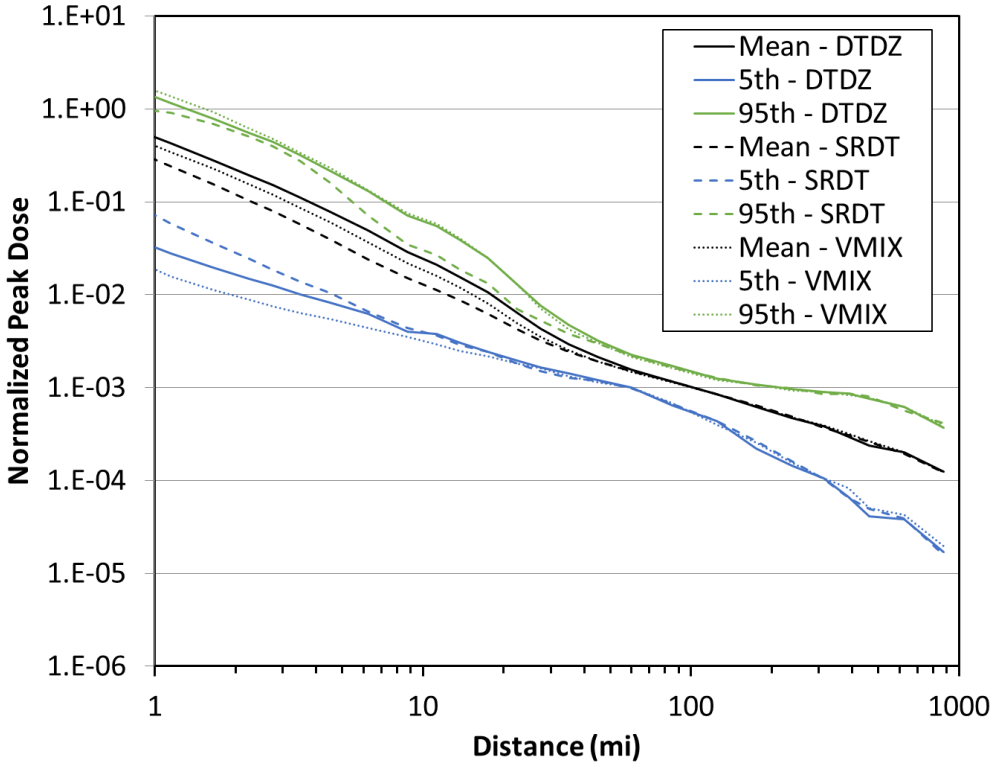

Figure 5-98. Peak dose comparison for three stability class methods (Site D, ST #1)

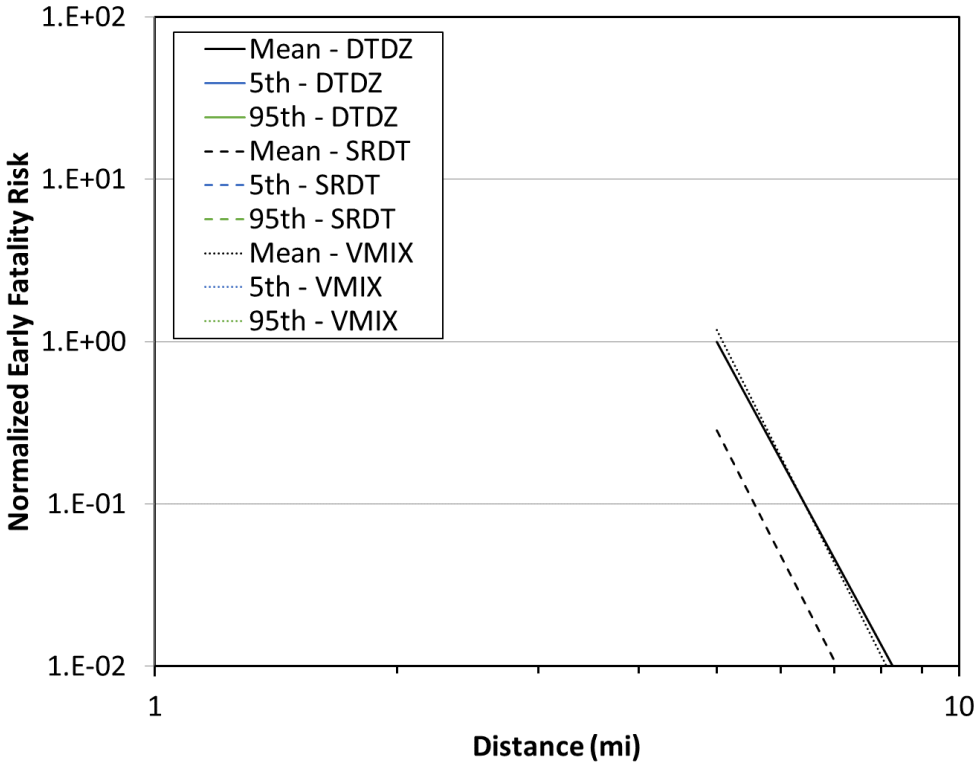

Figure 5-99. Early fatality risk comparison for three stability class methods (Site D, ST #1)

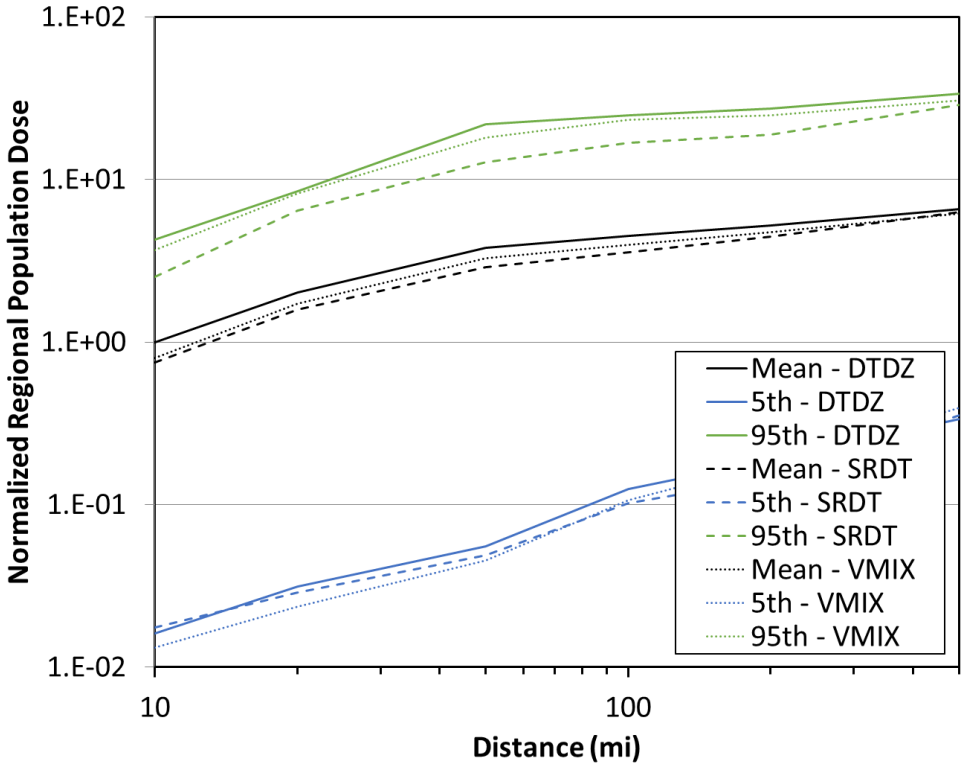

Figure 5-100. Population dose comparison for three stability class methods (Site D, ST #1)

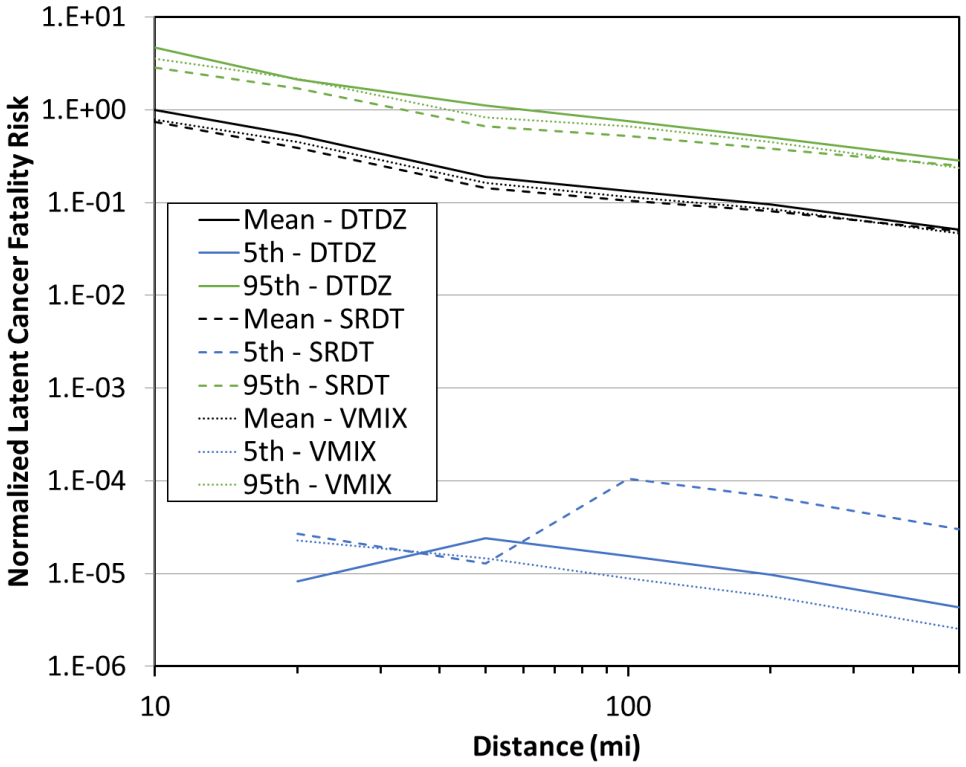

Figure 5-101. Latent cancer fatality risk comparison for three stability class methods (Site D, ST #1)

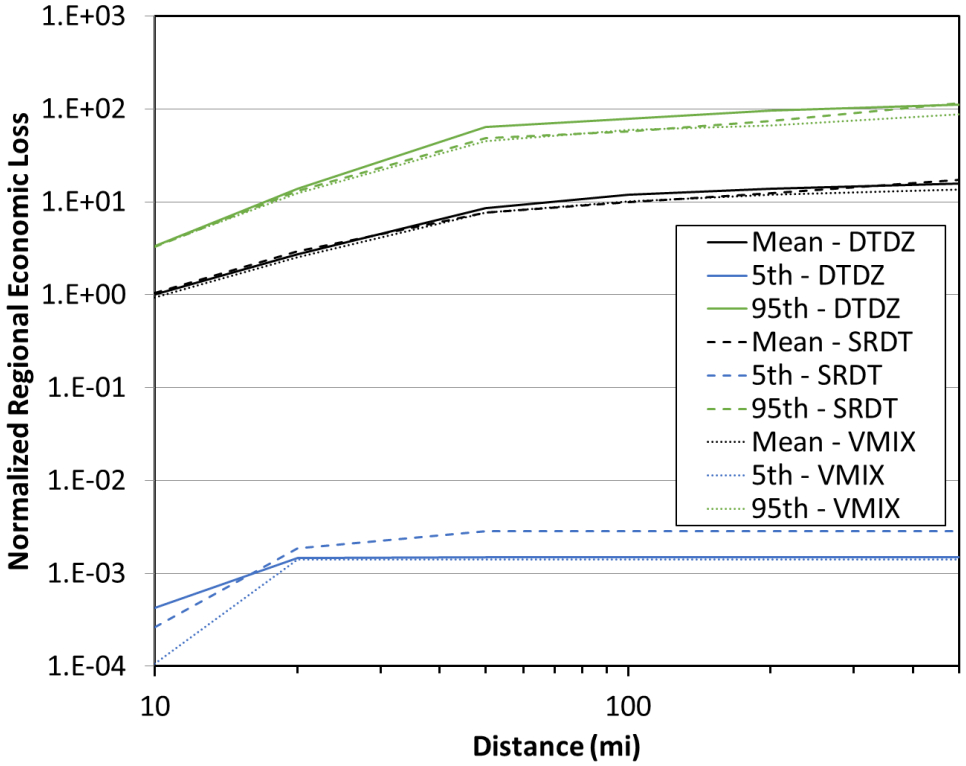

Figure 5-102. Economic loss comparison for three stability class methods (Site D, ST #1)

5.2.2.2. Source Term #2

Results for peak air concentration, peak ground deposition, land contamination area, peak dose, early fatality risk, population dose, latent cancer fatality risk, and economic loss (as described in Section 3.6) using the Gaussian ATD model at Site D with ST #2 are compared for the DTDZ, SRDT, and VMIX stability class methods in Figure 5-103 through Figure 5-110. The annual statistics for these measures are shown with different colors, where the mean values are in black, the 5th percentile values are shown in blue, and the 95th percentile values are shown in green. HYSPLIT results are shown as dashed lines and Gaussian model results are shown as solid lines. The normalized results are shown as a function of distance, rather than the ratio of Gaussian and HYSPLIT results, to allow for the trends with distance to be observed. Some results are zero for early fatality risk, so they cannot be shown on the log scale used in the figures. Discussion of the difference seen in these figures is provided below in Section 5.2.3.

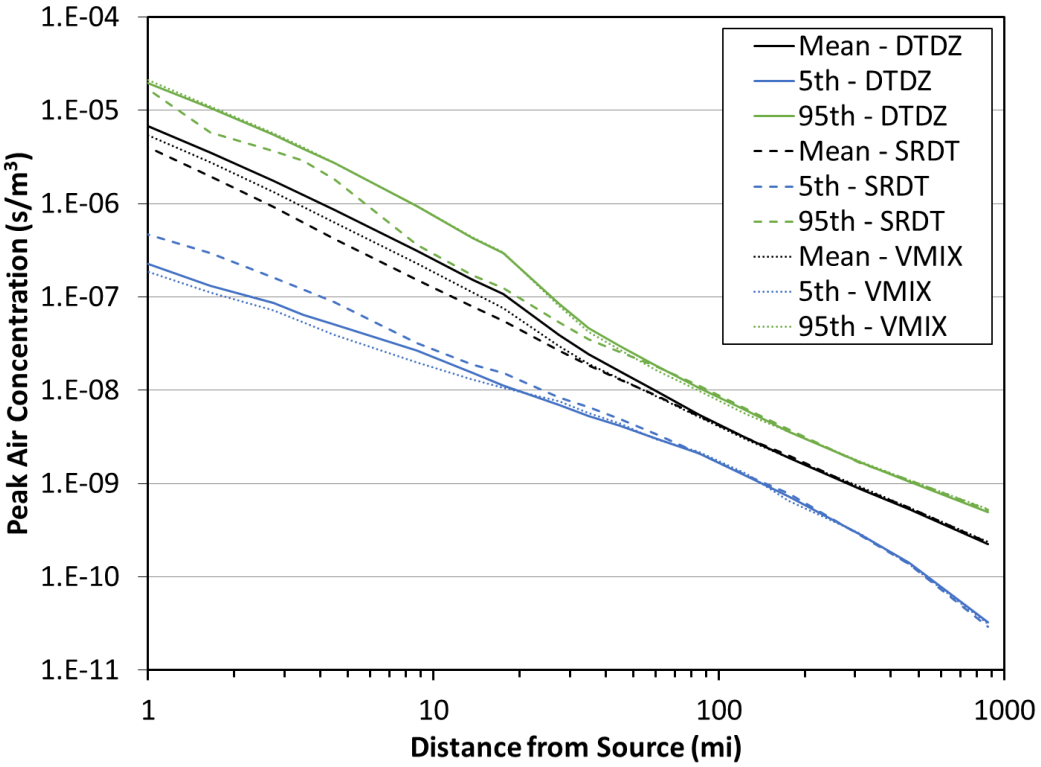

Figure 5-103. Peak air concentration comparison for three stability class methods (Site D, ST #2)

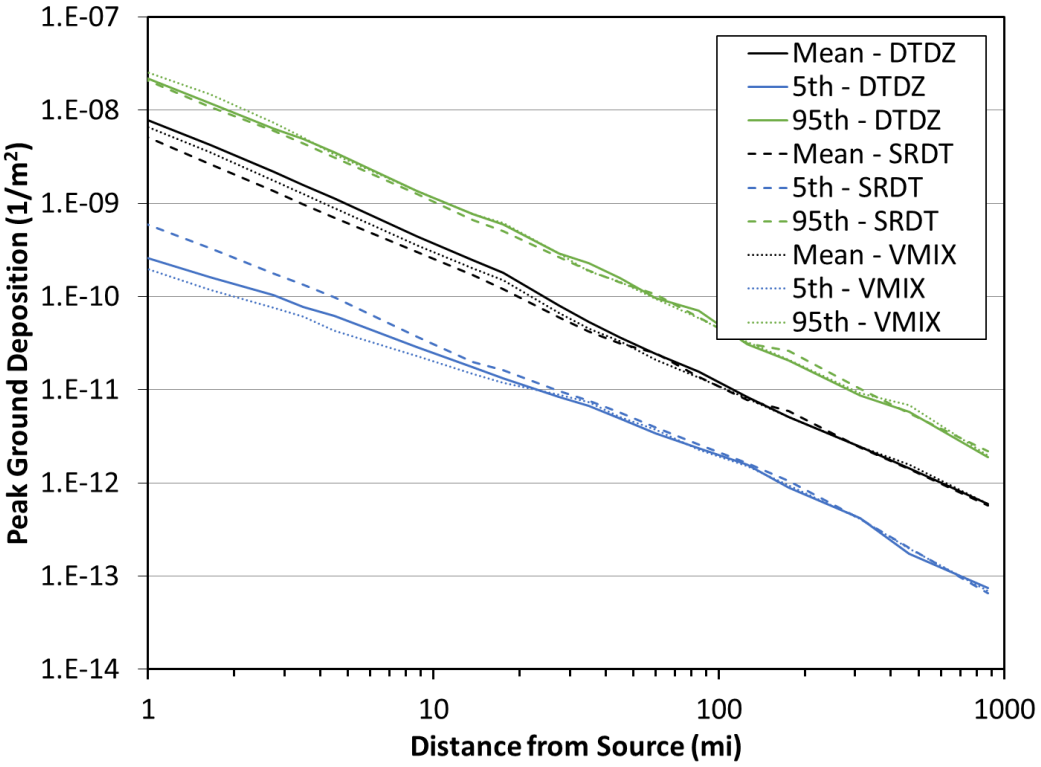

Figure 5-104. Peak ground deposition comparison for three stability class methods (Site D, ST #2)

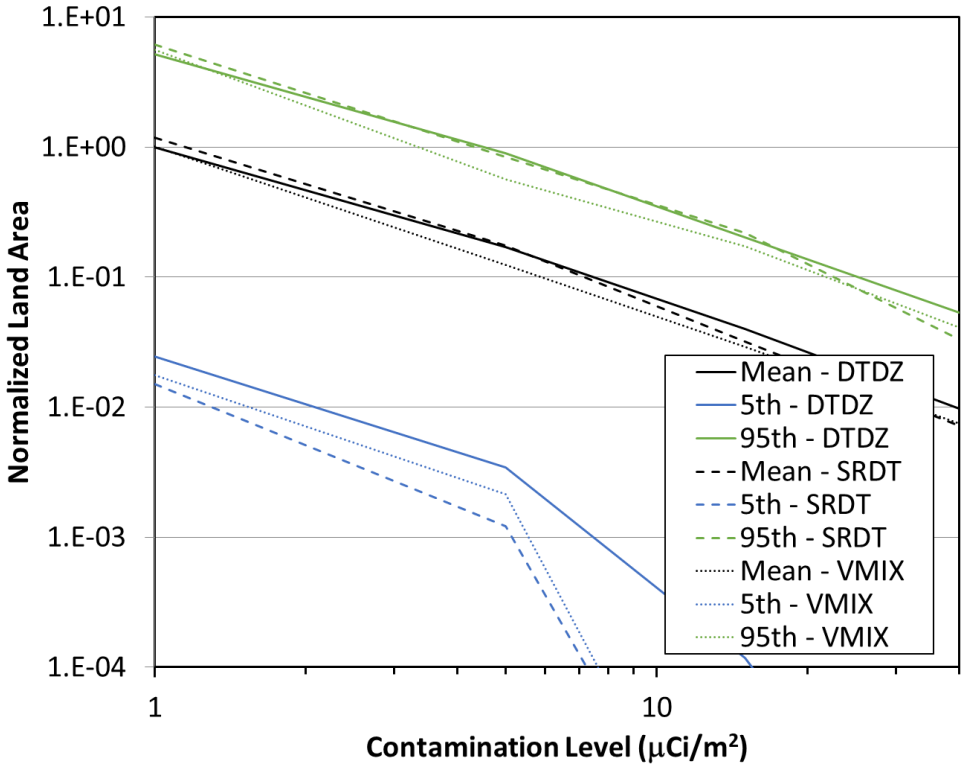

Figure 5-105. Land contamination area within 805 km (500 mi) comparison for three stability class methods (Site D, ST #2)

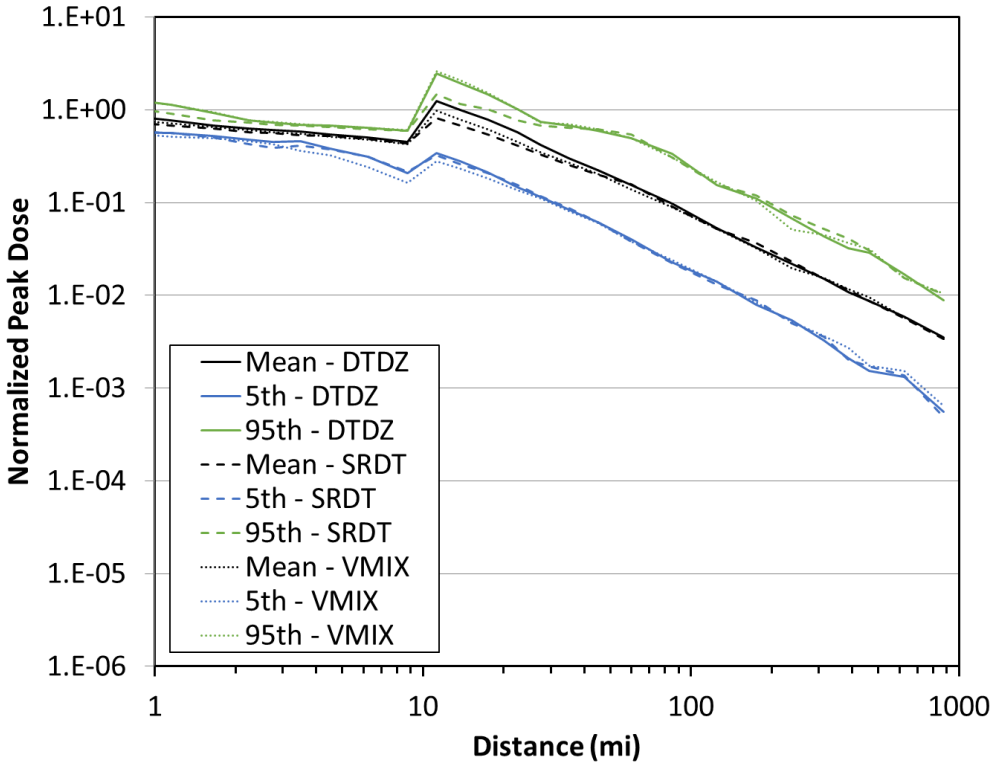

Figure 5-106. Peak dose comparison for three stability class methods (Site D, ST #2)

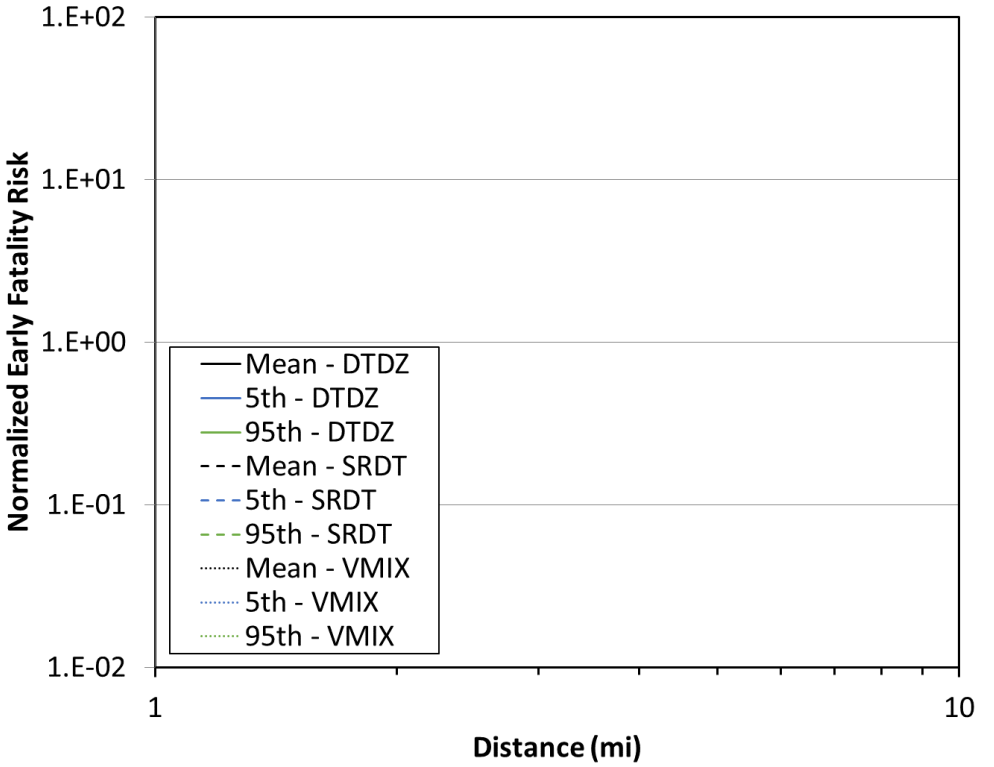

Figure 5-107. Early fatality risk comparison for three stability class methods (Site D, ST #2)

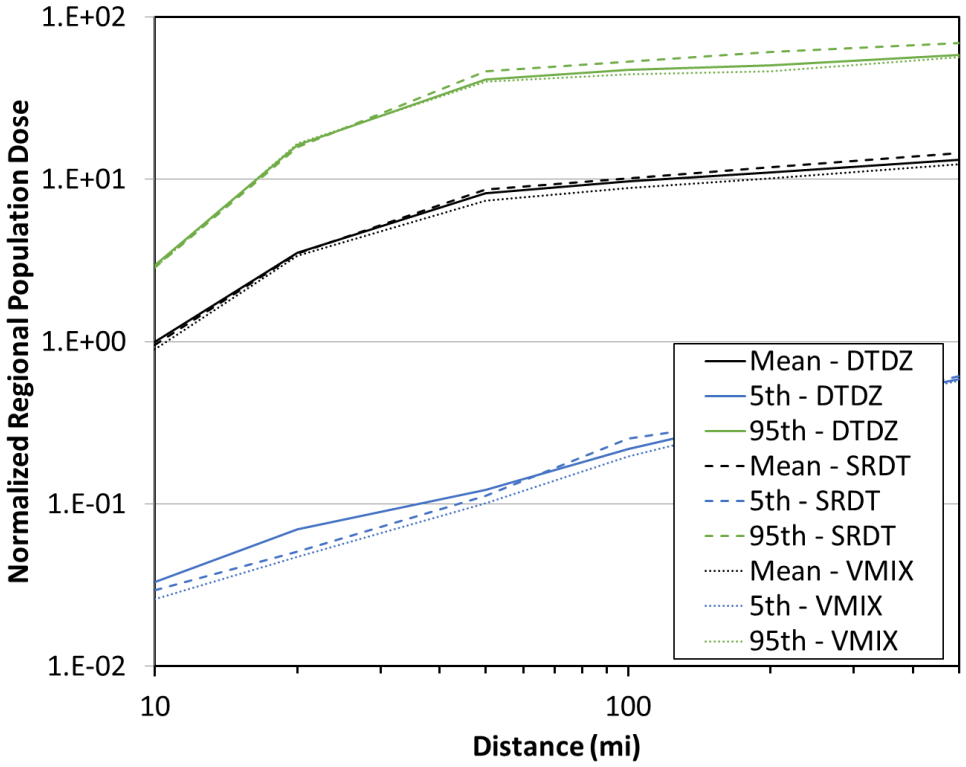

Figure 5-108. Population dose comparison for three stability class methods (Site D, ST #2)

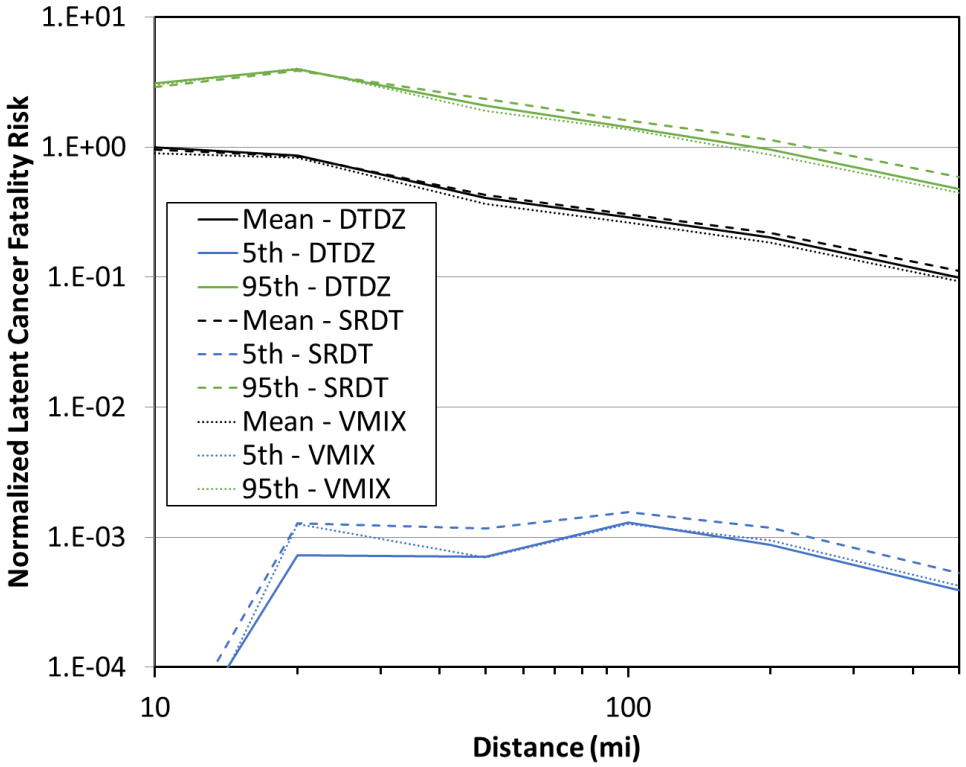

Figure 5-109. Latent cancer fatality risk comparison for three stability class methods (Site D, ST #2)

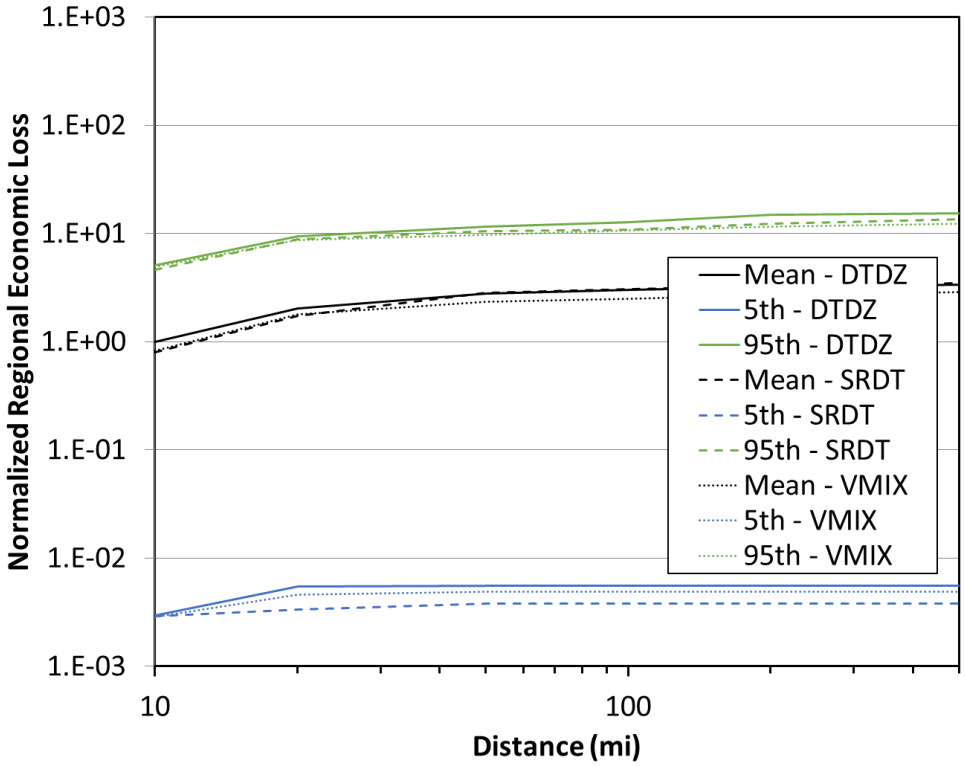

Figure 5-110. Economic loss comparison for three stability class methods (Site D, ST #2)

5.2.3. Interpretations of Stability Class Method Sensitivity

This section provides a comprehensive analysis of the results in the multiple figures presented in the previous sections (Sections 5.2.1 through 5.2.2). For those figures, the ratios of the annual average results obtained using the SRDT and VMIX stability class methods to those obtained using the DTDZ stability class method are determined for each output metric as a function of distance. The averages of these ratios, along with their minimums and maximums from the site out to 805 km (500 mi) are shown in Table 5-4 and Table 5-5, respectively. The columns represent the outputs in the figures presented above for all distances; i.e., there is no break down between nearfield and far field. For source term #2, EF risk was calculated as zero and so a ratio couldn't be calculated.

Table 5-4. Ratios of the Gaussian annual average results obtained using the SRDT stability class method to those using the DTDZ stability class method, shown as [Average (Minimum | Maximum)]

Site/ Source	Peak Air	Peak Ground	Peak Dose	Pop Dose	LCF Risk	Econ Loss	EF Risk	Land Area
A/1	0.8 (0.6|1.0)	0.9 (0.7|1.2)	0.8 (0.6|1.0)	0.9 (0.8|1.0)	0.8 (0.7|1.0)	1.0 (1.0|1.1)	0.7 (0.4|0.8)	1.1 (1.0|1.1)
D/1	0.7 (0.5|1.0)	0.8 (0.6|1.0)	0.7 (0.5|1.1)	0.8 (0.8|1.0)	0.8 (0.7|1.0)	1.0 (0.8|1.1)	0.2 (0.2|0.3)	1.5 (1.4|1.6)
A/2	0.8 (0.6|1.0)	0.9 (0.7|1.2)	0.9 (0.7|1.1)	0.9 (0.8|1.0)	0.9 (0.8|1.0)	0.8 (0.7|0.9)	a	0.9 (0.9|1.0)
D/2	0.7 (0.5|1.1)	0.8 (0.6|1.2)	0.9 (0.7|1.1)	1.0 (1.0|1.1)	1.0 (1.0|1.1)	1.0 (0.8|1.0)	a	0.9 (0.7|1.2)

[a]Data not available to compute ratio

Table 5-5. Ratios of the Gaussian annual average results obtained using the VMIX stability class method to those using the DTDZ stability class method, shown as [Average (Minimum | Maximum)]

Site/ Source	Peak Air	Peak Ground	Peak Dose	Pop Dose	LCF Risk	Econ Loss	EF Risk	Land Area
A/1	0.8 (0.6|1.0)	0.9 (0.7|1.1)	0.8 (0.7|1.1)	0.9 (0.8|1.0)	0.9 (0.8|1.0)	1.1 (1.1|1.1)	0.7 (0.4|0.8)	1.1 (1.0|1.2)
D/1	0.9 (0.7|1.1)	0.9 (0.8|1.1)	0.9 (0.7|1.1)	0.9 (0.8|0.9)	0.9 (0.8|0.9)	0.9 (0.9|0.9)	1.0 (0.7|1.2)	1.1 (1.0|1.2)
A/2	0.8 (0.7|1.0)	0.8 (0.7|1.0)	0.9 (0.7|1.1)	1.0 (0.9|1.0)	1.0 (0.9|1.0)	0.9 (0.8|1.0)	a	0.9 (0.8|1.1)
D/2	0.8 (0.7|1.1)	0.9 (0.8|1.1)	0.9 (0.8|1.1)	0.9 (0.9|1.0)	0.9 (0.9|1.0)	0.8 (0.8|0.9)	a	0.8 (0.7|1.0)

[a]Data not available to compute ratio

General results determined by examining the comparisons between the Gaussian ATD model calculations at Site A and Site D using the three stability class methods are discussed below. Caution should be used in generalizing these interpretations to other sites or consequence metrics. The interpretations in this section summarize the trends from the results above.

1. The level of agreement between annual average results from the Gaussian ATD model with the three methods to determine stability class is closer than it is in the previous comparison using different meteorological data sets. Most consequence metrics are well within 20% for the three methods used to estimate stability class.
2. The annual average results that show the largest differences occur at short distances (<30 km), while there are smaller differences at longer distances. This similarity at larger distances corresponds to the change from a distance- to a time-based dispersion function at 30 km (19 mi), as described previously. Time-based dispersion does not distinguish between stability classes and so the results become homogenized as distance increases beyond 30 km (19 mi).
3. The annual average results from the Gaussian ATD model with the DTDZ method generally produce the higher values (~10%) for the peak air concentration, peak ground deposition, peak dose, normalized regional population doses, and latent cancer fatality risk over the region.

5.3. Dispersion Model Beyond 30 km

The third sensitivity study examines the impact of turning off the time-based dispersion model in the Gaussian ATD model. Changes in slope of the peak air concentration and peak ground deposition versus distance are observed in the previous figures in this report for the Gaussian ATD model at the distance at which the Gaussian dispersion model shifts from a distance-based to time-based formulation (19 mi, 30 km). For this comparison, the benchmark Gaussian ATD results are labeled "Time." A sensitivity test was performed for Site A and Site D (labeled Distance) in which the transition from distance-based to time-based dispersion was switched off, i.e., distance-based dispersion was used over the entire domain. Comparisons of the results for these two Gaussian ATD model options (labeled Time and Distance) with results using the HYSPLIT ATD option are shown below, for both source terms and for all consequence metrics.

5.3.1. Site A

5.3.1.1. Source Term #1

Results for peak air concentration, peak ground deposition, land contamination area, peak dose, early fatality risk, population dose, latent cancer fatality risk, and economic loss (as described in Section 3.6) using the Gaussian ATD model (Time and Distance options) at Site A with ST #1 are

compared with each other and with the HYSPLIT ATD models in Figure 5-111 through Figure 5-118. The annual statistics for these measures are shown with different colors, where the mean values are in black, the 5th percentile values are shown in blue, and the 95th percentile values are shown in green. HYSPLIT results are shown as dashed lines and Gaussian model results are shown as solid lines. The normalized results are shown as a function of distance, rather than the ratio of Gaussian and HYSPLIT results, to allow for the trends with distance to be observed. Some results are zero for early fatality risk, so they cannot be shown on the log scale used in the figures. The early fatality risk for Time and Distance are identical and hence only the results from the Time and HYSPLIT model is visible in Figure 5-115. Discussion of the difference seen in these figures is provided below in Section 5.2.3.

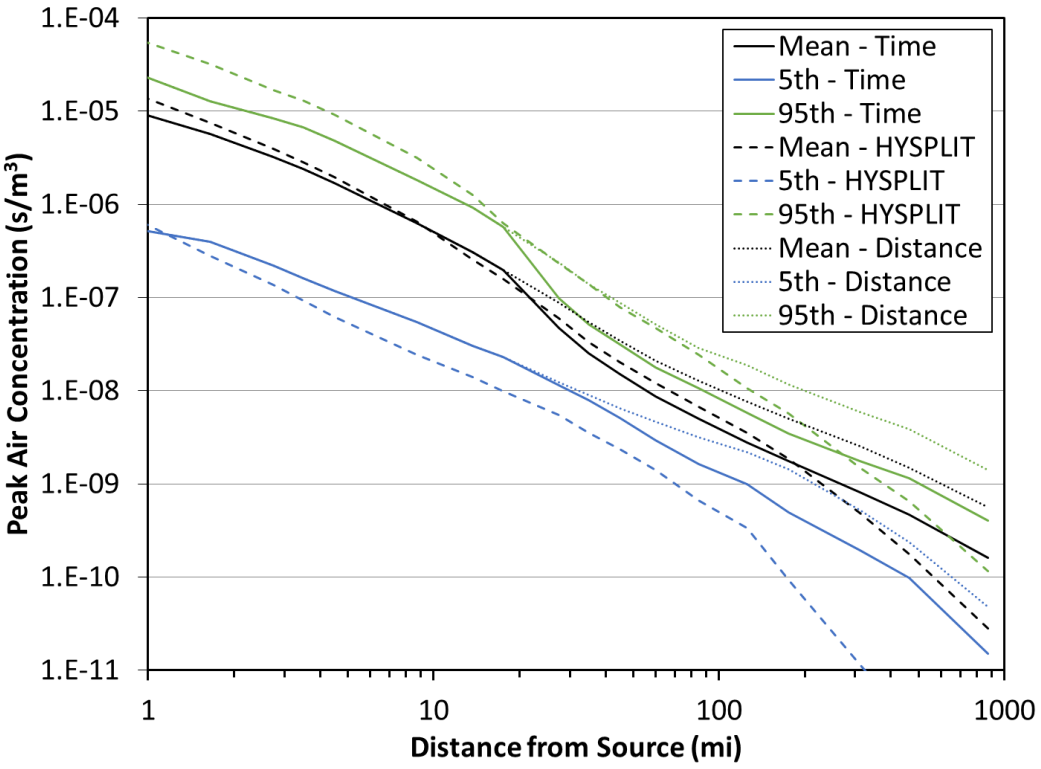

Figure 5-111. Peak air concentration comparison for two Gaussian ATD model options (Time and Distance) and the HYSPLIT ATD model (Site A, ST #1)

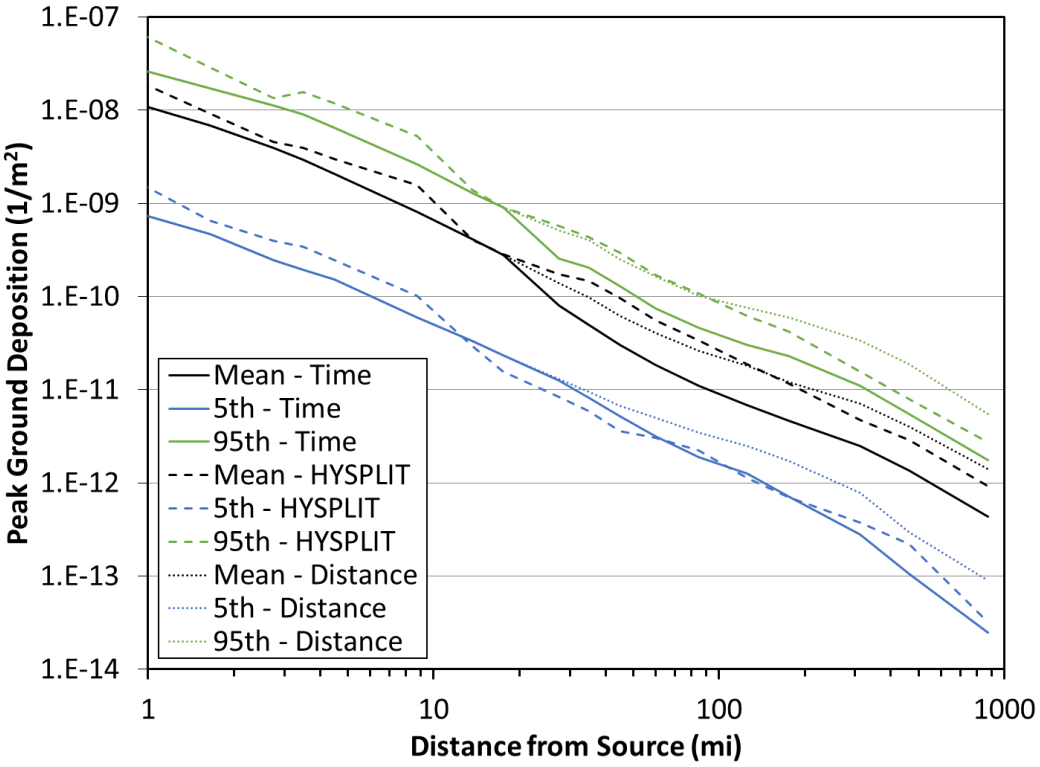

Figure 5-112. Peak ground deposition comparison for two Gaussian ATD model options (Time and Distance) and the HYSPLIT ATD model (Site A, ST #1)

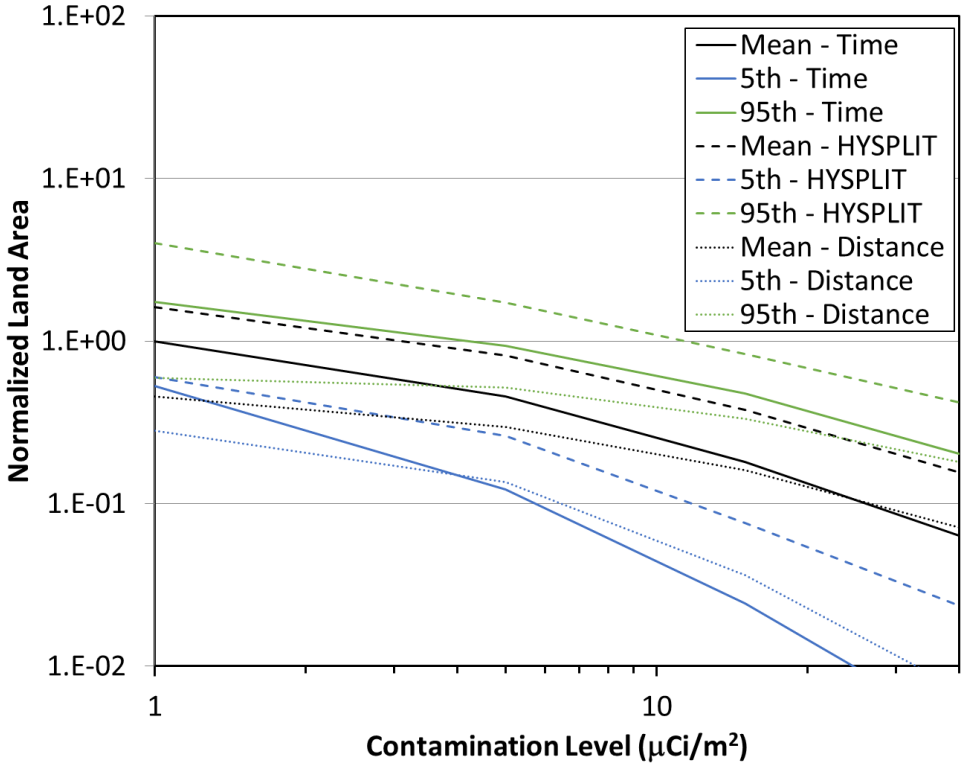

Figure 5-113. Land contamination area within 805 km (500 mi) comparison for two Gaussian ATD model options (Time and Distance) and the HYSPLIT ATD model (Site A, ST #1)

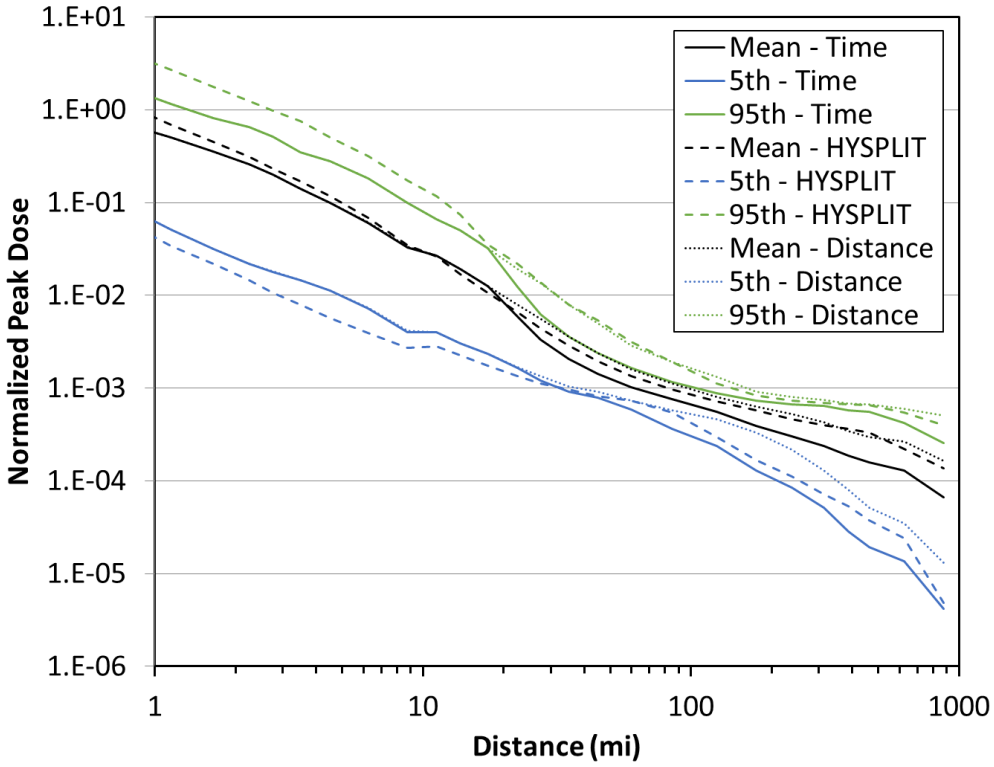

Figure 5-114. Peak dose comparison for two Gaussian ATD model options (Time and Distance) and the HYSPLIT ATD model (Site A, ST #1)

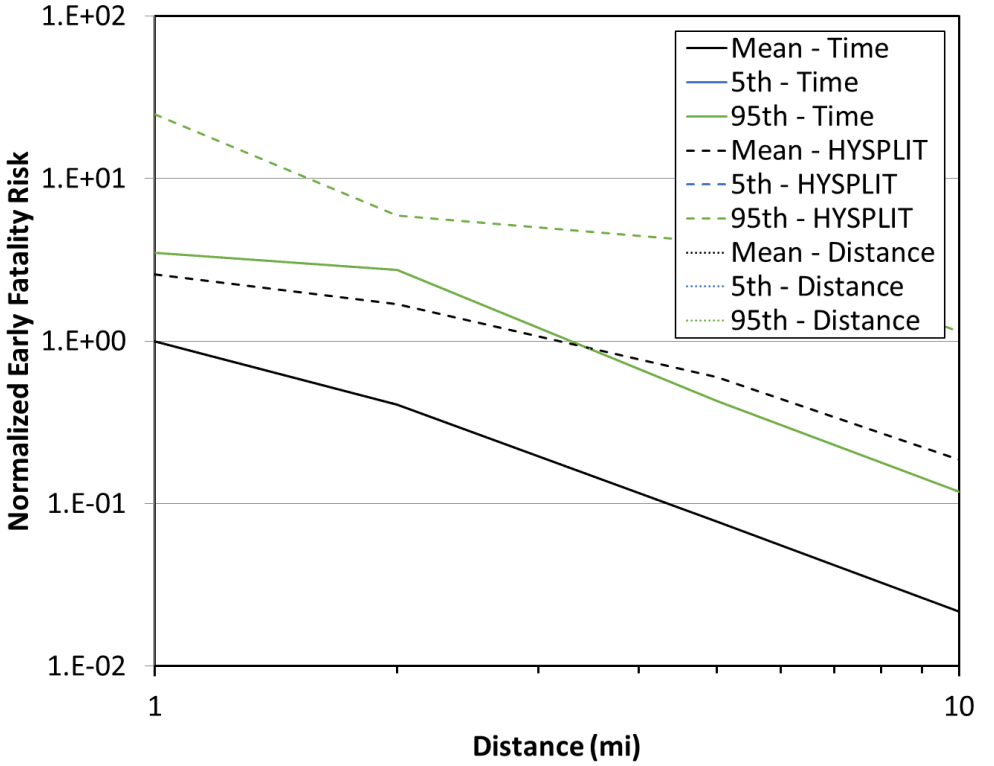

Figure 5-115. Early fatality risk comparison for two Gaussian ATD model options (Time and Distance) and the HYSPLIT ATD model (Site A, ST #1)

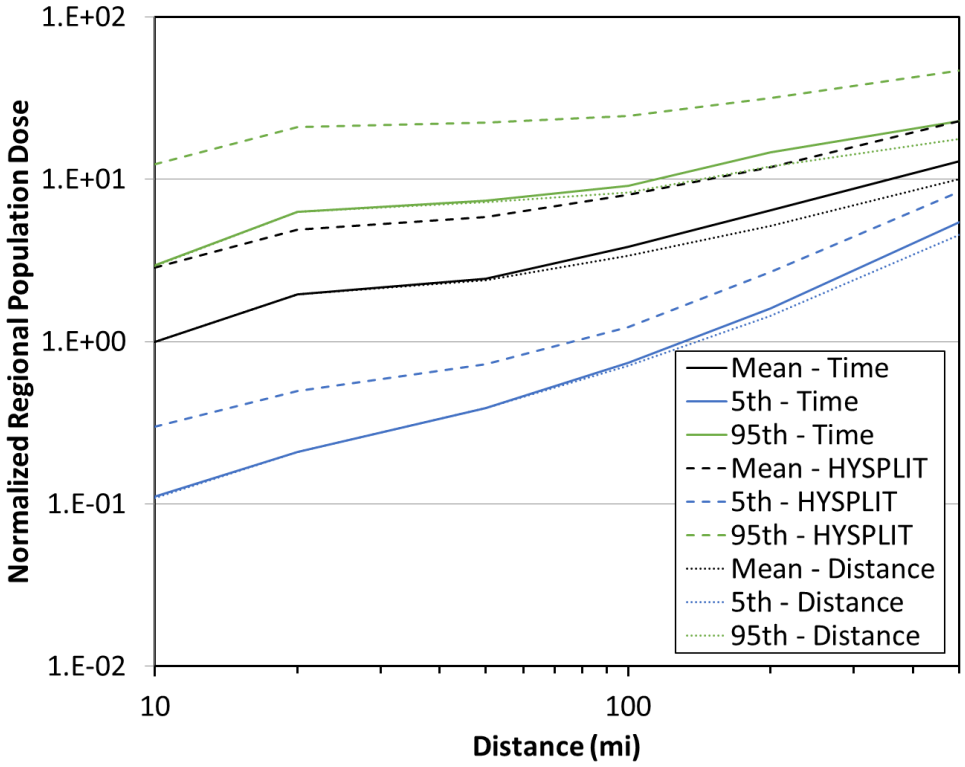

Figure 5-116. Population dose comparison for two Gaussian ATD model options (Time and Distance) and the HYSPLIT ATD model (Site A, ST #1)

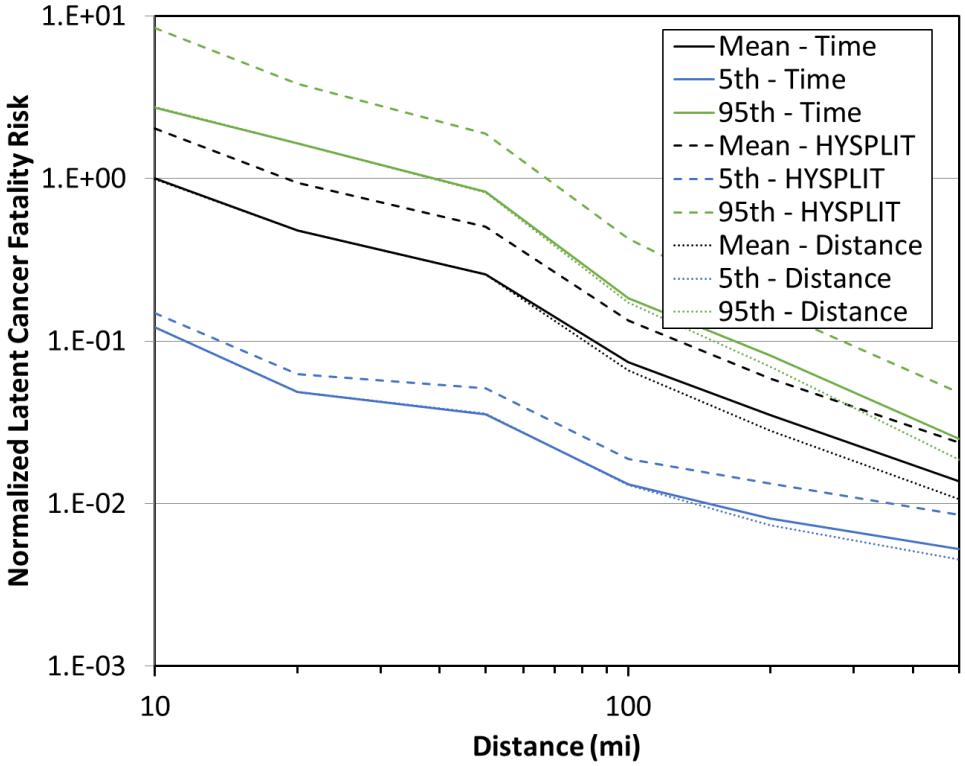

Figure 5-117. Latent cancer fatality risk comparison for two Gaussian ATD model options (Time and Distance) and the HYSPLIT ATD model (Site A, ST #1)

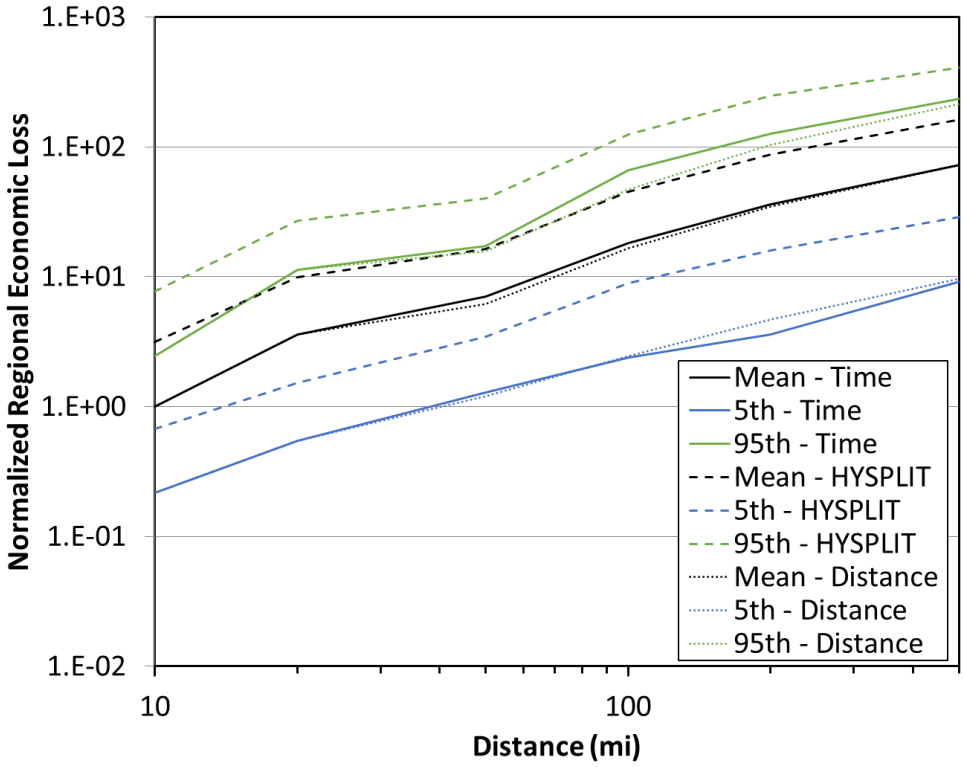

Figure 5-118. Economic loss comparison for two Gaussian ATD model options (Time and Distance) and the HYSPLIT ATD model (Site A, ST #1)

5.3.1.2. Source Term #2

Results for peak air concentration, peak ground deposition, land contamination area, peak dose, early fatality risk, population dose, latent cancer fatality risk, and economic loss (as described in Section 3.6) using the Gaussian ATD model (Time and Distance options) at Site A with ST #2 are compared with each other and with the HYSPLIT ATD models in Figure 5-119 through Figure 5-126. The annual statistics for these measures are shown with different colors, where the mean values are in black, the 5th percentile values are shown in blue, and the 95th percentile values are shown in green. HYSPLIT results are shown as dashed lines and Gaussian model results are shown as solid lines. The normalized results are shown as a function of distance, rather than the ratio of Gaussian and HYSPLIT results, to allow for the trends with distance to be observed. Some results are zero for early fatality risk, so they cannot be shown on the log scale used in the figures. Discussion of the difference seen in these figures is provided below in Section 5.2.3.

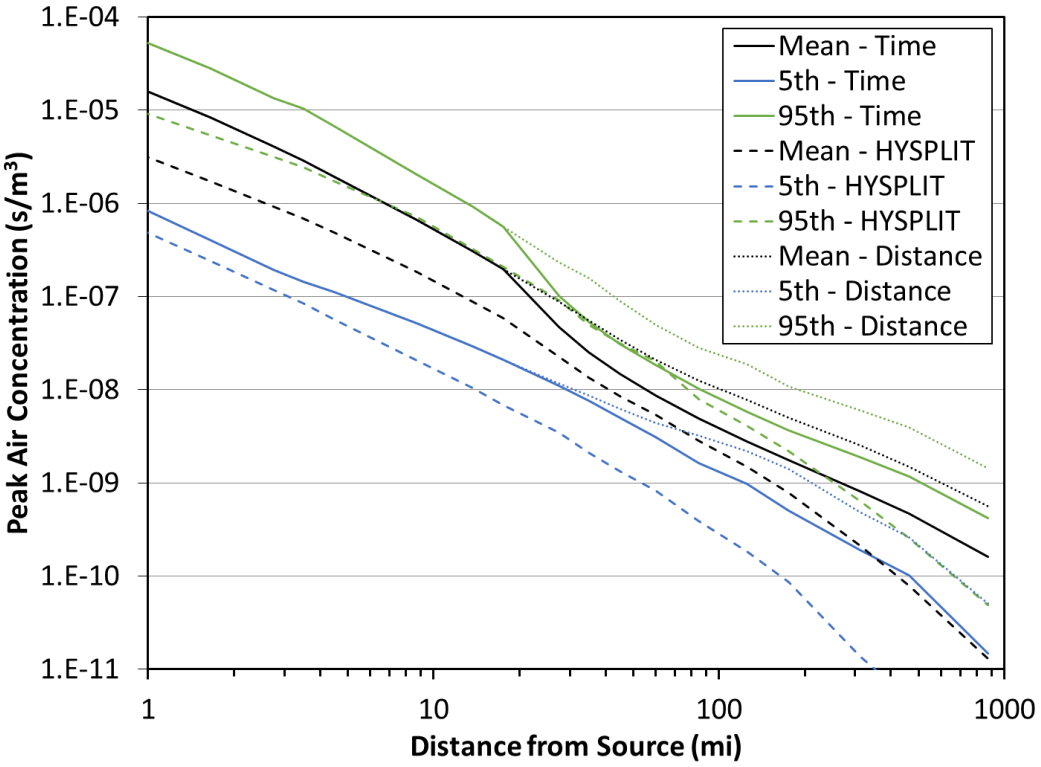

Figure 5-119. Peak air concentration comparison for two Gaussian ATD model options (Time and Distance) and the HYSPLIT ATD model (Site A, ST #2)

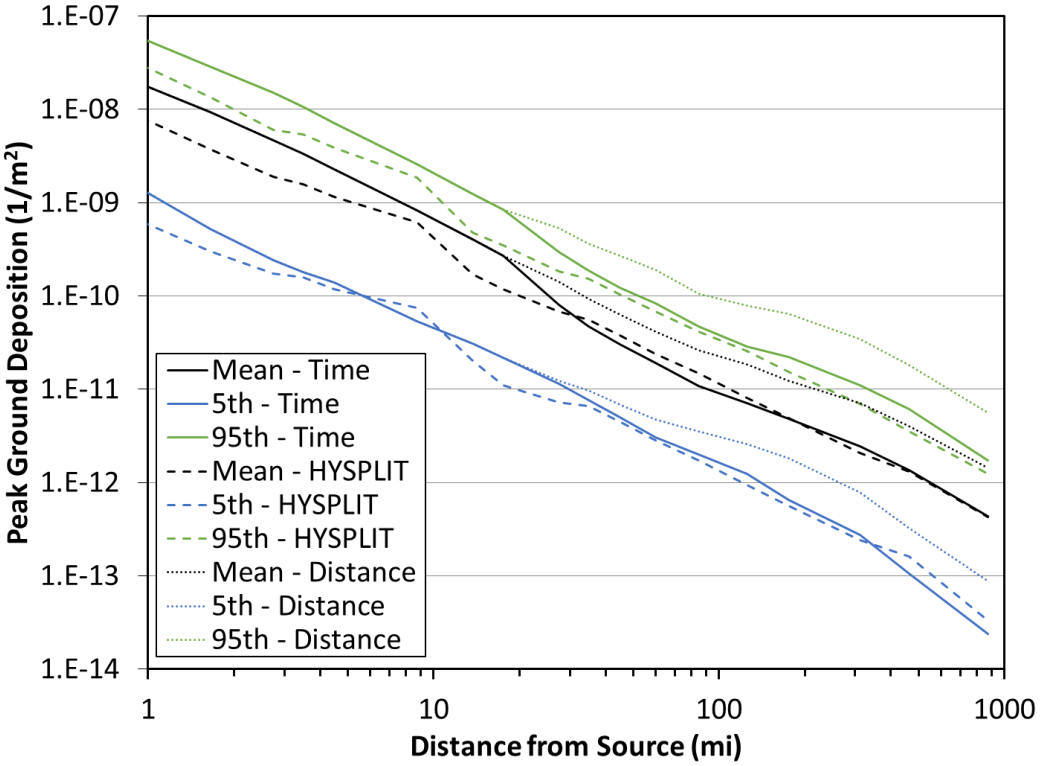

Figure 5-120. Peak ground deposition comparison for two Gaussian ATD model options (Time and Distance) and the HYSPLIT ATD model (Site A, ST #2)

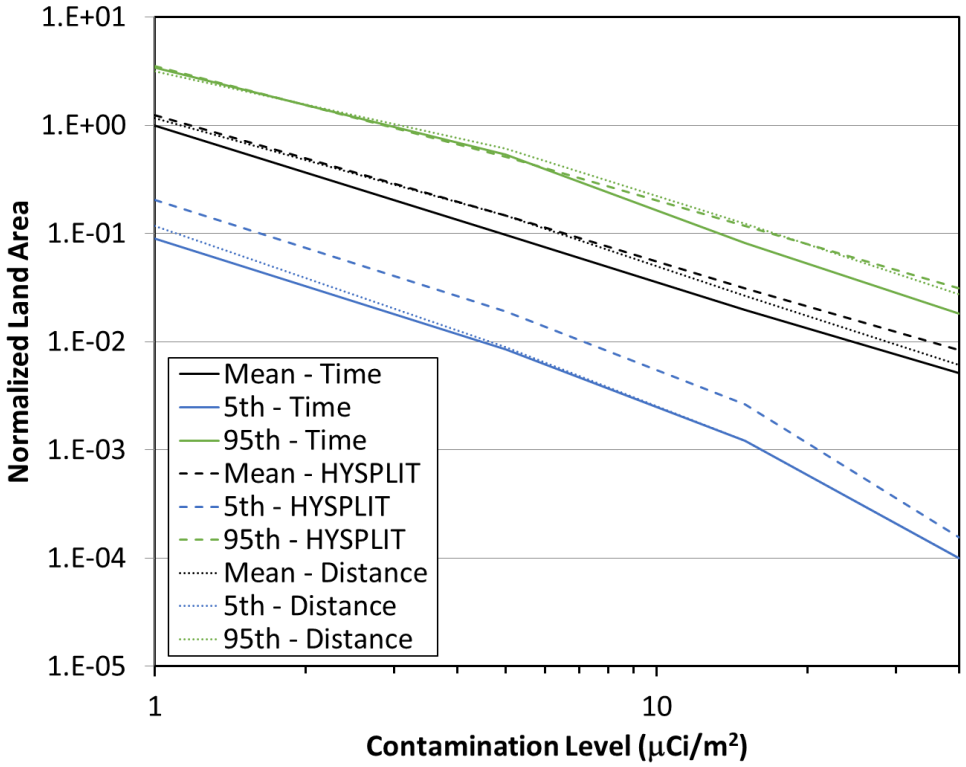

Figure 5-121. Land contamination area within 805 km (500 mi) comparison for two Gaussian ATD model options (Time and Distance) and the HYSPLIT ATD model (Site A, ST #2)

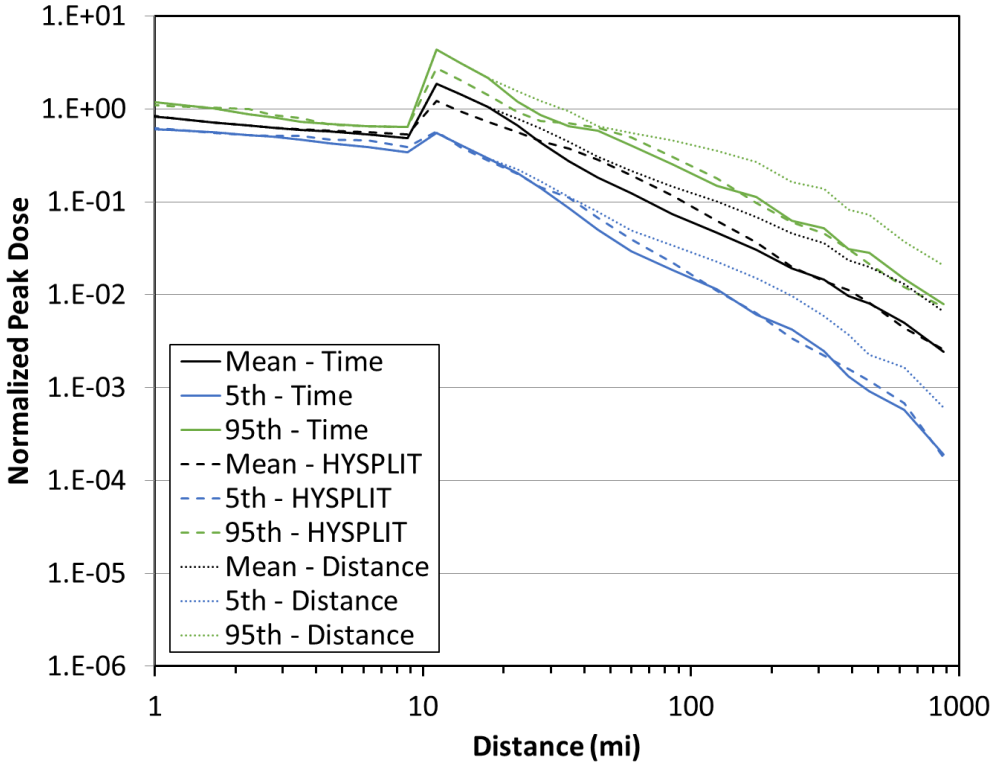

Figure 5-122. Peak dose comparison for two Gaussian ATD model options (Time and Distance) and the HYSPLIT ATD model (Site A, ST #2)

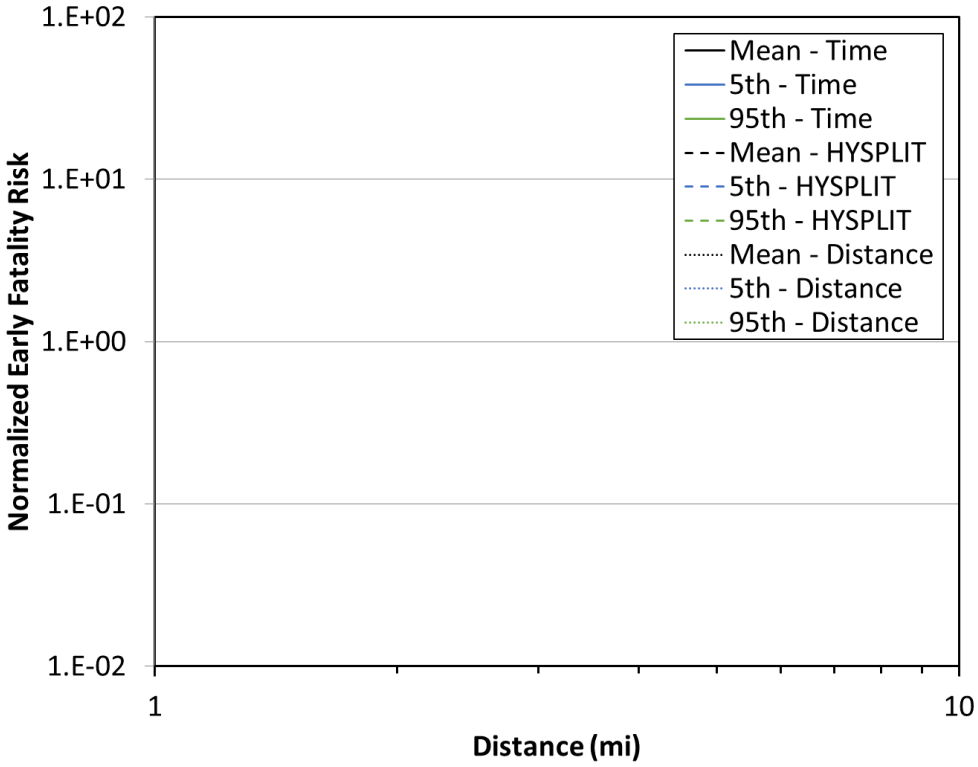

Figure 5-123. Early fatality risk comparison for two Gaussian ATD model options (Time and Distance) and the HYSPLIT ATD model (Site A, ST #2)

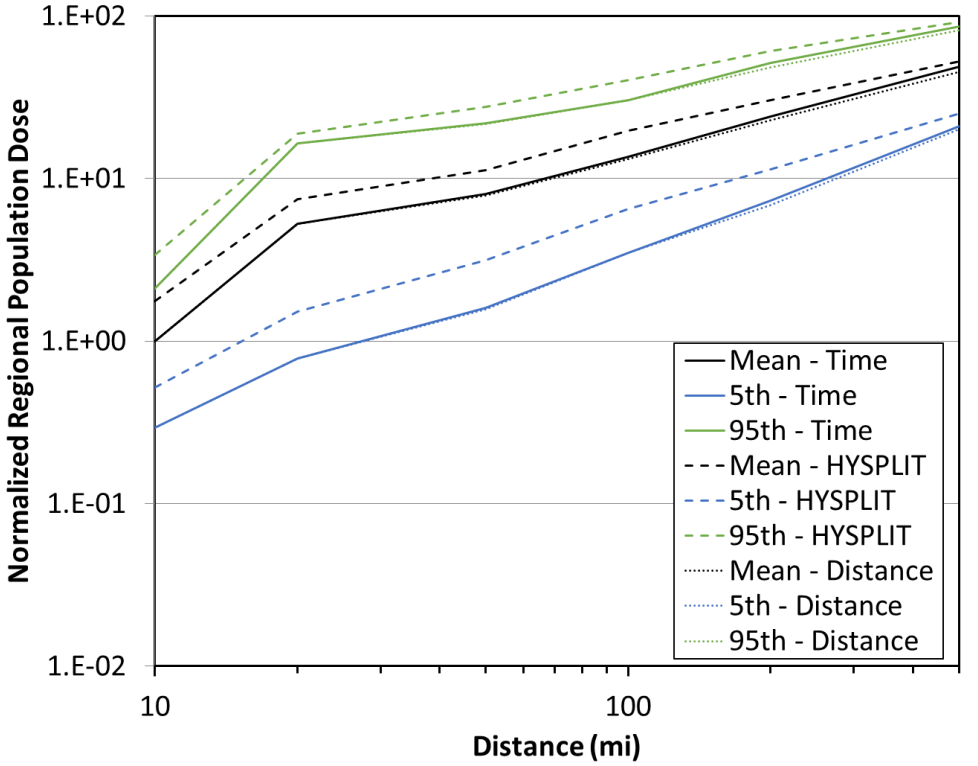

Figure 5-124. Population dose comparison for two Gaussian ATD model options (Time and Distance) and the HYSPLIT ATD model (Site A, ST #2)

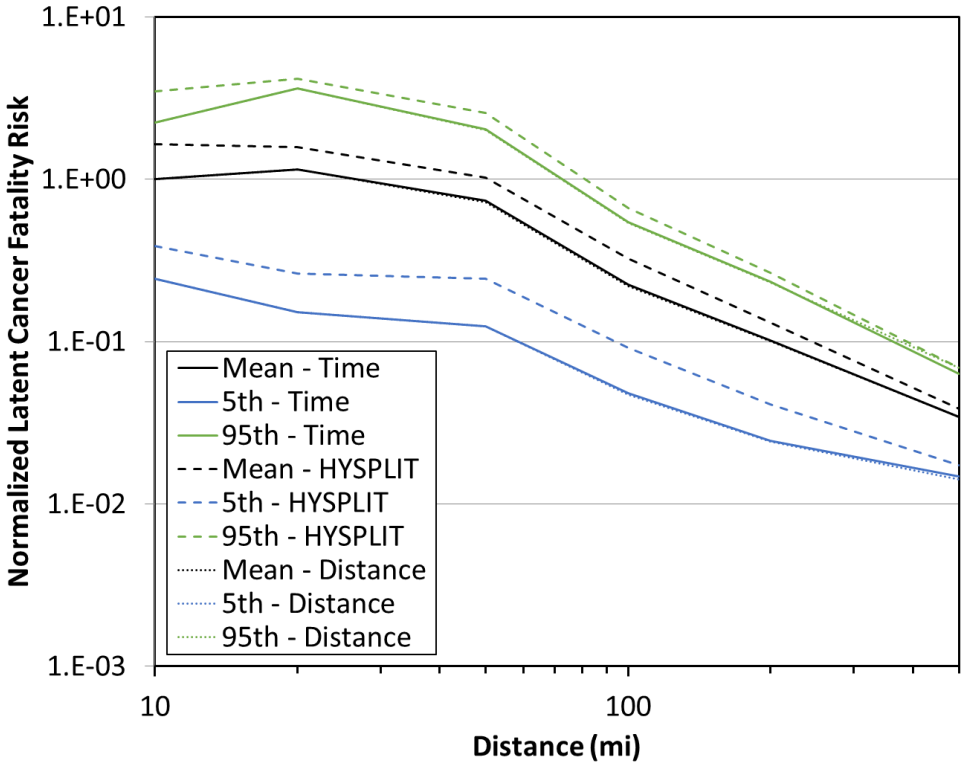

Figure 5-125. Latent cancer fatality risk comparison for two Gaussian ATD model options (Time and Distance) and the HYSPLIT ATD model (Site A, ST #2)

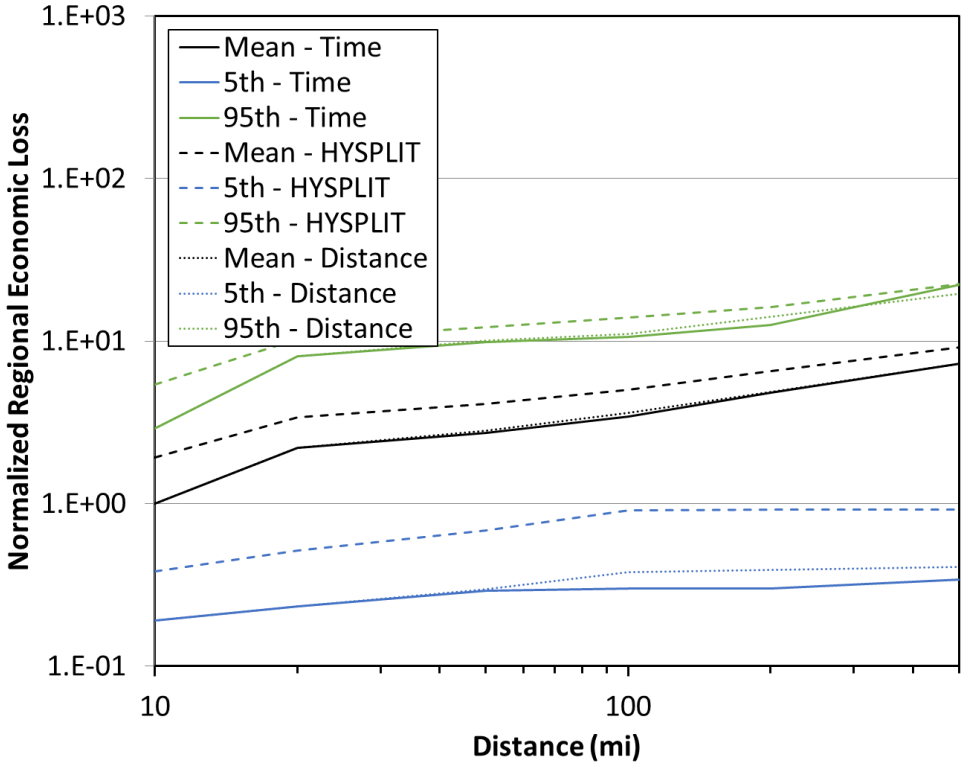

Figure 5-126. Economic loss comparison for two Gaussian ATD model options (Time and Distance) and the HYSPLIT ATD model (Site A, ST #2)

5.3.2. Site D

5.3.2.1. Source Term #1

Results for peak air concentration, peak ground deposition, land contamination area, peak dose, early fatality risk, population dose, latent cancer fatality risk, and economic loss (as described in Section 3.6) using the Gaussian ATD model (Time and Distance options) at Site D with ST #1 are compared with each other and with the HYSPLIT ATD models in Figure 5-127 through Figure 5-134. The annual statistics for these measures are shown with different colors, where the mean values are in black, the 5th percentile values are shown in blue, and the 95th percentile values are shown in green. HYSPLIT results are shown as dashed lines and Gaussian model results are shown as solid lines. The normalized results are shown as a function of distance, rather than the ratio of Gaussian and HYSPLIT results, to allow for the trends with distance to be observed. Some results are zero for early fatality risk, so they cannot be shown on the log scale used in the figures. Discussion of the difference seen in these figures is provided below in Section 5.2.3.

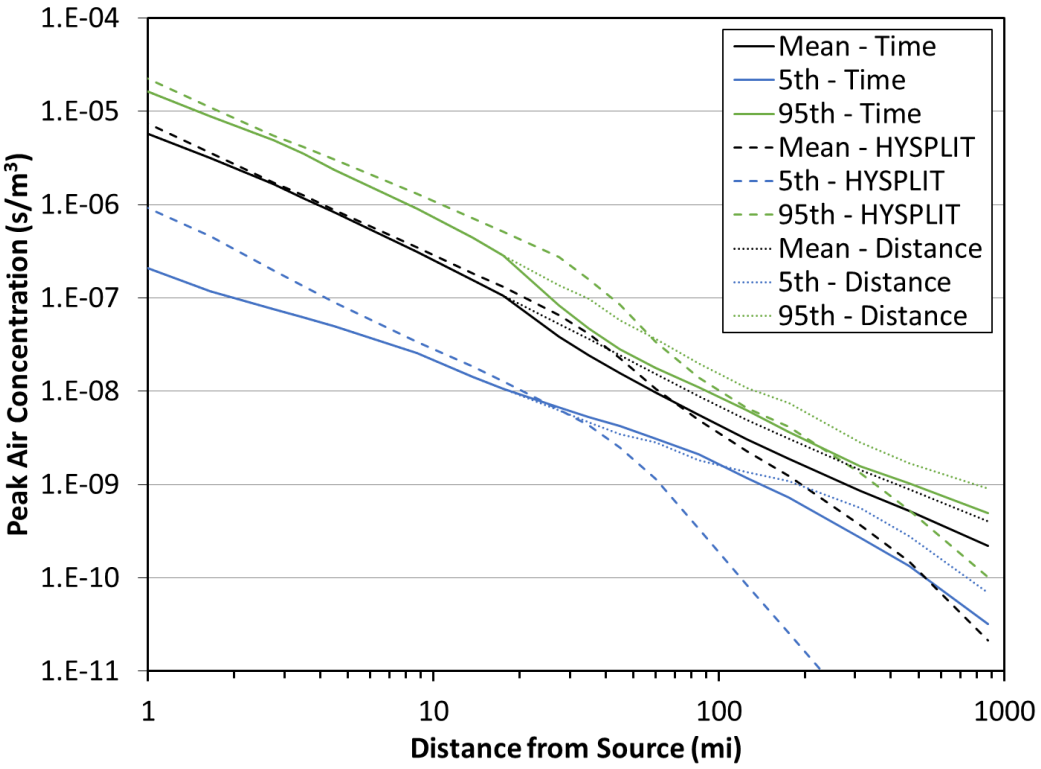

Figure 5-127. Peak air concentration comparison for two Gaussian ATD model options (Time and Distance) and the HYSPLIT ATD model (Site D, ST #1)

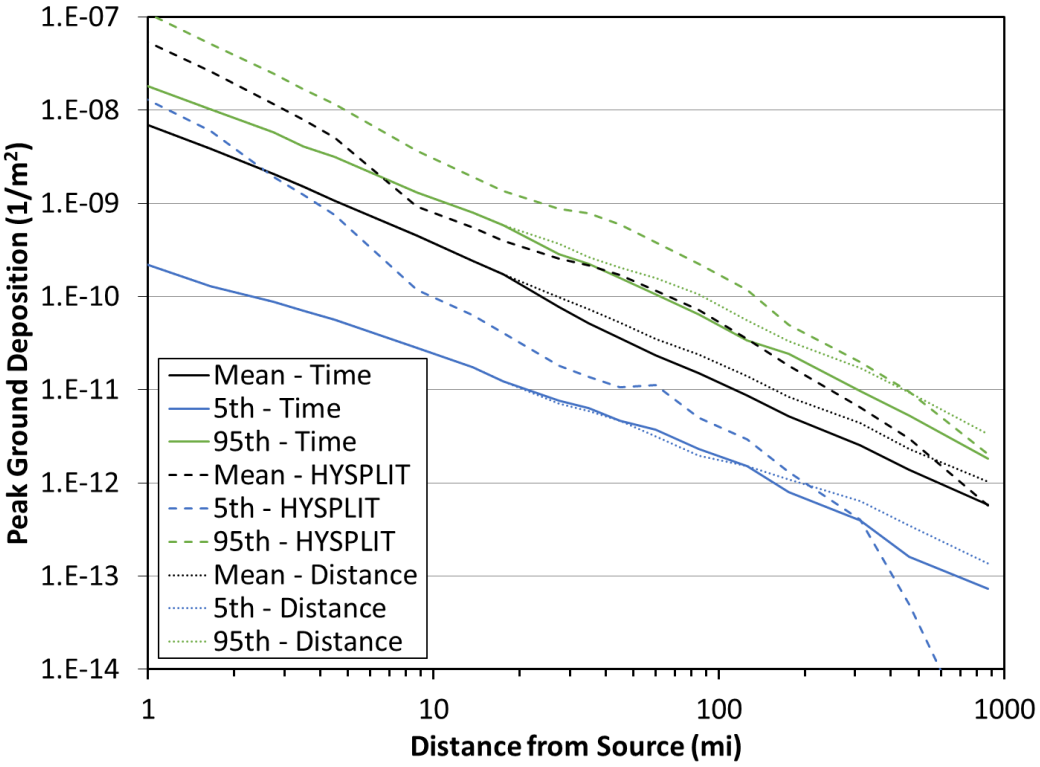

Figure 5-128. Peak ground deposition comparison for two Gaussian ATD model options (Time and Distance) and the HYSPLIT ATD model (Site D, ST #1)

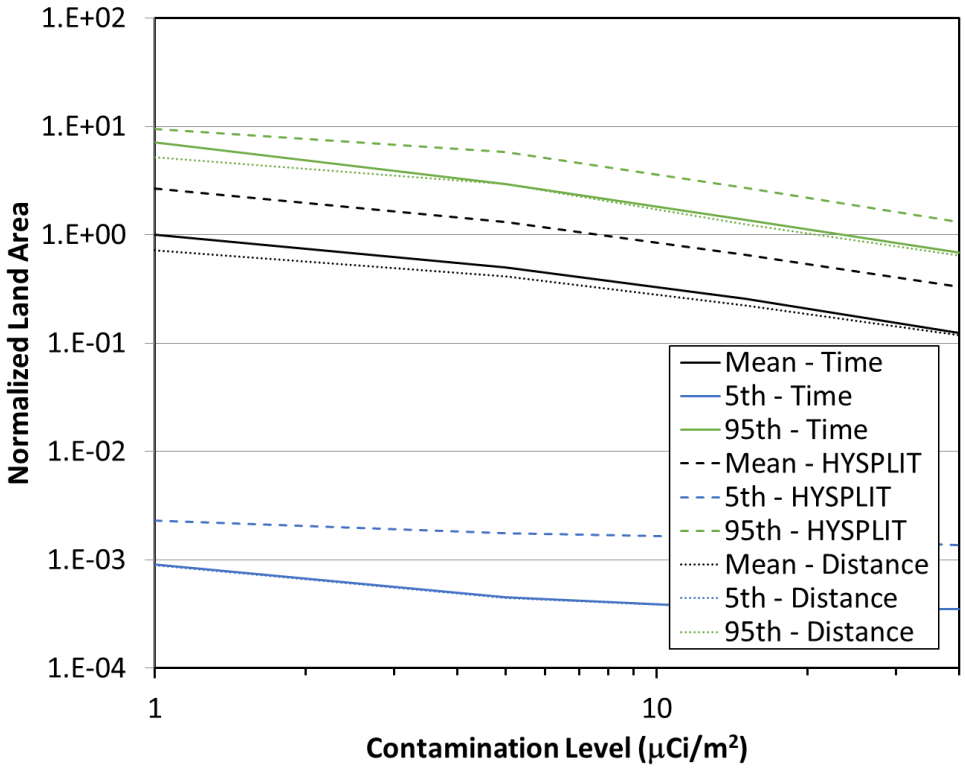

Figure 5-129. Land contamination area within 805 km (500 mi) comparison for two Gaussian ATD model options (Time and Distance) and the HYSPLIT ATD model (Site D, ST #1)

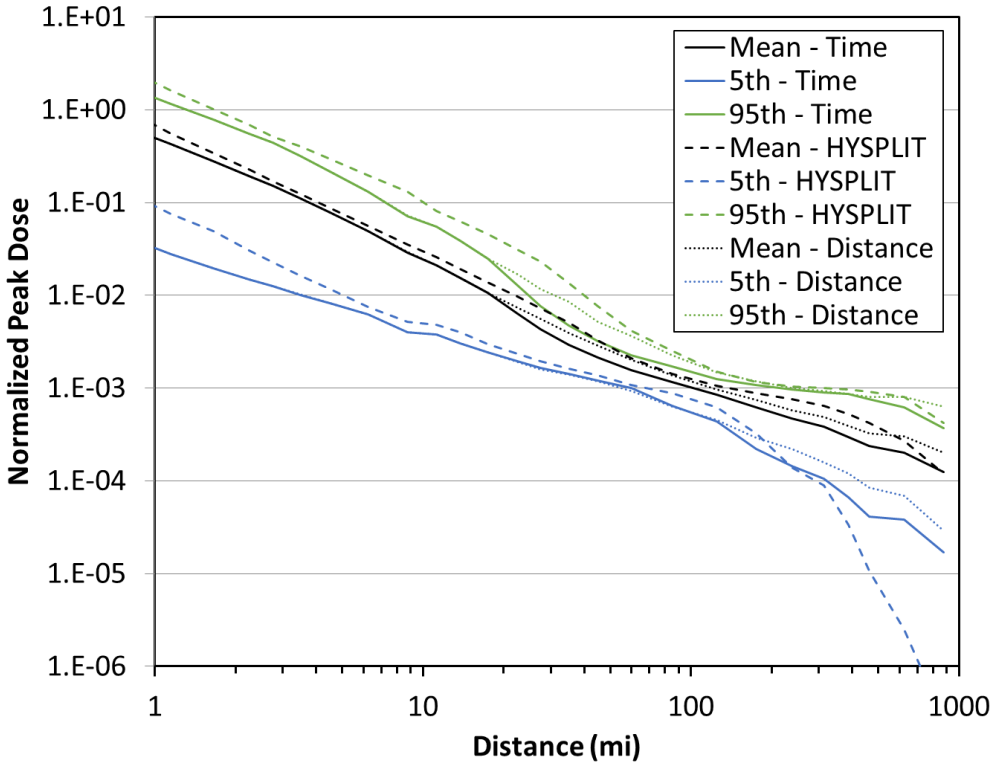

Figure 5-130. Peak dose comparison for two Gaussian ATD model options (Time and Distance) and the HYSPLIT ATD model (Site D, ST #1)

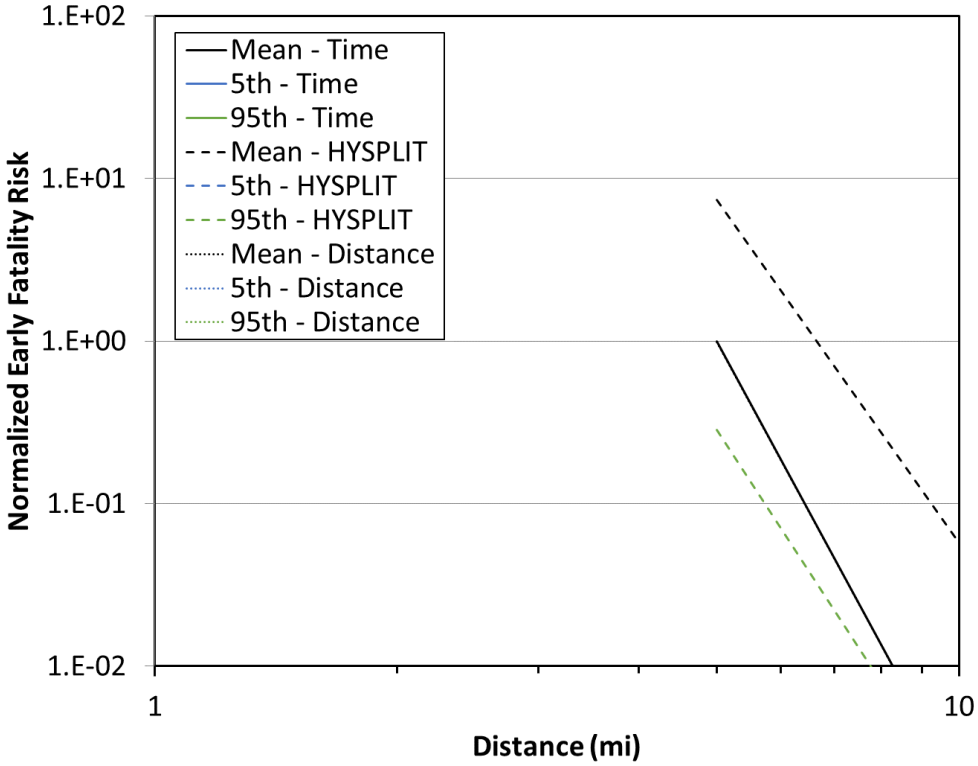

Figure 5-131. Early fatality risk comparison for two Gaussian ATD model options (Time and Distance) and the HYSPLIT ATD model (Site D, ST #1)

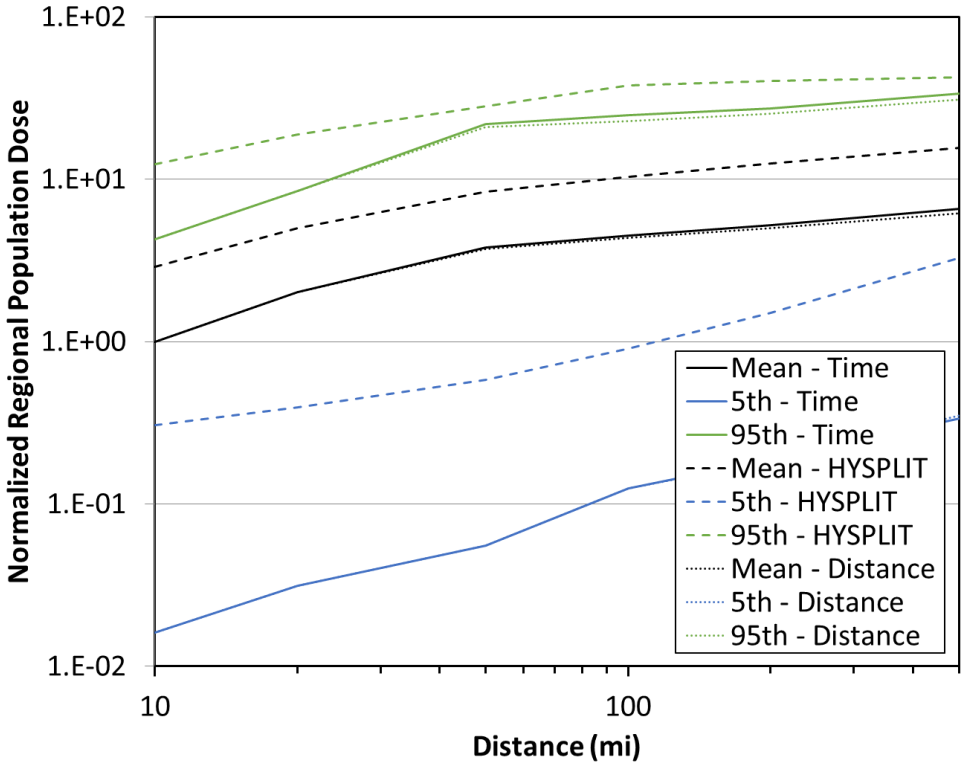

Figure 5-132. Population dose comparison for two Gaussian ATD model options (Time and Distance) and the HYSPLIT ATD model (Site D, ST #1)

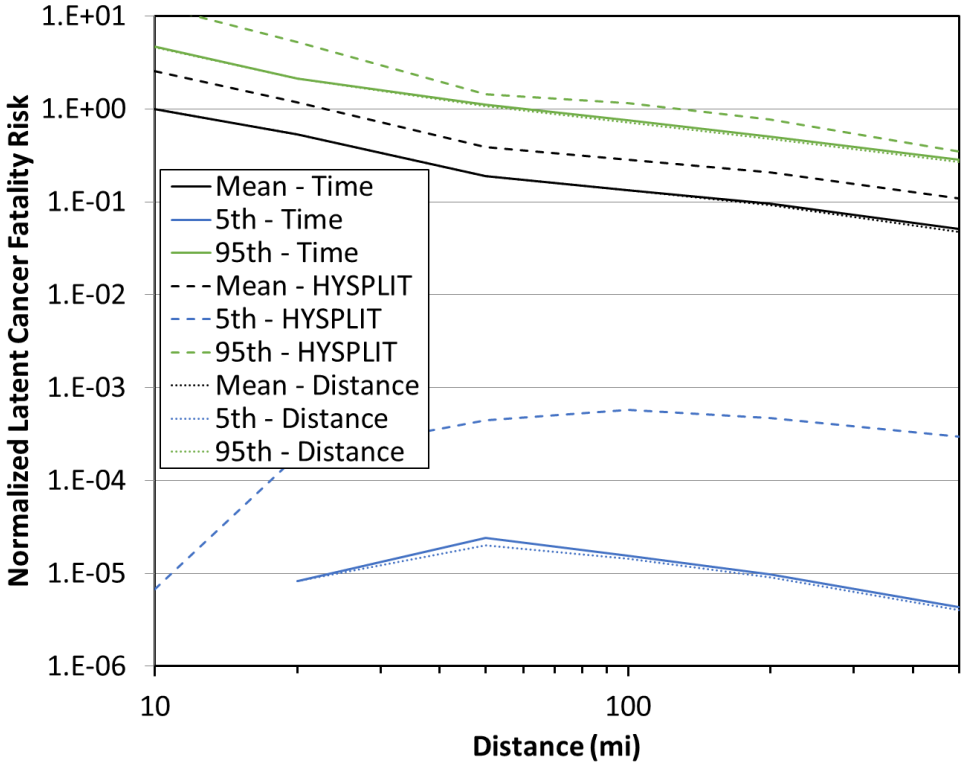

Figure 5-133. Latent cancer fatality risk comparison for two Gaussian ATD model options (Time and Distance) and the HYSPLIT ATD model (Site D, ST #1)

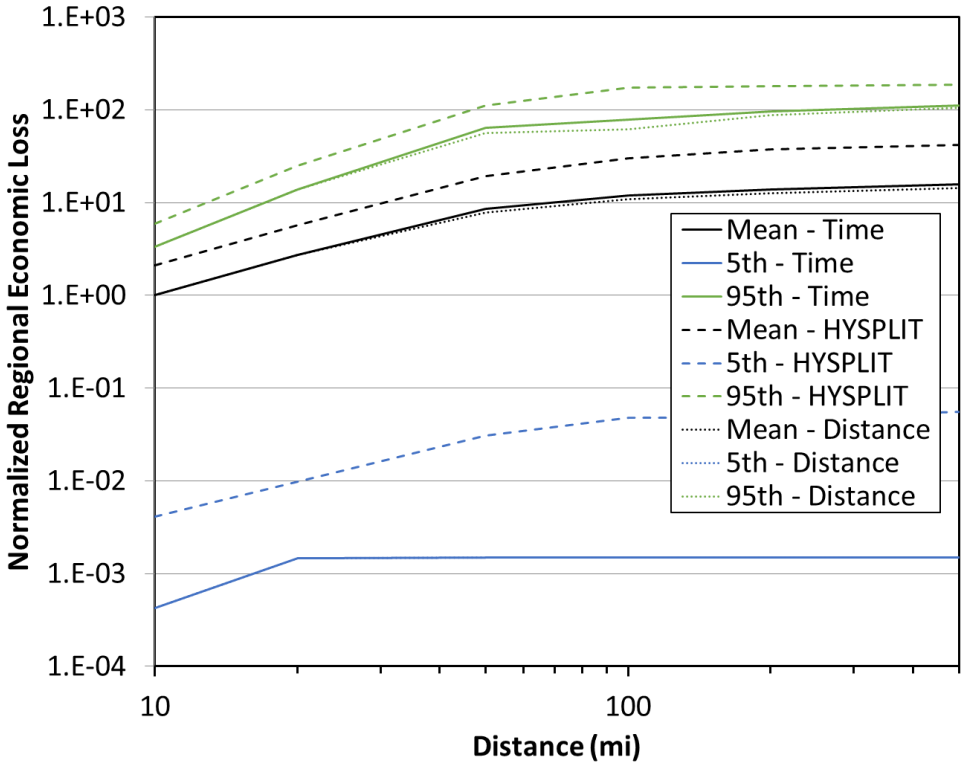

Figure 5-134. Economic loss comparison for two Gaussian ATD model options (Time and Distance) and the HYSPLIT ATD model (Site D, ST #1)

5.3.2.2. Source Term #2

Results for peak air concentration, peak ground deposition, land contamination area, peak dose, early fatality risk, population dose, latent cancer fatality risk, and economic loss (as described in Section 3.6) using the Gaussian ATD model (Time and Distance options) at Site D with ST #2 are compared with each other and with the HYSPLIT ATD models in Figure 5-135 through Figure 5-142. The annual statistics for these measures are shown with different colors, where the mean values are in black, the 5th percentile values are shown in blue, and the 95th percentile values are shown in green. HYSPLIT results are shown as dashed lines and Gaussian model results are shown as solid lines. The normalized results are shown as a function of distance, rather than the ratio of Gaussian and HYSPLIT results, to allow for the trends with distance to be observed. Some results are zero for early fatality risk, so they cannot be shown on the log scale used in the figures. Discussion of the difference seen in these figures is provided below in Section 5.2.3.

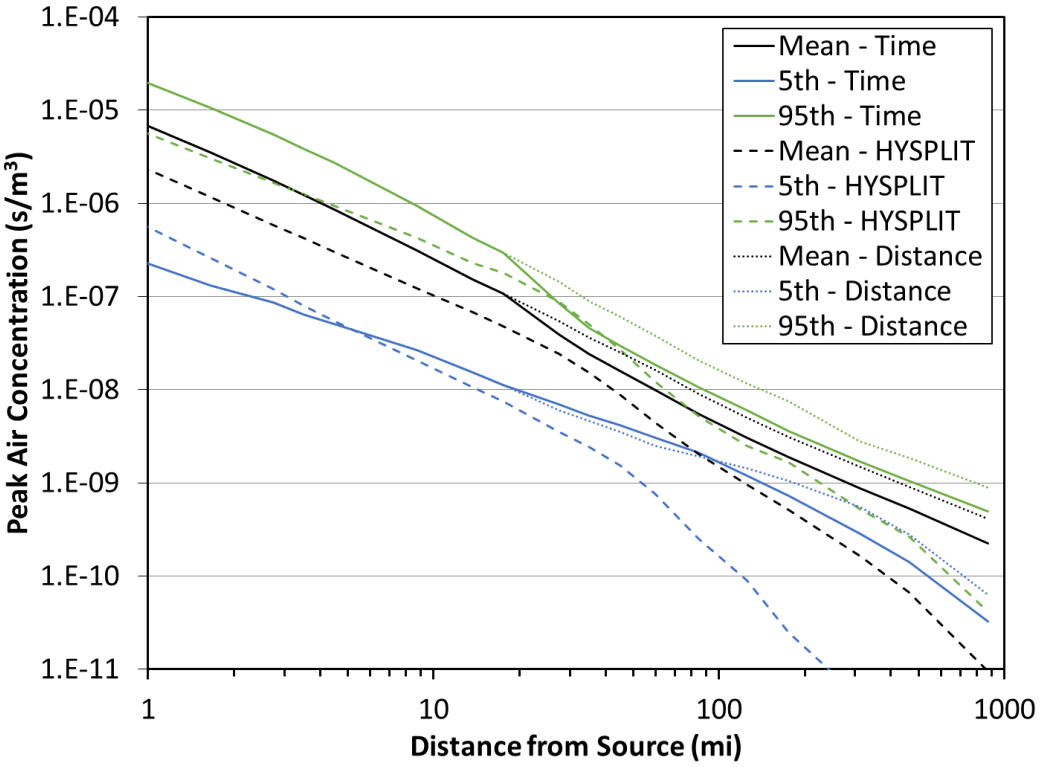

Figure 5-135. Peak air concentration comparison for two Gaussian ATD model options (Time and Distance) and the HYSPLIT ATD model (Site D, ST #2)

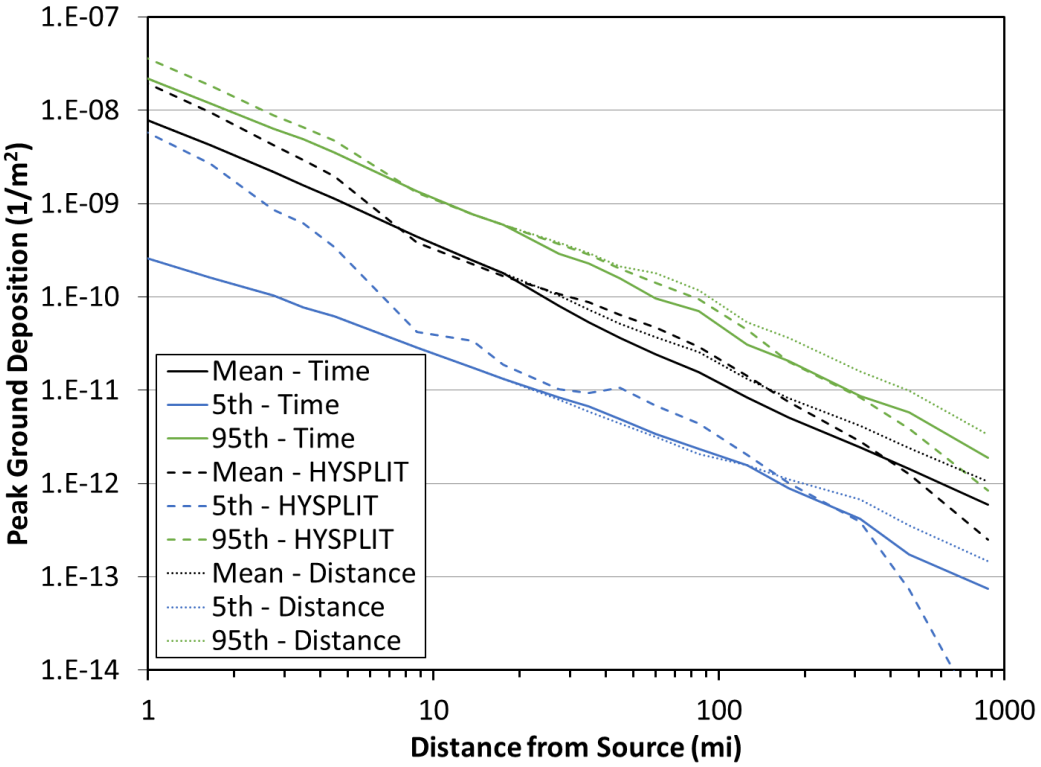

Figure 5-136. Peak ground deposition comparison for two Gaussian ATD model options (Time and Distance) and the HYSPLIT ATD model (Site D, ST #2)

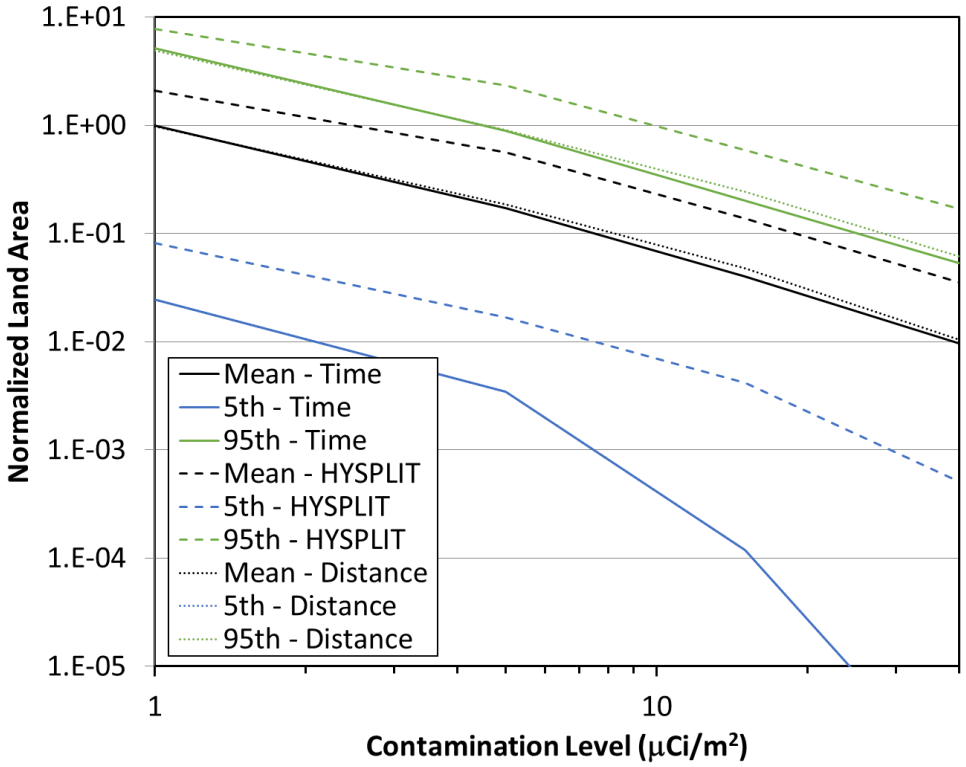

Figure 5-137. Land contamination area within 805 km (500 mi) comparison for two Gaussian ATD model options (Time and Distance) and the HYSPLIT ATD model (Site D, ST #2)

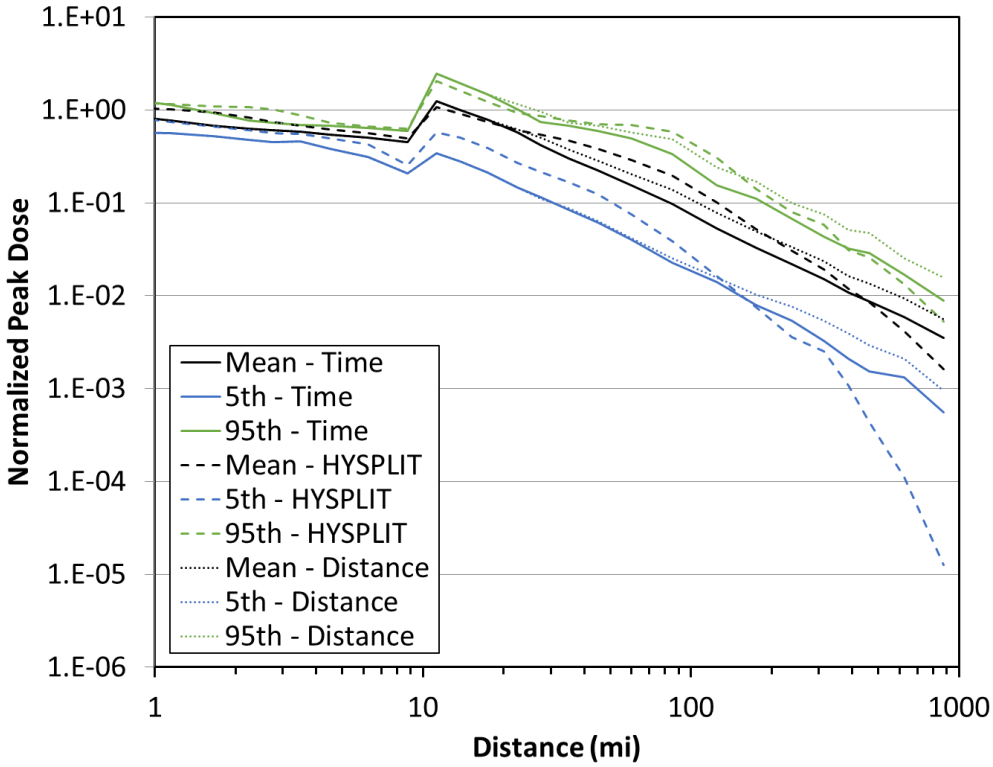

Figure 5-138. Peak dose comparison for two Gaussian ATD model options (Time and Distance) and the HYSPLIT ATD model (Site D, ST #2)

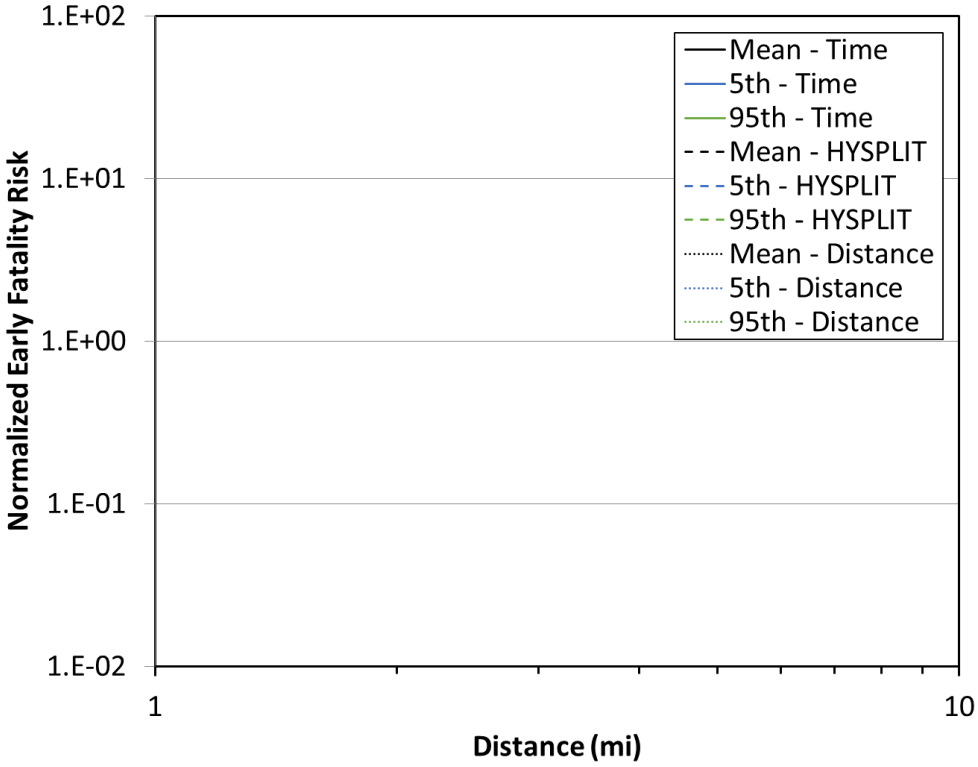

Figure 5-139. Early fatality risk comparison for two Gaussian ATD model options (Time and Distance) and the HYSPLIT ATD model (Site D, ST #2)

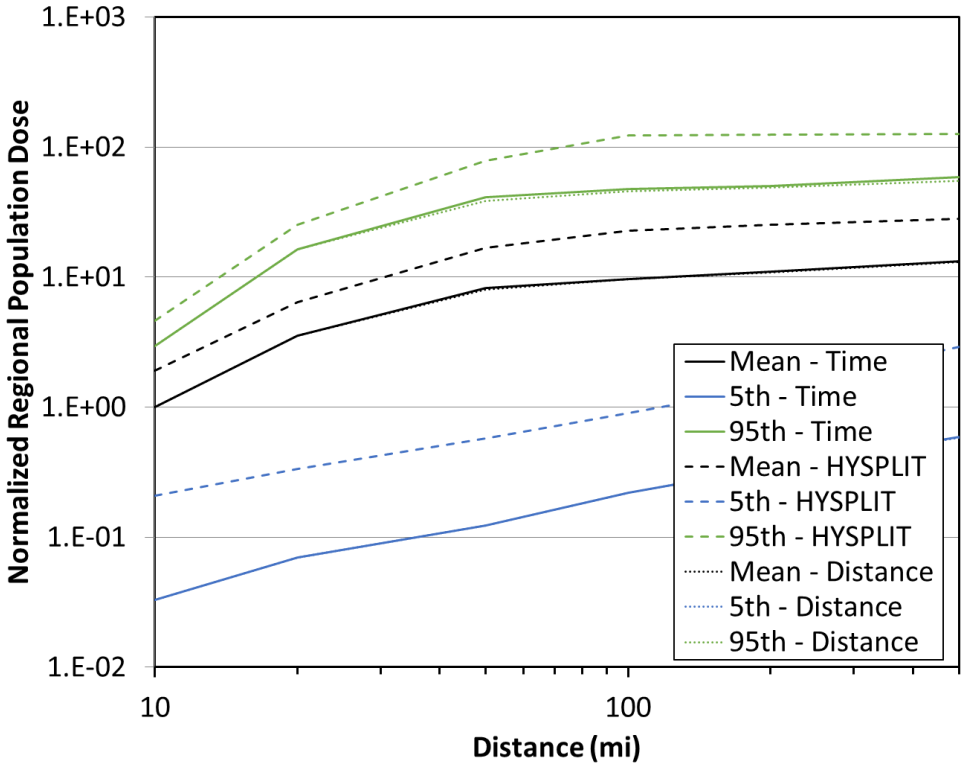

Figure 5-140. Population dose comparison for two Gaussian ATD model options (Time and Distance) and the HYSPLIT ATD model (Site D, ST #2)

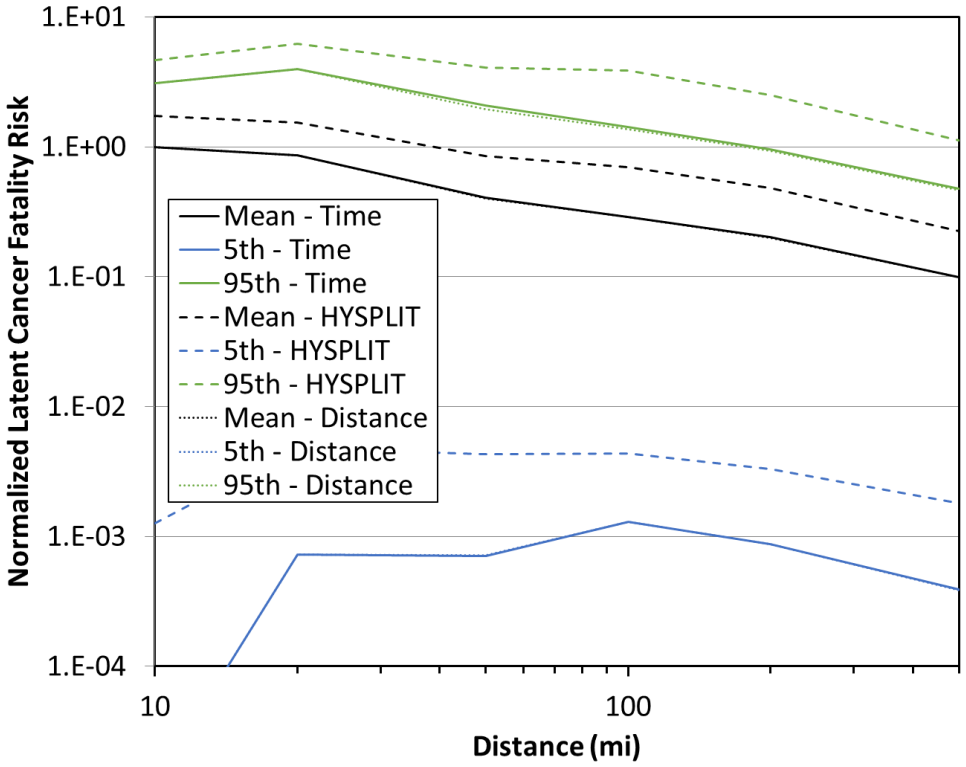

Figure 5-141. Latent cancer fatality risk comparison for two Gaussian ATD model options (Time and Distance) and the HYSPLIT ATD model (Site D, ST #2)

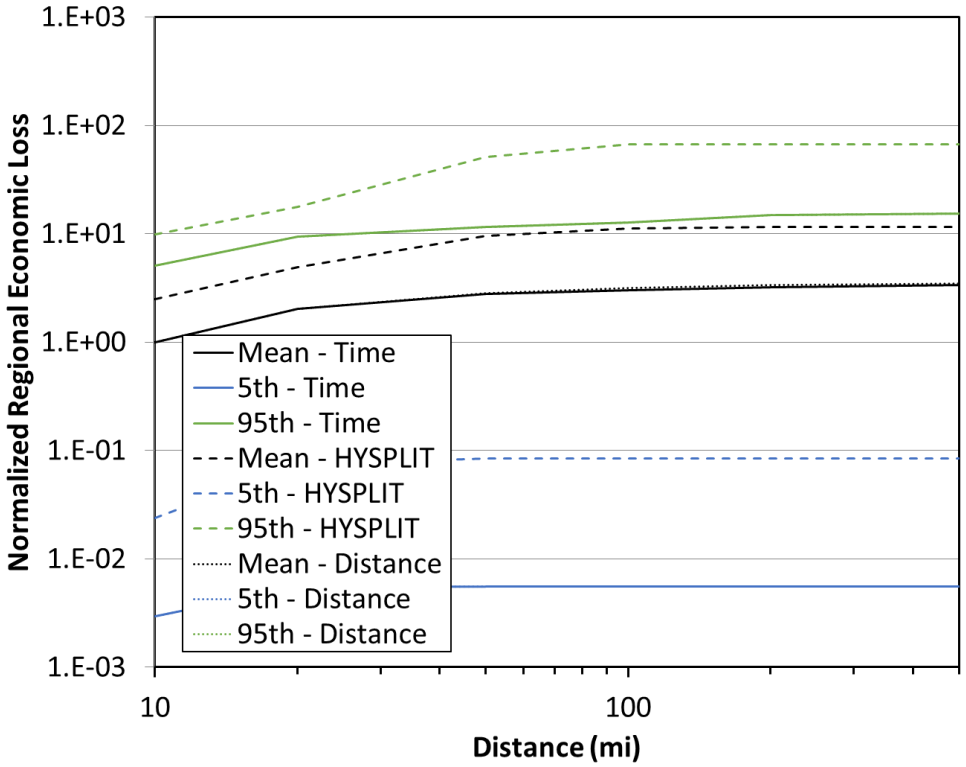

Figure 5-142. Economic loss comparison for two Gaussian ATD model options (Time and Distance) and the HYSPLIT ATD model (Site D, ST #2)

5.3.3. Interpretations of Dispersion Model Beyond 30 km Sensitivity

This section provides a comprehensive analysis of the results in the multiple figures presented in the previous sections (Sections 5.3.1 through 5.3.2). For those figures, the ratios of the annual average results for the Distance (Gaussian option using distance-based dispersion model throughout the domain) calculations to those for the Time (Gaussian option switching to time-based dispersion at 30 km [19 mi]) calculations are determined for each output metric as a function of distance. The averages of these ratios, along with their minimums and maximums from the site out to 805 km (500 mi) are shown in Table 5-6. The columns represent the outputs in the figures presented above for all distances; i.e., there is no break down between nearfield and far field. For source term #2, EF risk was calculated as zero and so a ratio couldn't be calculated.

Table 5-6. Ratios of the annual average results obtained using the Gaussian ATD model Distance option results to the Gaussian ATD model Time option results, shown as [Average (Minimum | Maximum)]

Site/ Source	Peak Air	Peak Ground	Peak Dose	Pop Dose	LCF Risk	Econ Loss	EF Risk	Land Area
A/1	1.9 (1.0|3.2)	1.8 (1.0|3.0)	1.3 (1.0|1.9)	0.9 (0.8|1.0)	0.9 (0.8|1.0)	1.0 (0.9|1.0)	1.0 (1.0|1.0)	0.8 (0.5|1.1)
D/1	1.3 (1.0|1.7)	1.3 (1.0|1.7)	1.1 (1.0|1.4)	1.0 (0.9|1.0)	1.0 (0.9|1.0)	0.9 (0.9|1.0)	1.0 (1.0|1.0)	0.8 (0.7|1.0)
A/2	1.9 (1.0|3.2)	1.8 (1.0|3.0)	1.5 (1.0|2.5)	1.0 (0.9|1.0)	1.0 (1.0|1.0)	1.0 (1.0|1.0)	a	1.3 (1.2|1.5)
D/2	1.3 (1.0|1.7)	1.3 (1.0|1.7)	1.2 (1.0|1.6)	1.0 (1.0|1.0)	1.0 (1.0|1.0)	1.0 (1.0|1.0)	a	1.1 (1.0|1.2)

[a]Data not available to compute ratio

General results determined by examining the comparisons between the Gaussian ATD model with the time-based dispersion option and with the distance-based dispersion option calculations for Site A and Site D for the two source terms are discussed below. Caution should be used in generalizing these interpretations to other sites or consequence metrics. The interpretations in this section summarize the trends from the results above.

1. The annual average results from the "Distance" Gaussian ATD model (i.e., without the time-based dispersion option) do not exhibit a change in slope in the peak air concentration and ground deposition at 30 km (19 mi). The peak air concentration and ground deposition values for the Gaussian ATD model results with the distance-based dispersion option are larger (with an average ratio of 1.6) than the results with the time-based dispersion option at distances beyond 30 km (19 mi).
2. The calculated annual average peak individual dose is higher (with an average ratio of 1.3) for the option of the Gaussian ATD model with the distance-based dispersion option compared to that with the time-based dispersion option.
3. The calculated regional population doses, latent cancer fatality risks, total regional economic loss, and early fatality risks for the Gaussian ATD model with the distance-based dispersion option are the same or slightly lower (with an average ratio of 0.9) than the results with the time-based dispersion option for both source terms.
4. The land areas that exceed various levels of contamination for the Gaussian ATD model with the distance-based dispersion option are lower (with an average ratio of 0.8) for ST #1 and higher (with an average ratio of 1.2) for ST #2 than the results with the time-based dispersion option.

This page left blank

6. SUMMARY

The nuclear accident consequence analysis code MACCS has traditionally modeled dispersion during downwind transport using a Gaussian plume segment model. The objective of this work is to supplement the Gaussian ATD model currently in MACCS with a new option using the HYSPLIT model. HYSPLIT/MACCS coupling has been implemented, with HYSPLIT as an alternative atmospheric dispersion option. The documentation of the implementation is provided to describe how the coupling was achieved and to show the results of verification tests performed on the HYSPLIT/MACCS coupling.

This report contains technical details of the HYSPLIT/MACCS coupling. The implementation strategy for incorporating HYSPLIT into MACCS is to provide a database of air concentration and ground deposition values, generated by HYSPLIT, that can be queried by MACCS for use in subsequent consequence calculations. The subsequent calculations in MACCS use the HYSPLIT-generated air concentration, and ground deposition values to calculate the same range of output quantities (dose, health effects, risks, etc.) that can be generated when using the MACCS Gaussian ATD model. MACCS is designed to determine those output quantities on a statistical basis over the course of a year. Based on the results from the verification test cases (agreement within 0.1%), the implementation of the HYSPLIT/MACCS coupling is confirmed.

A comparative analysis that involves running specific scenarios and sensitivity studies and comparing the results of the available modeling options is also documented in this report. This benchmarking exercise has several purposes. First, it serves as an initial analysis using the HYSPLIT/MACCS coupling to demonstrate the modeling results that can be obtained from using this new option. This provides a practical test of the implementation and provides information on the differences in the model input data and computational resources needed to exercise the new capability. Second, it serves as a further test of the hypothesis tested in (Molenkamp et al., 2004) that the results of a simple Gaussian plume segment model are sufficient for purposes of estimating expected values of consequence measures when averaged over a broad set of meteorological conditions (e.g., one year). Ultimately, the purpose of this benchmarking study is to illustrate the application of the new capabilities and inform decisions on when it may be appropriate to choose the Gaussian ATD model versus the HYSPLIT ATD model for specific applications.

The benchmark analysis is configured to explore the differences between the Gaussian and HYSPLIT ATD model results for a variety of NPP sites with prototypical input parameters. Sites were selected to represent a potentially diverse set of meteorological conditions, ranging from relatively simple to more complex wind fields. A variety of outputs were evaluated to inform a range of potential applications. For each output quantity, the mean and the 5^{th} and 95^{th} percentiles are used to quantify the range of the results. The ratio of the results from the Gaussian and HYSPLIT ATD models are calculated and discussed further below. Caution should be used in generalizing these conclusions to other sites and consequence metrics. Because some applications may be substantially different from these benchmarking comparisons, this study does not provide any general recommendations regarding which option may be generally identified as the preferred option. Users are encouraged to perform application-specific evaluations to determine which modeling approach best suits their needs in terms of model fidelity (HYSPLIT ATD model) versus computational expense (Gaussian ATD model).

Using the HYSPLIT ATD option adds substantial computational costs compared with the Gaussian ATD option. For example, for each site GenHysplit took 36 hours running on 720 processors to generate the HYSPLIT concentration files (*.ccd), generating a total of 35,136 files and storage of

500-600 GB per site. Another 14 hours were needed to run HyGridConvert for each site to generate the set of *.mcd files, which require ~200 GB more disc storage. Furthermore, the MACCS run time is longer when using the HYSPLIT ATD option. It is a function of the input/output speeds and depends on the communication speed between the device storing the *.mcd files and the computer running the calculations. The MACCS run time also depends on the number of plume segments in the source term. For example, it took about 5 hours for the MACCS/HYSPLIT calculations using ST #1 for each site; it took 28 hours using ST #2. The same calculations with MACCS using the Gaussian ATD option took 90 seconds for ST #1 and 22 minutes for ST #2.

The interpretations from the benchmark analysis are as follows:

1. The level of agreement between annual average results from the Gaussian and HYSPLIT ATD model is very similar to the results shown in NUREG/CR-6853 (Molenkamp et al., 2004), with the current study having a wider set of metrics and a longer distance range. It is important to note that this study examined only the comparison of annual statistics; the level of agreement between the two models may be quite different if these comparisons were evaluated for individual weather trials. Note the consistent trend in all metrics discussed below. On average, the HYSPLIT ATD model generally (but not always) predicts larger peak air concentrations and ground depositions than the Gaussian ATD model. The HYSPLIT ATD model also generally predicts larger consequences (e.g., doses, health effects, land areas contaminated, and economic effects). The differences between the Gaussian and HYSPLIT ATD model results was generally more pronounced with ST#1 than with ST#2. This shows that the level of agreement can be systematically affected by the source term being evaluated. The trends as a function of distance for the output quantities also agree between the two models:
    a. Annual average peak air concentrations are higher (with an average of 1.3) for the HYSPLIT ATD model compared with the Gaussian ATD model for ST #1 in the nearfield and at 4 out of 5 sites in the far field. For ST #2 the peak air concentration is always lower (with an average ratio of 0.5) for the HYSPLIT ATD model compared with the Gaussian ATD model in both the near and far field. This indicates that the nature of the source term has an impact on peak air concentration trends.
    b. Annual average peak ground depositions in the nearfield, are higher (with an average ratio of 2.1) at 4 out of 5 sites for ST #1 and lower (with an average ratio of 0.5) at 4 out of 5 sites for ST #2 for the HYSPLIT ATD model compared with the Gaussian ATD model. In the far field, they are the higher (with an average ratio of 2.9) at all five sites for ST #1 and higher (with an average ratio of 1.3) at 4 out of 5 sites for ST #2. This indicates that the nature of the source term has an impact on ground deposition trends.
    c. Annual average peak dose in the nearfield, are higher (with an average ratio of 1.3) for ST #1 and lower or equal (with an average ratio of 0.9) at 4 out of 5 sites for ST #2 for the HYSPLIT ATD model compared with the Gaussian ATD model. Peak dose is higher in all cases in the far field (with an average ratio of 1.6 and 1.3 for ST #1 and ST #2, respectively,) with the HYSPLIT ATD model.
    d. Annual average population doses in the nearfield are higher (with an average ratio of 2.8) for the HYSPLIT ATD model compared with the Gaussian ATD model for ST #1. For ST #2, the HYSPLIT ATD model predicts higher or equal (with an average ratio of 1.6) nearfield population doses. This indicates that there is a source term/site dependence in the trends of nearfield population dose predictions. For the far field, the HYSPLIT ATD

model predicts higher population doses in all cases (with an average ratio of 2.2 and 1.5 for ST #1 and ST #2, respectively).

e. Annual average latent cancer fatality risks are consistently higher (with an average ratio of 2.3 and 1.5 for ST #1 and ST #2, respectively,) for the HYSPLIT ATD model in the nearfield. They are also consistently higher (with an average ratio of 2.1 and 1.6 for ST #1 and ST #2, respectively,) in the far field as well.

f. Annual average economic loss in the nearfield is consistently predicted to be higher (with an average ratio of 2.6) for the HYSPLIT ATD model with ST #1. For ST #2, 4 out of 5 sites are higher (with an average ratio of 1.8) for the HYSPLIT ATD model. This indicates that there is a significant source term dependence on the trend for economic loss in the nearfield. For the far field, the HYSPLIT ATD model consistently predicts larger economic loss (with an average ratio of 2.4 and 1.9 for ST #1 and ST #2, respectively).

g. Annual average early fatality risk is predicted to be the larger (with an average ratio of 9.8) than the HYSPLIT ATD model for all cases for ST #1. All EF risks are predicted to be zero for ST #2.

h. Land contamination area is consistently predicted to be higher (with an average ratio of 2.4 and 1.8 for ST #1 and ST #2, respectively,) for the HYSPLIT ATD model with both STs.

2. While there are changes in trends between annual average results from the predictions of the Gaussian and HYSPLIT ATD models between the near and far fields for some of the consequence metrics considered in this study, there is no clear distance at which the Gaussian model seems to systematically diverge (greater than an order of magnitude) from the HYSPLIT ATD model. This highlights the difficulty in quantitatively identifying a specific distance limit beyond which Gaussian ATD models should not be used to estimate average annual consequences over variable weather. However, this study does not examine applications of Gaussian ATD models for specific weather sequences, where it is anticipated that these models may not produce acceptably accurate results at longer distances for some meteorological sequences (e.g., a sea breeze scenario or a cold front passage scenario). The process of averaging consequences over a full annual cycle of weather variability appears to largely compensate for inaccuracies in the use of Gaussian ATD models for specific weather sequences.
3. 5^{th} and 95^{th} percentile annual results shown in the benchmark results also follow the same trends for the Gaussian and HYSPLIT ATD models. However, they are often farther apart than the mean results, as expected.
4. Changes in annual average consequence results do not correlate directly with the changes in the annual average peak air concentration and peak ground deposition. For example, the far field, ST #2 results show an average ratio of 0.4 for the annual average peak air concentration and 0.7 for the annual average peak ground deposition, while the annual average peak individual dose had an average ratio of 0.9 and the annual average population dose had an average ratio of 1.6, both higher than either the annual average peak air concentration or peak ground deposition. The consequence output ratios show a strong dependence on sites and source terms.
5. The zero early fatality risks for ST #2 are due to the relatively small, delayed, and protracted nature of the source term. Early fatalities only occur when acute doses exceed a threshold level for a type of early fatalities. The delayed nature of the source terms calculated in the

SOARCA project allows time for radioactive decay of several shorter-lived radionuclides. The protracted nature of these source terms allows for wind shifts that reduce peak doses to any individual. Combined with relatively small releases of radionuclides, the analyses show that the possibility of early fatalities for these source terms is essentially zero.

6. One of the differences between ST #1 and ST #2 is that the rate of release of sensible heat in ST #1 is relatively large for the initial "puff" release (plume segment 1), which also carried most of the radionuclides. This should have caused more of the radionuclides to be carried further downwind than in ST #2. This may have accounted for at least some of the differences in trends between the two STs in the nearfield.

A set of sensitivity studies were conducted to test whether the differences seen between the HYSPLIT and Gaussian ATD calculations shown in the benchmark analysis are affected by: a) the source of the meteorological data set used for the HYSPLIT or Gaussian ATD calculations; b) the MacMetGen stability class determination method used to generate the MACCS-formatted meteorological file for the Gaussian ATD calculations (HYSPLIT ATD calculations do not use stability classes); and c) whether the long-range Gaussian dispersion model plume spread coefficients are expressed as a function of time or distance. It should be noted that the sensitivity studies are variants of the Gaussian model and don't affect the parameterization of the HYSPLIT model. The sensitivity to the source of the meteorological data set study includes HYSPLIT runs but does not change the parameterization of the HYSPLIT model. They are all therefore cases to test the hypothesis that trajectory averaging will result in reasonable agreement (approximately a factor of two) between the traditional MACCS Gaussian ATD model and the higher-fidelity MACCS/HYSPLIT coupled ATD model for computing consequence distributions.

The first sensitivity study investigates the potential differences that could arise in the results due to the choice of meteorological input data (NAM12, WRF27, and site observational data). The level of agreement between annual average results from the Gaussian ATD model for the three meteorological data sets is within plus or minus 50% with both source terms and for all consequence metrics. The trends in the level of agreement as a function of distance also agree between the three meteorological data set options. Differences resulting from the source of meteorological data are on the order of half the differences between the Gaussian and HYSPLIT ATD consequence metrics shown in the benchmark analyses.

The second sensitivity study explores the effect of the method used to estimate stability class on the model outputs. The level of agreement between annual average results from the Gaussian ATD model with the three methods to determine stability class is closer than it is in the previous comparison using different meteorological data sets. Most consequence metrics are well within 20% for the three methods used to estimate stability class. The annual average results that show the largest differences occur at short distances (<30 km), while there are smaller differences at longer distances. This similarity at larger distances corresponds to the change from a distance- to a time-based dispersion function at 30 km (19 mi), as described previously. Time-based dispersion does not distinguish between stability classes and so the results become homogenized as distance increases beyond 30 km (19 mi). The annual average results from the Gaussian ATD model with the DTDZ method generally produce the higher values (~10%) for the peak air concentration, peak ground deposition, peak dose, normalized regional population doses, and latent cancer fatality risk over the region.

The third sensitivity study examines the impact of turning off the time-based dispersion model in the Gaussian ATD model. Changes in slope of the peak air concentration and peak ground deposition versus distance are observed for the Gaussian ATD model results at the distance at

which the Gaussian dispersion model shifts from a distance-based to time- based formulation (19 mi, 30 km). The annual average results from the "Distance" Gaussian ATD model (i.e., without the time-based dispersion option) do not exhibit a change in slope in the peak air concentration and ground deposition at 30 km (19 mi). The peak air concentration and ground deposition values for the Gaussian ATD model results with the distance-based dispersion option are larger (with an average ratio of 1.6) than the results with the time-based dispersion option at distances beyond 30 km (19 mi). The calculated regional population doses, latent cancer fatality risks, total regional economic loss, and early fatality risks for the Gaussian ATD model with the distance-based dispersion option are the same or slightly lower (with an average ratio of 0.9) than the results with the time-based dispersion option for both source terms.

Based on the discussion above, the following conclusions are made:

- HYSPLIT is properly coupled with MACCS and is suitable for use when a higher fidelity atmospheric model is desired. This is demonstrated by a set of verification tests.
- In many of the scenarios evaluated in this analysis, the HYSPLIT ATD model predicts larger peak air concentrations and ground depositions than the Gaussian ATD model. For these scenarios, the HYSPLIT ATD model also generally (but not always) predicts larger consequences (e.g., doses, health effects, land areas contaminated, and economic effects). The higher HYSPLIT ATD model consequences are generally within a factor of two and hence the results of this analysis are consistent with the conclusions in (Molenkamp et al., 2004). However, this analysis extends those comparisons to a wider array of consequence measures, longer distances, multiple sites, and 5th and 95th percentile results in addition to the mean.
- The higher fidelity MACCS/HYSPLIT coupled model requires significantly more computational resources (~1 TB of storage and 100-200 times the computational run time) than the simple MACCS Gaussian plume segment model. This may be a consideration for resource intensive applications (e.g., evaluation of a large number of potential source terms or performance of uncertainty analyses) or for short-distance analyses where the Gaussian plume segment model may be considered more applicable.
- However, the computational resources needed to exercise the higher fidelity option are not prohibitive and, given the widespread availability of archived meteorological datasets, the new capabilities actually ease some of the input data burdens (i.e., development of high-quality meteorological data for multiple years for a specific site) associated with older models.

This page left blank

REFERENCES

[1] Bixler, N., E. Clauss, and C. Morrow (2013). Synthesis of Distributions Representing Important Non-Site-Specific Parameters in Offsite Consequence Analysis (NUREG/CR-7161; SAND2010-3380P). Albuquerque, NM: Sandia National Laboratories.

[2] Bixler, N., J. Jones, D. Osborn and S. Weber (2014). MACCS Best Practices as Applied in the State-of-the-Art Reactor Consequence Analyses (SOARCA) Project (NUREG/CR-7009). Albuquerque, NM: Sandia National Laboratories.

[3] Bixler, N., F. Walton, J. Leute, L. Eubanks, R. Haaker and K. McFadden (2021). MELCOR Accident Consequence Code System (MACCS): User's Guide and Reference Manual SAND2021-1588. Albuquerque, NM: Sandia National Laboratories 2021.

[4] Brenk, F.W., & K.J. Vogt (1981). "The Calculation of Wet Deposition from Radioactive Plumes". Nuclear Safety, Vol. 22, 362. 1981.

[5] Briggs, G.A. (1973). "Plume Rise Predictions". Environmental Research Laboratories, U.S. Department of Commerce, NOAA. 1973.

[6] Chamberlain, A.C. (1953). "Aspects of Travel and Deposition of Aerosol and Vapour Clouds". British Report AERE-HP/R 1261, Atomic Energy Research Establishment, Harwell, United Kingdom. 1953.

[7] Chanin, D.I., J. Sprung, L. Ritchie and H.-N. Jow, "MELCOR Accident Consequence Code System (MACCS). Volume 1: Users Guide (NUREG/CR-4691)," Sandia National Laboratories, Albuquerque, NM, 1990.

[8] Chanin, D.I., & M.L.Young (1998). Code Manual for MACCS2: Volume 1, User's Guide (NUREG/CR-6613). Albuquerque, NM: Sandia National Laboratories.

[9] Dobbins, R.C. (1979). "Atmospheric Motion and Air Pollution: An Introduction for Students of Engineering and Science". John Wiley & Sons, Inc. 1979.

[10] Draxler, R.R., & G.D. Hess (1997). Description of the HYSPLIT_4 modeling system. NOAA Tech. Memo. ERL ARL-224, Silver Spring, MD: NOAA Air Resources Laboratory.

[11] Draxler, R.R., & G.D. Hess (1998). An overview of the HYSPLIT_4 modeling system of trajectories, dispersion, and deposition. Aust. Meteor. Mag., 47, 295-308.

[12] Draxler, R.R. (1999). HYSPLIT4 user's guide. NOAA Tech. Memo. ERL ARL-230. Silver Spring, MD: NOAA Air Resources Laboratory.

[13] Hanna, S.R., et al. (1982). "Handbook on Atmospheric Diffusion". DOE/TIC-11223, U.S. Department of Energy, Washington DC. 1982.

[14] Hanna, S.R. (2002). "Meteorological Modeling in MACCS (Final Report P047)". Hanna Consultants, Kennebunkport, ME, March 22, 2002.

[15] Harper, F.T., S.C. Hora, M.L. Young, L.A. Miller, C.H. Lui, M.D. McKay, J.C. Helton, L.H.J Goossens, R.M. Cooke, J. Pasler-Sauer, B. Kraan, & J.A. Jones (1995). "Probabilistic Accident Consequence Uncertainty Analysis, Dispersion and Deposition Uncertainty Assessment, Volumes 1 and 2" (NUREG/CR-6244 / EUR 15855EN / SAND94-1453), US Nuclear Regulatory Commission, Washington, DC, and Commission of the European Communities, Brussels, Belgium, January 1995.

[16] Hosker, Jr., R.P. (1974). "Estimates of Dry Deposition and Plume Depletion over Forests and Grassland". in Physical Behavior of Radioactive Contaminants in the Atmosphere. Symposium Proceedings, International Atomic Energy Agency, Vienna. 1974.

[17] Jow, H.-N., J. Sprung, J. Rollstin, L. Ritchie, & D. Chanin (1990). *MELCOR Accident Consequence Code System (MACCS): Volume 2, Model Description (NUREG/CR-4691; SAND86-1562).* Albuquerque, NM: Sandia National Laboratories.

[18] Karlsson, S. (1982). "Dry Deposition – A Literature Review". Studsvik Energiteknik AB, Studsvik/NW-82/242. Sweden. 1982.

[19] Molenkamp, C., N. Bixler, C. Morrow, J. Ramsdell, & J. Mitchell (2004). Comparison of Average Transport and Dispersion Among a Gaussian, a Two-Dimensional, and a Three-Dimensional Model (NUREG/CR-6853). Livermore, CA, Albuquerque, NM, and Richland, WA,: Lawrence Livermore National Laboratory, Sandia National Laboratories, and Pacific Northwest National Laboraratory.

[20] National Oceanic and Atmospheric Administration (NOAA), Air Resources Laboratory (ARL), Weather Data Archive. Data retrieved at ftp://arlftp.arlhq.noaa.gov/archives/, January 2017.

[21] Ritchie, L. T., J. D. Johnson, and R. M. Blond (1983), Calculations of Reactor Accident Consequences Version 2 CRAC2: Computer Code, User's Guide, NUREG/CR-2326, SAND81-1994, Sandia National Laboratories, Albuquerque, NM.

[22] Skamarock, W.C., J.B. Klemp, J. Dudhia, D.O. Gill, D.M. Barker, M.G. Duda, X.-Y. Huang, W. Wang, & J.G. Powers (2008). A Description of the Advanced Research WRF Version 3. NCAR/TN-475+STR. National Center for Atmospheric Research, Boulder, CO, June 2008.

[23] Stein, A.F., R.R. Draxler, G.D. Rolph, B.J.B. Stunder, M.D. Cohen & F. Ngan (2015). NOAA's HYSPLIT Atmospheric Transport and Dispersion Modeling System, Bull. Amer. Meteor. Soc., 96, 2059-2077, http://dx.doi.org/10.1175/BAMS-D-14-00110.

[24] Tadmor, J., & Y. Gur (1969). Analytical Expressions for the Vertical and Lateral Dispersion Coefficients in Atmospheric Diffusion. Atmospheric Environment, Vol. 3, pp. 688–689.

[25] Turner, D.B., (1970). "Workbook of Atmospheric Dispersion Estimates (AP-26)". Office of Air Programs, U.S. Environmental Protection Agency, Research Triangle Park, NC.

[26] U. S. Environmental Protection Agency (EPA) (2000). Meteorological Monitoring Guidance for Regulatory Modeling Application. EPA-454/R-99-005. February 2000.

[27] U.S. Nuclear Regulatory Commission (NRC), 1975. NUREG-75/014; WASH-1400. "Reactor Safety Study: Appendix VI," U.S. Nuclear Regulatory Commission, Washington, DC, 1975.

[28] U. S. Nuclear Regulatory Commission (NRC), 1983. NUREG/CR-2300. "PRA Procedures Guide: A Guide to the Performance of Probabilistic Risk Assessments for Nuclear Power Plants. Final Report," U.S. Nuclear Regulatory Commission, Washington DC, 1983.

[29] U. S. Nuclear Regulatory Commission (NRC), 1990. NUREG-1150, "Severe Accident Risks: An Assessment for Five U.S. Nuclear Power Plants," U.S. Nuclear Regulatory Commission, Washington DC, 1990.

[30] U. S. Nuclear Regulatory Commission (NRC) (2007). Regulatory Guide 1.23, Rev. 1, "Meteorological Monitoring Programs for Nuclear Power Plants," U.S. Nuclear Regulatory Commission, Washington DC, March 2007.

[31] U. S. Nuclear Regulatory Commission (NRC), 2012. NUREG-1935, "State-of-the-Art Reactor Consequence Analyses (SOARCA) Report," U.S. Nuclear Regulatory Commission, Washington DC, 2012.

[32] Weber, S., & N.E. Bixler (2014). SecPop 4 User's Guide: Sector Population, Land Fraction, and Economic Estimation Program, Revision 2 (NUREG/CR-6525). Albuquerque, NM: Sandia National Laboratories.

This page left blank

APPENDIX A. GENHYSPLIT INPUT FILE EXAMPLE

This appendix contains a sample input file to GenHysplit. The options specified here are examples shown to illustrate how GenHysplit interacts with HYSPLIT. The user should determine the appropriate values to use for their specific application. The file below is configured to generate results for each hour between 0000 UTC January 1, 2008 through 2300 UTC December 31, 2008, at a release location of 25°26'6" N, 80°19'53" W, and at four specified release heights. This would generate 8,784 files (366 day × 24 hours) for each of the four release heights for a grand total of 35,136 .ccd files. Each file would contain the air concentration and ground deposition out to 1,610 km for ten aerosol sizes and one non-depositing aerosol. The air concentrations and ground depositions would be the average over each 15-minute increment from the start of release up to 120 hours (5 days) after the one-hour release. One of the HYSPLIT input file sets (CONTROL, EMITTIMES, SETUP.CFG) that would be generated is shown below. These HYSPLIT input files would be generated using the options specified in this sample GenHysplit input file for a release during the first hour (0) of the first day (January 1, 2008), at the first release height (10 m). The reader is directed to the HYSPLIT User's Guide (Draxler 1999) for the interpretation of the HYSPLIT input files.

A.1. Sample GenHysplit Input File

```
! ------------------------------------------------------------------------ !
! An input file for a GenHysplit run
! ------------------------------------------------------------------------ !
!
! ------------------------------------------------------------------------ !
! File Information
! ------------------------------------------------------------------------ !
! Meteorology directory
/scratch/sample/met/met_wrf_2008
! Meteorology file prefix

! Are the meteorology files generated with the stn2arl utility (0=no, 1=yes)
0
! HYSPLIT Directory
/home/sample/hysplit/hysplit_810/trunk
! Output Directory
/scratch/sample/ADT/GenHysplit/site_wrf
! ------------------------------------------------------------------------ !
! Run Information
! ------------------------------------------------------------------------ !
! Number of groups to run
1
! First and last day for each group [YYYYMMDD]
20080101        20081231
! Release Longitude [degrees minutes seconds direction (W or E)]
80      19      53      W
! Release Latitude [degrees minutes seconds direction (N or S)]
25      26      6       N
! Varying heights (=0) or varying power (=1)
0
! Release Heights [m] (truncated to increments of 10 m, max=9990 m)
10.0 50.0 100.0 200.0
! Heat release [MW] (truncated to increments of 0.1 MW, max=99.9 MW)
0.0
```

```
! Release horizontal area [m2]
0
! Run time after release [hr]
120
! Time increment for concentration output [minutes]
15
! Output Grid Type (0=rectangular, 1=polar)
1
! Output Grid Size [km] (distance from release location)
1610.0
! Base Grid Size [km] (distance from release location)
10
! Base Grid Spacing [km]
0.5
! Height for ground-level air concentration calculations [m]
50.0
! Modeling Approach (0=lagrangian particles, 1=gaussian puffs)
0
! Number of particles per aerosol size per minute
10
! Aerosol sizes [microns]
0.15332 0.28543 0.53138 0.98923 1.8416 3.4284 6.3825 11.882 22.120 41.179
! Aerosol densities [g/cm3]
1.0 1.0 1.0 1.0 1.0 1.0 1.0 1.0 1.0 1.0
! Deposition velocities (m/s) [0=internal calculation]
0.0 0.0 0.0 0.0 0.0 0.0 0.0 0.0 0.0 0.0
! Deposition configuration (1=wet and dry, 2=1 + neither wet nor dry, 3=2 + either no wet or no dry)
2
```

A.2. Sample HYSPLIT Input Files – 0000 UTC, January 1, 2008, 10 m

A.2.1. CONTROL

```
2008  1  1  0
1
25.435000 -80.331389 10.0
121
0
10000.0
12
/scratch/sample/met/met_wrf_2008/
20080101.ARL
/scratch/sample/met/met_wrf_2008/
20080102.ARL
/scratch/sample/met/met_wrf_2008/
20080103.ARL
/scratch/sample/met/met_wrf_2008/
20080104.ARL
/scratch/sample/met/met_wrf_2008/
20080105.ARL
/scratch/sample/met/met_wrf_2008/
20080106.ARL
/scratch/sample/met/met_wrf_2008/
20080107.ARL
/scratch/sample/met/met_wrf_2008/
20080108.ARL
```

/scratch/sample/met/met_wrf_2008/
20080109.ARL
/scratch/sample/met/met_wrf_2008/
20080110.ARL
/scratch/sample/met/met_wrf_2008/
20080111.ARL
/scratch/sample/met/met_wrf_2008/
20080112.ARL
11
GP00
0.00000
0.000
 0 0 0 0 0
GP01
0.00000
0.000
 0 0 0 0 0
GP02
0.00000
0.000
 0 0 0 0 0
GP03
0.00000
0.000
 0 0 0 0 0
GP04
0.00000
0.000
 0 0 0 0 0
GP05
0.00000
0.000
 0 0 0 0 0
GP06
0.00000
0.000
 0 0 0 0 0
GP07
0.00000
0.000
 0 0 0 0 0
GP08
0.00000
0.000
 0 0 0 0 0
GP09
0.00000
0.000
 0 0 0 0 0
GP10
0.00000
0.000
 0 0 0 0 0
9
25.43500 -80.33139
2.81250 0.50000

```
360.00000 10.00000
./
2008010100H001.cdump0
2
0.0 50.0
 0  0  0  0  0
 0  0  0 121  0
 0  0 15
25.43500 -80.33139
2.81250 1.00000
360.00000 20.00000
./
2008010100H001.cdump1
2
0.0 50.0
 0  0  0  0  0
 0  0  0 121  0
 0  0 15
25.43500 -80.33139
2.81250 2.00000
360.00000 40.00000
./
2008010100H001.cdump2
2
0.0 50.0
 0  0  0  0  0
 0  0  0 121  0
 0  0 15
25.43500 -80.33139
2.81250 4.00000
360.00000 80.00000
./
2008010100H001.cdump3
2
0.0 50.0
 0  0  0  0  0
 0  0  0 121  0
 0  0 15
25.43500 -80.33139
2.81250 8.00000
360.00000 160.00000
./
2008010100H001.cdump4
2
0.0 50.0
 0  0  0  0  0
 0  0  0 121  0
 0  0 15
25.43500 -80.33139
2.81250 16.00000
360.00000 320.00000
./
2008010100H001.cdump5
2
0.0 50.0
 0  0  0  0  0
```

```
 0  0  0 121  0
 0  0 15
25.43500 -80.33139
2.81250 32.00000
360.00000 640.00000
./
2008010100H001.cdump6
2
0.0 50.0
 0  0  0  0  0
 0  0  0 121  0
 0  0 15
25.43500 -80.33139
2.81250 64.00000
360.00000 1280.00000
./
2008010100H001.cdump7
2
0.0 50.0
 0  0  0  0  0
 0  0  0 121  0
 0  0 15
25.43500 -80.33139
2.81250 80.50000
360.00000 1610.00000
./
2008010100H001.cdump8
2
0.0 50.0
 0  0  0  0  0
 0  0  0 121  0
 0  0 15
11
0.153 1.000 1.000
0.0000E+00 100.000 0.000 0.000 0.000
0.000 8.0E-05 8.0E-05
0.00
0.00
0.285 1.000 1.000
0.0000E+00 100.000 0.000 0.000 0.000
0.000 8.0E-05 8.0E-05
0.00
0.00
0.531 1.000 1.000
0.0000E+00 100.000 0.000 0.000 0.000
0.000 8.0E-05 8.0E-05
0.00
0.00
0.989 1.000 1.000
0.0000E+00 100.000 0.000 0.000 0.000
0.000 8.0E-05 8.0E-05
0.00
0.00
1.842 1.000 1.000
0.0000E+00 100.000 0.000 0.000 0.000
0.000 8.0E-05 8.0E-05
```

```
0.00
0.00
3.428 1.000 1.000
0.0000E+00 100.000 0.000 0.000 0.000
0.000 8.0E-05 8.0E-05
0.00
0.00
6.383 1.000 1.000
0.0000E+00 100.000 0.000 0.000 0.000
0.000 8.0E-05 8.0E-05
0.00
0.00
11.882 1.000 1.000
0.0000E+00 100.000 0.000 0.000 0.000
0.000 8.0E-05 8.0E-05
0.00
0.00
22.120 1.000 1.000
0.0000E+00 100.000 0.000 0.000 0.000
0.000 8.0E-05 8.0E-05
0.00
0.00
41.179 1.000 1.000
0.0000E+00 100.000 0.000 0.000 0.000
0.000 8.0E-05 8.0E-05
0.00
0.00
0.000 0.000 1.000
0.0000E+00 100.000 0.000 0.000 0.000
0.000 0.0E+00 0.0E+00
0.00
0.00
```

A.2.2. EMITIMES

```
YYYY MM DD HH    DURATION(hhhh) #RECORDS
YYYY MM DD HH MM DURATION(hhmm) LAT LON HGT(m) RATE(/h)  AREA(m2) HEAT(w)
2008  1  1  0      121   11
2008  1  1  0   0   60  25.435000 -80.331389 10.00  1.000e+00 0.000e+00 0.000e+00
2008  1  1  0   0   60  25.435000 -80.331389 10.00  1.000e+00 0.000e+00 0.000e+00
2008  1  1  0   0   60  25.435000 -80.331389 10.00  1.000e+00 0.000e+00 0.000e+00
2008  1  1  0   0   60  25.435000 -80.331389 10.00  1.000e+00 0.000e+00 0.000e+00
2008  1  1  0   0   60  25.435000 -80.331389 10.00  1.000e+00 0.000e+00 0.000e+00
2008  1  1  0   0   60  25.435000 -80.331389 10.00  1.000e+00 0.000e+00 0.000e+00
2008  1  1  0   0   60  25.435000 -80.331389 10.00  1.000e+00 0.000e+00 0.000e+00
2008  1  1  0   0   60  25.435000 -80.331389 10.00  1.000e+00 0.000e+00 0.000e+00
2008  1  1  0   0   60  25.435000 -80.331389 10.00  1.000e+00 0.000e+00 0.000e+00
2008  1  1  0   0   60  25.435000 -80.331389 10.00  1.000e+00 0.000e+00 0.000e+00
2008  1  1  0   0   60  25.435000 -80.331389 10.00  1.000e+00 0.000e+00 0.000e+00
```

A.2.3. SETUP.CFG

```
&SETUP
tratio  = 0.75,
```

```
initd  = 0,
kpuff  = 0,
khmax  = 9999,
kmixd  = 0,
kmix0  = 250,
kzmix  = 0,
kdef  = 0,
kbls  = 1,
kblt  = 2,
conage  = 48,
numpar  = -600,
qcycle  = 0.00,
efile  = 'EMITIMES',
tkerd  = 0.18,
tkern  = 0.18,
ninit  = 1,
ndump  = 0,
ncycl  = 0,
pinpf  = '',
poutf  = 'PARDUMP',
mgmin  = 10,
kmsl  = 0,
maxpar  = 13200,
cpack  = 3,
cmass  = 0,
dxf  = 1.00,
dyf  = 1.00,
dzf  = 1.00,
ichem  = 0,
kspl  = 1,
krnd  = 6,
frhs  = 1.00,
frvs  = 0.01,
frts  = 0.10,
frhmax  = 3.00,
splitf  = 1.00,
delt  = 0.00,
/
```

This page left blank

APPENDIX B. PEER REVIEW SUMMARY

At the request of the NRC, a peer review was conducted to help the NRC and SNL evaluate whether the HYSPLIT/MACCS coupled model can be used for probabilistic consequence analyses as a "state-of-practice" model. The panel comprised of Damien Didier, head of the Environmental Dispersion Modeling for Accidental Consequences Section at the Institut de Radioprotection et de Sûreté Nucléaire; Dr. Steven Hanna, a consultant with extensive experience in atmospheric dispersion modeling; and Dr. Chris Owen, who is the Model Development Team lead for the US Environmental Protection Agency AERMOD Modeling System. The peer review panel was convened in March 2019 to review the coupling of HYSPLIT ATD results with MACCS and to evaluate the validity and interpretations of the benchmarking exercise. The reviewers were provided with a preliminary draft of the report as well as presentations covering the implementation of the HYSPLIT coupling and the results of the benchmarking exercise. A detailed set of review questions was also provided to focus the scope of desired peer review feedback. Following the meeting, the peer reviewers provided comments on the document as well as their initial response to the set of review questions. The reviewers were supportive of adding the new capabilities to MACCS but had a number of comments related to model descriptions, design and interpretation of the benchmarking exercises, and the conclusions. A summary of the initial peer review feedback is shown in Table B-1.

Table B-1. High-level summary of initial peer review feedback

Indicator	Comment	Response
General Comments		
GC1	Skepticism of using the Gaussian model at distances as long as 1000 mi.	Added discussion for distance selection to Sections 1.1, 3.0 and 3.3
GC2	Benchmarking results indicate smaller differences than expected.	Added discussion regarding expectation of smaller differences in Section 1.1, 3.0, 4.0 and 4.7
GC3	Approach is state-of-the-art science	Acknowledged
Basic Models		
BM1	Choice of HYSPLIT and its validation	Added discussion on choice of HYSPLIT and its validation to Section 1.3.2
BM2	Discussion of Gaussian model	Enhanced discussion of Gaussian model in Section 1.3.1
BM3	Details of the implementation of the HYSPLIT model with MACCS	Added more details for HYSPLIT/MACCS coupling in Section 2.1
BM4	Description of use of HYSPLIT model results in MACCS	Added more details for HYSPLIT/MACCS coupling in Section 2.1
BM5	Discussion of plume rise	Added plume rise discussion to model descriptions in Section 1.3.1 and 1.3.2. Added discussion of model differences to Section 3.4.2.1
BM6	Discussion of MacMetGen, especially method for determining stability class	Added more details to MacMetGen discussion in Section 2.1.4
BM7	Description of weather sampling options	Added section on weather sampling, which is Section 1.4
BM8	Description of radioactive decay and ingrowth	Added decay and ingrowth discussion to Section 2.1.3

Indicator	Comment	Response
Verification and Benchmarking		
VB1	Better discussion of cases and results	Added intention/objective of verification, benchmark, and sensitivity studies to Section 1.1 and then within their respective sections (2.2, 3.0, 4.0, and 5.0)
VB2	Spatial plotting of air and ground concentrations	Updated verification cases, comparisons are much clearer in Section 2.2
VB3	Use of quantitative acceptance criteria	Added quantitative criteria for verification test in Section 2.2. Added discussion of why acceptance criteria are not applicable to benchmark in Section 4.0. Added quantitative comparisons to Sections 4.7, 5.1.3, 5.2.3, and 5.3.3.
VB4	Discussion of averaging time	Added discussion in Section 2.1.1 and included example GenHysplit and HYSPLIT input files in Appendix A
VB5	Better discussion/description of quantities in plots	Revisited discussion of quantities in plots in Section 2.2 and 3.1
VB6	Conclusions are not well explained	Updated conclusion discussions in Sections 4.6, 5.1.3, 5.2.3, and 5.3.3
VB7	Add areas and distances as output metrics	Rearranged land contamination to atmospheric dispersion output in Sections 2, 4 and 5
VB8	Add one more site	For sensitivity studies, added Site D to Section 5
Additional Verification and Justification of Parameter Choices		
AV1	Verification of the HYSPLIT implementation is not adequately established.	Completely redid verification tests (Section 2.2)
AV2	More sensitivity studies to evaluate importance of HYSPLIT model choices	Discussed using HYSPLIT defaults in Section 3.4 and added HYSPLIT input files to Appendix A
AV3	Reasons for differences in HYSPLIT results with polar and Cartesian coordinates	Removed from discussion
AV4	Treatment of aerosol size distributions, neglecting agglomeration in the atmosphere	Added text for source of aerosol distributions used in Section 3.4
AV5	Treatment of near-field modeling	Not addressed in this document but addressed separately
AV6	Number of years of weather data	Not addressed in this document
AV7	Number of Lagrangian particles	Updated discussion in Section 3.4.2.2

In response to this initial feedback, the report was revised to improve the documentation, provide additional analyses to verify the correct coupling of MACCS and HYSPLIT, and to more clearly explain the purpose and interpretation of the model comparison studies. A revised draft was provided to the panel prior to the final meeting in June 2020. The reviewers provided their feedback on the revised draft. The reviewers noted that:

- Overall, there was a significant, global improvement of the document from the previously reviewed version.

- There are several improvements needed to enhance the document in terms of clarity, discussion of results, and interpretation of model comparison studies.
- There should be more recognition that consequence outputs are correlated with atmospheric dispersion outputs; for example, if peak concentrations increase, then peak radiological doses likely increase.
- It is important to recognize that many results obtained using the HYSPLIT ATD model are larger on average than the results obtained using the Gaussian ATD model.
- It is important to emphasize that MACCS is typically used to estimate annual average results and is not typically used to develop real-time results from short-term releases.
- The implementation of the HYSPLIT atmospheric dispersion model results into MACCS appear satisfactory.
- The ability to incorporate HYSPLIT model results is a major improvement in the capabilities of MACCS simulations and provides a state-of-the-art alternative.

Both the initial and final feedback from the peer review panel were considered in creating the final report.

This page left blank

APPENDIX C. ORIGINAL BENCHMARK ANALYSIS RESULTS

The benchmark analysis was originally performed using earlier versions of the software during the development phase of the capabilities. The codes and versions for the software used in the original comparative analyses are shown in Table C-1. The results of the original analysis were presented to the peer review panel. The trends and results of the original analysis are similar to the results shown in Section 4, and are provided here for completeness.

Table C-1. Software used in original benchmark analyses

Code	Version
GenHysplit	1.1.0
HyGridConvert	1.1.0
HYSPLIT	810
MacMetGen	1.0.0
MACCS	3.10.0.15
SecPop	4.3.0
WinMACCS	3.10.9

C.1. Site A

C.1.1. Source Term #1

The original comparisons between the Gaussian and HYSPLIT ATD model results for Site A, ST #1 (from Sample Problem A), for peak air concentration, peak ground deposition, land contamination area, peak dose, early fatality risk, population dose, latent cancer fatality risk, and economic loss (as described in Section 3.6) are shown in Figure C-1 through Figure C-8. The annual statistics for these measures are shown with different colors, where the mean values are in black, the 5th percentile values are shown in blue, and the 95th percentile values are shown in green. HYSPLIT results are shown as dashed lines and Gaussian model results are shown as solid lines. The normalized results are shown as a function of distance, rather than the ratio of Gaussian and HYSPLIT results, to allow for the trends with distance to be observed. Some results are zero for early fatality risk, so they cannot be shown on the log scale used in the figures. Note that the change in slope at about 19 mi for the Gaussian plume segment curves is caused by the switch from distance- to time-based dispersion models. A summary of the difference seen in these figures is provided below in Section C.6.

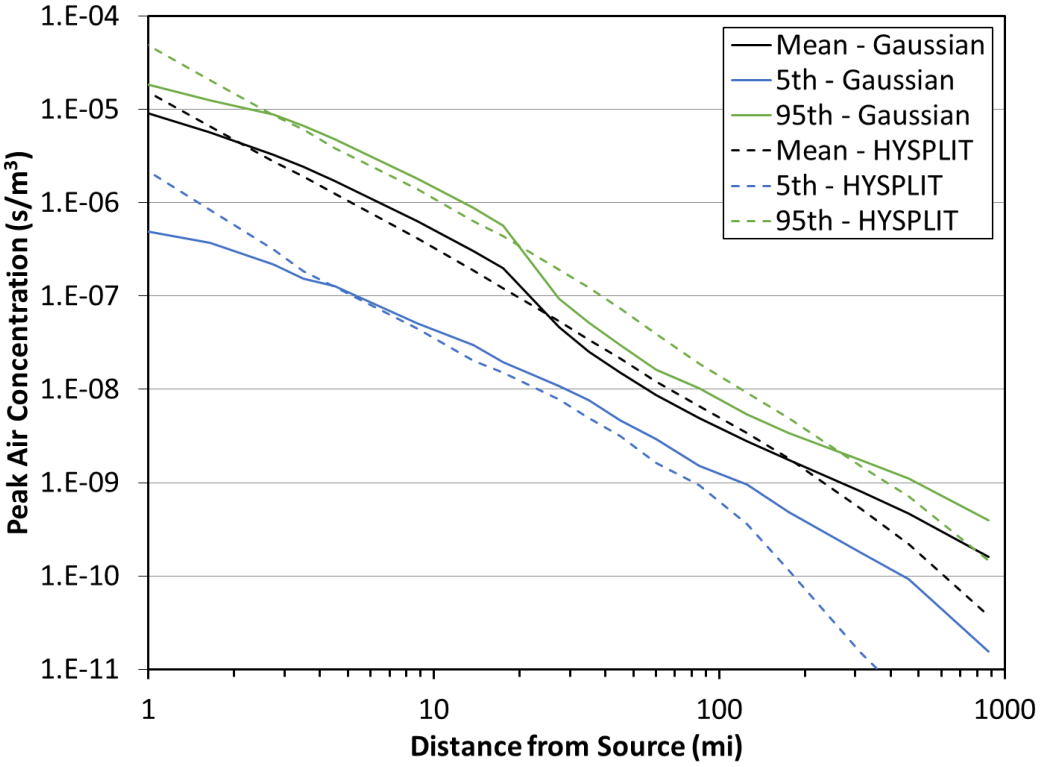

Figure C-1. Original benchmark Site A, ST #1, peak air concentration original comparison

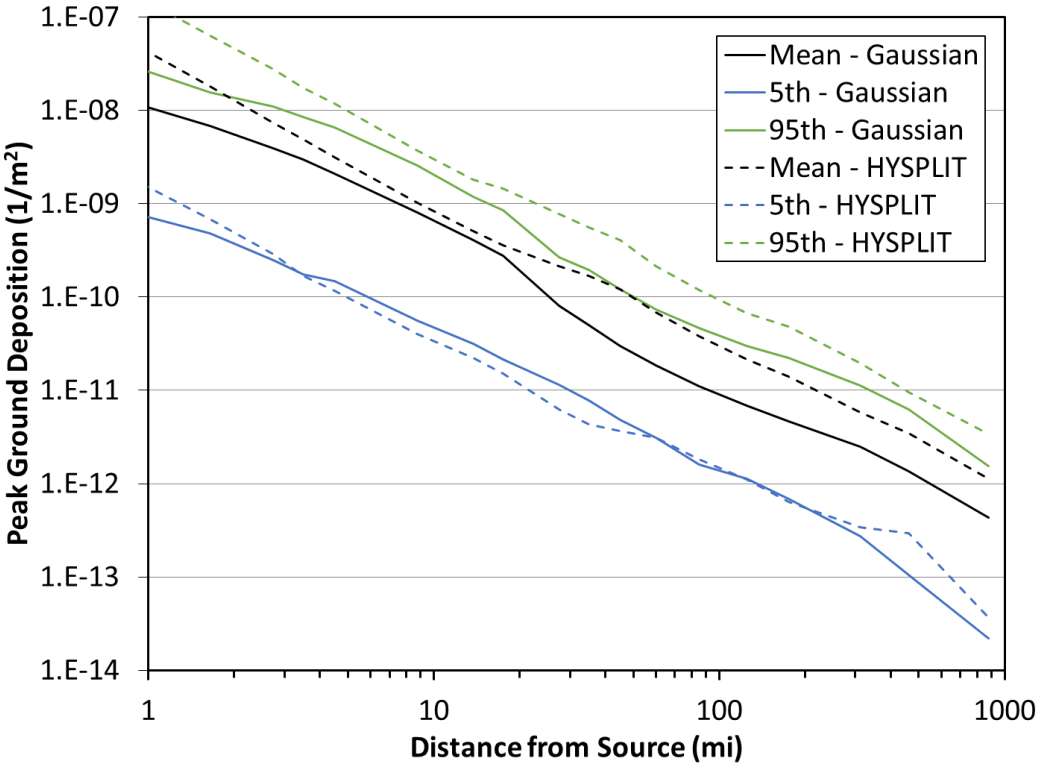

Figure C-2. Original benchmark Site A, ST #1, peak ground deposition original comparison

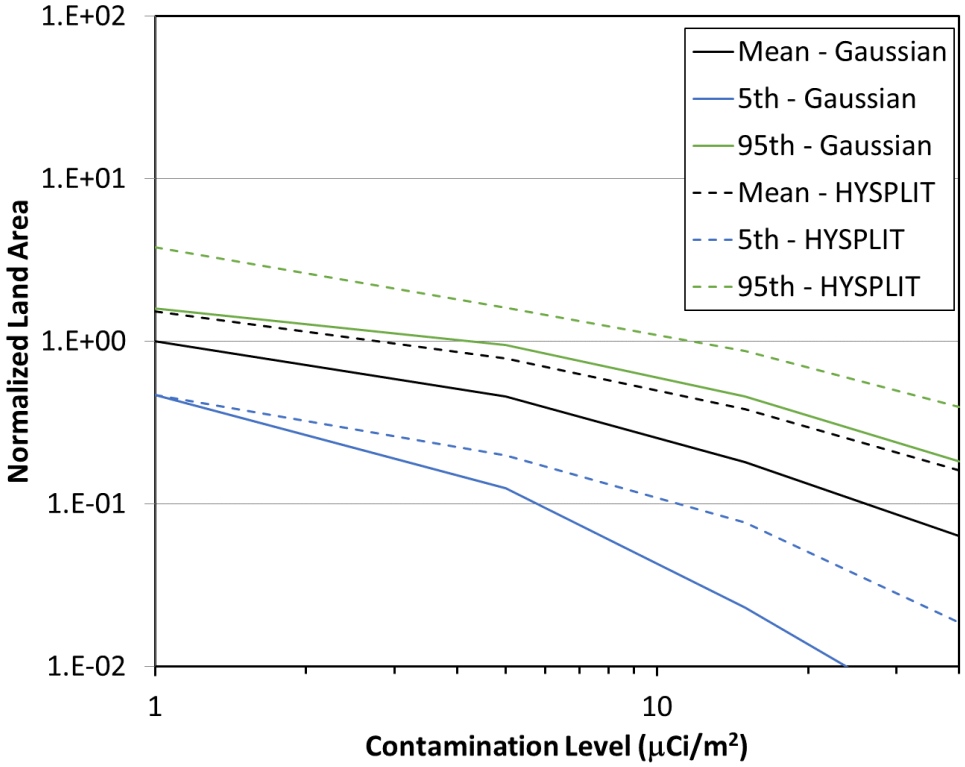

Figure C-3. Original benchmark Site A, ST #1, land contamination area within 805 km (500 mi) original comparison

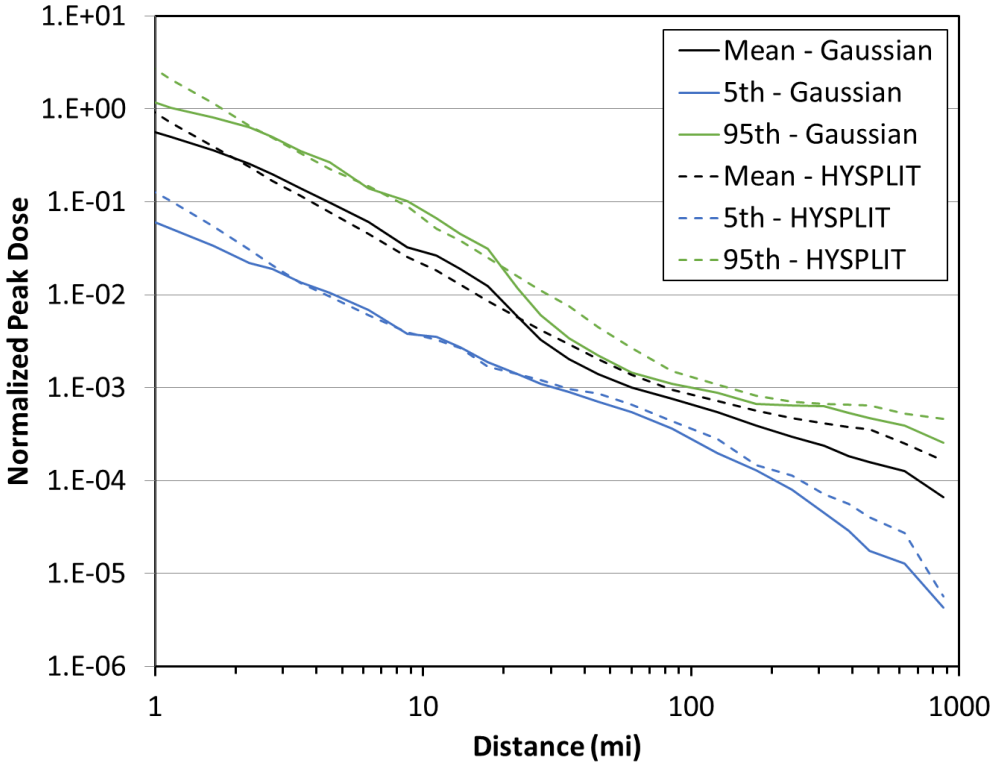

Figure C-4. Original benchmark Site A, ST #1, peak dose original comparison

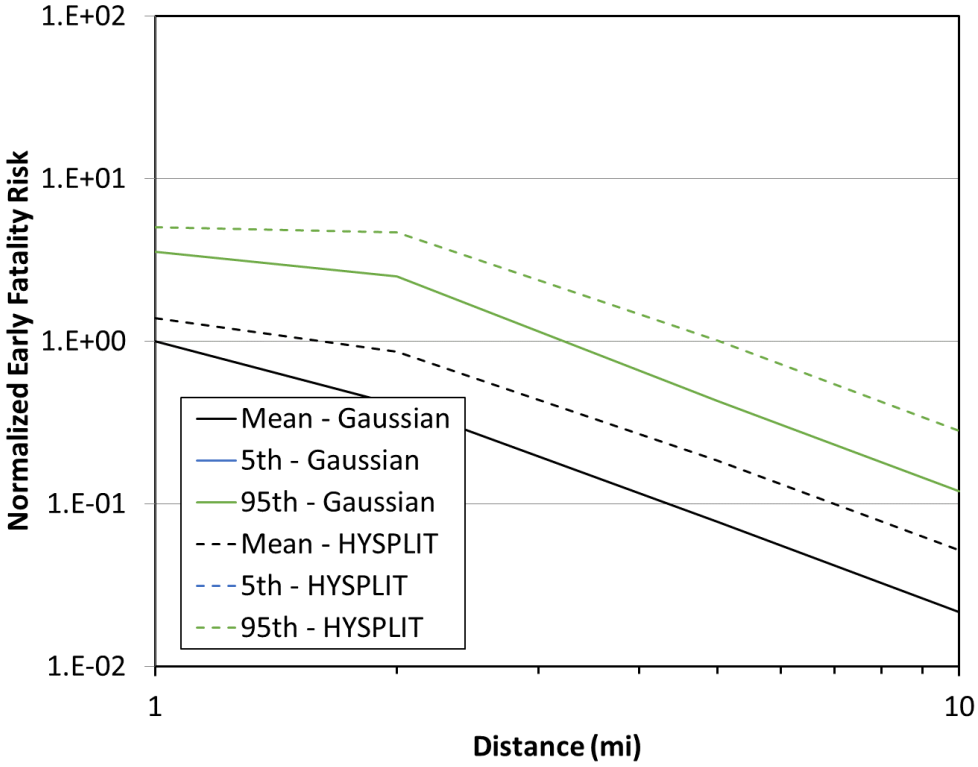

Figure C-5. Original benchmark Site A, ST #1, early fatality risk original comparison

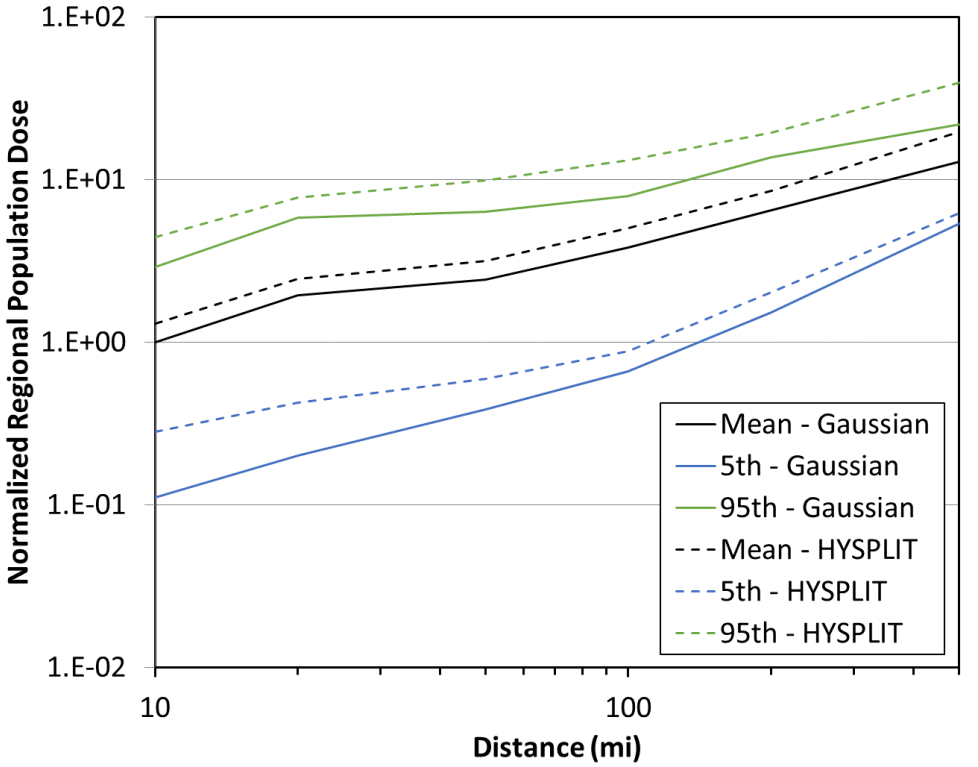

Figure C-6. Original benchmark Site A, ST #1, population dose original comparison

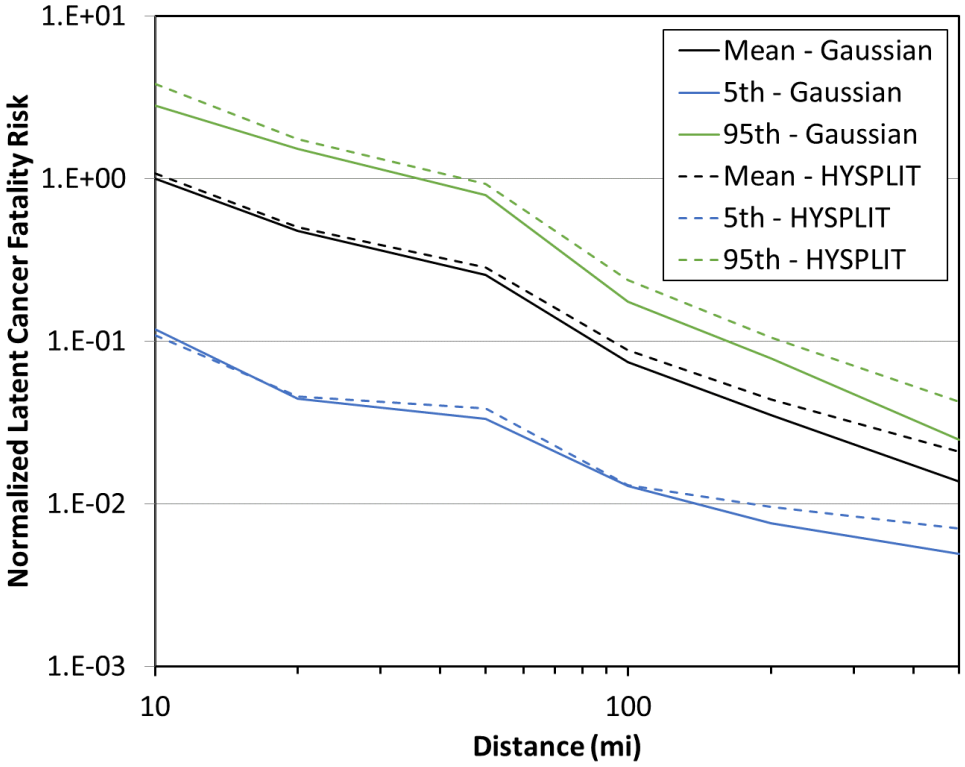

Figure C-7. Original benchmark Site A, ST #1, latent cancer fatality risk original comparison

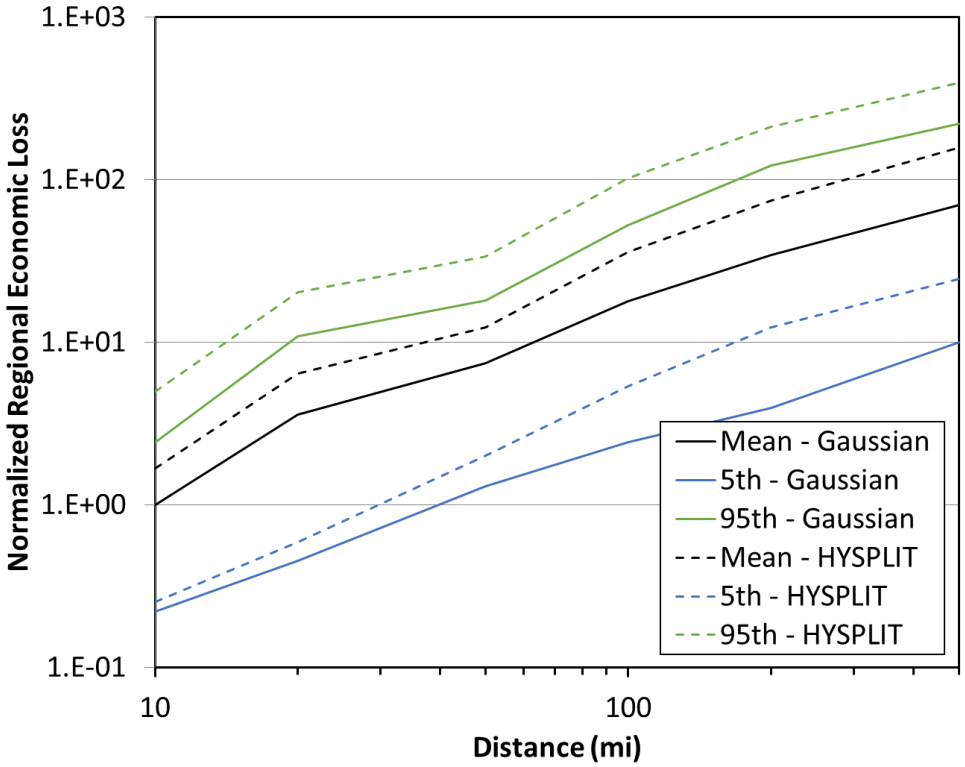

Figure C-8. Original benchmark Site A, ST #1, economic loss original comparison

C.1.2. Source Term #2

The original comparisons between the Gaussian and HYSPLIT ATD model results for Site A, ST #2 for peak air concentration, peak ground deposition, land contamination area, peak dose, early fatality risk, population dose, latent cancer fatality risk, and economic loss (as described in Section 3.6) are shown in Figure C-9 through Figure C-16. The annual statistics for these measures are shown with different colors, where the mean values are in black, the 5th percentile values are shown in blue, and the 95th percentile values are shown in green. HYSPLIT results are shown as dashed lines and Gaussian model results are shown as solid lines. The normalized results are shown as a function of distance, rather than the ratio of Gaussian and HYSPLIT results, to allow for the trends with distance to be observed. Some results are zero for early fatality risk, so they cannot be shown on the log scale used in the figures. In Figure C-13, the single, normalized curve for the HYSPLIT ATD mean early fatality risk represents extremely small (essentially zero) values; the corresponding Gaussian results are zero. Note that the sharp jumps in peak dose in Figure C-12 and some other figures below correspond to evacuation of the population within 10 miles but not beyond. A summary of the difference seen in these figures is provided below in Section C.6.

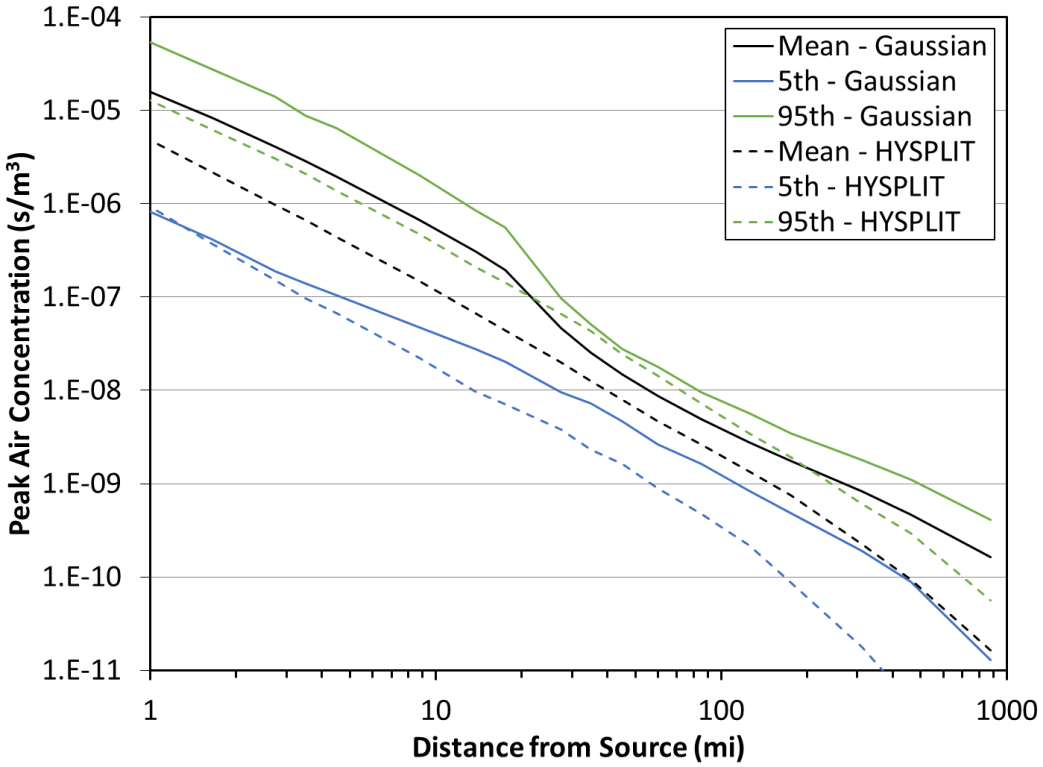

Figure C-9. Original benchmark Site A, ST #2, peak air concentration original comparison

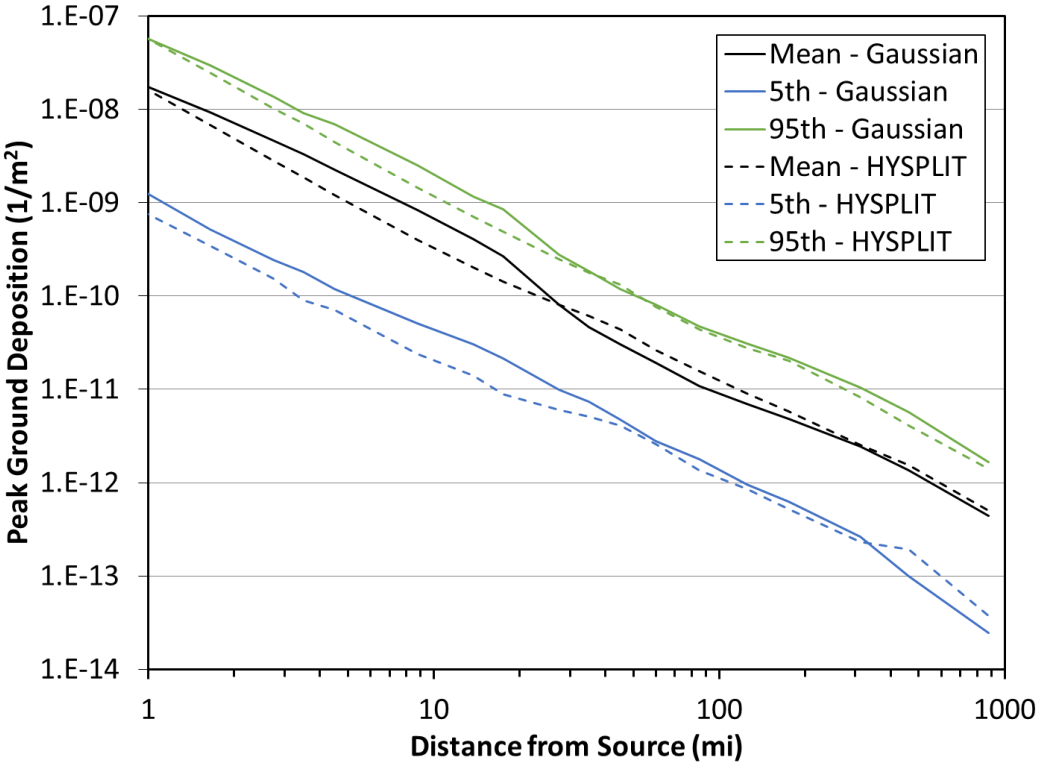

Figure C-10. Original benchmark Site A, ST #2, peak ground deposition original comparison

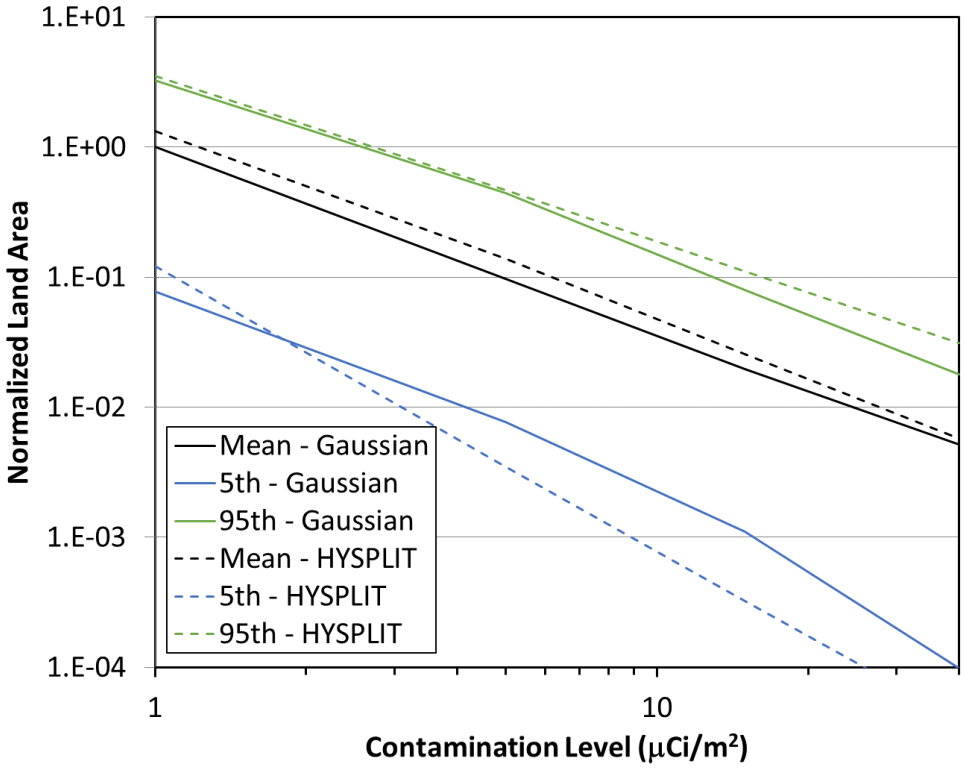

Figure C-11. Original benchmark Site A, ST #2, land contamination area within 805 km (500 mi) original comparison

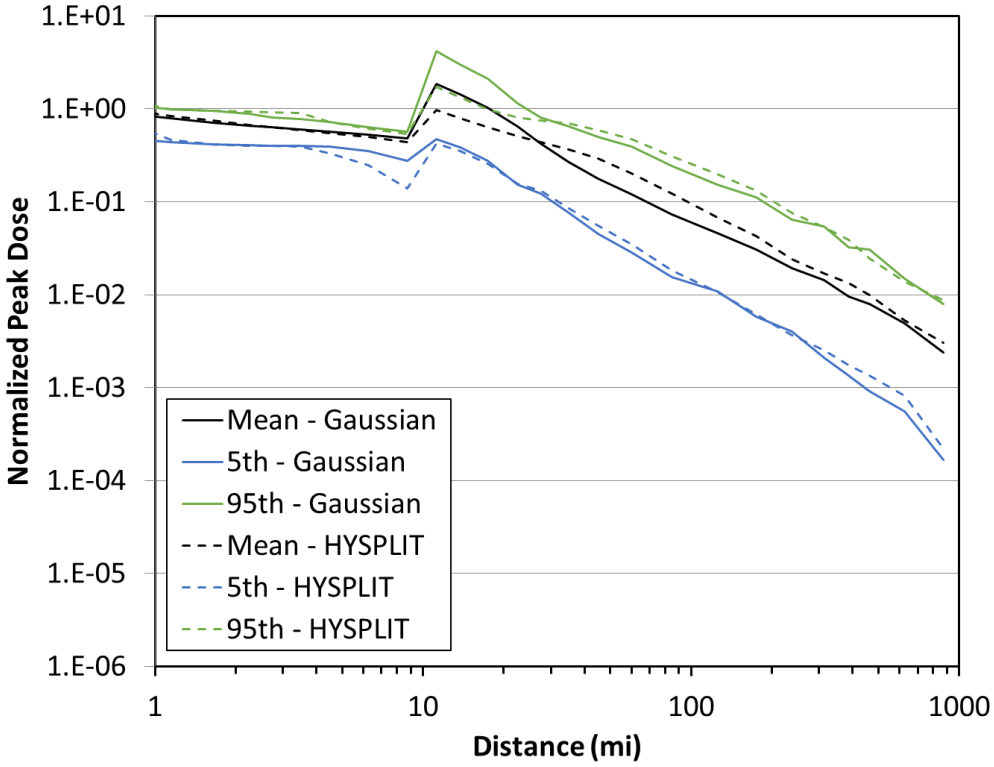

Figure C-12. Original benchmark Site A, ST #2, peak dose original comparison

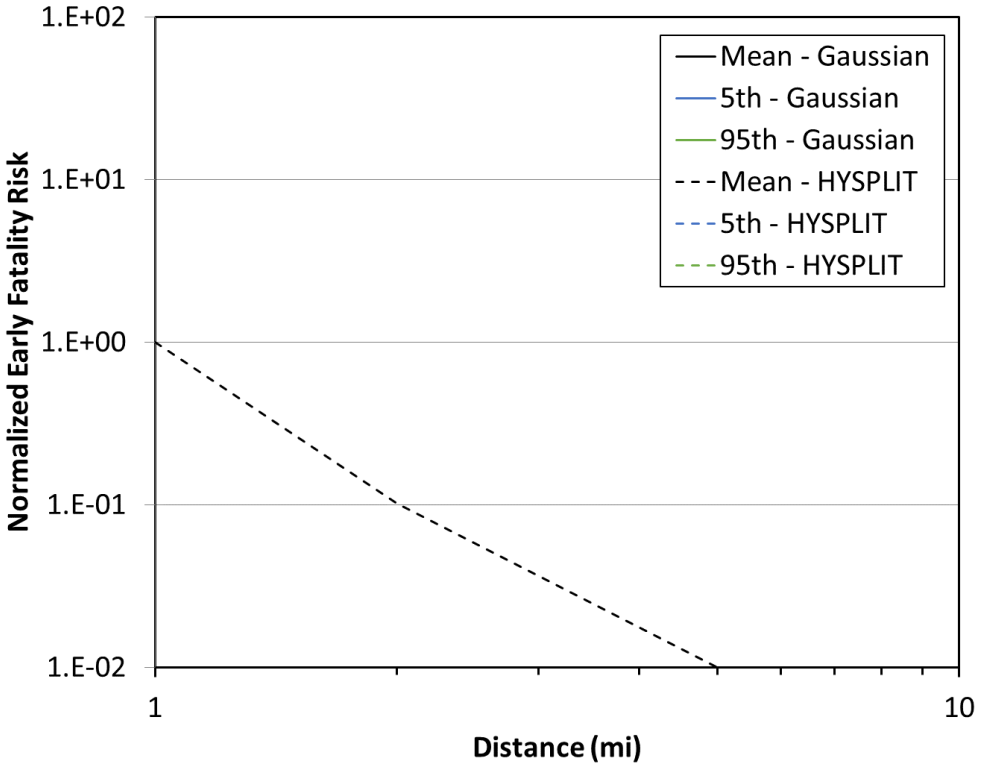

Figure C-13. Original benchmark Site A, ST #2, early fatality risk original comparison

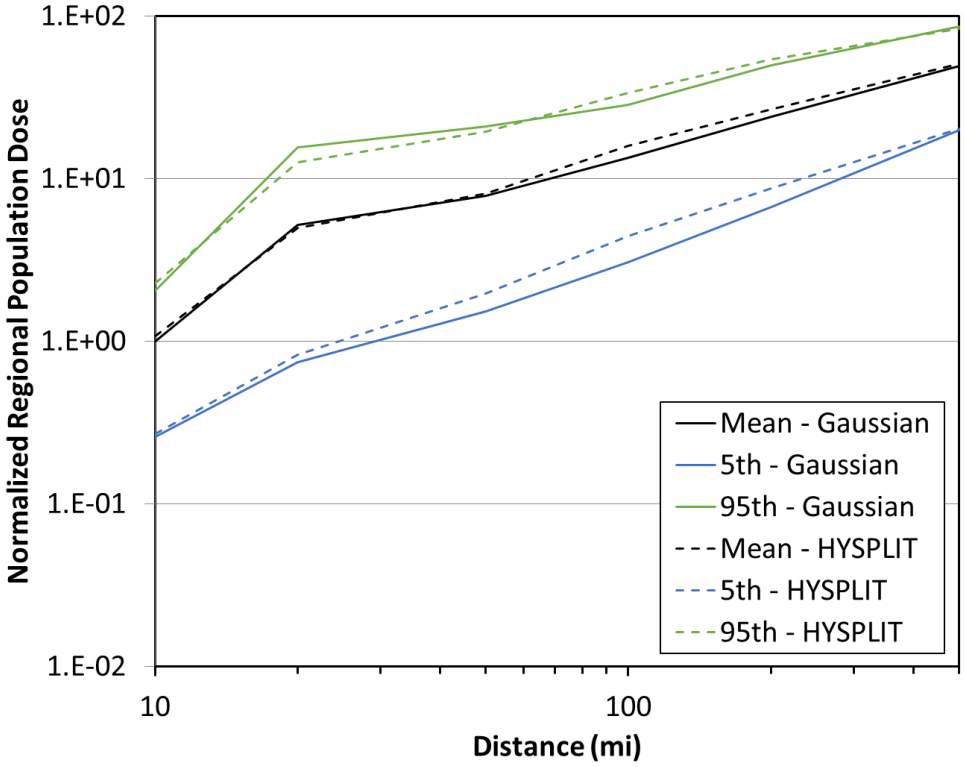

Figure C-14. Original benchmark Site A, ST #2, population dose original comparison

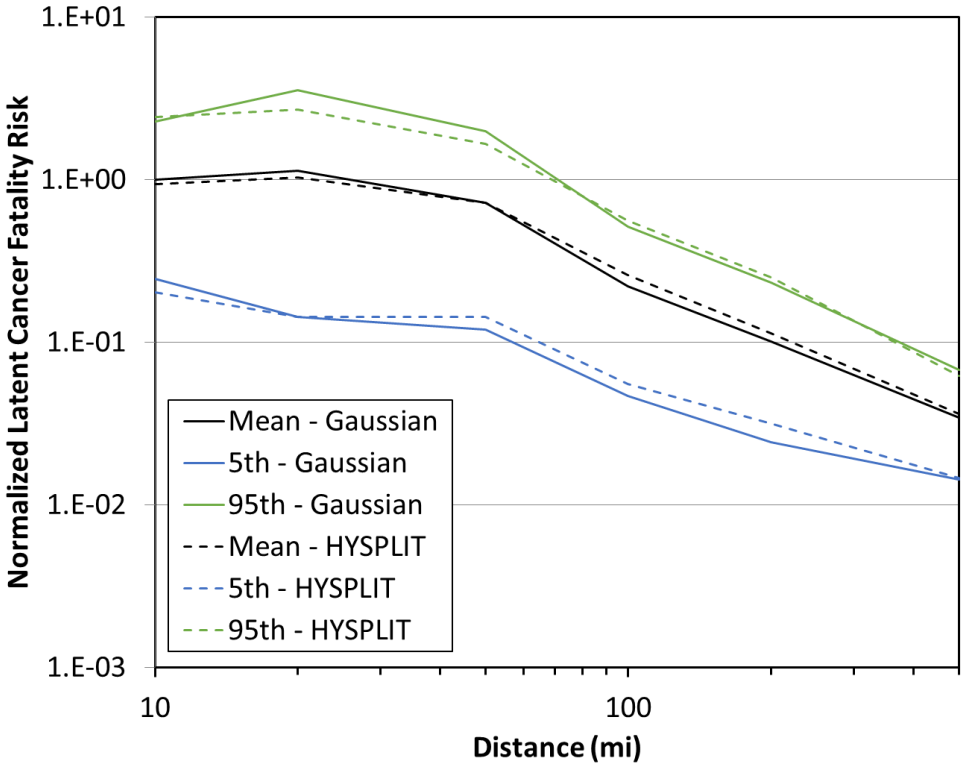

Figure C-15. Original benchmark Site A, ST #2, latent cancer fatality risk original comparison

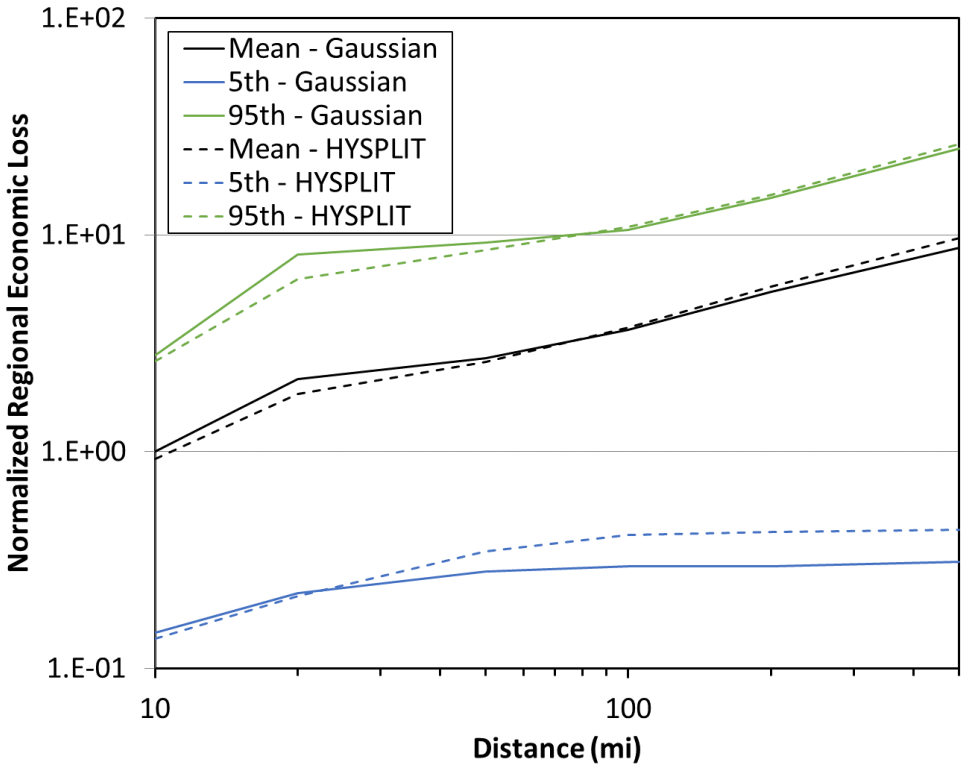

Figure C-16. Original benchmark Site A, ST #2, economic loss original comparison

C.2. Site B

C.2.1. Source Term #1

The original comparisons between the Gaussian and HYSPLIT ATD model results for Site B, ST #1 for peak air concentration, peak ground deposition, land contamination area, peak dose, early fatality risk, population dose, latent cancer fatality risk, and economic loss (as described in Section 3.6) are shown in Figure C-17 through Figure C-24. The annual statistics for these measures are shown with different colors, where the mean values are in black, the 5th percentile values are shown in blue, and the 95th percentile values are shown in green. HYSPLIT results are shown as dashed lines and Gaussian model results are shown as solid lines. The normalized results are shown as a function of distance, rather than the ratio of Gaussian and HYSPLIT results, to allow for the trends with distance to be observed. Some results are zero for early fatality risk, so they cannot be shown on the log scale used in the figures. For Site B, there are no individuals within two miles of the site, which results in a calculated zero fatality risk. A summary of the difference seen in these figures is provided below in Section C.6.

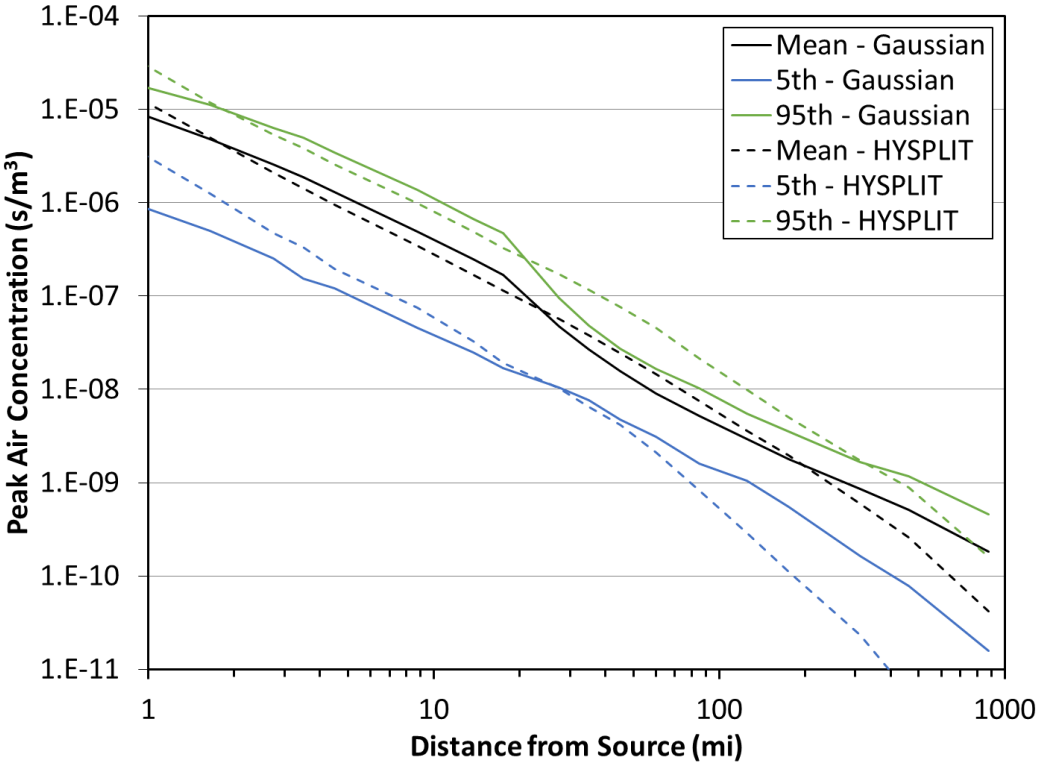

Figure C-17. Original benchmark Site B, ST #1, peak air concentration original comparison

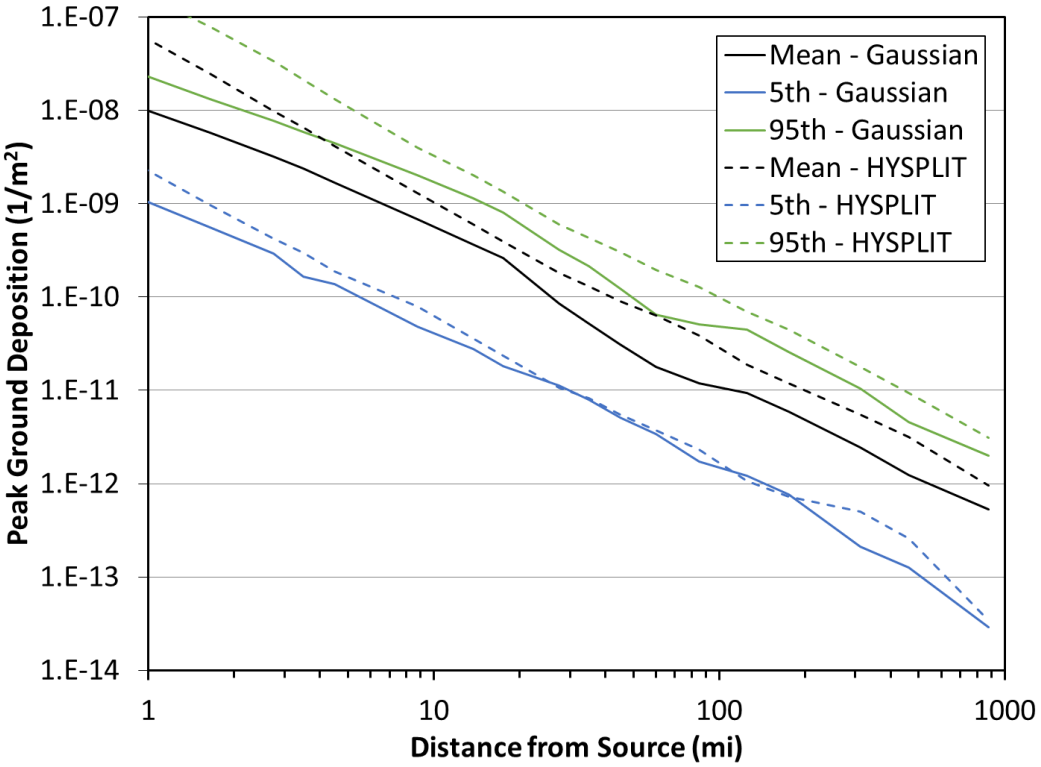

Figure C-18. Original benchmark Site B, ST #1, peak ground deposition original comparison

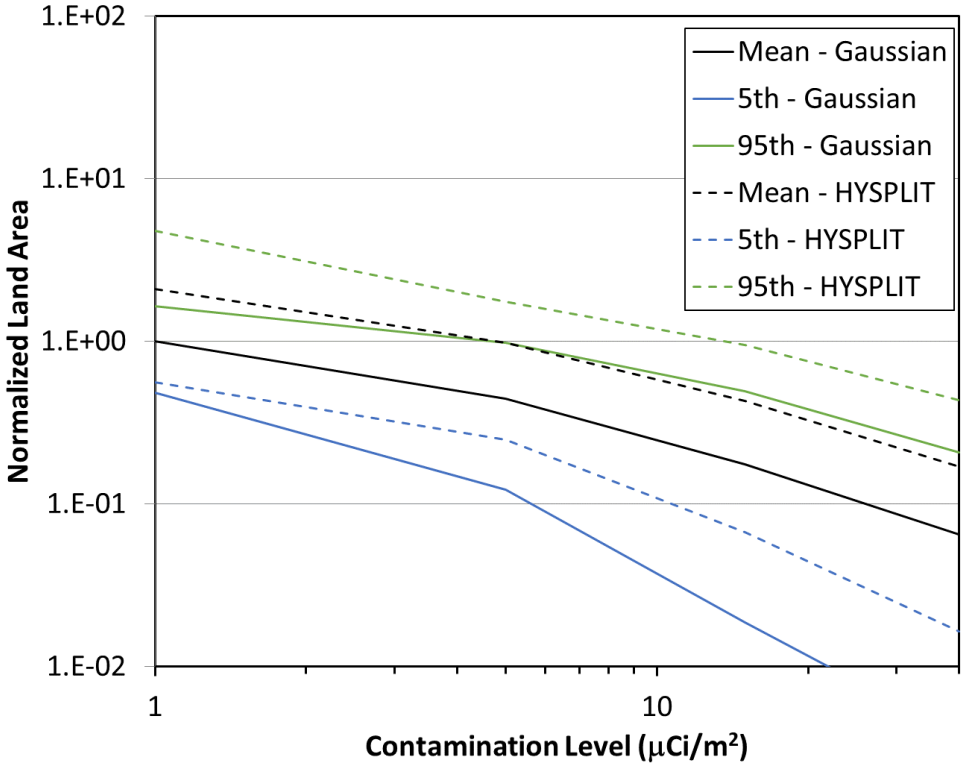

Figure C-19. Original benchmark Site B, ST #1, land contamination area within 805 km (500 mi) original comparison

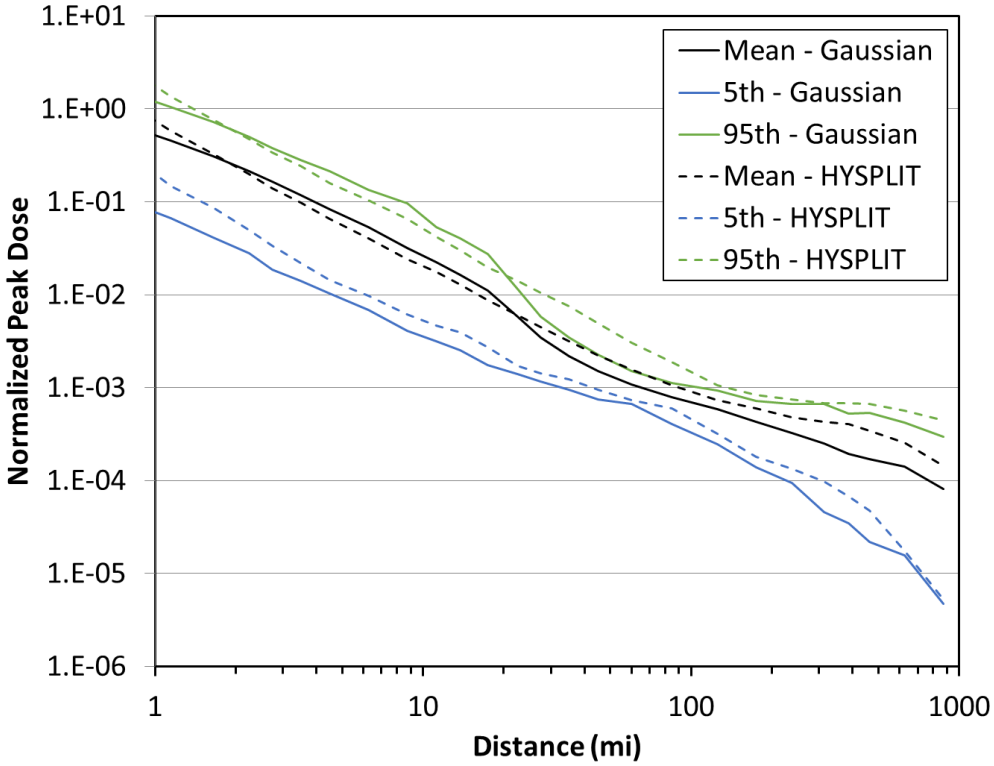

Figure C-20. Original benchmark Site B, ST #1, peak dose original comparison

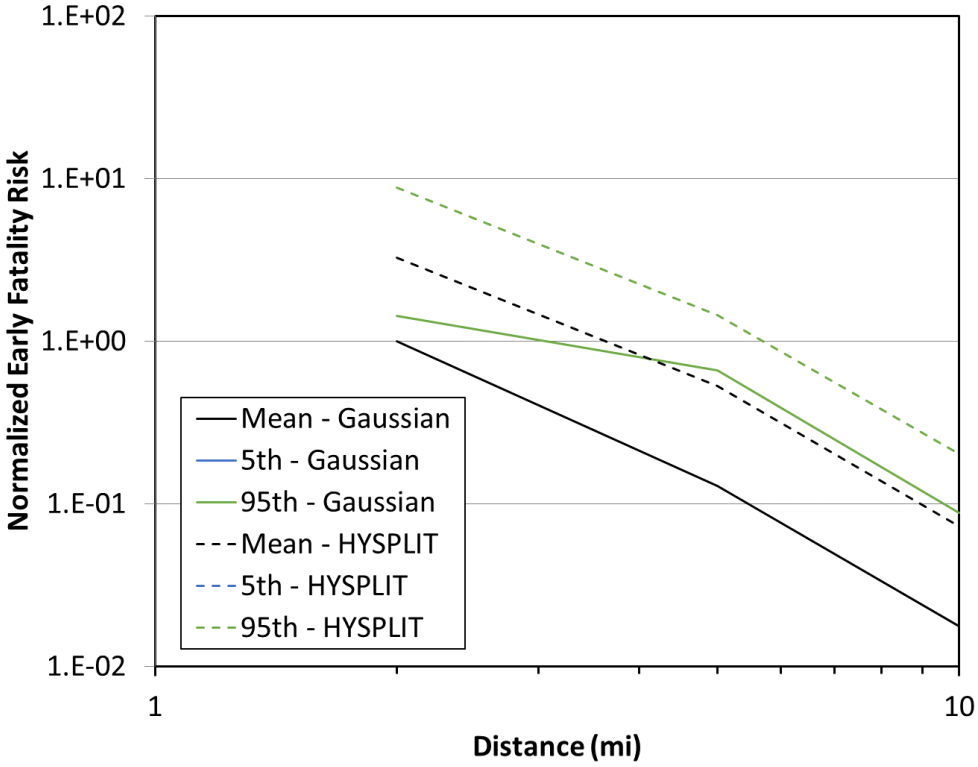

Figure C-21. Original benchmark Site B, ST #1, early fatality risk original comparison

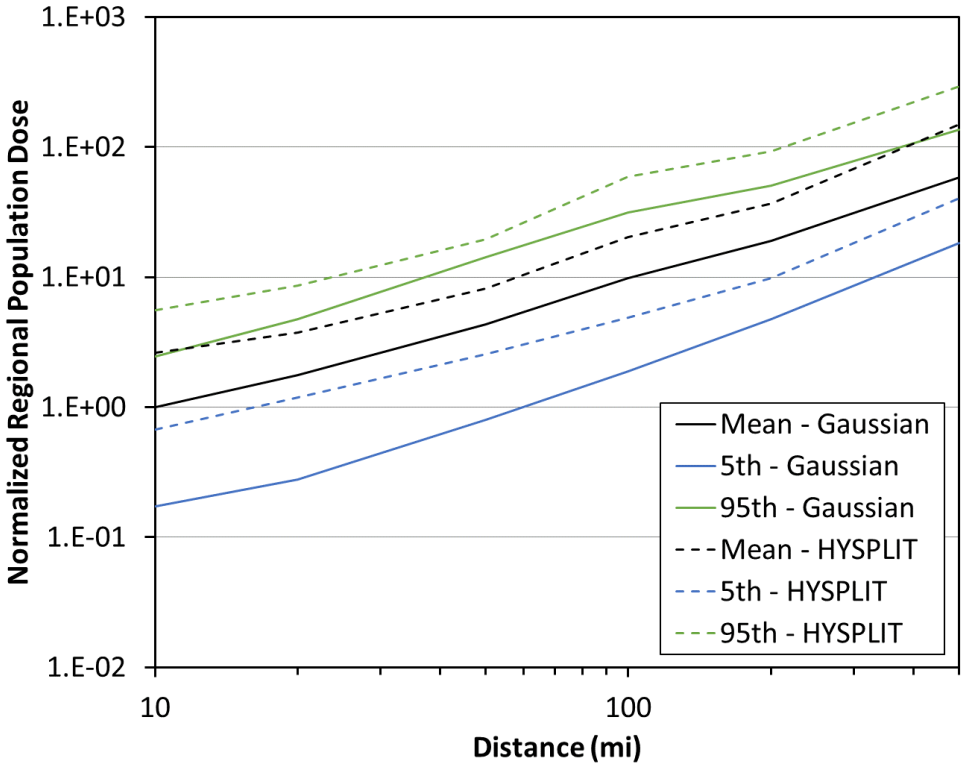

Figure C-22. Original benchmark Site B, ST #1, population dose original comparison

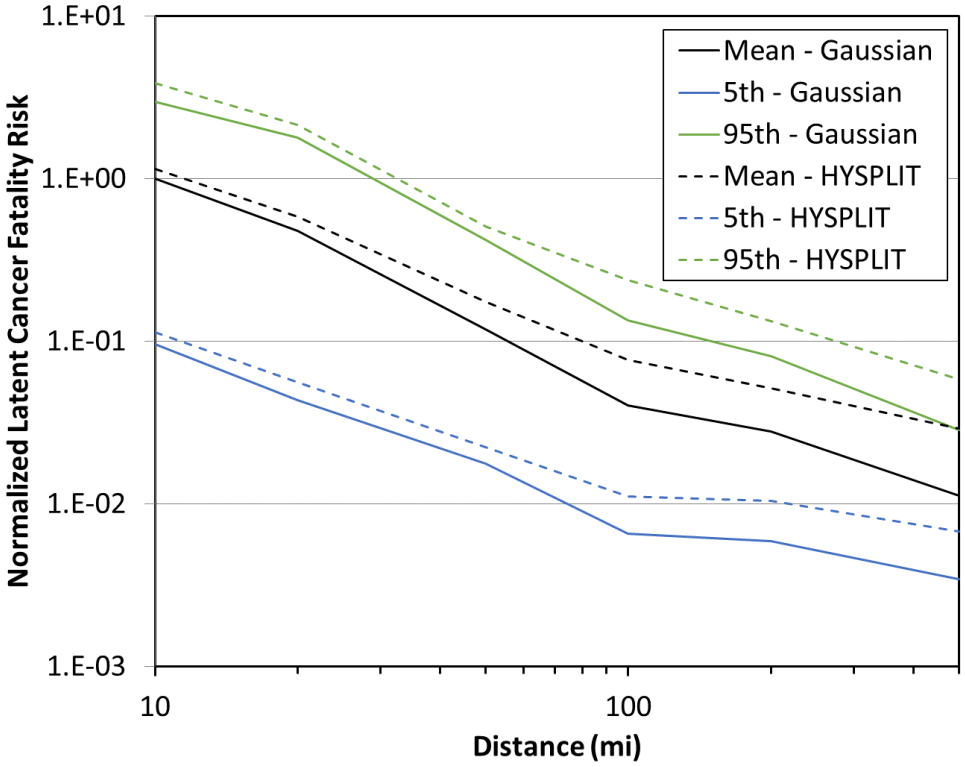

Figure C-23. Original benchmark Site B, ST #1, latent cancer fatality risk original comparison

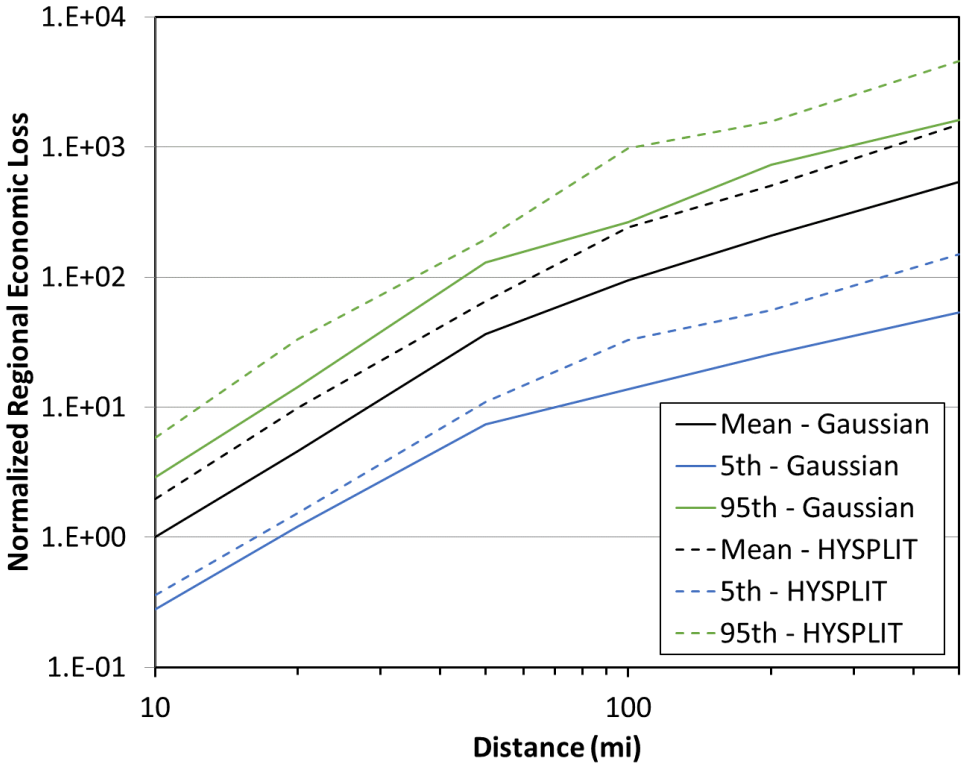

Figure C-24. Original benchmark Site B, ST #1, economic loss original comparison

C.2.2. Source Term #2

The original comparisons between the Gaussian and HYSPLIT ATD model results for Site B, ST #2 for peak air concentration, peak ground deposition, land contamination area, peak dose, early fatality risk, population dose, latent cancer fatality risk, and economic loss (as described in Section 3.6) are shown in Figure C-25 through Figure C-32. The annual statistics for these measures are shown with different colors, where the mean values are in black, the 5th percentile values are shown in blue, and the 95th percentile values are shown in green. HYSPLIT results are shown as dashed lines and Gaussian model results are shown as solid lines. The normalized results are shown as a function of distance, rather than the ratio of Gaussian and HYSPLIT results, to allow for the trends with distance to be observed. Some results are zero for early fatality risk, so they cannot be shown on the log scale used in the figures. A summary of the difference seen in these figures is provided below in Section C.6.

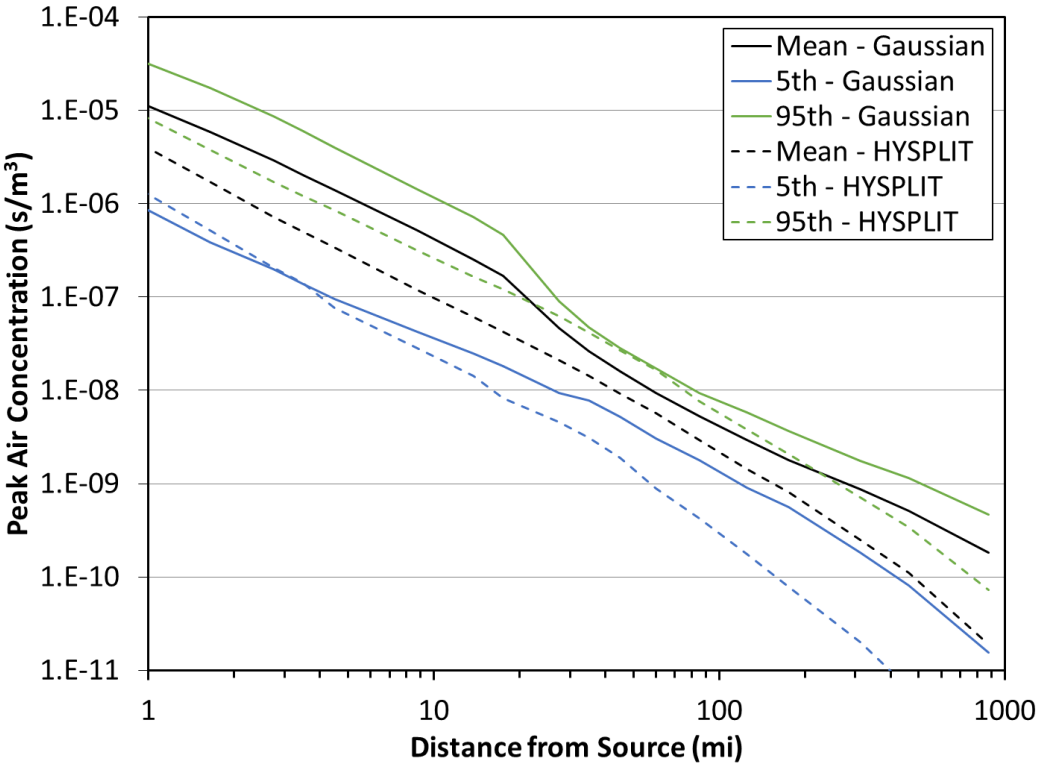

Figure C-25. Original benchmark Site B, ST #2, peak air concentration original comparison

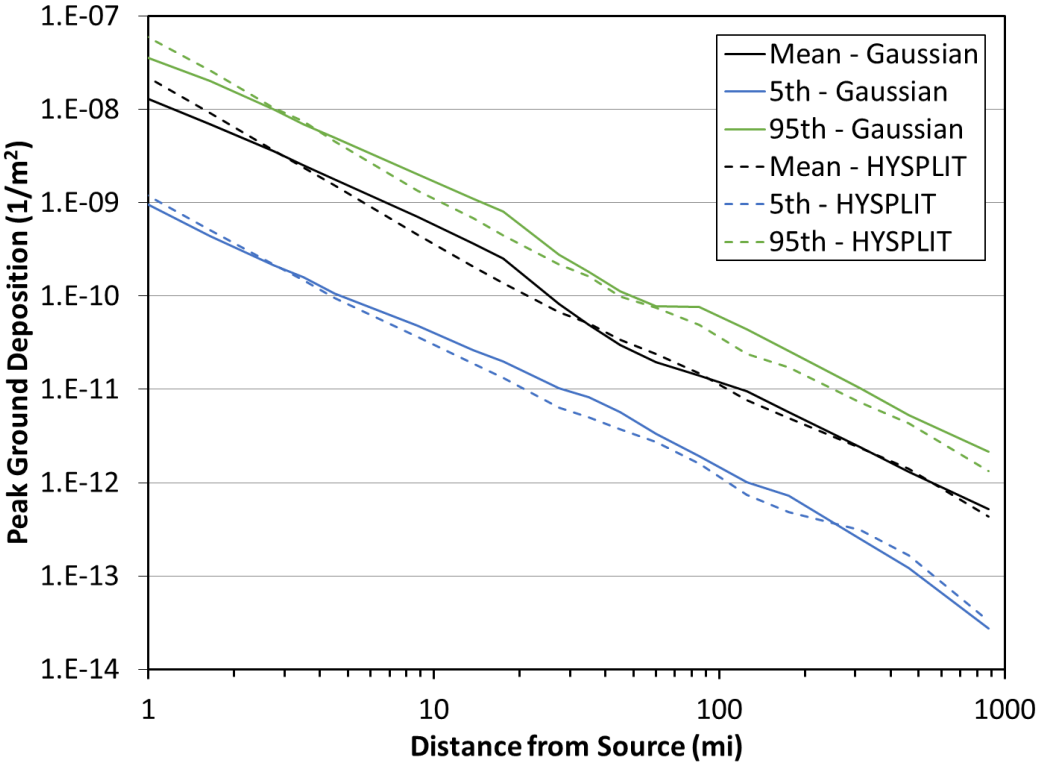

Figure C-26. Original benchmark Site B, ST #2, peak ground deposition original comparison

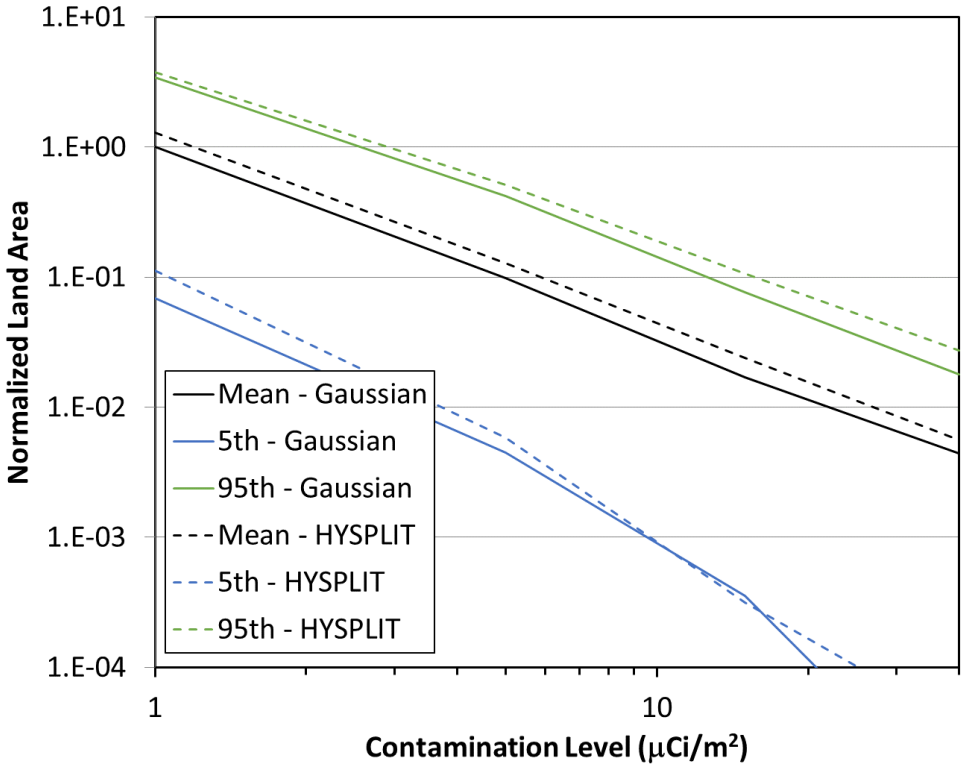

Figure C-27. Original benchmark Site B, ST #2, land contamination area within 805 km (500 mi) original comparison

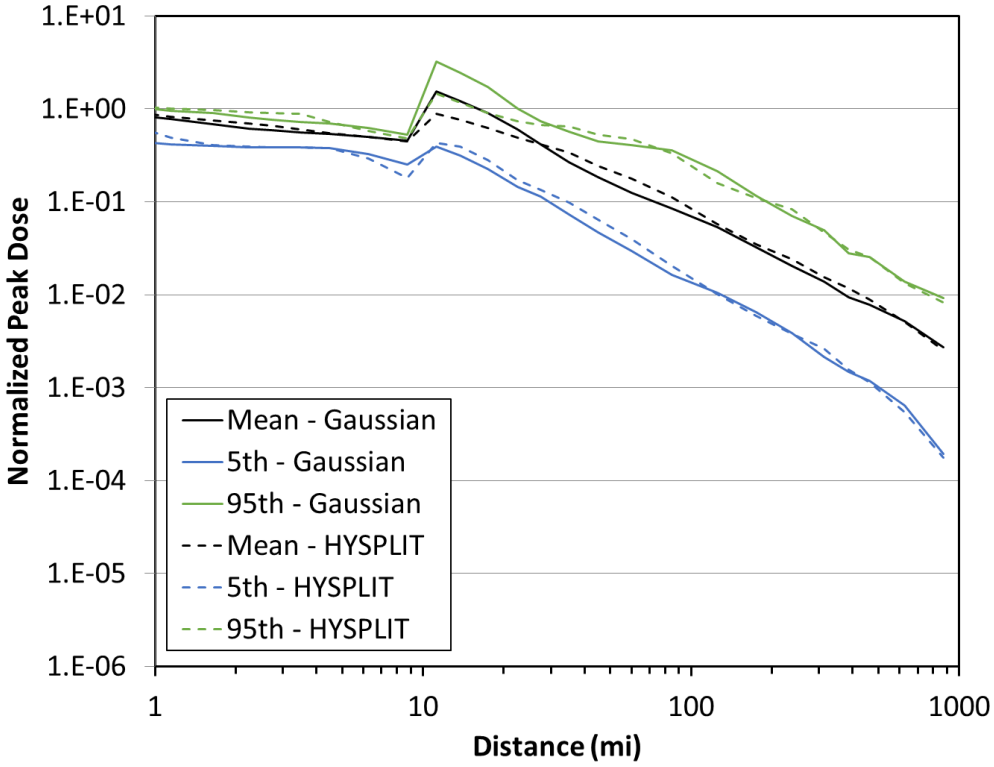

Figure C-28. Original benchmark Site B, ST #2, peak dose original comparison

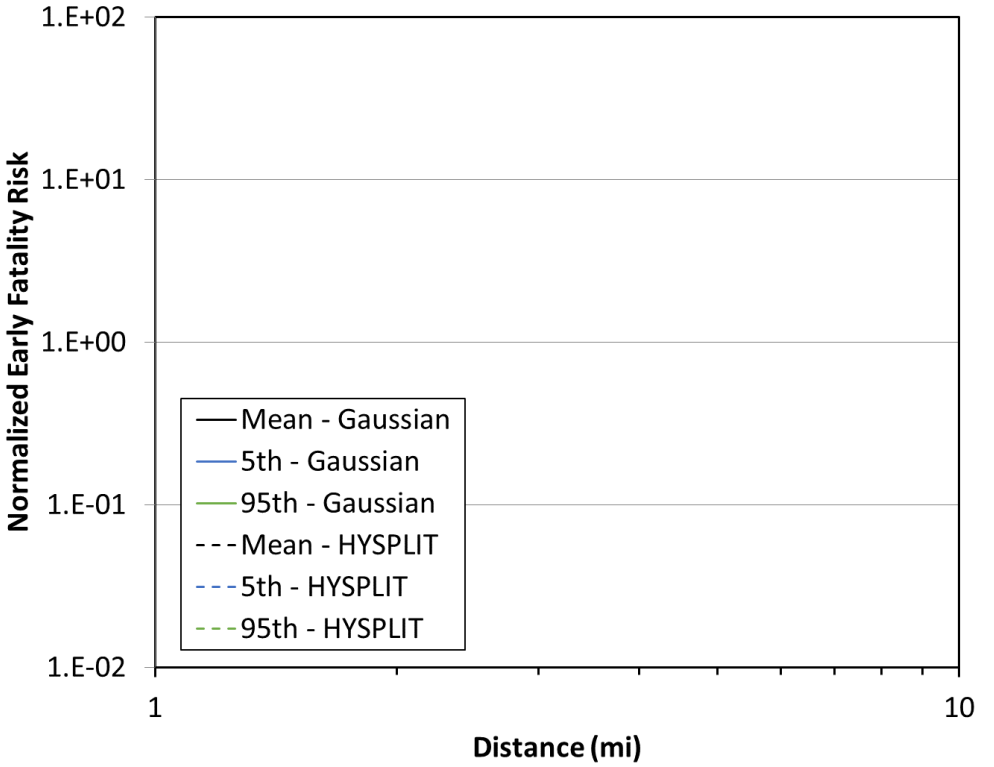

Figure C-29. Original benchmark Site B, ST #2, early fatality original comparison

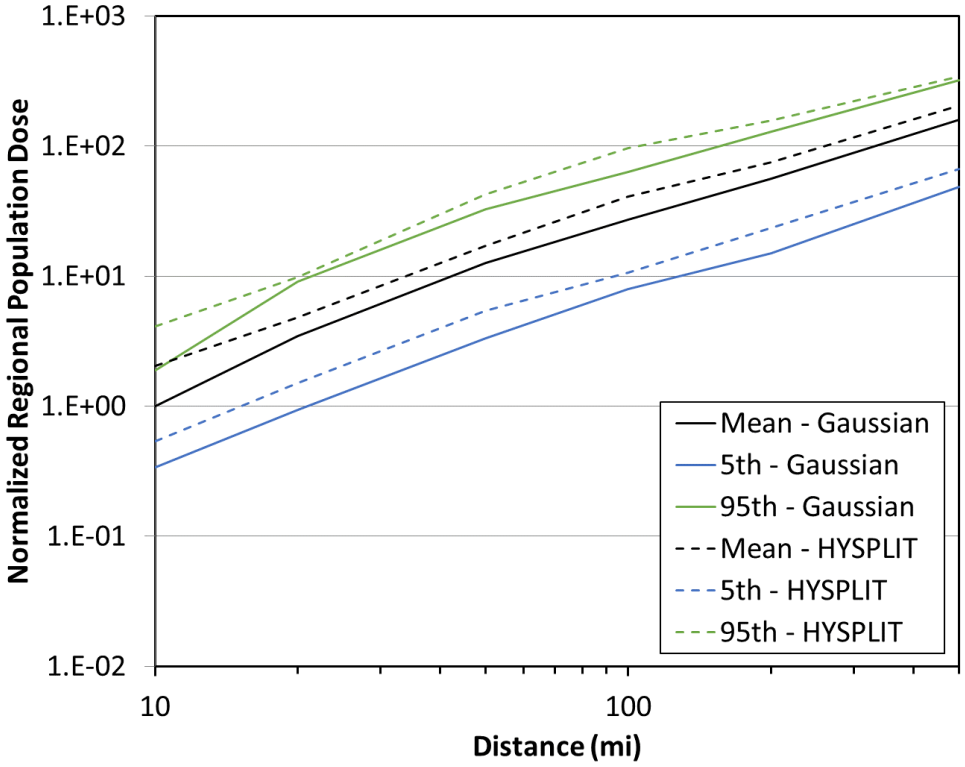

Figure C-30. Original benchmark Site B, ST #2, population dose original comparison

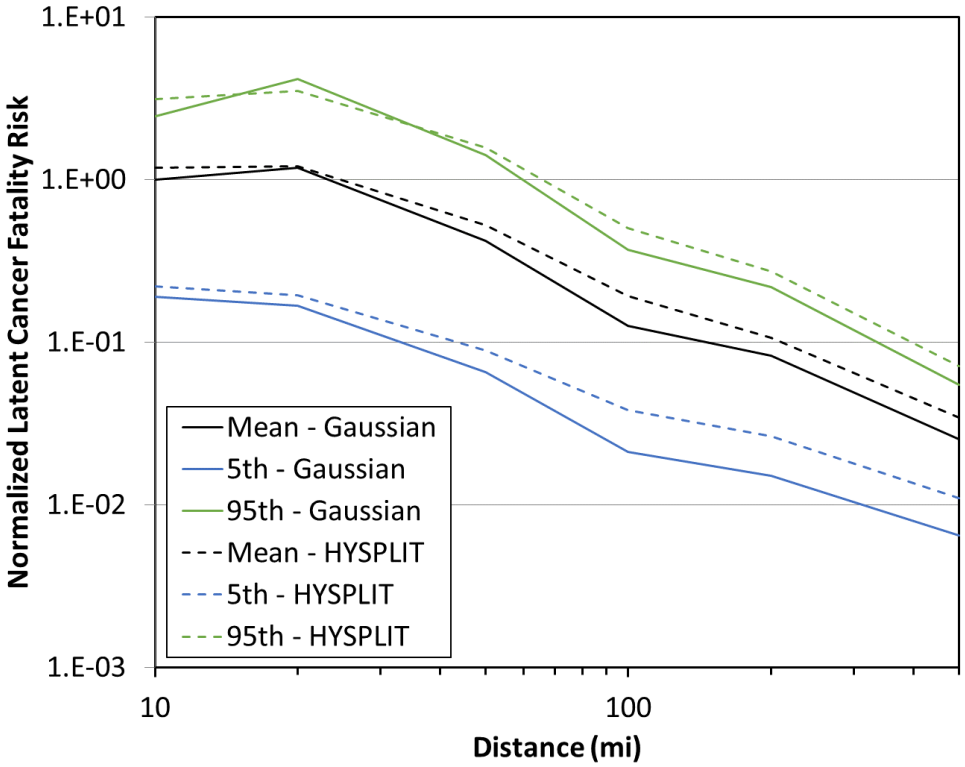

Figure C-31. Original benchmark Site B, ST #2, latent cancer fatality risk original comparison

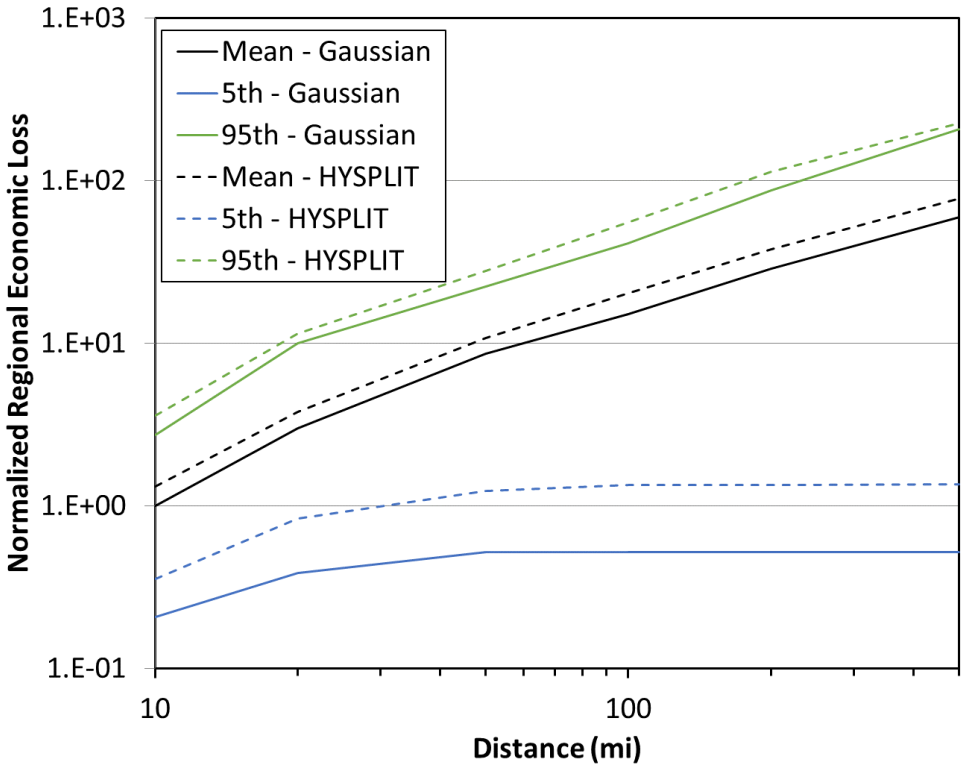

Figure C-32. Original benchmark Site B, ST #2, economic loss original comparison

C.3. Site C

C.3.1. Source Term #1

The original comparisons between the Gaussian and HYSPLIT ATD model results for Site C, ST #1 for peak air concentration, peak ground deposition, land contamination area, peak dose, early fatality risk, population dose, latent cancer fatality risk, and economic loss (as described in Section 3.6) are shown in Figure C-33 through Figure C-40. The annual statistics for these measures are shown with different colors, where the mean values are in black, the 5th percentile values are shown in blue, and the 95th percentile values are shown in green. HYSPLIT results are shown as dashed lines and Gaussian model results are shown as solid lines. The normalized results are shown as a function of distance, rather than the ratio of Gaussian and HYSPLIT results, to allow for the trends with distance to be observed. Some results are zero for early and latent cancer fatality risk, so they cannot be shown on the log scale used in the figures. A summary of the difference seen in these figures is provided below in Section C.6.

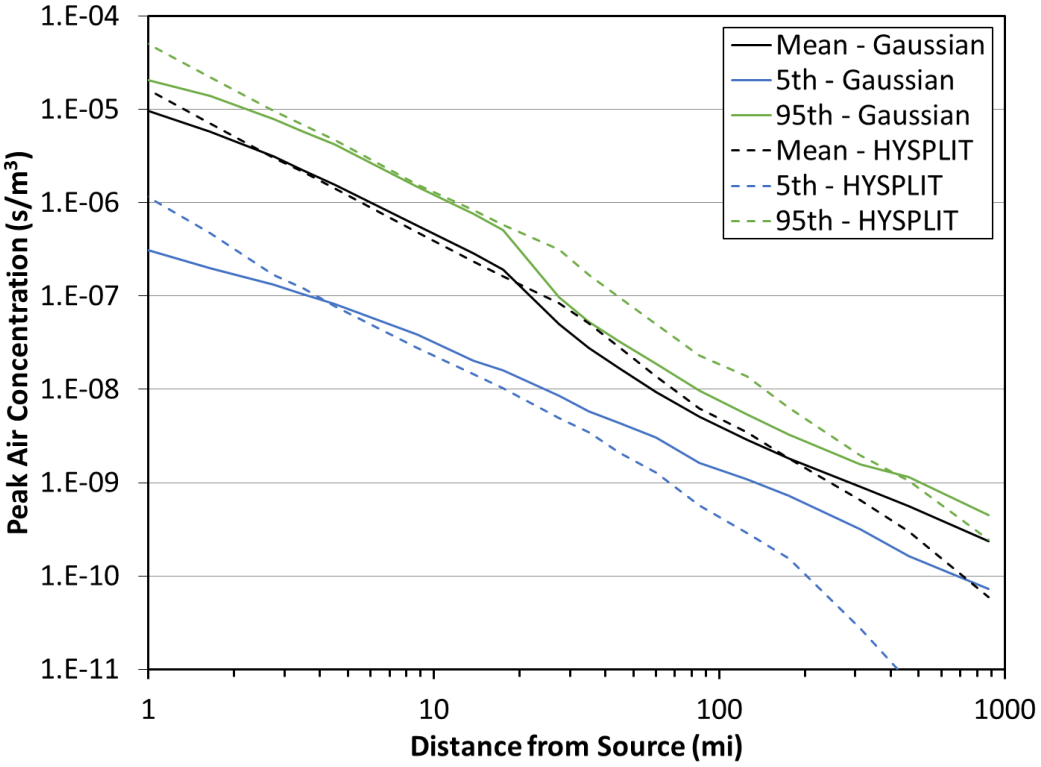

Figure C-33. Original benchmark Site C, ST #1, peak air concentration original comparison

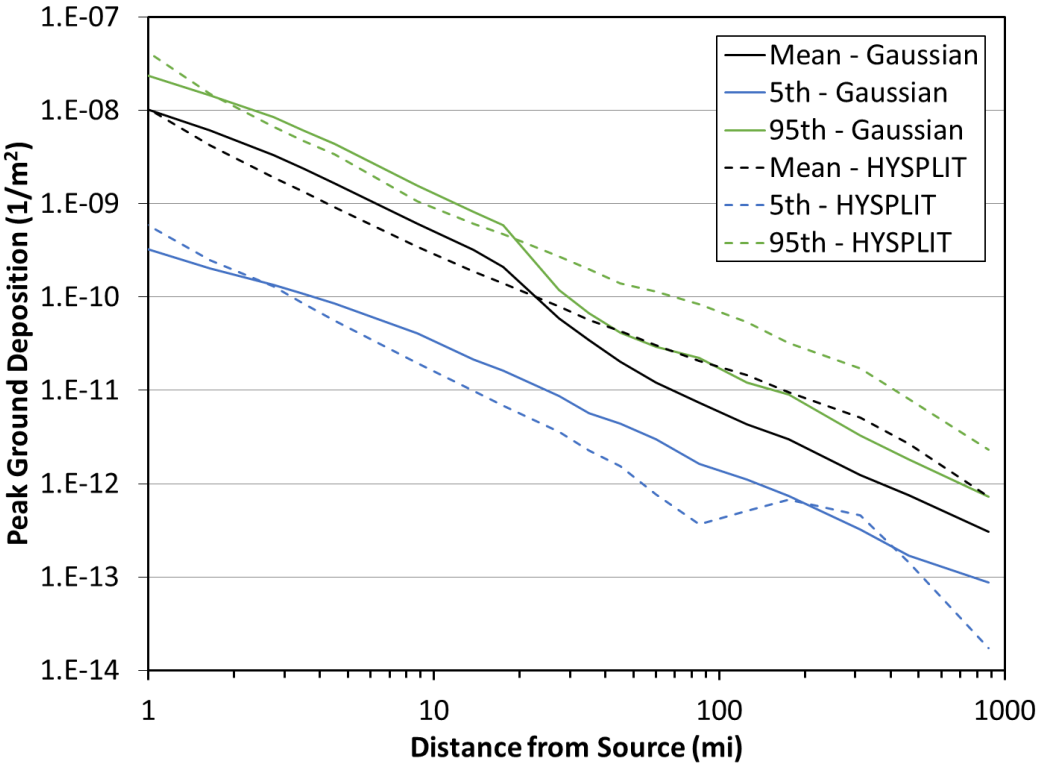

Figure C-34. Original benchmark Site C, ST #1, peak ground deposition original comparison

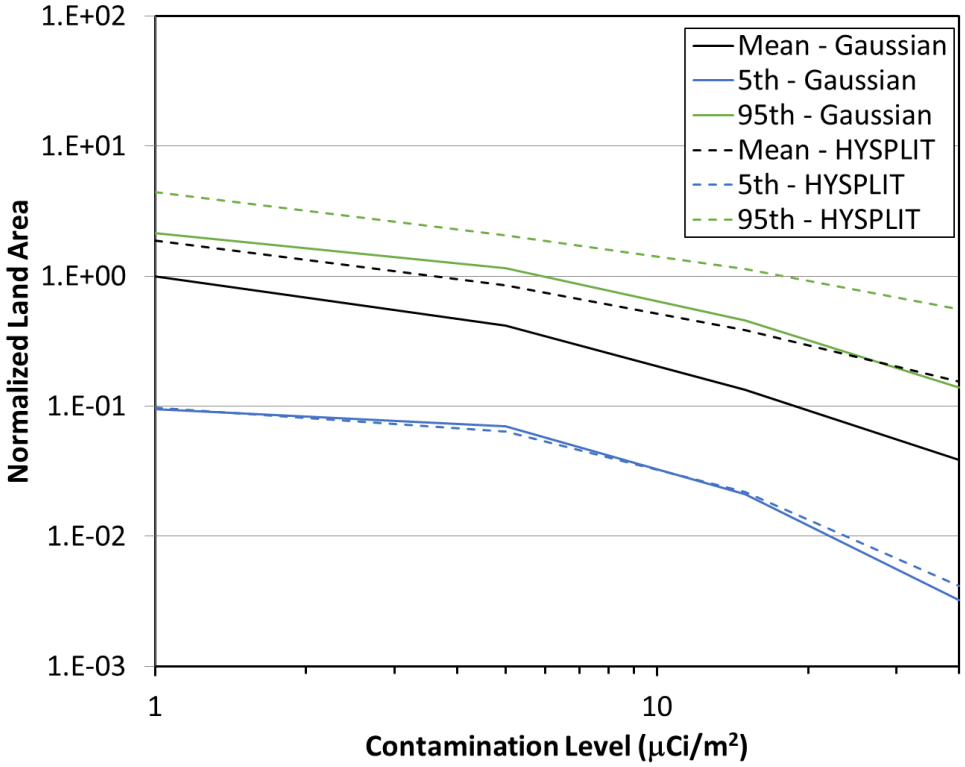

Figure C-35. Original benchmark Site C, ST #1, land contamination area within 805 km (500 mi) original comparison

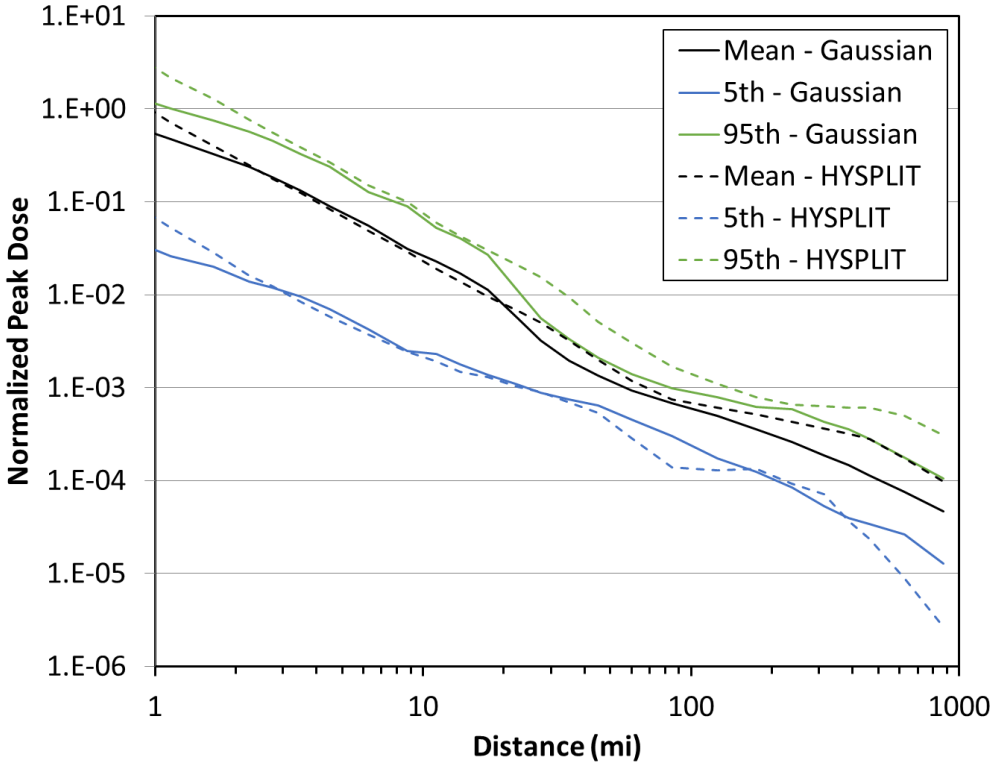

Figure C-36. Original benchmark Site C, ST #1, peak dose original comparison

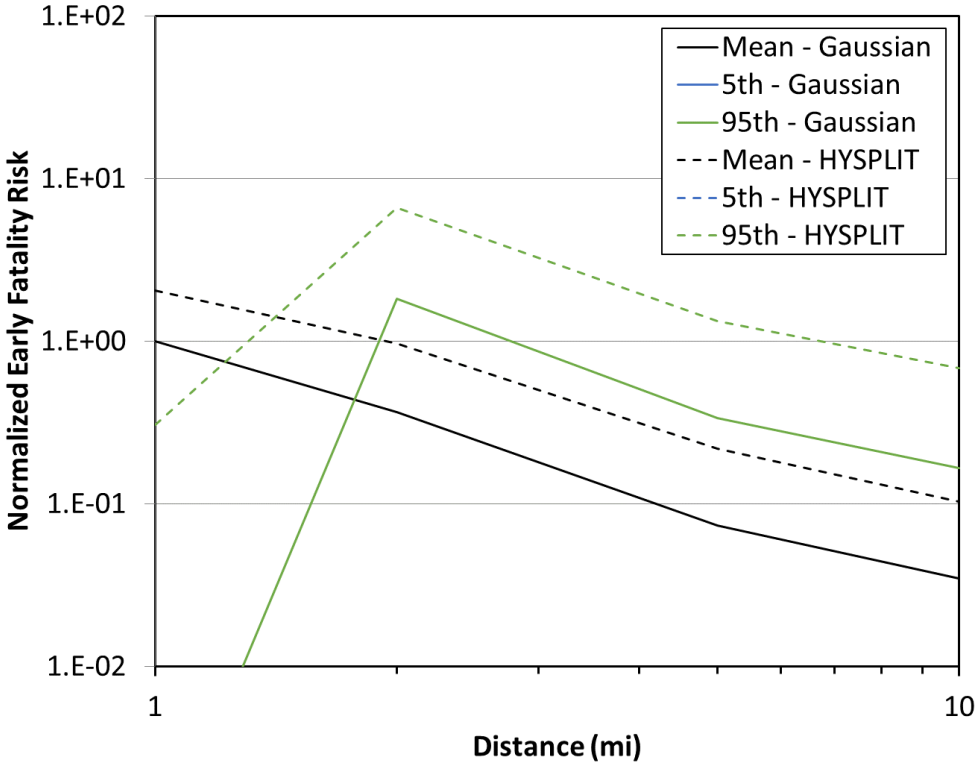

Figure C-37. Original benchmark Site C, ST #1, early fatality original comparison

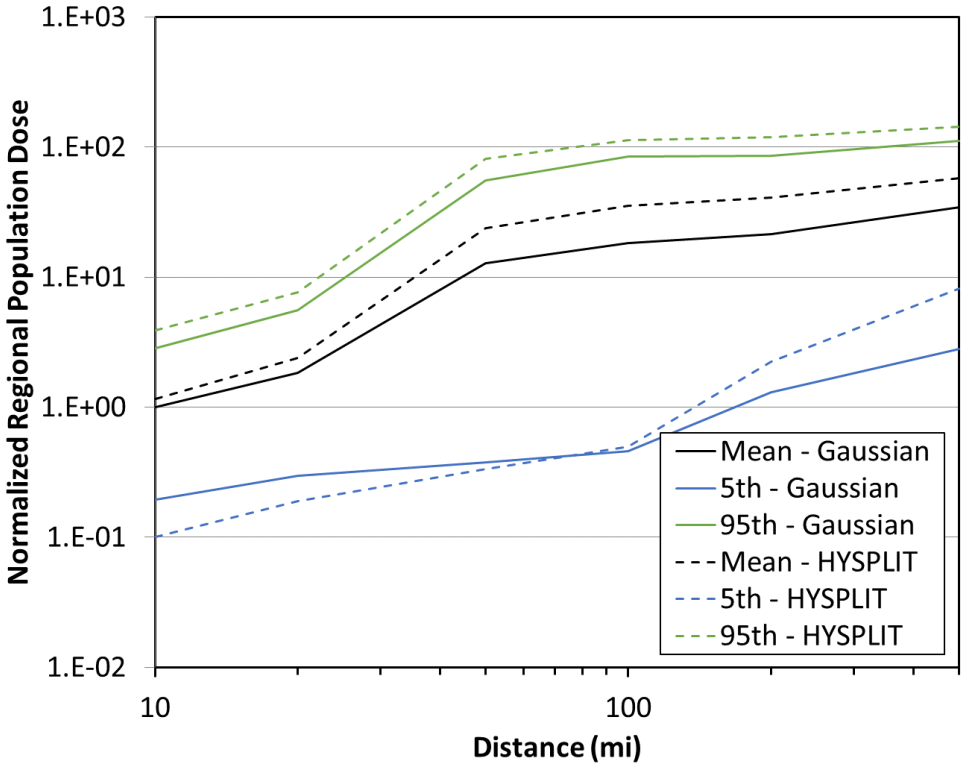

Figure C-38. Original benchmark Site C, ST #1, population dose original comparison

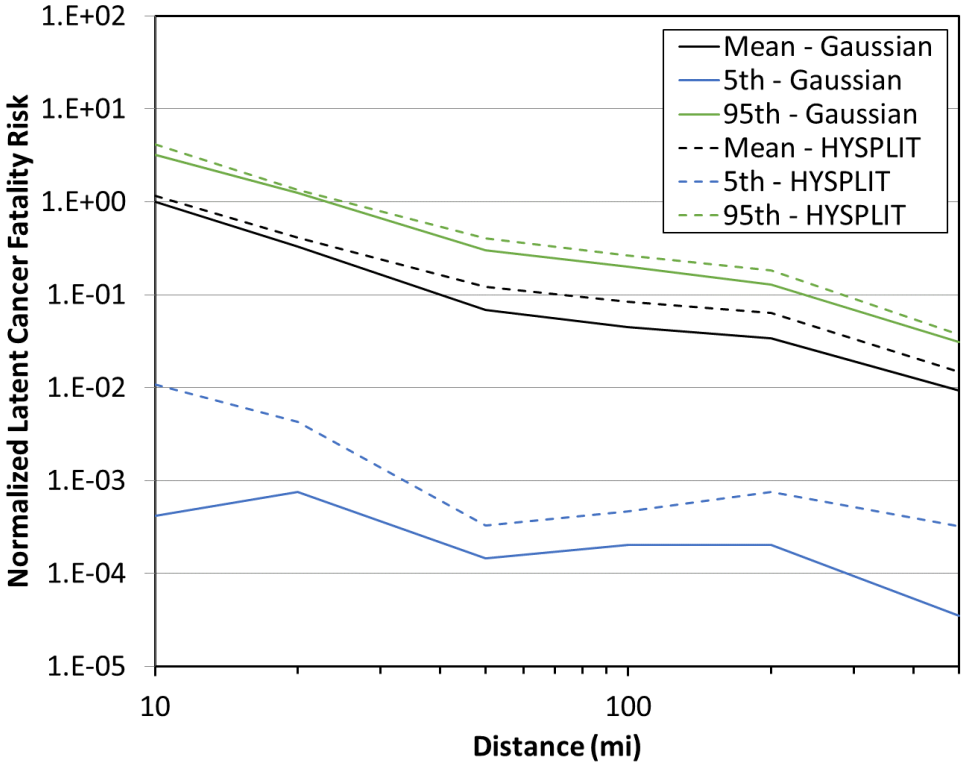

Figure C-39. Original benchmark Site C, ST #1, latent cancer fatality risk original comparison

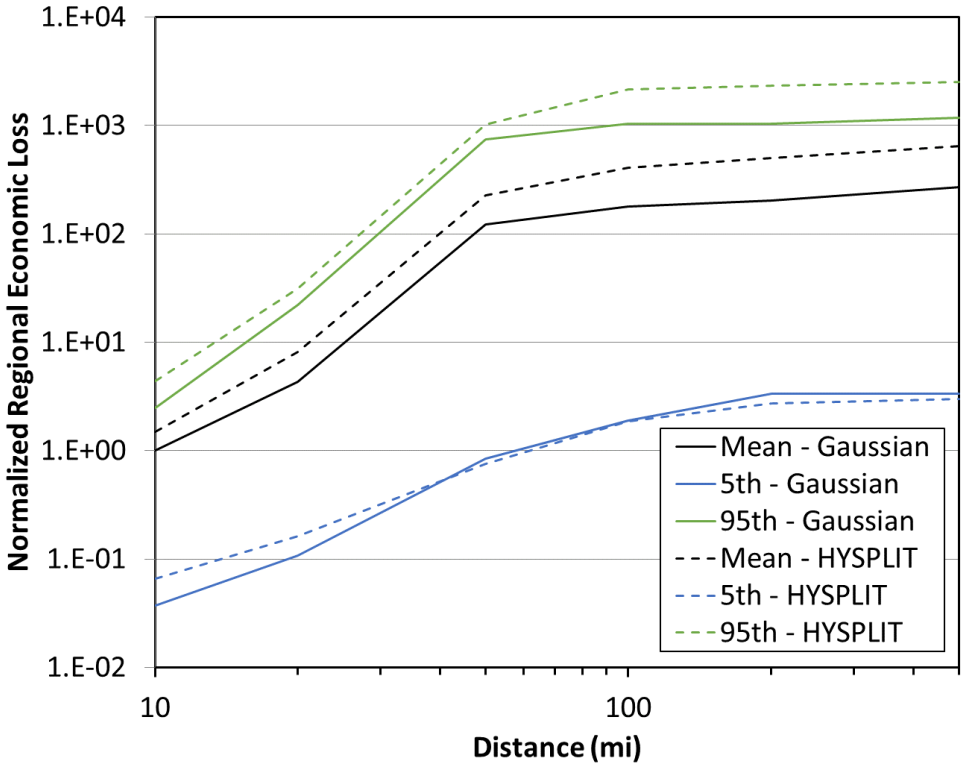

Figure C-40. Original benchmark Site C, ST #1, economic loss original comparison

C.3.2. Source Term #2

The original comparisons between the Gaussian and HYSPLIT ATD model results for Site C, ST #2 for peak air concentration, peak ground deposition, land contamination area, peak dose, early fatality risk, population dose, latent cancer fatality risk, and economic loss (as described in Section 3.6) are shown in Figure C-41 through Figure C-48. The annual statistics for these measures are shown with different colors, where the mean values are in black, the 5th percentile values are shown in blue, and the 95th percentile values are shown in green. HYSPLIT results are shown as dashed lines and Gaussian model results are shown as solid lines. The normalized results are shown as a function of distance, rather than the ratio of Gaussian and HYSPLIT results, to allow for the trends with distance to be observed. Some results are zero for early fatality risk, so they cannot be shown on the log scale used in the figures. A summary of the difference seen in these figures is provided below in Section C.6.

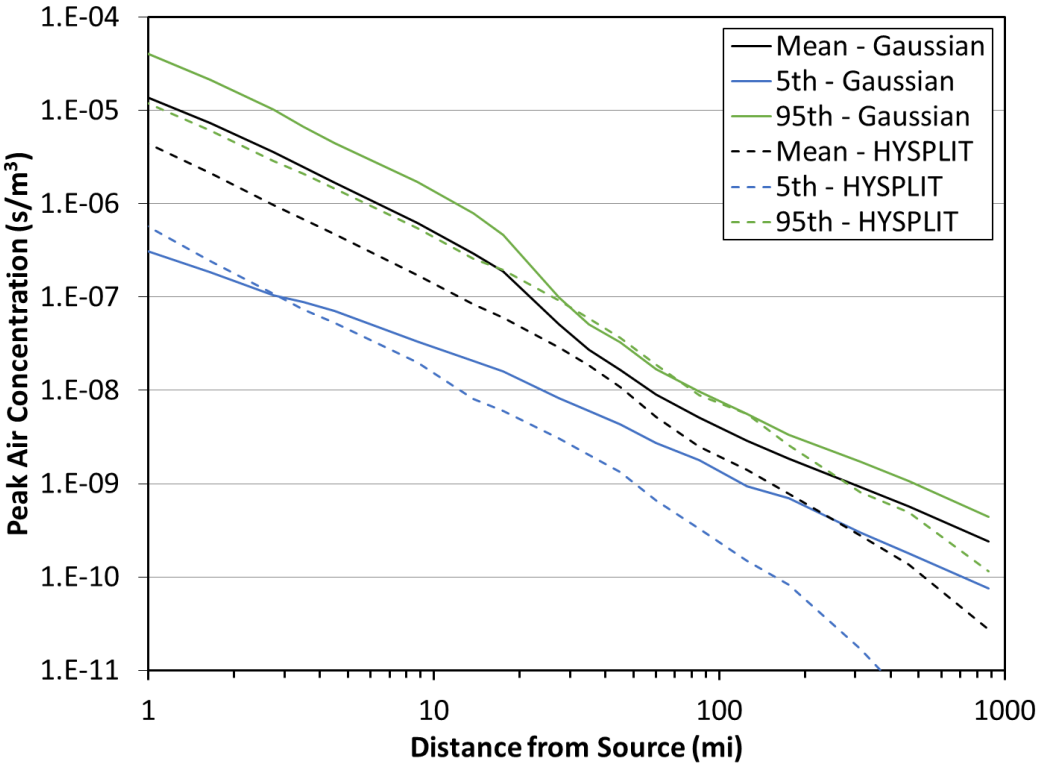

Figure C-41. Original benchmark Site C, ST #2, peak air concentration original comparison

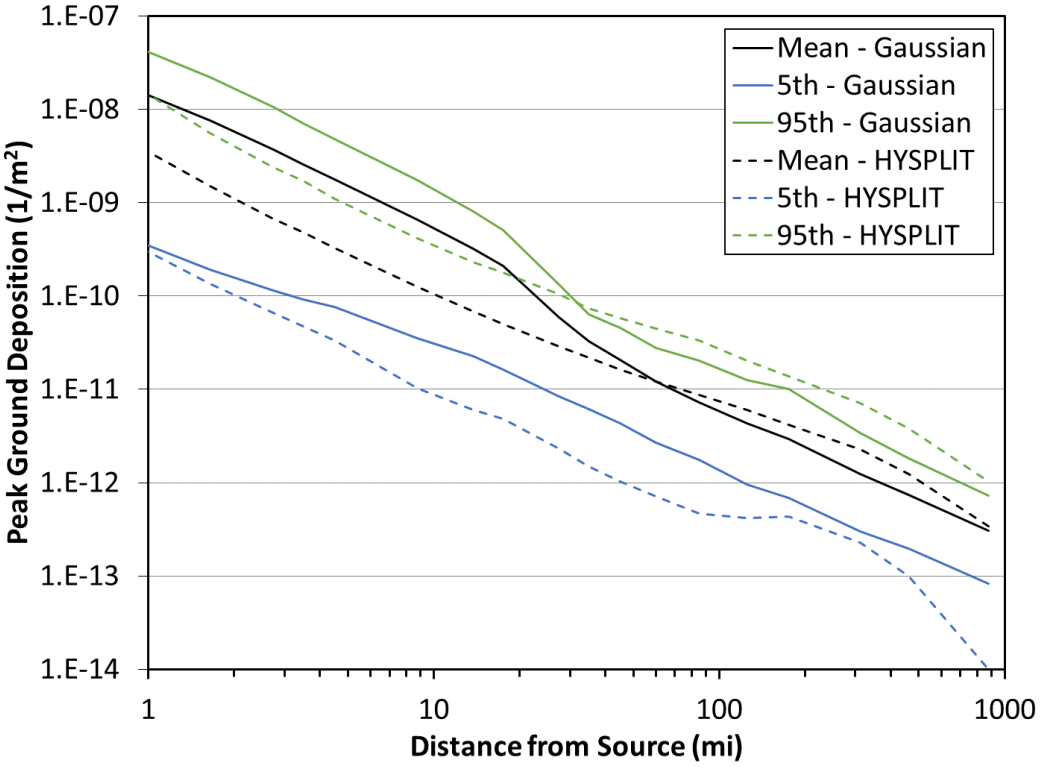

Figure C-42. Original benchmark Site C, ST #2, peak ground deposition original comparison

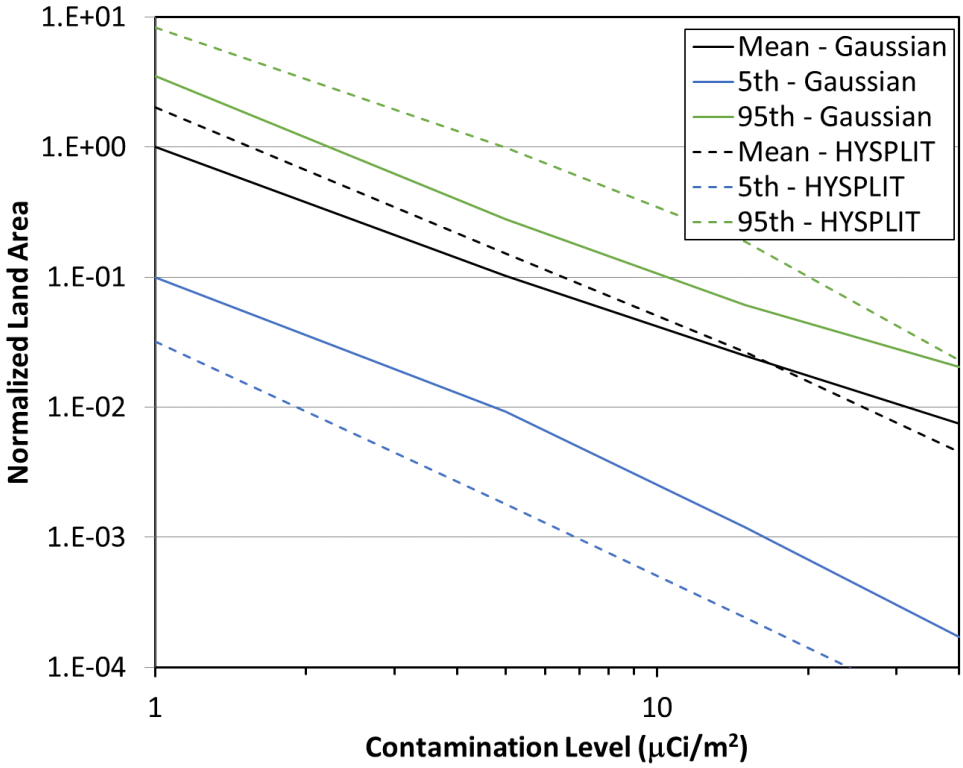

Figure C-43. Original benchmark Site C, ST #2, land contamination area within 805 km (500 mi) original comparison

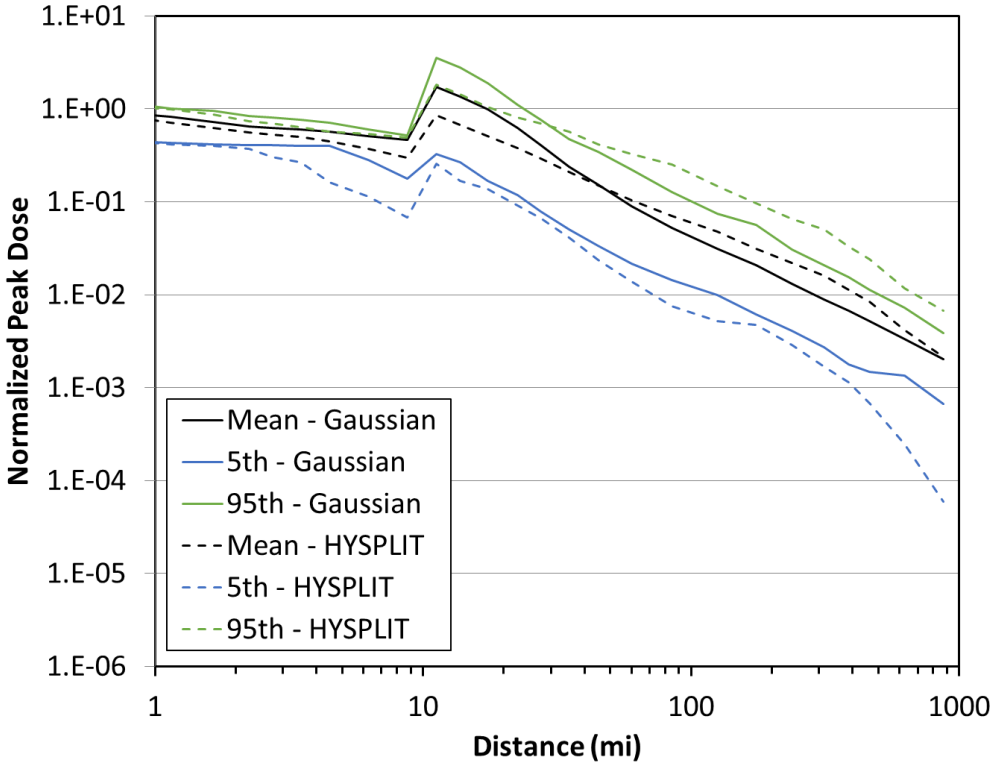

Figure C-44. Original benchmark Site C, ST #2, peak dose original comparison

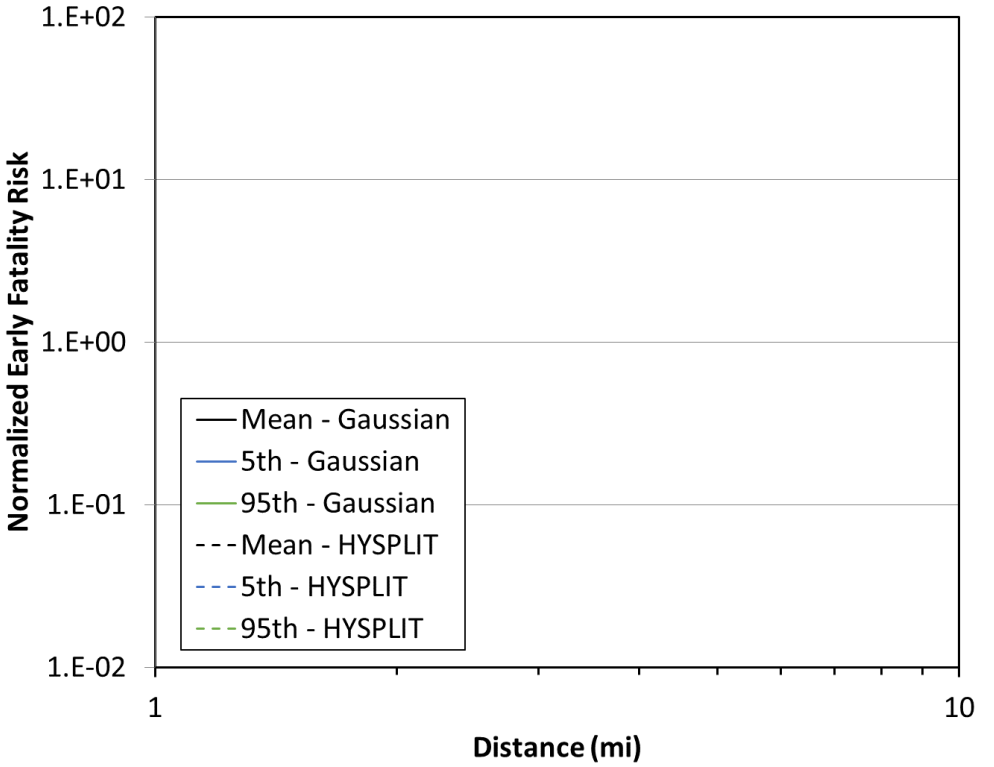

Figure C-45. Original benchmark Site C, ST #2, early fatality risk original comparison

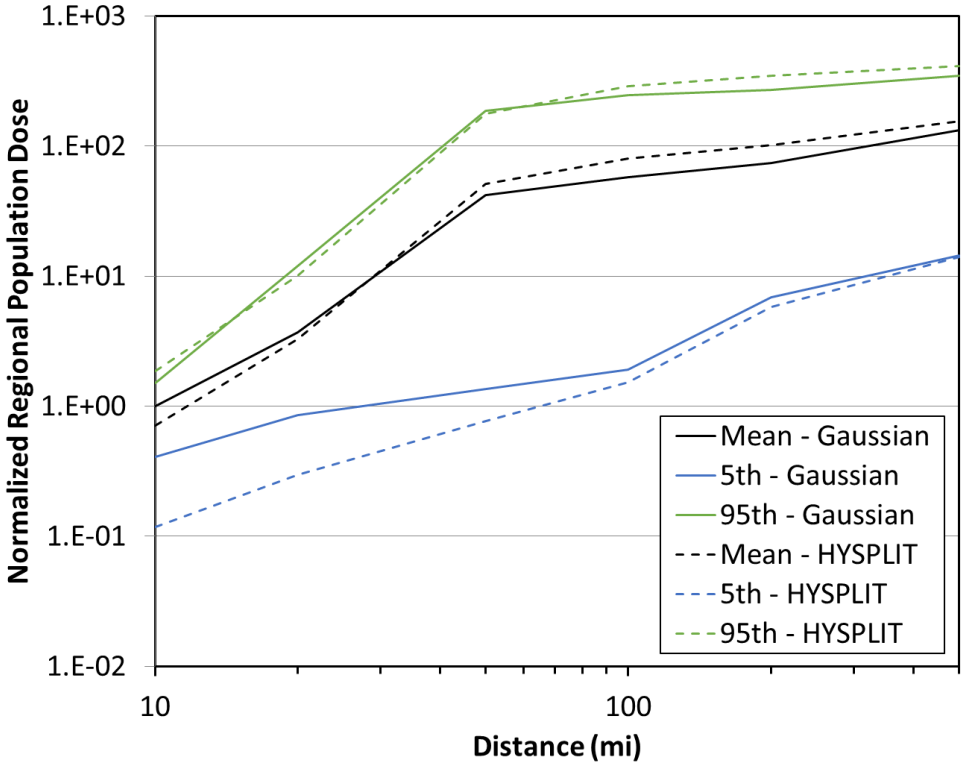

Figure C-46. Original benchmark Site C, ST #2, population dose original comparison

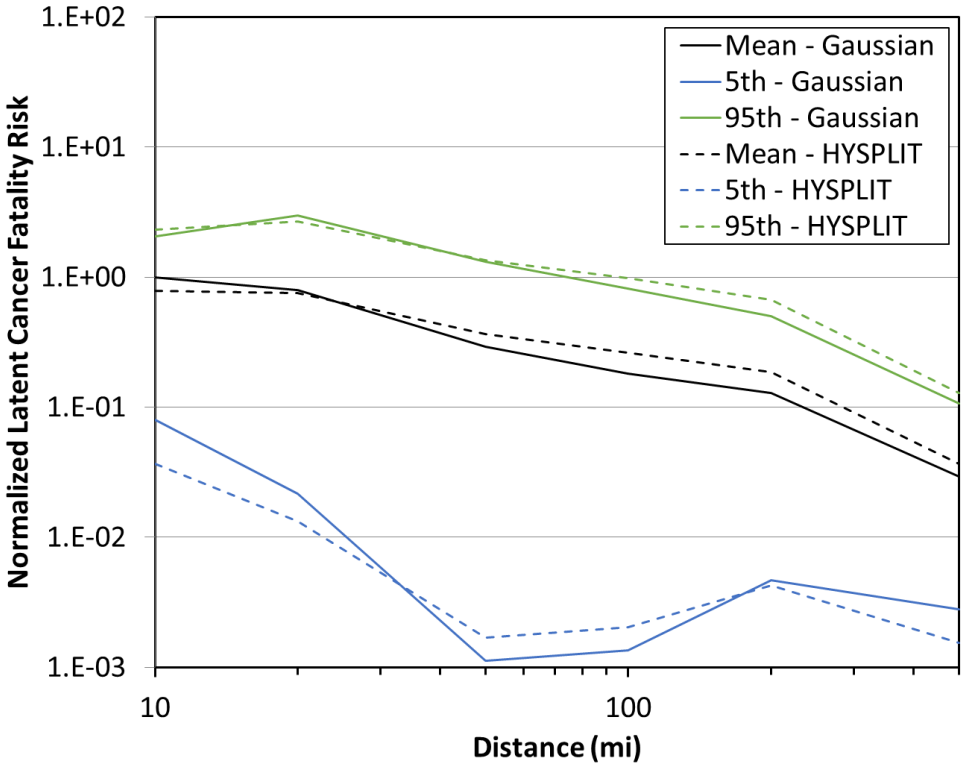

Figure C-47. Original benchmark Site C, ST #2, latent cancer fatality risk original comparison

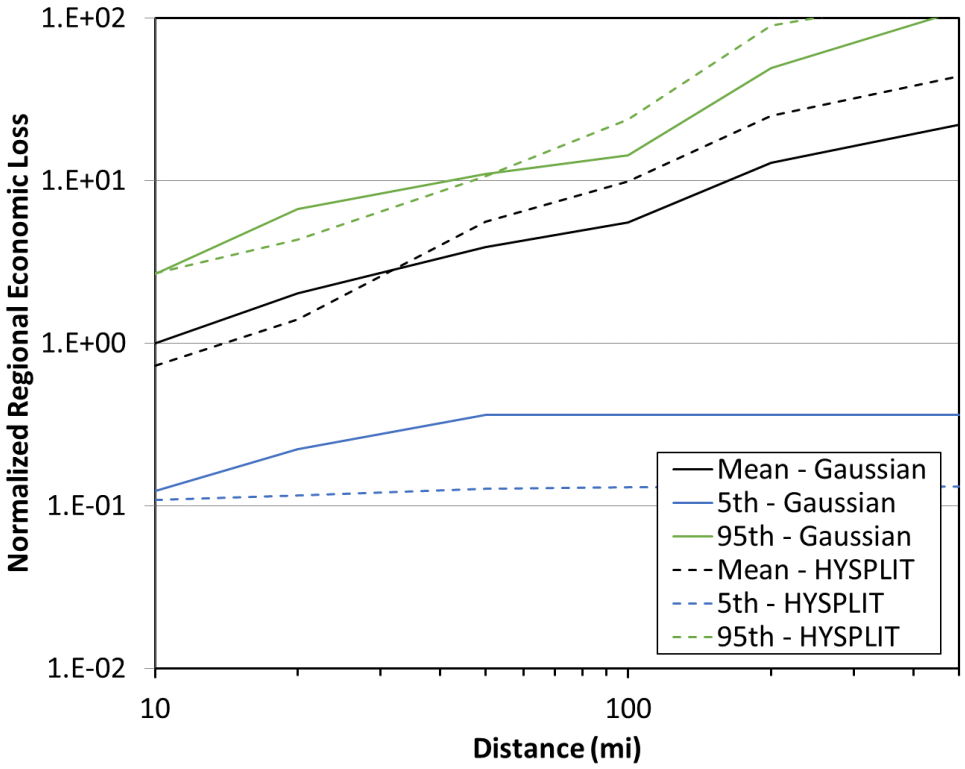

Figure C-48. Original benchmark Site C, ST #2, economic loss original comparison

C.4. Site D

C.4.1. Source Term #1

The original comparisons between the Gaussian and HYSPLIT ATD model results for Site D, ST #1 for peak air concentration, peak ground deposition, land contamination area, peak dose, early fatality risk, population dose, latent cancer fatality risk, and economic loss (as described in Section 3.6) are shown in Figure C-49 through Figure C-56. The annual statistics for these measures are shown with different colors, where the mean values are in black, the 5th percentile values are shown in blue, and the 95th percentile values are shown in green. HYSPLIT results are shown as dashed lines and Gaussian model results are shown as solid lines. The normalized results are shown as a function of distance, rather than the ratio of Gaussian and HYSPLIT results, to allow for the trends with distance to be observed. Some results are zero for early and latent cancer fatality risk, so they cannot be shown on the log scale used in the figures. For Site D, there are no individuals within five miles of the site, which results in a calculated zero early fatality risk at shorter distances. A summary of the difference seen in these figures is provided below in Section C.6.

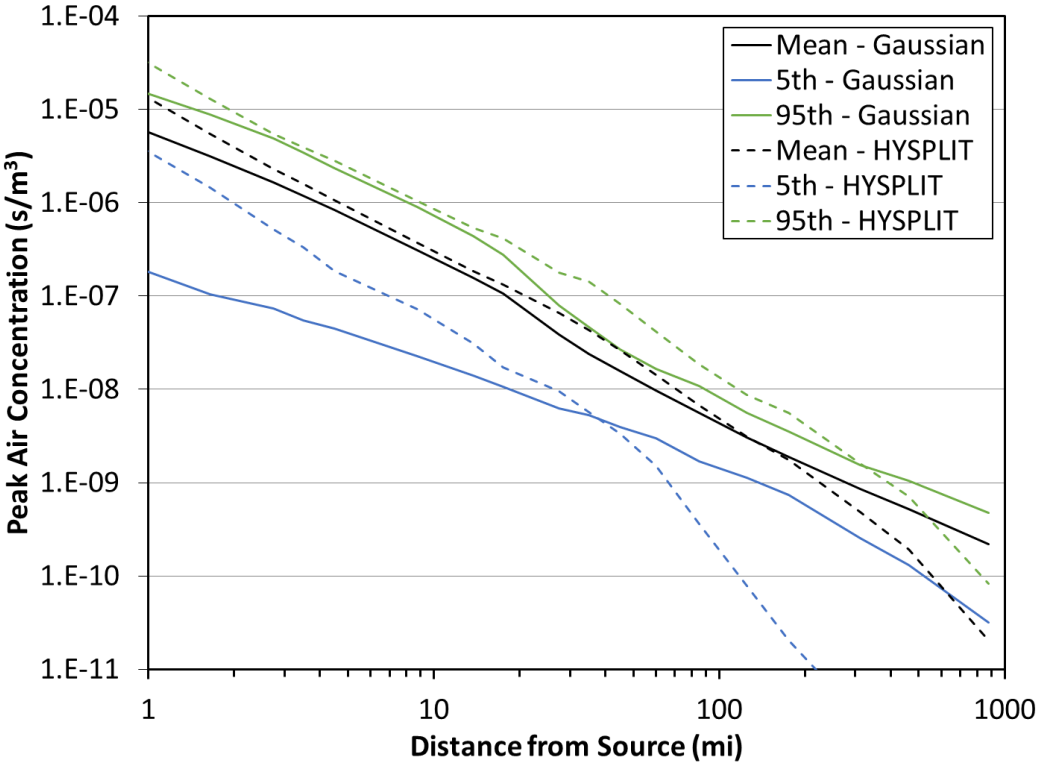

Figure C-49. Original benchmark Site D, ST #1, peak air concentration original comparison

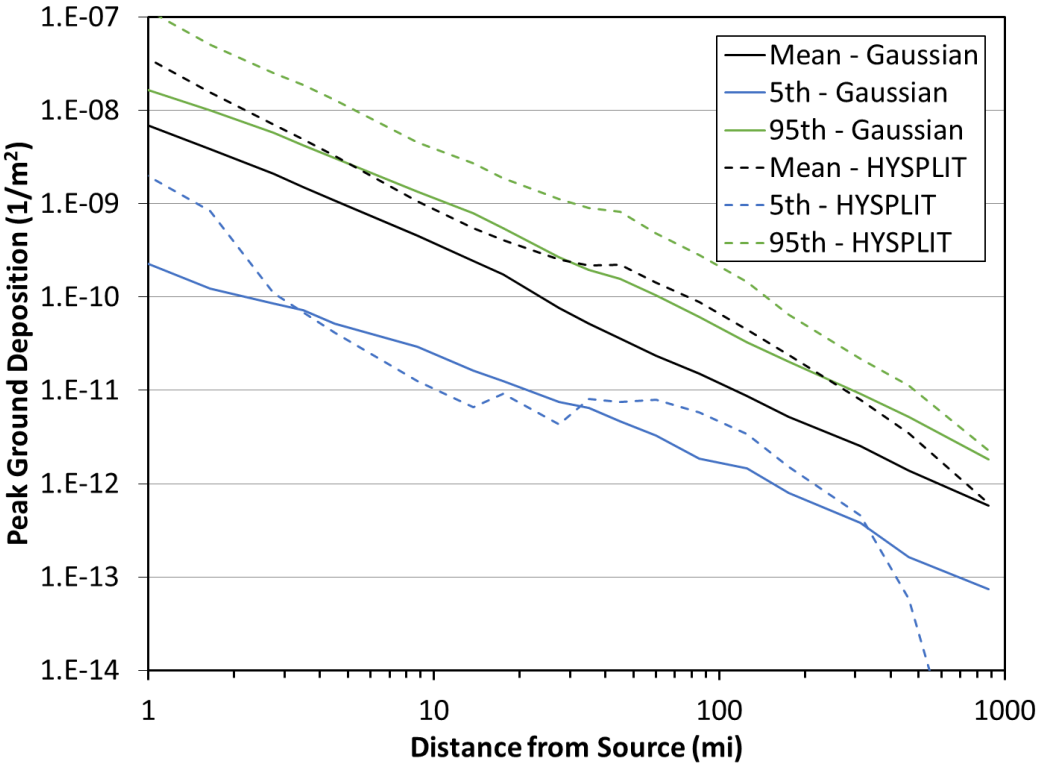

Figure C-50. Original benchmark Site D, ST #1, peak ground deposition original comparison

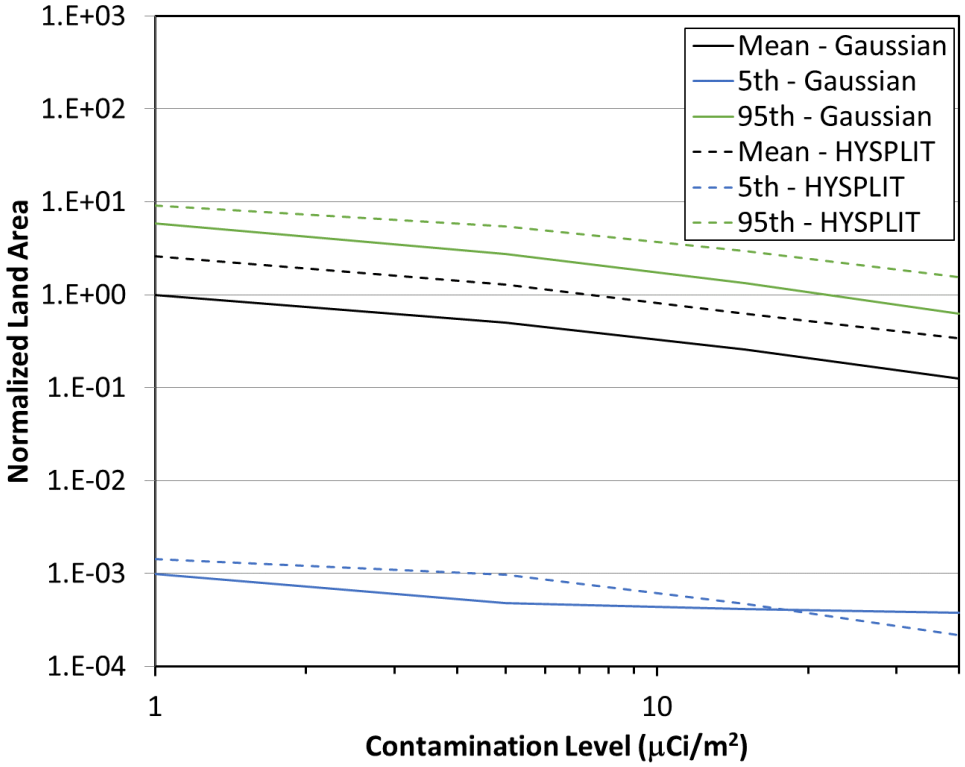

Figure C-51. Original benchmark Site D, ST #1, land contamination area within 805 km (500 mi) original comparison

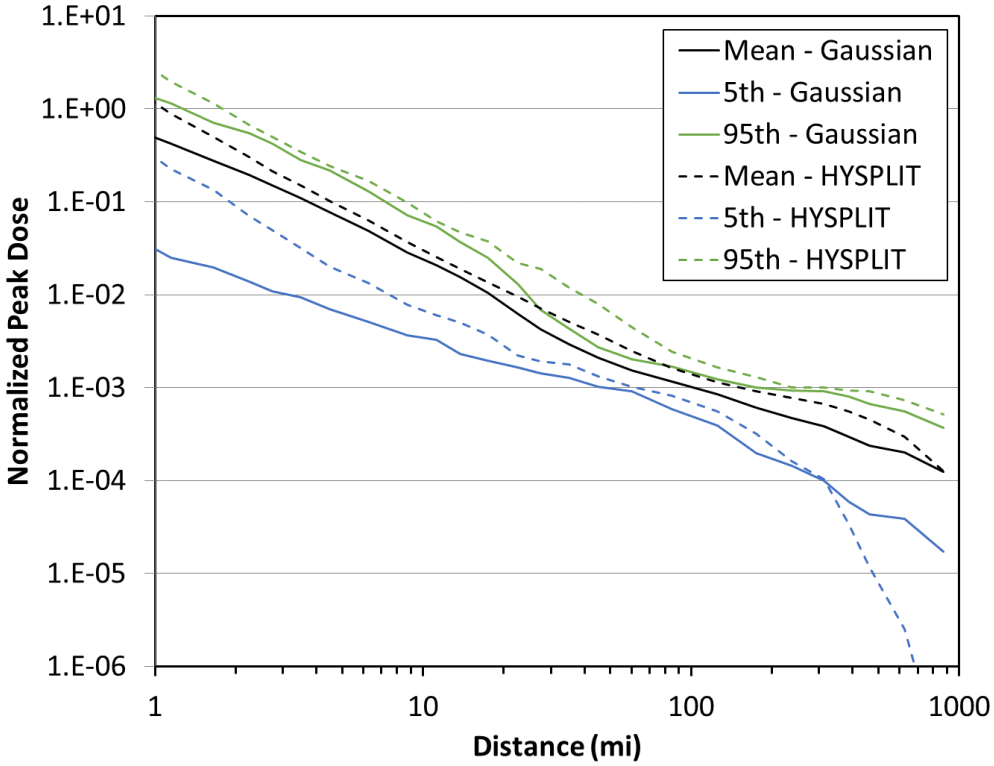

Figure C-52. Original benchmark Site D, ST #1, peak dose original comparison

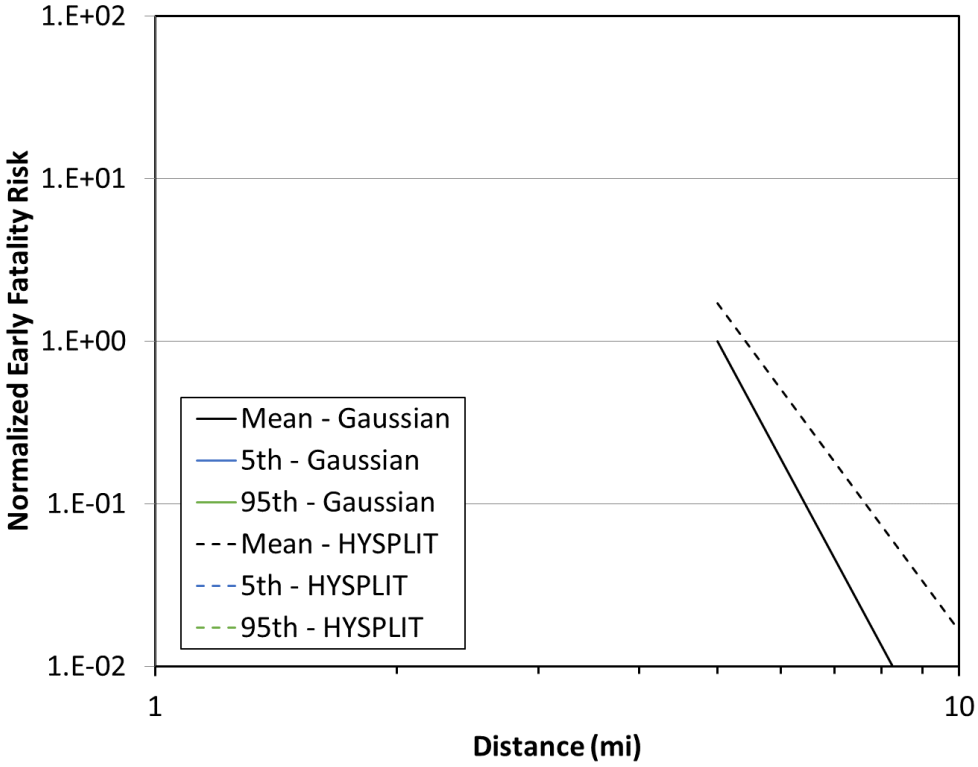

Figure C-53. Original benchmark Site D, ST #1, early fatality risk original comparison

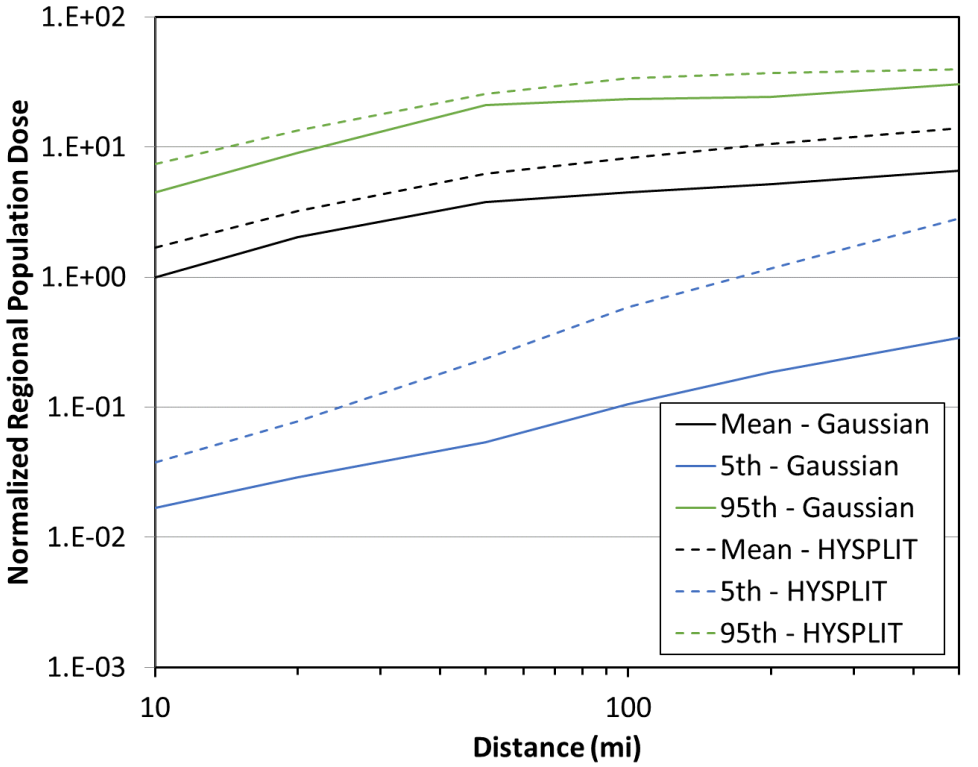

Figure C-54. Original benchmark Site D, ST #1, population dose original comparison

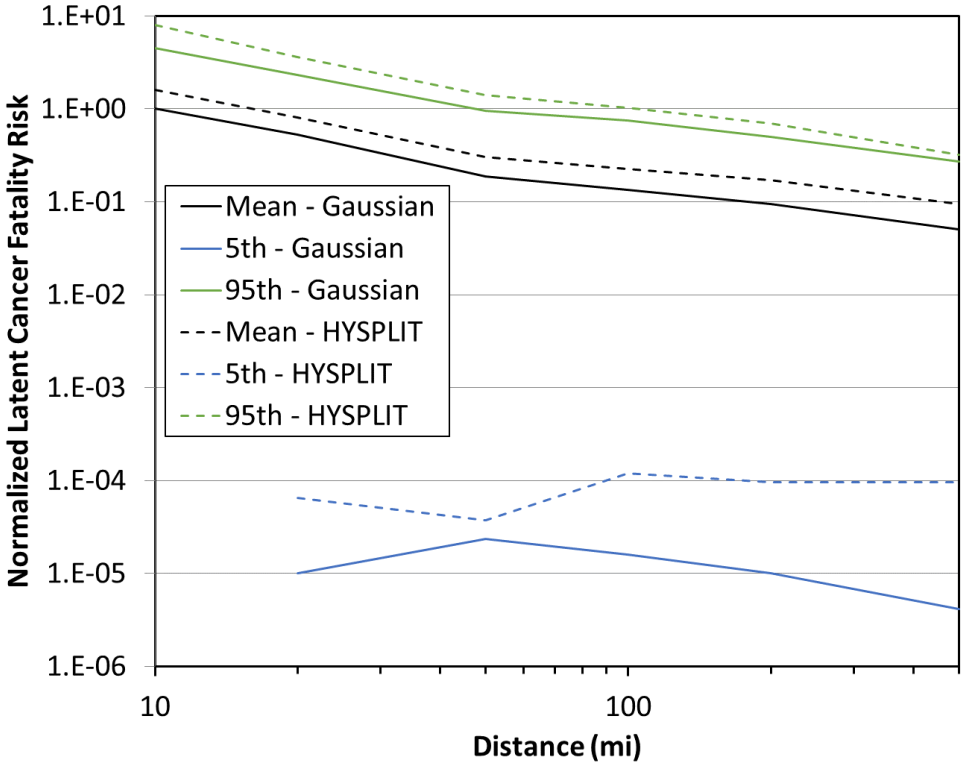

Figure C-55. Original benchmark Site D, ST #1, latent cancer fatality risk original comparison

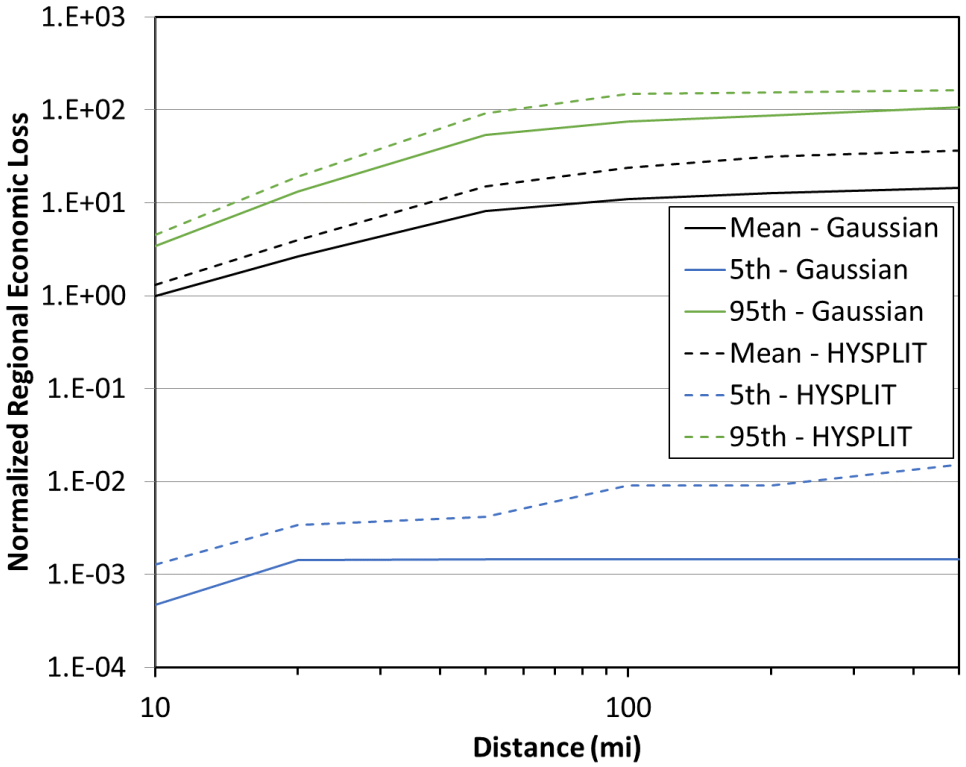

Figure C-56. Original benchmark Site D, ST #1, economic loss original comparison

C.4.2. Source Term #2

The original comparisons between the Gaussian and HYSPLIT ATD model results for Site D, ST #2 for peak air concentration, peak ground deposition, land contamination area, peak dose, early fatality risk, population dose, latent cancer fatality risk, and economic loss (as described in Section 3.6) are shown in Figure C-57 through Figure C-64. The annual statistics for these measures are shown with different colors, where the mean values are in black, the 5th percentile values are shown in blue, and the 95th percentile values are shown in green. HYSPLIT results are shown as dashed lines and Gaussian model results are shown as solid lines. The normalized results are shown as a function of distance, rather than the ratio of Gaussian and HYSPLIT results, to allow for the trends with distance to be observed. Some results are zero for early fatality risk, so they cannot be shown on the log scale used in the figures. A summary of the difference seen in these figures is provided below in Section C.6.

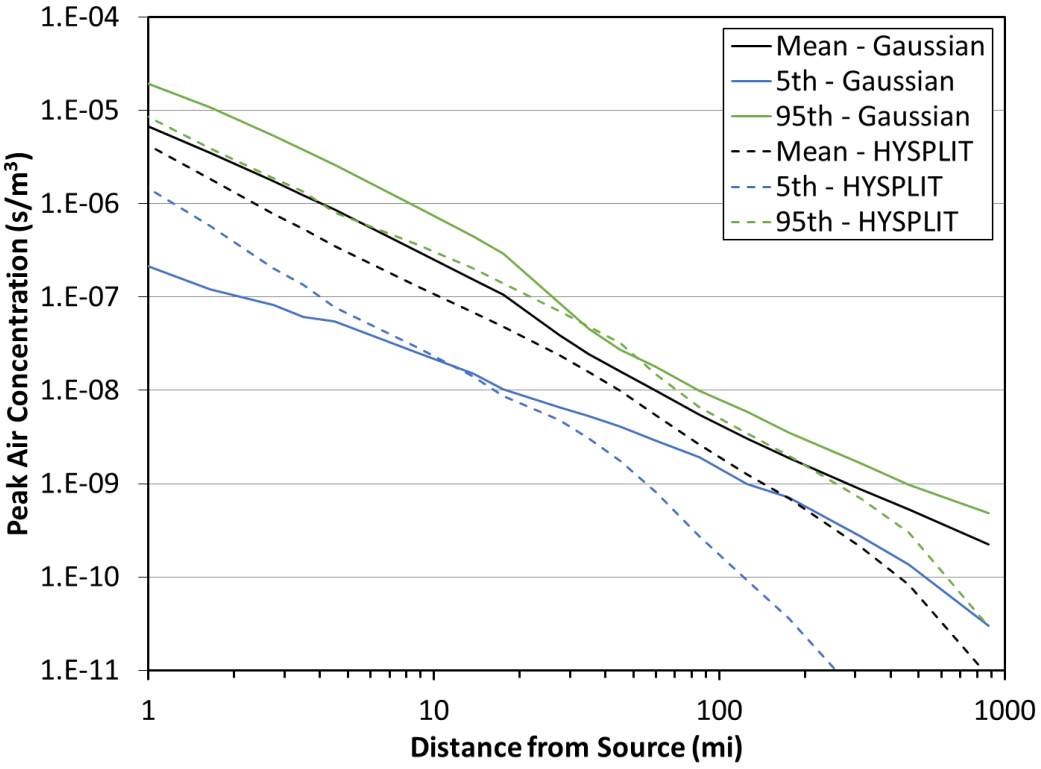

Figure C-57. Original benchmark Site D, ST #2, peak air concentration original comparison

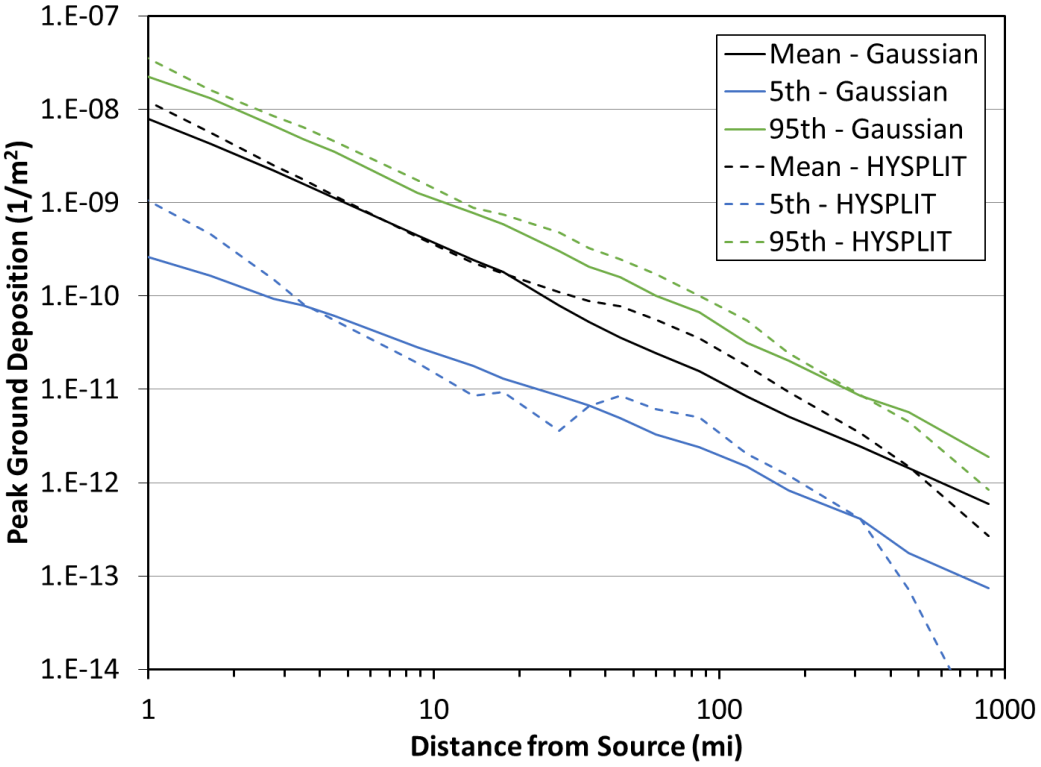

Figure C-58. Original benchmark Site D, ST #2, peak ground deposition original comparison

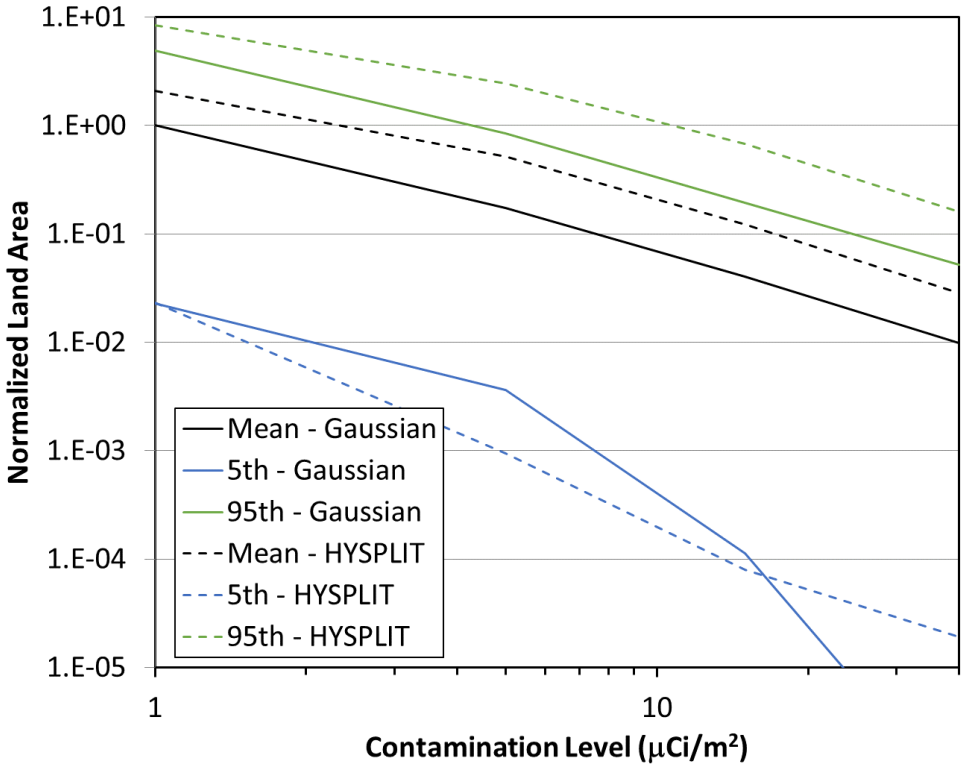

Figure C-59. Original benchmark Site D, ST #2, land contamination area within 805 km (500 mi) original comparison

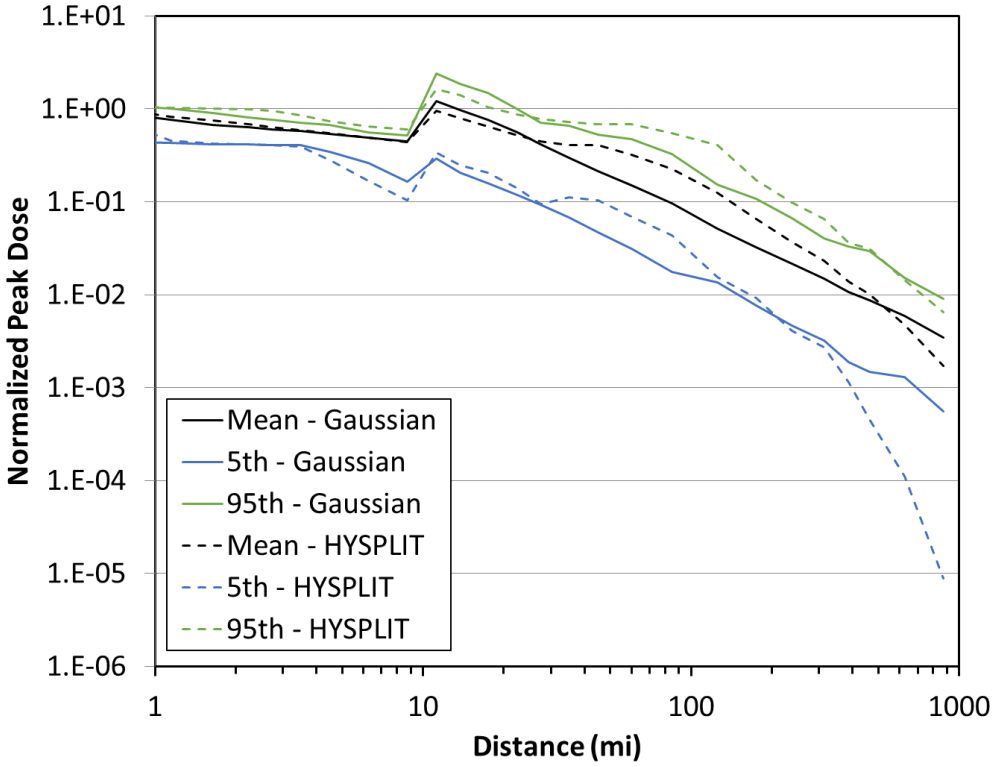

Figure C-60. Original benchmark Site D, ST #2, peak dose original comparison

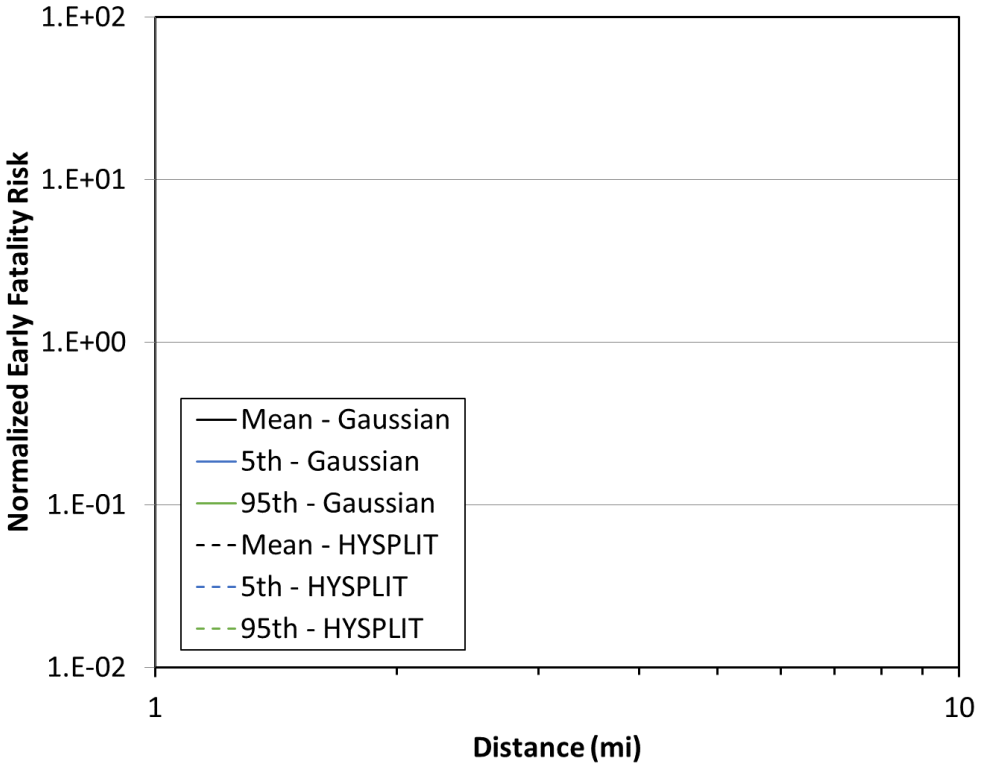

Figure C-61. Original benchmark Site D, ST #2, early fatality risk original comparison

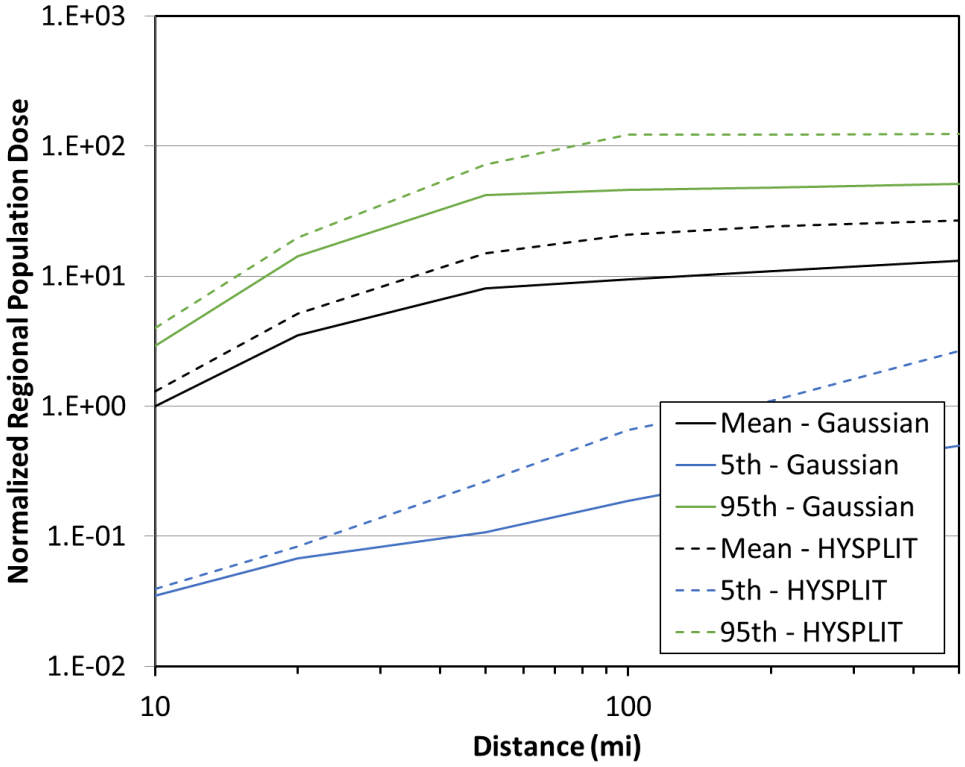

Figure C-62. Original benchmark Site D, ST #2, population dose original comparison

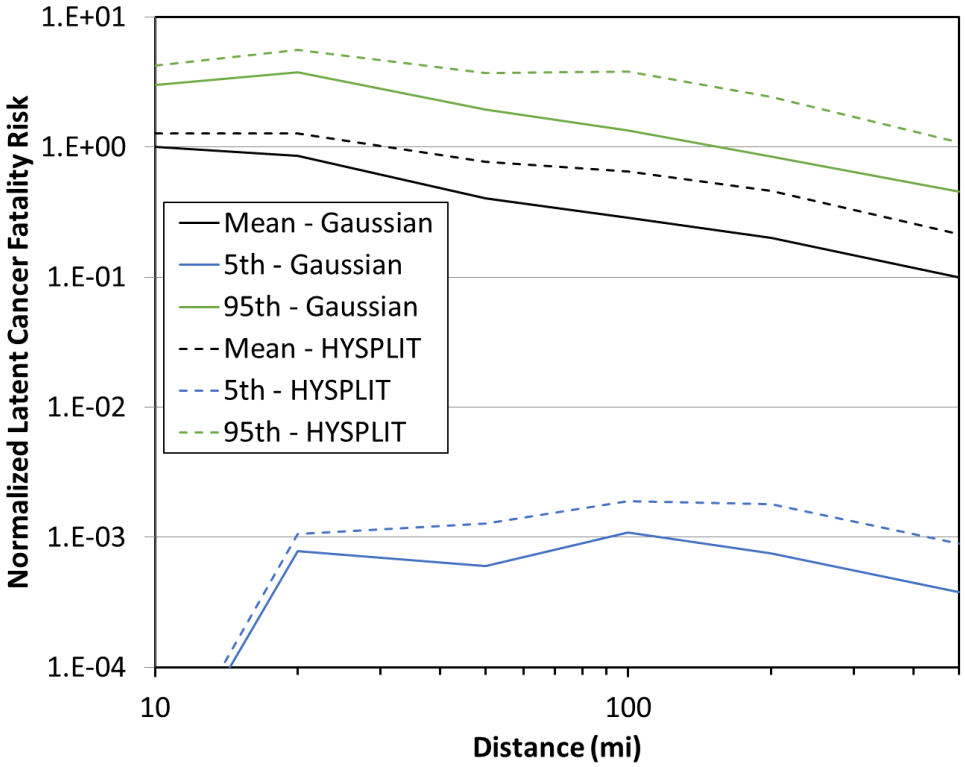

Figure C-63. Original benchmark Site D, ST #2, latent cancer fatality risk original comparison

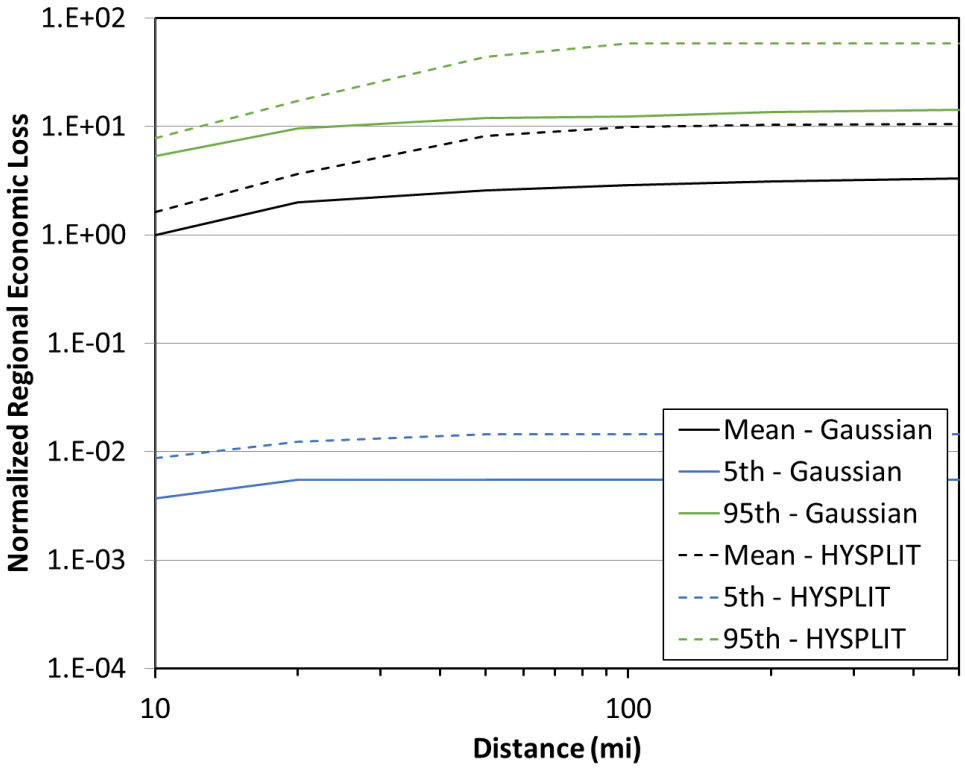

Figure C-64. Original benchmark Site D, ST #2, economic loss original comparison

C.5. Site E

C.5.1. Source Term #1

The original comparisons between the Gaussian and HYSPLIT ATD model results for Site E, ST #1 for peak air concentration, peak ground deposition, land contamination area, peak dose, early fatality risk, population dose, latent cancer fatality risk, and economic loss (as described in Section 3.6) are shown in Figure C-65 through Figure C-72. The annual statistics for these measures are shown with different colors, where the mean values are in black, the 5th percentile values are shown in blue, and the 95th percentile values are shown in green. HYSPLIT results are shown as dashed lines and Gaussian model results are shown as solid lines. The normalized results are shown as a function of distance, rather than the ratio of Gaussian and HYSPLIT results, to allow for the trends with distance to be observed. Some results are zero for early and latent cancer fatality risk, so they cannot be shown on the log scale used in the figures. A summary of the difference seen in these figures is provided below in Section C.6.

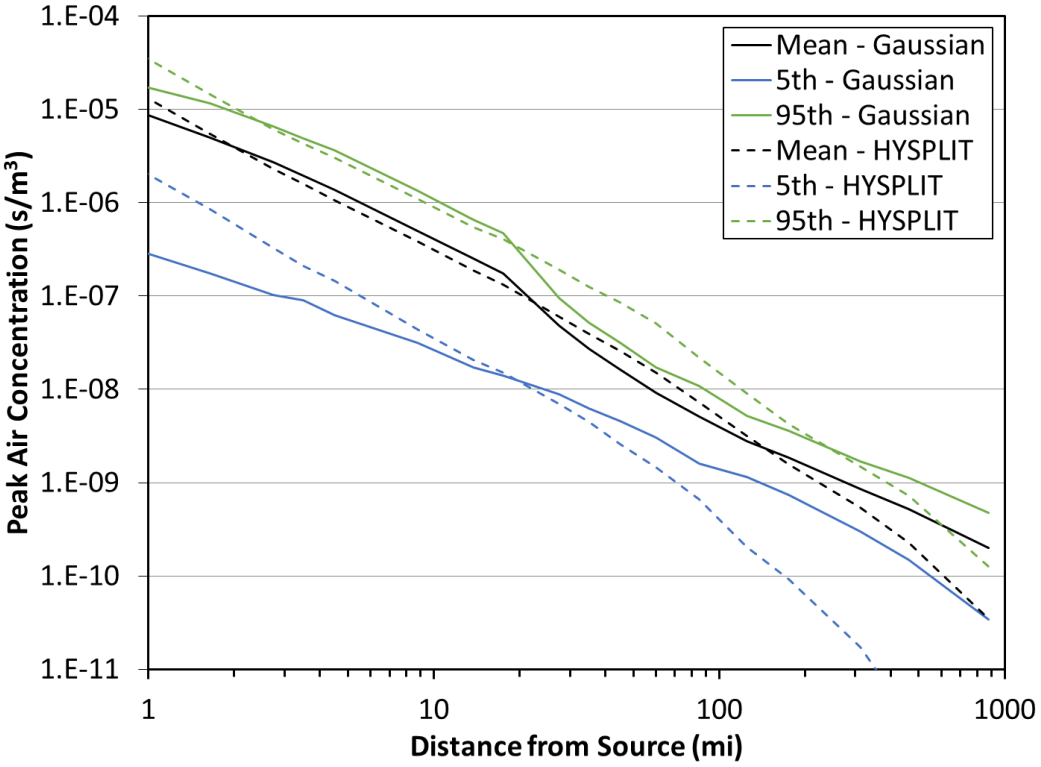

Figure C-65. Original benchmark Site E, ST #1, peak air concentration original comparison

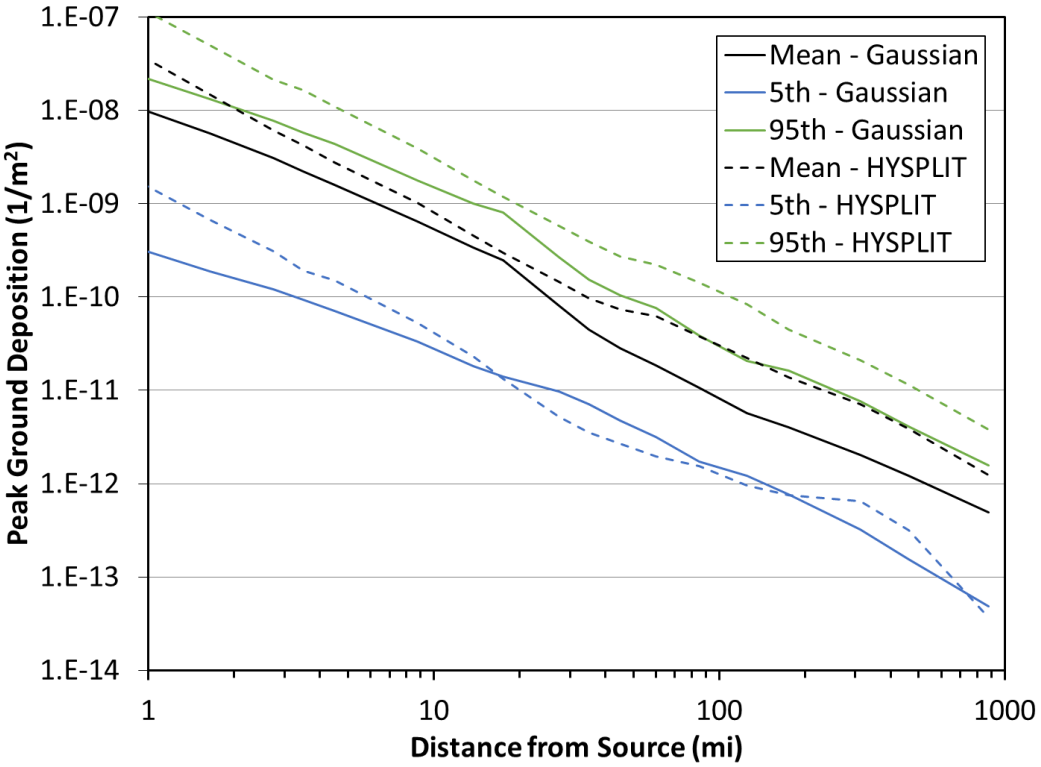

Figure C-66. Original benchmark Site E, ST #1, peak ground deposition original comparison

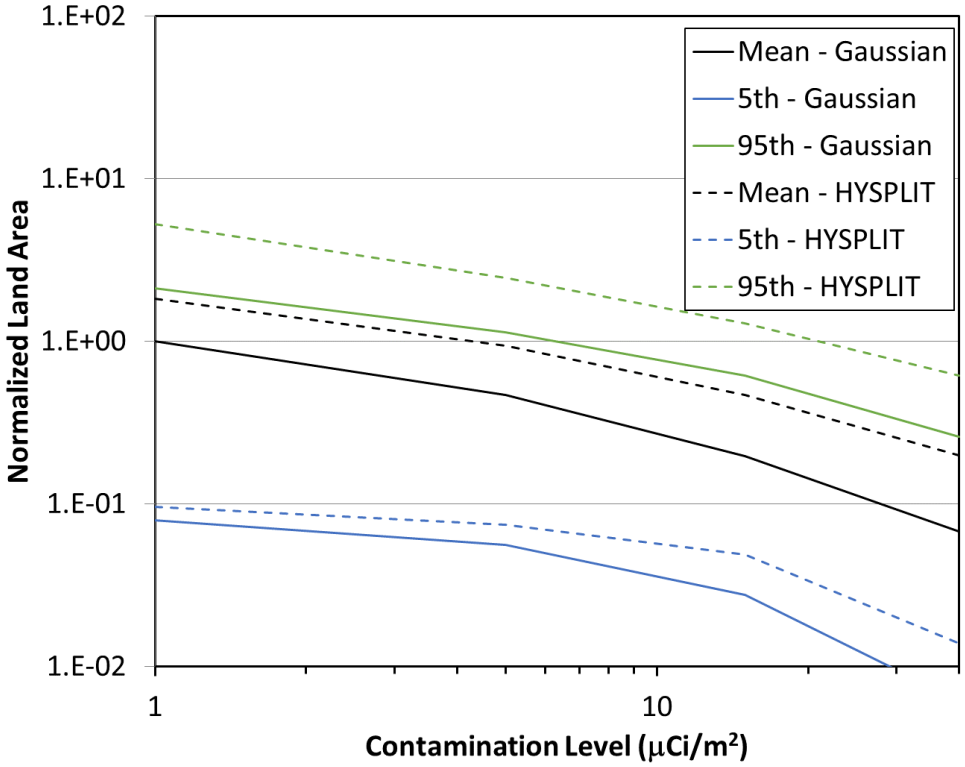

Figure C-67. Original benchmark Site E, ST #1, land contamination area within 805 km (500 mi) original comparison

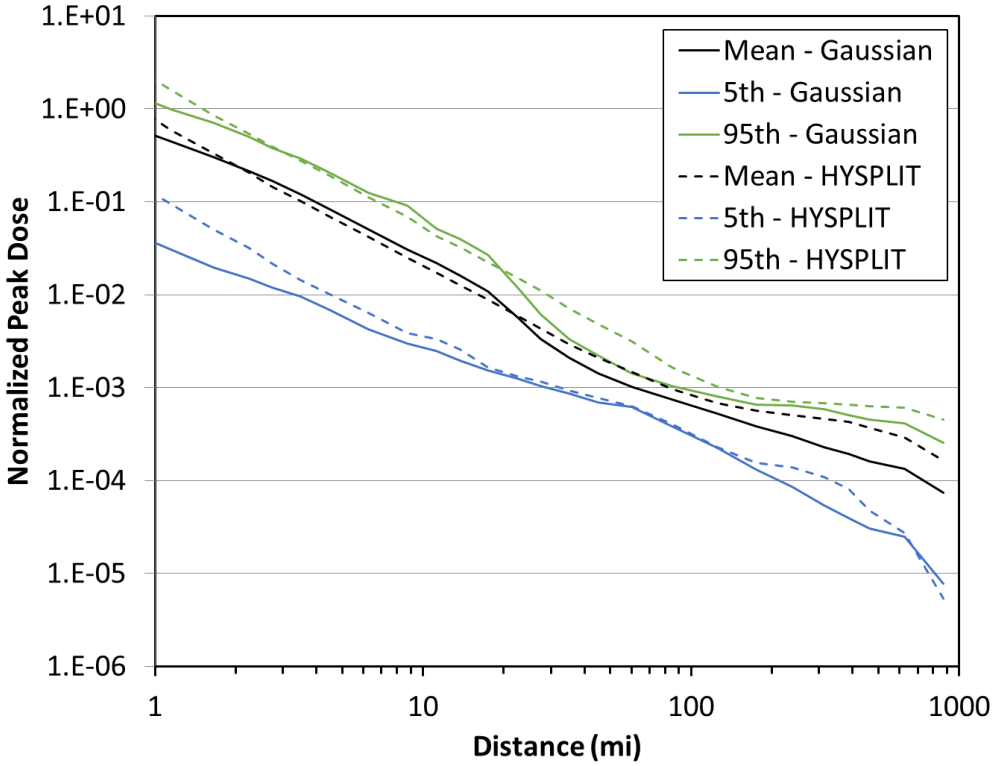

Figure C-68. Original benchmark Site E, ST #1, peak dose original comparison

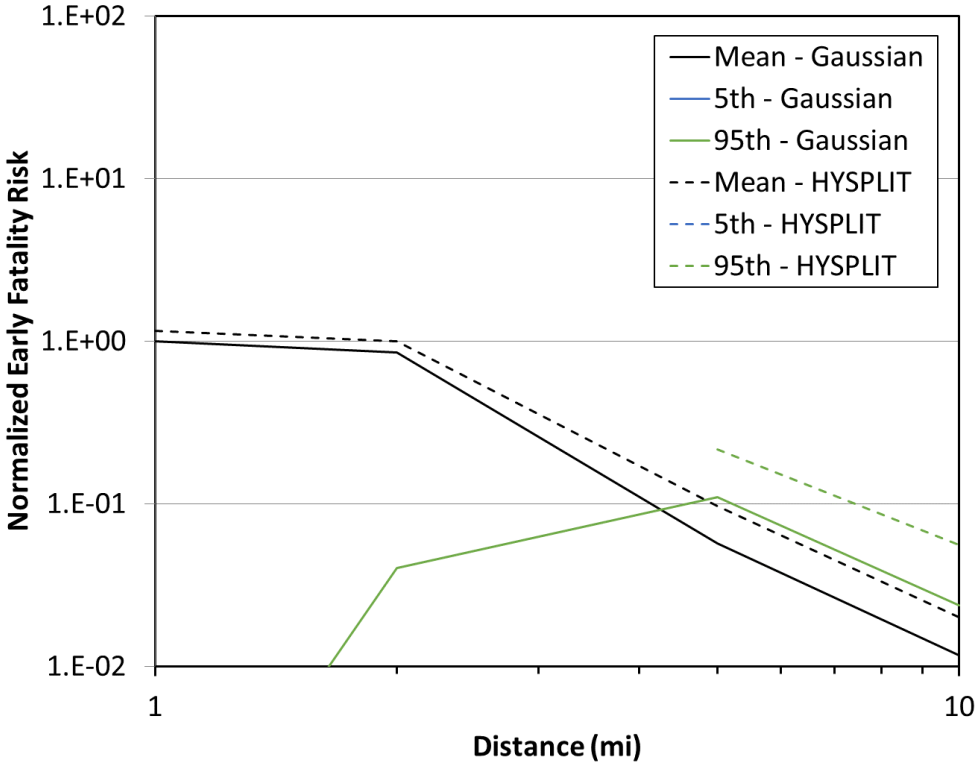

Figure C-69. Original benchmark Site E, ST #1, early fatality risk original comparison

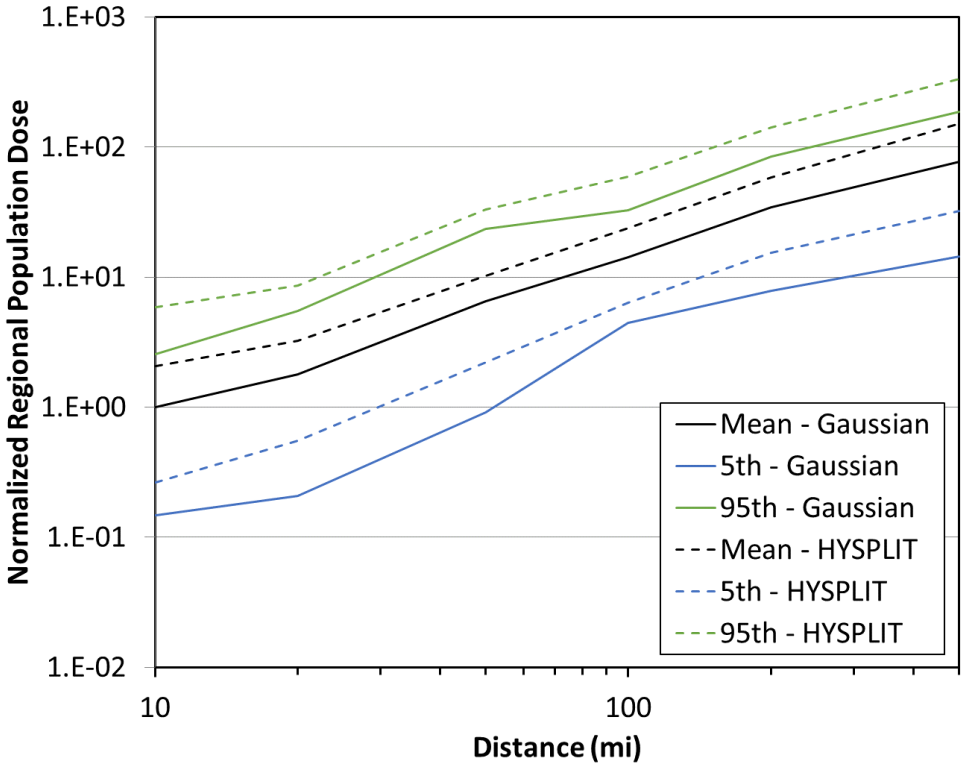

Figure C-70. Original benchmark Site E, ST #1, population dose original comparison

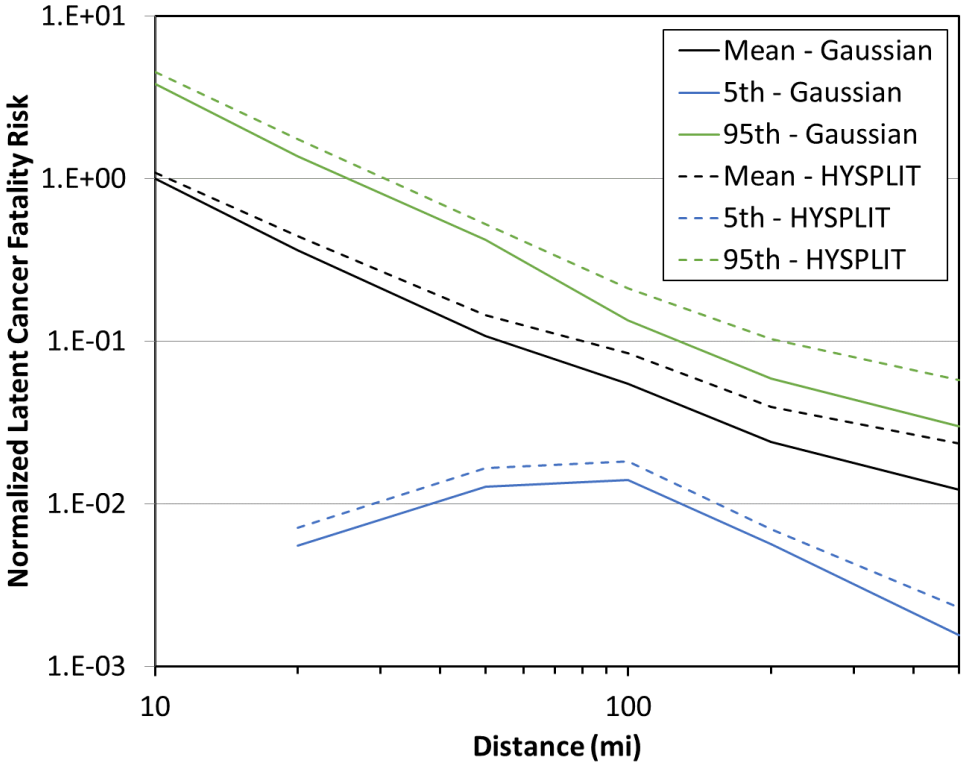

Figure C-71. Original benchmark Site E, ST #1, latent cancer fatality risk original comparison

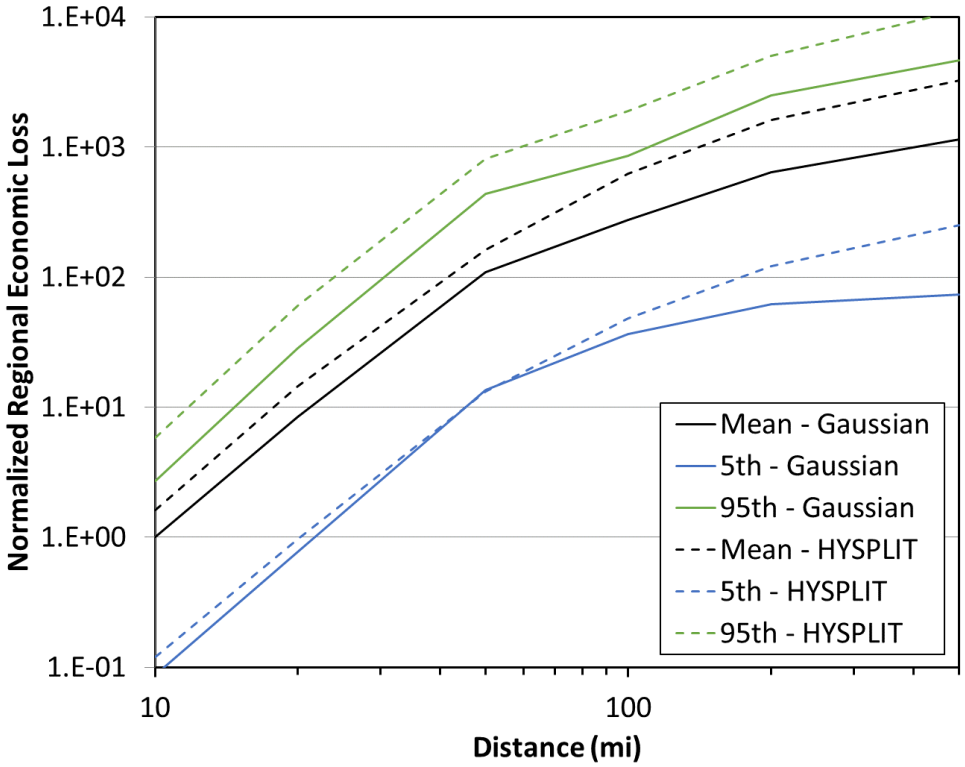

Figure C-72. Original benchmark Site E, ST #1, economic loss original comparison

C.5.2. Source Term #2

The original comparisons between the Gaussian and HYSPLIT ATD model results for Site E, ST #2 for peak air concentration, peak ground deposition, land contamination area, peak dose, early fatality risk, population dose, latent cancer fatality risk, and economic loss (as described in Section 3.6) are shown in Figure C-73 through Figure C-80. The annual statistics for these measures are shown with different colors, where the mean values are in black, the 5th percentile values are shown in blue, and the 95th percentile values are shown in green. HYSPLIT results are shown as dashed lines and Gaussian model results are shown as solid lines. The normalized results are shown as a function of distance, rather than the ratio of Gaussian and HYSPLIT results, to allow for the trends with distance to be observed. Some results are zero for early and latent cancer fatality risk, so they cannot be shown on the log scale used in the figures. A summary of the difference seen in these figures is provided below in Section C.6.

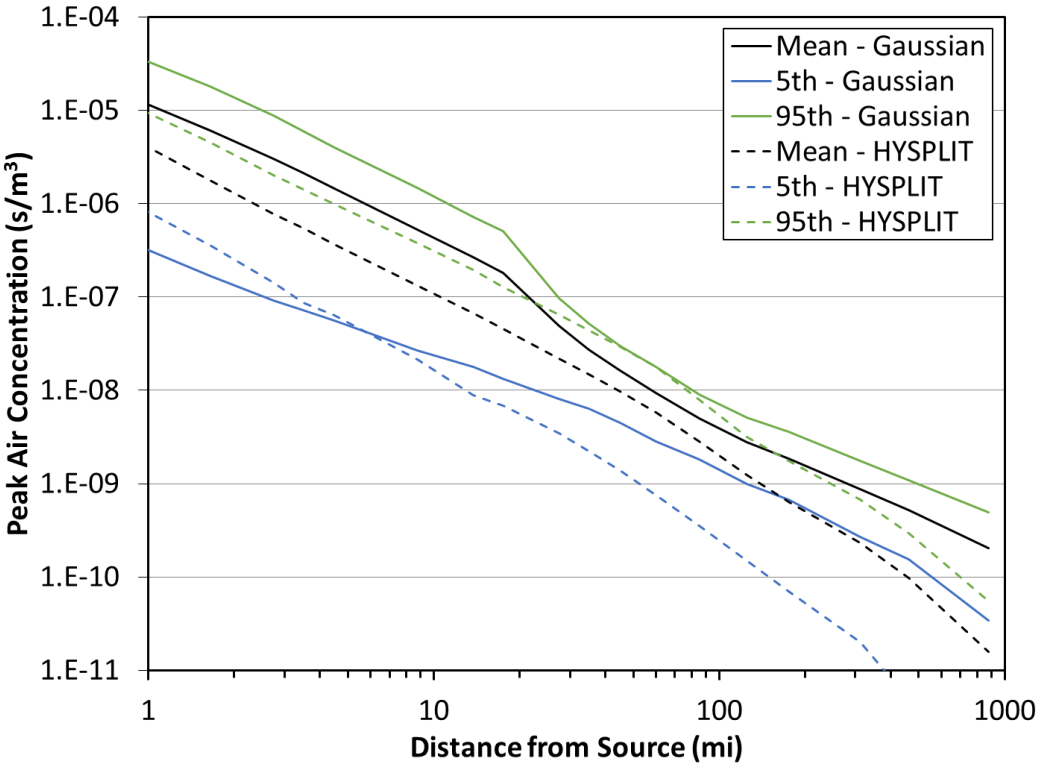

Figure C-73. Original benchmark Site E, ST #2, peak air concentration original comparison

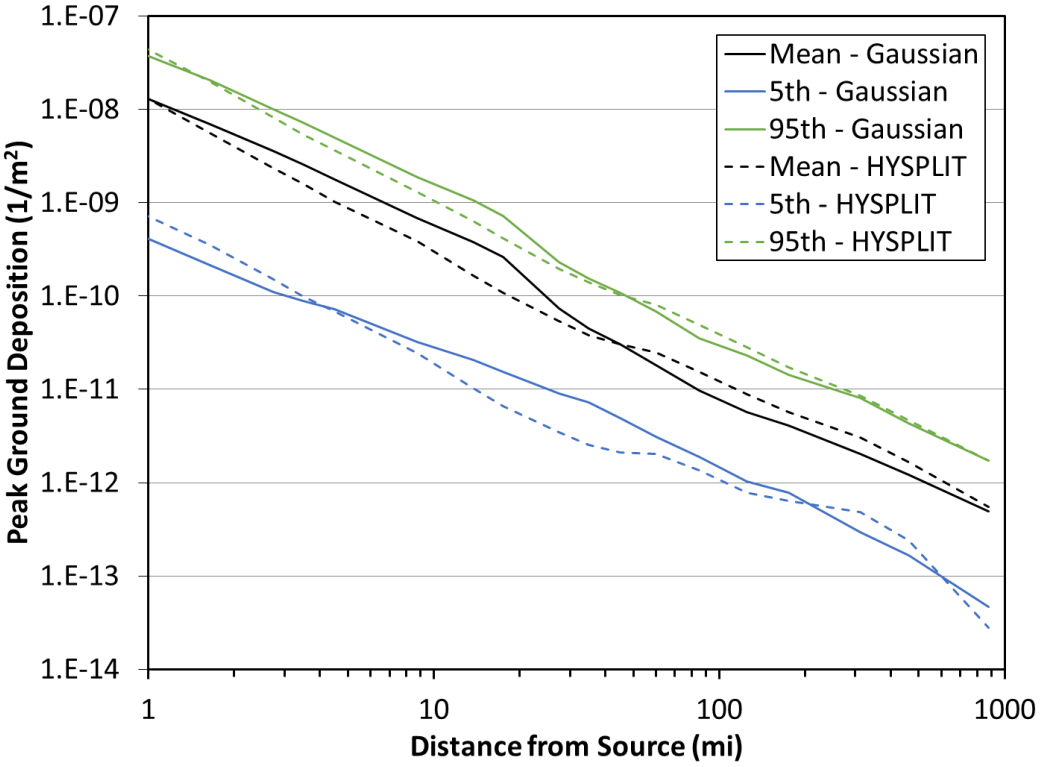

Figure C-74. Original benchmark Site E, ST #2, peak ground deposition original comparison

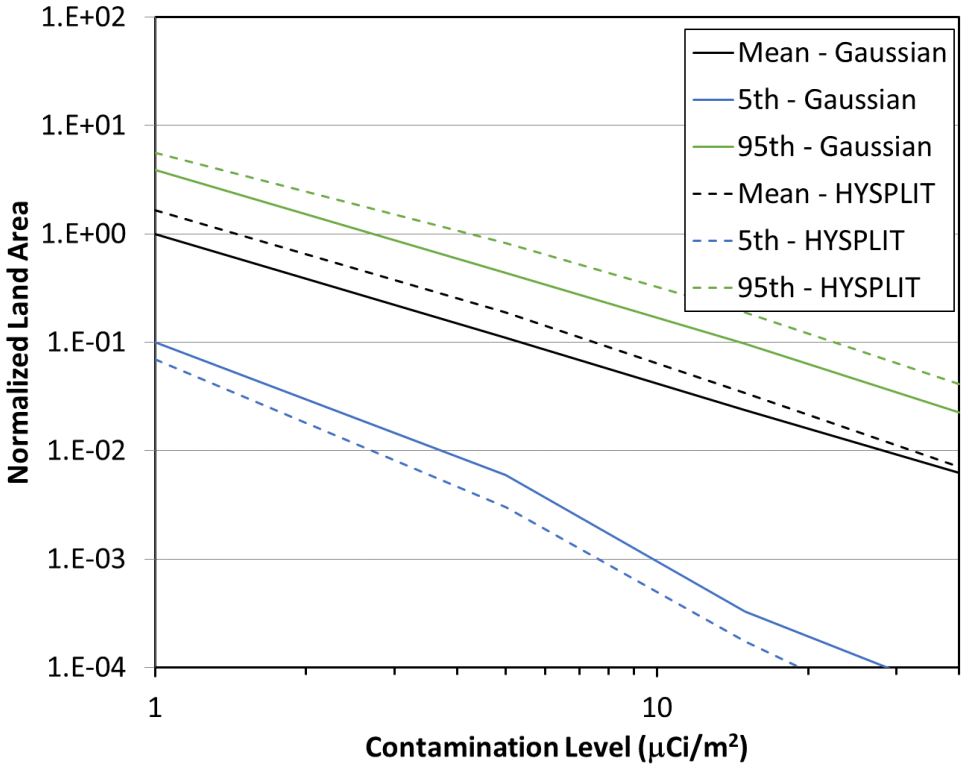

Figure C-75. Original benchmark Site E, ST #2, land contamination area within 805 km (500 mi) original comparison

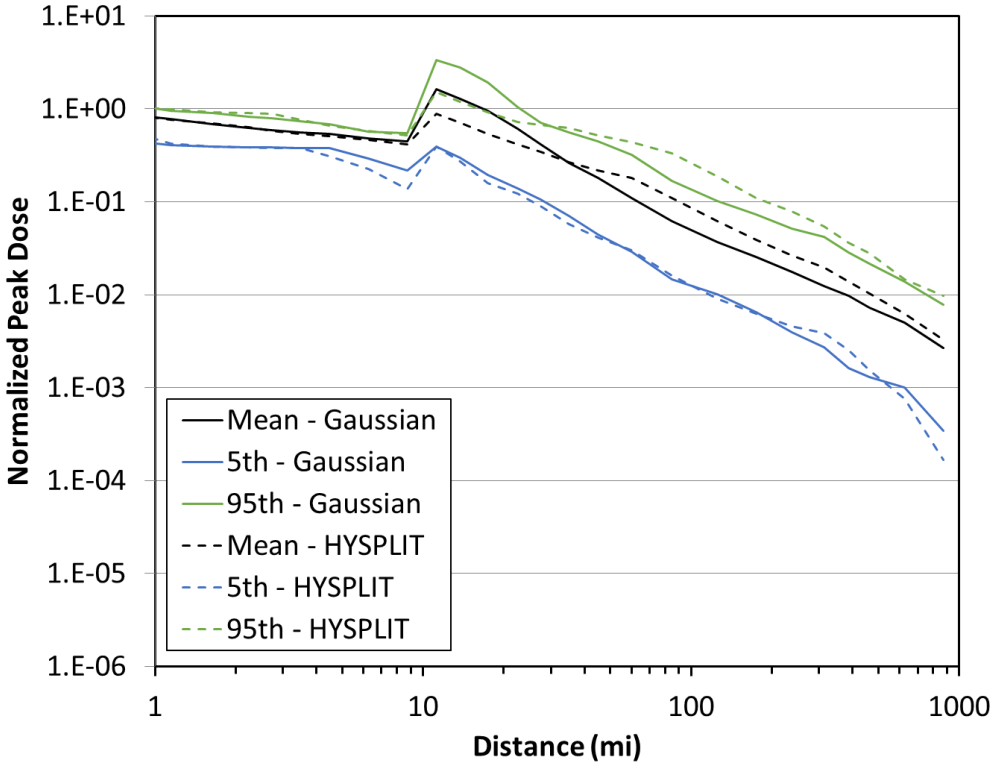

Figure C-76. Original benchmark Site E, ST #2, peak dose original comparison

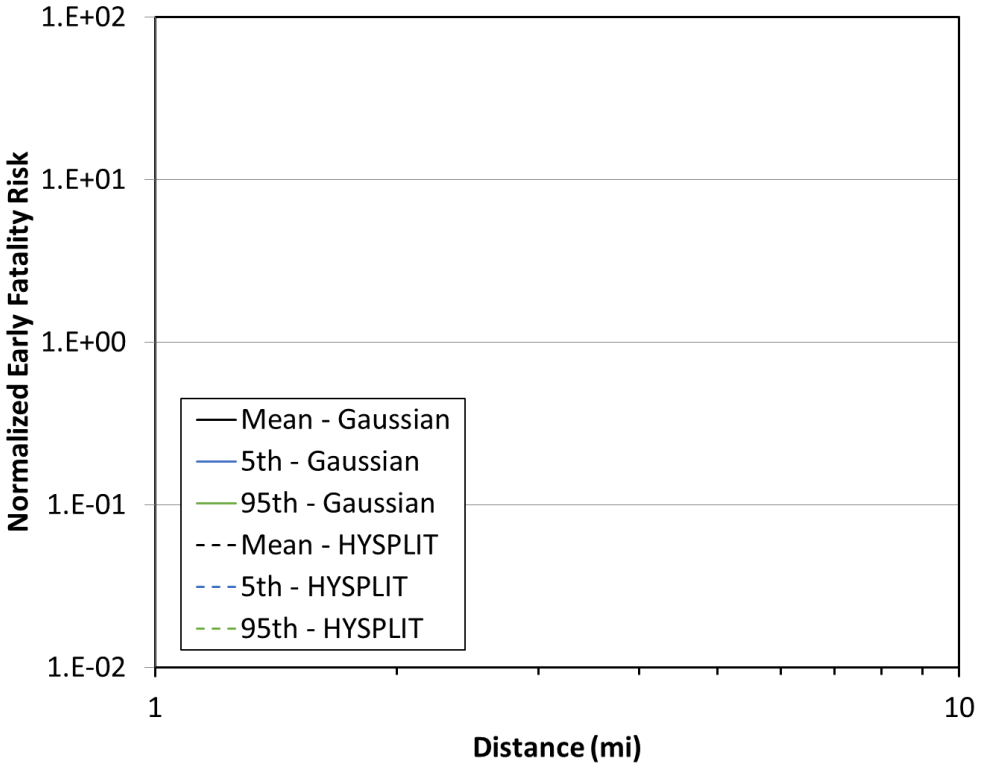

Figure C-77. Original benchmark Site E, ST #2, early fatality risk original comparison

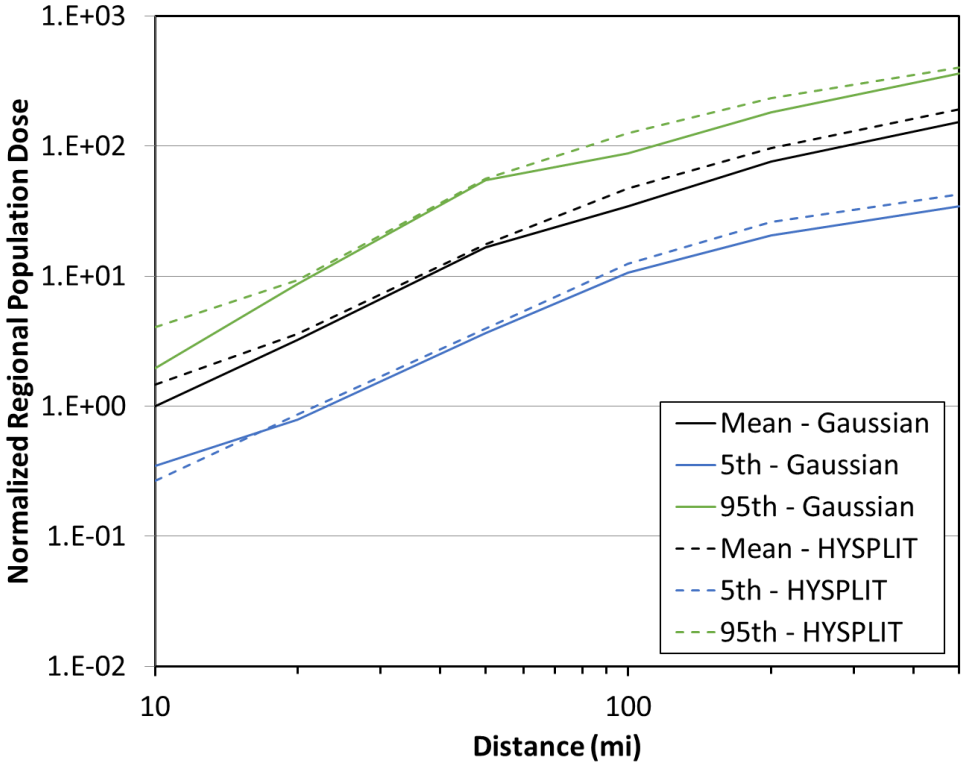

Figure C-78. Original benchmark Site E, ST #2, population dose original comparison

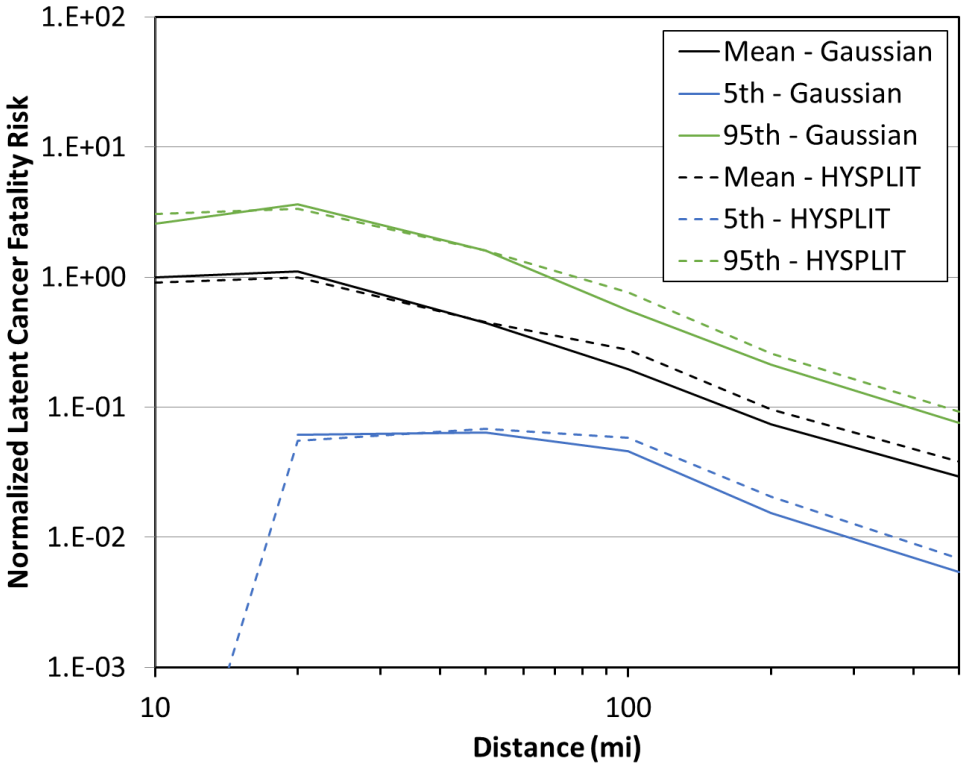

Figure C-79. Original benchmark Site E, ST #2, latent cancer fatality risk original comparison

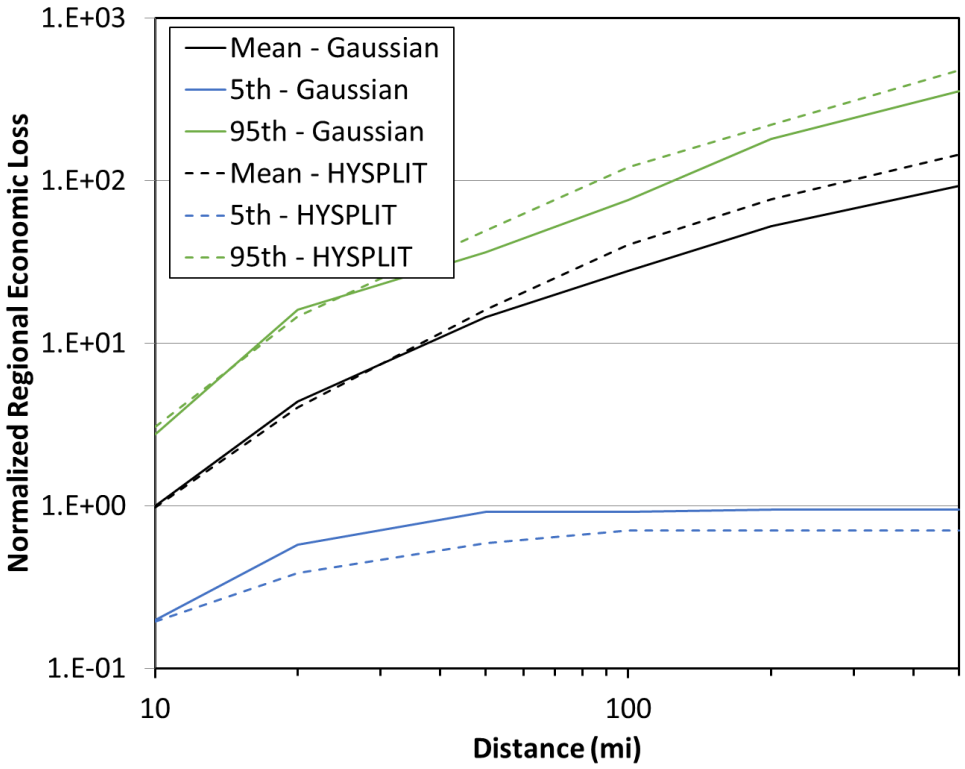

Figure C-80. Original benchmark Site E, ST #2, economic loss original comparison

C.6. Summary of Original Benchmark Results

This section provides a summary of the results in the multiple figures presented in the previous sections (Sections C.1through C.5). For these figures, the ratios of the annual average results over the weather variability for the HYSPLIT model to the Gaussian model are calculated for each output metric as a function of distance. The averages of these ratios, along with their minimums and maximums are delineated between nearfield (here defined to be from the site out to a radius of 48 km [30 mi]) and far field (beyond 48 km [30 mi] from the site out to 805 km [500 mi]) below in Table C-2 and Table C-3, respectively. EF risk is purely a nearfield result and hence is only shown in Table C-2. The land areas contaminated above a specific level are not delineated by distance and so are only shown in the far field results in Table C-3. For source term #2, EF risk was calculated as zero and so a ratio couldn't be calculated.

Table C-2. Nearfield ratios of the mean results for the HYSPLIT ATD model to the Gaussian ATD model, shown as [Average (Minimum | Maximum)], from the original benchmark analysis

Site/ Source	Near Field						
	Peak Air	Peak Ground	Peak Dose	Pop Dose	LCF Risk	Econ Loss	EF Risk
A/1	0.8 (0.6|1.1)	1.8 (1.2|2.7)	0.9 (0.7|1.4)	1.3 (1.3|1.3)	1.1 (1.0|1.1)	1.7 (1.7|1.8)	2.1 (1.4|2.4)
B/1	0.8 (0.7|1.2)	2.5 (1.5|4.2)	0.9 (0.7|1.3)	2.4 (2.1|2.6)	1.2 (1.1|1.2)	2.1 (2.0|2.1)	3.1 (1.0|4.1)
C/1	1.0 (0.8|1.7)	0.7 (0.6|1.3)	1.0 (0.8|1.6)	1.2 (1.2|1.3)	1.2 (1.2|1.2)	1.7 (1.5|1.9)	2.7 (2.1|3.0)
D/1	1.4 (1.2|1.7)	3.0 (2.3|4.0)	1.5 (1.2|2.1)	1.6 (1.6|1.7)	1.6 (1.5|1.6)	1.4 (1.3|1.5)	3.3 (1.0|9.5)
E/1	0.9 (0.8|1.3)	1.8 (1.2|2.6)	0.9 (0.8|1.3)	1.9 (1.8|2.1)	1.2 (1.1|1.2)	1.7 (1.6|1.7)	1.4 (1.2|1.7)
A/2	0.3 (0.2|0.4)	0.6 (0.5|1.0)	0.9 (0.5|1.1)	1.0 (1.0|1.1)	0.9 (0.9|0.9)	0.9 (0.9|0.9)	a
B/2	0.3 (0.2|0.5)	0.8 (0.5|1.3)	0.9 (0.6|1.1)	1.7 (1.4|2.1)	1.1 (1.0|1.2)	1.3 (1.3|1.3)	a
C/2	0.3 (0.3|0.6)	0.2 (0.2|0.5)	0.7 (0.5|0.9)	0.8 (0.7|0.9)	0.9 (0.8|0.9)	0.7 (0.7|0.7)	a
D/2	0.5 (0.4|0.6)	1.1 (0.9|1.4)	1.0 (0.8|1.1)	1.4 (1.3|1.5)	1.4 (1.3|1.5)	1.7 (1.6|1.8)	a
E/2	0.3 (0.3|0.4)	0.6 (0.4|0.8)	0.8 (0.5|1.0)	1.3 (1.1|1.5)	0.9 (0.9|0.9)	1.0 (0.9|1.0)	a

[a]Data not available to compute a ratio

Table C-3. Far field ratios of the mean results for the HYSPLIT ATD model to the Gaussian ATD model, shown as [Average (Minimum | Maximum)], from the original benchmark analysis

Site/ Source	Far Field						
	Peak Air	Peak Ground	Peak Dose	Pop Dose	LCF Risk	Econ Loss	Land Area
A/1	1.1 (0.5|1.4)	3.2 (2.3|4.0)	1.6 (1.2|2.3)	1.4 (1.3|1.5)	1.3 (1.1|1.5)	2.0 (1.7|2.2)	2.0 (1.5|2.5)
B/1	1.2 (0.5|1.6)	2.6 (2.0|3.5)	1.6 (1.2|2.1)	2.1 (1.9|2.5)	2.0 (1.5|2.6)	2.4 (1.8|2.8)	2.3 (2.1|2.6)
C/1	1.2 (0.5|1.8)	2.9 (1.6|4.1)	1.6 (1.1|2.5)	1.8 (1.7|1.9)	1.8 (1.6|1.9)	2.2 (1.8|2.4)	2.7 (1.9|4.0)
D/1	1.1 (0.4|1.8)	4.7 (2.6|6.2)	1.7 (1.3|1.9)	1.9 (1.7|2.1)	1.7 (1.6|1.9)	2.3 (1.8|2.5)	2.6 (2.5|2.7)
E/1	1.1 (0.4|1.6)	3.2 (2.2|3.9)	1.7 (1.3|2.3)	1.7 (1.6|2.0)	1.6 (1.3|1.9)	2.3 (1.5|2.8)	2.3 (1.8|2.9)
A/2	0.4 (0.2|0.5)	1.3 (1.0|1.5)	1.4 (1.2|1.7)	1.1 (1.0|1.2)	1.1 (1.0|1.2)	1.0 (1.0|1.1)	1.3 (1.1|1.4)
B/2	0.5 (0.2|0.6)	1.0 (0.8|1.2)	1.2 (1.1|1.4)	1.4 (1.3|1.5)	1.4 (1.2|1.5)	1.3 (1.2|1.4)	1.3 (1.3|1.4)
C/2	0.5 (0.2|0.7)	1.2 (0.7|1.8)	1.4 (0.9|1.8)	1.3 (1.2|1.4)	1.3 (1.2|1.4)	1.8 (1.4|2.0)	1.3 (0.6|2.0)
D/2	0.4 (0.2|0.6)	1.8 (1.0|2.3)	1.8 (1.2|2.4)	2.1 (1.9|2.2)	2.2 (1.9|2.3)	3.3 (3.2|3.5)	2.7 (2.1|3.0)
E/2	0.4 (0.2|0.6)	1.3 (0.8|1.6)	1.5 (1.0|1.8)	1.2 (1.0|1.4)	1.3 (1.0|1.4)	1.4 (1.1|1.6)	1.5 (1.1|1.7)

This page left blank

DISTRIBUTION

Email—Internal

Name	Org.	Sandia Email Address
Daniel Clayton	8855	djclayt@sandia.gov
Jennifer Leute	8855	jeleute@sandia.gov
John Fulton	8855	jdfulto@sandia.gov
Technical Library	1911	sanddocs@sandia.gov

Email—External

Name	Company Email Address	Company Name
Keith Compton	Keith.Compton@nrc.gov	U.S. Nuclear Regulatory Commission
Salman Haq	Salman.Haq@nrc.gov	U.S. Nuclear Regulatory Commission

This page left blank

This page left blank

Sandia National Laboratories is a multimission laboratory managed and operated by National Technology & Engineering Solutions of Sandia LLC, a wholly owned subsidiary of Honeywell International Inc. for the U.S. Department of Energy's National Nuclear Security Administration under contract DE-NA0003525.